Andrea Longobardo

SAMPLE RETURN MISSIONS

The Last Frontier of Solar System Exploration

ELSEVIER

Sample Return Missions

Sample Return Missions

The Last Frontier of Solar System Exploration

Edited by

ANDREA LONGOBARDO
INAF-IAPS, Rome, Italy

ELSEVIER

Elsevier
Radarweg 29, PO Box 211, 1000 AE Amsterdam, Netherlands
The Boulevard, Langford Lane, Kidlington, Oxford OX5 1GB, United Kingdom
50 Hampshire Street, 5th Floor, Cambridge, MA 02139, United States

Notices

Knowledge and best practice in this field are constantly changing. As new research and experience broaden our understanding, changes in research methods, professional practices, or medical treatment may become necessary.

Practitioners and researchers must always rely on their own experience and knowledge in evaluating and using any information, methods, compounds, or experiments described herein. In using such information or methods they should be mindful of their own safety and the safety of others, including parties for whom they have a professional responsibility.

To the fullest extent of the law, neither the Publisher nor the authors, contributors, or editors, assume any liability for any injury and/or damage to persons or property as a matter of products liability, negligence or otherwise, or from any use or operation of any methods, products, instructions, or ideas contained in the material herein.

British Library Cataloguing-in-Publication Data
A catalogue record for this book is available from the British Library

Library of Congress Cataloging-in-Publication Data
A catalog record for this book is available from the Library of Congress

ISBN: 978-0-12-818330-4

Publisher: Candice Janco
Acquisitions Editor: Peter Llewellyn
Editorial Project Manager: Allison Hill
Production Project Manager: Sruthi Satheesh
Cover Designer: Christian Bilbow

Typeset by Aptara, New Delhi, India

CONTENTS

Contributors

Masanao Abe
Japan Aerospace Exploration Agency, Institute of Space and Astronautical Science, Astromaterials Science Research Group

Jérôme Aléon
Institut de Minéralogie, de Physique des Matériaux et de Cosmochimie, Sorbonne Université, Museum National d'Histoire Naturelle, CNRS, Université Pierre et Marie Curie, Institut de Recherche pour le Développement, Paris

Alice Aléon-Toppani
Université Paris-Saclay, CNRS, Institut d'Astrophysique Spatiale, Orsay, France

Allan Bennett
Public Health England, Porton Down, Wiltshire, UK

Lucy Berthoud
University of Bristol, Queen's Building, University Walk, Clifton, UK; Thales Alenia Space UK Limited, Bristol

Janet Borg
Université Paris-Saclay, CNRS, Institut d'Astrophysique Spatiale, Orsay, France

John C. Bridges
Space Research Centre, Michael Atiyah Building, University of Leicester, Leicester, UK

Donald E. Brownlee
Department of Astronomy, University of Washington, Seattle, WA, USA

Rosario Brunetto
Université Paris-Saclay, CNRS, Institut d'Astrophysique Spatiale, Orsay, France

Don Burnett
Geological and Planetary Sciences, California Institute of Technology, Pasadena, CA

John Robert Brucato
Istituto Nazionale di Astrofisica - Osservatorio Astrofisico di Arcetri (INAF-OAA), L.go E. Fermi, Firenze, Italy

Vincenzo Della Corte
INAF-IAPS, Roma, Italy

Vinciane Debaille
Laboratoire G-Time, Université Libre de Bruxelles (ULB), Département Géosciences, Environnement et Société, Bruxelles, Belgium

Fabrizio Dirri
INAF-IAPS, Rome, Italy

Zahia Djouadi
Université Paris-Saclay, CNRS, Institut d'Astrophysique Spatiale, Orsay, France

Heather L. Enos
Lunar and Planetary Laboratory, University of Arizona, Tucson, AZ, USA

Ludovic Ferrière
Naturhistorisches Museum Wien, Vienna, Austria

Luigi Folco
Dipartimento di Scienze della Terra, Università di Pisa, Pisa, Italy; CISUP, Centro per l'Integrazione della Strumentazione dell'Università di Pisa, Pisa, Italy

Frédéric Foucher
CNRS, Centre de Biophysique Moélculaire, CNRS, Centre de Biophysique Moléculaire, Orléans, France

Ian A. Franchi
PSSRI, The Open University, Milton Keynes, UK

Akira Fujiwara
Japan Aerospace Exploration Agency

Matthieu Gounelle
Institut de Minéralogie, de Physique des Matériaux et de Cosmochimie, Sorbonne Université, Museum National d'Histoire Naturelle, CNRS, Université Pierre et Marie Curie, Institut de Recherche pour le Développement, Paris

Monica M. Grady
PSSRI, The Open University, Milton Keynes, UK

John Holt
Space Research Centre, Michael Atiyah Building, University of Leicester, Leicester, UK

Aurore Hutzler
Lunar and Planetary Institute, USRA, Houston, TX, USA; Astromaterials Research and Exploration Sciences, NASA JSC, Houston, TX, USA

Eric A. Jerde
Department of Physics, Earth Science, and Space Systems Engineering, Morehead State University, Morehead, KY, USA

Amy Jurewicz
Arizona State University Center for Meteorite Studies/School of Earth and Space Exploration, c/o Dartmouth College, Department of Earth Sciences, Hanover, NH

Junichiro Kawaguchi
Japan Aerospace Exploration Agency

Dante S. Lauretta
Lunar and Planetary Laboratory, University of Arizona, Tucson, AZ, USA

Stefano Leuko
German Aerospace Centre, Institute of Aerospace Medicine, Radiation Biology, Köln, Germany

Andrea Longobardo
INAF-IAPS, Rome, Italy

Jonathan I. Lunine
Department of Astronomy, Cornell University

Yves Marrocchi
CRPG, CNRS, Université de Lorraine, Vandoeuvre-lès-Nancy, France

Andrea Meneghin
Istituto Nazionale di Astrofisica - Osservatorio Astrofisico di Arcetri (INAF-OAA), L.go E. Fermi, Firenze, Italy

Ernesto Palomba
INAF-IAPS, Rome, Italy

Anjani T. Polit
Lunar and Planetary Laboratory, University of Arizona, Tucson, AZ, USA

Thomas Pottage
Public Health England, Porton Down, Wiltshire, UK

Yuqi Qian
Planetary Science Institute, School of Earth Sciences, China University of Geosciences, Wuhan, China

Dan Reisenfeld
Los Alamos National Laboratory, Los Alamos, NM, USA

Petra Rettberg
German Aerospace Centre, Institute of Aerospace Medicine, Radiation Biology, Köln, Germany

Heather L. Roper
Lunar and Planetary Laboratory, University of Arizona, Tucson, AZ, USA

Alessandra Rotundi
Università degli studi di Napoli Parthenope, Napoli, Italy

Sara S. Russell
Department of Earth Sciences, The Natural History Museum, London, UK

Scott A. Sandford
NASA-Ames Research Center, Astrophysics Branch, Moffett Field, CA, USA

Caroline L. Smith
Department of Earth Sciences, The Natural History Museum, London, UK; School of Geographical and Earth Sciences, University of Glasgow, Glasgow, UK

Evgeny Slyuta
Vernadsky Institute of Geochemistry and Analytical Chemistry RAS, Moscow, Russia

Shogo Tachibana
UTokyo Organization for Planetary and Space Science (UTOPS), University of Tokyo, Tokyo, Japan; Institute of Space and Astronautical Science, Japan Aerospace Exploration Agency (JAXA), Sagamihara, Kanagawa, Japan

Elizabeth J. Tasker
Institute of Space and Astronautical Science, Japan Aerospace Exploration Agency

Akira Tsuchiyama
Ritsumeikan University and Guangzhou Institute of Geochemistry

John Vrublevskis
Thales Alenia Space UK Limited, Bristol

Qian Wang
Lunar Exploration and Space Engineering Center, China National Space Administration, Beijing, China

Qiong Wang
Lunar Exploration and Space Engineering Center, China National Space Administration, Beijing, China

Frances Westall
CNRS, Centre de Biophysique Moélculaire, CNRS, Centre de Biophysique Moléculaire, Orléans, France

Roger C. Wiens
Los Alamos National Laboratory, Los Alamos, NM, USA

Catherine W.V. Wolner
Lunar and Planetary Laboratory, University of Arizona, Tucson, AZ, USA

Long Xiao
Planetary Science Institute, School of Earth Sciences, China University of Geosciences, Wuhan, China

Makoto Yoshikawa
Japan Aerospace Exploration Agency

Jutta Zipfel
Senckenberg Gesellschaft für Naturforschung, Frankfurt am Main, Germany

Michael E. Zolensky
XI2, NASA-Johnson Space Center, Houston, TX, USA

CHAPTER 1

Introduction

Andrea Longobardo
INAF-IAPS, Rome, Italy

Which were the processes occurred in the early stages of our Solar System? Which the processes that led to emergence of life? These two fundamental key-questions identified by the worldwide Planetary Science community are requiring thorough scientific investigations, which in turn take advantage of technological improvements.

Small bodies, such as satellites, asteroids and comets, are the most suitable targets to deepen these issues, because they are the least altered bodies from their state in the solar nebula and therefore best preserve information on the Solar System early stages. Nevertheless, the recent discoveries about the astrobiological potential of Mars make the Red Planet another important scientific target to investigate the development of life in the Solar System.

Prior to space exploration, the information on small bodies was derived on ground observations, whose results were generally limited to global (e.g., shape, size, rotation period) and average (optical, spectroscopic and photometric) properties. Except for the Moon, that was explored in-situ by means of both robotic and crewed missions since 1960s (with the first hard landing occurred in 1959), the small bodies features at small spatial scale (i.e., at cm-scale and lower) could only be inferred from meteorites: the ground-based observations were often sufficient to link different meteorite classes with related parent bodies.

However, meteorites are affected by the terrestrial environment, both during their entrance in atmosphere, when they experience heating (caused by atmosphere friction) and interact with atmospheric gases, and after their fall, when they are altered by salts, water and oxygen, therefore do not provide ground truth.

Planetary in-situ exploration overcomes this issue, allowing analysis of samples directly on the target body. In-situ missions were addressed to the Moon, Mars and Venus from the 60s to the 80s and then extended to small bodies other than the Moon (satellites, asteroids and comets). While these missions do not suffer the samples alteration, they have to deal with the limitations proper of space missions. The limited mass/power/volume spacecraft budget forces a selection of experiments to be performed on the target body. Moreover, in-situ measurements are performed by means of instrumentation/technologies available at the time of the mission, without possibility to repeat or improve them.

Sample Return Missions
DOI: 10.1016/C2018-0-03374-5

Sample return combines the advantages of in-situ planetary measurements (ground truth) and meteorite laboratory experiments (repeatibility, continuous sample availability, possibility to take advantage of technology improvements). The first extraterrestrial samples were returned from the Moon, during the Moon race between U.S. and U.S.S.R. between 60s and 70s. While the astronauts landed on the Moon during the NASA's Apollo program brought back an enormous amount of lunar material, the Soviet Luna program performed the first robotic extraterrestrial sampling. The following sample return missions were performed more than 20 years later, with the NASA's Genesis and Stardust missions which returned solar wind particles and cometary dust, respectively. With the new century, the Japan Aerospace Exploration Agency (JAXA)'s Hayabusa mission performed the first asteroid sample return. Sample return missions were increasingly considered from the planetary science community, new technologies were studied and developed to this end, new actors (Europe and China) appeared in this scenario.

At the time of writing, two missions just returned their samples to Earth (the JAXA/Hayabusa2 and the Chinese Chang'e 5), one is ongoing but already sampled its target (the NASA/OSIRIS-Rex), while another mission is to be launched in the next years (the Japanese MMX).

It is clear that the sample return is the last frontier of Solar System exploration. Nevertheless, in view of the enormous advantages offered, this type of mission requires a special care from its planning until their end, given the technical challenges requested by approach and sampling operations. These operations have to take into account several body and sample properties, such as body gravity, terrain hardness, sample size, and require an assessment of security and risks related to the available technology and to the sampling site characteristics. After return to Earth, the first duty is to safely transport the samples from the landing site to the curation laboratory, avoiding their contamination from the terrestrial environment (or, in the case of samples potentially hosting lifeforms, to the terrestrial environment). The following sample analysis and storage operations should also guarantee the samples integrity and purity.

The development of sample return missions obviously goes together with creation and improvement of curation facilities devoted to acceptance, study and preservation of these scientifically precious samples, as well as with progress of sample collection/analysis techniques and instrumentation.

This book provides a snapshot at 2020 of sample return from the Solar System, under both a scientific and an engineering perspective. The book describes the past and ongoing missions with their main achieved results, the operating curation facilities, the state of art of sample collection, transport, analysis and preservation techniques, and future plans in terms of designed/proposed missions, facility concepts and technique developments.

The first part (Chapters 2–10) focuses on sample return space missions.

The NASA's Apollo program (Jerde, Chapter 2) was the first to bring extraterrestrial samples back to Earth. Specifically, the six human landings on the Moon between

1969 and 1972 returned 376 kg of lunar rocks (basalts, breccias, glasses, anorthosites). This allowed to unveil the history of the Moon: the original crust, made of anorthosite, formed 4.5–4.1 Ga through plagioclase crystallization and flotation from a magma ocean; impacts formed large basins until 3.8 Ga; most of these basins were filled by basalts, erupted as a consequence of secondary melting of deeper portions of the crystallized magma ocean; this volcanic activity occurred until 3 Ga, followed by other sporadic events.

The Luna program (Slyuta, Chapter 3) was the lunar exploration Soviet program, simultaneous to Apollo. This program holds several records (first artificial planet and Moon satellite, first extraterrestrial hard landing and first Moon soft landing, first Moon far side images, panoramas and gamma-ray survey) and included three robotic sample return missions (Luna 16, Luna 20 and Luna 24). The latter brought back basalts of different size (both coarse and fine) and composition (medium- and low- titanium, high-aluminium) from the lunar maria, while anorthosites were returned from a highland region.

The NASA's Stardust mission (Sandford et al., Chapter 4) was the first to collect and return cometary (from 81P/Wild2, a Jupiter family comet) and interplanetary dust. These samples were brought back in 2006 and their analysis strongly improved our knowledge of comet formation processes. In particular, the mission highlighted that 81P/Wild2 was made of a mixture of materials formed in different locations of the protosolar disk and processed differently, then assembled in a cometary body and subsequently poorly altered. The outcoming scenario was that comets are more complex than what was previously thought.

The NASA's Genesis mission (Wiens et al., Chapter 5) represents a stand-alone among sample return missions: it was not addressed to a specific planetary body, but aimed at studying solar cosmoschemistry by collecting over 887 days (2001–2004) and returning different types of solar wind particles. Despite the non-nominal landing on Earth (the sample return capsule crashed due to a parachute deployment failure), it was possible to analyse several samples (mainly by noble gas and secondary ion mass spectrometry) and to reveal new solar cosmochemistry insights, i.e., the lower mass number of solar oxygen and nitrogen isotopes with respect to the terrestrial ones (due to solar-nebula photochemical self-shielding), the occurrence of solar noble gases in the lunar regolith, new constraints on theories of solar wind acceleration and fractionation.

The first sample return from an asteroid was performed by the JAXA's Hayabusa mission (Yoshikawa et al. Chapter 6), launched in 2003, arrived to Itokawa (a small near-Earth asteroid) in 2003 and returned back to Earth in 2010 with thousands of small grains. Remote observations by means of four scientific instruments revealed the absence of craters and the occurrence of many boulders on the asteroid surface. Even if the sampling was not performed as planned and despite the problems expe-

rienced after the second touchdown, a lot of information on the Itokawa's origin and evolution was provided by combining remote sensing data and measurements on returned samples.

Hayabusa was followed by Hayabusa2 (Tachibana, Chapter 7), which was launched on 2014 and succeeded two landing operations to sample Ryugu, a carbonaceous near-Earth asteroid. The Hayabusa2 observations revealed that Ryugu is a top-shape rubble pile body, darker than most of meteorite samples, spectrally uniform and globally covered by weakly hydrated silicates. The spacecraft has recently delivered the reentry capsule to the Earth. Analysis of returned samples will unveil the reason of the weak hydration (thermal dehydration or weak aqueous alteration), as well as the nature of carbonaceous asteroids and the sample record of origin and evolution of the Solar System and of the asteroid itself.

NASA is also conducting a sample return mission from a near-Earth asteroid, Bennu. The OSIRIS-REx (Origins, Spectral Interpretation, Resource Identification, and Security–Regolith Explorer) mission (Lauretta et al., Chapter 8) reached its target in December 2018, revealing a body completely different than expected, with rough and rugged terrains, which is going to complicate the sampling operations. For this reason, the mission team modified the mission profile, being however able to select primary and backup sampling site. To date, the mission characterized the Bennu's physical, chemical and geological properties, with particular attention to the sampling site's context, and performed one sampling operation in October 2020. The departure from Bennu is scheduled in 2021 and the return to Earth in 2023.

The first Chinese sample return mission was launched in November 2020. Chang'e 5 (Xiao et al., Chapter 9) landed and sampled (by a drill and a robotic arm) the Moon's Rümker region, covered by young basalts, returning to Earth 1.7 kg of lunar material in December 2020. The China National Space Administration (CNSA) will manage the sample operations and storage. The procedures of sample preliminary analysis and curation at the primary storage center, of sample storage and of allocation for research analysis have been defined.

Chapter 10 (Tasker and Lunine) is dedicated to planned missions and proposed/under evaluation mission concepts. The JAXAs Martian Moon eXplorer (MMX) will be launched in 2024 and will be the first to obtain and return a sample from Phobos: its results will constrain the origin of this Martian satellite. JAXA is also considering OKEANOS (Oversize Kite-craft for Exploration and AstroNautics in the Outer Solar System), that aims at sampling a Trojan asteroid: the combination with results obtained by the other JAXA sample return missions (MMX and the two Hayabusa) would allow the reconstruction of organics and volatile movement across the early Solar System. On the NASA side, the CAESAR (Comet Astrobiology Exploration SAmple Return) mission has been proposed to return a sample from the nucleus of 67P/Churyumov-Gerasimenko comet, in order to expand the knowledge of this comet after its exploration by the ESA/Rosetta mission.

The second part of the book (Chapters 11–13) is devoted to curation facilities.

The Johnson Space Center (Longobardo and Hutzler, Chapter 11) is the largest and the oldest complex of laboratories for curation and storage of returned samples. It is curating samples since 1969 and includes laboratories for each past and ongoing sample return mission. The Johnson Space Center staff's expertise resulted in the definition of protocols for handling, processing and storing extraterrestrial samples.

The JAXA Planetary Material Sample Curation Facility (Abe, Chapter 12), led by the JAXA's ISAS (Institute for Space Center), is more recent. It accepted the samples returned by Hayabusa and will also curate Hayabusa2 and OSIRIS-REx samples. The Itokawa samples are here characterized, and then catalogued and distributed to researchers for upcoming analyses.

Currently, a European curation facility for extraterrestrial returned samples does not exist. Nevertheless, an European Commission funded project under the Horizon 2020 Research and Innovation program, named EUROCARES (European Curation of Astromaterials Returned from the Exploration of Space), reviewed the current state-of-art curational practises and defined the steps to create a fully operative European facility in view of future sample return missions. The project is presented in Chapter 13 (Smith et al.).

The third part of the book (Chapters 14–18) focuses on techniques and technologies applied to returned samples.

A review of sample collection techniques adopted in past and present missions, together with techniques used to collect interplanetary and stratospheric extra-terrestrial dust and with technologies under study for future Mars and Moon sampling, is given in Chapter 14 (Della Corte and Rotundi).

Sample recovery and transport are crucial procedures, that have to avoid sample contamination from and to (in the case of samples hosting life forms) terrestrial environment. Chapter 15 (Dirri et al.) describes the landing sites considered so far and their influence on these procedures, the techniques and technologies used for sample transport from landing site to laboratories and among laboratories, and the regulatory issues to take into account in the case of transport of critical samples (i.e., those potentially including biological molecules).

Techniques and instruments used to analyze, characterize and study returned extraterrestrial samples are the focus of Chapter 16 (Brunetto et al.). Their purpose is to maximize the scientific return and minimize the sample loss: this is achieved by defining a multi-analytical sequence from less to more destructive techniques. The return of samples from ongoing missions will probably refine these techniques.

Chapter 17 presents containment procedures and technologies applied on returned samples (Meneghin and Brucato): their aim is to preserve the samples, maintaining their conditions as close as possible to their parent body and implementing clean and sterile environments. A special care would be required in the case of samples returned from

Mars, that are considered "restricted", i.e., potentially hosting or having hosted life. This poses the problem of "backward contamination" (i.e., from samples to humans) and requires the development of specific sample preservation procedures.

The last chapter Longobardo. Chapter 18 summarizes the lessons learned so far by sample return mission and the future perspectives.

PART I

Space missions

CHAPTER 2

The Apollo program

Eric A. Jerde
Department of Physics, Earth Science, and Space Systems Engineering,
Morehead State University, Morehead, KY, USA

Chapter Outlines

Sample Return Missions
DOI: 10.1016/C2018-0-03374-5

2.1 Introduction

The Apollo program stands alone in the history of spaceflight. It was the culmination of a decade of engineering innovation, tests, and lead-up manned and unmanned flights. Much of the procedural experience actually owes its existence to the flights of Gemini in the mid-1960s, which developed techniques for rendezvous and extra-vehicular activity (EVA) operations. It is truly stunning to comprehend the scope of the endeavor to reach the Moon. There were 9 flights in the Ranger program to impact the Moon, 7 Surveyors to soft land on the Moon, 5 Lunar Orbiters, 10 manned Gemini flights, and the 11 Apollo flights, including the six landings. There were also numerous lesser flights to test rocket stages and two full-up tests of the Saturn V itself. It is safe to say that it is unlikely that the world will witness spaceflight at this pace again.

Outside of technological innovations such as electronic miniaturization, which led to the development of calculators and eventually personal computers, probably the greatest thing gained from Apollo is that humans became comfortable working in space. The basic procedures for missions and EVAs were developed during Apollo and have served the Space Shuttle and International Space Station.

2.2 Early planning and strategies

2.2.1 Landing site selection

Initial ideas for landing sites were concerned mainly with smoothness of terrain to allow for the safest possible outcome. The Lunar Orbiter program utilized five orbiters, launched between August 1966 and August 1967. These spacecraft provided high-resolution imagery of potential landing sites, identifying the relatively craterless and boulder-free region used for the first landing in Mare Tranquillitatis (Apollo 11).

Additional concerns existed over the potential threat of surface dust thickness that might impair surface operations. Indeed, the general nature of the surface properties was of great interest. To address this, a series of soft-landers were created, namely the Surveyor series of lunar probes. Seven of these were launched between May 1966 and January 1968. Two failed before landing, but five were successful, and demonstrated that surface dust would not be a hindrance, except perhaps during the actual landing when it might obscure the surface due to entrainment in rocket exhaust.

Along with the identification of potential landing sites, analysis was needed as to the orbital dynamics associated with reaching landing sites. The Apollo program managers had decided to use a "lunar-orbit-rendezvous" process, where an initial orbit about the Moon would be established by the combination of the lunar lander (LM) and the command/service module (CSM). The issue that arises with this, particularly for any extended surface operations is that once the lander has descended to the surface, the rotation of the Moon moves the lander "out of plane" of the orbiting CSM. After a few days, this rotation can potentially make it difficult for the lander to rendezvous with

Table 2.1 Identified Landing Sites (Binder and Roberts, 1970.)
Originally Proposed Landing Sites

Identified Site	Apollo Mission	Lunar Coordinates*
Mare Tranquillitatis	Apollo 11	0.6742°N; 23.4731°E
Surveyor III	Apollo 12	3.0128°S; 23.4219°W
Mare So. Of Kepler	A-12 alternate	*8.1°N; 38.0°W (Kepler)*
Fra Mauro	Apollo 14	3.6459°S; 17.4719°W
Littrow	Apollo 17	20.1911°N; 30.7655°E
Censorinus		*0.4°S; 32.7°E*
Tycho		*43.3°S; 11.4°W*
Copernicus Central Peak		*9.6°N; 20.1°W*
Descartes	Apollo 16	8.9734°S; 15.5011°E
Marius Hills		*14°N; 56°W*
Hadley-Apennine	Apollo 15	26.1324°N; 3.6333°E

*Actual Apollo LM locations from Wagner et al. (2017). Italics are for the general feature, since no specific site was identified.

the CSM without the ability to significantly change the plane of orbit, a maneuver that requires significant energy and thus fuel. This problem is minimized when the inclination of the established lunar orbit is nearly that of the latitude of the landing site. Early missions utilized transfer trajectories that had a low inclination to the lunar equator, and this restricted potential landing sites to those of low latitudes. Higher latitude sites would have required very short stay times or increased "plane change" capability, which was not feasible in early Apollo landings. A detailed description of the orbital dynamics associated with the Apollo missions is given in Enderson (1965).

Given the basic constraints and needs of the initial, rather limited, science objectives, eleven potential landing sites were identified (Table 2.1, Fig. 2.1). Six of these were utilized for the Apollo landings. The emergency associated with Apollo 13 and the cancellation of the originally planned Apollo 18, 19, and 20 flights eliminated landing sites from the program.

2.2.2 Science gains in importance

As an almost completely unexplored planetary object, the initial scientific objectives were very basic, namely to return samples of a variety of rock types, and characterize the basic geology of the region surrounding each site. However, prior to even the first of the Apollo flights, a more comprehensive science plan was developed.

The initial goal of Apollo was "to land a man on the Moon and return him safely to the Earth" as set forth by U.S. President John Kennedy in May 1961. The initial work to make this a reality was mainly concerned with the monumental engineering challenges to be overcome, given that the United States experience in spaceflight was only three years old, and none of that experience was beyond Earth orbit. The return of samples was probably always in the mix, but more organized geological strategies were still far off.

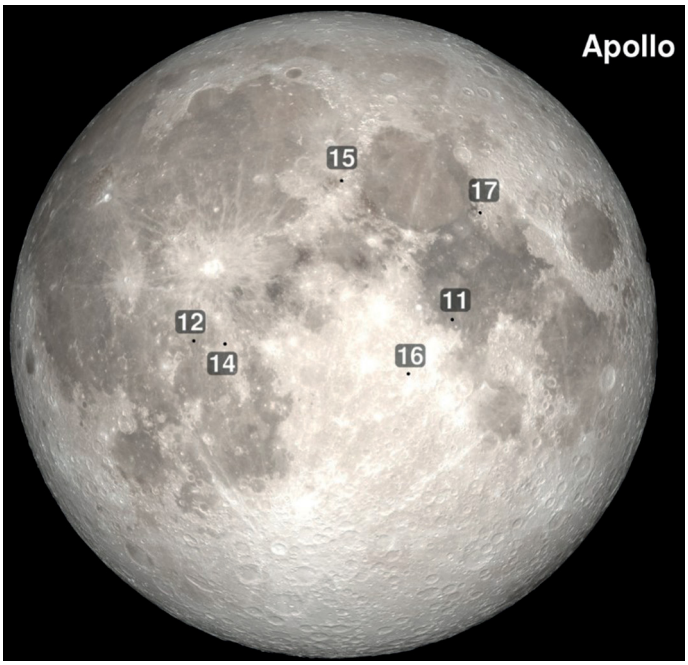

Fig. 2.1 The six Apollo lunar landing sites. *(NASA Goddard Spaceflight Center).*

Even during Apollo 11, there was not really much of a detailed sampling strategy. The "contingency" sample was collected in the first minutes of the initial extra-vehicular activity (EVA). Then, during the remainder of the approximately two hours on the surface, a "bulk" sample was collected by Neil Armstrong via 22 – 23 individual scoops at various places around the lunar module. These two samples comprised approximately 85 percent of the returned sample material. The remaining 15 percent were a few individual rocks and two short cores driven into the surface using a hammer.

Based on the success of Apollo 11 in terms of human performance, and results from the initial sample analysis, more detailed plans emerged for Apollo 12 and 14. By the time of Apollo 15, science became the focus of the EVAs (three EVAs on each of the last three missions, including extended traverses with a lunar roving vehicle). Within the typical Apollo constraints due to orbital mechanics and fuel, the landing site selection was based on science.

During the debriefing after each mission, modifications were made to future missions to address specific issues that were discovered. The discovery during the first landing, Apollo 11, of the nature of the regolith, with abundant fine material along with pebble- and cobble-sized fragments that made sampling difficult, led to the development of the lunar "rake" for subsequent missions (Fig. 2.2). This tool was basically a sieve that permitted the gathering of a set of rocks separated from the finer material, and

Fig. 2.2 Lunar rake used to separate rocks from the surface regolith. *(NASA photograph AS16-116–18690).*

greatly aided the collection of a wide variety of rock types. The Apollo 12 astronauts, with their two, more extended EVAs, suggested that the need for food may not arise during an EVA, but thirst was a problem. This led to the development of a system by which astronauts could get sips of water or orange juice during EVAs.

In all missions it was noted that while leg fatigue was not an issue, hand grip became progressively more difficult because the pressure suit tended to force open the glove due to the vacuum on the lunar surface. As such, the astronauts had to work against this force and physically "grip" things even for the most menial of tasks, leading to tired hands. This was particularly true for the final three missions.

2.2.3 Other constraints

There were numerous constraints on the collection of samples. The ultimate planning constraint was astronaut safety, and this limited EVA duration. The fundamental rule was that consumables would dictate the length (Loftus et al., 1969). This led to lunar surface exploration being broken down into periods of active scientific work, and travel times, whether walking or, in the later missions, driving. Aside from the setting up of scientific instruments, which was generally in the vicinity of the lunar module, sample collecting was designed to be at pre-determined locations, or "stations". For a given EVA, the furthest station was done first, and the astronauts worked their way back toward the Lunar Module (LM).

There were additional constraints in that the two astronauts had to be in visual contact with each other at all times and were not permitted to be out of contact with each other or with the Mission Control Center for more than five minutes at a time. As a further constraint, at no time could the astronauts be further from the LM than walking distance with the pressure suit consumables (oxygen and water – both drinking and cooling water). This even extended to the rover traverses where at times the astronauts were many kilometers from the LM. All these constraints led to a timeline that provided limited time at any given site, and thus limited the amount of sample material collected. If something notable was discovered, like the orange soil at Apollo 17, extended time would be allotted, but it would be at the expense of time elsewhere. In a few cases, entire stations that had been planned were dropped.

Even though the astronauts found that working on the lunar surface was not difficult, it was found that fatigue did play a role. During a traverse made by the Apollo 14 astronauts, they got very tired from exertion while walking up a slope in an attempt to reach the rim of Cone Crater. This had also been found on Apollo 12, and short rest periods were taken during EVAs.

2.3 Experiments not related to geologic sampling

The so-called "Moon rocks" are generally remembered by the public. However, there were many additional experiments to investigate lunar processes and features (see Sullivan, 1994).

During each mission, the first extravehicular activity (EVA) consisted of obtaining contingency samples, and then deploying a set of experiments. Among these, there were experiment packages, known as the Early Apollo Surface Experiments Package (EASEP) on Apollo 11, and the Apollo Lunar Surface Experiments Package (ALSEP) on the remaining flights. These carried a variety of instruments to gather data for radio transmission to Earth. Other geophysical experiments included both active and passive seismic experiments, gravimeters (one of which was transported on the lunar rover and periodically read by the astronauts on Apollo 17), heat flow probes to measure the amount of internal heat coming out of the Moon, and a variety of magnetometers to characterize the inherent lunar magnetic field as well as local fields. Surface electrical properties and soil mechanics were also measured.

On Apollo 12, 14, and 15, a Cold Cathode Ion Gauge was deployed to measure the density of neutral particles in order to determine the amount of gas present at the lunar surface. On Apollo 17, a more discerning mass spectrometer, the Lunar Atmosphere Composition Experiment, actually measured the composition of the lunar atmosphere.

Experiments to measure particles and fields included a Charged Particle Lunar Environment Experiment, Cosmic Ray Detector Experiments, Solar Wind Composition and Solar Wind Spectrometer Experiments, and a Suprathermal Ion Detector Experiment.

Another set of items placed on the Moon represent the only experiments still used today. Laser Ranging Retroreflectors were placed at the Apollo 11, 14, and 15 landing

sites to permit short-pulse laser measurements of the distance to the Moon from the Earth. This can also measure the effects of lunar libration, Earth rotation wobbles, and the Moon's recession from the Earth due to tidal dissipation. These reflectors are completely passive, requiring no energy, and have suffered no appreciable degradation since deployment during the Apollo era.

2.4 Tools & photography

A large variety of tools were utilized during the Apollo missions. Tool design posed a unique set of constraints, since they had to be designed for use by astronauts in pressure suits, using gloves that were bulky and hard to manipulate (the internal pressure of the suits tended to keep them in an extended position, requiring constant pressure to grip anything). In addition, any sampling tool or container had to be able to withstand the hard vacuum of the lunar environment, as well as the lunar thermal range of approximately 100–400 K. Additional constraints on tool materials were placed due to considerations of sample contamination. Materials were to avoid the use of Pb, U, Th, Li, Be, B, K, Rb, Sr, noble gases, rare earths, and also needed to be sterilized. Aluminum alloy 6061 and 300 series stainless steel were the primary materials used. The only plastic material that met criteria was Teflon and was used for sample bags. Additional details of the tools and equipment used in sampling are given in Allton (1989).

Photography on the lunar surface was used to document activities, location of samples, nature of the surface, and other items of interest. The missions utilized 70 mm Hasselblad cameras that had film cartridges that could be interchanged easily by astronauts in pressure suits. Such switching of film could be done even when the film was only partially used, and this permitted changing of film from black & white to color, and to compensate for varying lighting conditions. Over the course of the six landings, 45 cartridges of film were used, and over 5500 photographs were taken.

For sampling of rocks and driving tubes, a hammer was developed that had a resemblance to a typical terrestrial rock hammer (Fig. 2.3). Over the course of the six Apollo landings, two different weights were used: a lighter hammer (860 g mass) for Apollo 11

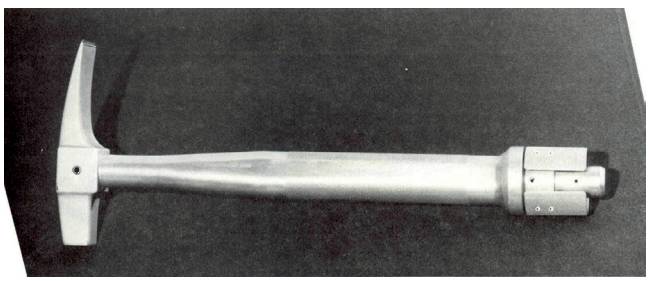

Fig. 2.3 Hammer of a lightweight variety used on Apollo 11 and 12. *(NASA photograph S69-31847)*.

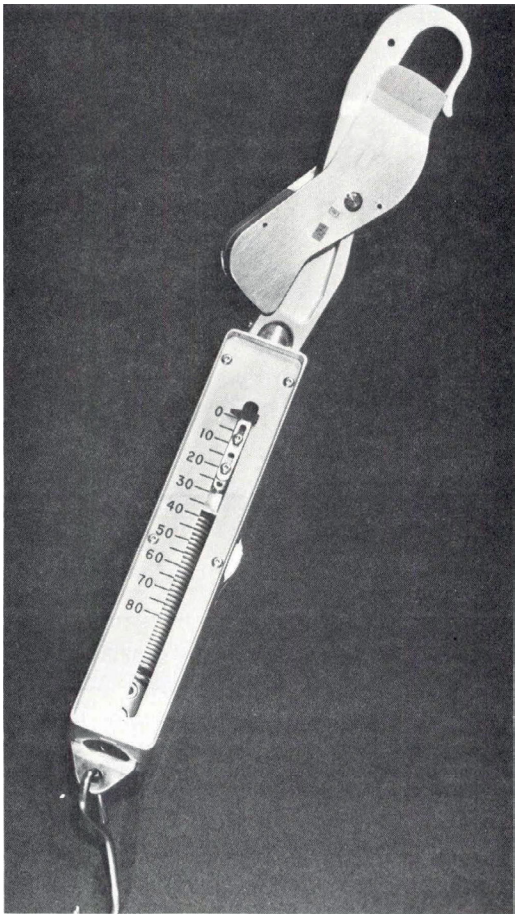

Fig. 2.4 Spring scale used to determine the mass of samples on the lunar surface. *(NASA photograph S70-36083)*.

and 12, and hammers of 1300 g for the following missions. One of the features of the heavier hammers was a larger area on the side of the head, which facilitated driving of core tubes. Weighing the bags of samples was accomplished through the use of a spring scale (Fig. 2.4). This scale was calibrated to provide the correct mass in the one-sixth g of the lunar environment.

2.5 The Apollo samples

2.5.1 Documented versus undocumented

To fully document a sample, down-sun and cross-sun photographs were taken of a rock to be sampled prior to disturbance. After collection, a down-sun photograph was taken. Ideally, a gnomon would be in the field of view of the photographs. The gnomon (Fig. 2.5)

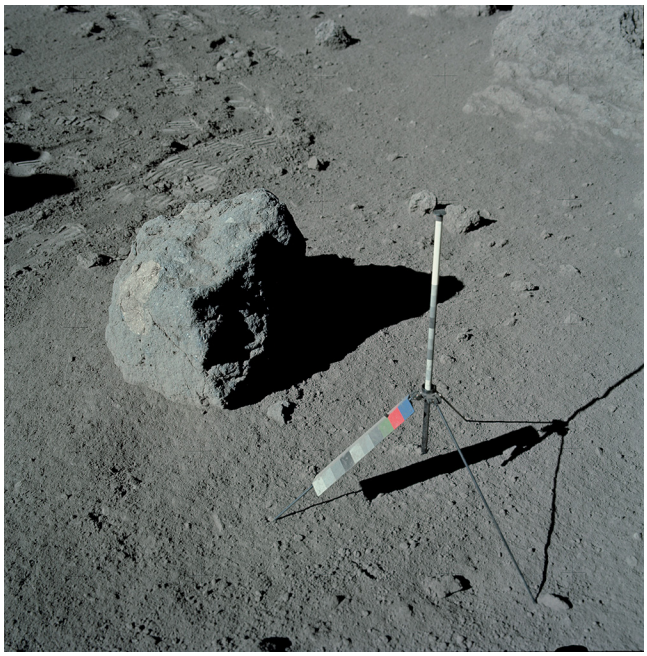

Fig. 2.5 Gnomon used for photographic references of slope, reflectance, color, and vertical. *(NASA photograph AS17-137–20963)*.

served as a measurement scale, had a hinged vertical component that showed local vertical. It also served as a reflectivity reference and as a color scale. All these features permitted a determination of the lighting and surface features prior to astronaut disturbance when the sample was actually bagged. Such sampling allowed the precise orientation to be worked out and depth of burial, which would aid in determining how long the rock had been at that location, and its exposure history.

However useful, the documented sample technique had the disadvantage of being time consuming. Since there was a detailed timeline for each EVA, excess time spent at one location meant the loss of time at another, so in practice there were not as many documented samples as perhaps many of the earthbound scientists would have liked. Instead, many samples were obtained as so-called "selected" samples, where an astronaut would pick up a sample and bag it while discussing its characteristics and setting. This technique permitted the collection of many more samples and a greater variety of samples than would have been possible through detailed documentation and photography. A summary of the samples returned from the six Apollo landings is given in Table 2.2.

2.5.2 "Contingency" samples

On Apollos 11, 12, 14, and 15, a sample was taken very soon after the initial steps on the surface. A special scoop was used to collect about a kilogram of material (Fig. 2.6).

Table 2.2 Apollo Sample Collection Summary.
(compiled from Astromaterials Acquisition and Curation Office – NASA).

	Apollo 11	Apollo 12	Apollo 14	Apollo 15	Apollo 16	Apollo 17	Apollo Total
Number of EVAs	1	2	2	3	3	3	14
Total Duration (hr:min)	2:32	7:45	9:23	18:35	20:14	22:04	80:33
Original Number of samples	67	68	207	414	767	756	2279
Total Mass (kg)	21.6	34.3	41.8	76.3	92.5	109.4	375.9
Sample Status (as of 2016)							
Pristine samples (percent of original)							
Rocks	57.6	78.7	79.4	75.4	85.6	88.5	81.8
Fines	72.2	66.6	86.3	83.8	87.3	90.7	84.3
Cores	54.7	55.4	62.0	73.0	78.3	81.1	77.2
Total	65.5	76.2	81.3	76.7	85.3	88.6	82.1
Lithologies (percent of original mass)							
Rocks							
Anorthosite				0.4	0.2	3.4	1.1
Basalt	22.0	77.6	0.8	38.4		29.3	24.8
Breccia	22.9	2.9	67.6	38.0	75.4	33.3	45.0
Other					0.2	0.3	0.1
Fines	54.6	18.2	30.7	17.2	16.6	26.9	23.6
Cores	0.5	1.2	0.9	6.1	7.6	6.7	5.3

This sample was set aside at the lunar module, so that in the event of an emergency requiring a rapid departure, there would be at least some material retrieved from the site.

2.5.3 Regolith or "Soil"

The uppermost portion of the lunar surface is fine, powdery and includes fragments sized up to several centimeters. Although often referred to as lunar soil, there is no organic component, and no weathering products as found on Earth. Therefore the term "soil" is not strictly correct and this portion of the lunar surface has been more cor-

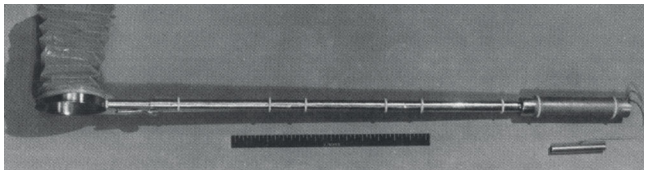

Fig. 2.6 Scoop used to obtain contingency sample on Apollo 11, 12, 14, and 15 missions. *(NASA photograph S68-54937).*

rectly termed "regolith". However, the word "soil" continues to be used, even in official descriptions of the Apollo samples (Heiken et al., 1991).

The regolith was sampled in bulk and sieved samples. A large metal scoop was used for the bulk sample and did not sort material at all. For sampling of the various pebbles and cobbles in the regolith, the rake developed after Apollo 11 could be fitted with a wire end that would retain the particles and pieces above about a centimeter in size (Fig. 2.2). This was a very efficient way to obtain a large variety of different rock types as the regolith is composed of fragments both fractured in place and delivered to the site via impacts at great distance.

For the general purposes of discussion, lunar scientists reserve the term "soil" for the size fraction <1 mm. The regolith generally corresponds to pebble or cobble-bearing sands. There are no terrestrial-style erosion processes, so in all cases the material is poorly sorted. The components of the regolith are varied, but are quite diagnostic, and include fragments of igneous rocks (both intrusive and extrusive), igneous and impact glass, meteoritic material, and agglutinates (the most diagnostic one). Agglutinates are common in the soil, are glassy and vesicular, and are caused by the impact of micrometeoroids (Fig. 2.7).

The constant bombardment of the upper regolith results in the deposit of nanophase Fe, both as blebs 4–33 nm across (e.g., Tsay et al., 1971) and in thin layers or patinas on mineral grains (e.g., Keller and McKay, 1997). This iron is in the reduced metallic, Fe^0, state. This leads to a ferromagnetic resonance signal, the intensity of which (I_s) increases with increased Fe. When I_s is normalized to the total Fe, expressed as FeO, this I_s/FeO ratio provides a measure of the exposure age (termed "maturity") of the soil. In this way, a history of the surface, and in cores a history with depth, can be deciphered.

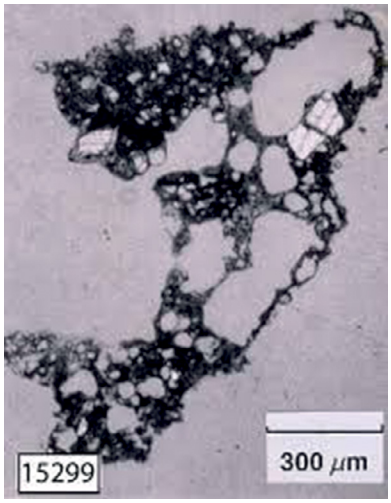

Fig. 2.7 Photomicrograph of a lunar agglutinate from Apollo 15. *(Meyer, 2003)*.

Table 2.3 Apollo Core Sample Summary.
(compiled from Astromaterials Acquisition and Curation Office – NASA).

	Apollo 11		Apollo 12		Apollo 14		Apollo 15		Apollo 16		Apollo 17	
Core Type	#	Depth (cm)	#	Depth (cm)	#	Depth (cm)	#	Depth (cm)	#	Depth (cm)	#	Depth (cm)
2 cm Drive												
Single	2	13.5 10.0	2	19.3 17.4	2	16.5 12.5						
Double			1	41.1	1	40.0						
4 cm Drive												
Single							1	38.5	1	~27	2	18.4 34.5
Double							2	66.0 67.0	4	65.4 63.1 65.6 62.3	3	56.0 68.2 51.3
2 cm Drill							1	242	1	216	1	286

2.5.4 Core samples

At all of the Apollo landing sites, cores of varying lengths were obtained of the lunar regolith (Table 2.3). They represent the only opportunity to sample and study the in situ relationships of regolith structure and stratigraphy. Early missions (Apollo 11, 12, and 14) used tubes 2 cm in diameter, and drove these into the ground with hammers. The core tubes were of "single core" and "double core" types, with the double cores being two cores threaded together to increase the depth sampled. Although able to accommodate cores up to 31.6 cm long, the rocky nature of the regolith made driving of the cores difficult, and the single core lengths only ranged from 10 to 19.3 cm. Two cores were obtained with double cores, and these were 40.0 and 41.1 cm. During the Apollo 15, 16, and 17 missions, drive tubes were increased to 4 cm in diameter, and these improved sampling depths. There were 13 drive cores obtained with the larger diameter tubes, ranging from 18.4 cm to 68.2 cm in length. Until November 2019, four of these tubes (one from Apollo 16 and three from Apollo 17) had never been opened, and were still encased in the vacuum sample holders with which they were packaged on the lunar surface (https://curator.jsc.nasa.gov/lunar/index.cfm). On 5 Nov 2019, sample 73001 was opened for the first time. Sample 73002 is expected to be opened later in 2020. These two samples represented the two portions of a double core drive tube, and it is possible that any gas trapped in 73002 on the Moon can be sampled at the time of opening.

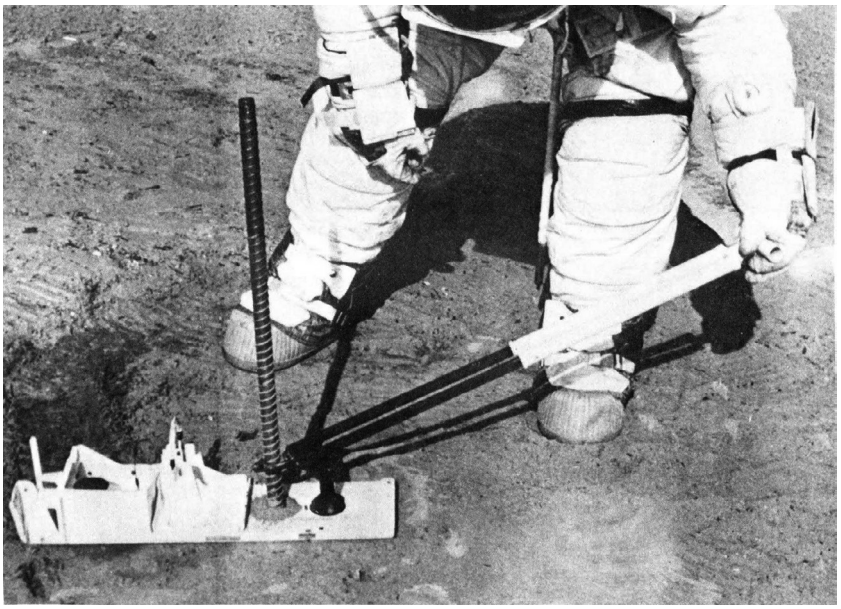

Fig. 2.8 Treadle used to remove long core tubes from the lunar regolith. *(Allton, 1989)*.

For the Apollo 15, 16, and 17 missions, cores were drilled into the regolith with multiple sections of 2 cm tubes. This provided cores over two meters long, with the longest being almost 3 m during the Apollo 17 mission. For all these drill tubes, extraction of the cores proved to be very difficult, and a special tool was used to pry them back out of the regolith (Fig. 2.8).

All of these cores permit study of the regolith history by analyzing the material with depth. Since exposure to space at the surface leads to cosmic ray damage to minerals, it is possible to obtain "cosmic ray exposure ages" for the regolith, and obtain a history and some indication of the timing between major regolith depositing events. Many of the cores have sections that have been epoxy-impregnated, which permits study of structures and properties of various components without concern over disturbance of the loose material falling out.

2.5.5 Rocks

Except for the Apollo 11 landing, where over 70 percent of the sample was "bulk" (Kramer et al., 1977), rocks comprised two-thirds or more of the samples returned from each mission. While small numbers of other types are present, the bulk of returned lunar rocks can be broadly categorized into three groups: anorthosites, basalts, and breccias.

The Moon can be divided into light-colored (albedo values from 11 percent to 18 percent) and darker regions (albedo values from 7 percent to 10 percent). The darker portions correspond to lower elevation, and generally correlate with large, circular

basins. They are less cratered and are therefore younger than the lighter-colored "highlands", which are crater-saturated. The highlands are considered the oldest regions on the Moon. Therefore lunar highlands rocks are the primary way to infer the early geologic history of the Moon, which was one of the reasons a highlands site was chosen for Apollo 16. A potentially confounding process that was ubiquitous early in the history of the Moon is meteoroid bombardment. Materials delivered through this bombardment usually had significant amount of iron-nickel metal within them, and these carried high abundances of other "siderophile" elements that are associated with iron. These would have included elements such as iridium, osmium, platinum, and gold. Since these elements do not play a significant role in the evolution and crystallization of the rocks such as anorthosites and basalts, the presence of elevated levels of siderophile elements can be used to assess the level of contamination by meteoritic material. Lunar highlands rocks are thus classified as "pristine" if they display little contamination, and "non-pristine" if they are contaminated by meteoritic material (Warren and Wasson, 1977). Only pristine varieties are confidently used for genetic interpretation.

Anorthosites are defined as coarse-grained (phaneritic) igneous rocks, mainly composed of plagioclase feldspar. This mineral can be found on Earth in a continuous compositional series from calcium-rich ($CaAl_2Si_2O_8$) to sodium-rich varieties ($NaAlSi_3O_8$). The molar ratio of Ca to Na, given as Ca/(Ca + Na) and termed the "An number", is used to characterize the plagioclase mineral. The Ca-endmember plagioclase is anorthite. The plagioclase in lunar rocks is predominantly calcium-rich (An_{90} or greater). Lunar anorthosites fall into two subgroups, the "ferroan" anorthosites, and the Mg-suite (magnesium-rich) rocks. The ferroan anorthosites are not strictly iron-rich as the name might imply. For igneous rocks that contain plagioclase that is highly calcium-rich, the typical mafic minerals that might be present (olivine and/or pyroxene) would be expected to have magnesium/iron (Mg/Fe) ratios that are very high. However, in ferroan anorthosites, the accompanying mafics have Mg/Fe significantly lower than expected, while the Mg-suite of rocks have mafics with more typical Mg/Fe (Fig. 2.9).

Anorthosites are a rare rock type on Earth, and the discovery of anorthosite as numerous fragments in lunar rocks was one of the early surprises from the Apollo samples. The search for anorthositic rocks became one of the objectives of the last three missions. Each of these returned larger samples of anorthosite, which has broadened the understanding of lunar history.

Basalts arguably represent the most common igneous rock on rocky planetary surfaces. They generally represent lava flows originating as partial melting of mantle materials in planets and larger satellites and asteroids. Since the geochemical relationships of melting of mantle materials are well understood, basalts are key materials for interpreting the nature of mantle materials since we cannot sample them directly. The basic mineralogy of basalt is comprised of plagioclase feldspar and pyroxene. Olivine is a common accessory mineral in some basalt suites. Basalt forms the surface of the

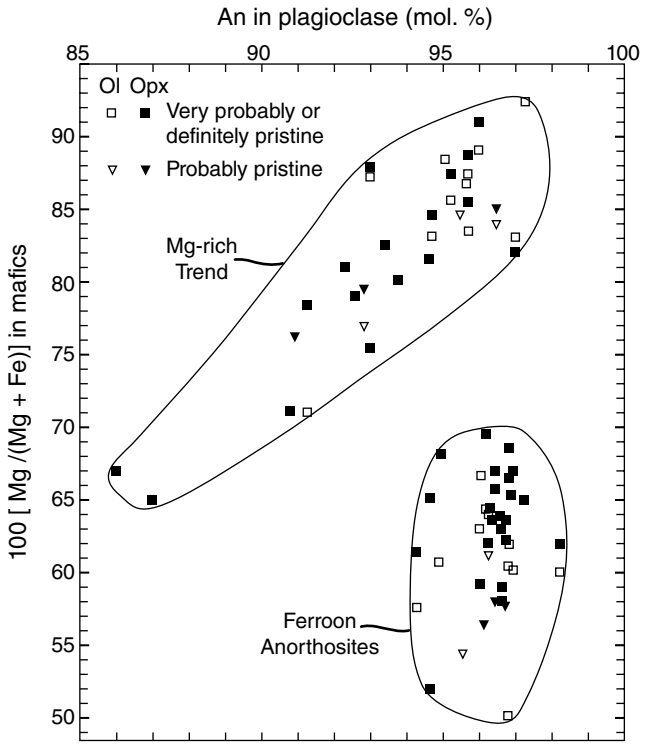

Fig. 2.9 ***Mg/(Mg+Fe) vs An content in plagioclase for "pristine" highlands rocks***. The ferroan anorthosites are distinct from the more typical igneous trend of the Mg-suite rocks. *(Figure. from Warren and Wasson, 1980)*.

darker regions of the lunar nearside. These were originally referred to as "seas" in early astronomy ("maria" in latin), and represent about 17 percent of the surface area of the Moon. Basalts were returned in various amounts from all Apollo sites except Apollo 16, which was a highlands landing site. The maria have considerably fewer craters, are thus smoother than the lighter highlands, and were therefore the target of the first mission (Apollo 11) which landed in Mare Tranquillitatis. Lunar basalts have a wide variety of compositions in both elemental and mineralogical senses. As with terrestrial basalts, multiple classification systems have been suggested for lunar basalts (Taylor et al., 1991; Neal and Taylor, 1992; Papike, 1998). The most useful discriminator among lunar basalts is the TiO_2 content (often combined with Al_2O_3 and K_2O as secondary discriminators), and three broad groups have been established: high-Ti (>9 wt percent TiO_2), low-Ti (1.5–9 wt percent TiO_2), and very-low Ti (<1.5 wt percent TiO_2) basalts. An advantage of using Ti to classify basalts is that Ti can be mapped using remote-sensing techniques, and orbital missions since the 1990s have mapped the Ti distribution on the lunar surface. This permits more comprehensive modeling of the origins and distribution of this important set of lunar materials. From such remote-sensing it has become clear that the

Apollo (and also Soviet Luna) missions likely have not sampled the full range of lunar basalt compositions.

Breccia is a rock type composed of fragments of other rocks. In the entire set of returned Apollo samples 45 percent of the 267 kg of rocks returned were breccias (Table 2.2). These rocks represent materials fractured and transported from elsewhere by the extensive bombardment of asteroidal and meteoritic material onto the Moon throughout its history. Breccias have an important function in the geologic study of the Moon since through their fragments they provide sample materials from locations remote to those of the six Apollo landings.

Among breccias themselves, there are multiple types. Lunar breccias are classified as either *monomict*, with fragments of a single rock type, and *polymict*, where the fragments represent multiple rock types. There are a few *dimict* breccias where two types of rock are found within them. The materials represented within breccias can either be rock fragments, impact melt that has recrystallized, and impact melt that has remained glassy.

Another, minor, type of breccia is the regolith (or soil) breccia. This type of material is lithified regolith, with fragments typically found in the regolith along with impact glass, volcanic glass, and other debris. Regolith breccias generally form via small impacts. There have been 53 regolith breccias identified among the samples returned by the six Apollo missions (Fruland, 1983). These modified soil samples permit the study of soil characteristics of an area slightly greater than that sampled through astronaut traverses.

Miscellaneous rocks include plagioclase that is more sodium-rich than the ferroan anorthosites and the Mg-suite rocks. This group, referred to as the Alkali Suite, includes anorthosites, along with those that have significant amounts of mafic material (pyroxene) and are termed gabbronorites and norites. These are all from the Apollo 12 and Apollo 14 samples, which is suggestive that they may be related to KREEP (Shervais and McGee, 1998).

Some rare rock types (granite, quartz monzodiorite) have been described (e.g., Shervais and McGee, 1998; Neal et al., 1989; Jolliff, 1991; Snyder et al., 1992, 1994). These were identified as fragments in Apollo 14 breccias. They are enriched in incompatible trace elements and have been interpreted as having formed from KREEP-related rocks.

2.5.6 Glass

Glass is a common component of the regolith and some rocks. Indeed, glassy material, termed "agglutinates", is a key diagnostic of lunar regolith (Fig. 2.7). Due to the lack of water in lunar materials, glass remains stable for timescales that are on the order of the actual age of the Moon itself. Glass forms during both impact and volcanic processes and is found in many forms in the lunar rocks brought back by the Apollo missions. Since impact melts form through melting of large batches of material, these glasses provide an opportunity to obtain "average" compositions for their source material.

The discovery of green glass beads in samples from Apollo 15 was significant in that these represent volcanic pyroclastic materials erupted in "fire fountains". Orange glass was famously discovered at the Apollo 17 station 4 site, and yellow and red glass varieties have also been found. These glass beads are generally less than 1 mm across, and uniform in composition both within the beads themselves and among the population of beads in a given sample. The lunar glass beads are also enriched in volatile materials. Such characteristics separate them from impact glasses, and suggest that these materials formed as a spray of volcanic material which chilled quickly after eruption. This preserved original compositions, providing information about the source regions.

2.5.7 KREEP

Samples from Apollo 12 included glass that was enriched in incompatible trace elements (Hubbard et al., 1971). The characteristic enrichment of potassium, rare earth elements, and phosphorus (K, REE and P) led to the assignment of the term "KREEP" to glass fragments that displayed this composition. In current lunar studies, the term "KREEP" or the adjective "KREEPy" are used to describe any material with the same or similar pattern of enrichments as those originally described. Apollo 14 provided numerous samples with the KREEP "signature", and although KREEP is not truly a "rock" that can be pointed to, this material is now considered to be a significant composition among the Apollo sample set.

2.6 Transport & storage

2.6.1 Packaging on the Moon

The "bulk" sample obtained during the Apollo 11 EVA was simply bagged and put into an aluminum container with an indium vacuum seal for return to Earth. Following missions used a system of numbered bags of various sizes and other containers. Packaging on the lunar surface was aided by the vacuum and was remarked upon by the astronauts as being quite easy. Sample bags were made of Teflon and came in dispensers that made it easier to manipulate them with the pressure suit gloves. The samples were returned in large "rock boxes" that continued to use a metal seal of soft indium that deformed to seal the box when closed on the Moon.

2.6.2 Lunar Receiving Laboratory

In the initial phases of the Apollo Program, the principal goal was simply to get astronauts to the Moon and return them safely and therefore a very little effort was spent thinking about any scientific investigations. Geoscientists and others, however, made a strong case that, while astronaut safety was paramount, there was a great opportunity to collect geological samples and perhaps perform some other experiments at the same time. As a result, discussions began in 1963 about the nature of a facility that could

receive, house, process, and distribute sample portions to scientists. From a geoscientist's perspective, protecting any lunar samples from terrestrial contamination was the primary concern. However, even as early as 1960 some concern had been raised about the possibility that some unknown type of lunar organism might pose a hazard to life on the Earth. There was a vigorous debate over this issue, and though it was understood that the chances were remote of any true risk of so-called "back contamination", it was deemed a prudent and even moral duty to provide for protection. This protection, along with the "traditional" protections against "forward contamination" of the lunar samples made the planning and design of the Lunar Receiving Laboratory (LRL) very complex and led to many internal debates and delays (Mangus and Larsen, 2004).

Construction at the Manned Spaceflight Center in Houston took approximately a year and finished in late 1967. The next 18–21 months were spent installing the various systems needed for sample processing (vacuum systems for initial sample handling and nitrogen-purged glove boxes for additional handling) and the quarantine areas for the astronauts and other equipment. These all had to undergo detailed certification with the deadline of being ready for the first lunar sample return mission in July 1969. Although the exact date for the first sample return was not known until Spring 1969, the LRL was considered ready in late June 1969.

2.7 Curation

2.7.1 Numbering system

A fundamental five-digit generic number is assigned to each sample actually retrieved from the lunar surface. This five-digit generic is followed by a number that identifies the specific "split" from the generic, and is separated by a comma (e.g., 12018,14). The first two digits of the generic identify the mission number with 10 = Apollo 11, 12 = Apollo 12, 14 = Apollo 14, 15 = Apollo 15; 6x = Apollo 16, and 7x = Apollo 17. For the Apollo 11, 12, and 14 samples, the last three digits were assigned without regard to the sample type or location at which it was obtained. Beginning with Apollo 15, this was modified to provide information about location (the third number), and these were assigned in the order of the traverses. The Apollo 16 and 17 EVAs had specific stations around which sampling activity took place, and these station numbers were used for the second number in the generic (e.g., sample 74220 is from Apollo 17, station 4).

For Apollo 15, 16 and 17, the fifth digit of the generic was assigned to identify the sample from a sample bag on the basis of its typology (0–4 for fraction of fines and 5–9 for rocks) and its size: 0 for unsieved, 1 for <1mm, 2 for 1–2 mm, 3 for 2–4 mm, 4 for 4–10 mm, 5 for > 10 mm. In cases where additional rocks were in the same sample bag, the numbers 6–9 were assigned. In the atypical cases where more than five rocks were in the same bag, the fourth digit was simply incremented and the numbers 5–9 used again in the fifth digit. In this way, every rock received a unique generic number.

Once a sample is processed and subdivided, the specific number, separated by a comma, is assigned. The primary, undivided sample is usually given the specific of "0" (e.g., 12018,0). Further splits (e.g., thin sections, chips, other pieces) are given the next higher specific number for that generic sample. While this system seems arcane and confusing, it does provide a ready means to track samples and data. Further details are provided through a number of sources (https://www.lpi.usra.edu/lunar/samples/; https://curator.jsc.nasa.gov/lunar/index.cfm).

2.7.2 Allocation process

While allocation of lunar samples is open to all who wish to study them (regardless of citizenship), because of the limited amount of sample material there are very rigorous and specific requirements that must be fulfilled. The allocation process is outlined in detail in the Lunar Sample Allocation Guidebook (Lofgren, 2007). This process requires a favorable peer review of the proposed research. This can be through a successful research proposal to NASA or to another government or non-profit agency, or reprints of peer-reviewed articles that pertain to the specific research methods and capabilities of the applicant. It further must be approved by the Curation and Analysis Planning Team for Extraterrestrial Materials (CAPTEM), which also takes into account information about sample accountability and security while in the custody of researchers.

2.7.3 Status of Apollo collection

The current status of each lunar sample is available through the website of the Astromaterials Acquisition and Curation Office of NASA (https://curator.jsc.nasa.gov/lunar/index.cfm). A significant portion of the Apollo sample collection has never been studied, and has only been cataloged. From a curation standpoint, the term "pristine" is used for samples that have never been exposed to Earth's atmosphere, and are either still in vacuum as packaged on the lunar surface or have never left nitrogen-filled cabinets in the curation facility.

2.8 Major findings

2.8.1 Extreme antiquity

The first remarkable discovery from the lunar samples was the extreme antiquity of the lunar rocks. The samples returned from Apollo 11 were mainly components of a bulk sample scooped from 22 or 23 places on the surface. The fragments contained within this regolith sample yielded ages of approximately 3.6 – 3.85 Ga. This is a similar age to oldest terrestrial rocks for which there are more than isolated samples. With the Apollo 12 mission, younger ages were found for the basaltic rocks, but these were still quite ancient, 3.15–3.2 Ga. The later missions provided samples of highland rocks which far exceeded terrestrial ages. Ferroan anorthosites range from 4.35- ~ 4.5 Ga, and the other plutonic highlands rocks of the Mg-suite range from ~4.1 to 4.5 Ga.

The basalts of Apollo 12 were the youngest lunar samples identified, until the discovery of a fragment in a lunar meteorite that was determined to be 2.86 Ga (Borg, et al., 2004). Further studies using crater size-frequency has led to the interpretation of locations where basalts may be as young as 1.2 Ga (Hiesinger, et al., 2003) or even 100 Ma (Braden, et al., 2014). While these are compelling, the findings from the Apollo sample collection point to the bulk of thermal activity being early in lunar history.

2.8.2 Water

One of the questions that Apollo set out to answer was the presence and role of water in the lunar landscape. Indeed, when the Apollo 17 astronauts reported seeing orange soil during EVA 2, scientists on Earth rejoiced in the assumption of hydrothermal activity, which often leads to bright-colored rocks due to exotic sulfides. However, this was determined to be incorrect when the orange soil was found to be composed of orange glass beads. Indeed, in none of the Apollo samples was there any definitive evidence for indigenous water. The compound FeOOH was occasionally found in some rocks from every mission, and sometimes described as "rust" (e.g., Taylor et al., 1973). Although ostensibly demonstrating the presence of water, this material was shown to be the result of terrestrial contamination (Taylor et al., 1973).

More recently, infrared spectroscopy studies found evidence of small amounts (a few ppm) of water in lunar anorthosites (Hui et al., 2013). Based on this finding, Hui et al. (2013) interpreted an amount of water in the lunar magma ocean of approximately 320 ppm. While this is not a lot of water by terrestrial standards, it would imply that at the final crystallization stage of the magma ocean, water contents could have reached over 1 percent, making water a significant factor in the origin of lunar basalts, which also have recently had water detected within them (e.g., Saal et al., 2008; Hauri et al., 2011).

2.8.3 Anorthosite – magma ocean

Another surprise from the Apollo samples was the abundance of anorthosite, a comparatively rare rock on Earth. Anorthosite is predominantly plagioclase, and the lunar samples were also surprising in that the plagioclase within them was highly anorthitic, being very close to the calcium rich endmember composition (i.e., contained very little sodium). This lack of sodium, a volatile element, is one of the pieces of evidence that the Moon's origin involved significant heating.

The presence of anorthosite as a significant crustal component led to the suggestion that the original crust may have formed through flotation of plagioclase within a large magma chamber (Wood et al., 1970; Smith et al., 1970). By the end of the 1970s, the concept of a "large" magma chamber had assumed a global scale, and the Lunar Magma Ocean had appeared as the paradigm for early igneous processes on the Moon. This model (summarized in Warren, 1985) has the early Moon undergoing significant

melting soon after formation. The actual depth of the magma ocean (a few hundred kilometers or the entire mantle) is still debated, but the basic tenet is that during crystallization of this magma ocean the mafic silicates (olivine and pyroxene) sank to bottom of the magma, and the plagioclase feldspar floated to the top, forming the primitive anorthositic crust. In this scenario, the ferroan anorthosites represent this ancient, primitive crust.

Into this crust, intruded rocks were then seen as the Mg-suite and alkali-suite among the Apollo samples. The ages of these rocks, which overlap those of the ferroan anorthosites, but extend to younger ages is consistent with this. The details concerning the relative abundance of anorthosite, the contribution of more mafic-rich rocks, and the exact structure of the magma ocean are questions still being addressed in the literature. Ambiguity is no doubt fostered by the fact that most of the "rocks" sampled and analyzed are only fragments < 1cm, derived from the regolith or breccias.

2.8.4 Basalt – later volcanism

Lunar basalts show a wide variation in compositions, and a wider range in ages. On Earth, basalts represent partial melts from the mantle, and thus provide constraints on the mantle's composition. Although volumetrically small (< 1 percent of the crustal volume – Head and Wilson, 1992), the lunar mare basalts provide significant information about the lunar interior composition during a second era of melting and igneous activity that began shortly before the end of activity related to the magma ocean crystallization. The lavas were very low in water contents, and this, along with generally low SiO_2 contents and high temperatures, means that lunar mare basalts had very low viscosities. The result was that the basalts formed highly effusive flows that filled large swaths of impact basins very quickly.

One of the perhaps surprising discoveries about lunar basalts is that these compositions appear to be unique to the Moon. There are no terrestrial basalts that are similar in composition to those on the Moon, which are higher in FeO and MgO, and lower in CaO, Al_2O_3, and Na_2O. Indeed, meteoritic samples of basalt (even those from Mars) are also very different from lunar basalts. The low Na_2O likely reflects the general depletion in the Moon of volatile elements (Taylor, 1982), but the significantly lower CaO and Al_2O_3 reflect a mantle source that is unusual. The flotation of calcium-rich plagioclase to form the lunar crust would have removed calcium and aluminum from the residua of the magma ocean. Given this Lunar Magma Ocean paradigm, the mare basalts are viewed as having formed not by melting of a primitive lunar mantle, but by secondary melting of the mafic-rich residua of magma ocean crystallization (Shearer et al., 2006).

The majority of mare basalts occupy the major impact basins on the Moon. The ages of the basalts and highlands rocks have permitted the development of meteoroid flux models for the Moon, which then provide for the determination of ages for the various basin-forming events. This work resulted in the determination that most large

basins formed between 4.0 – 3.8 Ga. Whether this represents simply the tail end of the Solar System accretion process (e.g., Neukum et al., 2001), or an actual increase in large impacts to form a "cataclysmic bombardment" (e.g., Cohen et al., 2000) is still an open question.

2.8.5 Glass – interior implications

As with terrestrial volcanoes, pyroclastic deposits are associated with the mare volcanics. Given that the mare magmas were very low viscosity (Weill et al., 1971), volatiles such as CO_2 would be released essentially explosively, resulting in "fire fountains". Evidence for this process is seen in the numerous small glass beads of varying color. These glasses are high in MgO and are properly termed "picritic". Such materials are similar to the ultramafic komatiites extruded on Earth early in its history. The glass beads provide compositions of the extrusive material that solidified immediately and have not undergone any crystallization and possible modification from the original composition, and thus are interpreted to be the best examples of primary magma compositions (Delano, 1986). The volcanic glasses, like the mare basalts, indicate an origin from a source depleted in CaO and Al_2O_3 compared to an undifferentiated, more "typical" mantle composition.

2.8.6 KREEP – lunar magma ocean significance

KREEP material was first identified at the Apollo 12 site and has a significant presence in Apollo 14, 15 and 17 samples, providing a profound constraint on the origin and evolution of the later basaltic rocks. The ultimate origin of KREEP is thought to be as the very final residuum of lunar magma ocean crystallization. The actual residual material has been termed "urKREEP" – using the German prefix "ur" to mean primeval – by Warren and Wasson (1979) and would have been FeO- and trace-element rich.

The origin of KREEP basalts may represent partial melting of rocks in the lower crust, including urKREEP, resulting in the unusual composition of these basalts. Models of KREEP basalt formation (Warren, 1988; Snyder et al., 1995) suggest that they may represent parent magmas to the Mg-suite and, particularly, the related alkali-suite of highland rocks.

2.8.7 Understanding of lunar and solar system processes

Prior to the Apollo era, there was extensive debate over the origin of the craters on the Moon. There was no definitive evidence to determine whether they were of volcanic or impact origin. Unequivocal evidence of impacts in the returned samples (brecciation, glass fragments, crushed minerals, the fragmental nature of the regolith) along with the detailed photographic data led to a profound change in thinking. By the end of the Apollo program in December 1972, it was understood that impacts were the predominant surficial geologic process on the Moon.

Indeed, along with the photographic evidence of the Mariner probes to Mars, it was Apollo that has established the role of impacts in planetary evolution in general. This has continued to be the case to this day, when spacecraft have visited all the terrestrial planets and many of the asteroids and satellites in the outer solar system and confirmed that impacts have been a key process in Solar System history.

The Lunar Magma Ocean model has served well as a model for lunar geologic activity. The scope of this process has now been extended, and magma oceans are invoked routinely as a "standard" feature of early planetary evolution, even on the Earth (e.g., Solomatov, 2015). It is understood that the large number of impacts associated with accretion of planets, in addition to planetary differentiation (core formation) and decay of radioactive isotopes led to a tremendous amount of heat retained in early planetary bodies. This would lead to extensive melting of the outer portion of these bodies, i.e., a magma ocean.

2.8.8 Origin of the Moon

Throughout history, the four basic models for the ultimate origin of the Moon were: 1) Fission, where the Moon spun out of the Earth and has been receding from Earth ever since (Darwin, 1879), 2) Capture, where the Moon represents an exotic object that was captured by Earth early in Solar System history (Gerstenkorn, 1955), 3) Co-accretion, where the Moon and the Earth formed simultaneously, with the Moon already in orbit about the Earth (Schmidt, 1959), and 4) the Giant Impact, where an early Earth was impacted by a Mars-sized object, and the resultant debris coalesced to form the Moon (Daly, 1946; Hartmann and Davis, 1975).

The Apollo samples demonstrated that the Moon was depleted in volatiles, had a magma ocean early in its history, and possesses stable isotopes in its rocks that are essentially identical to the Earth (unlike all other Solar System materials sampled by the meteorites). These geological findings are present along with other considerations such as the very low density of the Moon due to a very small iron core and its orbit being very close to the Earth's equatorial plane. All this information led to a consensus in favor of the Giant Impact model (Hartmann et al., 1986), that has remained the consensus model, although details are still debated about the nature of the impactor, how close to Earth it ultimately had formed, how directly it had struck Earth, and other chemical details.

2.8.9 Working in the lunar environment

While the various scouting work by the Surveyor landers and the Lunar Orbiters had demonstrated that many initial fears about working on the surface were unfounded, several practical issues were discovered that will require consideration prior to the next crews landing on the Moon. Besides issues with suit mobility and difficulties related to having to work against the pressure-opened suit gloves, the astronauts all found that the

lunar dust was an ever-present nuisance. By the end of the three EVAs on each of the final missions, the suits were extensively soiled, and the astronauts expressed concerns over possible fouling of the various seals of the gloves and helmet, and even worried about problems within the lunar module itself.

These issues are due to basic characteristics of the lunar dust. Eighty percent or more of the dust at the surface is <250 μm, with perhaps 50 percent being <75 μm (Heiken, 1975). An aggravating factor is that, due to the extremely dry nature of the regolith, there can be a significant static charge, leading to the dust clinging to surfaces. The astronauts noted this, and on missions beginning with Apollo 14 carried brushes among their tools to periodically clean items such as camera lenses, their visors, and the suits themselves.

The presence of significant agglutinates and other glass also makes the problem worse by making the fine dust extremely abrasive. This could easily become a problem on longer missions with many EVAs. The abrasive nature of the lunar dust also led to a situation referred to by Apollo 17 astronaut Harrison Schmitt as "lunar dust hay fever." He noted that the dust brought into the lunar module led to watery eyes, throat congestion, and sneezing. This is likely due to the irritating nature of the glass-rich dust, as well as the high chemical reactivity of the lunar components.

2.9 Future lunar sampling

There are still many outstanding questions that might be addressed via future sample-return missions to the Moon. Some of these are related to gaps in our understanding left by the Apollo samples, and others are related to discoveries and insights that have been made exclusive of the samples in the intervening decades.

The discovery of small amounts of water in lunar samples and in the regolith has led to a realignment of thinking about lunar processes. One of the focal points of inquiry relates to the presence and potential quantity of water ice in regions near the poles that are permanently shadowed. Such regions are commonly discussed for the initial targets of the next phase of lunar exploration.

There are several questions remaining that were generated by analysis of the Apollo samples. How recently was basaltic volcanism active? What compositional ranges for lunar basalts exist? These can only be answered through landings and sampling of a wider range of sites on the Moon, such as the Marius Hills, which may be examples of volcanoes that have extruded lavas in the comparatively recent past (say 1 Ga or so). Landings on presumably basaltic materials on the far side (e.g., Tsiolkovsky, Mare Moscoviense) would shed light on the variability in mare basalt compositions, although landings on the far side pose extreme logistical challenges related to communication. The Chinese lander, Chang'e 4 in 2019, was the first ever to land on the far side and return data via a relay satellite in lunar orbit. At this point, this is the only mission to visit the far side surface of the Moon.

Searching for deep crustal rocks may answer questions about the nature of the magma ocean, the extent of an anorthositic crust, and other early igneous processes. The possibility of such rocks was the reasoning behind the selection of the central peaks of Tycho or Copernicus as potential landing sites. The fact that there were only six Apollo landings necessarily means that our understanding of the Moon is incomplete. A polygon drawn to connect the six landing sites has an area that is only 1.4 percent of the entire lunar surface. If the three Luna sample-return sites are included, it is still only 2.7 percent of the lunar surface. Just about anywhere that samples can be obtained is likely to be helpful in continuing to understand the history of our nearest planetary neighbor.

References

Allton, J.H., 1989. Catalog of Apollo lunar surface geological sampling tools and containers. NASA, 99p JSC-23454.

Binder, A.B., Roberts, D.L., 1970. Criteria for lunar landing site selection. Astro Sciences Center, Report P-30, IIT Research Institute, 50p.

Borg, L.E., Shearer, C.K., Asmerom, Y., Papike, J.J., 2004. Prolonged KREEP magmatism on the Moon indicated by the youngest dated lunar igneous rock. Nature 432, 209–211.

Braden, S.E., Stopar, J.D., Robinson, M.S., Lawrence, S.J., van der Bogert, C.H., Hiesinger, H., 2014. Evidence for basaltic volcanism on the Moon within the past 100 million years. Nat. Geosci. **7**, 787–791.

Cohen, B.A., Swindle, T.D., Kring, D.A., 2000. Support for the lunar cataclysm hypothesis from lunar meteorite impact melt ages. Science 290, 1754–1756.

Daly, R.A., 1946. Origin of the Moon and its topography. Proc. Am. Philos. Soc. 90, 104–119 9, 81-104.

Darwin, G., 1879. On the procession of a viscous spheroid and on the remote history of the Earth. Phil. Trans. R. Soc. London 170, 447–538.

Delano, J., 1986. Pristine lunar glasses: criteria, data, and implications. Proc. Lunar Planet Sci. Conf., 16th, J. Geopys. Res. 91, D201–D213.

Enderson, L.W., 1965. A Study of lunar landing sites and associated stay times. NASA TN D-2795, 36p.

Fruland, R.M., 1983. Regolith breccia workbook. NASA planetary materials branch publ. No. 66. NASA JSC 19045, 260p.

Gerstenkorn, H., 1955. Uber gezeitenreibung beim zweikorper-problem. Zeit. Astrophys. 36, 245–274.

Hartmann, W.K., Phillips, R.J., Taylor, G.J. (Eds.), 1986. Origin of the Moon. Lunar and Planetary Institute, Houston, 781p.

Hartmann, W.K., Davis, D.R., 1975. Satellite-sized planetesimals and lunar origin. Icarus 24, 504–515.

Hauri, E.H., Weinreich, T., Saal, A.E., Rutherford, M.C., Van Orman, J.A., 2011. High pre-eruptive water contents preserved in lunar melt inclusions. Science 333, 213–215.

Head, J.W., Wilson, L., 1992. Lunar mare volcanism: stratigraphy, eruption conditions, and the evolution of secondary crusts. Geochim. Cosmochim. Acta 56, 2155–2175.

Heiken, G.H., 1975. Petrology of lunar soils. Rev. Geophys. Space Phys. 13, 567–587.

Heiken, G.H., Vaniman, D.T., French, B.M., 1991. Lunar sourcebook: a user's guide to the Moon. Cambridge University Press, New York, 736p.

Hiesinger, H., Head III, J.W., Wolf, U., Jaumann, R., Neukum, G., 2003. Ages and stratigraphy of mare basalts in oceanus procellarum, mare nubium, mare cognitum, and mare insularum. J. Geophys. Res. 108 (E7), 5065.

Hubbard, N.J., Gast, P.W., Meyer, C., Nyquist, L.E., Shih, C.-.Y., Weismann, H., 1971. Chemical composition of lunar anorthosites and their parent liquids. Earth Planet Sci. Lett. 13, 71–75.

Hui, H., Peslier, A.H., Zhang, Y., Neal, C.R., 2013. Water in lunar anorthosites and evidence for a wet early Moon. Nat. Geosci. 6, 177–180.

Jolliff, B.L., 1991. Fragments of quartz monzodiorite and felsite in Apollo 14 soil particles. Proc. Lunar Planet Sci. Conf. 21, 101–118.

Keller, L., McKay, D., 1997. The nature and origin of rims on lunar soil grains. Geochim. Cosmochim. Acta 61, 2331–2340.
Kramer, F.E., Twedell, D.B., Walton Jr., W.J.A., 1977. Apollo-11 lunar sample information catalogue (revised). NASA JSC 12522, 478p.
Lofgren, G.E., 2007. Lunar Sample Allocation Handbook. Astromaterials Acquisition and Curation Office. NASA Johnson Space Center, Houston, 48p.
Loftus, J.P., Hodge, J.D., McDivitt, J.A., Faget, M.A., Craft Jr., C.C., Slayton, D.K., Calio, A.J., Berry, C.A., 1969. Apollo lunar exploration missions (ALEM) program and mission definition. NASA SPD-9P-052, 190.
Mangus, S., Larson, W., 2004. Lunar receiving laboratory project history. NASA/CR-2004-208938, 66.
Meyer, C., 2003. Lunar petrographic thin section set study guide. Astromaterials Curation. NASA JSC, Houston, 66.
Neal, C.R., Taylor, L.A., 1992. Petrogenesis of mare basalts: a record of lunar volcanism. Geochim. Cosmochim. Acta 56, 2177–2211.
Neal, C.R., Taylor, L.A., Patchen, A.D., 1989. High alumina (HA) and very high potassium (VHK) basalt clasts from Apollo 14 breccias, Part 1-mineralogy and petrology: evidence of crystallization from evolving magmas. Proc. Lunar Planet Sci. Conf. 19, 137–145.
Neukum, G., Ivanov, B., Hartmann, W.K., 2001. Cratering records in the inner solar system. In: Kallenbach, R., Geiss, J., Hartmann, W.K. (Eds.), Chronology and evolution of Mars. Kluwer, pp. 55–86.
Papike, J.J., Ryder, G., Shearer, C.K., 1998. Lunar Samples. Rev Mineral 36, 5.1–5.234.
Saal, A.E., Hauri, E.H., Cascio, M.L., Van Orman, J.A., Rutherford, M.C., Cooper, R.F., 2008. Volatile content of lunar volcanic glasses and the presence of water in the Moon's interior. Nature 454, 192–195.
Schmidt, O.Y., 1959. A theory of the origin of the Earth. Lawrence and Wishart, London, pp. 139.
Shearer, C.K., Hess, P.C., Wieczorek, M.A., Pritchard, M.E., Parmentier, E.M., Borg, L.E., Longhi, J., Elkins-Tanton, L.T., Neal, C.R., Antonenko, I., Canup, R.M., Halliday, A.N., Grove, T.L., Hager, B.H., Lee, D-C., Wiechert, U., 2006. Thermal and magmatic evolution of the Moon. In: Jolliff, B.L., Wieczorek, M.A., Shearer, C.K., Neal, C.R. (Eds.), New Views of the Moon, Rev. Mineral, 60, 365–518.
Shervais, J.W., McGee, J.J., 1998. Ion and electron microprobe study of troctolites, norite, and anorthosites from Apollo 14: evidence for urKREEP assimilation during petrogenesis of Apollo 14 Mg-suite rocks. Geochim. Cosmochim. Acta 62, 3009–3023.
Smith, J.V., Anderson, A.T., Newton, R.C., Olsen, E.J., Wyllie, P.J., Crewe, A.V., Isaacson, M.S., Johnson, D., 1970. Petrologic history of the moon inferred from petrography, mineralogy, and petrogenesis of apollo 11 rocks, Proc. Apollo 11 Lunar Sci. Conf., 897–925.
Snyder, G.A., Taylor, L.A., Halliday, A.N., 1995. Chronology and petrogenesis of the lunar highlands alkali suite: cumulates from KREEP basalt crystallization. Geochim. Cosmochim. Acta 59, 1185–1203.
Snyder, G.A., Taylor, L.A., Jerde, E.A., Riciputi, L.R., 1994. Evolved QMD melt parentages for lunar highlands alkali suite cumulates: evidence from ion-probe rare-earth element analyses of individual minerals. Lunar Planet Sci. XXV, 1311–1312.
Snyder, G.A., Taylor, L.A., Neal, C.R., 1992. A chemical model for generating the sources of mare basalts: combined equilibrium and fractional crystallization of the lunar magmasphere. Geochim. Cosmochim. Acta 56, 3809–3823.
Solomatov, V., 2015. Magma oceans and primordial mantle differentiation. In: Schubert, G., (ed.) Treatise of Geophysics (2nd Edition), Elsevier, v. 9, 81-104.
Sullivan, T.A., 1994. Catalog of Apollo experiment operations. NASA Reference Publication 1317, 161.
Taylor, L.A., Mao, H.K., Bell, P.M., 1973. "Rust" in the Apollo 16 rocks. Proc. Lunar Sci. Conf. 4th, 829–839.
Taylor, L.A., Warren, P., Ryder, G., Delano, J., Pieters, C., Lofgren, G., 1991. Lunar rocks. In: Heiken, G.H., Vaniman, D.T., French, B.M. (Eds.), Lunar sourcebook: a user's guide to the Moon. Cambridge University Press, New York, pp. 183–284.
Taylor, S.R., 1982. Planetary science: a lunar perspective. Lunar and Planetary Institute, Houston, pp. 481.
Tsay, F.-.D., Chan, S.I., Manatt, S.L., 1971. Ferromagnetic resonance of lunar samples. Geochim. Cosmochim. Acta 35, 865–875.
Wagner, R.V., Nelson, D.M., Plescia, J.B., Robinson, M.S., Speyerer, E.J., Mazarico, E., 2017. Coordinates of anthropogenic features on the Moon. Icarus 283, 92–103.

Warren, P.H., 1985. The magma ocean concept and lunar evolution. Ann. Rev. Earth Planet. Sci. 13, 201–240.
Warren, P.H., 1988. The origin of pristine KREEP: effects of mixing between urKREEP and the magmas parental to the Mg-rich cumulates. Proc. Lunar Planet Sci. Conf. 18, 233–241.
Warren, P.H., Wasson, J.T., 1977. Pristine nonmare rocks and the nature of the lunar crust. Proc. Lunar Science Conf. 8th, 2215–2235.
Warren, P.H., Wasson, J.T., 1979. The origin of KREEP. Rev. Geophys. Space Phys. 17, 73–88.
Warren, P.H., Wasson, J.T., 1980. Early lunar petrogenesis, oceanic and extraoceanic. Proc. Conf. Lunar Highlands Crust, 81–99.
Weill, D.F., Grieve, R.A., McCallum, I.S., Bottinga, Y., 1971. Mineralogy-petrology of lunar samples: microprobe study of samples 12021 and 12022; viscosity of melts of selected lunar compositions. Proc. Lunar Sci. Conf. 2nd, 413–430.
Wood, J.A., Dickey, J.S., Marvin, U.B., Powell, B.N., 1970. Lunar anorthosites and a geophysical model of the Moon. Proc. Apollo 11 Lunar Sci. Conf., 965–988.

CHAPTER 3

The Luna program

Evgeny Slyuta
Vernadsky Institute of Geochemistry and Analytical Chemistry RAS, Moscow, Russia

Chapter Outlines

Much in the Luna program was done for the first time in the history of space research, but one of the most important scientific tasks was lunar samples return by the Luna-16, Luna-20, and Luna-24 automatic spacecrafts. The full cycle of lunar samples return is considered: drilling and soil sampling on the lunar surface, delivery, acceptance and primary processing of lunar soil in the ground-based receiving complex, research methods and the major scientific results. Studies revealed medium-titanium fine- and coarse-grained basalts in the Mare Fecunditatis, low-titanium and high-aluminum basalts in the Mare Crisium, and rocks of anorthosite-troctolite-norite series in a Highland region. The last spacecraft Luna-24 on August 22, 1976 on Earth actually completed the first stage of the Moon's exploration with spacecrafts.

3.1 The beginning

The exploration of the Moon with spacecraft began with the successful launch by the Soviet Union on January 2, 1959 of the Luna-1 station (Soviet space rocket, 1959)

Sample Return Missions
DOI: 10.1016/C2018-0-03374-5

Table 3.1 Spacecrafts of the Luna program that have successfully completed the scientific task.

No	Spacecraft	Launch date	Launch target
1	Luna 1	02.01.1959	Hard landing on the Moon
2	Luna 2	12.09.1959	Hard landing on the Moon
3	Luna 3	04.10.1959	Flyby around the Moon
4	Zond 3	18.07.1965	Flyby around the Moon
5	Luna 9	31.01.1966	Soft landing on the Moon
6	Luna 10	31.03.1966	Moon orbital artificial satellite
7	Luna 12	22.10.1966	Moon orbital artificial satellite
8	Luna 13	21.12.1966	Soft landing on the Moon
9	Zond 6	10.11.1968	Flyby around the Moon
10	Zond 7	08.08.1969	Flyby around the Moon
11	Luna 16	12.09.1970	Lunar sample return
12	Zond 8	20.10.1970	Flyby around the Moon
13	Luna 17	10.11.1970	Lunokhod 1
14	Luna 20	14.02.1972	Lunar sample return
15	Luna 21	08.01.1973	Lunokhod 2
16	Luna 24	09.08.1976	Lunar sample return

(Table 3.1). After completing the work of the third stage of a rocket at a distance of 113,000 km from Earth, an experiment was conducted with an artificial comet to visually indicate the station flight path. Ionized sodium vapor of 1 kg was scattered into space, forming an extended flickering cloud of orange color. The cloud brightness was comparable to 7th star magnitude, making it observable from Earth for 3 min (Bulletin, 1965). The station did not hit the Moon. The miss was caused by a delay in the command of the ground-based radio control system to disable the second stage. Luna-1 flew near the Moon at a distance of 5000–6000 km and made its first important scientific discovery: the Moon did not have a magnetic field. On January 5, 1959, due to the exhaustion of power sources, communication with the spacecraft ceased. Around January 7–8, 1959, Luna-1 entered the heliocentric orbit and became the world's first artificial planet in the Solar system.

The total weight of the sealed container with scientific equipment amounted to 361.3 kg (Marov and Huntress, 2013). The container had a spherical shape with a diameter of 80 cm and consisted of two hemispheres (Fig. 3.1). The following scientific equipment was located on the station's case: 1) four proton traps in the form of three concentric electrodes for studying gas component and solar corpuscular radiation; 2) a triaxial fluxgate magnetometer on a remote rod; 3) piezoelectric sensors for studying meteor particles; 4) Cherenkov detector for detecting high-energy particles; 5) two gas-discharge Geiger counters for studying ionizing cosmic

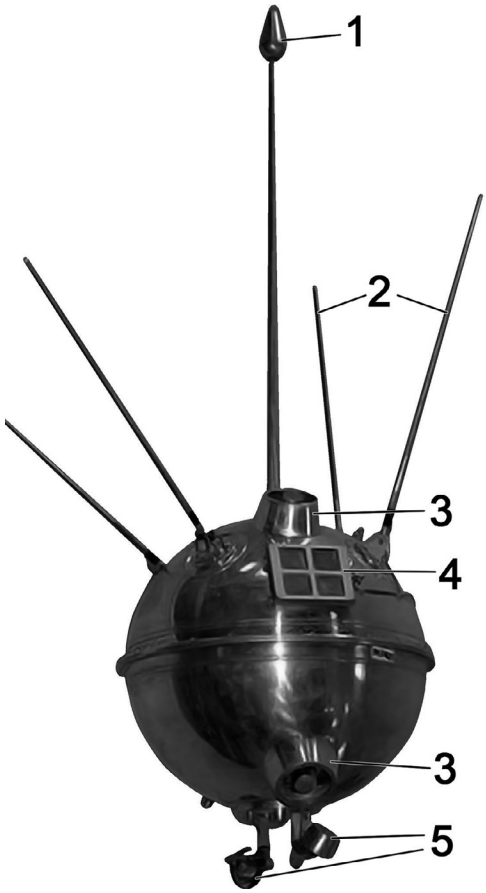

Fig. 3.1 General view of the Luna-1 spacecraft: 1 - a magnetometer; 2 - a whip antennas; 3 - proton traps; 4 - a micrometeorite sensor; 5 - tape antennas.

radiation (one counter was placed on the surface of the hull, the second inside the hull); 6) two scintillation counters with photomultipliers on crystals for detecting photons in cosmic radiation.

The Luna-2 spacecraft was launched on September 12, 1959. The mission main objective was to reach the Moon's surface and make a hard landing. At a distance of 156,000 km from the Earth, a sodium cloud was ejected, which was observed for 5–6 min, had a brightness comparable to a 4.5 star magnitude, and which visually indicated the trajectory of the spacecraft (Bulletin, 1965). On September 14, the station fell on the Moon's surface at a speed of 3.3 km s^{-1}, making a hard landing. The moment of fall was recorded due to cessation of radio signals. Seconds after the fall

of the spacecraft, the observatories in Hungary (Budapest and Baja) and Sweden (Uppsala) noticed a dust cloud on the lunar surface on the northern slopes of the Apennines at the station's fall place (~30° N, 0° E). The fall area was on the east coast of the Mare Serenitatis. Inside the case, there were two ribbons and two spherical pennants, consisting of pentagonal medallions with the inscription "USSR September 1959", which upon impact should have split and fly apart on the surface (TASS message, 1959). The sealed container Luna-2 was the same as at the Luna-1 station with a similar set of scientific equipment (Fig. 3.2). The mission was successful. Scientific instruments confirmed the absence of a magnetic field on the Moon and the presence of radiation belts about the Earth. For the first time, the existence of the outer region of the Earth's ionosphere at heights from 2000 km to 20,000 km from the Earth's surface was discovered. The ionic component of the solar wind outside the magnetosphere was also measured for the first time. These measurements confirmed the hydrodynamic theory of the solar wind, proposed in 1958 by the American physicist Eugene Parker and harshly criticized by physicists.

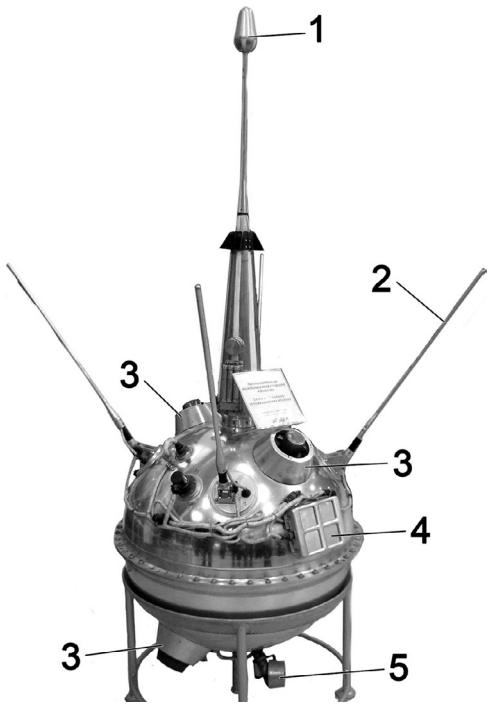

Fig. 3.2 General view of the Luna-2 spacecraft: 1 - a magnetometer; 2 - whip antennas; 3 - proton traps; 4 - a micrometeorite sensor; 5 - tape antennas. *(Photo by the author with the permission of the Museum of S.P. Korolev Rocket and Space Corporation Energia).*

3.2 "The Dark Side of the Moon"

The Luna-3 spacecraft was launched a month later on October 4, 1959. The spacecraft was entered into a geocentric orbit with a flyby around the Moon with an apogee of 480,000 km and a perigee of about 47,500 km and an orbital period of 16 days (Bulletin, 1965). On October 7, from a distance from 65,200 to 68,400 km, the station repeatedly photographed the Moon Far Side for 40 min. Image transmission was carried out in two modes, i.e., slower transmission at large distances and faster at close distances when approaching to the Earth.

The station weighing 278.5 kg had the shape of a cylinder with length of 130 cm and a diameter of 120 cm (Fig. 3.3) (Marov and Huntress, 2013). The complex of scientific equipment was similar to Luna-1 and Luna-2 (Fig. 3.2). The "Yenisei" TV-complex was located inside the body behind the porthole, which was closed by two semicircular covers that opened before photographing the Moon. The camera had two lenses with focal lengths of 200 mm and 500 mm and relative apertures of 1:5.6 and 1:9.5. A 200 mm lens provided an image of the full Moon disk, and a 500 mm lens gave a larger image of a portion of the Moon disk (The first photographs, 1959). To obtain negatives with the better exposure, the exposure of various frames during photography was changed automatically. The heat-resistant 35 mm film was developed and fixed in one solution. After processing, the film entered a special cassette for image transfer. In November 1959, for unexplained reasons, communication with the station suddenly ceased. It is assumed that in March 1960 the SC burned out in the Earth's atmosphere, making 11 revolutions around the Earth.

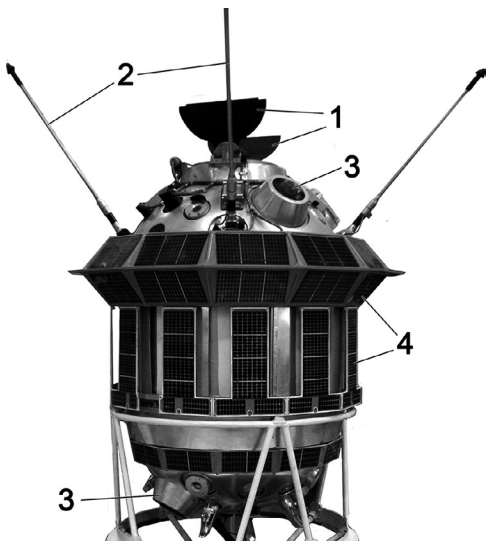

Fig. 3.3 General view of the Luna-3 spacecraft: 1 - porthole covers; 2 - whip antennas; 3 - proton traps; 4 - solar panels. *(Photo of the author with the permission of the Museum of S.P. Korolev Rocket and Space Corporation Energia).*

Luna-3 for the first time in human history glanced at the invisible from Earth the Moon Far Side. A snapshot of the century, as it was later called worldwide, was published in the Pravda newspaper on October 27, 1959 (The third Soviet space rocket, 1959) (Fig. 3.4). The obtained images revealed 107 features. The twelve largest craters were named after the most prominent scientists. Asymmetry (dichotomy) of the visible and reverse hemispheres of the Moon was discovered. Another great mystery in the history of mankind – "And what is there, on the Moon Far Side?" – ceased to exist.

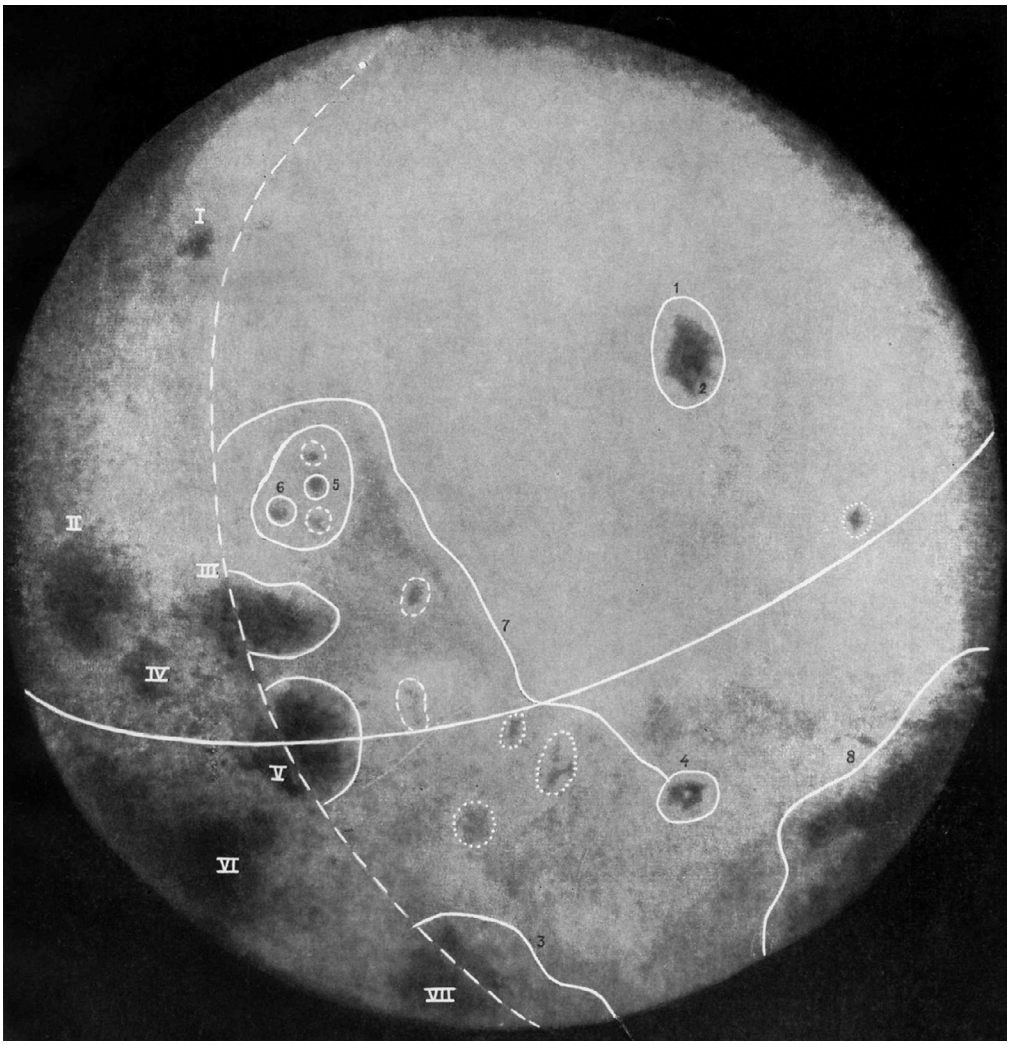

Fig. 3.4 Image of the Moon Far Side according to the Luna-3 spacecraft *(The third Soviet space rocket, 1959)*: 1 - Mare Moscovience; 2 - Astronaut Bay in the Mare Moscovience; 3 - Mare Australe; 4 - crater Tsiolkovsky; 5 - crater Lomonosov ; 6 - crater Joliot-Curie; 7 - Soviet mountain range; 8 - Mare Ingenii. Objects on the Moon Near Side: I - Mare Humboldtianum; II - Mare Crisium; III - Mare Marginis; IV - Mare Undarum; V - Mare Smythii; VI - Mare Fecunditatis; VII - Mare Australe continued on the Moon Far Side.

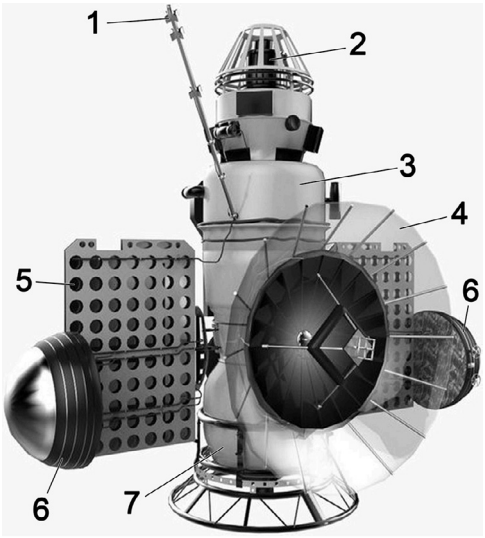

Fig. 3.5 General view of the spacecraft Zond-3: 1 - a magnetometer; 2 - a correction engine; 3 - an orbital compartment; 4 - a parabolic antenna; 5 - solar panels; 6 - radiators of the temperature control system; 7 - a planetary compartment.

The Zond-3 spacecraft (Fig. 3.5), which was launched on July 18, 1965, continued photographing the Moon Far Side. Photographing was carried out on July 20 at a distance from 11,570 km to 9220 km from the lunar surface. During photographing, 28 frames were received (Fig. 3.6). Of these, 23 are photoimages and 3 are frames exposed using an ultraviolet spectrograph (Atlas, 1967). Some pictures could be combined into stereo pairs. Communication with the station was maintained until March 1966. In addition to scientific instruments for measuring radiation and magnetic field, an ultraviolet spectrograph,

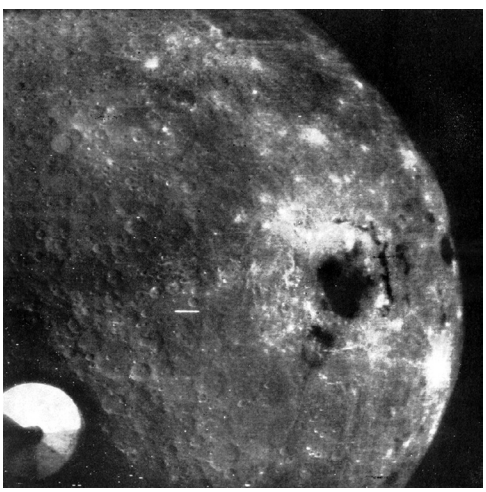

Fig. 3.6 The 26th image frame of the Moon according to the spacecraft Zond-3 *(Atlas, 1967)*.

a camera with automatic film processing and an optical-mechanical scanning device for transmitting images were placed on the spacecraft. Each frame was transmitted with its decomposition into 1100 lines with a clarity of 860 elements. The camera was equipped with a lens with a focal length of 106.4 mm and a relative aperture of 1:8. Images of the western part of the Moon Far Side, including the part of the Mare Orientale that is invisible from the Earth were obtained. The length of this previously unexplored territory was approximately 70° in longitude, i.e. about one third of the surface of the Moon Far Side (Fig. 3.7). Together with images, the surface spectra of the Moon were obtained in the ultraviolet (1900–2700 angstroms) and infrared (3–4 μm) ranges.

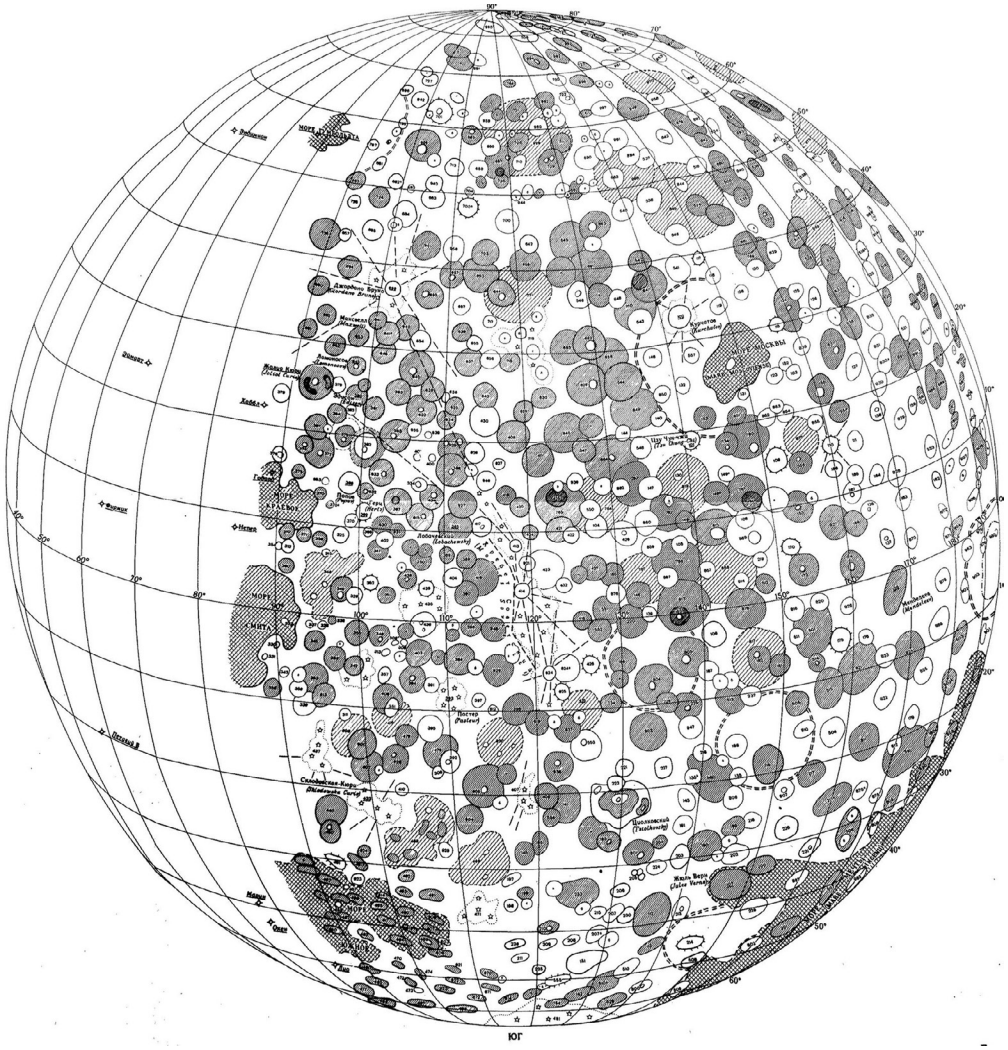

Fig. 3.7 A schematic map of the Western sector of the Moon Far Side, compiled by the Sternberg State Astronomical Institute and Central Research Institute of Geodesy, Aerial Surveying and Cartography based on the data of the Zond-3 spacecraft *(Atlas, 1967)*.

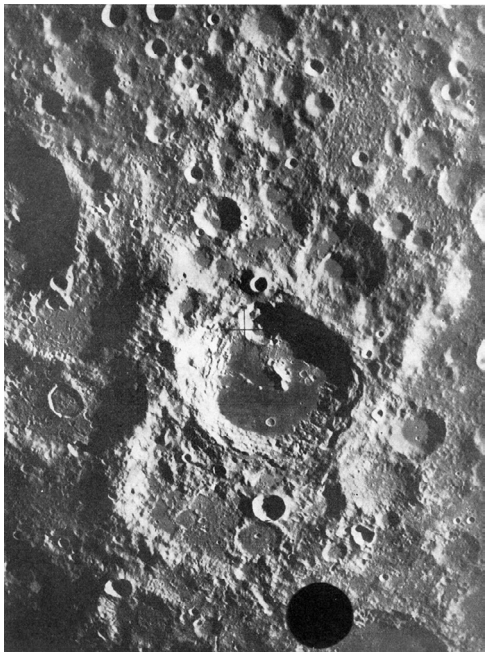

Fig. 3.8 ***Image frame of the far side of the moon according to the spacecraft Zond-8 (Atlas, 1975).*** In the center is Aitken Crater (16.8° S, 173.4° E) of 135 km in diameter.

Photographing of the Moon continued with the spacecrafts Zond-6, Zond-7, and Zond-8, launched on November 10, 1968, August 8, 1969, and October 20, 1970, respectively. The main goal of these missions was testing an automatic version of a manned spacecraft for flights to the Moon (Marov and Huntress, 2013). Stations circled the Moon at distances of 2000–3000 km from its surface and returned to Earth. A precision aerial camera with a focal length of 403 mm was installed at stations. The shooting was carried out through a porthole on 190 mm black-and-white and color films. The film was returned to the Earth in a descent module and processed in laboratory conditions, which allowed us to obtain high-quality images with good resolution (Fig. 3.8) (Atlas, 1975).

3.3 First lunar surface panoramas

The Luna-9 automatic station was launched on January 31, 1966. The station made a soft landing on the lunar surface in the morning of February 3, 1966 on the western coast of the Oceanus Procellarum, specifically at - 7°08′ N, 64°22′ W. It was the first controlled soft landing of an automatic machine from planet Earth on the surface of another celestial body and another world. The general designer of the project, Sergei

Pavlovich Korolev, who was looking forward to this event with great impatience, did not live to see it only 20 days.

The properties of the lunar soil were unknown. The landing module was separated from the propulsion system. Elastic bags located around the landing module were inflated with compressed gas and softened the impact on a hard surface, and also excluded immersion in the alleged deep dust layer (Gold's hypothesis). The opened petals provided a stable position of the station and tilted the station from the vertical by 16°, which made it possible to obtain a microrelief image directly in front of the station. The transmission of panoramic images was carried out on February 4, 5 and 6 at Sun height above the horizon of 7°, 13°, 27° and 42° (The first panoramas, 1966). A small random shift of the station on soil by 9 cm made it possible to obtain stereo pairs of images. On February 7, 1966, communication with the station ceased.

The station consisted of three main parts: a landing module in the form of a spherical sealed container weighing 100 kg and a diameter of 58 cm (Marov and Huntress, 2013), a braking propulsion system and compartments with flight control equipment (Fig. 3.9). The following scientific equipment was installed in the landing module:

1. Counters of cosmic radiation.
2. Three dihedral mirrors for stereoscopic imaging of six narrow sections of the lunar surface and determining the distance to objects in panoramic images.
3. Luminance standards for assessing the lunar rocks albedo.
4. Optical-mechanical scanning television system for transmitting a still image. The full panorama consisted of 6,000 lines and was transmitted within 100 min.

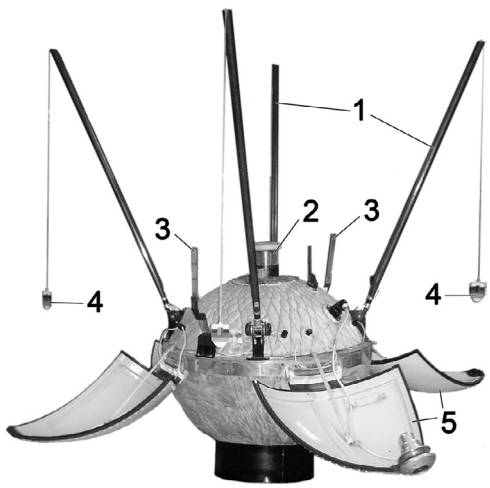

Fig. 3.9 General view of the Luna-9 landing spacecraft: 1 - whip antennas; 2 - a television system; 3 - trihedral mirrors for stereo imaging; 4 - brightness standards; 5 - petal antennas. *(Photo by the author with permission of the Lavochkin association's museum)*.

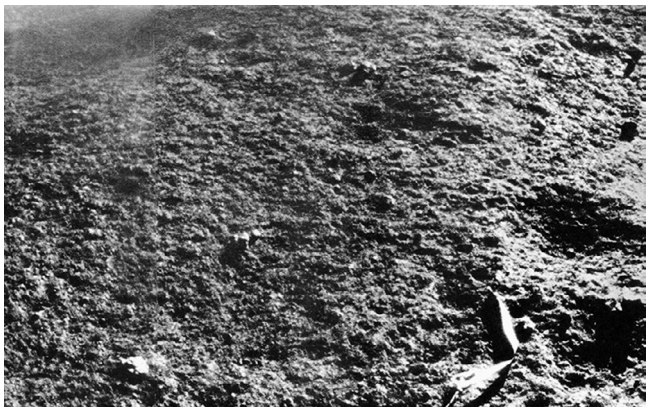

Fig. 3.10 A fragment 3 of the panorama III of the lunar surface according to the Luna-9 spacecraft *(The first panoramas, 1966)*.

The first panoramic images of the lunar landscape and several stereo pairs were obtained (Fig. 3.10). Images were taken from a distance from 85 cm (with a resolution of 1.5–2 mm) to the visible horizon of about 1.5 km (with an apparatus height of 58 cm). Lunar soil turned out to be quite dense with high bearing capacity. It was first established that the intensity of radiation on the lunar surface is mainly determined by cosmic rays. Secondary radiation due to nuclear reactions from cosmic rays on soil particles was also discovered.

The next Soviet station Luna-13 (Fig. 3.11), launched on December 21, 1966, soft landed on a lunar surface 6 h 29 min before sunrise on December 24, 1966 again in the Oceanus Procellarum, at -18°52′ N, 62°03′ W. During the first transmission of images, the height of the Sun above the horizon was 6°, during the second -19° and during the third -32° (The first panoramas, 1969). After transmitting the last, fifth lunar panorama

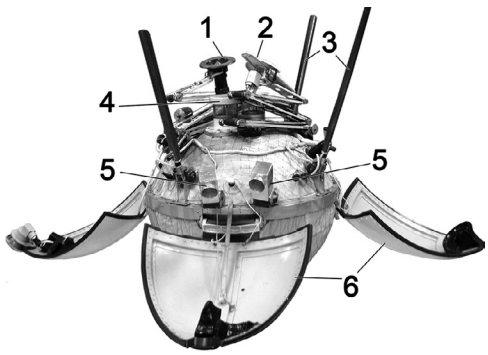

Fig. 3.11 General view of the Luna-13 landing spacecraft: 1 - a penetrometer with folded device for lowering to the lunar surface; 2 - a gamma-densitometer with folded device for lowering to the lunar surface; 3 - whip antennas; 4 - a television system; 5 - radiometers; 6 - petal antennas. *(Photo by the author with permission of the Lavochkin association's museum)*.

on December 28, 1966, communication with the station ceased. With respect to Luna-9, the additional scientific instruments were installed:

1. The penetrometer for assessing the mechanical strength of the lunar soil. A small jet engine with a force of about 6 kg introduced a titanium conical tip into the ground.
2. A gamma-densitometer for determining the density of lunar soil down to 15 cm deep, which consisted of a gamma radiation source and three gas-discharge counters with a protective screen from the source radiation.
3. Radiometer for measuring heat flux from the surface.
4. Dynamometer for detecting a dynamic load depending on soil hardness during landing.

In addition to five panoramic images of lunar surface transmitted to the Earth (Fig. 3.12), the station also performed the first direct measurements density, physical and mechanical properties and thermal characteristics of lunar soil. New data on the intensity of cosmic radiation on a lunar surface also were obtained.

3.4 The first gamma-survey of the lunar surface

The Luna-10 started on March 31, 1966, and on April 3 the station entered a lunar orbit with a pericenter of 350 km, an apocenter of 1017 km, an inclination of 71°54', and an orbital period of 2 h 58 min. After turning off the brake engine, the compartment with

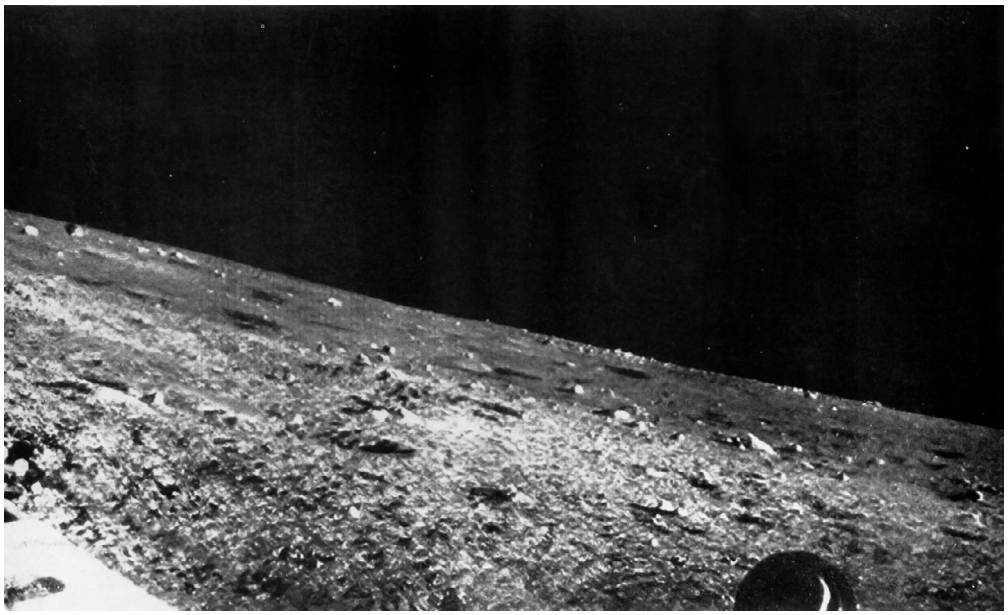

Fig. 3.12 A fragment 6 of the panorama II of the lunar surface according to the Luna-13 spacecraft (*The first panoramas, 1969*).

scientific and radio equipment was separated. The active existence of the station lasted 56 days. During this time, the station made 460 orbits around the Moon. The last radio communication session took place on May 30, 1966. The Luna-10 spacecraft became the first artificial Moon satellite.

The station consisted of two main parts: a detachable sealed container with scientific and radio equipment and a propulsion system with instrument compartments (Fig. 3.13). A detachable container weighed 245 kg (Marov and Huntress, 2013). The following scientific devices were installed on the Luna-10:

1. Three-component magnetometer with sensitivity 15 times higher than one on the Luna-2.
2. Scintillation gamma-spectrometer for studying gamma radiation from the lunar surface in the energy range 0.3–3.0 MeV (Fig. 3.14).
3. Counters of soft x-ray photons for measuring x-ray fluorescence radiation of lunar rocks.

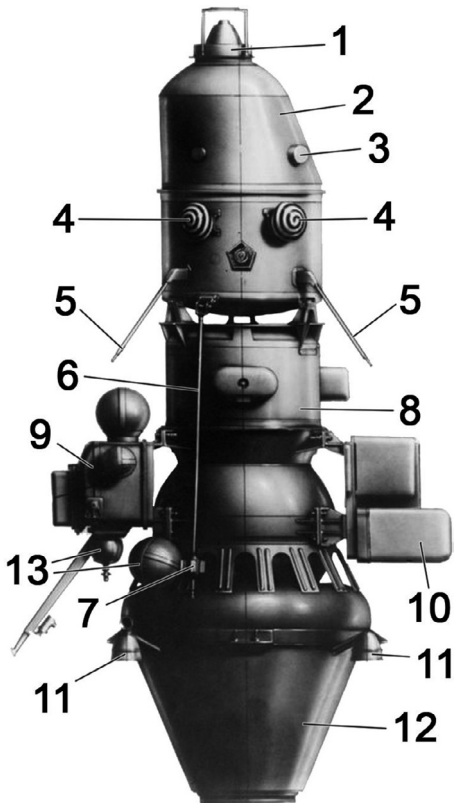

Fig. 3.13 General view of the Luna-10 spacecraft: 1 - a gamma spectrometer; 2 - a detachable artificial Moon satellite; 3 - a proton trap; 4 - antennas; 5 - whip antennas; 6 - a magnetometer arm; 7 - a magnetometer; 8 - service module; 9 - an astroorientation system; 10 - measuring radio equipment; 11 - an orientation engine; 12 - the main engine; 13 - gas tank.

Fig. 3.14 General view of the gamma spectrometer for the Luna-10 spacecraft. *(Photo by the author. With the permission of the Vernadsky Institute).*

4. Counters for recording solar radiation and cosmic rays, as well as to detect the Moon's ionosphere.
5. Ion traps for recording flux of ions and electrons of solar wind.
6. Piezoelectric sensors with an area of about 1 m^2 for recording meteor particles with a mass exceeding 10^{-8} g.
7. Infrared sensor to determine the integral thermal radiation of the Moon.

More than 40 sessions of measurements of the lunar surface's gamma radiation were conducted. It was found that 90 percent of lunar radiation is caused by nuclear reactions under the influence of cosmic rays, and only 10 percent - due to the natural radiation of potassium, uranium and thorium in lunar rocks (Vinogradov et al., 1966; Surkov, 1977). Variations of gamma radiation due to the natural radioactivity of lunar rocks in different regions did not exceed 40 percent. It was established that the content of natural radioactive elements in lunar maria rocks corresponds to terrestrial basalts, and in lunar Highlands to terrestrial ultrabasic rocks. The mass and the shape of the Moon were also clarified. The measured spatial density of meteoroid particles in the satellite's orbit was about 100 times higher than in interplanetary space.

Imaging and geochemical mapping of the lunar surface was successfully continued by Luna-12, launched on October 22, 1966. On October 25, Luna-12 entered a near-moon orbit with pericenter 100 km, apocenter 1740 km and orbital period 3 h 25 min. Imaging of the Oceanus Procellarum and the Mare Imbrium was carried out from a distance of 100–340 km. The best image resolution reached was 15–20 m. Among the features imaged from the mission, there were the bright rays of the Aristarchus crater. On January 19, 1967 on the 602 orbit communication with the station was terminated.

Luna-12 spacecraft had an undetachable container with service and scientific instruments (Fig. 3.15). Additional scientific equipment with respect to Luna-10 included a

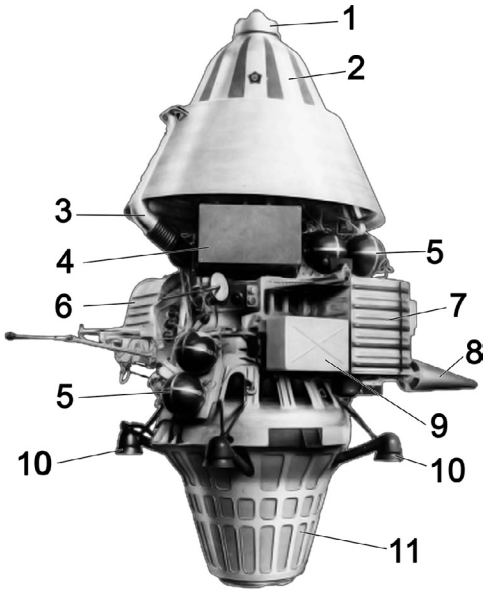

Fig. 3.15 General view of the Luna-12 spacecraft: 1 - a gamma spectrometer; 2 - an instrument compartment; 3 - a radiator of a temperature control system; 4 - a chemical battery; 5 - a gas tank; 6 - a photo-television device; 7 - an astroorientation system; 8 - an antenna; 9 - an electronic unit of the astroorientation system; 10 - an orientation engine; 11 - the main engine.

US-3 spectrophotometer to record the lunar surface in the UFS range, a radio astronomy equipment "Cassiopeia KYA-4" for observation of long-wave space radio emission and two TV-cameras, with focal lengths of 500 mm and 110 mm, respectively. The film stock (42 frames) was designed for one shooting session lasting 64 min. The frame size was 24 by 24 mm. The image size was 1100 by 1100 elements.

The inclination of the orbit, different from the inclination of the Luna-10 station, made it possible to study gamma and x-ray radiation from lunar rocks for previously unexplored regions of the Moon. The content of potassium, uranium, and thorium in lunar rocks of mare and Highland, previously measured by the Luna-10 spacecraft, was confirmed. An increased concentration of small secondary impact craters on rays of Aristarchus crater was found.

3.5 Lunokhod

The launch of the Luna-17 spacecraft with Lunokhod-1 took place on November 10, 1970. The spacecraft made a soft landing on the lunar surface on November 17 in the Mare Imbrium area south of Sinus Iridium (landing point coordinates -38°17′ N, 35° W). Remote control of the lunokhod was carried out by a group of 5 people, i.e. the commander, driver, navigator, flight engineer and operator (Vinogradov, 1971). Given the time delay of the passage of signals and commands, the time for making and executing

decisions ranged from 4 to 20 s. This significantly reduced the average speed of the lunokhod, which did not exceed 0.143 km h^{-1}. In the first two lunar days, a reconnaissance scientific survey was conducted to obtain the main characteristics of the lunar surface. Before sunrise on December 5 and 6, an experiment on laser ranging from the Crimean Astrophysical Observatory of the USSR Academy of Sciences was conducted.

Lunokhod overcame craters with slope steepness up to 20° without changing course. According to updated data (Karachevtseva et. al, 2013), the lunar rover passed 9930 m in 11 lunar days (Fig. 3.16). The last communication session took place on September 14, 1971 to prepare the lunokhod for a lunar night. On the lunar morning of September 30, 1971 the signal from the lunokhod was not received longer.

Lunokhod consisted of a sealed instrument compartment with equipment mounted on a self-propelled eight-wheeled chassis (Fig. 3.17). The lunokhod total weight was 756 kg. On top was a lid that during the lunar day opened and served as a solar panel battery, and closed at night and prevented the emission of heat from the instrument compartment. The following scientific equipment was installed on board the lunokhod:

1. Four TV-cameras with optical-mechanical panoramic scan with an angle of 30°.
2. Two small-frame TV-cameras for controlling the movement with a wide-angle lens with a focal length of 6.7 mm, a viewing angle in the horizontal plane of 50°, and in the vertical -38° The camera axis was tilted down 15° The distance between the cameras was 400 mm, which made it possible to obtain stereo pairs of images. In normal mode, only one of the cameras worked.
3. A current sensor of traction electric motor-wheel, a roll and trim sensor, a sensor of wheel revolutions and a sensor of the traveled distance (ninth wheel) to assess soil physical properties and lunokhod passability.
4. A cone-lobate penetrator. The penetrator was introduced into the soil with a force of up to 20 kg to a depth of 50–100 mm. Angle of cone rotation was up to 90°, and torque was up to 0.5 kg.
5. An active X-ray fluorescence spectrometer RIFMA with an X-ray source based on ^{3}H for studying chemical composition of lunar soil.
6. Two Geiger gas discharge counters and six semiconductor silicon counters for studying solar wind and low-energy cosmic rays.
7. A collimator x-ray telescope RT-1 with an angular aperture of 3.3° for study of cosmic x-ray radiation. Telescope axis was directed along vertical axis of the lunokhod. Radiation receivers were two proportional photon counters, the lateral and lower surfaces of which were covered by a lead screen.
8. French laser corner reflector for conducting experiments on laser ranging and determining the distance to the Moon. Due to thermal deformations of the prisms at high temperature, the reflector could only work on lunar night.

Lunokhod-1 transmitted over 211 high-quality panoramic images and more than 25,000 individual images of the lunar surface. Data on the physicomechanical properties

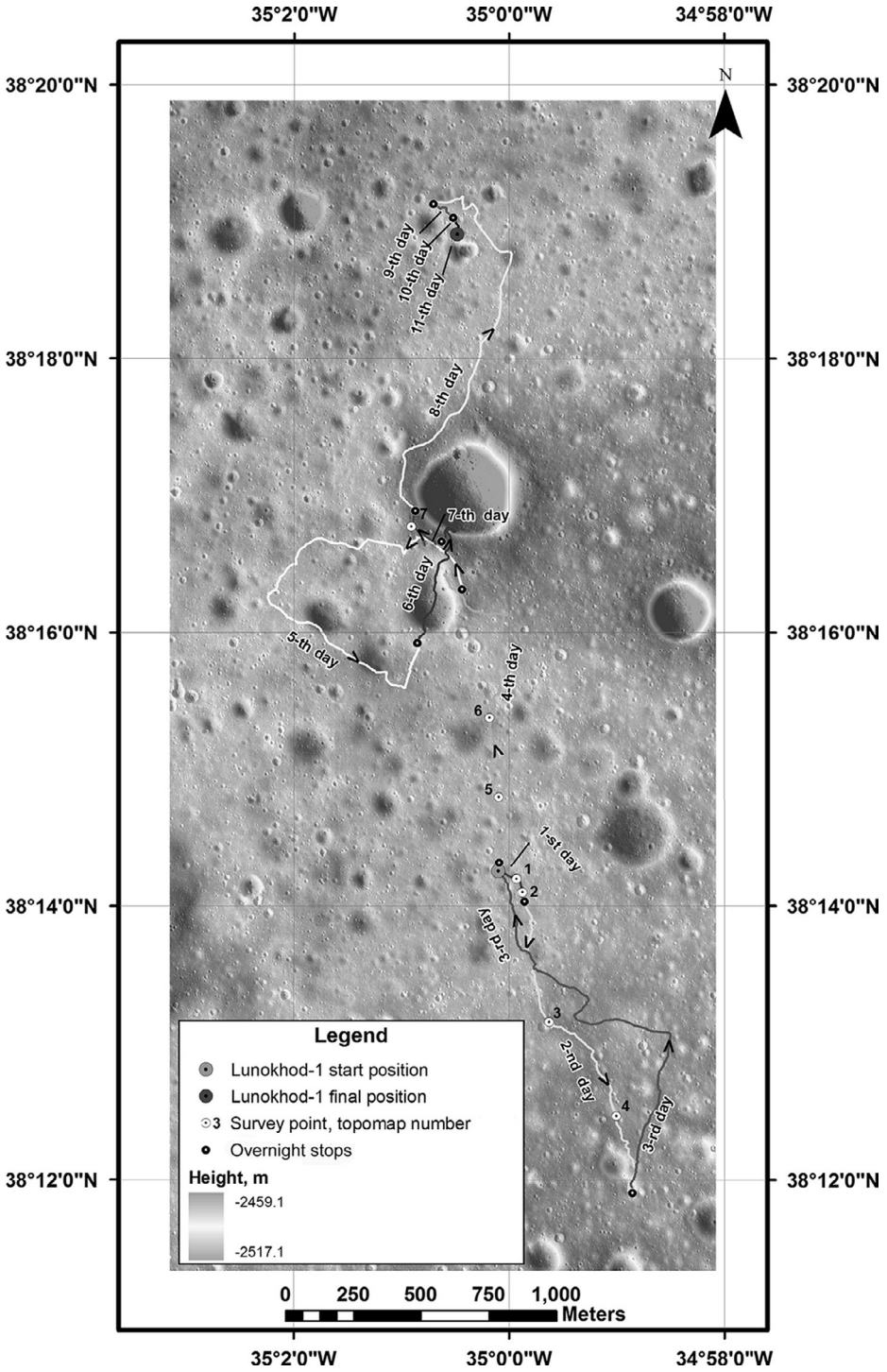

Fig. 3.16 ***Map of Lunokhod-1 traverse (orthomosaic DEM) by (Karachevtseva et. al, 2013).*** For interpretation of the references to color in this figure legend, the reader is referred to the web version of (Karachevtseva et. al, 2013).

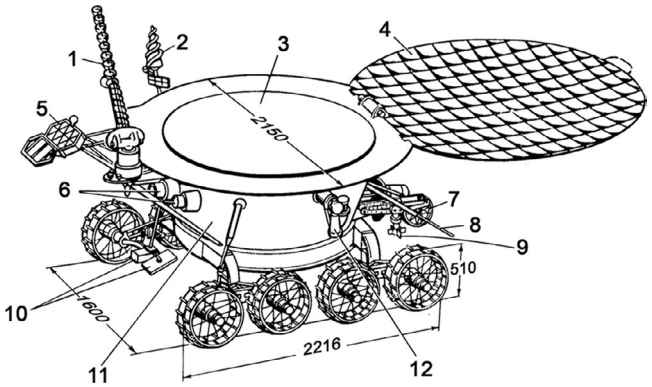

Fig. 3.17 General view of the Lunokhod-1: 1 - a pointed antenna; 2 - an omnidirectional antenna; 3 - a radiator-cooler; 4 - a solar battery; 5 - a laser corner reflector; 6 - small-frame TV-cameras; 7 - the ninth wheel; 8 - a whip antenna; 9 - a cone-lobate penetrator; 10 - X-ray fluorescence spectrometer RIFMA; 11 - a sealed instrument compartment; 12 - TV-cameras.

and chemical composition of lunar soil were obtained (Barsukov, 1978). A high resolution geomorphological and topographic mapping of lunar surface along the route was carried out. Data on the degree of isotropy of the background of x-ray radiation at small angular apertures of the x-ray telescope were obtained. Large-scale variations of solar wind for each lunar day were studied. Because of a simultaneous laser location session from the Crimean Astrophysical Observatory (USSR) and from the Pic du Midi Observatory (France), the distance to the reflector on the lunokhod was measured with an accuracy of ±3 m.

The launch of the Luna-21 spacecraft with the Lunokhod-2 was carried out on January 8, 1973 from the Baikonur Cosmodrome. On November 16, 1973, the station made a soft landing on the lunar surface in the eastern part of the Mare Serenitatis, in the Lemonnier crater at coordinates 25.999° N, 30.407° E (Karachevtseva et al., 2017). On the first lunar day (January 16–24, 1973), the lunokhod traveled 1148 m to the nearest crater with a diameter of about 250 m (Fig. 3.18). Then, the lunokhod moved east along the coast of Lemonier Crater. Lunokhod examined western and eastern sides the Fossa Recta. In total, the lunokhod traveled 39,105 m in five lunar days and studied lunar plain with an area of 14 by 8 km. The Lunokhod-2 mission was completed on May 10, 1973 at a point with coordinates 25.832° N, 30.922° E (Fig. 3.18).

The onboard equipment and design of Lunokhod-2 was similar to the Lunokhod-1. The total mass of Lunokhod-2 was 836 kg, i.e., 80 kg more than Lunokhod-1 (Kemurdzhian, 1993). New arsenide-galium panels replaced solar panels. The average operating speed of the lunar rover was twice (0.354 km h^{-1}) that of the Lunokhod-1. A set of scientific equipment from Lunokhod-1 was supplemented with a three-component ferromagnetometer on a remote arm (length 1.5 m) and a third frontal small-sized camera for navigation.

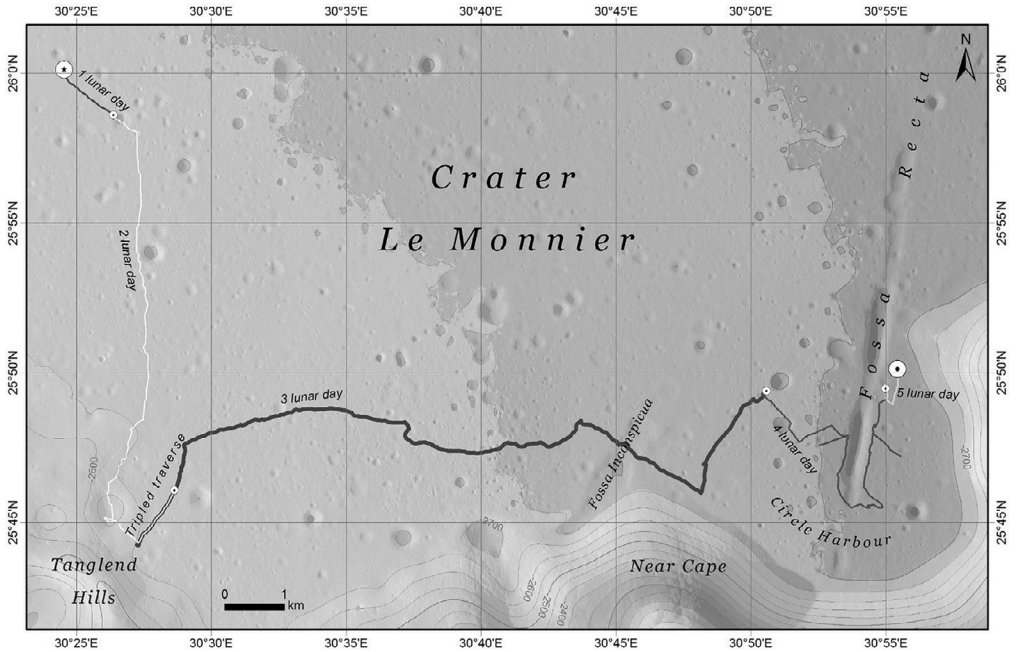

Fig. 3.18 Hypsometric map of the Lunokhod-2 study area, based on new DEM and orthomosaic by *(Karachevtseva et al., 2017)*.

Lunokhod-2 transmitted over 90 lunar panoramas and 80,000 frames to the Earth, which were used for large-scale geomorphological and topographic mapping along the lunokhod route (Florensky et al., 1974; Bazilevsky et al., 1984). Data were obtained on the physicomechanical properties of lunar soil at various sections of the route (Cherkasov and Shvarev, 1975). Data on a chemical composition of lunar soil were obtained at 23 observation points (Kocharov and Viktorov, 1974). Magnetic field profiles were made through fresh craters and through the Fossa Recta tectonic graben (Ivanov et al., 1976). Landslide phenomena on the crater slopes were recorded and studied (Kuzmin, 1975).

3.6 Lunar samples return

3.6.1 Luna-16

The launch of the Luna-16 spacecraft with the first drilling rig on board took place on September 12, 1970. On September 17, the station entered a circular orbit around the Moon, and on September 20, the SC landed within the Mare Fecunditatis at a point with coordinates -0°41′ S, 56°18′ E (Outstanding achievements, 1970). The spacecraft consisted of three main modules - the landing platform with a drilling soil intake device, the Moon-Earth space rocket, and the returned apparatus with a container for lunar soil (Fig. 3.19). The total weight of the lander was 1880 kg (Marov and Huntress, 2013). In

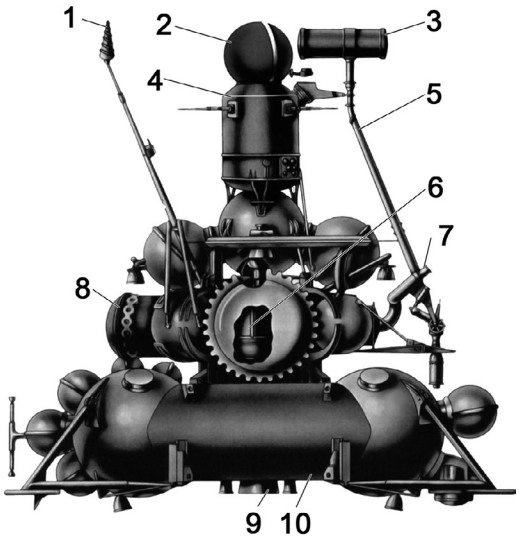

Fig. 3.19 ***General view of the Luna-16 spacecraft.*** 1 - an antenna; 2 - a returned apparatus; 3 - a drilling rig; 4 - an instrument compartment of the Moon-Earth space rocket; 5 - a lever to move the drilling rig; 6 - the Moon-Earth rocket engine; 7 - a TV-camera (telefotometer); 8 - an instrument compartment of the landing plataform; 9 - a landing platform engine; 10 - a landing platform.

the instrument compartment of the landing platform, in addition to service equipment, scientific instruments for temperature and radiation measurements were also placed. To land on the lunar surface, shock absorbing supports were installed.

The soil intake device consisted of three main parts:

1. A drilling rig with electric drives and a core drill for drilling to a depth of 35 cm and sampling lunar soil of various densities and hardness - from the loosest soil to massive basalt (Fig. 3.20).
2. A lever to move the drilling rig to the lunar surface and from the surface to the receiving container of the returned apparatus.
3. A drive moving the lever in the vertical and horizontal planes.

Two TV-cameras transmitted information to the Earth about the drilling site and drilling tool easily penetrated into the lunar soil. At the end of the set depth, the drill rested against a solid rock, into which it deepened by five mm. A rock density was measured depending on the drilling speed. After drilling, a drill with lunar soil was pulled into the drilling rig housing. The lever lifted the drill with lunar soil to the receiving container of the returned apparatus. The drill was separated from the rig. The airtight lid of the receiving container slammed shut. The station was on the Moon for 26 h 25 min. During this period, temperature and radiation measurements also was carried out.

Having completed soil sampling, the Luna-16 on September 21 was launched to the Earth, using its landing stage as a launch platform (Fig. 3.21). Before entering the atmosphere of the Earth on September 24, the returned apparatus was separated from the instrument compartment. The brake parachute opened at an altitude of 14.5 km, and

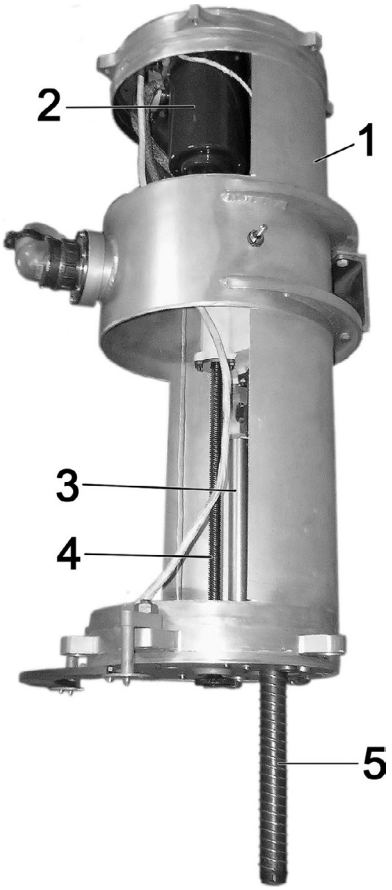

Fig. 3.20 General view of the drilling rig on the spacecraft Luna-16: 1 – a rig housing; 2 – an electric motor; 3 – a rotation drive; 4 – a feed screw; 5 – a core drill. Photo by the author with permission of the Lavochkin association's museum.

the dome of the main parachute opened at an altitude of 11 km. At the same moment, radio transmitters of the station turned on. The station's signal was detected and its descent by parachute was visually observed from helicopters and search service aircraft. On September 24, 1970, the returned apparatus made a soft landing on the USSR territory, 80 km southeast of Dzhezkazgan city. The mass of the lunar soil delivered to the Earth was 101 gs (Vinogradov, 1974).

3.6.2 Luna-20

The following Luna-20 spacecraft was launched on February 14, 1972. On February 21, the station descended to the lunar surface 130 km north of Luna-16 landing site on Highland between the Mare Fecunditatis and the Mare Crisium, and a few kilometers west from the Apollonius Crater (landing site coordinates - 3°32′ N, 56°33′ E)

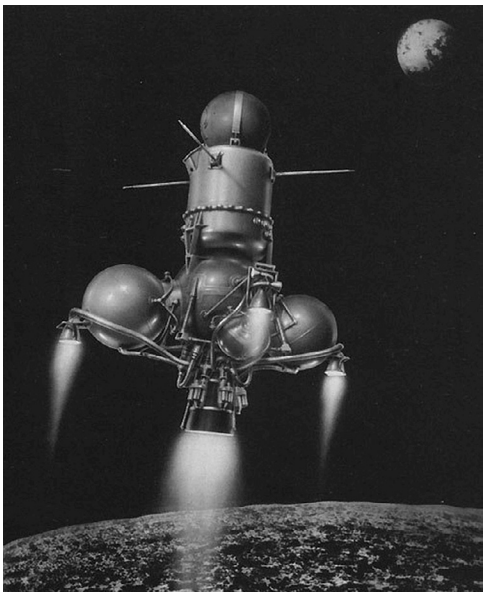

Fig. 3.21 General view of the Moon-Earth rocket of the Luna-16 spacecraft *(Outstanding achievements, 1970)*.

(Barsukov and Surkov, 1979). The landing speed in Highlands was reduced with respect to previous Luna spacecrafts, resulting in the softest landing. Unlike the Luna-16, which landed on a lunar night, the Luna-20 landed on a lunar day.

Using two telephotometers, the station transmitted images to the Earth to select a location for drilling (Surkov, 1972). The soil-sampling device was the same as on the Luna-16. A lever lowered the drill rig to the lunar surface. The drill easily overcame the first centimeters of soil, and then the resistance grew. The drill rig at critical moments by an additional mechanical drive was raised and lowered again. Drilling was carried out in several stages with intermediate stops. After drilling, the drill was drawn into the drilling rig and, using a lever, was placed into a return capsule and closed with a sealed lid. This operation was monitored using telephotometers. All operations were carried out by commands from the Earth. Once completed the program, the station with a capsule with soil started from the lunar surface on February 23. The mass of the return rocket was 512 kg. The spacecraft approached Earth on February 25. The returned apparatus landed 40 kms from Dzhezkazgan (Kazahstan). Lunar soil from the lunar Highland (mass of 55 gs) was delivered to the Earth.

As at the Luna-16 station, the returned apparatus weighing 35 kg consisted of three compartments (Fig. 3.22) (Marov and Huntress, 2013). In the largest compartment, there were radio direction-finding transmitters, chemical batteries and on-board control devices. The second sector housed a parachute, four elastic antennas of direction-finding transmitters and two gas-filled elastic balloons, which provided the necessary position on the Earth's surface after landing (Fig. 3.23). A receiving container for lunar soil samples was in the third compartment.

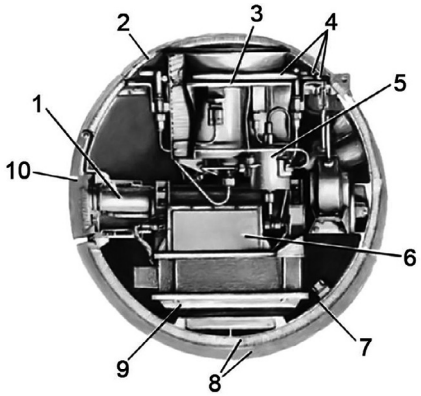

Fig. 3.22 The returned apparatus of the Luna-20: 1 - a soil container; 2 - a parachute compartment lid; 3 - a parachute compartment; 4 - antennas; 5 - an antenna switch; 6 - transmitters; 7 - the body of the returned apparatus; 8 - a thermal insulation; 9 - a chemical battery; 10 - a lid.

3.6.3 Luna-24

The Luna-24 station was launched on August 9, 1976. The station, in controlled descent mode soft landed on a lunar night on August 18, in the southeastern region of the Mare Crisium and 300 kms northeast of the Luna-20. The coordinates of the landing site are 12°45′ N, 62°12′ E (Barsukov, 1980).

The next-generation drilling rig LB-09 (Fig. 3.24) was designed for one-time drilling of lunar soil in automatic mode to a depth of 3 m and for sampling soil with

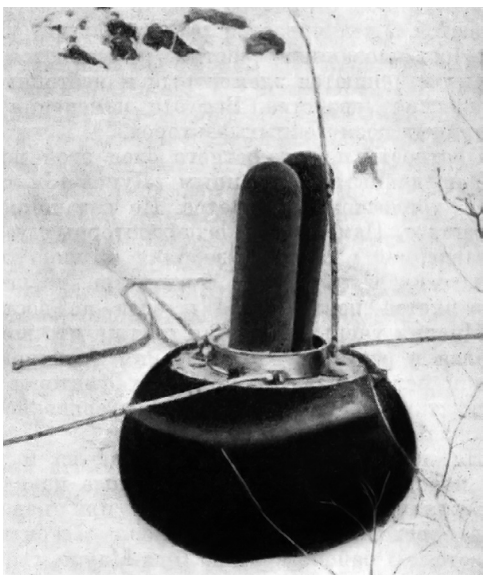

Fig. 3.23 The returned apparatus of the spacecraft Luna-20 after landing.

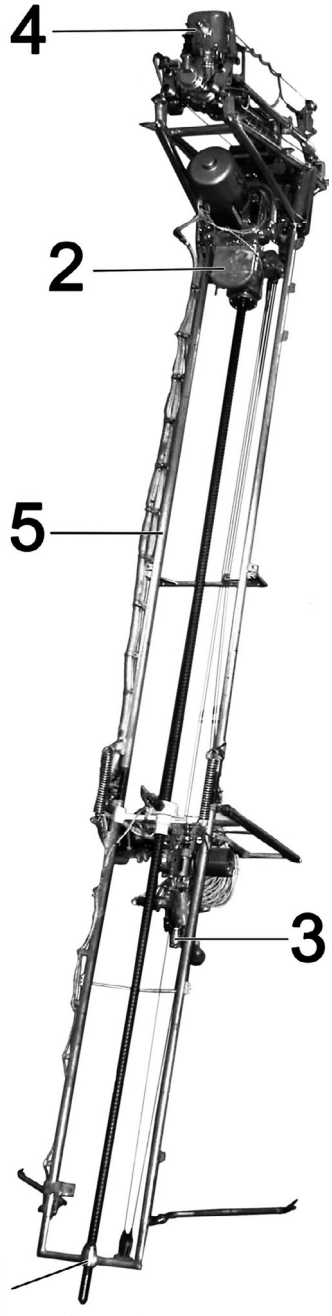

Fig. 3.24 ***General view of the drilling rig LB-09.*** 1 - a drilling tool; 2 - a drill head; 3 - a feed mechanism; 4 - a reloading mechanism; 5 - a frame.

Table 3.2 Technical specifications of LB-09 drilling rig.

Parameter	Value
Height, m	3.2
Mass, kg	55
Core diameter, mm	10.0
Mass of core, g	170
Working stroke of the soil sampling tool, mm	2500
Average power consumption, W	550
The drilling speed of the lunar soil, cm min^{-1}	15
Drilling time to full depth, h	1.0

undisturbed stratification (Table 3.2). A drilling rig was developed in Barmin KBOM, on the instructions of the Director of Vernadsky Institute Academician A.P. Vinogradov. The LB-09 drilling rig consisted of the following main units:

1. A drilling rig with an elastic sampler and a 2-stage crown for drilling lunar soil;
2. The drill head to create a rotational and shock-rotational modes;
3. The feed mechanism for moving the drill head and pressing with a given force of the drilling tool to the lunar soil during drilling;
4. The mechanism for reloading an elastic sampler from a drilling tool, placing it in a drum and loading it into the returned apparatus;
5. A farm for attaching a drilling rig to the landing stage;
6. A control unit for monitoring the operation of the drilling rig.

The drilling process was carried out according to an autonomous program (Sokolov et al., 1976). During drilling, an automatic transition from rotational to shock-rotational drilling was provided, depending on the resistance of lunar rock. To a depth of 1.2 m, the rotational mode was applied, and deeper periodically there was a change of modes. A well was drilled at an angle of about 30° from the vertical to a depth of 2.25 m. An elastic sampler, which was located inside the drill rod, during drilling, was filled with soil. After drilling, the elastic sampler was wound on a drum with a diameter of 80 mm (Fig. 3.25), which was loaded into a sealed container of the returned apparatus.

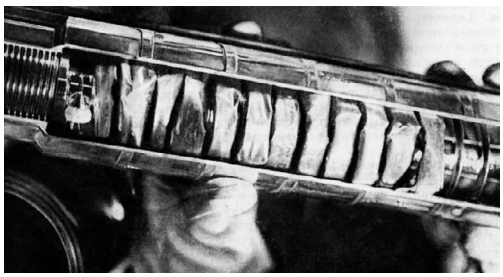

Fig. 3.25 Reception drum with a flexible sampler. *With the permission of the Vernadsky Institute.*

A rocket with soil samples was launched from the Moon on August 19. The station approached the Earth on August 22. The capsule with soil landed on August 22 in the calculation zone 200 kms from the city of Surgut (Russia). A column of lunar soil 218 cm long and of 170.1 gs was delivered (Barsukov, 1980).

3.7 Ground-based receiving complex for lunar soil

Sealed containers with lunar soil were delivered to a special laboratory of the Vernadsky Institute of the USSR Academy of Science, where a ground-based reception complex was located. The complex was developed taking into account all the requirements for safe long-term storage and preliminary investigation of the lunar soil, aimed at excluding contamination with the Earth's material (dust, atmospheric gases, etc.). The receiving complex consisted of three receiving chambers for opening containers with samples in ultrahigh vacuum, for opening containers in a medium of high-purity helium and for preliminary studies and packaging of samples in a medium of high-purity nitrogen, respectively.

A specially developed chamber of ultra-high vacuum (HVC) allowed opening containers and exploring properties of lunar soil in a vacuum of 10^{-13} Torr (Fig. 3.26). The low pressure of the background gases made it possible to preserve and measure natural characteristics of the substance for hundreds of hours. HVC was made of stainless steel

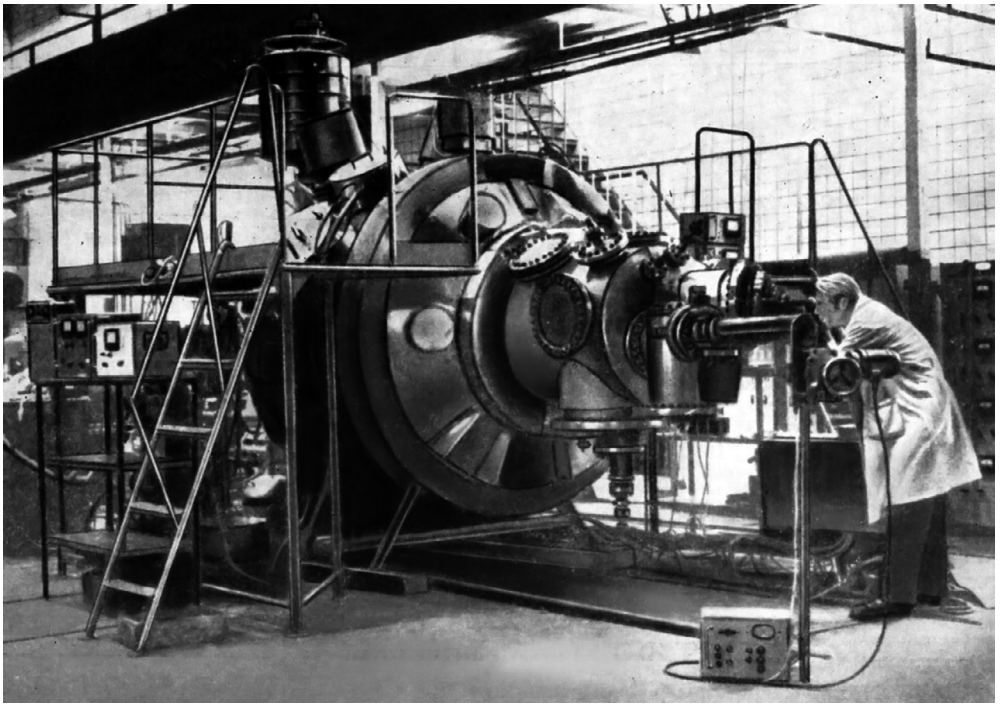

Fig. 3.26 General view of an ultra-high vacuum chamber. *With the permission of the Vernadsky Institute.*

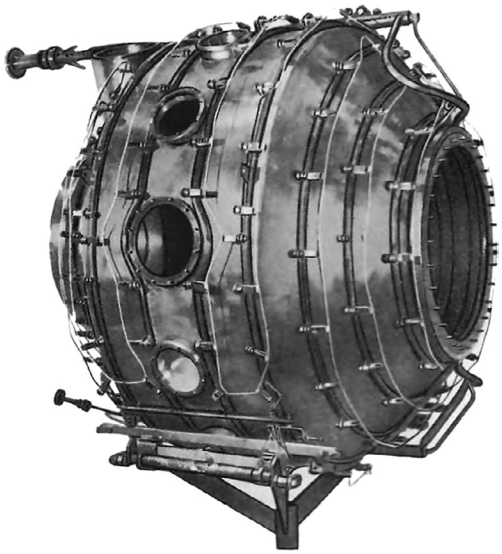

Fig. 3.27 General view of a pumping chamber of the ultra-high vacuum chamber. *With the permission of the Vernadsky Institute.*

and consisted of pumping and research chambers, connected by flanges of 700mm diameter. The pumping chamber ensured the creation of an ultrahigh oil-free vacuum at a pumping speed of 600,000 L s^{-1} due to the removal of gases by a constantly renewable titanium film that was sprayed onto a screen cooled to the temperature of liquid nitrogen (Surkov et al., 1971). The housing of the pumping chamber was a cylinder with a diameter of 1800 mm and a length of 2500 mm. A copper screen was placed inside the case, cooled to a temperature of −196° C (Fig. 3.27).

The research chamber housed mechanisms and apparatus for opening containers and studying extraterrestrial matter (Fig. 3.28). After pumping the chamber to ultra-high vacuum, the container with soil was opened and the soil transferred to the table for study by a manipulator. The table could be installed in one of three positions - for

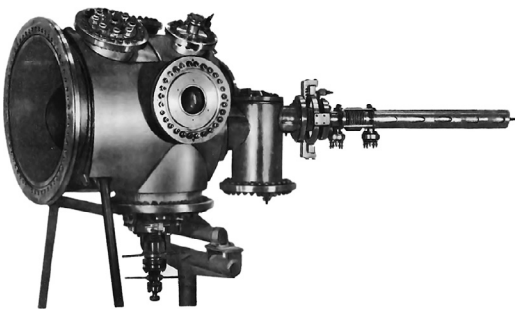

Fig. 3.28 General view of a research chamber of the ultra-high vacuum chamber. *With the permission of the Vernadsky Institute.*

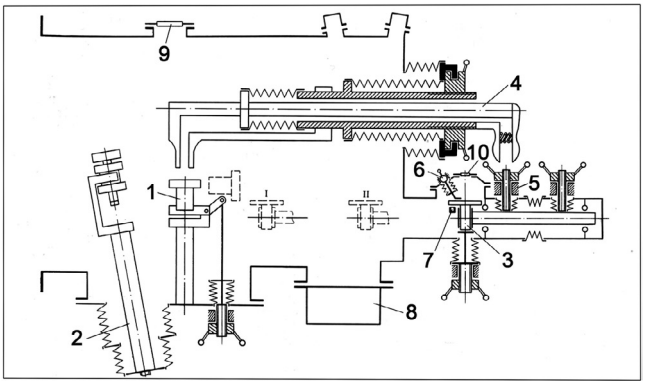

Fig. 3.29 ***Diagram of a research chamber of the ultra-high vacuum chamber.*** 1 - container with soil; 2 - device for opening the container; 3 - a table for studying samples; 4 - a manipulator; 5 - a mechanism for moving the table; 6 - a small manipulator; 7 - a small container for samples; 8 - a device for studying the physico-mechanical properties of soil samples; 9 - a viewing large window; 10 - a viewing small window. *(With the permission of the Vernadsky Institute).*

unloading the container (Fig. 3.29), position I), for mass-spectrometric studies (position II) and for studying with optical instruments (position III). In position III, individual fragments of soil using a small manipulator could be oriented and moved under the lenses of devices. Using the same manipulator, soil samples could be placed in small containers pre-installed on the table. A soil sample could also be transferred using the main manipulator to a device for studying the physical and mechanical properties. Observations of operations were made through sight glasses.

The second receiving lunar chamber was intended for opening containers with soil, its initial inspection, studying the chemical and mineral composition, magnetic, thermal, electrical, and other characteristics in a medium of high purity helium. The chamber was made of stainless steel, has been preserved, and is currently located in the laboratory of geochemistry of the Moon and planets of the Vernadsky Institute RAS (Fig. 3.30).

The receiving lunar chamber consists of a working chamber, a gateway device, a glove device, a vacuum pumping system and an inert gas inlet (Surkov et al., 1972). The working chamber has a cylindrical shape. The chamber diameter is 1200 mm, the length is 1600 mm. The working chamber has a hinged lid with a diameter of 500 mm (Fig. 3.31). On the cover flange, it was possible to mount the device to study the physical and mechanical properties of the soil. Inside the chamber there were placed devices and tools for opening containers and working with the substance, packaging containers, scales, sensors and other devices (Fig. 3.32). Operators worked in the cell using three glove devices. During long-term storage of the soil, the gloves were insulated from the working chamber by vacuum closures and from the atmosphere by caps. The design of glove devices allows for vacuum degassing of gloves with two-sided pumping with closed caps and closures. To study the composition of residual gases in the volume of the chamber, mass spectrometers (chronotron and omegatron) were used. The gateway

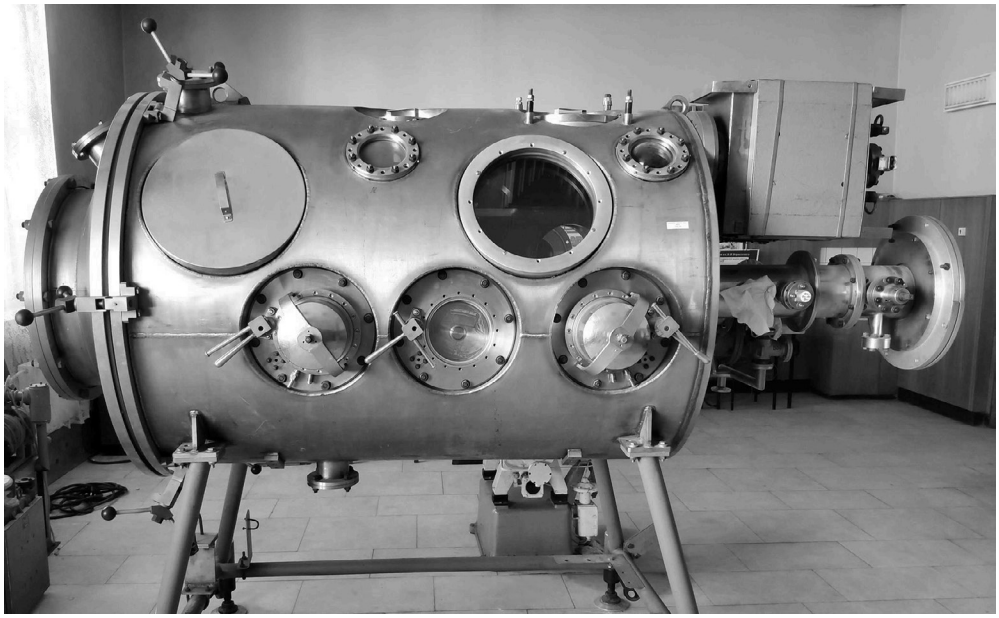

Fig. 3.30 ***General view of a receiving lunar chamber.*** At the top of the camera, there are small windows for lighting and large viewing windows, below are three glove devices, to the right is a gateway. *(Photo by the author. With the permission of the Vernadsky Institute)*.

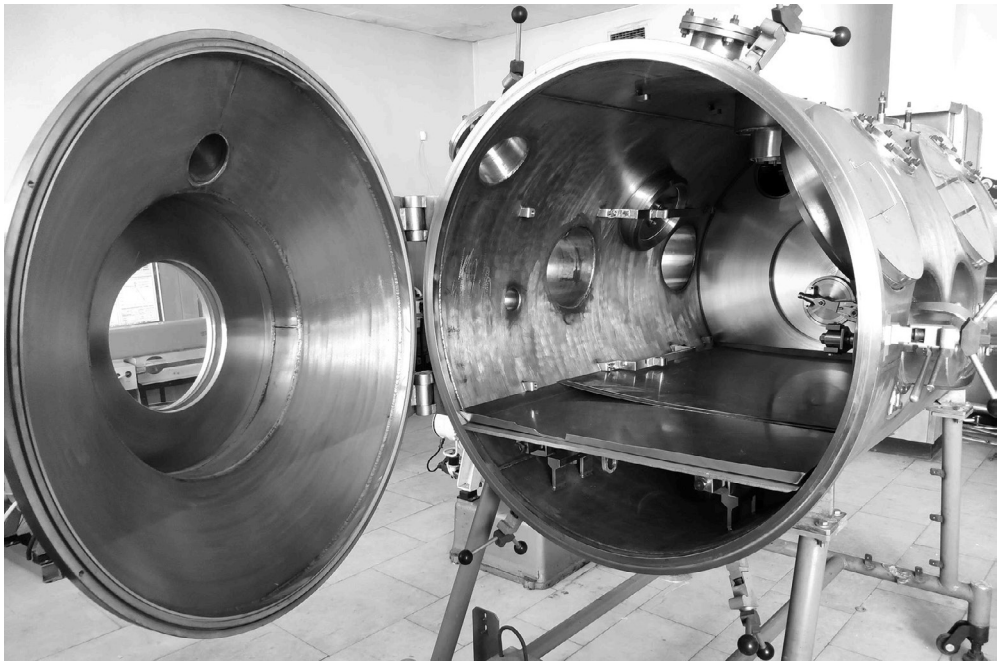

Fig. 3.31 A hinged lid of the receiving lunar chamber. *(Photo by the author. With the permission of the Vernadsky Institute)*.

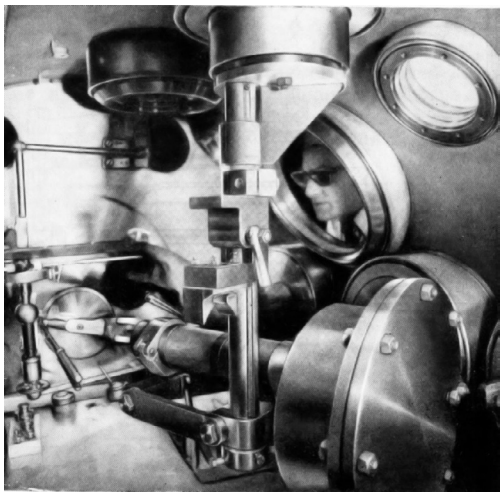

Fig. 3.32 An opening tool for a container with lunar soil in the receiving lunar chamber. *(With the permission of the Vernadsky Institute)*.

is designed to transfer tools and containers with soil into the chamber and vice versa without violating the conditions in the working chamber. A temperature sterilizer with an operating temperature of 800° C was installed in the pre-pumping line to destroy microorganisms that could be present in space material. The minimum pressure that was achieved in the chamber was 2×10^{-6} Torr.

A special research chamber for the primary processing, sieving, packaging and preliminary studies of lunar samples in a high-purity nitrogen atmosphere, was made from plexiglass (Fig. 3.33) (Vinogradov, 1974). The chamber in the drum form with a diameter

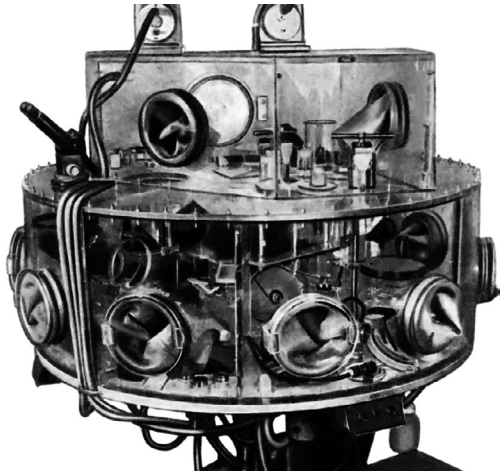

Fig. 3.33 General view of a special research chamber with a high-purity nitrogen atmosphere. *(With the permission of the Vernadsky Institute)*.

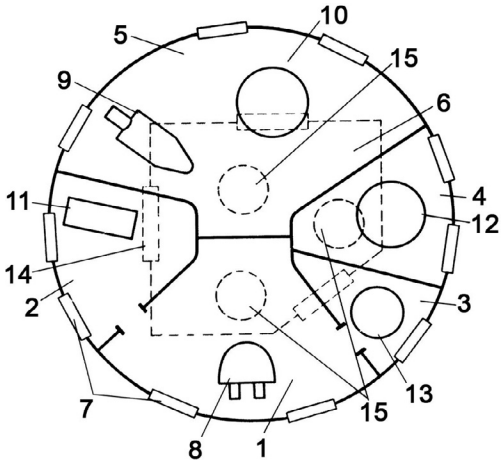

Fig. 3.34 Diagram of a special research chamber: 1 – a compartment for packaging and preliminary studies; 2 – a weighing compartment; 3 – a grinding and sieving compartment; 4 – a cutting compartment; 5 – a compartment for the thin sections manufacture; 6 – a gateway (dotted line); 7 – gloves; 8 – a binocular microscope MBS-2; 9 – a microscope MIN-8; 10 – a grinding and polishing wheel; 11 – cup and torsion scales; 12 - a diamond saw; 13 - a ball vibrating mill and a sieve analyzer; 14 – an external hatch; 15 - internal hatches of the gateway. *(With the permission of the Vernadsky Institute)*.

of 1600 mm and a height of 500 mm could rotate around the vertical axis by 355° Along the perimeter of the drum were placed 10 glove devices (Fig. 3.34), which allowed two or three researchers to work with samples simultaneously. One of the drum halves was divided into three compartments: a compartment with cup and torsion scales, a compartment for packaging and preliminary studies with small sample containers and a binocular microscope, as well as a compartment with a ball vibrating mill and a sieve analyzer with nylon nets with square cells of 900, 450, 200, 125 and 83 μm in size. The second half was divided into two compartments: a compartment with one glove for cutting billet sections with a diamond saw, and a grinding and polishing compartment with the necessary tools including a microscope for inspection. A gateway with two glove devices for input and output of samples from both compartments of the chamber was placed on top.

3.8 Primary processing of the lunar soil and major results

3.8.1 Luna-16

A container with lunar soil delivered by the Luna-16 was subjected to sterilization and dosimetric measurements, which showed a level of gamma radiation comparable to terrestrial basalts. To exclude contact of terrestrial microorganisms with lunar soil, a receiving lunar chamber was sterilized by hydrogen peroxide sublimation in a vacuum before opening the container. First, a vacuum was created with a pressure of 2×10^{-5} Torr, and then the chamber was filled with highly purified helium to atmospheric pressure.

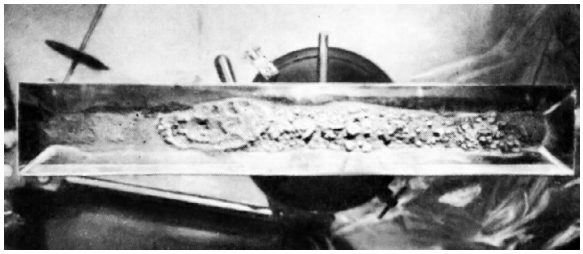

Fig. 3.35 Lunar soil delivered by Luna-16, on a tray in the receiving lunar chamber. *(With the permission of the Vernadsky Institute).*

The operator took out a drill from the container, which turned out to be covered with a thin layer of lunar regolith. The drill was completely filled with soil. The drill with soil was first weighed and then gently poured onto the tray with preserving the depth distribution of the soil (Fig. 3.35), on which the soil was examined and repeatedly photographed through a viewing window at different illumination and magnification, and at different angles.

The soil was a dark gray uniform color with no apparent layering and had a loose fine-grained structure with a noticeable adhesion (sticking) between particles with the formation of small lumps. Granularity increased with depth and coarse-grained material was observed at a depth of about 35 cm. Based on granularity, 5 intervals were defined from fine-grained at the top to coarse-grained at depth: A (1–8 cm), B (8–15 cm), C (15–28 cm), G (28–33 cm) and D (33–35 cm) (Vinogradov, 1974). A small soil sample was selected for toxicological and biological studies (Outstanding achievements, 1970) (Vinogradov, 1974). Until the end of these studies, the lunar soil was in the receiving chamber in quarantine. After quarantine and preliminary inspection and description of the main properties, the soil was packaged in special stainless steel containers (Fig. 3.36), which were transferred to the research chamber.

Fig. 3.36 ***A sealed stainless steel container for storing and transporting samples of lunar soil.*** Sizes: height is 80 mm, a cover diameter is 60 mm, and a bottom diameter is 70 mm. Mass is 1452 g. *(Photo by the author. With the permission of the Vernadsky Institute).*

The lunar soil in an airtight container was placed into research chamber gateway, and then to the packing compartment, where the soil was examined under a binocular microscope, sieved into fractions and weighed. In the same compartment, preliminary studies of the physical and mechanical properties of the soil were carried out. At this stage, samples were taken from a fraction of less than 83 μm and from a gross sample for chemical composition studies. Particles of more than 900 μm and particles from a fraction of 450–900 μm and, as well as samples mass of 1–2 mg from fractions of more than 200 μm, 127–200 μm and 83–127 μm were selected, fixed in the plane of thin sections and were studied under microscope and electron microprobe. The remaining samples allocated for further various studies were packaged in small glass containers or sealed ampoules. A few particles 4–6 mm in size were preserved as characteristic samples of lunar rocks. The main part of the soil was placed in a special storage located at the Vernadsky Institute for long-term storage and future research.

As a result of preliminary studies in the soil, three sets of particles were identified, i.e. fine-grained basalts with glass, coarse-grained basalts of the gabbroid type, and fused particles, such as breccias, slags, agglutinates, glass particles and balls of various shapes, monomineral grains and others (Fig. 3.37). In basalts, the main minerals were anorthite, pyroxenes, ilmenite, and less commonly olivine. The content of anorthosites was insignificant, whereas monomineral grains are mainly represented by plagioclase

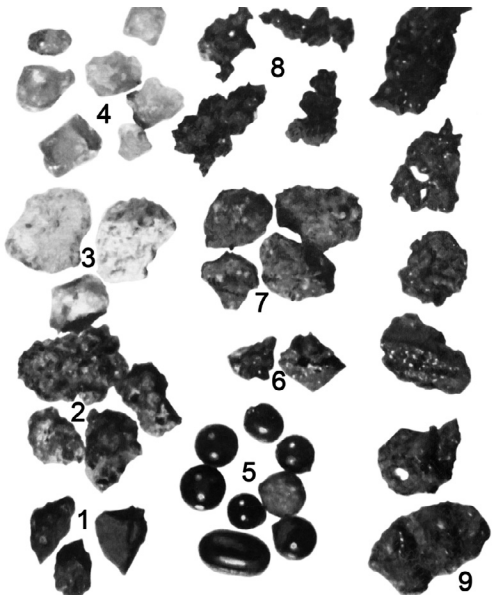

Fig. 3.37 Particles of lunar soil from the fraction 0.45 mm, magnification 30: 1 - basalt; 2 - coarse-grained basalt (gabbro); 3 - anorthosites; 4 - homogeneous glass and mineral grains; 5 - glass balls; 6 - brown glass; 7 - breccia; 8 - sintered particles; 9 - slag and fused particles. *(With the permission of the Vernadsky Institute)*.

(anorthite), olivine, pyroxene (augite), spinel, ilmenite and iron particles. The results of comprehensive studies lunar soil delivered by Luna-16 were published in the collections (Vinogradov, 1974; Pomeroy and Hubbard, 1977), and in many other scientific publications.

3.8.2 Luna-20

A container with lunar soil delivered by Luna-20 spacecraft was also opened in the receiving lunar chamber with a helium atmosphere. The drill with soil was removed from the container. Soil only partially filled the drill, and the total length of the soil column was estimated at about 15–20cm. Therefore, the soil mass turned out to be almost two times less than in the Luna-16 sample. The primary preparation and preliminary study of the soil was carried out according to the same methodology as for the Luna-16 sample. The soil was carefully poured into a special receiving tray with a metric ruler (Fig. 3.38). Although the drill rod was filled a little more than half, the mixing of the soil during transportation was insignificant, and the main stratification of the layers with different particle size distribution was preserved. The first thing that scientists noticed was the light gray color of the soil, which was much lighter than the soil delivered from the Mare Fecunditatis. Melted vitrified particles (agglutinates) were observed significantly less. Relatively large white particles 4–6 mm in size against a background of fine-grained mass were observed near marks on the tray ruler of 29, 32 and 35 cm.

Fig. 3.38 Lunar soil delivered by Luna-20 on a tray in the receiving lunar chamber. *(With the permission of the Vernadsky Institute).*

The soil column on the tray was divided into four equal zones (layers) from the surface to a depth of L2001, L2002, L2003, and L2004, from which samples were taken for research (Barsukov and Surkov, 1979). Microscopic examination of soil samples showed that, unlike the Luna-16, Apollo-11, and Apollo-12 soil, fragments of crystalline rocks and minerals with well-preserved faces and cleaved surfaces predominate in the sample (Vinogradov, 1972; 1979). Glass balls and slag breccias were rarely observed.

After a preliminary study of the particle morphology, about 200 fragments of rocks and minerals from fractions of more than 450 μm and more than 900 μm were collected and transparently polished sections for petrographic and mineralogical studies in transmitted and reflected light were prepared. Complex sections, which contained 200–400 particles, were made from fractions of 83–127 μm, 127–200 μm, 200–450 μm and from samples L2002 and L2004. Because of a preliminary study, it was found that the main minerals of fragments of Highland rocks are the main plagioclase (mainly anorthite), olivine and pyroxenes. According to the mineral composition and the main minerals ratio, the rocks belong to the anorthosite-troctolite-norite series. A few fragments of maria basalts were represented by ilmenite and anorthite basalts. The presence of anorthosite in soil samples delivered by Apollo 11 from the Mare Tranquilitatis, and having mainly basalt composition, made it possible to speculate on the anorthosite composition of the Moon primary crust. However, direct confirmation of anorthosite composition of the Highland crust was obtained after the study of samples delivered by the Luna-20 from the Highland region (Tarasov et al., 1979). The results of comprehensive studies were published in the collection (Pomeroy and Hubbard, 1977; Barsukov and Surkov, 1979), and in many other scientific publications.

3.8.3 Luna-24

A container with lunar soil removed from the returned Luna-24 spacecraft was delivered to the Vernadsky Institute on August 3, 1976. The container was cleaned of possible contaminants and dosimetric measurements were carried out. Soil acceptance was carried out in the same chamber as Luna-16 and Luna-20 samples. The container was opened, the drum was removed with an elastic soil sampler wound on it (Fig. 3.25), and elastic sampler was unwound from the drum and laid in a spiral groove (Fig. 3.39). Magnetic susceptibility measurements with a step of 30 mm to assess filling degree of the sampler with soil, as well as maturity degree of the soil depending on iron content in regolith particles, were carried out during the sampler laying. Subsequent x-ray photography confirmed the good filling of the sampler with soil along its entire length (Fig. 3.40). Inclusions of small stones were observed at the very top of the sampler. Dust traces in the sampler were observed at a distance of 47 cm from its beginning, then soil amount increased and complete filling of the sampler was observed from 58 cm. After a preliminary study of the X-ray image, the elastic sampler was cut into separate intervals for further studies. The sampler was placed on trays of 35 cm in a length. Before

Fig. 3.39 An elastic sampler with lunar soil in a spiral groove. *(With the permission of the Vernadsky Institute).*

opening, each tray was photographed in x-rays to assess the soil movement inside the sampler. At the extreme tray, the sampler was opened lengthwise, cut off and carefully removed (Fig. 3.41). A new tray was inserted between the first tray and the spiral-mounted sampler (Fig. 3.42). All seven trays with soil samples were weighed with an accuracy of 0.1 g. Soil samples were photographed in different ranges of the visible and infrared spectra to determine the photometric characteristics.

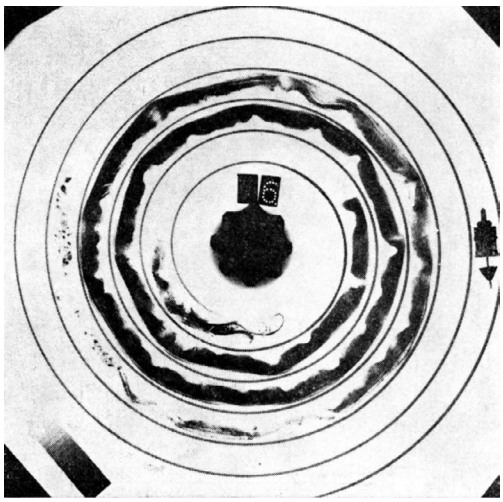

Fig. 3.40 X-ray image of the elastic sampler with lunar soil in a spiral groove. *(With the permission of the Vernadsky Institute).*

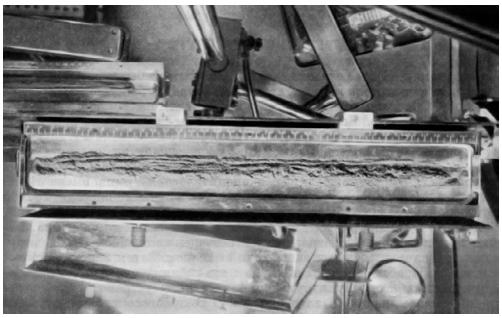

Fig. 3.41 A sample of lunar soil delivered by Luna-24 on one of the seven trays in the receiving lunar chamber. *(With the permission of the Vernadsky Institute)*.

The color of the soil changed depending on the lighting from brown to dark gray. In general, the soil was a lighter color than a typical mare soil from the Mare Fecunditatis. There were six clearly visible layers in the soil column, which differed in particle size and color. A noticeable heterogeneity of the soil was observed at depth, especially in the lower part of the column. The layers of lighter color, apparently, were ejections from craters located on the Mare Crisium coast in highland, and the dark gray layers that prevailed apparently had mare basaltic origin.

Samples from trays were taken of two types: small samples weighing 150–200 mg along the entire length of each tray to study soil changes in a column for its stratification, and

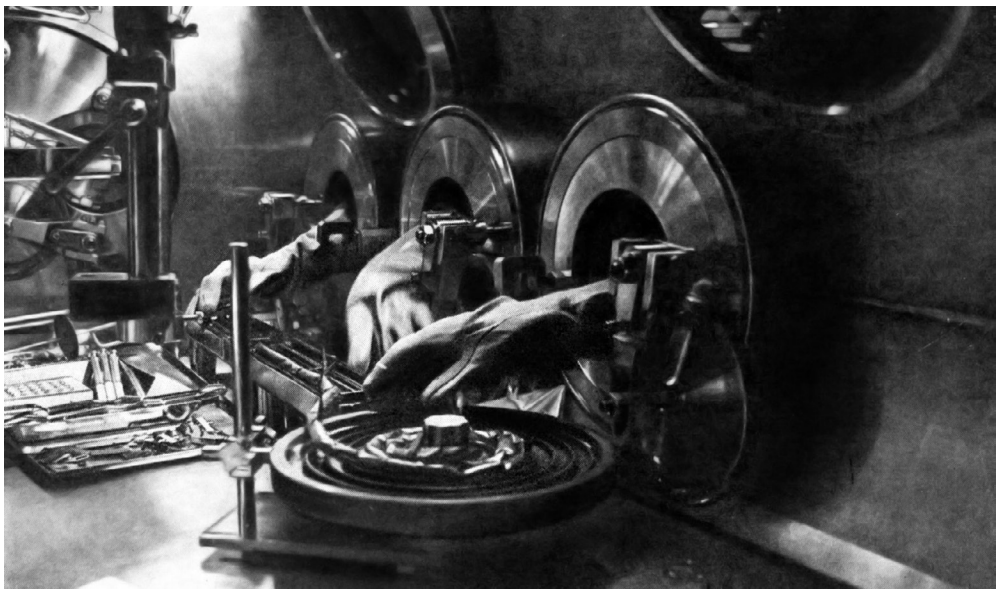

Fig. 3.42 Opening of an elastic sampler with lunar soil in the receiving lunar chamber. *(With the permission of the Vernadsky Institute)*.

basic samples weighing about 2 g from 3–4 cm intervals from individual layers for integrated research. Special samples were also taken. In total, no more than half of the material along the soil column was selected. The samples were placed in special containers made of stainless steel, fluoroplastic or glass, which were removed through gateway and transferred to a research chamber with a nitrogen atmosphere, in which further preparatory work was carried out - sieving into fractions, weighing and taking aliquots from fractions.

The sample number consisted of six digits: the first two digits are the KA number (24), the next three digits indicate the depth on the soil column in centimeters, and the sixth digit after the decimal point indicated the interval of the soil column in centimeters from which the sample was taken. After the dash, the number of the fraction was indicated (indicating the sample size), and after the decimal point, the aliquot number issued from this sample, i.e., 24,118.4–2.12 (Barsukov, 1980). As a result of sieving, 6 number fractions were obtained: 1 - ⟨74 μm, 2 - 74–94 μm, 3 - 94–200 μm, 4 - 200–375 μm, 5 - 375–900 μm, 6 -⟩ 900 μm. The serial numbers of large particles from the sixth fraction, which were studied individually, were indicated after the dash. Zero instead of the fraction number after the dash was indicated for gross samples that were not sieved for fractions.

At the initial stage, predominantly non-destructive methods were used to study the chemical composition of lunar soil samples (Zolotov, 1976). A sample of 10–20 mg soil powder was pressed in a tablet form and subjected to x-ray analysis, first with a defocused electron beam for averaged content of 10–12 basic rock-forming elements, then microanalysis of individual particles and minerals with an electron beam focused to 1 μm. Then, the method of spark spectrometry was used, which allowed to estimate the content of at least 60 elements. The study of large particles weighing more than 10–20 mg was carried out according to a special program. Particles were often divided into several fragments for complex studies. All fractions and particles were stored in special containers in pure nitrogen atmosphere.

It was found that igneous rocks at the Mare Crisium are characterized by a high content of aluminum (up to 19 percent Al_2O_3) and iron (16–20 percent FeO), a low content of titanium (about 1 percent) and alkalis, and are represented by a new type of basalt compared to rocks from the Mare Fecunditatis - a high-alumina, low-titanium mare basalt with a low alkali content. The content in the regolith of Highland anorthosite rocks is insignificant, i.e. about 2 percent. The results of comprehensive studies were published in the collection (Merill and Papike, 1977; Barsukov, 1980), and in many other scientific publications.

3.9 International exchange of lunar soil samples

The Soviet government and Soviet scientists actively handed samples of lunar soil, delivered under the Luna program, to the scientific laboratories of foreign countries. The first samples of lunar soil delivered by Luna-16 were given to representatives of the

French Embassy in the USSR on April 6, 1971, and then to eight laboratories in France. On July 5, 1972, lunar soil sample delivered by Luna-20 was handed to the president of the French National Center for Space Research, Jean-Francois Deniss. Academician A.P. Vinogradov at the Vernadsky Institute on December 19, 1972 additionally handed to French scientists soil samples delivered by Luna-16 and Luna-20. The new director of the Vernadsky Institute V.L. Barsukov on February 10, 1977 gave a lunar soil sample delivered by Luna-24 to a colleague from the Paris University Dr K. Allegre.

On June 10, 1971, an exchange of lunar samples delivered by Luna-16, Apollon-11 and Apollo-12 took place in Moscow between the Academy of Sciences of the USSR and NASA. On August 1, 1973, US Chargé d'Affaires in the USSR Mr A. Dubs passed a lunar soil sample delivered by Apollo-17 to the Chairman of the Supreme Council Presidium of the USSR N.V. Podgorny. On April 13, 1974, Soviet scientists exchanged with NASA representatives samples of lunar soil delivered by Luna-20 and Apollo 15. On December 15, 1976, Soviet scientists handed over to the American Professor Duke lunar samples delivered by Luna-24.

On August 24, 1972 Vice-President of the USSR Academy of Sciences Academician A.P. Vinogradov, handed Luna-16 and Luna-20 soil samples to the representative of the London Royal Society, Professor James Lighthill. Lunar soil samples delivered by the Luna-24 were offered to the member of the London Royal Society, Dr J. Eglinton by Vernadsky Institute Director V.L. Barsukov in Moscow on May 27, 1977.

On April 30, 1971, at the Vernadsky Institute, soil samples delivered by Luna-16 were given to the Deputy Chairman of the Czechoslovak Academy of Sciences, Academician Bogumir Rositsky. The transferred sample was divided into 1300 registered particles and studied at four institutes and laboratories of the Higher Chemical and Technological School in Prague and at the Mining Institute in Ostrava. On June 10, 1977 director of the Vernadsky Institute V.L. Barsukov handed to the Czechoslovak counterpart Dr A. Tsymbalnikova another sample delivered by Luna-24.

Lunar soil samples were also offered for research in scientific laboratories in Hungary. The Luna-20 samples handing to German scientists took place on May 12, 1973 at the USSR Embassy in Berlin. Luna-16 soil sample were handed over to the GDR scientists on May 26, 1974. In addition, on November 16, 1977, samples of lunar soil delivered by all three Soviet stations were given to the Secretary General of the Academy of Sciences of the GDR, K. Grothe.

On December 12, 1972 Luna-16 and Luna-20 soil samples were handed to the Indian Academy of Sciences by Academician A.P. Vinogradov. Soil sample from Mare Crisium (Luna-24) was handed from the Vernadsky Institute director V.L. Barsukov to the Indian scientist Dr N. Bandari on March 3, 1977.

On December 25, 1972, samples of lunar soil delivered by the Luna-16 were also handed over to the Minister of Higher Education and Scientific Research of the Republic of Iraq, Dr Hisham al-Shawi.

3.10 Conclusions

The delivery of lunar soil under the Luna program made it possible to study various types of lunar rocks in the eastern part of the Moon Near Side. There are medium-titanium fine-grained and coarse-grained basalts of the gabbroid type in the Mare Fecunditatis, low-titanium basalts with a high content of aluminum and iron in the Mare Crisium, and rocks of anorthosite-troctolite-norite series in the Highland region. The Luna program also for the first time demonstrated with high scientific efficiency that soil can be delivered from another celestial body in an automatic mode. Obviously, at the present stage of the Solar system study, this method is the most promising and low-cost for delivering soil not only from comets and asteroids, but also from the Mars, Venus, Mercury and satellites of planets.

Acknowledgments

I thank Vladislav Makovchuk for help in the processing and preparation of figures.

References

Atlas of the Moon Far Side. P., 1967. Nauka, Moscow 2, 236 in Russian.

Atlas of the Moon Far Side. P., 1975. Nauka, Moscow 3, 240 in Russian.

Barsukov V. L. (Ed.), 1978. Mobile laboratory on the Moon Lunokhod-1. P. 2. Nauka, Moscow. 184 p. (in Russian).

Barsukov V.L., and S Yu.A. (Eds.), 1979. Soil from the Moon highland region Nauka, Moscow. 708 p. (in Russian).

Barsukov,V.L. (Ed.), 1980. Lunar Soil from the Mare Crisium. Nauka, Moscow, p. 360 in Russian.

Bazilevsky, A.T., Grebennik, N.P., Gromov, V.V., Dmitriev, A.D., Kemurdzhian, A.L., Polosukhin, V.P., Semenov, P.S., Florensky, K.P., 1984. The dependence of the physico-mechanical properties of lunar soil on the features of the relief and processes in the area of the Lunokhod-2. Kosmicheskie Issledovaniya V. 22 (2), 243–251 in Russian.

Bulletin of optical observation stations of artificial Earth satellites No. 45, 1965. Astronomical council of the USSR academy of sciences. Moscow, 140 in Russian.

Cherkasov, I.I., Shvarev,V.V., 1975. Soil of the moon. Nauka, Moscow, p.142 in Russian.

Florensky, K.P., Bazilevsky, A.T., Gurshteyn, A.A., Zasetsky, V.V., Pronin, A.A., Polosukhin, V.P., 1974. Geological and morphological analysis of the "Lunokhod-2"work area. Doklady (Reports) USSR Acad. Sci. V. 214 (1), 75–78 in Russian.

Ivanov, B.A., Okulessky, B.A., Bazilevsky, A.T., 1976. An impulsive magnetic field from shock-induced polarization in lunar rocks as a possible cause of field anomalies associated with craters. Sov. Astron. Lett.,V. 2 (3), 101–102.

Karachevtseva, I., Oberst, J., Scholten, F., A., K., Shingareva, K., Cherepanova, E., Gusakova, E., Haase, I., Peters, O., Plescia, J., Robinson, M., 2013. Cartography of the Lunokhod-1 landing site and traverse from LRO image and stereo-topographic data. Planet. Space Sci. V. 85, 175–187.

Karachevtseva, I.P., Kozlova, N.A., Kokhanov, A.A., Zubarev, A.E., Nadezhdina, I.E., Patratiy, V.D., Konopikhin, A.A., Basilevsky, A.T., Abdrakhimov, A.M., Oberst, J., Haase, I., Jolliffe, B.L., Plescia, J.B., Robinson, M.S., 2017. Cartography of the Luna-21 landing site and lunokhod-2 traverse area based on lunar reconnaissance orbiter camera images and surface archive TV-panoramas. Icarus V. 283, 104–121.

Kemurdzhian, A.L. (Ed.), 1993. The Rovers. Mashinostroenie, Moscow, p. 400 in Russian.

Kocharov, G.E., Viktorov, S.V., 1974. Chemical composition of the lunar surface in the area of the Lunokhod-2. Doklady (Reports) USSR Acad. Sci. V. 214 (1), 71–74 in Russian.

Kuzmin, R.O., 1975. Landslide phenomena in regolith on the slopes of the lunar topography. Proceedings of the USSR Acad. Sci., Geological Ser 10, 65–72 in Russian.
Marov, M.Y., Huntress, W.T., 2013. Soviet robots in the Solar system. Technology and discovery, Moscow, Fizmatlit, p. 612 in Russian.
Mare Crisium: the view from Luna 24. In: Merill, R.B., Papike, J.J. (Eds.), Proceedings of the Conference on Luna 24, Houston Texas, December 1-3, 1977. Pergamon Press, New York, p. 709.
Outstanding achievements of our cosmonautics, 1970. Pravda newspaper October 4in Russian.
Pomeroy, J.H., Hubbard, N.J. (Eds.), 1977. The Soviet-American conference on cosmochemistry of the Moon and planets. P. 1, 2. NASA, Washington, D.C., p. 929.
Sokolov, S., Barsukov, V., Vladimirov, B., 1976. On the route Earth - Moon. Pravda newspaper October 13 (in Russian).
Soviet space rocket, 1959. Pravda newspaper January 12 (in Russian).
Surkov Yu, A., 1972. Drilling in the lunar mountains. Pravda newspaper February 27 (in Russian).
Surkov Yu, A., Kheifets, A.B., Rudnitsky, E.M., Danilov, K.D., Glotov, V.A., Shvarev, V.V., 1972. A chamber for working with extraterrestrial matter in an inert gas environment. Kosmicheskie Issledovaniya. V. 10 (5), 766–770 in Russian.
Surkov Yu., A., 1977. Gamma spectrometry in space research. Atomizdat, Moscow, p. 240 in Russian.
Surkov Yu., A., A.B., K., Rudnitsky, E.M., Danilov, K.D., Glotov, V.A., 1971. The study of extraterrestrial matter in an inert gas medium and ultrahigh vacuum. USSR Acad. Sci., Moscow, 15 in Russian.
Tarasov, L.S., Ivanov, A.V., Florensky, K.P., Rode, O.D., Nazarov, M.A., 1979. Lithological and morphological characteristics of lunar regolith from the Apollonius highland region. In: Barsukov, V.L., Surkov Yu, A. (Eds.), Soil from the Moon highland region. Nauka, Moscow, p. 62–73 in Russian.
TASS message, 1959. About the first results of launching a space rocket to the Moon. Pravda newspaper September 21 (in Russian).
The first panoramas of the lunar surface, 1966. Nauka, Moscow, p. 130 in Russian.
The first panoramas of the lunar surface. P. 2, 1969. Nauka, Moscow, p. 104 in Russian.
The first photographs of the Moon Far Side, 1959. USSR Acad. Sci., Moscow 38 in Russian.
The third Soviet space rocket, 1959. Pravda newspaper October 27 (in Russian).
Vinogradov, A.P. (Ed.), 1971. Mobile laboratory on the Moon Lunokhod-1. Nauka, Moscow, p. 128 in Russian.
Vinogradov, A.P., 1972. Soil of the lunar mountains. Pravda newspaper May 04 (in Russian).
Vinogradov, A.P. (Ed.), 1974. Lunar soil from the Mare Fecunditatis. Nauka, Moscow, p. 624 (in Russian).
Vinogradov, A.P., 1979. Preliminary data on lunar soil delivered by the Luna-20 automatic station. In: Barsukov, V.L., Surkov Yu., A. (Eds.), Soil from the Moon highland region. Nauka, Moscow, pp. 7–17 in Russian.
Vinogradov, A.P., Surkov, Y.A., Chernov, G.M., 1966. Studies of the intensity and spectral composition of gamma radiation of the Moon at the automatic station Luna-10. Doklady (Reports) USSR Acad. Sci. V. 170 (3), 561–564 in Russian.
Zolotov, Y., 1976. Portrait of the lunar soil. Pravda newspaper September 5 (in Russian).

CHAPTER 4

The Stardust sample return mission

Scott A. Sandford[a], **Donald E. Brownlee**[b], **Michael E. Zolensky**[c]
[a]NASA-Ames Research Center, Astrophysics Branch, Moffett Field, CA, USA
[b]Department of Astronomy, University of Washington, Seattle, WA, USA
[c]XI2, NASA-Johnson Space Center, Houston, TX, USA

Chapter Outlines

4.1 Introduction

The *Stardust* spacecraft was the first mission to return solid samples from a body beyond the Moon. As the fourth NASA Discovery mission, it retrieved samples from the comet 81P/Wild 2, that is believed to have formed at the outer fringe of the solar nebula. The return of these samples provides unprecedented opportunities to compare astronomical (remote sensing) and sample analysis (ground truth) information for a known primitive solar system body. The samples make it possible to compare materials from the outer Solar System with sample-derived and astronomical data for asteroids, the parents of most meteorites, which formed much closer to the Sun. The samples returned by *Stardust* are the first primitive collected materials from a known body, and as such they provide contextual insight for all primitive meteoritic samples.

4.2 Mission overview

4.2.1 The target – comet 81P/Wild 2

Wild 2 is a Jupiter-family comet that has only been in its present orbit since 1974. Before 1974, it resided in an orbit with perihelion at 4.9 AU (near Jupiter's orbit)

Sample Return Missions
DOI: 10.1016/C2018-0-03374-5

and aphelion at 25 AU. This orbit had probably been stable for at least a few centuries (Sekanina 2003; Krolikowska and Suztowicz 2006). In 1974, a close encounter with Jupiter diverted Wild 2 into its current orbit, with perihelion at 1.58 AU and aphelion near 5.2 AU. Thus, 81P/Wild 2 is probably a "fresh" comet whose surface may have only recently been subjected to moderate solar heating. Wild 2 samples are expected to be remnants from the Kuiper Belt region of the solar nebula.

While 81P's history suggested it is an ideal object for the collection of primitive solar system materials, its selection as the target for *Stardust* depended largely on the comet's favorable orbit. A systematic search for comet flyby sample return opportunities showed that 81P/Wild 2 provided a trajectory to a "fresh" dusty comet with an encounter speed as low as 5.4 km/s (Tsou et al. 1994; Yen and Hirst 1997). Wild 2 met all four imperatives for the required *Stardust* trajectory: a dusty comet, a low comet encounter speed, reachable using a Delta II vehicle, and a small delta V requirement during flight.

4.2.2 Launch, orbital trajectory, and return

Stardust's trajectory allowed it to execute several scientific tasks during flight. *Stardust* was launched from Cape Canaveral on 7 February 1999. During its 7-year mission, *Stardust* made three heliocentric revolutions, all with perihelia at 1.0 AU. After the first revolution, the spacecraft performed an Earth Gravity Assist that raised its orbital aphelion to 2.7 AU and changed the orbital inclination to match Wild 2's orbit. The flyby encounter with 81P/Wild 2 and sample collection occurred at an encounter speed of 6.12 km/sec on 2 January 2004. The spacecraft returned to Earth on 15 January 2006. During the inbound portions of the orbits, the spacecraft's trajectory roughly paralleled that of contemporary interstellar dust particles entering the Solar System, resulting in a reduced relative speed with these particles. This allowed for 246 days of collection of contemporary interstellar dust on the back side of the sample tray assembly during two of the orbits. The trajectory also allowed for a flyby of the asteroid Annefrank on 2 November 2002 (Duxbury et al. 2004). After return of the sample capsule, the main spacecraft was diverted to a close encounter with comet 9P/Tempel 1 where it imaged the crater made by the Deep Impact mission (Veverka et al. 2013).

4.2.3 Spacecraft description

A description of the hardware components of *Stardust* can be found in Brownlee et al. (2003) (Fig. 4.1). The spacecraft carried several instruments including a camera (Newburn et al. 2003), a dust flux monitor (Tuzzolino et al. 2003), and a dust analyzer (Kissel et al. 2003). The primary 'instrument' was a deployable dust collector that used low density aerogel as a collecting medium (Tsou et al. 2003). The aerogel collection area is divided up into 130 2 × 4 cm rectangular and 2 trapezoidal cells (Fig. 4.2). The variable aerogel density for the Wild 2 collection side was 5 mg/ml to 50 mg/ml and was 2 mg/ml to 20 mg/ml for the interstellar capture cells on the collector's back side. In addition, pure,

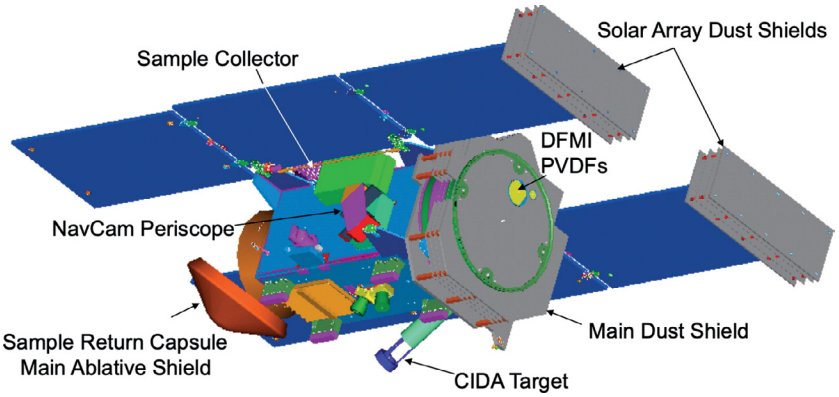

Fig. 4.1 ***Schematic of the Stardust spacecraft showing the positions of the onboard instruments.*** The gray portions of the diagram represent the leading edge Whipple shields that protected the spacecraft from cometary dust impacts.

100 micron thick aluminum foils wrapped the walls of the aerogel frames to facilitate cell removal, and the foils exposed portions were good targets for acquisition of dust impact craters. The Wild 2 and interstellar trays were mounted back to back and had a total exposed aerogel surface area of 1039 cm^2 and 1037 cm^2, respectively. The total exposed aluminum foil is about 15 percent of the exposed aerogel surface area.

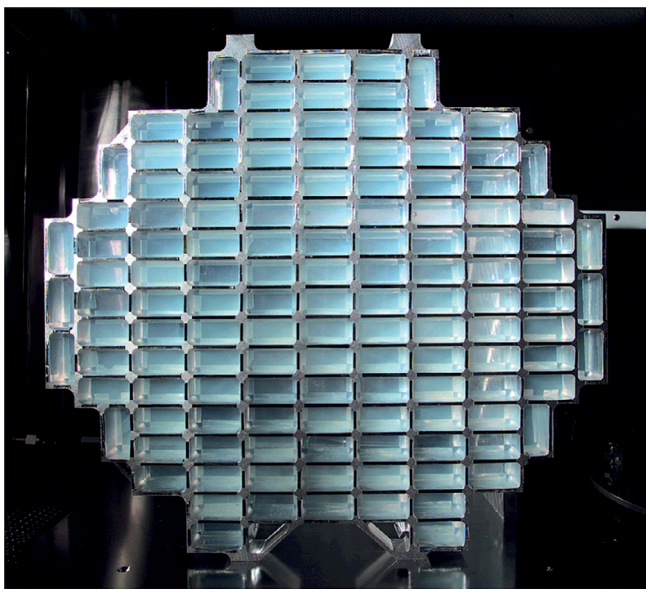

Fig. 4.2 ***The cometary collector tray contained multiple individual aerogel tiles.*** A second interstellar aerogel collector tray was placed back-to-back with the cometary tray.

4.3 Results

4.3.1 Flyby observations

An overview of the *Stardust* flyby of 81P/Wild 2 on 2 January 2004 can be found in Tsou et al. (2004). *Stardust* flew 236.4 ± 1 km from the comet's center when the comet was 1.86 AU from the Sun and the encounter occurred as planned. All the onboard instruments obtained data during the flyby and the deployed aerogel collector collected particles from the comet's coma.

4.3.1.1 Camera images

The *Stardust* camera obtained 72 images of the nucleus of 81P/Wild 2 during the flyby (Tsou et al. 2004). Close encounter imaging was done with a camera that covered the spectral range 380 nm - 1000 nm without filters using two exposure times - 10 ms for nucleus imaging alternated with 100 ms for nucleus tracking (Fig. 4.3).

Stereoscopic images of the nucleus show a diverse and complex variety of landforms not seen from earlier comet flybys of 1P/Halley and 19P/Borrelly. These include craters, excavation zones, flat-floored depressions, surface crusts, landslides, lineaments, terraces, spires/pinnacles (some 100 m in height), steep cliffs, overhangs, and small bright patches (potential vents or exposed ice). Wild 2 does not have smooth plains as seen on other comet surfaces. Most surface features are likely associated with ice sublimation processes. A triaxial ellipsoidal fit of the images yielded principal nucleus radii of 1.65 × 2.00 × 2.75 km (± 0.05 km). The longer exposures were used to identify the orientations and the approximate source locations of at least 20 collimated and partially overlapping jets of dust emitted from the nucleus.

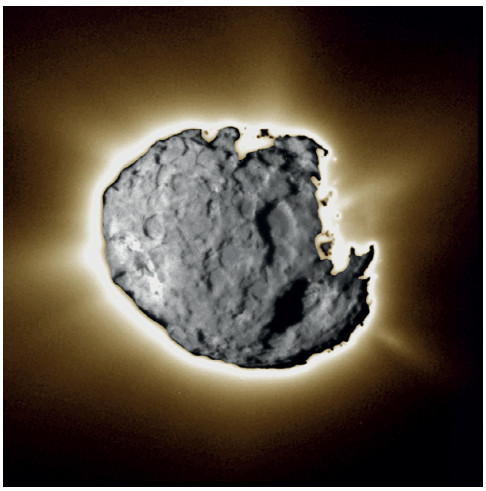

Fig. 4.3 A ***composite figure.*** made by superimposing long and short exposure images of the nucleus of 81P/Wild 2. The short exposure shows the surface features of the nucleus and the long exposure shows the gas/dust jets of gas emitted by the nucleus.

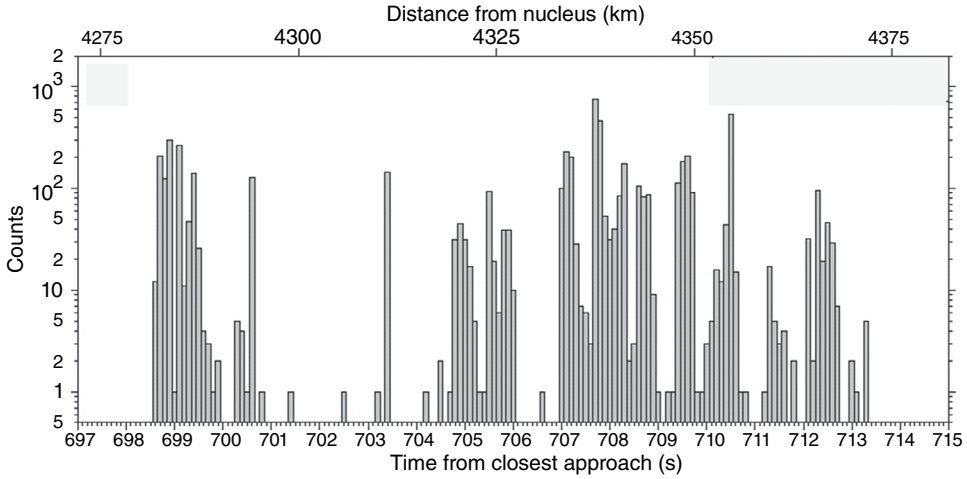

Fig. 4.4 Eighteen seconds of data from the Dust Flux Monitor taken when the spacecraft was ~4300 km from the nucleus of 81P/Wild 2, showing the variable impact rate seen as the spacecraft passed through the comet's coma *(adapted from Clark et al. 2004)*.

4.3.1.2 Dust flux monitor data

During the flyby the dust detectors recorded particle impacts of masses ranging from 10^{-11} to $> 10^{-4}$ g. The impact distribution along *Stardust's* flight path was extremely non-uniform. Dust impacts occurred in short "bursts" that could contain nearly a thousand particles separated by intervals in which no dust arrived at all (Tuzzolino et al. 2004) (Fig. 4.4). The most likely explanation for this behavior is the ejection of larger particle aggregates from the nucleus that fragmented as they moved out into the coma (Clark et al. 2004). At least seven impacting particles were big enough (the largest ~4 mm in diameter) to penetrate the spacecraft's front bumper shield and be detected by the flux monitor's acoustic sensors (Green et al. 2004). These data indicated that the expected samples were successfully collected by the aerogel collector during the flyby.

4.3.2 Results obtained from returned samples

The *Stardust* Sample Return Capsule (SRC) returned to Earth at the Utah Test and Training Range on January 2, 2006 and was quickly recovered (Fig. 4.5). The SRC was transported to a temporary cleanroom where it was opened and the sample canister was removed and placed in a container purged by curatorial grade N_2. The canister was flown to NASA's Johnson Space Center and opened in a cleanroom made specifically to receive and curate the samples. Samples removed from the aerogel collector were subjected to a 6 month preliminary examination by prearranged teams that studied the chemical, physical, spectral, and isotopic nature of the samples before the samples were made available for general distribution to the science community.

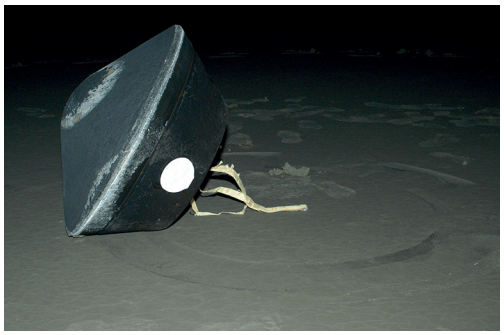

Fig. 4.5 The Stardust Sample Return Capsule as found during its recovery from the Utah Test and Training Range.

An extensive effort was made to assess contamination of the returned samples and concluded that contamination during the design, construction, and flight of the spacecraft, and during and after recovery of the SRC did not contribute significant material to the collectors (Sandford et al. 2010). The largest concern is associated with contaminant particles and structural carbon within the original aerogel, although these materials can generally be distinguished from the returned cometary samples.

4.3.2.1 Physical nature of the dust

One of the first science results from the returned samples was that Wild 2 contains a diverse range of particles. The aerogel capture track geometries clearly showed the presence of both strong solid materials that produced long thin tracks and friable particles that produced wide (bulbous) tracks (Brownlee et al. 2006; Burchell et al. 2008) (Fig. 4.6). Many of the grains are polymineralic. Except for surface abrasion, most grains >2 μm are well preserved, while many of the smaller ones were altered or destroyed during high speed capture into aerogel (Brownlee et al. 2006). Some submicron grains did survive capture, but it is clear that others melted and dissolved into melted aerogel lining track walls. The preferential destruction of the finest grained fraction affects the completeness of our full understanding of the comet's mineralogical composition.

4.3.2.2 Elemental composition

During the preliminary analyses of Wild 2 samples, results from the aerogel and foils were combined to seek a "comprehensive" elemental analysis of the Wild 2 particles (Flynn et al. 2006). Twenty-three tracks were analyzed by synchrotron X-ray Fluorescence (SXRF) to determine abundances for elements heavier than P. One track was also split lengthwise and analyzed by time-of-flight–secondary ion mass spectrometry (TOF-SIMS) analysis for some lighter elements, particularly Mg and Al (the silica aerogel prevented measurement of Si and O). Residues in 7 Al foil craters were also analyzed by scanning electron microscopy using energy-dispersive X-ray analyses (SEM-EDX)

Fig. 4.6 ***Cometary particles impacting Stardust aerogel collector tiles created several types of tracks.*** Single, strong particles created long, thin carrot tracks like the one on the left of the image. Weaker aggregate particles came apart during impact and produced more bulbous tracks like the two in the center of the image. Particles in this image entered from above and the surface of the aerogel is at the top of the image.

and TOF-SIMS. These 'bulk' compositions are compared to the elemental composition of CI chondrites, which were generally thought to represent the closest analogues to cometary material (Gounelle et al. 2006).

Since the mineralogy of the tracks varied so widely, it was difficult to arrive at a 'bulk' composition for the overall collected sample. Many terminal particles were dominated by a single mineral, generally olivine, pyroxene, or Fe-Ni-Zn sulfide (Zolensky et al. 2006) and the fraction of the total Fe detected in the studied terminal particles varied from 0 percent to almost 60 percent. The spatial distributions of other elements in each track were similarly varied. Thus, terminal particle analysis provides uncertain information on the bulk elemental composition of Wild 2.

The mean composition of the Wild 2 coma dust was calculated by Flynn et al. (2006) by summing the measured abundance of each element over all 23 analyzed tracks. It was found that approximately 90 percent of the material in an entering cometary grain ended up being distributed along the tracks, with only ~10 percent being present in the terminal grains. The Fe-normalized mean element abundances of Wild 2

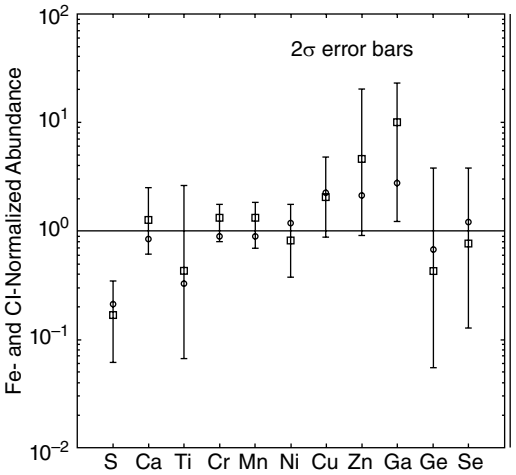

Fig. 4.7 ***CI- and Fe-normalized mean composition determined by summing the 23 whole-track analyses (squares) and by summing the same data set except for the particle having the highest Fe content (circles).*** The vertical bars show the degree of diversity of the mean composition (after Flynn et al. 2006). The horizontal line represents CI abundances.

tracks gathered in this fashion for Ca, Ti, Cr, Mn, Ni, Ge, and Se (Fig. 4.7) are consistent with CI values at the 2σ confidence level. Ge and Se were detected in only a few particles, so their values are very uncertain. Sulfur is depleted relative to CI values, and Cu, Zn, and Ga are enriched.

Westphal et al. (2009) reported additional compositional measurements of the Wild 2 tracks, based on SXRF measurements of the relative concentrations of the chemical state of iron. They reported significantly higher S/Fe atom ratios of > 0.31, which is higher than in most chondritic meteorites.

Analyses of impact residue in 7 Al foil craters provided additional element-to-Si ratios, although only Mg, Si, and Fe were detected in all analyzed craters. The Si-normalized mean composition detected in four craters has an abundance difference from CI of less than 50 percent for Mg, Ca, and Fe. An observed S depletion is consistent with track results. Residues in five craters were also analyzed by TOF-SIMS. The Si-normalized mean abundances are consistent with CI for Mg, Ca, and Ni, but small depletions were seen for Cr and Fe, consistent with the SEM-EDX results. Li, Na, and K appeared to be enriched.

Flynn et al. (2006) analyzed ~300 ng of Wild 2 dust and the material appears depleted in S and Fe relative to Si and enriched in the moderately volatile minor elements Cu, Zn, and Ga relative to CI. These trends were previously reported in the fine-grained, anhydrous chondritic IDPs (Schramm et al. 1989; Flynn et al. 1996). However, the abundances of Cu, Zn, and Ga are not well determined in the latter, suggesting that Wild 2 particles and anhydrous IDPs may better reflect the composition of the solar nebula.

4.3.2.3 Mineralogy

Before the return of *Stardust* samples there were a number of different opinions concerning what Wild 2 coma dust would be like. Possibilities included (a) materials very similar or identical to anhydrous chondritic interplanetary dust particles (IDPs) (Bradley 2014), (b) amorphous nebular condensate silicates (Rietmeijer et al. 2009), (c) products of annealing of nebular condensates (Kimura et al. 2011), or (d) materials largely made up of presolar grains with direct interstellar heritage (Engelhardt et al. 2017). Wild 2 could have also been an interstellar visitor like 1I/'Oumuamua (Jewitt et al. 2017). The actual Wild 2 samples did not match any of these possibilities.

The mineral chemistry of the collected samples is a remarkably complex mix of unequilibrated phases. The most abundant phases are the ferromagnesian silicates olivine and pyroxene (Fig. 4.8), and are similar to materials found in most anhydrous chondritic

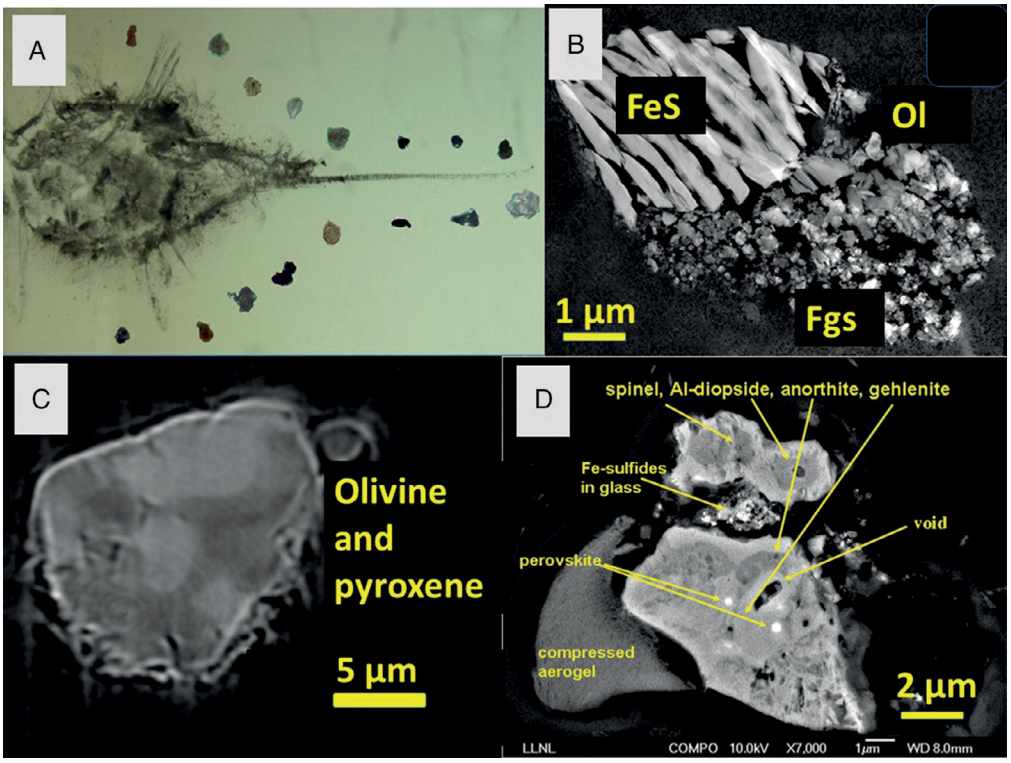

Fig. 4.8 ***Wild 2 coma grains.*** (A) Transmitted light view of track 35 (1.5 mm long) with images of extracted grains shown alongside; grains vary from 8–23 µm in diameter and are not shown to scale. (B) Back-scattered electron image of a terminal grain from track 57. The troilite (FeS) and olivine (ol) crystals apparently shielded the fine-grained material (Fgm) from destruction during capture (after Brownlee et al. 2006). (C) X-ray computed tomographic image of a terminal grain from track 35 identified by Nakamura et al. (2008) as a chondrule, containing olivine and pyroxene. (D) Back-scattered electron image of a CAI terminal grain from track 25 (Inti) (after Zolensky et al. 2006).

IDPs and unequilibrated or unaltered chondrites. The samples also contained chondrule fragments (Nakamura et al. 2008). The expectation that amorphous silicates and fine-grained annealed products of these minerals would predominate in Wild 2 grains was clearly incorrect, at least for micron and larger grains.

The major element compositional range of olivine, a reflection of the formation conditions and thermal history of astromaterials, is the largest of any known astromaterial, and the distribution is very flat, with no expected peak for forsterite (Frank et al. 2014). Comparisons of Wild 2 samples with other available astromaterials initially proved to be difficult since Wild 2 samples require study, by necessity, at the micron size scale - a scale for which there was a lack of comparable information for most other astromaterials. Subsequent detailed measurement of olivine compositions in chondrite matrix revealed how unique the range is for Wild 2 samples (Frank et al. 2014; Joswiak et al. 2014a; Brownlee and Joswiak 2017; Defouilloy et al. 2017). The flat olivine compositional distribution for Wild 2 samples indicates no thorough heating of the samples occurred after they were accreted into the comet. It also suggests that the formation regions of the olivine in Wild 2 samples differed from that of any of the carbonaceous chondrites. In addition, Wild 2 grains include a population of Ca-enriched, Mn-depleted olivine crystals not found in any other known astromaterial (Frank et al. 2014). Wild 2 also contains low-iron, manganese-enriched forsterites (called LIME olivines) that are commonly found in IDPs and carbonaceous chondrites and proposed to be early nebular condensates (Klock et al. 1989; Ebel et al. 2012).

In contrast to the major elements, Frank et al. (2014) reported *depletion* of Cr from the FeO-rich olivines in Wild 2, comparable to that attributed to mild thermal metamorphism petrologic grade (3.05–3.2) chondrites. Since Cr is highly mobile under thermal metamorphism as low as 200 °C, it is a sensitive indicator of heating events and it shows greater depletion in smaller grains (Grossman and Brearley 2005). Thus, olivine minor element compositions suggest that some, but not all, Wild 2 materials experienced thermal metamorphism prior to incorporation into their ice-rich parent body. Unfortunately, it is unclear whether the mineralogical criteria for thermal metamorphism derived from coarser chondrule silicates in ordinary and carbonaceous chondrites can be applied to the fine-grained Wild 2 samples. It is also not known what the initial Cr contents of olivine were across various early solar system environments.

The measured Mn content in >200 of Wild 2 olivine grains having a broad range of Fe content show distinctly different trends than seen in olivines from specific chondrite groups (Frank et al. 2014; Brownlee and Joswiak 2017), suggesting that comet olivine formed in a broader range of environments than these specific chondrite groups.

Comprehensive results for Wild 2 pyroxenes have not yet been published, but a number of Wild 2 particles, named "Kool" grains (Kosmochloric high-Ca pyroxene and FeO-rich olivine), contain assemblages of FeO-rich olivines, Na- and Cr-rich clinopyroxenes (usually augites), poorly-crystallized albite or albitic glass, and spinel (Joswiak

et al. 2009; 2012). Kool grains have been reported in some chondritic IDPs. The textures, grain sizes, and mineral assemblages of these grains are consistent with high temperature formation processes, rather than direct condensation or thermal annealing of amorphous condensates. The O isotopic composition of one Wild 2 Kool grain has been reported, and is comparable to some type II (FeO-rich) chondrule olivines from OC, R, and CR chondrites (Krot et al. 2006; Connolly and Huss 2010; Kita et al. 2010; Isa et al. 2011). However, actual Kool grains have not yet been observed in chondrites.

The discovery of high temperature materials like chondrule and CAI (Ca-Al-rich inclusions) fragments (Fig. 4.8C,D) among Wild 2 grains was unexpected and contrary to the idea that comets formed in isolation from the inner Solar System (Zolensky et al. 2006; McKeegan et al. 2006; Joswiak et al. 2012, 2014a,b). CAIs containing olivines, pyroxenes, sulfides, and refractory oxides have been reported from at least 5 different particle tracks, suggesting that these high-temperature components constitute ~2 percent of the collected sample (Joswiak et al. 2017). Mineral assemblages, chemistries, and bulk particle compositions indicate these grains are most similar to fine grained CAIs in carbonaceous chondrites.

Some Wild 2 grains have igneous mineralogies, textures, and bulk oxygen isotope compositions consistent with an origin as fragments of chondrules like those found in carbonaceous chondrites (Nakamura et al. 2008; Matzel et al. 2010; Joswiak et al. 2012; Ogliore et al. 2012; Gainsforth et al. 2015). The abundance of chondrule fragments in Wild 2 is > 5–10 percent and could be much higher. The exact relationships of Wild 2 chondrules to those in chondrites is not known, although the similarities are striking. It remains to be determined if Wild 2 chondrules and CAIs sample the same populations of components found in chondrites (Westphal et al. 2017). Regardless, they must have formed via high temperature processes (Gainsforth et al. 2015). These igneous materials probably require large scale mixing in the early Solar System, although there are proposals for high-temperature processes in the outer Solar System (Sanborn et al. 2017; Kruijer et al. 2017). The common presence of these materials in interplanetary dust particles of likely cometary origin suggests that they are common in comets.

Wild 2 samples include abundant sulfides. These are predominantly troilite (FeS), pyrrhotite $Fe_{(1-x)}S$, with lesser pentlandite (ideally $(FeNi)_9S_8$), but the occurrence of unusual sulfides (including ZnS) implies complex sulfide formation processes (Zolensky et al. 2006; Westphal et al. 2009; Schrader et al. 2016). The rare presence of cubanite ($CuFe_2S_3$) has been interpreted as evidence for possible rare aqueous processing (Berger et al. 2011), although a primary origin for this phase is also possible. Wild 2 Fe-Ni sulfides plot within the Fe-Ni-S ternary plot as two modes: either pyrrhotite/troilite, or pentlandite, with few compositions between (Zolensky et al. 2006). This limits the extent of possible aqueous processing since the aqueous alteration seen in hydrous IDPs produces assemblages bridging the gap between the pure end member phases. Understanding the sulfide mineralogy in the returned samples is complicated by the presence of FeS formed by melting of pre-existing grains during capture in the aerogel.

Chondritic meteorites often contain materials resulting from the activity of aqueous fluids (Zolensky and McSween 1988; Brearley 2006). Searches in Wild 2 samples for minerals unambiguously requiring formation via aqueous fluids have largely been unsuccessful. A possible exception is the cubanite grain mentioned above. Another is a magnesium carbonate reported by Mikouchi et al. (2007). Several Ca carbonates have also been reported, but these were ascribed to contamination from aerogel impurities. Magnetite and chromite have been reported from Wild 2 grains (Changela et al. 2012; Bridges et al. 2015). In chondrites and IDPs such phases have been proposed to result from aqueous alteration and oxidation of metal and Fe-Ni sulfides (Kerridge et al. 1979; Zolensky and McSween 1988), but they can also be produced in the absence of aqueous fluids (Lauretta and Schmidt 2009). The lack of phyllosilicates in analyzed Wild 2 materials could be ascribed to post-alteration thermal neomorphism impact shock or to capture heating, but heated phyllosilicates have characteristic textures (Nakamura 2005; Tonui et al. 2014) not observed in the Wild 2 materials. Thus, there is currently no unambiguous evidence for liquid water having been present on the comet.

GEMS (Glass with Embedded Metal and Sulfides) are common sub-micron sized assemblages in anhydrous chondritic IDPs, but found in only one meteorite (Ningqiang) (Rietmeijer 1994; Bradley 1994; Zolensky et al. 2003). They have been variously proposed to be radiation-damaged early nebular solids or preserved presolar materials, and they have been vigorously searched for in Wild 2 materials. A few Wild 2 components have been proposed to be GEMS (e.g., Gainsforth et al. 2016), but since very similar silica-sulfide rich aggregates are a major byproduct of the capture process of chondritic materials in silica aerogel (Barrett et al. 1992), an unambiguous identification of a true GEMS assemblage has proven to be elusive (Ishii 2019). GEMS are easily degraded by modest heating and it is possible that Wild 2 contained abundant submicron GEMS that were melted to form the silica-rich melt on track walls. It is also possible that Wild 2 does not contain GEMS.

4.3.2.4 Organics

Comets may have had a significant role in delivering volatiles and organics to the early Earth and these materials may have played a role in the origin of life (Oró 1961; Chyba and Sagan 1992). Considerable emphasis was placed on searching for organics in the returned samples (Sandford 2008, 2009). This task was made difficult by the small sizes of the samples, the complexity of the organic materials present, the fact that organics fared relatively poorly during hypervelocity collection, and the presence of structural carbon in the aerogel collection material. Nonetheless, it was possible to identify cometary organics in the samples by the presence of non-terrestrial D/H and $^{15}N/^{14}N$ isotope ratios or by clear associations with surrounding mineral grains.

Organics found in Wild 2 samples show a heterogeneous and unequilibrated distribution in both abundance and composition. Some of the organics are similar, but not

identical, to those in IDPs and carbonaceous meteorites, but there is evidence for additional organic materials not found in meteorites (Sandford et al. 2006). These additional organics are more labile, richer in oxygen and nitrogen, and aromatic-poor compared with meteoritic organics.

Comparisons with IDPs and meteorite organics are problematic since the hypervelocity impacts associated with aerogel collection resulted in the destruction and alteration of some of the collected organics. IR mapping of tracks shows that the aerogel surrounding some (but not all) tracks contains excess absorption by aliphatic $-CH_3$ and $-CH_2-$ groups, suggesting that some of the organic material in the arriving particles was vaporized during impact and redistributed into the surrounding aerogel (Sandford et al. 2006; Bajt et al. 2009). It is therefore difficult to determine the actual abundance ratio of organics to mineral phases in the original particles.

Infrared spectra of individual particles and organic regions within them show absorption bands of $-CH_3$, $-CH_2-$, $C{=}O$, and CC groups (Keller et al. 2006; Sandford et al. 2006; Rotundi et al. 2008; Bajt et al. 2009). The observed aliphatic CH stretching features of *Stardust* particles resemble those seen in IDPs in terms of peak shapes, positions, and the $-CH_2-/-CH_3$ band depth ratio, but differ somewhat from those seen in primitive carbonaceous chondrite meteorites like Orgueil and Murchison.

The presence of aromatic organics is seen in both IR and Raman spectra of collected particles (Keller et al. 2006; Sandford et al. 2006; Rotundi et al. 2008). Raman spectra of Wild 2 samples are dominated by the aromatic D and G bands near 1360 and 1590 Δcm^{-1} and are superimposed on a fluorescence background of variable intensity. The D and G band parameters of the samples indicate the presence of amorphous carbonaceous materials that scatter across the entire meteoritic field, but are best matched to the range seen in IDPs.

The technique of X-ray Absorption Near Edge Spectroscopy (XANES) has been very useful for the analysis of *Stardust* samples (Sandford et al. 2006; Cody et al. 2008; Matrajt et al. 2008; Wirick et al. 2009). C-XANES spectra of *Stardust* samples look similar to those of meteoritic organics and most closely resemble those of IDPs. C-, N-, and O-XANES spectra reveal considerable chemical complexity across the range of organic samples analyzed. The cometary organics contain low concentrations of aromatic and/or olefinic carbon relative to aliphatic and heteroatom-containing functional groups, e.g., amide, carboxyl, and alcohol/ethers. The atomic ratios for N/C and O/C derived from XANES data reveal a wide range in heteroatom content and these ratios are higher than those seen in primitive meteoritic organic matter (Fig. 4.9). The wide range in chemistry, both in elemental abundances and specific organic functional groups, suggests that the comet Wild 2 organics likely have multiple origins.

Organic species have also been detected using two-step laser desorption / laser ionization mass spectrometry (L^2MS) (Sandford et al. 2006; Clemett et al. 2010). L^2MS

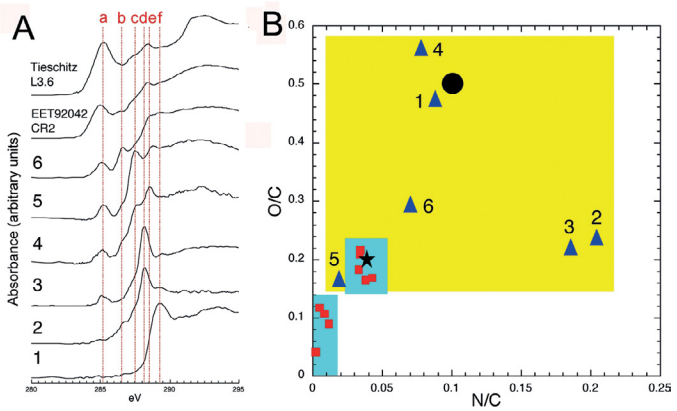

Fig. 4.9 (A) XANES data from different Wild 2 grains show a range of spectra. Specific organic functional groups are highlighted in the figure. on the left (dashed lines a to f): (a) *C* = *C* at ~ 285.2 eV; (b) *C* = *C*–O at ~ 286.5 eV; (c) *C* = *O* at ~ 287.5 eV; (d) N–*C* = *O* at 288.2 eV; (e) O–*C* = *O* at 288.6 eV; and (f) C–O at 289.5 eV (B) Wild 2 particles (numbered triangles) show unusually high N/C and O/C ratios relative to chondritic organic matter (squares). Average values for comet Halley particles and stratospheric IPDs are marked by the black star and the solid circle, respectively *(figure adapted from Sandford et al. 2006)*.

mass spectra obtained from individual particles and aerogel along impact tracks show the presence of multiple polycyclic aromatic hydrocarbons (PAHs) and their alkylated derivatives. Two distinct populations of PAHs can be distinguished. In the first population, benzene and naphthalene (1- to 2-ring PAHs) and their alkylated variants are seen in the absence of moderate mass (3- to 6-ring) PAHs. These distributions are uncharacteristic of meteorites and IDPs, but closely resemble the pyrolysis products of meteoritic macromolecular organics and have been observed in high-power laser L^2MS measurements of aerogel tiles (Spencer et al. 2009). This suggests that many lower mass PAHs may not be cometary but instead originate from impact processing of C original to the aerogel. The second population of PAHs has a more complex compositional distribution in which the dominant observed species are naphthalene ($C_{10}H_8$; 2 rings), phenanthrene ($C_{14}H_{10}$; 3 rings), and pyrene ($C_{16}H_{10}$; 4 rings), along with their alkylated homologs extending up to at least C4-alkyl. This second distribution resembles that found in matrix material in the Murchison carbonaceous chondrite and some IDPs (Clemett et al. 1993, 2010).

Amines and amino acids have also been detected. These were not found in individual cometary grains, but were instead detected within the general volume of aerogel tiles using liquid chromatography with UV fluorescence detection and time of flight mass spectrometry (LC-FD/ToF-MS). Glavin et al. (2008) detected a suite of amines and amino acids, including glycine, in acid-hydrolyzed, hot-water extracts of *Stardust* aerogels and Al foils above background levels. Most of the primary amines detected were also present in the flight aerogel witness tile that was not exposed to the comet,

indicating that they were terrestrial in origin. However, excesses of methylamine (MA) and ε-amino-n-caproic acid (EACA) in comet-exposed aerogel suggested that these volatile amines were captured from comet 81P/Wild 2 and present in an acid-hydrolyzable bound form in the aerogel (Glavin et al. 2008). Subsequently, Elsila et al. (2009) showed that the EACA had a $\delta^{13}C$ value of $-25 \pm 2‰$, indicating a terrestrial origin (EACA is likely due to contamination from the Nylon-6 used to bag samples during curation). In contrast, glycine was observed to have a $\delta^{13}C$ value of $+29 \pm 6‰$, which strongly suggests an extraterrestrial origin. This represents the first detection of a cometary amino acid.

4.3.2.5 Isotopes

Isotopically anomalous grains are found in Wild 2 grains at approximately the same level as in chondritic IDPs and the most pre-solar-rich chondrites (Stadermann et al. 2008). Thus, the composition of Wild 2 is *not* dominated by isotopically anomalous presolar grains.

The isotopically anomalous presolar grain abundance in Wild 2 samples has been best measured by detailed SIMS analysis of craters in Al foil that surrounded each aerogel cell. These indicate pre-capture abundances of 600–830 ppm for O-rich presolar grains and at least 45 ppm for SiC grains larger than 300 nm (Floss et al. 2013). This abundance is at the upper level for that reported for chondritic IDPs and higher than found in most chondrites. If the comet contains isotopically normal interstellar grains there is no existing method to determine their abundance.

High precision oxygen isotope analyses reveal the range of compositions of the returned silicates. Many silicates fit a pattern of oxygen composition vs. Fe content that is similar to CR chondrite olivine (Defouilloy et al. 2017). The oxygen isotope compositions reveal components with affinities to carbonaceous and ordinary chondrites, the presence of relict grains in chondrules, and ^{16}O-rich materials that include CAIs and Mg-rich condensates.

Organic materials in meteorites and IDPs often show non-terrestrial values for D/H and $^{15}N/^{14}N$ (Messenger 2000; Keller et al. 2004; Busemann et al. 2006) and the same is true for the organic materials returned from Wild 2, showing a large excesses in D and ^{15}N (McKeegan et al. 2006; Matrajt et al. 2008). These isotopic anomalies demonstrate conclusively that the associated organics are not terrestrial contaminants and provide insights into the types of environments and processes involved in their formation.

The distribution of anomalous enrichments of D and ^{15}N in *Stardust* samples are highly heterogeneous and the range of excesses span a similar range as that seen in IDPs. The two anomalies do not directly correlate in either location or magnitude; materials are seen that contain none, one, or both of the D and ^{15}N excesses. The decoupling of D and ^{15}N anomalies and the variable magnitudes of the effects suggest that they were formed by multiple interstellar/protostellar processes and environments that predate the formation 81P/Wild 2 (Sandford et al. 2001; McKeegan et al. 2006). Their presence also

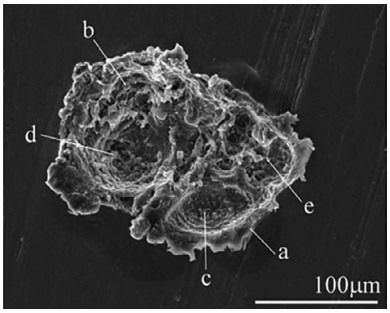

Fig. 4.10 ***Wild 2 particle impact crater in Al foil.*** The impactor was a loose aggregate composed of Mg silicate, Ca bearing silicate, chondritic, and sulfide components that produced the complex multi-pit crater lined with comet residue *(Kearsley et al. 2008)*.

indicates that these organics have experienced little alteration since their incorporation into the cometary nucleus.

4.3.2.6 Craters

While the aerogel collectors were *Stardust*'s primary means of capturing cometary samples, the forward facing aluminum foils that held aerogel capture cells in place were also exposed to the incoming flux of cometary particles. Particles impacting the foil created hypervelocity impact craters that could be individually studied (Hörz et al. 2006). The morphologies of these craters indicated that they were made by particles varying from individual dense mineral grains to loosely bound, polymineralic aggregates.

Residual impactor material was found in some craters and was studied by energy dispersive X-ray microanalysis (Kearsley et al. 2008). These showed that some particles included coarse (>10 μm) mafic silicate grains dominated by a single mineral species of density around 3–4 g cm^{-3} (such as olivine). Other grains were porous, low-density aggregates from a few nanometers to 100 μm, with an overall density that may be lower than 1 g cm^{-3}, containing mixtures of silicates, sulfides, and possibly glass. In one large aggregate crater (Fig. 4.10), the combined diverse residue composition is similar to CI chondrites. On the whole, the inferred mineral assemblages are very similar to the most common species reported from aerogel tracks.

4.3.2.7 Interstellar particles

Contemporary interstellar dust grains passing through our Solar System were first observed by detectors aboard the Ulysses spacecraft (Grün et al. 1994) and subsequently verified by data from detectors on board the Galileo, Cassini, and Helios spacecraft (Krüger et al. 2019). The original goal of the *Stardust* mission was to collect some of this "fresh" interstellar dust, although this dropped to a secondary goal as the mission developed. The Ulysses and the other spacecraft data indicated that the maximum size of the interstellar grains would be ~ 1 μm and that they would be relatively rare. The

effort to collect interstellar dust suffered from the fact that *Stardust's* dust collection periods occurred close to solar maximum, when the flux of interstellar grains to the inner Solar System is lowest. As a result, only a dozen grains spread across the entire Stardust Interstellar Particle Experiment (ISPE) aerogel collector were expected to be collected.

It was not clear when the spacecraft was launched how such minuscule and dispersed grains would be recognized and analyzed. Fortunately, Prof. Andrew Westphal (UC Berkeley), developed a plan for the public to locate the grains through one of the largest distributed planetary science efforts in history. The returned ISPE aerogel cells were scanned using an automated system, which recorded millions of microscope focusing 'movies' across each aerogel cell. These movies were placed online and more than 20,000 volunteers (self-named "dusters") searched them for traces of captured ISPE grains. Over half of the ISPE aerogel tray has been scanned in this effort (Westphal et al. 2014a,b).

Using this procedure, features of special interest were identified and a subset considered to have the greatest possibility of being interstellar grains were removed from the aerogel cells. These were mounted between 70 nm thick sheets of Si_3N_4 for protection. The resulting mounts were transparent to synchrotron X-rays, permitting analyses to be performed on the grains while still encased in aerogel. Analytical techniques used included Scanning Transmission X-ray Microscopy (STXM), Fourier Transform Infrared Spectroscopy (FTIR), X-Ray Fluorescence spectroscopy (XRF), and X-Ray Diffraction (XRD) (Westphal et al. 2014a). These analyses were carefully chosen to be non-destructive to the interstellar candidate grains. The chemistry of the majority of these samples were found to be consistent with secondary impact ejecta from *Stardust's* solar panels or sample return capsule, injected into the aerogel when interplanetary dust particles or comet coma grains impacted on these parts of the spacecraft.

Westphal et al. (2014a) reported on the mineralogy and bulk composition of the first three recognized *probable* interstellar grains (Fig. 4.11). Sample *I1043,1,30,0,0* (named "Orion") is a mixture of shocked forsteritic olivine (Fo >90), spinel, iron metal nanoparticles and one additional unidentified iron-bearing phase. Elemental abundances, normalized to magnesium and the composition of CI meteorites, show ten-fold enrichments in Al and Cu, depletions for Si, Ca and near normal Fe, Cr, Mn, and Ni. Sample *I1047,1,34,0,0* ("Hylabrook") contains shocked, partially amorphized, olivine (Fo >80) with a rim of poorly crystalline Mg-silicate, amorphous alumina, amorphous metal oxides (Cr and Mn), and an Fe-bearing oxide phase which may include reduced iron nanoparticles. The major elements Mg, Si and Fe are present in CI-like relative proportions; Mg-normalized minor heavy elemental abundances show depletions in Ca and Ni, and enrichments in Cr, Mn, and Cu, relative to CI. The nature of the third candidate, Sample *I1003,1,40,0,0* ("Sorok"), is less certain. The capture track morphology was consistent with an interstellar grain, but no Fe, Mg, or Al were detected by SXRF. Either the grain was relatively Fe-poor compared to Orion and Hylabrook, or relatively little of the original projectile survived capture.

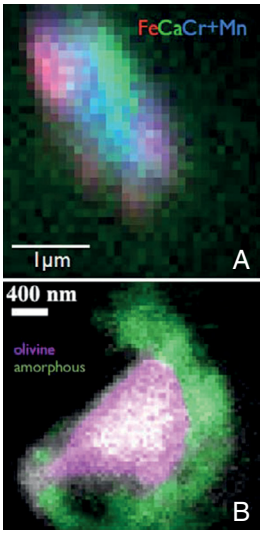

Fig. 4.11 ***Element maps of two of the first recognized probable ISPE grains derived from SXRF measurements.*** (A) Map of Sample I1043,1,30,0,0 (Orion). Blue is olivine, purple is spinel, and green is an unidentified Ca-bearing phase. (B) Map of I1047,1,34,0,0 (Hylabrook). Pink is olivine, and green is an amorphous phase. *(figure is after Westphal et al. 2014a)*.

A search for interstellar particle impact craters was also made on the Al metal foils surrounding the aerogel cells (Westphal et al. 2014a,b). Twenty-five crater-like features were identified during an automated scanning electron microscope-based search. Elemental analysis by Auger electron spectroscopy and/or energy dispersive X-ray spectroscopy (EDS) indicated that 21 of these features were secondaries from impacts on the spacecraft solar panels or defects in the foil. The remaining four impact craters (*I1044N,3*; *I1061N,3*; *I1061N,5*; and *I1061N,4*) have residues consistent with an extraterrestrial origin, consisting of Fe-, Mg-silicates, and/or Fe with associated S. Oxygen isotopic measurements of two of the crater residues were found to be consistent with solar system values, the remaining two craters could not be analyzed for O.

None of the compositional, isotopic, or mineralogic information from these samples (aerogel tracks or craters in Al foil) *requires* an interstellar origin. The strongest evidence for an interstellar origin comes from the directionality of the features. None of tracks for the interstellar candidates in the aerogel were in the angular range where IDPs should have their maximum flux. The ISPE track directions are slightly different from those expected from Ulysses and Galileo dust data, but a slightly shifting interstellar dust radiant hypothesized by Westphal et al. (2014a) would permit an interstellar dust origin for these tracks. Westphal et al. (2014a) used a statistical argument based on the expected flux of interplanetary dust vs. interstellar dust grains impacting the Al foils (from Landgraf et al. 1999) to similarly argue that all four of the potential Al craters mentioned above were most likely from interstellar impacts.

To summarize, several grains captured in ISPE aerogel and several residues found in craters in adjacent Al have been proposed to be of interstellar origin. However, no definitive evidence has yet been collected from any *Stardust* samples of an interstellar origin.

4.4 Conclusions

The *Stardust* mission was the first mission to bring back to Earth samples from outside the Earth-Moon system. The samples collected from the coma of Comet 81P/Wild 2 contained an enormous diversity of solar system materials in terms of elemental composition, mineralogy, organics, and isotopic structures. This diversity revolutionized our understanding of the processes and environments operant in the early protosolar nebula. Key points resulting from the study of the returned materials include:

- Comets clearly do not consist solely of presolar materials. Indeed, isotopically anomalous presolar grains are rare in Wild 2 samples for >μm solid grains. Many of the materials in the returned samples show evidence for high temperature formation in the protosolar nebula and are similar to the materials found in primitive meteorites.
- The returned comet dust is primitive. The returned materials do not appear to have been significantly altered after their incorporation into the comet. This has preserved a heterogeneity that demonstrates that these materials come from a wide variety of formation environments and have different detailed histories. The comet silicates seem to represent a more diverse sampling of nebular environments than seen in specific meteorite groups, unlike chondrite groups whose defining properties partially relate to regional differences in their source regions. Comets are likely to contain a broader mix of materials from nebular environments dispersed in both time and space.
- Large scale mixing must have occurred in the early protosolar disk. While comets may live predominantly in the outer Solar System, the composition of Wild 2 samples suggests they contain significant amounts of material that formed or was altered much closer to the Sun. Indeed, nearly all of the collected particles >2 μm in size are high temperature materials that include CAIs, chondrule fragments, and condensates.
- The elemental composition, mineralogy, isotopic patterns, etc. of Wild 2 particles are similar, but not identical to, primitive meteorites and anhydrous IDPs. They cannot be related to any specific meteorite group, but contain components found in various groups.
- Organics are present but severely under-represented in the returned samples due to their collection at hypervelocity. Material like meteoritic IOM is present, but there is evidence that comets may contain an additional, less aromatic organic component.

It seems unlikely that identification of chondrule and CAI fragments, measurement of the abundance of isotopically anomalous pre-solar grains, and a quantitative and detailed understanding of the complex mix materials formed in numerous nebular materials could ever have been known without the laboratory study of returned comet samples

Acknowledgements

This work was supported by the National Aeronautics and Space Administration through the NASA Emerging Worlds Program under Cooperative Agreement Notice NNH17ZDA001N issued through the Science Mission Directorate.

References

Bajt, S., Sandford, S.A., Flynn, G.J., Matrajt, G., Snead, C.J., Westphal, A.J., Bradley, J.P., 2009. Infrared spectroscopy of Wild 2 particle hypervelocity tracks in Stardust aerogel: evidence for the presence of volatile organics in comet dust. Meteoritics and Planetary Science 44, 471–484.

Barrett, R.A., Zolensky, M.E., Horz, F., Lindstrom, D.J., Gibson, E.K., 1992. Suitability of silica aerogel as a capture medium for interplanetary dust. In: Ryder, G., Sharpton, V. (Eds.), Proceedings of the 19th Lunar and Planetary Science Conference, 203–212.

Berger, E.L., Zega, T.J., Keller, L.P., Lauretta, D.S., 2011. Evidence for aqueous activity on comet 81P/Wild 2 from sulfide mineral assemblages in Stardust samples and CI chondrites. Geochim. Cosmochim. Acta 75, 3501–3513.

Bradley, J.P., 1994. Chemically anomalous, pre-accretionally irradiated grains in interplanetary dust from comets. Science 265, 925–929.

Bradley, J.P., 2014. Early grains in the solar nebula—interplanetary dust particles. In: Meteorites and Cosmochemical Processes, H.D., Holland, K.K., Turekian (Eds.), Treatise on Geochemistry, 2nd ed., vol. 1, Oxford:Elsevier–Pergamon, pp. 287–308 .

Brearley, A.J., 2006. The action of water. In: Lauretta, D.S., McSween, H.Y. (Eds.), Meteorites and the Early Solar System II, 584–624.

Bridges, J.C., Hicks, L.J., MacArthur, J.L., Price, M.C., Burchell, M.J., Franchi, I.A., Gurman, S.J., 2015. Magnetite in Stardust terminal grains: evidence for hydrous alteration in the Wild 2 parent body. European Planetary Science Congress 2015, held 27 September - 2 October 2015 in Nantes. France, id.EPSC2015-866.

Brownlee, D., Tsou, P., Aléon, J., Alexander, C.M.O'.D., Araki, T., Bajt, S., Baratta, G.A., Bastien, R., Bland, P., Bleuet, P., Borg, J., Bradley, J.P., Brearley, A., Brenker, F., Brennan, S., Bridges, J.C., Browning, N.D., Brucato, J.R., Bullock, E., Burchell, M., Busemann, H., Butterworth, A., Chaussidon, M., Cheuvront, A., Chi, M., Cintala, M.J., Clark, B.C., Clemett, S.J., Cody, G., Colangeli, L., Cooper, G., Cordier, P., Daghlian, C., Dai, Z., d'Hendecourt, L., Djouadi, Z., Dominguez, G., Duxbury, T., Dworkin, J.P., Ebel, D.S., Economou, T.E., Fakra, S., Fairey, S.A.J., Fallon, S., Ferrini, G., Ferroir, T., Fleckenstein, H., Floss, C., Flynn, G., Franchi, I.A., Fries, M., Gainsforth, Z., Gallien, J.-P., Genge, M., Gilles, M.K., Gillet, P., Gilmour, J., Glavin, D.P., Gounelle, M., Grady, M.M., Graham, G.A., Grant, P.G., Green, S.F., Grossemy, F., Grossman, L., Grossman, J.N., Guan, Y., Hagiya, K., Harvey, R., Heck, P., Herzog, G.F., Hoppe, P., Hörz, F., Huth, J., Hutcheon, I.D., Ignatyev, K., Ishii, H., Ito, M., Jacob, D., Jacobsen, C., Jacobsen, S., Jones, S., Joswiak, D., Jurewicz, A., Kearsley, A., Keller, L.P., Khodja, H., Kilcoyne, A.L.D., Kissel, J., Krot, A., Langenhorst, F., Lanzirotti, A., Le, L., Leshin, L.A., Leitner, J., Lemelle, L., Leroux, H., Liu, M.-C., Luening, K., Lyon, I., MacPherson, G., Marcus, M.A., Marhas, K., Marty, B., Matrajt, G., McKeegan, K., Meibom, A., Mennella, V., Messenger, K., Messenger, S., Mikouchi, T., Mostefaoui, S., Nakamura, T., Nakano, T., Newville, M., Nittler, L.R., Ohnishi, I., Ohsumi, K., Okudaira, K., Papanastassiou, D.A., Palma, R., Palumbo, M.E., Pepin, R.O., Perkins, D., Perronnet, M., Pianetta, P., Rao, W., Rietmeijer, F.J.M., Robert, F., Rost, D., Rotundi, A., Ryan, R., Sandford, S.A., Schwandt, C.S., See, T.H., Schlutter, D., Sheffield-Parker, J., Simionovici, A., Simon, S., Sitnitsky, I., Snead, C., Spencer, M.K., Stadermann, F.J., Steele, A., Stephan, T., Stroud, R., Susini, J., Sutton, S.R., Suzuki, Y., Taheri, M., Taylor, S., Teslich, N., Tomeoka, K., Tomioka, N., Toppani, A., Trigo-Rodríguez, J.M., Troadec, D., Tsuchiyama, A., Tuzzolino, A.J., Tyliszczak, T., Uesugi, K., Velbel, M., Vellenga, J., Vicenzi, E., Vincze, L., Warren, J., Weber, I., Weisberg, M., Westphal, A.J., Wirick, S., Wooden, D., Wopenka, B., Wozniakiewicz, P., Wright, I., Yabuta, H., Yano, H., Young, E.D., Zare, R.N., Zega, T., Ziegler, K., Zimmerman, L., Zinner, E., Zolensky, M., 2006. Comet 81P/Wild 2 under a microscope. Science 314, 1711–1716.

Brownlee, D.E., Joswiak, D.J., 2017. Diversity of the initial rocky planetary building materials at the edge of the solar system. Meteoritics and Planetary Science 52, 471–478.
Brownlee, D.E., Tsou, P., Anderson, J.D., Hanner, M.S., Newburn, R.L., Sekanina, Z., Clark, B.C., Hörz, F., Zolensky, M.E., Kissel, J., McDonnell, J.A.M., Sandford, S.A., Tuzzolino, A.J., 2003. STARDUST: comet and interstellar dust sample return mission. J. Geophys. Res. 108, #E10, (8111), pp. 1–1 to 1–15.
Burchell, M.J., Fairey, S.A.J., Wozniakiewicz, P., Brownlee, D.E., Hörz, F., Kearsley, A.T., et al., 2008. Characteristics of cometary dust tracks in Stardust aerogel and laboratory calibrations. Meteoritics and Planetary Science 43, 23–40.
Busemann, H., Young, A.F., Alexander, C.M.O'D., Hoppe, P., Mukhopadhyay, S., Nittler, R.N., 2006. Interstellar chemistry recorded in organic matter from primitive meteorites. Science 312, 727–730. DOI:10.1126/science.1123878.
Changela, H.G., Bridges, J.C., Gurman, S.J., 2012. Extended X-ray absorption fine structure (EXAFS) in Stardust tracks: constraining the origin of ferric iron-bearing minerals. Geochim. Cosmochim. Acta 98, 282–294. DOI:10.1016/j.gca.2012.04.036.
Chyba, C., Sagan, C., 1992. Endogenous production, exogenous delivery and impact-shock synthesis of organic molecules: an inventory for the origins of life. Nature 355, 125–132.
Clark, B.C., Green, S.F., Economou, T.E., Sandford, S.A., Zolensky, M.E., McBride, N., Brownlee, D.E., 2004. Release and fragmentation of aggregates to produce heterogeneous lumpy coma streams. J. Geophys. Res. 109, #E12, (E12S03), 13 pages.
Clemett, S., Maechling, C., Zare, R., Swan, P., Walker, R., 1993. Identification of complex aromatic molecules in individual interplanetary dust particles. Science 262, 721.
Clemett, S.J., Sandford, S.A., Nakamura-Messenger, K., Hörz, F., McKay, D.S., 2010. Complex aromatic hydrocarbons in Stardust samples collected from the comet 81P/Wild-2. Meteoritics and Planetary Science 45, 701–722.
Cody, G.D., Ade, H., Alexander, O'D.C.M., Araki, T., Butterworth, A., Fleckenstein, H., Flynn, G., Gilles, M.K., Jacobsen, C., Kilcoyne, A.L.D., Messenger, K., Sandford, S.A., Tyliszczak, T., Westphal, A.J., Wirick, S., Yabuta, H., 2008. Quantitative organic and light-element analysis of comet 81P/Wild 2 particles using C-, N-, and O- μ-XANES. Meteoritics and Planetary Science 43, 353–365.
Connolly, H.C., Huss, G.R., 2010. Compositional evolution of the protoplanetary disk: oxygen isotopes of type-II chondrules from CR2 chondrites. Geochim. Cosmochim. Acta 74, 2473–2483.
Defouilloy, C., Nakashima, D., Joswiak, D., Brownlee, D., Tenner, T., Kita, N., 2017. Origin of crystalline silicates from Comet 81P/Wild 2: combined study on their oxygen isotopes and mineral chemistry. Earth Planet. Sci. Lett. 465, 145–154.
Duxbury, T.C., Newburn, R.L., Acton, C.H., Carranza, E., McElrath, T.P., Ryan, R.E., Synnott, S.P., You, T.H., 2004. Asteroid 5535 Annefrank size, shape, and orientation: Stardust first results. J. Geophys. Res. 109, E02002. DOI:10.1029/2003JE002108.
Ebel, D.S., Weisberg, M.K., Beckett, J.R., 2012. Chemical stability of low-iron, manganese-enriched olivine in astrophysical environments. Meteoritics and Planetary Science 47, 585–593.
Elsila, J.E., Glavin, D.P., Dworkin, J.P., 2009. Cometary glycine detected in samples returned by Stardust. Meteoritics and Planetary Science 44, 1323–1330.
Engelhardt, T., Jedicke, R., Vereš, P., Fitzsimmons, A., Denneau, L., Beshore, E., Meinke, B., 2017. An observational upper limit on the interstellar number density of asteroids and comets. Astron. J. 153, 133, 11p.
Floss, C., Stadermann, F.J., Kearsley, A.T., Burchell, M.J., Ong, W.J., 2013. The abundance of solar system grains in comet 81P/Wild 2. Astrophys. J. 763, 140–151.
Flynn, G.J., Bajt, S., Sutton, S.R., Zolensky, M., Thomas, K.L., Keller, L.P., 1996. The abundance pattern of elements having low nebular condensation temperatures in the IDPs: evidence for a new type of chondritic material. In: Gustafson, B., Hanner, M. (Eds.), Physics, Chemistry and Dynamics of Interplanetary Dust. Astronomical Society of the Pacific, pp. 291–294.
Flynn, G.J., Bleuet, P., Borg, J., Bradley, J., Brenker, F., Brennan, S., Bridges, J., Brownlee, D.E., Bullock, E., Clark, B.C., Dai, Z.R., Daghlian, C., Djouadi, Z., Fakra, Sirine, Ferroir, T., Floss, C., Franchi, I.A., Gainsforth, Z., Gallien, J.-P., Gillet, Ph., Grant, P.G., Graham, G.A., Green, SimonF., Grossemy, F., Heck, P., Herzog, G.F., Hoppe, P., Hörz, F., Huth, J., Ignatyev, K.I., Ishii, H.A., Joswiak, D., Kearsley, A.T., Khodja, H., Lanzirotti, A., Leitner, J., Lemelle, L., H, Leroux, Luening, K., MacPherson, G., Marhas, K.K., Marcus, M.A., Matrajt, G., Nakamura, T., Nakano, T., Newville, M., Papanastassiou, D.A., Pianetta, P., Rao, W., Rietmeijer, F.J.M., Rost, D., Schwandt, C.S., See, T.H., Sheffield-Parker, J., Simionovic, A.,

Sitnitsky, I., Snead, C.J., Stadermann, F.J., Stephan, T., Stroud, R.M., Susini, J., Suzuki, Y., Sutton, S.R., Taylor, S., Teslich, N., Troadec, D., Tsou, P., Tsuchiyama, A., Uesugi, K., Westphal, A., Wozniakiewicz, P., Vicenzi, E., Vincze, L., Zolensky, M.E., 2006. Elemental compositions of comet 81P/Wild 2 samples collected by Stardust. Science 314, 1730–1733.

Frank, D.R., Zolensky, M.E., Le, L., 2014. Olivine in terminal particles of Stardust aerogel tracks and analogous grains in chondrite matrix. Geochim. Cosmochim. Acta 142, 240–259.

Gainsforth, Z., Butterworth, A.L., Jilly-Rehak, C.E., Westphal, A.J., Brownlee, D.E., Joswiak, D., Ogliore, R.C., Zolensky, M.E., Bechtel, H.A., Ebel, D.S., Huss, G.R., Sandford, S.A., White, A.J., 2016. Possible GEMS and ultrafine grained polyphase units in comet Wild 2. Lunar and Planetary Science Conference, LPI Contribution No. 1903, p.2366.

Gainsforth, Z., Butterworth, A.L., Stodolna, J., Westphal, A.J., Huss, G.R., Nagashima, K., Ogliore, R., Brownlee, D.E., Joswiak, D., Tyliszczak, T., Simionovici, A.S., 2015. Constraints on the formation environment of two chondrule-like igneous particles from comet 81P/Wild 2. Meteoritics and Planetary Science 50, 976–1004.

Glavin, D.P., Dworkin, J.P., Sandford, S.A., 2008. Detection of cometary amines in samples returned by Stardust. Meteoritics and Planetary Science 43, 399–413.

Gounelle, M., Spurný, P., Bland, P.A., 2006. The atmospheric trajectory and orbit of the Orgueil meteorite. Meteoritics and Planetary Science 41, 135–150.

Green, S.F., McDonnell, J.A.M., McBride, N., Colwell, M.T.S.H., Tuzzolino, A.J., Economou, T.E., Tsou, P., Clark, B.C., Brownlee, D.E., 2004. The dust mass distribution of comet 81P/Wild 2. J. Geophys. Res. 109, E12S04. DOI:10.1029/2004JE002318.

Grossman, J.N., Brearley, A.J., 2005. The onset of metamorphism in ordinary and carbonaceous chondrites. Meteoritics and Planetary Science 40, 87–122.

Grün, E., Gustafson, B., Mann, I., Baguhl, M., Balogh, A., Morfill, G.E., Staubach, P., Taylor, A., Zook, H.A., 1994. Interstellar dust in the heliosphere. Astronomy & Astrophysics 286, 915–924.

Hörz, F., Bastien, R., Borg, J., Bradley, J.P., Bridges, J.C., Brownlee, D.E., Burchell, M.J., Chi, M., Cintala, M.J., Dai, Z.R., Djouadi, Z., Dominguez, G., Economou, T.E., Fairey, S.A.J., Floss, C., Franchi, I.A., Graham, G.A., Green, S.F., Heck, P., Hoppe, P., Huth, J., Ishii, H., Kearsley, A.T., Kissel, J., Leitner, J., Leroux, H., Marhas, K., Messenger, K., Schwandt, C.S., See, T.H., Snead, C., Stadermann, F.J., Stephan, T., Stroud, R., Teslich, N., Trigo-Rodríguez, J.M., Tuzzolino, A.J., Troadec, D., Tsou, P., Warren, J., Westphal, A., Wozniakiewicz, P., Wright, I., Zinner, E., 2006. Impact features on Stardust: implications for comet 81P/Wild 2 Dust. Science 314, 1716–1719.

Isa, J., Rubin, A.E., Marin-Carbonne, J., McKeegan, K.D., Wasson, J.T., 2011. Oxygen-isotopic compositions of r-chondrite chondrules. 42nd Lunar and Planetary Science Conference, LPI Contribution No. 1608, p.2623.

Ishii, H.A., 2019. Comparison of GEMS in interplanetary dust particles and GEMS-like objects in a Stardust impact track in aerogel. Meteoritics and Planetary Science 54, 202–219.

Jewitt, D., Luu, J., Rajagopal, J., Kotulla, R., Ridgway, S., Liu, W., Augusteijn, T., 2017. Interstellar interloper 1I/2017 U1: observations from the NOT and WIYN telescopes. Astrophysical Journal Letters 850, L36.

Joswiak, D.J., Brownlee, D.E., 2014a. Refractory-rich materials in comets: CAIs, Al-rich chondrules and AOAs from comet Wild 2 and a giant cluster interplanetary dust particle (IDP) of probable cometary origin and comparison to refractory-rich objects in chondrites. 45th Annual Lunar and Planetary Science Conference, abstract no. 2282.

Joswiak, D.J., Brownlee, D.E., Matrajt, G., Westphal, A.J., Snead, C.J., 2009. Kosmochloric Ca-rich pyroxenes and FeO-rich olivines (Kool grains) and associated phases in Stardust tracks and chondritic porous interplanetary dust particles: possible precursors to FeO-rich type II chondrules in ordinary chondrites. Meteoritics and Planetary Science 44, 1561–1588. DOI:10.1111/j.1945-5100.2009.tb01192.x.

Joswiak, D.J., Brownlee, D.E., Matrajt, G., Westphal, A.J., Snead, C.J., Gainsforth, Z., 2012. Comprehensive examination of large mineral and rock fragments in Stardust tracks: mineralogy, analogous extraterrestrial materials, and source regions. Meteoritics and Planetary Science 47, 471–524. DOI:10.1111/j.1945-5100.2012.01337.x.

Joswiak, D.J., Brownlee, D.E., Nguyen, A.N., Messenger, S., 2017. Refractory materials in comet samples. Meteoritics and Planetary Science 52, 1612–1648.

Joswiak, D.J., Nakashima, D., Brownlee, D.E., Matrajt, G., Ushikubo, T., Kita, N.T., Messenger, S., Ito, M., 2014b. Terminal particle from Stardust track 130: probable Al-rich chondrule fragment from comet Wild 2. Geochim. Cosmochim. Acta 144, 277–298.

Kearsley, A.T., Borg, J., Graham, G.A., Burchell, M.J., Cole, M.J., Leroux, H., Bridges, J.C., F. Wozniakiewicz, P.J., Bland, P.A., Bradley, J.P., Dai, Z.R., Teslich, N.T., Hoppe, P., Heck, P.R., Huth, J., Stadermann, F.J., Floss, C., Marhas, K., Stephan, T., Leitner, J., 2008. Dust from comet Wild 2: interpreting particle size, shape, structure, and composition from impact features on the Stardust aluminum foils. Meteoritics and Planetary Science 43, 41–73.

Keller, L.P., Bajt, S., Baratta, G.A., Borg, J., Bradley, J.P., Brownlee, D.E., Busemann, H., Brucato, J.R., Burchell, M., Colangeli, L., d'Hendecourt, L., Djouadi, Z., Ferrini, G., Flynn, G., Franchi, I.A., Fries, M., Grady, M.M., Graham, G.A., Grossemy, F., Kearsley, A., Matrajt, G., Nakamura-Messenger, K., Mennella, V., Nittler, L., Palumbo, M.E., Stadermann, F.J., Tsou, P., Rotundi, A., Sandford, S.A., Snead, C., Steele, A., Wooden, D., Zolensky, M., 2006. Infrared spectroscopy of comet 81P/Wild 2 samples returned by Stardust. Science 314, 1728–1731.

Keller, L.P., Messenger, S., Glynn, G.J., Clemett, S., Wirick, S., Jacobsen, C., 2004. The nature of molecular cloud material in interplanetary dust. Geochim. Cosmochim. Acta 68, 2577–2589. DOI:10.1016/j.gca.2003.10.044.

Kerridge, J.F., Mackay, A.L., Boynton, W.V., 1979. Magnetite in CI carbonaceous meteorites - origin by aqueous activity on a planetesimal surface. Science 205, 395–397. DOI:10.1126/science.205.4404.395.

Kimura, Y., Nuth, J.A., Tsukamoto, K., Kaito, C., 2011. Laboratory annealing experiments of refractory silicate grain analogs using differential scanning calorimetry. Meteoritics and Planetary Science 46, 92–102.

Kissel, J., Glasmachers, Grün, A., Henkel, E., Höfner, Haerendel, H., von Hoerner, G., Hornung, H., Jessberger, K., Krueger, E.K., Möhlmann, F.R., Greenberg, D., Langevin, J.M., Silen, Y., Brownlee, J., Clark, D., Hanner, B.C., Hörz, M.S., Sandford, F., Sekanina, S., Tsou, Z., Utterback, P., Zolensky, N.G., Heiss, M., Ch., 2003. Cometary and interstellar dust analyzer for comet Wild 2. J. Geophys. Res. 108, #E10, (8114), 4-1 to 4-8.

Kita, N., et al., 2010. High precision SIMS oxygen three isotope study of chondrules in LL3 chondrites: role of ambient gas during chondrule formation. Geochim. Cosmochim. Acta 74, 6610–6635.

Klöck, W., Thomas, K.L., McKay, D.S., Palme, H., 1989. Unusual olivine and pyroxene composition in interplanetary dust and unequilibrated ordinary chondrites. Nature 339, 126–128.

Krolikowska, M., Suztowicz, S., 2006. Non-gravitational motion of the Jupiter-family comet 81P/Wild 2. Astronomy & Astrophysics 448, 401–409.

Krot, A., et al., 2006. Aluminum-magnesium and oxygen isotope study of relict Ca-Al-rich inclusions in chondrules. Astrophys. J. 639, 1227–1237.

Krüger, H., Strub, P., Altobelli, N., Sterken, V., Srama, R., Grün, E., 2019. Interstellar dust in the solar system: model versus in-situ spacecraft data. Astronomy & Astrophysics 626, A37.

Kruijer, T., Burkhardt, C., Budde, G., Kleine, T., 2017. Age of Jupiter inferred from the distinct genetics and formation times of meteorites. Proc. Natl Acad. Sci. 114, 6712–6716.

Landgraf, M., Müller, M., Grün, E., 1999. Prediction of the in-situ dust measurements of the Stardust mission to comet 81P/Wild 2. Planet. Space Sci. 47, 1029–1050.

Lauretta, D.S., Schmidt, B.E., 2009. Oxidation and minor elements from an iron-nickel-chromium-cobalt-phosphorus alloy in 17.3% CO_2-H_2 gas mixtures at 700-1000 °C. Oxid. Met. 71, 219–235.

Matrajt, G., Ito, M., Wirick, S., Messenger, S., Brownlee, D.E., Joswiak, D., Flynn, G., Sandford, S., Snead, C., Westphal, A., 2008. Carbon Investigation of two Stardust particles: a TEM, NanoSIMS, and XANES study. Meteoritics and Planetary Science 43, 315–334.

Matzel, J.E.P., Ishii, H.A., Joswiak, D., Hutcheon, I.D., Bradley, J.P., Brownlee, D., et al., 2010. Constraints on the formation age of cometary material from the NASA Stardust mission. Science 328, 483–486.

McKeegan, K.D., Aléon, J., Bradley, J., Brownlee, D., Busemann, H., Butterworth, A., et al., 2006. Isotopic compositions of cometary matter returned by Stardust. Science 314, 1724–1727.

Messenger, S., 2000. Identification of molecular-cloud material in interplanetary dust particles. Nature 404, 968–971.

Mikouchi, T., Tachikawa, O., Hagiya, K., Ohsumi, K., Zolensky, M., 2007. Mineralogy and crystallography of comet 81P/Wild 2 particles returned by the Stardust mission. Lunar And Planetary Science XXXVIII. The Lunar and Planetary Institute. Abstract #1946.

Nakamura, T., 2005. Post-hydration thermal metamorphism of carbonaceous chondrites. J. Mineral. Petrol. Sci. 100, 260–272.

Nakamura, T., Noguchi, T., Tsuchiyama, A., Ushikubo, T., Kita, N., Valley, J., Zolensky, M.E., Kakazu, Y., Sakamoto, K., Mashio, E., Uesugi, K., Nakano, T., 2008. Chondrule-like objects in short-period comet 81P/Wild 2. Science 321, 1664–1667.

Newburn Jr., R.L., Bhaskaran, S., Duxbury, T.C., Fraschetti, G., Radey, T., Schwochert, M., 2003. Stardust imaging camera. J. Geophys. Res. 108 (E10), 8116. DOI:10.1029/2003JE002081.

Ogliore, R.C., Huss, G.R., Nagashima, K., Butterworth, A.L., Gainsforth, Z., Stodolna, J., et al., 2012. Incorporation of a late-forming chondrule into comet Wild 2. Astrophysical Journal Letters, 745, L19.

Oró, J., 1961. Comets and the formation of biochemical compounds on the primitive earth. Nature 190, 389.

Rietmeijer, F.J., Pun, A., Nuth, J.A., 2009. Dust formation and evolution in a Ca-Fe-SiO-H2-O2 vapour phase condensation experiment and astronomical implications. Mon. Not. R. Astron. Soc. 396, 402–408.

Rietmeijer, F.J.M., 1994. Searching for a principal component mixing model for chondritic interplanetary dust particles: the use of size analyses. 25th Lunar and Planetary Science Conference, 1129–1130.

Rotundi, A., Baratta, G.A., Borg, J., Brucato, J.R., Busemann, H., Colangeli, L., d'Hendecourt, L., Djouadi, Z., Ferrini, G., Franchi, I.A., Fries, M., Grossemy, F., Keller, L.P., Mennella, V., Nakamura, K., Nittler, L.R., Palumbo, M.E., Sandford, S.A., Steele, A., Wopenka, B., 2008. Combined micro-raman, micro-infrared, and field emission scanning electron microscope analyses of comet 81P/Wild 2 particles collected by Stardust. Meteoritics and Planetary Science 43, 367–397.

Sanborn, M., Yin, Q.-.Z., Goodrich, C., Zolensky, M., Fioretti, A., 2017. A case for nebula scale mixing between non-carbonaceous and carbonaceous chondrite reservoirs: testing the grand tack model with chromium isotopic composition of Almahata Sitta stone 91a. 80th Annual Meeting of the Meteoritical Society. Abstract #6277.

Sandford, S.A., 2008. Organics in the samples returned from comet 81P/Wild 2 by the Stardust spacecraft. In: Kwok, S., Sandford, S. (Eds.), *Organic Matter in Space*, Proceedings of IAU Symposium #251, Cambridge Univ. Press, Cambridge, pp. 299–307.

Sandford, S.A., 2009. Organics in the samples returned by the Stardust spacecraft from comet 81P/Wild 2. In bioastronomy 2007 - molecules, microbes, and extraterrestrial life, astronomical society of the pacific conference series, Vol. 420. In: Meech, K.J., Keane, J.V., Mumma, M.J., Siefert, J.L., Werthimer, D.J. (Eds.), Proceedings of meeting held 16-20 July 2007, San Juan, Puerto Rico. ASP: San Francisco, CA. pp. 113–119.

Sandford, S.A., Aléon, J., Alexander, C.M.O'.D., Araki, T., Bajt, S., Baratta, G.A., Borg, J., Bradley, J.P., Brownlee, D.E., Brucato, J.R., Burchell, M.J., Busemann, H., Butterworth, A., Clemett, S.J., Cody, G., Colangeli, L., Cooper, G., d'Hendecourt, L., Djouadi, Z., Dworkin, J.P., Ferrini, G., Fleckenstein, H., Flynn, G.J., Franchi, I.A., Fries, M., Gilles, M.K., Glavin, D.P., Gounelle, M., Grossemy, F., Jacobsen, C., Keller, L.P., Kilcoyne, A.L.D., Leitner, J., Matrajt, G., Meibom, A., Mennella, V., Mostefaoui, S., Nittler, L.R., Palumbo, M.E., Papanastassiou, D.A., Robert, F., Rotundi, A., Snead, C.J., Spencer, M.K., Stadermann, F.J., Steele, A., Stephan, T., Tsou, P., Tyliszczak, T., Westphal, A.J., Wirick, S., Wopenka, B., Yabuta, H., Zare, R.N., Zolensky, M.E., 2006. Organics captured from comet 81P/Wild 2 by the Stardust spacecraft. Science 314, 1720–1724.

Sandford, S.A., Bajt, S., Clemett, S.J., Cody, G.D., Cooper, G., DeGregorio, B.T., De Vera, V., Dworkin, J.P., Elsila, J.E., Flynn, G.J., Glavin, D.P., Lanzirotti, A., Limero, T., Martin, M.P., Snead, C.J., Spencer, M.K., Stephan, T., Westphal, A., Wirick, S., Zare, R.N., Zolensky, M.E., 2010. Assessment and control of organic and other contaminants associated with the Stardust sample return from Comet 81P/Wild 2. Meteoritics and Planetary Science 45, 406–433.

Sandford, S.A., Bernstein, M.P., Dworkin, J.P., 2001. Assessment of the interstellar processes leading to deuterium enrichment in meteoritic organics. Meteoritics and Planetary Science 36, 1117–1133.

Schrader, D.L., Davidson, J., McCoy, T.J., 2016. Widespread evidence for high-temperature formation of pentlandite in chondrites. Geochim. Cosmochim. Acta 189, 359–376.

Schramm, L., Brownlee, D., Wheelock, M., 1989. Major element composition of stratospheric micrometeorites. Meteoritics and Planetary Science 24, 99–112.

Sekanina, Z., 2003. A model for comet 81P/Wild 2. Journal of Geophysical Research (Planets) 108, 8112.

Spencer, M.K., Clemett, S.J., Sandford, S.A., McKay, D.S., Zare, R.N., 2009. Organic compound alteration during hypervelocity collection of carbonaceous materials in aerogel. Meteoritics and Planetary Science 44, 15–24.

Stadermann, F.J., Hoppe, P., Floss, C., Heck, P.R., Hörz, F., Huth, J., et al., 2008. Stardust in Stardust—the C, N, and O isotopic compositions of Wild 2 cometary matter in Al foil impacts. Meteoritics and Planetary Science 43, 299–313.

Tonui, E., Zolensky, M., Hiroi, T., Nakamura, T., Lipschutz, M., Wang, M.-S., Okudaira, K., 2014. Petrographic, chemical and spectroscopic evidence for thermal metamorphism in carbonaceous chondrites I: CI and CM chondrites. Geochim. Cosmochim. Acta 126, 284–306.

Tsou, P., Brownlee, D.E., Anderson, J.D., Bhaskaran, S., Cheuvront, A.R., Clark, B.C., Duxbury, T., Economou, T., Green, S.F., Hanner, M.S., Hörz, F., Kissel, J., McDonnell, J.A.M., Newburn, R.L., Ryan, R.E., Sandford, S.A., Sekanina, Z., Silen, J., Tuzzolino, A.J., Vellinga, J.M., Zolensky, M.E., 2004. STARDUST encounters comet 81P/Wild 2. J. Geophys. Res. 109, #E12, (E12S01), 8 pages.

Tsou, P., Brownlee, D.E., Sandford, S.A., Hörz, F., Zolensky, M.E., 2003. Wild 2 and interstellar sample collection and earth return. J. Geophys. Res. 108, #E10, (8113), pp. 3–1 to 3–21.

Tsou, P., Yen, C.-.W., Albee, A.L., 1994. Low-encounter speed comet coma sample return missions, paper presented at the GFSC flight mechanics/estimation theory symposium, Goddard Space Flight Cent. Greenbelt, Md., 17 May 1994.

Tuzzolino, A.J., Economou, T.E., Clark, B.C., Tsou, P., Brownlee, D.E., Green, S.F., McDonnell, J.A.M., McBride, N., Colwell, M.T.S.H., 2004. Dust measurements in the coma of comet Wild 2 by the dust flux monitor instrument. Science 304, 1776–1780.

Tuzzolino, A.J., Economou, T.E., McKibben, R.B., Simpson, J.A., McDonnell, J.A.M., Burschel, M.J., Vaughan, B.A.M., Tsou, P., Hanner, M.S., Clark, B.C., Brownlee, De.E., 2003. Dust flux monitor instrument (DFMI) for the Stardust mission to comet Wild 2, J. Geophys. Res. 108 (E10), 8115. DOI:10.1029/2003JE002086.

Veverka, J., Klaasen, K., A'Hearn, M., Belton, M., Brownlee, D., Chesley, S., Clark, B., Economou, T., Farquhar, R., Green, S.F., Groussin, O., Harris, A., Kissel, J., Li, J.-Y., Meech, K., Melosh, J., Richardson, J., Schultz, P., Silen, J., Sunshine, J., Thomas, P., Bhaskaran, S., Bodewits, D., Carcich, B., Cheuvront, A., Farnham, T., Sachett, S., Wellnitz, D., Wolf, A., 2013. Return to comet Tempel 1: overview of Stardust-NExT results. Icarus 222, 424–435.

Westphal, A.J., Bechtel, H.A., Brenker, F.E., Butterworth, A.L., Flynn, G.J., Frank, D.R., Frank, D.R., Gainsforth, Z., Hillier, J.K., Postberg, F., Simionovici, A.S., Sterken, V.J., Stroud, R.M., Allen, C., Anderson, D., Ansari, A., Bajt, S., Bastien, R.K., Bassim, N., Borg, J., Bridges, J., Brownlee, D.E., Burchell, M., Burghammer, M., Changela, H., Cloetens, P., Davis, A.M., Doll, R., Floss, C., Grün, E., Heck, P.R., Hoppe, P., Hudson, B., Huth, J., Hvide, B., Kearsley, A., King, A.J., Lai, B., Leitner, J., Lemelle, L., Leroux, H., Leonard, A., Lettieri, R., Marchant, W., Nittler, L.R., Ogliore, R., Ong, W.J., Price, M.C., Sandford, S.A., Tresseras, J.-A.S., Schmitz, S., Schoonjans, T., Silversmit, G., Solé, V.A., Srama, R., Stadermann, F., Stephan, T., Stodolna, J., Sutton, S., Trieloff, M., Tsou, P., Tsuchiyama, A., Tyliszczak, T., Vekemans, B., Vincze, L., Von Korff, J., Wordsworth, N., Zevin, D., Zolensky, M.E., 2014b. Final reports of the Stardust interstellar preliminary examination. Meteoritics and Planetary Science 49, 1720–1733.

Westphal, A.J., Bridges, J.C., Brownlee, D.E., Butterworth, A.L., de Gregorio, B.T., Dominguez, G., Flynn, G.J., Gainsforth, Z., Ishii, H.A., Joswiak, D., Nittler, L.R., Ogliore, R.C., Palma, R., Pepin, R.O., Stephan, T., Zolensky, M.E., 2017. The future of Stardust science. Meteoritics and Planetary Science 52, 1859–1898.

Westphal, A.J., Fakra, S.C., Gainsforth, Z., Marcus, M.A., Ogliore, R.C., Butterworth, A.L., 2009. Mixing fraction of inner solar system material in comet 81P/Wild2. Astrophys. J. 694, 18–28.

Westphal, A.J., Stroud, R.M., Bechtel, H.A., Brenker, F.E., Butterworth, A.L., Flynn, G.J., Frank, D.R., Gainsforth, Z., Hillier, J.K., Postberg, F., Simionovici, A.S., Sterken, V.J., Nittler, L.R., Allen, C., Anderson, D., Ansari, A., Bajt, S., Bastien, R.K., Bassim, N., Bridges, J., Brownlee, D.E., Burchell, M., Burghammer, M., Changela, H., Cloetens, P., Davis, A.M., Doll, R., Floss, C., Grün, E., Heck, P.R., Hoppe, P., Hudson, B., Huth, J., Kearsley, A., King, A.J., Lai, B., Leitner, J., Lemelle, L., Leonard, A., Leroux, H., Lettieri, R., Marchant, W., Ogliore, R., Ong, W.J., Price, M.C., Sandford, S.A., Tresseras, J.-A.S., Schmitz, S., Schoonjans, T., Schreiber, K., Silversmit, G., Solé, V.A., Srama, R., Stadermann, F., Stephan, T., Stodolna, J., Sutton, S., Trieloff, M., Tsou, P., Tyliszczak, T., Vekemans, B., Vincze, L., Von Korff, J., Wordsworth, N., Zevin, D., Zolensky, M.E., 2014a. Evidence for interstellar origin of seven dust particles collected by the Stardust spacecraft. Science 345, 786–791.

Wirick, S., Flynn, G.J., Keller, L.P., Nakamura-Messenger, K., Peltzer, C., Jacobsen, C., Sandford, S., Zolensky, M., 2009. Organic matter from comet 81P/Wild 2, IDPs, and carbonaceous meteorites; similarities and differences. Meteoritics and Planetary Science 44, 1611–1626.

Yen, C.-.W., E. Hirst, E., 1997. Stardust mission design, paper presented at the astrodynamics specialist conference, paper 97-07. Am. Astron. Soc., Sun Valley, Idaho, 4–7 Aug. 1997.

Zolensky, M., Nakamura, K., Weisberg, M.K., Prinz, M., Nakaura, T., Ohsumi, K., Saitow, A., Mukai, M., Gounelle, M., 2003. A primitive dark inclusion with radiation-damaged silicates in the Ningqiang carbonaceous chondrite. Meteoritics and Planetary Science 38, 305–322.

Zolensky, M.E., McSween Jr., H.Y., 1988. Aqueous alteration. In: Kerridge, J.F., Matthews, M. (Eds.), Meteorites and the Early Solar System. Univ. of Arizona Press, Tucson, pp. 114–143.

Zolensky, M.E., Zega, T.J., Yano, H., Wirick, S., Westphal, A.J., Weisberg, M.K., Weber, I., Warren, J.L., Velbel, M.A., Tsuchiyama, A., Tsou, P., Toppani, A., Tomioka, N., Tomeoka, K., Teslich, N., Taheri, M., Susini, J., Stroud, R., Stephan, T., Stadermann, F.J., Snead, C.J., Simon, S.B., Simionovici, A., See, T.H., Robert, F., Rietmeijer, F.J.M., Rao, W., Perronnet, M.C., Papanastassiou, D.A., Okudaira, K., Ohsumi, K., Ohnishi, I., Nakamura-Messenger, K., Nakamura, T., Mostefaoui, S., Mikouchi, T., Meibom, A., Matrajt, G., Marcus, M.A., Leroux, H., Lemelle, L., Le, L., Lanzirotti, A., Langenhorst, F., Krot, A.N., Keller, L.P., Kearsley, A.T., Joswiak, D., Jacob, D., Ishii, H., Harvey, R., Hagiya, K., Grossman, L., Grossman, J.N., Graham, G.A., Gounelle, M., Gillet, P., Genge, M.J., Flynn, G., Ferroir, T., Fallon, S., Ebel, D.S., Dai, Z.R., Cordier, P., Clark, B., Chi, M., Butterworth, A.L., Brownlee, D.E., Bridges, J.C., Brennan, S., Brearley, A., Bradley, J.P., Bleuet, P., Bland, P.A., Bastien, R., 2006. Mineralogy and Petrology of Comet Wild 2 Nucleus Samples. Science 314, 1735–1740.

CHAPTER 5

The Genesis Solar-Wind Mission: first deep-space robotic mission to return to earth

Roger C. Wiens[a], Dan Reisenfeld[a], Amy Jurewicz[b], Don Burnett[c]
[a]Los Alamos National Laboratory, Los Alamos, NM, USA
[b]Arizona State University Center for Meteorite Studies/School of Earth and Space Exploration, c/o Dartmouth College, Department of Earth Sciences, Hanover, NH
[c]Geological and Planetary Sciences, California Institute of Technology, Pasadena, CA

Chapter Outlines

5.1 Introduction and purpose of the Genesis mission

Conceived in the 1990s and executed in the early 2000s, the Genesis mission was a revolutionary extension of earlier concepts in the study of solar-system cosmochemistry. In the 20th century it was argued that, because the sun contains >99 percent of the material in the solar system, its composition represents that of the material from which the planets formed, the original solar nebula. So "solar abundances" became a baseline for understanding the relative compositions of the solar system's planetary bodies. Originally, solar abundances were derived from telescopic observations of absorption lines in the solar spectrum. Later, the primitive carbonaceous-chondrite (C1) meteorite compositions were discovered to have remarkable similarities to the solar abundances obtained telescopically (e.g., Anders, 1971). The ability to analyze these samples in the laboratory provided the potential for more accurate "solar" compositions. In the ensuing decades, cosmochemists tabulated solar abundances based on C1 meteorites for all but

Sample Return Missions
DOI: 10.1016/C2018-0-03374-5

the highly volatile elements (e.g., Anders and Grevesse, 1989). The C1 solar abundances were an improvement over astronomical spectroscopic data but they were skewed by parent-body aqueous alteration that had leached and mobilized some elements (e.g., Bunch and Chang, 1980).

With the advent of the Apollo lunar missions, the opportunity arose to capture solar wind (SW) and return it to Earth for analysis (Signer et al., 1965). The SW Composition experiments (SWC), exposed on the Moon, yielded the first laboratory analyses of solar material. Helium and neon isotope ratios provided the first clue that the Earth had experienced the loss of its primary atmosphere (Geiss et al., 1972), revealing the process of hydrodynamic escape of atmospheres of the terrestrial planets. Unfortunately, the study of SW implanted in the SWC foils was limited to helium, neon, and argon. Analyses of SW in lunar soils and breccias have been carried out mostly for the noble gases, nitrogen, and carbon (e.g., Wieler, 2016). However, these observations left many questions unanswered due to the passage of time and concomitant diffusion of SW, and erosion of collection surfaces, as well as potential addition of indigenous lunar materials.

A SW collection experiment of significantly longer duration using purer substrates without contamination by lunar dust could provide solar abundances of many more elements and isotopes. Work began in the late 1980s with studies to determine whether collector materials of sufficient purity existed to allow precise measurement of minor SW elements (Jurewicz et al., 2003). The second step was to determine whether techniques existed to measure these minute fluences (Burnett et al., 2003). A competing concept was to measure these fluences in space using spacecraft instruments. Several spectrometers were developed and flown on the Advanced Composition Explorer, WIND, and Solar and Heliospheric Observatory (SOHO) missions that could determine SW elemental and isotopic abundances up to iron in the periodic table (Hovestadt et al., 1995; Gloeckler et al., 1995, 1998). However, these instruments were limited in dynamic range and accuracy, falling short of permil (part per thousand) accuracies desired for isotope ratios by an order of magnitude in many cases. These spectrometers did not advance further and so, by the late 1990s, sample return appeared to be the best method to achieve the desired measurement objectives. At that time, NASA was developing a medium-cost line of planetary science missions, above the Explorer class (roughly $100M), but below the New Frontiers (roughly $1B) class of missions. The Genesis mission could fit within this Discovery class of missions.

Although the ultimate goal was to study the solar elemental and isotopic composition with as great an accuracy as possible, specific measurement goals were delineated, given in brief in Table 5.1 (Burnett et al., 2003, 2011, 2019). Solar isotope ratios were ranked as the highest priority, primarily because cosmochemical isotopic compositions are known at parts-per-thousand levels or better, whereas relative elemental compositions are generally known at the percent levels. Astronomical observations of solar absorption lines for isotope ratios are significantly more difficult than for elemental abundances in comparison to the accuracies obtained for each in meteoritic material.

Table 5.1 Prioritized solar-wind measurement objectives for the Genesis mission.

Priority	Objective*
1	O Isotopes
2	N Isotopes in Bulk Solar Wind
3	Noble Gas Elements and Isotopes
4	Noble Gas Elements and Isotopes in Different Regimes
5	C Isotopes
6	C Isotopes in Different Regimes
7	Mg, Ca, Ti, Cr, Ba Isotopes
8	Mass 80–100 and 120–140 Elemental Abundance Patterns
9	Survey of Solar-Terrestrial Isotopic Differences
10	Noble Gas and N, Elements and Isotopes for Higher Energy Solar Particles
11	Li, Be, B Elemental and Isotopic Abundances
12	F Abundance
13	Pt-Group Elemental Abundances
14	Key S-Process Heavy Elements
15	Heavy-Light Element Comparisons
16	Solar Rare Earth Element Abundance Pattern
17	Comparison of Solar and Chondritic Elemental Abundances
18	Radioactive Nuclei in the Solar Wind

*Measurement of bulk solar wind except where noted.

The isotopic ratios of many non-volatile elements are observed to be constant across various meteorite classes as well as the measured planetary bodies: the Moon, Earth, Mars, and other parent bodies sampled by meteorites. However, this was not the case for volatile elements including the noble gases, oxygen, nitrogen, and carbon. These appear to show telltale clues to the formation of the planets and the evolution of the solar nebula. Oxygen in particular showed enrichments of pure ^{16}O in calcium-aluminum inclusions (CAIs)—the most primitive objects in the solar system (e.g., Clayton et al., 1973). Differentiated bodies, represented by meteorites from Mars, Vesta, and several other classes of differentiated meteorites, also show small but significant differences in their bulk ^{16}O abundances (e.g., Clayton, 2003). Researchers widely believed that these heterogeneities, if understood relative to the average solar-system oxygen isotopic composition, would provide a significant clue to the conditions in the early solar nebula (e.g., Wiens et al., 1999).

Nitrogen and carbon isotopic systems, while showing significant heterogeneity among solar-system objects and lunar samples, are not as understandable in terms of the source and nature of these heterogeneities (e.g., Wieler, 2016), in part due to the fact that each of these elements possess only two stable isotopes, which do not allow distinction between mass-dependent and other types of fractionation.

Among the noble gases from measured solar-system objects, several components could be deduced. Relative consistency between lunar-regolith samples, the Apollo SWC experiments (e.g., Geiss et al., 1972), and gas-rich meteorites showing a solar component provided some confidence in understanding the major planetary noble gas components (e.g., Ozima et al., 1998). However, more precise values for SW isotopic and elemental noble gas abundances were needed for more accurate modeling of hydrodynamic escape of planetary atmospheres (e.g., Lillis et al., 2015).

Beyond these solar isotope-ratio measurement goals, the list of measurement objectives for Genesis (Table 5.1) included a range of solar-physics, space-plasma, and cosmochemical objectives, all of which were related to obtaining the solar composition at an accuracy needed to address a number of cosmochemical mysteries. One fascinating cosmochemical question was whether the Sun accreted solid-forming elements and volatile elements without preference, which could be tested against theoretical slow neutron-capture-process (s-process; Burbidge et al., 1957) nuclide production rates in certain atomic mass regimes (Wiens et al., 1991). To probe the processes behind the formation and acceleration of the SW from the Sun, mission objectives included measuring abundances of elements and isotopes in different SW regimes. This required in-situ determination of these regimes based on plasma velocity, density, and direction in real time, and deployment of separate collectors for each regime.

5.2 Mission and spacecraft design

The fundamental constraints for a SW sample return mission are that: a) it must collect a sufficient amount of SW outside the Earth's magnetosphere, and b) it must return these samples to Earth. To address the question of "how much is enough?", the mission team had to balance mission constraints against measurement necessities. The Apollo SW collection durations were up to ~48 h (Geiss et al., 1972). A dedicated mission should collect at least several orders of magnitude more. However, an excessively long mission (by the standards of the time) would increase the risk of failure during flight as well as the risk to mission selection, as the NASA leadership of that era expected a rapid return on its investment. The team decided on a > 2-year collection, resulting in a mission duration of just over 3 years.

In terms of mission design, the experiment had already been studied as part of a Mars or lunar sample-return mission. However, once the Discovery-class missions were established, a relatively logical trajectory for an independent SW return mission became clear: The metastable Earth-Sun L1 point is a very easy point from which to return, and in fact, Earth return could be initiated easily every six months. The spacecraft would always be relatively close to Earth (compared to some heliocentric trajectories), facilitating communications, while the Earth's magnetotail would not interfere with SW collection. The Genesis trajectory is shown in Fig. 5.1.

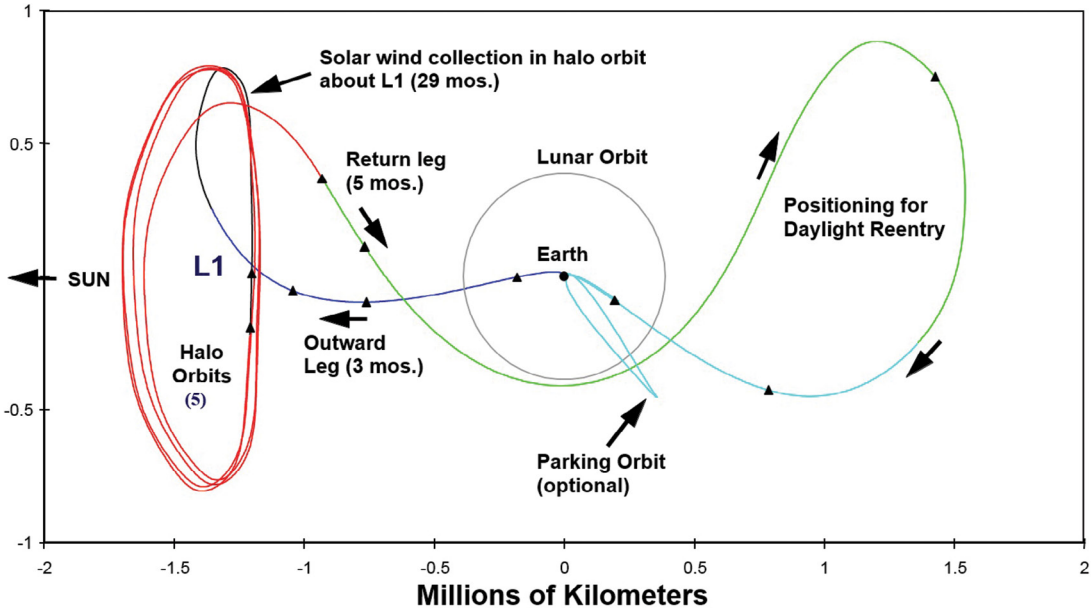

Fig. 5.1 ***The Genesis spacecraft trajectory shown in an Earth-Sun reference frame from above the ecliptic.*** The x-axis represents distance sunward or anti-sunward of the Earth; the y-axis represents distance forward or behind a line connecting the Earth and Sun. The outbound phase is shown in blue, the science collection phase is shown in red, and the return phase in green. The lunar orbit is shown for reference; the Moon did not play a significant role in the trajectory. The optional parking orbit (cyan) was considered in case of inclement weather at the time of return, but was not used. (NASA/JPL-Caltech.)

The spacecraft's design focused on the return capsule (Fig. 5.2). The goal was to return as much material as possible within the size and weight constraints of the Discovery-class mission. A 1.62 m diameter, 210 kg capsule fit easily within the Delta II 7326 rocket's payload faring. The capsule was encased in carbon-carbon heat shielding and a silicone-based ablative material (SLA-561). A hinged clamshell mechanism allowed the capsule to open for SW collection. The spacecraft was spin stabilized.

Inside the capsule, a canister housed most of the SW collectors, acting as a contamination barrier. The canister opened as a clamshell to expose ultrapure collection substrates to the SW (Fig. 5.2). A stack of four collector arrays were designed to collect three different SW regimes (low-speed or interstream wind, high-speed or coronal-hole wind, and coronal mass ejections; e.g., Neugebauer, 1991). The top array in the stack was exposed at all times, for collection of "bulk" SW. Each regime array rotated out from under the bulk collector array while conditions were right for collecting its respective type of SW.

Another important instrument resided inside the canister: the SW Concentrator (Fig. 5.2). It was a 40 cm diameter aperture reflecting ion telescope that concentrated, by an average factor of >20x, SW ions of oxygen and some heavier elements, focusing them onto a 28 mm diameter target (Nordholt et al., 2003; Wiens et al., 2003; Wiens et al., 2013).

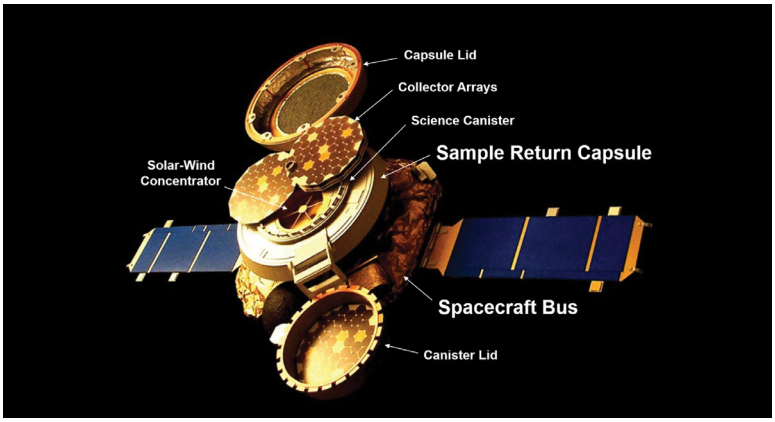

Fig. 5.2 ***Genesis spacecraft, shown in its science collection configuration.*** Sample collectors were exposed in the capsule lid, the science canister lid, and on four retractable arrays. The SW concentrator was also housed in the science canister. (NASA)

The SW collection substrates consisted mostly of hexagons fabricated from 100 mm diameter wafers of high-purity silicon, sapphire, aluminum on sapphire, silicon on sapphire, and diamond-like carbon, as well as other materials (Jurewicz et al., 2003). The Concentrator target consisted of SiC, diamond-like carbon, and ^{13}C labeled synthetic diamond (Nordholt et al., 2003).

These materials were selected for both purity and analyzability by the most sensitive analytical techniques including secondary ion mass spectrometry (SIMS), resonance ionization mass spectrometry (RIMS), noble gas mass spectrometry, and various nuclear techniques. SW fluxes for elements other than hydrogen and helium are extremely low, for example at ~2.5e5 oxygen ions/cm^2/s (Burnett et al., 2003), which necessitated the long exposure, the high purity of the collector materials, spacecraft measures to minimize surface contamination, and, in the case of some elements, the use of the Concentrator.

Two other instruments were mounted on the spacecraft bus outside the capsule: the Genesis Ion Monitor (GIM) and Genesis Electron Monitor (GEM; Barraclough et al., 2003). With use of an onboard algorithm (Neugebauer et al., 2003; Reisenfeld et al., 2013), these instruments determined the SW regime in real time based on speed, temperature, He/H, and electron directionality. The collector arrays were deployed based on the determination of regime, and the Concentrator voltages were optimized based on speed and plasma temperature.

5.3 Mission, re-entry, and recovery

The Genesis spacecraft was launched on August 8, 2001. It reached the L1 region and deployed its SW collectors on November 30, 2001. Two issues occurred during the

mission that ultimately had minimal effect, though they were concerns at the time. During turn-on, the SW Concentrator's proton-rejection grid (Nordholt et al., 2003) could not achieve its maximal electrical potential. This grid was to prevent excessive hydrogen fluence to the target, which would potentially cause diffusive loss of the elements of interest. The grid potential was to be adjusted between 0.5 and 3.5 kV in real time based on SW speed. Since the highest potential was rarely needed, a new algorithm was developed and uploaded to allow rejection of >85 percent of the protons, sufficient to maintain the integrity of the SW collectors. Another issue encountered during flight was the failure of a thermal paint designed to radiate heat when the capsule was open. The capsule's thermal design was challenging due to the insulating nature of the heat shield at the rear (shadowed side) of the capsule and the exposure of bare metal surfaces to collect SW on the sunward side. To balance this, white paint was applied around the science canister on the inside of the capsule. However, it did not perform as anticipated, resulting in interior capsule temperatures of >65 °C. The primary concern was the re-entry system's battery, precipitating a rapid program to test similar batteries to failure. The capsule battery's temperature near the end of the science collection phase still had ~10 °C of margin.

The Genesis collection phase coincided with the declining phase of the solar cycle. This period was more active than expected, resulting in Genesis collecting a significantly larger fraction of coronal hole (CH) SW than predicted (Reisenfeld et al., 2013). This was a boon to the analysis, as the CH material is the least fractionated relative to the solar composition. A solar storm in October 2003 caused Genesis to go into safe mode for 11 days, representing the only relatively long period without active collection, although the bulk collectors were still exposed during this time.

The return phase began with successful stowing of the collectors and closing of the capsule on April 1, 2004. Re-entry and landing were desired to occur on the sunlit side of the Earth, and so an Earth swing-by and a pass near the L2 point was needed (Fig. 5.1). The return to Earth was uneventful up to the landing itself, which occurred on September 8, 2004 at the Utah Test and Training Range (UTTR). The capsule was released several hours before entry, giving time for the spacecraft bus to divert to avoid Earth. The capsule was equipped with accelerometers to sense deceleration, initiating a timer that would deploy a drogue chute and then a subsonic parafoil. Due to the fragile nature of the collectors, helicopters were deployed to capture the capsule in mid-air as it descended. Unfortunately, the accelerometers had been installed upside down (Genesis Mishap Investigation Board Report, 2006) and so the parachutes never deployed. The capsule landed at ~310 km/hr on its side in a slightly wet portion of the Utah salt flats. A popular account of the landing is given in Wiens (2013).

As soon as the area around the sample return capsule was deemed to be safe, the science canister containing the samples was removed from the damaged capsule and lifted onto a tarp. It was transported to a temporary clean room in a UTTR facility, which

had been set up to receive the returned capsule (Zeigler and Modders, 2016). Damaged collector arrays and individual collector pieces were carefully photographed, inventoried and then prepared for transport to Johnson Space Center (JSC). The crash caused most of the passive collector substrates to shatter; only one intact wafer survived. Many small fragments that were loosely attached to the wreckage fell onto the tarp during transport of the canister to the clean room. Many of these were put on the sticky side of post-its or into plastic (biological) well plates and then packed with bits of clean-room cloth to keep them from moving and scratching during transport. Once at JSC, it took approximately four weeks to archive all spacecraft and collector materials that were found at the landing site, as well as samples of the UTTR dirt for comparison. Thankfully, wafers from the different collector arrays each have a characteristic thickness, so they could be identified and categorized after the crash according to the solar-wind regime to which they were exposed. Of the >10,000 fragments, many are useable for SW composition analysis, aided by the fact that most of the analytical techniques require relatively small surface areas. However, techniques requiring large surface areas (e.g., radiochemical neutron activation) are no longer viable.

Curation of the samples is ongoing at the NASA Astromaterials Research and Exploration Science Division at Johnson Space Center. Solar-Wind Concentrator targets were mostly intact in spite of the crash. Only a few important measurements have been made on the Concentrator targets, so most of that material remains. Passive collector materials of several millimeters diameter are available for analyses, with bulk SW samples being more plentiful than regime substrates.

5.4 Results and scientific discoveries

5.4.1 Isotopic compositions

5.4.1.1 Oxygen and nitrogen

Analysis of oxygen isotopes from the Genesis Concentrator required unique efforts. These included the construction and characterization of a dedicated instrument, the "Mega-SIMS," a hybrid SIMS and accelerator mass spectrometer, which was required to separate OH and H_2O interferences from ^{17}O and ^{18}O (Mao et al., 2008). For SIMS analyses of typical oxygen abundances, these interferences can be small and well constrained. However, for nanomoles of SW oxygen and desired precision of a fraction of a percent, the dedicated system was necessary. Another dedicated effort was the characterization of instrumental fractionation of the SW Concentrator. In addition to modeling (Wiens et al., 2003; 2013), SW neon isotopes from specific (sub-mm) locations on the Concentrator target facilitated this correction (Heber et al., 2007, 2011).

The SW oxygen isotopic results are summarized in Fig. 5.3 (McKeegan et al., 2011). As mentioned earlier, solar-system objects are characterized by a diversity of oxygen

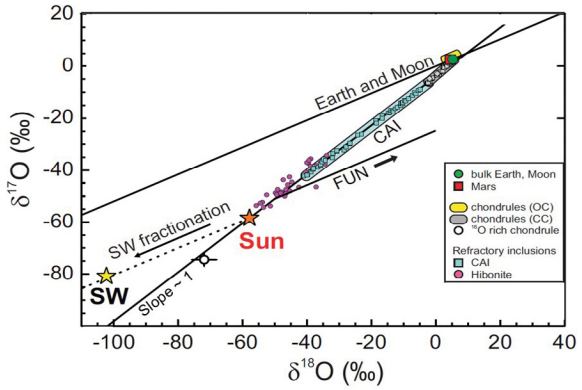

Fig. 5.3 ***SW oxygen isotopic composition measured in the Genesis Concentrator targets and the inferred solar composition relative to the Earth, Moon, and other materials (after McKeegan et al., 2011).*** Axes represent deviations of $^{18}O/^{16}O$ and $^{17}O/^{16}O$ relative to standard mean ocean water (SMOW) in parts per thousand. The yellow and orange stars identify the solar-wind and solar oxygen isotopic compositions, respectively. Fractionation occurring during formation and acceleration of the SW results in a difference between solar and SW compositions. Most known solar-system materials, including the Earth, Moon, Mars, and ordinary chondrites, are enriched equally in ^{17}O and ^{18}O relative to the Sun. Some primitive solar-system materials including calcium-aluminum inclusions (CAIs), hibonite, and chondrules from carbonaceous chondrites lie along a line of equal ^{17}O and ^{18}O enrichment from the Sun, trending toward the terrestrial composition. Some primitive materials experienced fractionation and unidentified nuclear (FUN) effects, causing them to trend to the right of the Earth-Sun line.

isotopic compositions, usually plotted as $^{18}O/^{16}O$ and $^{17}O/^{16}O$ deviations in parts per thousand (permil, ‰) from standard mean ocean water. On this plot, mass-dependent fractionations occurring in most chemical and kinetic reactions plot along a curve approximated by a slope of one-half (e.g., "Earth and Moon" line). Bulk Mars and ordinary chondrites are close to bulk Earth on this plot, though in detail they are clearly distinct. By contrast, refractory inclusions in carbonaceous chondrites display a trend along a slope-one line intersecting near the bulk Earth composition and extending upward to other refractory materials (not shown). Individual CAI compositions are plotted along with hibonite compositions (McKeegan et al., 2011, and references therein).

The mean Genesis-derived SW composition, after correction for Concentrator and SIMS fractionations, is shown in Fig. 5.3 as the yellow star labeled "SW". Correction for isotopic fractionation of the SW relative to the Sun, and for gravitational settling within the Sun over 4.5 Ga, are relatively uncertain but are approximately of the magnitude that would result in the ancient solar composition near the slope-one line ("Sun"). This suggests that the inner solar system— the materials above and to the right along the slope-one line in Fig. 5.3, including bulk Earth, Moon, Mars, and other bodies sampled so far—experienced an enrichment of equal fractions of ^{17}O and ^{18}O relative to the Sun and the solar nebula.

The $^{17,18}O$-enriched composition of the terrestrial planets is consistent with a photochemical self-shielding hypothesis (e.g., Clayton, 2003) in which carbon monoxide—the dominant O-carrying gas in the nebula—is dissociated by solar ultraviolet photons during its active T-Tauri phase. Wavelengths specific to $C^{16}O$ dissociation were extinguished relatively near the Sun by this reaction, leaving $C^{16}O$ unaffected at greater distances. $C^{18}O$ and $C^{17}O$ are ~ 500 and 2500 times less abundant, respectively, and so the wavelengths specific to their dissociation were not extinguished. The result was a region of the solar system, supposedly corresponding to the distances of the terrestrial planets and an unknown distance beyond them, in which $C^{17}O$ and $C^{18}O$ were readily dissociated while $C^{16}O$ was not. The heavy atomic oxygen was free to bind with hydrogen and adsorb to dust grains that eventually formed the terrestrial planets.

The SW nitrogen isotopic composition was measured in a somewhat similar way to that of oxygen, using the Genesis Concentrator target. In this case, a conventional SIMS instrument was able to make the measurement, observing a SW $^{15}N/^{14}N$ ratio of $2.18.10^{-3}$, and implying a nascent solar composition that is ~ 383‰ depleted in ^{15}N relative to the terrestrial atmosphere (Marty et al., 2011). While other explanations are possible, this result is also consistent with photochemical self-shielding in the early solar system. The reason for the stronger fractionation of nitrogen relative to oxygen has been suggested to be due to the difference in chemical reactivity between atomic O and N following vacuum ultraviolet photodissociation from CO and N_2, respectively (Shi et al., 2017).

5.4.1.2 Noble gases

Noble gas measurements of Genesis SW samples provided two important results: a) repudiation of the existence of a postulated second, higher-energy implanted component along with SW in lunar regolith samples, and b) improved accuracy of isotopic and elemental abundances. Extraction of noble gases from lunar samples has been typically performed by step-wise heating of the samples in a closed system. Observations of isotopically heavier releases at higher temperatures were postulated to represent a more deeply-implanted (e.g., higher-energy) solar component (e.g., Benkert et al., 1993) although observations by spacecraft instruments indicate that the flux of high-energy particles is currently orders of magnitude lower than would be required to explain these observations. The Genesis mission flew a dedicated substrate to test this observation: a "bulk metallic glass" was intended to simulate the lunar materials. Stepped heat-extraction experiments of this sample showed a progression toward isotopically heavier releases, just as in the lunar samples. Modeling of the results showed that diffusion induced by stepped heating results in this pattern of increasingly heavy isotopic releases from a single implanted component, e.g., normal SW (Grimberg et al., 2006), obviating the need to invoke a separate high-energy component.

Genesis sample measurements have improved the accuracy of SW noble gas compositions. There is excellent agreement between three laboratories on nearly all of the noble gas measurements (Meshik et al., 2014). Key compositional measurements for bulk SW include $^{3}He/^{4}He = (4.64\pm0.09) \bullet 10^{-4}$, $^{20}Ne/^{22}Ne = 13.78 \pm 0.03$, $^{21}Ne/^{22}Ne = 0.0329 \pm 0.0001$ (Heber et al., 2009), $^{36}Ar/^{38}Ar = 5.5005 \pm 0.0040$, $^{86}Kr/^{84}Kr = 0.3012 \pm 0.0004$, $^{129}Xe/^{132}Xe = 1.0405 \pm 0.0010$ (Meshik et al., 2014; see also Crowther and Gilmour; 2013), and $^{4}He/^{20}Ne/^{36}Ar/^{84}Kr/^{132}Xe = (656\pm5)/(42.1 \pm 0.3)/(2390\pm120)/(9.9 \pm 0.3)$ (Heber et al., 2009; Vogel et al., 2011). These values provide an accurate contemporary record of SW flux for comparison with lunar regolith samples that were exposed in different epochs (Wieler, 2016). No significant changes are observed in SW flux or composition over the last several hundred million years (Vogel et al., 2011; Meshik et al., 2014). However, for more ancient lunar soils, Vogel et al. (2011) and Wieler (2016) suggest the Kr/Xe ratio is up to a factor of two lower for unknown reasons.

Isotopes of He, Ne, and Ar from different SW regime samples provide constraints for SW acceleration models. Heber et al. (2012) observed heavy isotope depletion in the slow SW relative to the fast wind, of 63.1 ± 2.1‰ for He, 4.2 ± 0.5‰ for Ne, and 2.6 ± 0.5‰ for Ar. Previous SW acceleration models did not model mass-dependent fractionation due to the dominance of fractionation by atomic properties, especially first ionization potential (FIP), as will be discussed below. However, the recent observation of isotopic and elemental (Pilleri et al., 2015) fractionation by mass has led to new theories (e.g., Laming, 2015, Laming et al., 2017) that use recently reported mass-dependent variations.

5.4.1.3 Other isotopes

Efforts have focused on quantifying isotopic differences between SW regimes relative to terrestrial Mg (Jurewicz et al., 2020) as a way to constrain SW acceleration theories. The advantage for Mg is that the inner solar system's Mg isotopic composition is homogeneous and very well defined, providing an excellent baseline with which to compare the SW composition.

Other isotopic measurements that will likely be made in the near future include carbon and iron. The iron isotopic composition, like that of Mg, could be used to constrain theories of SW acceleration. The carbon isotopic composition could be more interesting, as carbon was present in both solid and gaseous phases in the early solar nebula, and so it may be another element to display symptoms of photochemical self-shielding. Like nitrogen, carbon has only two stable isotopes, so it is more difficult than oxygen to decipher the origins of isotopic differences. Carbon analyses must be done on unconcentrated SW samples, as the Concentrator targets all contain carbon. Finally, one other element that might be analyzed for isotopic composition is sulfur. The Concentrator targets might be used for sulfur, but with its higher mass-to-charge, it is on the margin of elements for which it can be used (Wiens et al., 2013).

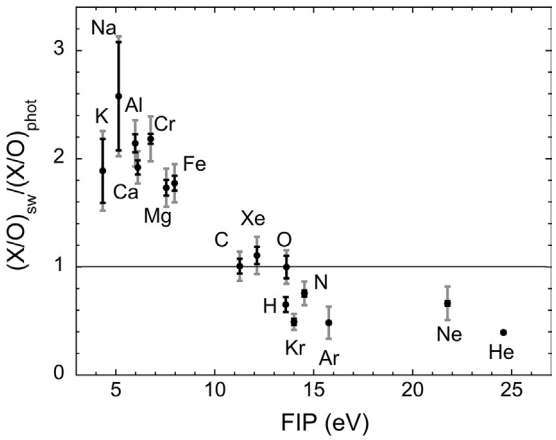

Fig. 5.4 ***Solar wind abundances from Genesis bulk sample analyses, ratioed to photospheric abundances of Asplund et al. (2009) and Scott et al. (2015a, 2015b).*** Species are normalized to oxygen. Black error bars give uncertainty in Genesis measurement; grey error bars give uncertainties in photospheric abundances. The Genesis results are K and Na, Rieck et al. (2016); Ca, Al and Cr, Heber et al. (2014); Fe and Mg, Jurewicz et al. (2011); C, N and O, Heber et al. (2013); Kr and Xe, Meshik et al. (2014); and H, Koeman-Shields et al. (2016).

5.4.2 Elemental compositions

Most, if not all, elements observed in the SW are fractionated relative to their solar abundance. The degree of fractionation depends on a number of factors, but appears to be primarily governed by the so-called first ionization potential, or FIP, effect. The prevailing models for SW acceleration all require particles to be ionized before entrainment in the SW. In the Sun's chromosphere, at the base of the corona, the atmosphere is only partially ionized, but as particles diffuse upward and the density falls, the ionization fraction increases as photo-ionization dominates over recombination. Since low-FIP elements have a higher ionization fraction than high-FIP elements, low-FIP elements are more readily accelerated and are more abundant in the SW.

SW elemental abundances derived from the Genesis samples are more tightly constrained than abundance measurements performed in situ by SW instruments; thus, they have more accurately documented the FIP effect. SW elemental abundances determined by Genesis for bulk SW are plotted as a function of FIP in Fig. 5.4. To illustrate SW fractionation, the SW abundances are plotted relative to photospheric abundances estimated either from photospheric absorption lines (low- and intermediate-FIP elements) or coronal abundances (high-FIP elements) (Asplund et al., 2009; Scott et al., 2015a, 2015b). The figure clearly shows the FIP effect: low-FIP elements cluster at a fractionation value of around two, whereas intermediate-FIP elements are generally around one, where oxygen is used for normalization. All of the noble gases except xenon are depleted, closer to 0.5, while nitrogen is intermediate. Black error bars give

uncertainties in the Genesis measurements; grey error bars give uncertainties in photospheric abundances. The fractional uncertainties in Genesis sample measurements range from 2 percent for Ca to 20 percent for Na.

It is clear from Fig. 5.4 that FIP alone cannot explain SW elemental fractionation, as even elements with very similar FIP show statistically meaningful differences. A deeper look reveals that elemental abundances vary with SW speed and with phase of the solar cycle (Lepri et al., 2013; Pilleri et al., 2015; Heidrich-Meisner et al., 2018). As mentioned above, Pilleri et al. report that there may be a secondary mass-dependent effect that affects how abundances vary with SW speed. Currently there is an effort to analyze Genesis regime-specific samples for elements other than the noble gases, such as C, N, and O, to better constrain the mass dependent effect (Rieck et al., 2019).

A goal of the Genesis elemental analysis effort is to provide better constraints on SW acceleration theory. The hope is to advance theory to the point where solar elemental abundances can be derived from SW abundances, particularly for the elements that are too sparse to be measured by in situ spacecraft. One very promising type of theory suggests that the "ponderomotive force" acting in the lower corona is primarily responsible for SW acceleration (Laming, 2015). The ponderomotive force is a second-order mechanism that arises from magnetic wave reflections at the top of the chromosphere where the density falls precipitously. This force acts to accelerate ions toward regions of increased wave activity. Thus, the higher intensity magnetic field waves present in the corona results in ionized particles being accelerated upward from the chromosphere into the corona. Genesis elemental abundances have recently been used to help constrain this model (Laming et al., 2017).

5.5 Conclusions

True to its name, the Genesis mission provided key cosmochemical clues to the conditions present at the beginning of the solar system. As a multidisciplinary mission, its results have also yielded important details for solar physics and for the study of SW generation and acceleration.

Not all the goals of Table 5.1 are fulfilled, and a number of these studies are still in progress or expected shortly (Burnett et al., 2019). These include attempts to understand solid-gas fractionation in the solar nebula (e.g., Wiens et al., 1991), solar-wind carbon isotopic composition, and extension of isotopic results to other elements such as iron.

The Genesis mission speaks to the resiliency of sample return missions: despite the crash landing, much of the science proposed for the mission has been accomplished. The mission continues to provide new results as the analytical techniques advance.

Acknowledgements

Support by NASAs office for Laboratory Analysis of Returned Samples (LARS) through grants NNH15AZ67I and NNH17ZDA001N is gratefully acknowledged. We thank the many people over the years who made the Genesis mission a success SDG.

Permissions

Fig. 5.1 is public domain, credited to NASA/JPL-Caltech, although it was also used in Burnett et al., 2003. Permission has been granted from Springer.

Fig. 5.2 is public domain, credited to NASA

Fig. 5.3 is after McKeegan et al., 2011. Permission from AAAS has been registered.

Fig. 5.4 is original.

References

Anders, E., 1971. How well do we know "cosmic" abundances?. Geochim. Cosmochim. Acta 35, 516–522.

Anders, E., Grevesse, N., 1989. Abundances of the elements: meteoritic and solar. Geochim. Cosmochim. Acta 53, 197–214.

Asplund, M., Grevesse, N., Sauval, A.J., Scott, P., 2009. The chemical composition of the sun. Ann. Rev. Astron. Astrophys 47, 481–522. doi:10.1146/annurev.astro.46.060407.145222.

Barraclough, B.L., Dors, E.E., Abeyta, R.A., Alexander, J.F., Ameduri, F.P., Baldonado, J.R., Bame, S.J., Casey, P.J., Dirks, G., Everett, D.T., Gosling, J.T., Grace, K.M., Guerrero, D.R., Kolar, J.D., Kroesche Jr, J.L., Lockhart, W.L., McComas, D.J., Mietz, D.E., Roese, J., Sanders, J., Steinberg, J., Tokar, R.L., Urdiales, C., Wiens, R.C., 2003. Genesis electron and ion spectrometers. Spa. Sci. Rev. 105, 627–660.

Benkert, J.-P., Baur, H., Signer, P., Wieler, R., 1993. He, Ne, and Ar from the solar wind and solar energetic particles in lunar ilmenites and pyroxenes. J. Geophys. Res. 98, 13147–13162.

Bunch, T.E., Chang, S., 1980. Carbonaceous chondrites—II. Carbonaceous chondrite phyllosilicates and light element geochemistry as indicators of parent body processes and surface conditions. Geochim. Cosmochim. Acta 44, 1543–1577.

Burbidge, E.M., Burbidge, G.R., Fowler, W.A., Hoyle, F., 1957. Synthesis of the elements in stars. Rev. Modern Phys. 29, 548–650.

Burnett, D.S., 2011. Solar composition from the Genesis discovery mission. Proc. Nat. Acad. Sci 108, 19147–19151. doi:10.1073/pnas.1014877108.

Burnett, D.S., Barraclough, B.L., Bennett, R., Neugebauer, M., Oldham, L.P., Sasaki, C.N., Sasaki, C.N., Sevilla, D., Smith, N., Stansbery, E., Sweetnam, D., Wiens, R.C., 2003. The Genesis Discovery Mission: return of solar matter to earth. Spa. Sci. Rev. 105, 509–534.

Burnett, D.S., Jurewicz, A.J.G., Woolum, D.S., 2019. The future of Genesis science. Met. Planet. Sci. doi:10.1111/maps.13266.

Clayton, R.N., 2003. Oxygen isotopes in the solar system. Spa. Sci. Rev. 106, 19–32.

Clayton, R.N., Grossman, L., Mayeda, T., 1973. A component of primitive nuclear composition in carbonaceous meteorites. Science 182, 485–488.

Crowther, S.A., Gilmour, J.D., 2013. The Genesis solar xenon composition and its relationship to planetary xenon signatures. Geochim. Cosmochim. Acta 123, 17–34.

Geiss, J., Buehler, F., Cerutti, H., Eberhardt, P., Filleux, C., 1972. Solar Wind Composition Experiment. Apollo 16 Prelim. Sci. Rep., NASA SP-315, 1–14.

Genesis Mishap Investigation Board Report, 2006. https://ntrs.nasa.gov/search.jsp?R=20060008607.

Gloeckler, G., Balsiger, H., Bürgi, A., Bochsler, P., Fisk, L.A., Galvin, A.B., Geiss, J., Gliem, F., Hamilton, D.C., Holzer, T.E., Hovestadt, D., Ipavich, F.M., Kirsch, E., Lundgren, R.A., Ogilvie, K.W., Sheldon,

R.B., Wilken, B., 1995. The solar wind and suprathermal ion composition investigation on the WIND spacecraft, Spa. Sci. Rev. 71, 79–124.

Gloeckler, G., Cain, J., Ipavich, F.M., Tums, E.O., Bedini, P., Fisk, L.A., Zurbuchen, T., Bochsler, P., Fischer, J., Wimmer-Schweingruber, R.F., Geiss, J., Kallenbach, R., 1998. Investigation of the composition of solar and interstellar matter using solar wind and pickup ion measurements with SWICS and SWIMS on the ACE spacecraft, Spa. Sci. Rev. 86, 497–539.

Grimberg, A., Baur, H., Bochsler, P., Buehler, F., Burnett, D.S., Hays, C.C., Heber, V.S., Jurewicz, A.J.G., Wieler, R., 2006. Solar wind neon from Genesis: implications for the lunar noble gas record. Science 314, 1133–1135.

Heber, V.S., Baur, H., Bochsler, P., McKeegan, K.D., Neugebauer, M., Reisenfeld, D.B., Wieler, R., Wiens, R.C., 2012. Isotopic mass fractionation of solar wind: evidence from fast and slow solar wind collected by the Genesis mission. Astrophys. J. 759, 121. doi:10.1088/0004-637X/759/2/121.

Heber, V.S., Burnett, D.S., Duprat, J., Guan, Y., Jurewicz, A.J.G., Marty, B., McKeegan, K.D., 2013. Carbon, nitrogen, and oxygen abundances in the bulk solar wind and calibration of absolute abundances. Lunar Planet. Sci. XXXXIV, 2540.

Heber, V.S., McKeegan, K.D., Smith, S., Jurewicz, A.J.G., Olinger, C., Burnett, D.S., Guan, Y., 2014. Accurate analysis of shallow solar wind ion implants by SIM backside depth profiling. Lunar Planet. Sci. XXXXV, 1203.

Heber, V.S., Wieler, R., Baur, H., Olinger, C., Friedmann, T.A., Burnett, D.S., 2009. Noble gas composition of the solar wind as collected by the Genesis mission. Geochim. Cosmochim. Acta 73, 7414–7432.

Heber, V.S., Wiens, R.C., Jurewicz, A.J.G., Vogel, N., Baur, H., McKeegan, K., Wieler, R., Burnett, D.S., 2011. Genesis concentrator target: isotopic and elemental fractionation of implanted solar wind characterized and quantified by noble gases. Met. Planet. Sci. doi:10.1111/j.1945-5100.2011.01170.x.

Heber, V.S., Wiens, R.C., Reisenfeld, D.B., Allton, J.H., Baur, H., Burnett, D.S., Olinger, C., Wiechert, U., Wieler, R., 2007. The Genesis solar wind Concentrator target: mass fractionation characterised by Ne isotopes. Spa. Sci. Rev 130, 309–316. doi:10.1007/s11214-007-9179-1.

Heidrich-Meisner, V., Berger, L., Wimmer-Schweingruber, R.F., 2018. Disparity among low first ionization potential elements. Astron. & Astrophys. A79, 619. doi:10.1051/0004-6361/201833454.

Hovestadt, D., Hilchenbach, M., Bürgi, A., Klecker, B., Laeverenz, P., Scholer, M., Grünwaldt, H., Axford, W.I., Livi, S., Marsch, E., Wilken, B., Winterhoff, H.P., Ipavich, F.M., Bedini, P., Coplan, M.A., Galvin, A.B., Gloeckler, G., Bochsler, P., Balsiger, H., Fischer, J., Geiss, J., Kallenbach, R., Wurz, P., Reiche, K.-U., Gliem, F., Judge, D.L., Ogawa, H.S., Hsieh, K.C., Mobius, E., Lee, M.A., Managadze, G.G., Verigin, M.I., Neugebauer, M., 1995. CELIAS – Charge, element and isotope analysis system for SOHO. Solar Phys 162, 441–481.

Jurewicz, A.J.G., Burnett, D.S., Wiens, R.C., Friedmann, T.A., Hays, C.C., Hohlfelder, R.J., Nishiizumi, K., Stone, J.A., Woolum, D.S., Becker, R., Butterworth, A.L., Campbell, A.J., Ebihara, M., Franchi, I.A., Heber, V., Hohenberg, C.M., Humayun, M., McKeegan, K.D., McNamara, K., Meshik, A., Pepin, R.O., Schlutter, D., Wieler, R., 2003. The Genesis solar-wind collector materials. Spa. Sci. Rev 105, 535–560.

Jurewicz, A.J.G., Burnett, D.S., Woolum, D.S., McKeegan, K.D., Heber, V., Guan, Y., Humayun, M., Hervig, R., 2011. Solar-wind Fe/Mg and a comparison with CI chondrites. Lunar Planet. Sci. XXXXII, 1917.

Jurewicz, A.J.G., Rieck, K.D., Hervig, R., Burnett, D.S., Wadhwa, M., Olinger, C.T., Wiens, R.C., Laming, J.M., Guan, Y., Huss, G.R., Reisenfeld, D.B., Williams, P., 2020. Magnesium isotopes of the bulk solar wind from Genesis diamond-like carbon films. Met. Planet. Sci 55, 352–375. doi:10.1111/maps.13439.

Koeman-Shields, E.C., Huss, G.R., Ogliore, R.C., Jurewicz, A.J.G., Burnett, D.S., Nagashiima, K., Olinger, C.T., 2016. Hydrogen fluence calculated from Genesis collectors. Lunar Planet. Sci. XXXXVII, 2800.

Laming, J.M., 2015. The FIP and inverse FIP effects in solar wind stellar coronae. Living Rev. Sol. Phys. 12, 2. doi:10.1007/lrsp-2015-2.

Laming, J.M., Heber, V.S., Burnett, D.S., Guan, Y., Hervig, R., Huss, G.R., Jurewicz, A.J.G., Koeman-Shields, E.C., McKeegan, K.D., Nittler, L.R., Reisenfeld, D.B., Rieck, K.D., Wang, J., Wiens, R.C., Woolum, D.S., 2017. Determining the elemental and isotopic composition of the pre-solar nebula from Genesis data analysis: the case of oxygen. Astrophys. J. Lett. 85. doi:10.3847/2041-8213/aa9bf0.

Lepri, S.T., Landi, E., Zurbuchen, T.H., 2013. Solar wind heavy ions over solar cycle 23: ACE/SWICS measurements. Astrophys. J., 768. doi:10.1088/0004-637X/768/1/94.

Lillis, R.J., Brain, D.A., Bougher, S.W., Leblanc, F., Luhmann, J.G., Jakosky, B.M., Modolo, R., Fox, J., Deighan, J., Fang, X., Wang, Y.C., Lee, Y., Ma Dong, Y., Cravens, T., Andersson, L., Curry, S.M.,

Schneider, N., Combi, M., Stewart, I., Clarke, J., Grebowsky, J., Mitchell, D.L., Yelle, R., Nagy, A.F., Baker, D., Lin, R.P., 2015. Characterizing atmospheric escape from Mars today and through time, with MAVEN. Space Sci. Rev. 195, 357–422.

Mao, P.H., Burnett, D.S., Coath, C.D., Jarzebinski, G., McKeegan, K.D., 2008. MegaSIMS: a SIMS/AMS hybrid for measurement of the Sun's oxygen isotopic composition. Appl. Surf. Sci. 255, 1461–1464.

Marty, B., Chaussidon, M., Wiens, R.C., Jurewicz, A.J.G., Burnett, D.S., 2011. A ^{15}N-poor isotopic composition for the solar system as shown by Genesis solar wind samples. Science 332, 1533–1536. doi:10.1126/science.1204656.

McKeegan, K.D., Kallio, A.P.A., Heber, V.S., Jarzebinski, G., Mao, P.H., Coath, C.D., Kunihiro, T., Wiens, R.C., Nordholt, J.E., Moses Jr., R.W., Reisenfeld, D.B., Jurewicz, A.J.G., Burnett, D.S., 2011. The oxygen isotopic composition of the Sun inferred from captured solar wind. Science 332, 1528–1532. doi:10.1126/science.1204636.

Meshik, A., Hohenberg, C., Pravdivtseva, O., Burnett, D.S., 2014. Heavy noble gases in solar wind delivered by Genesis mission. Geochim. Cosmochim. Acta 127, 326–347.

Neugebauer, M., 1991. The quasi-stationary and transient states of the solar wind. Science 252, 404–409.

Neugebauer, M., Steinberg, J.T., Tokar, R.L., Barraclough, B.L., Dors, E.E., Wiens, R.C., Gingerich, D.E., Luckey, D., Whiteaker, D.B., 2003. Genesis on-board determination of the solar wind flow regime. Spa. Sci. Rev. 105, 661–679.

Nordholt, J.E., Wiens, R.C., Abeyta, R.A., Baldonado, J.R., Burnett, D.S., Casey, P., Everett, D.T., Lockhart, W., McComas, D.J., Mietz, D.E., MacNeal, P., Mireles, V., Moses, R.W., Jr., Neugebauer, M., Poths, J., Reisenfeld, D.B., Storms, S.A., Urdiales, C., 2003. The Genesis Solar Wind Concentrator. Spa. Sci. Rev 105, 561–599.

Ozima, M., Wieler, R., Marty, B., Podosek, F.A., 1998. Comparative studies of solar, Q-gases and terrestrial noble gases, implications on the evolution of the solar nebula. Geochim. Cosmochim. Acta 62, 301–314.

Pilleri, P., Reisenfeld, D.B., Zurbuchen, T.H., Lepri, S.T., Shearer, P., Gilbert, J.A., von Steiger, R., Wiens, R.C., 2015. Variations in solar wind fractionation as seen by ACE/SWICS and the implications for Genesis mission results. Astrophys. J. 812. doi:10.1088/0004-637X/812/1/1.

Reisenfeld, D.B., Wiens, R.C., Steinberg, J.T., Raines, J., Zurbuchen, T., Barraclough, B.L., 2013. Solar wind conditions and composition during the Genesis mission as measured by in situ spacecraft. Spa. Sci. Rev. doi:10.1007/s11214-013-9960-2.

Rieck, K., Jurewicz, A.J.G., Burnett, D.S., Hervig, R.L., Williams, P., Guan, Y., 2016. Bulk solar wind Na and K measured in Genesis collectors. Lunar Planet. Sci. XXXXVII, 2922.

Rieck, K.D., Ogliore, R.C., Jurewicz, A.J.G., Burnett, D.S., Guan, Y., Wiens, R.C., 2019. Measuring solar wind C and O abundances in Genesis regime collectors using SIMS ion imaging depth profiling. Lunar Planet. Sci. L, 2944.

Scott, P., Asplund, M., Grevesse, N., Bergemann, M., Sauval, A.J., 2015b. The elemental composition of the Sun: II. The iron group elements Sc to Ni. Astron. & Astrophys 573, A26. doi:10.1051/0004-6361/201424110.

Scott, P., Grevesse, N., Asplund, M., Sauval, A.J., Lind, K., Takeda, Y., Collet, R., Trampedach, R., Hayek, W., 2015a. The elemental composition of the sun: I. intermediate mass elements Na to Ca. Astron. & Astrophys. 573, A25. doi:10.1051/0004-6361/201424109.

Shi, X., Yin, Q.-.Z., Gao, H., Chang, Y.-.C., Jackson, W.M., Wiens, R.C., Ng, C.-Y., 2017. Branching ratios in vacuum ultraviolet photodissociation of CO and N_2: implications for oxygen and nitrogen isotopic compositions of the solar nebula. Astrophys. J. 850, 48. doi:10.3847/1538-4357/aa8ee7.

Signer, P., Eberhardt, P., Geiss, J., 1965. Possible determination of the solar wind composition. J. Geophys. Res. 70, 2243.

Vogel, N., Heber, V.S., Baur, H., Burnett, D.S., Wieler, R., 2011. Argon, krypton, and xenon in the bulk solar wind as collected by the Genesis mission. Geochim. Cosmochim. Acta 75, 3057–3071.

Wieler, R., 2016. Do lunar and meteoritic archives record temporal variations in the composition of solar wind noble gases and nitrogen? A reassessment in the light of Genesis data. Chem. Erde 76, 463–480. doi:10.1016/j.chemer.2016.06.001.

Wiens, R.C., 2013. Red Rover: Inside the Story of Robotic Space Exploration from Genesis to the Mars Exploration Rover Curiosity. Basic Books, New York.

Wiens, R.C., Burnett, D.S., Neugebauer, M., Pepin, R.O., 1991. Solar-wind krypton and solid/gas fractionation in the early solar nebula. Geophys. Res. Lett. 18, 207–210.
Wiens, R.C., Huss, G.R., Burnett, D.S., 1999. The solar oxygen isotopic composition: predictions and implications for solar nebula processes. Meteoritics and Planetary Science 34, 99–108.
Wiens, R.C., Neugebauer, M., Reisenfeld, D.B., Moses Jr., R.W., Nordholt, J.E., 2003. Genesis solar wind concentrator: computer simulations of performance under solar wind conditions. Spa. Sci. Rev. 105, 601–626.
Wiens, R.C., Reisenfeld, D.B., Olinger, C., Wurz, P., Heber, V., Burnett, D.S., 2013. The Genesis solar wind concentrator: flight and post-flight conditions and modeling of instrumental fractionation. Spa. Sci. Rev. 175, 93–124. doi:10.1007/s11214-013-9961-1.
Zeigler, R.A., Modders, B.W., 2016. Genesis Utah Processing https://curator.jsc.nasa.gov/genesis/utahprocessing.cfm#tabs-5.

CHAPTER 6

The Hayabusa mission

Makoto Yoshikawa[a], Junichiro Kawaguchi[a], Akira Fujiwara[a], Akira Tsuchiyama[b]
[a]Japan Aerospace Exploration Agency
[b]Ritsumeikan University and Guangzhou Institute of Geochemistry

Chapter Outlines

6.1 Introduction

The Hayabusa mission was planned by ISAS (Institute of Space and Astronautical Science), Japan, to execute the first asteroid sample return. The development of Hayabusa was proposed to the Japanese government in 1995, and the project started in 1996. The spacecraft was built and launched by ISAS, which was unified into the Japan Aerospace Exploration Agency (JAXA) after the launch. The mission code name was MUSES-C, and after the launch on May ninth, 2003 by the M-V vehicle from Uchinoura, Japan, it was given the name of "Hayabusa", whose literal meaning is falcon. It arrived at its target asteroid (25143) Itokawa on September 12th, 2005, and returned to the Earth on June 13th, 2010.

The main purpose of the mission was to demonstrate the following key technologies required for future planetary missions: (1) interplanetary cruise via ion engines as primary propulsion, (2) autonomous navigation and guidance using optical measurements, (3) sample collection from an asteroid surface under micro gravity, (4) direct reentry for sample recovery from interplanetary orbit, and (5) combination

Sample Return Missions
DOI: 10.1016/C2018-0-03374-5

of low thrust and gravity assist (Kawaguchi, 1986; 2003; Kawaguchi et al., 2002). In addition, Hayabusa carried other new technology objectives, such as bi-propellant small thrust reaction control system (20N), X-band up/down communication, complete CCSDS (Consultative Committee for Space Data Systems) packet telemetry, duty guaranteed heater control electronics, wheel unloading via ion engines, PN (Pseudo-Noise)-code ranging, lithium ion re-chargeable battery, multi-junction solar cell.

The original and backup target asteroids were the near-Earth asteroids (4660) Nereus and (10302) 1989 ML. However, when the spacecraft development started, the project faced mass capability issues, the launch was delayed and Nereus was replaced by 1989 ML as the primary target body. In 2000, a launch mishap occurred for an astronomical satellite. As a result, the launch of the MUSES-C was shifted half a year and the target asteroid was again switched to a different object, (25143) 1998 SF36, which was renamed Itokawa later. Itokawa is also a near-Earth asteroid and it is an S-type asteroid about 500 m in length. Therefore, Hayabusa was also the first spacecraft that explored a sub km sized asteroid.

However, the Hayabusa voyage entailed many hardships, most of which not anticipated before launch. The most important operation was the touchdown to get the surface material of Itokawa. The first touchdown resulted in an emergency landing. The second touchdown seemed successful but the sampling was not done as planned. Moreover, Hayabusa had very serious damages after the second touchdown: the fuel leaked, the attitude could not be controlled, and the communication stopped. However, the team was able to overcome these hardships. According to the original scenario, the spacecraft should have released a small reentry capsule in June of 2007, when it would have returned back to the Earth. However, due to the unexpected incidents mentioned above, the flight was extended and returned home in June 2010. The flight duration became seven years. Anyway, Hayabusa was able to bring back the surface material of an asteroid successfully for the first time. This chapter gives an overview of Hayabusa mission. A more detailed summary can be found in Yoshikawa et al. (2015).

6.2 Spacecraft and operations

6.2.1 Spacecraft system

Hayabusa was a small probe of dimensions 1.0 m × 1.6 m × 1.1 m and wet mass of 510 kg, including 70 kg of chemical fuel for the Reaction Control System (RCS) and 60kg of Xe propellant for the ion engines. It was a three-axis stabilized spacecraft (Fig. 6.1) with a fixed High Gain Antenna (HGA) and Solar Array Panel (SAP). SAP generated 2.6 kW of electric power at a 1 au distance from the Sun. Most of the instruments were on the bottom surface and to be pointed to the asteroid surface when the spacecraft descended and touched down on the surface. The ion engine

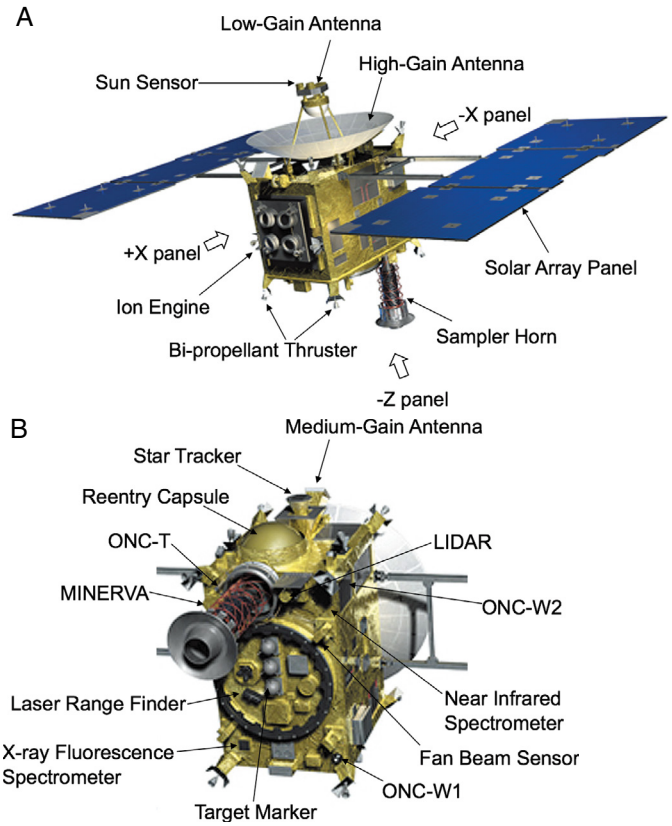

Fig. 6.1 The instruments of Hayabusa Spacecraft *(© JAXA)*.

thruster apertures were located on a side panel (+*X* panel) while the reentry capsule and star tracker were on the -X panel.

The ion engine system consisted of four thruster heads located on a two-axis gimbal plate such that the thrust could always penetrate the center of gravity and the attitude could eliminate the disturbance torque. The special characteristics of the ion engines were the use of microwave discharge to generate plasma and of a CC (carbon-carbon) composite for the grids. Since there were no electrodes in the system, the life of the thruster was greatly extended to eighteen thousand hours.

On both ±*X* panels there were Medium Gain Antennas (MGA) that enabled the spacecraft to communicate with ground stations while the ion engines were turned on, and the HGA was not pointed to the Earth. There was a sun angle sensor and a Low Gain Antenna (LGA) at the top of the HGA. The communication system adopted X-band for both up and down links.

When approaching Itokawa, the spacecraft released a target marker, illuminated by a flash lamp aboard the spacecraft at a 1 Hz frequency, so that it could be detected by the

optical navigation camera by subtracting two images (acquired with lamp on and off, respectively). The major purpose of the target marker was to enable the spacecraft to autonomously identify lateral velocity, crucial in soft landing operations. The spacecraft then stopped RCS firings and touchdown was performed in free fall manner in order to avoid surface contamination.

A sample collection horn, a funnel-like device, extended down from the -Z panel. To avoid the problems of anchoring and drilling, the Hayabusa mission planned a sampling via a projectile shot, which could cope with a variety of surface conditions. The ejected fragments were then guided through the Sampler Horn. The length of the horn was about a meter, sufficient to prevent the tip of SAP from hitting the asteroid's surface. The ejected sample would reach the canister, which would be pushed into the reentry capsule for recovery. The expected collected sample amount was up to ~1 g.

When the spacecraft returned to Earth, the reentry point needed to be in the southern hemisphere to maintain a shallow reentry flight path. As a result, the recovery location was situated in the Woomera Prohibited Area in Southern Australia. The reentry capsule had a diameter of 400 mm and a mass of about 20 kg and included a thermal protection shield, a sample container and a sequencer including beacon transmitter. The heat shield shells were designed to be separated from the instrument section when the parachute deployed.

The Hayabusa scientific payload consisted of four instruments: ONC (optical navigation camera), LIDAR (laser altimeter), NIRS (Near Infrared Spectrometer), and XRS (X-ray Fluorescence Spectrometer). ONC included three cameras: one telescopic camera called ONC-T or AMICA (Asteroid Multi-band Imaging Camera), and two wide angle cameras called ONC-W1 and ONC-W2. Hayabusa also had a small rover, MINERVA (Micro/Nano Experimental Robot Vehicle Asteroid).

6.2.2 Mission operations

From the mission beginning, the flight was not easy and was full of incidents. The spacecraft experienced the largest solar flare ever happened and consequent degradation of a solar cell, eventual loss of two out of the three reaction wheels, a fuel gas eruption and consequent loss of attitude, loss of communication with the ground for seven weeks, loss of lithium ion battery, on-board chemical engines, ion engines and three out of the four neutralizers, and failure of the sample collection.

On September 12th, 2005, the spacecraft arrived at the home position located 20 km above Itokawa's surface. The spacecraft had started a mapping and imaging operation for more than a month and then performed descent maneuvers to practice and confirm the touchdown scenario. During this period the spacecraft released a surface robot, MINERVA, that, due to the very subtle but inaccurate operation controlled from the ground, went away from the asteroid. Thus, the MINERVA operation largely failed, but the relay capability was successful and a photo of the solar paddle of Hayabusa taken by MINERVA was relayed back to the ground.

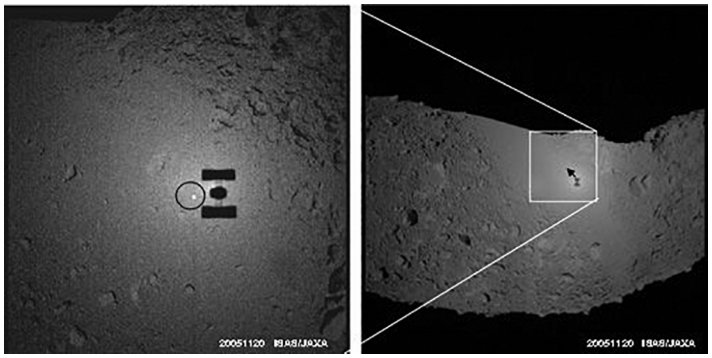

Fig. 6.2 ***The shadow of Hayabusa on the surface of Itokawa at the first touchdown.*** The white dot in the circle is the target maker released. This image was taken on November 20th, 2005. *(© JAXA)*.

A sophisticated autonomous maneuver was successfully performed when Hayabusa performed its first touchdown attempt on November 20th, 2005. At the first touchdown, the spacecraft deployed the target marker and everything seemed ready for shooting a projectile (Fig. 6.2). However, the obstruction detection sensor onboard detected a reflection from some small particles, probably aloft above the surface, and the sample collection shot was not directed. The spacecraft bounced a few times and settled down on the surface near the polar region waiting for commands from the ground for almost thirty minutes. The spacecraft lifted off when the emergency lift command was sent from the ground.

The second touchdown was attempted on November 25th, 2005. During this attempt, a new target marker was not deployed because of the possibility that the spacecraft could detect two target markers at the same time, resulting in confusion. The guidance accuracy was well developed and the expected landing accuracy was sufficiently high. The spacecraft clearly photographed the target marker placed one week before when the spacecraft made its first touchdown. The spacecraft touched down as planned and the projectile shot was directed from the inboard computer, and the sampling was thought performed perfectly. However, it was revealed later that the shooting pyro control circuit was turned to safe mode and the projectile was not fired. Fortunately, the recovered capsule carried back many particles caught by static electricity when the spacecraft descended to the surface two times.

When the spacecraft fired RCS thrusters on the top panel to decelerate the ascent speed while lifting off, one of the thrusters started leaking fuel. This put the spacecraft in Safe-Hold mode. All of the hydrazine leaked out and the RCS became unusable for the remainder of the mission. Another big gas eruption made the spacecraft tumble, and from the beginning of December 2005, radio communication was lost for seven weeks.

The tumbling precluded solar power and the spacecraft power was turned completely off. The on-board battery probably maintained the system just for 40 min.

The project team built a rescue operation plan to wake the spacecraft up. Fortunately, the spacecraft was designed to settle into a single spin motion around the maximum moment of inertia, the Z-axis. So, once the gas eruption stopped, the attitude settled into a single spin whose rotation axis was fixed to a particular direction with respect to the background sky. There was a 60–70 percent probability for the spacecraft to acquire solar power together with the omni-antenna aperture open toward Earth. The project team devised the operation contents so that the command could be heard at any high spin rate and attitude, regardless of the antenna profile gaps. The ground team monitored for any signal from the spacecraft. The miracle restoration occurred at the end of January 2006, when the carrier signal was received at JAXAs deep space antenna. The spacecraft was rotating in opposite spin direction owing to the gas eruption torque. The spin rate was high and the radio signal was intermittent.

The project team started recovery operations immediately. The biggest challenge was the reorientation of the spacecraft attitude to the Earth with the lowered spin motion. The operation started by initial Sun acquisition using the coarse Sun sensor. Ion engines were used to decelerate the spin motion by exhausting Xe gas with no electric acceleration. It took five months to properly correct the spacecraft attitude. There was the constant threat of loss of solar power, since the spacecraft spin direction was frozen in the inertial frame and the Sun direction shifts 90 ° over three months. The operation also had severe time constraints. Thus, the project team gave up on returning in 2007 and amended the flight sequence planning the return in 2010.

While the spacecraft was restored and restarted receiving telemetry, the biggest anticipated obstacle was how to perform the attitude control to point the spacecraft to the Sun and its ion engines aperture properly to the intended direction with no fuel. Hayabusa was equipped with ion engines independently of RCS, and it carried an additional propulsion system, even though its thrust was very weak and was never really intended for impulsive maneuvers. With the gimbaled table on which ion engines were mounted, the angular momentum of the spacecraft was managed in the Y and Z axes. Since the ion engine thrust was along X-axis, no propulsion torque was available around that axis. Therefore, the project team used solar radiation torque to maintain the spacecraft spin direction, keeping it automatically pointed toward the Sun.

The spacecraft's ion engine drive performed successfully from 2007 to 2009. However, the engines reached the end of their life in November of 2009, when all four engines became inoperable due to the death of the neutralizers and/or the ion sources. Among the four engines, three neutralizers were broken and it was therefore not possible to extract electrons from them. However, there was a single intact neutralizer left, Neutralizer-A. Engine-A had remained un-driven from launch, since the engine had a problem found in its radio frequency cable, and the ion source-A did not work well and had been left unused. Engine-A was not still usable, but it was decided to use its neutralizer combined with the other ion sources B, C, and D, even though the engines were

Fig. 6.3 ***Hayabusa's Reentry.*** The reentry capsule is seen in the most right. The body of the spacecraft was disintegrated and burned out. This image was captured from the video taken by NASA. *(© NASA).*

not designed to function in such across connection configuration. Thus, the project team could successfully drive engine-B with neutralizer-A. It was a miracle restoration.

The ion engine cruise lasted till the end of March 2010. The reentry required accurate trajectory corrections. These were applied in five segments started from April to June 2010 aiming at reentry on June 13th, 2010. The Trajectory Correction Maneuvers (TCMs) actually took 250 hrs 46 min 40 s just for 13.54 m/*sec* delta-V. There was a stringent attitude constraint in Hayabusa. The ion engines heads were aligned to the X-axis only, while the power source solar array panels were fixed to the Z-axis. Orbital control via ion engines only was a big challenge. The project team performed the successive TCMs via ion engine operation. The final TCM was performed to accurately target the touchdown point (within several kilometers) within the recovery area where the ground staff was deployed to locate the capsule landing point via radio signal.

On June 13th, 2010, Hayabusa returned home and a small reentry capsule containing the asteroid samples separated from the spacecraft three hours prior to its own reentry. Hayabusa plunged in to the atmosphere over the Australian desert (Fig. 6.3). The deployment of the parachute was designed to be triggered not only by a given time but also by the peak acceleration detected onboard. The primary capsule direction-finding system consisted of three sets of double UHF antenna arrays that precisely identified the signal direction. The combination of the signal confirmed the possible landing area within five to ten kilometers, and a helicopter was used to find the sample return container. The capsule was discovered within 30 min of the reentry, about 500 m from the presumed location. The recovered capsule was placed inside a special container filled with nitrogen and shipped to Japan for sample removal (Kawaguchi, 2010a, 2010b; Kawaguchi et al., 2011).

On June 18th, 2010, the reentry capsule arrived at ISAS and then it was brought into the curation facility. The disintegration of the capsule was carried out and the sample picking up operation started from July sixth, 2010. Then sample analysis started.

6.3 Scientific results: in-situ observations

6.3.1 Global properties of Itokawa

Itokawa has dimensions of 535 × 294 × 209 m, a mean diameter of 320 m (in agreement with ground observations estimates), a spin period of 12.1h and revolves with retrograde rotation (details in Fujiwara et al., 2006). There is no apparent short-term precession of the spin pole, which shows that enough time has passed for the asteroid to be dynamically relaxed after the last large impact event. No satellites were found by AMICA images (Fuse et al., 2008) which is consistent with past optical and radar observations. Using LIDAR and navigation data (Abe et al., 2006b; Mukai et al., 2007), the asteroid mass was determined to be 3.51×10^{10} kg. Coupled with the volume of Itokawa, estimated from the 3-D shape models (Demura et al., 2006), the bulk density is estimated to be 1.9 g/cm^3.

Itokawa has a bifurcated shape like a floating sea otter (Fig. 6.4, Fig. 6.5, Fig. 6.6). The smaller part is called the "head" and the larger part is called the "body". The size of the ellipsoids fitted to the body and to the head are 490 × 310 × 260 m and 230 × 200 × 180 m, respectively (Demura et al., 2006). The appearance of the surface was different from any other asteroids so far observed by spacecraft, including Ida, Mathilde and Eros, whose surfaces are globally covered with a thick regolith layer and many craters.

The surface of Itokawa is divided into two distinct types of terrain: *rough terrain* consisting of numerous boulders, and *smooth terrain*, which shows the existence of a smoother regolith layer. Rough terrain (Fig. 6.7), makes up ~80 percent of the surface (Saito et al., 2006). The smooth terrain is distributed into two distinct regions: the "MUSES-C", i.e., the wide region extending around the "breast" on the "body", where the spacecraft landed for sampling, and "Sagamihara" around the north-polar region

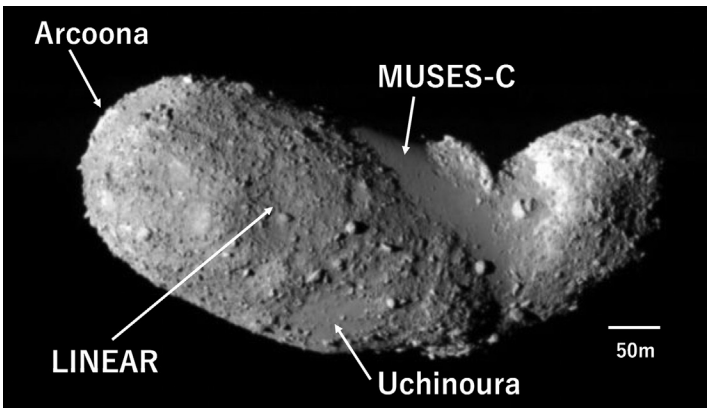

Fig. 6.4 ***The east side of Itokawa.*** The bottom is north. The spacecraft landed on the smooth terrain near MUSES-C. *(© JAXA).*

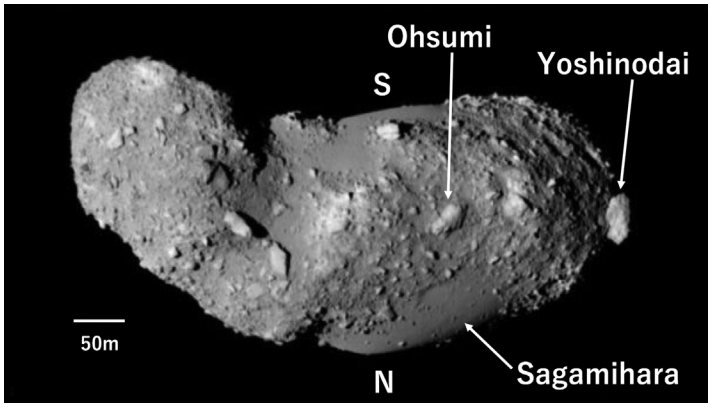

Fig. 6.5 ***The western side of Itokawa.*** South is up (head) and north is down (bottom) due to retrograde rotation. On this side large boulders are more abundant than the eastern side. Yoshinodai is the largest boulder. *(© JAXA)*.

near the "back" of the body. Close-up viewing of the MUSES-C regio (Fig. 6.8) shows that the smooth terrain is composed of cm- to mm-scale fragmental debris and pebbles (Yano et al., 2006). Most grains in the MUSES-C regio are larger than those observed in the close-up view of Eros' surface, and there is a strong depletion of fine grains on Itokawa compared with Eros. The boundaries between the rough and smooth terrains are relatively sharp, but a gradient of boulder number density and some evidence of movement of the surface material are evident (Miyamoto et al., 2007)

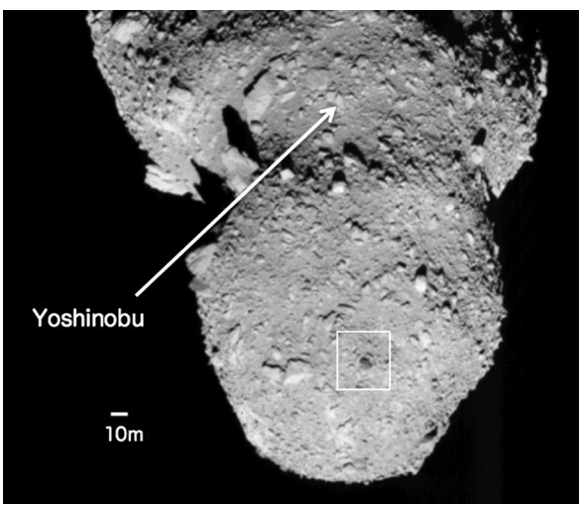

Fig. 6.6 ***"Back head" viewed from top.*** The large depression at the "neck" is Yoshinobu. On the top of "head" a black boulder is evident (inside the square). Scale bar is 10 m. *(© JAXA)*.

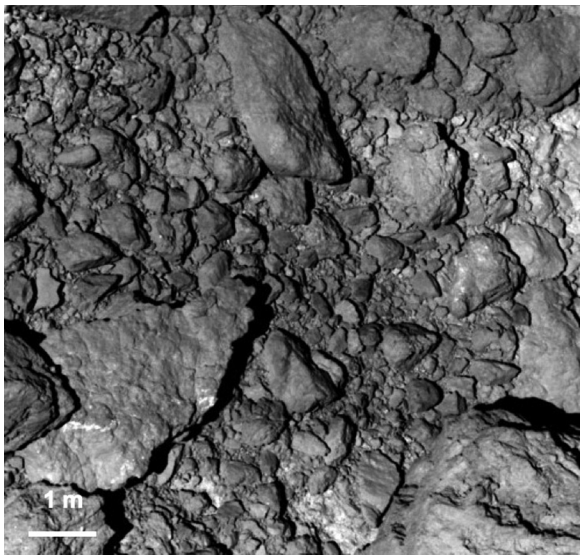

Fig. 6.7 ***Close-up view of rough terrain.*** Irregular plate-like fragments are characteristic of impact spalls. *(© JAXA)*.

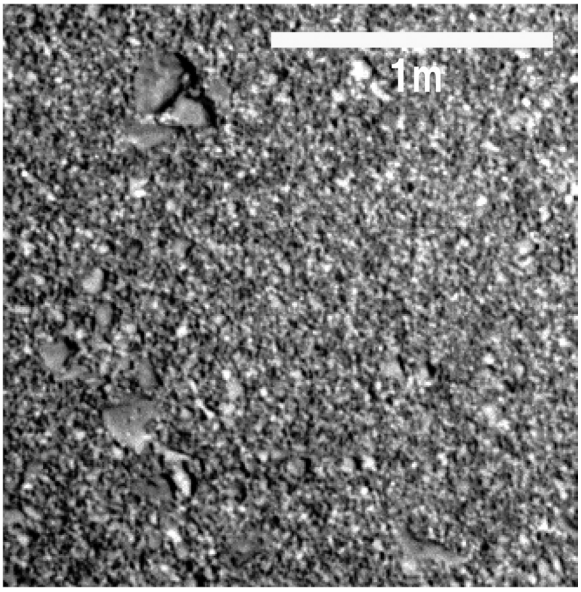

Fig. 6.8 Close-up view of MUSES-C regio. *(© JAXA)*.

6.3.2 Shape and YORP effect

Three-dimensional numerical shape models of Itokawa were developed using different methods, and based on these, potential and slope maps were constructed (Fujiwara et al., 2006; Demura et al., 2006; Gaskell et al., 2006). Toward the head and body, the potential increases, while low potential regions exist near the neck and northern areas on the body. The surface has slopes less than 8° in two areas - an isolated region around the north pole and the MUSES-C regio. In these regions, regolith maintains its smoothness down to at least cm to mm grain sizes (Fig. 6.8). A surface region with zero slopes is considered to be an energetically relaxed shape to the surface normal. This would be consistent with the existence of a loose regolith layer. Hence the accumulation of small grains could be explained by transport of these grains across the surface through seismic shaking induced by impacts (Miyamoto et al., 2007) or by tidal disturbance from close planetary encounters or electrostatic levitation.

The YORP effect (radiative spin-up/spin-down effect) was proposed for Itokawa based on ground-based observation (Vokrouhlický et al., 2004; Scheeres et al., 2007). Scheeres et al. (2007) reported that Itokawa was spinning with a period of 6.5 h 100 to 180 thousand years ago and has slowed to the current spin state in the absence of a disturbing event. This rotation rate is fast enough for the head and body to have gone into mutual orbit. However, the theoretical YORP value (spin-up or spin-down rate) is sensitive to the resolution of the shape model and lies in the range from -2 to -3×10^{-7} rad day^{-2} (Ďurech, et al., 2008). The observed change of rotation rate -9.0×10^{-8} rad day^{-2} (Kitazato et al., 2007) and upper limit $\sim1.5 \times 10^{-7}$ rad day^{-2} (Ďurech, et al., 2008) are slightly lower than the expected value. To solve this inconsistency, the possibility of density inhomogeneity for Itokawa was suggested (Scheeres and Gaskell, 2008). Lowry et al. (2014) measured an acceleration of rotation 3.54×10^{-8} rad day^{-2} (equivalent to a decrease of the rotation period of ~45 ms year^{-1}). From thermophysical analysis they found that the center-of-mass must be shifted by ~21m along the long axis of the asteroid to reconcile the observed YORP strength with theory. From these results, they proposed that Itokawa is composed of two bodies of very different bulk densities, 1750 ± 110 kg m^{-3} and 2850 ± 500 kg m^{-3}, and was formed by their merging via either reaccumulation following a catastrophic disruption of a larger, partially differentiated body, or the collapse of a binary system.

6.3.3 Boulders and craters

Most boulders are found in the rough terrain, while in the smooth terrain boulders appear buried by regolith. The average number density of boulders larger than 5 m is 10^3/km^2 (Michikami et al., 2008), which is slightly larger than that on the surface of

Eros. A black boulder is found at the top of the head where the gravitational potential is the highest (Fig. 6.6), which was assigned as the prime meridian (longitude 0°, Fujiwara et al., 2006). It measures about 6 m and has unusually low brightness. Three other smaller similar boulders were also found (Hirata and Ishiguro, 2011).

The largest boulder (50 × 30 × 20 m), named Yoshinodai (Saito et al., 2006), is located near the "right foot" of the "body" (Fig. 6.5). There are several boulders with sizes larger than a few tens of meters on the western side while large boulders are less abundant on the eastern side. There are several large pinnacles at the neck region on the western side (Fig. 6.5), believed to have resulted from landside from the higher gravitational potential of the "head" to the lower potential region of the "neck" to "breast" region. Considering the experimental relationship between impact crater and excavated fragment sizes (Gault et al., 1963), the large boulders are the likely relics formed in some cataclysmic event related to the formation of Itokawa's current configuration.

Many crater-like depressions are found on Itokawa but most of them have a shape that does not look like a crater as clearly as those found on other asteroids' surfaces. Hirata et al. (2009) listed 38 crater candidates on Itokawa's surface: five of them (Yoshinobu (Fig. 6.6), Arcoona, LINEAR, Uchinoura (Fig. 6.4), and Ohsumi (Fig. 6.5)) have diameters larger than 100 m. Most of the crater-like depressions are shallower than craters on other planetary bodies. Large craters have flat or convex floors affected by the pre-impact local surface curvature as shown in laboratory impact experiments (Fujiwara, et al., 1993). Many small craters are found on the smooth terrains on Itokawa, and those are also shallow.

Careful observation of the "head" and "body" shows that these surfaces are composed of many facets (Saito et al., 2006; Demura et al., 2006). There is a possibility that some facets could be the exposed surfaces of large fragments embedded near the asteroid's surface.

6.3.4 Regolith

Past impacts by interplanetary projectiles would have repeatedly fragmented and released Itokawa's surface material since most of the excavated finer particles would have velocities much higher than Itokawa's escape velocity. In impact experiments, fragments having velocities less than this escape velocity are limited to a very small number of the largest fragments. Hence one could suppose that fine-grained regolith was gradually lost and the surface became covered with large boulders.

In spite of this expectation, a significant amount of regolith mm to cm grain size is present on Itokawa, although the constituent particle size may be larger than that on larger asteroids. This is a remarkable result given that Itokawa is very small. One probable scenario for this reason is that regolith grain existed from the initial formation of the head and body and it has been gradually depleted through cratering. If the strength of Itokawa is weak, the excavated materials have lower speeds (Onose and Fujiwara,

2004) and will accumulate on the surface. Barnouin-Jha et al. (2008) estimated that this strength should be less than 100Pa. This value is small compared with loosely consolidated breccia (~ 1kPa) and is higher than typical values for lunar regolith (~ a few Pa). Another probable scenario for production of small particles is larger blocks crack due to thermal fatigue (Dombard et al., 2010; Delbo et al., 2014).

Moreover, regolith grains may be continuously produced if Itokawa is composed of boulder aggregates of various sizes and has considerable macro-porosity. Such a structure would not only reduce the shock effect during impacts but could also help to produce fine fragments in the shallow interior near the aggregated body's surface, if the characteristic size of the aggregate boulders is roughly comparable with the projectile sizes. This process would also produce shallow crater-like deposits. Thus, a considerable amount of grains would be retained within the interior of the asteroid, and the fine particles could easily migrate through spacing between larger boulders toward low potential regions like MUSES-C triggered by seismic shaking.

Albedo and color maps were made in the visible and near infrared (Saito et al., 2006; Ishiguro et al., 2007). Visible and near-infrared reflectance spectra show typical S-type characteristics with a broad absorption band near 1 μm (Abe et al., 2006a; Saito et al., 2006). Slight albedo and spectral variations were observed across the surface and ascribed to space weathering (Hiroi et al., 2006): darker regions are interpreted as being more space-weathered, since brighter regions probably indicate areas newly exposed by impacts or shaking.

6.3.5 Rubble-pile structure

The Itokawa's bulk density of 1.9 g cm^{-3} is considerably lower than the ~2.6 g cm^{-3} determined for other S-type asteroids. Assuming Itokawa's composition is like LL chondrites and that Itokawa's grain density is similar to the bulk density of LL chondrites (3.2 g cm^{-3}), the macro porosity of Itokawa is estimated to be 41 percent (Fujiwara et al., 2006; Abe et al., 2006b), suggesting a rubble pile structure (Fujiwara et al., 2006).

The ellipsoidal shapes of the head and body are also suggestive of a rubble-pile structure, because an ellipsoid is the configuration that an aggregated body takes under self-gravitation and centrifugal force. However, the fact that the current shape of Itokawa is not gravitationally relaxed to a single ellipsoid means that the head and body acquired some strength before the contact of these bodies (Shrama, 2010). There are no conspicuous long linear structures on Itokawa (Fujiwara et al., 2006; Hirata et al., 2009), which is consistent with Itokawa being an aggregate of rubbles of size less 50 m. In fact, numerical simulations of catastrophic disruptions of asteroids and fragment reaccumulations were able to produce aggregate objects whose shape resemble that of Itokawa (Michel and Richardson, 2013), suggesting that Itokawa is the product of reaccumulations of small fragments generated by the disruption of a larger parent body.

The existence of a thermally-insulating layer consisting of gravel on the smooth terrain (Yano et al., 2006) and many boulders in the rough terrain is also suggestive of rubble-pile structure and this is consistent with ground-based thermal inertia measurements (Mueller et al., 2005): Itokawa's thermal inertia of 350 $Jm^{-2}s^{-0.5}K^{-1}$ is at least an order of magnitude higher than large main-belt asteroids (5–25 $Jm^{-2}s^{-0.5}K^{-1}$) and the Moon (50 $Jm^{-2}s^{-0.5}K^{-1}$).

Thus, Itokawa is the first observationally verified rubble-pile body, although the existence of rubble piles was predicted long ago and more recently through numerical simulations of asteroid disruptions. This supports speculation that most asteroids larger than about 150 m may be rubble piles.

6.4 Scientific results: sample analysis

6.4.1 Sample collection and curation

The Hayabusa spacecraft made two touchdowns on Itokawa's area named MUSES-C regio (Fig. 6.4), but no bullets were shot. However, thousands of very small particles were recovered in the two sample catcher rooms of the sample container, i.e., A and B, corresponding to the second and first touchdown, respectively (Nakamura et al., 2011).

The sample container was opened in the clean chamber at the Planetary Material Sample Curation Facility of JAXA (PMSCF/JAXA). All the processes for sample transfer and storage were performed under high-purity nitrogen atmosphere. Several methods were used to remove particles from the sample containers, such as electrostatic needle, Teflon spatula, tapping the container with a very clean screwdriver to drop particles onto a quartz (silica glass) disk, and picking up the particles sticking on the cover lid of sample Catcher B (Nakamura et al., 2011; Yada et al., 2014a,b). Relatively larger particles (up to 300 μm) were safely collected from the quartz plates (Fig. 6.9). Gas in the sample container was also sampled during the opening procedure: the noble gas elemental ratio is essentially identical to terrestrial atmosphere, suggesting atmospheric contamination across the capsule O-ring seal (Okazaki et al., 2011).

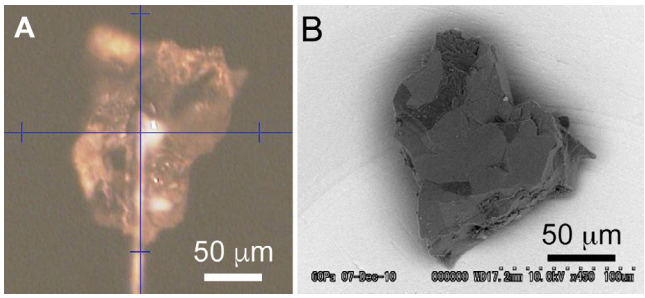

Fig. 6.9 ***Optical microscope image (A) and SEM image (B) of a particle (RA-QD02-0010) collected by the Hayabusa spacecraft.*** This particle is mainly composed of olivine. *(A : © Tsuchiyama, B : © JAXA).*

Initial descriptions of harvested particles were performed using a scanning electron microscope equipped with an energy dispersive X-ray spectrometer (SEM/EDX) at PMSCF/JAXA (Yada et al., 2014a). Analyses were made using low vacuum, low beam current mode without a conductive coating. The particles were grouped into four categories: Category 1 particles are composed mainly of olivine, pyroxene and feldspar; Category 2 particles consist of additional minerals, i.e. troilite, pentlandite, Fe-Ni metal, phosphates, and chromite; Category 3 particles are composed mainly of carbon-bearing phases; and Category 4 particles are contaminants such as aluminum, quartz glass, and stainless steel. The collected samples are stored in a clean chamber at PMSCF/JAXA, in a clean nitrogen atmosphere. By agreement, 1/10 of the harvested samples were transferred to NASAs curation facility at the Johnson Space Center in Houston (Longobardo and Hutzler, 2021).

6.4.2 Sample analysis

The Itokawa particles were the first samples returned from a known asteroid and related geological context. It has long been accepted that most meteorites originate from asteroids. In particular, ground-based observations indicate that the materials on S-type asteroid Itokawa are similar to thermally metamorphosed LL ordinary chondrites belonging to petrologic type 5 to 6 (i.e. LL5-6), which suffered limited space weathering. Itokawa samples thus provide a direct validation of the relation between S-type asteroids and ordinary chondrite meteorites. They can also be compared with other extraterrestrial regolith, particularly lunar regolith materials sampled by the Apollo and Luna mission, and studied to understand surface processes on an asteroid, such as regolith formation and space weathering. Exotic materials, including organic-rich matter brought by impacts on the asteroid's surface, might also be included in the samples. The returned samples from Itokawa are ideal for such examination because they come from a known source, they have experienced minimal contamination from the Earth's atmosphere and organic materials, and the surface structure of the samples has been preserved.

Sixty-five particles 30–180 μm in size removed from the quartz disks were examined by the Hayabusa preliminary analysis teams (HASPET) in the year following recovery on Earth (Nakamura et al., 2011; 2012; Tsuchiyama 2014a). The total volume of 48 particles examined by X-ray microtomography was approximately 4×10^6 μm^3, corresponding to a sphere about 100 μm in radius or 15 μg in mass (Tsuchiyama et al., 2014b). This may suggest that the total mass of samples collected by the spacecraft is roughly 100 μg although the exact amount is not known. Sixty particles were divided among the two HASPET groups; one for sequential analysis from non-destructive to progressively more destructive methods (mainstream group) and the other for the characterization of space weathering, noble gases, and carbonaceous and organic materials, while minimizing contamination (Fig. 6.10).

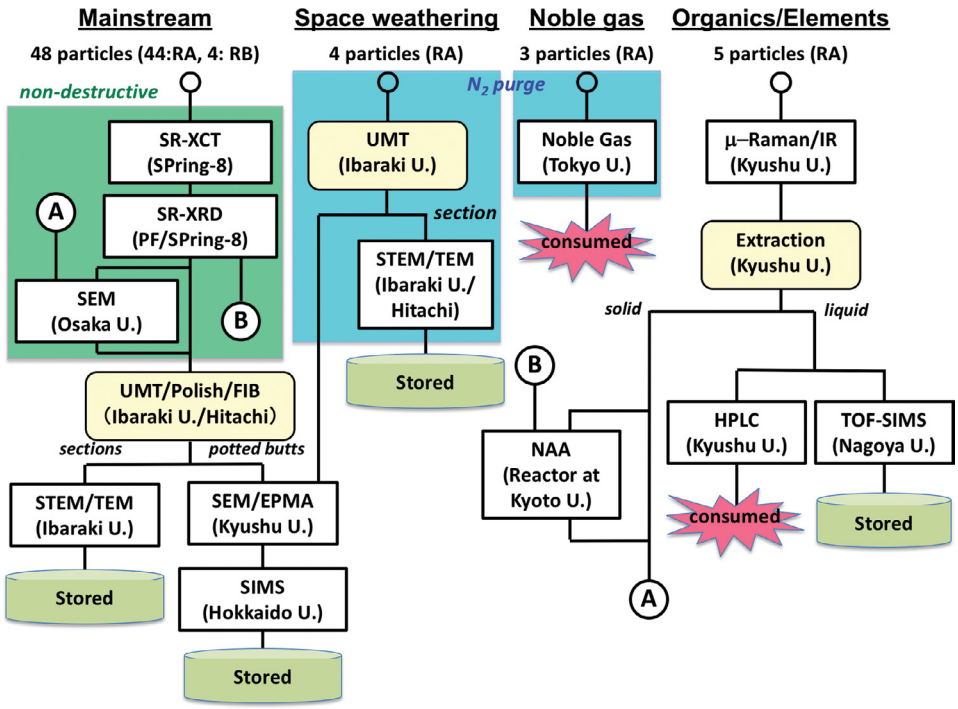

Fig. 6.10 ***The flowchart of Hayabusa preliminary sample analysis.*** RA and RB mean catcher room A and B, respectively. SR-XCT: SR (synchrotron radiation)-based X-ray computed tomography, SR-XRD: SR-based X-ray diffraction, SEM: scanning electron microscopy, UTM: ultra-microtome, FIB: focused ion beam micro-sampling, Hitachi: Hitachi High-Technologies Co., (S)TEM: (scanning) transmission electron microscopy, EPMA: electron-probe microanalysis, SIMS: secondary ion mass spectroscopy, m-Raman/IR: micro-Raman and infrared spectroscopy, Extraction: extraction by dichloromethane/methanol solution, NAA: neutron activation analysis, HPLC: high-precision liquid chromatography, TOF-SIMS: time-of-flight secondary ion mass spectroscopy. A and B show connections of the analytical flows, respectively. *(© Tsuchiyama)*.

Forty-eight particles were examined by the mainstream group (Nakamura et al., 2011). First, X-ray microtomography (XCT) and X-ray diffraction (XRD) were applied to obtain three-dimensional (3D) structures (Tsuchiyama et al., 2011, 2013a, 2014b) and mineral phases together with their specific crystallographic structures (Nakamura et al., 2011, 2014; Tanaka et al., 2014), respectively. The use of these nondestructive analyses is one of the key features of the Hayabusa initial analysis strategy involving sequential studies. The 3D distribution of minerals provided critical information about where a particle should be cut to ensure that the subsequent destructive analyses examined the optimal areas of the minerals exposed in the cross sections. Then, the particles were polished or sectioned using an ultra-microtome (UMT) or focused ion beam (FIB) and analyzed by transmission electron microscopy (TEM) to examine the nanostructures (Nakamura et al., 2011; Noguchi et al., 2011, 2014a). Some sections were examined by

optical microscopy and field-emission scanning electron microscopy (FE-SEM) coupled with electron back-scattered diffraction (EBSD) (Zolensky et al., 2012), and the chemical compositions of minerals were measured by electron probe microanalyzer (EPMA) (Nakamura et al., 2011, 2014). Subsequently, oxygen and magnesium isotope compositions of minerals together with some minor element compositions were determined using secondary ion mass spectroscopy (SIMS) (Yurimoto et al., 2011a, b). The surface nanomorphologies of eight particles were also observed by FE-SEM before sectioning (Matsumoto et al., 2012, 2013, 2014; Tsuchiyama et al., 2012, 2013b).

For the analysis of space weathering, TEM observations of ultrathin sections from twelve particles were performed (Noguchi et al., 2011, 2014a). Some sections were prepared by an UMT in a purged nitrogen atmosphere to avoid oxidation of Fe nanoparticles. The isotopic compositions of noble gases in three different particles were measured by laser ablation mass spectrometry (Nagao et al., 2011). The surface of five different particles was examined nondestructively by micro-Raman and micro-infrared spectroscopy to seek carbonaceous materials (Kitajima et al., 2011). These particles were then rinsed with a small amount of dichloromethane/methanol solution, and the extracts were examined using high-precision liquid chromatography (HPLC) to seek amino acids or using time-of-flight secondary ion mass spectrometry (TOF-SIMS) to analyze other organic compounds, including a search for polycyclic aromatic hydrocarbons (Naraoka et al., 2012). Neutron activation analysis (NAA) of one particle was made after rinsing (Ebihara et al., 2011). Lately, two additional samples were examined by NAA (Ebihara et al., 2015). Unconsumed samples were returned to PMSCF/JAXA after initial analysis.

Five different particles were independently studied by Nakamura et al. (2012). The surface micro-nano morphologies of these particles were first observed by FE-SEM, and then FIB sections of them were observed using optical microscopy and FE-SEM; the elemental and oxygen isotope compositions were measured by EPMA and SIMS, respectively.

6.4.3 Results

The Hayabusa samples mainly consist of olivine, Ca-poor and Ca-rich pyroxenes, plagioclase, and troilite with small amounts of kamacite, taenite, chromite, K-feldspar (sanidine), apatite and merrillite. The chemical compositions of minerals fall within the compositional range of LL ordinary chondrites (Nakamura et al., 2011, 2012, 2014; Mikouchi et al., 2014: Noguchi et al., 2014b; Ebihara et al., 2015). The oxygen isotope compositions of the minerals are consistent with equilibrated LL chondrites (Yurimoto et al., 2011a; Nakashima et al., 2013). The modal abundances are also consistent with LL chondrites (Tsuchiyama et al., 2011, 2014b). The $Fe^{3+}/(Fe^{2+}+Fe^{3+})$ ratio of plagioclase, determined by SR-XANES (synchrotron radiation-based X-ray absorption near edge structure) is approximately 0.5, indicating formation under a relatively oxidizing envi-

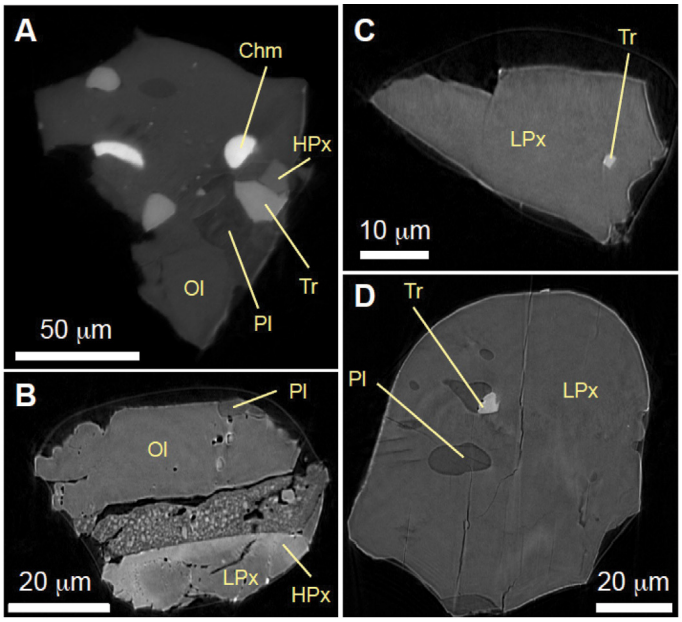

Fig. 6.11 ***Slice images of Itokawa particles obtained by microtomography for samples RA-QD02-0031 (A), RA-QD02-0048 (B), RA-QD02-0038 (C), and RA-QD02-0042 (D) (from Tsuchiyama et al., 2014a).*** Ol: olivine, LPx: low-Ca pyroxene, HPx: high-Ca pyroxene, Pl: plagioclase, Chm: chromite, Tr: troilite. The image contrast corresponds to the X-ray linear attenuation coefficient of the minerals. The bright edges of objects are artifacts resulting from X-ray refraction contrast.

ronment, again consistent with LL chondrites (Mikouchi et al., 2014). Based on mineral abundances and chemical compositions, the bulk chemical composition (Nakamura et al., 2011, 2014) and the bulk density of the samples (3.4 g/cm^3) (Tsuchiyama et al., 2011, 2014b) were found to be consistent with LL chondrites. The Fe/*Sc* and Ni/Co ratios by NAA are consistent with those of ordinary chondrites. Depletion of Ir, which may be the result of condensation in the early solar nebula before chondrite formation, was also reported (Ebihara et al., 2011).

The textures of the samples were examined by X-ray tomography (Tsuchiyama et al., 2011, 2014b) and FE-SEM (Nakamura et al., 2011, 2012, 2014). About 90 percent of the Itokawa particles examined exhibit triple junctions at the boundaries between coarse silicates (Fig. 6.11A) or almost monomineralic features (Figs. 6.11C, D). Minerals have almost homogeneous chemical compositions, indicating that they have been thermally annealed, as LL5/LL6 chondrites (Nakamura et al., 2011, 2014). Their microtextures, including porosity (1.5 percent in average), grains size, voids and cracks, are also similar to LL5/LL6 (Tsuchiyama et al., 2011, 2014b). Most of the remaining Itokawa particles (~ 10 percent), which are made of fine silicate grains and/or have more heterogeneous chemical compositions (Fig. 6.11B), are similar to LL4 chondrites (Nakamura

et al., 2011, 2014; Tsuchiyama et al., 2011). No differences were found between particles from sample catcher rooms A and B (Nakamura et al., 2014; Noguchi et al., 2014b; Tsuchiyama et al., 2014b). The above results clearly show that the Itokawa's surface correspond to equilibrated LL chondrites. This provides the first direct link between one class of asteroids and one group of meteorites.

The maximum sample temperature reached in the past was estimated to be about 800 °C from the chemical compositions of an equilibrated mineral pair of Ca-poor and Ca-rich pyroxenes (Nakamura et al., 2011). Crystallization temperatures of plagioclase based on crystal structure range from ~ 800 °C (Nakamura et al., 2011; Mikouchi et al., 2014) to 655–660 °C (Tanaka et al., 2014). The latter indicates the temperature during prograde metamorphism. If a small body like Itokawa was heated to 800 °C, even its interior would have cooled very fast. Based on a heating model calculation using the extinct nuclide 26Al as a heat source, the original Itokawa parent body diameter should have been larger than 20 km (Nakamura et al., 2011), and accreted between 1.9 and 2.2 Myr after CAI formation (Wakita et al., 2014), which is consistent with the 26Al–26 Mg isotope evidence (Yurimoto et al., 2011b). The LL4 Itokawa particles probably formed near the original parent-body surface.

We can draw up a scenario for the Itokawa parent body as follows. (1) Formation of the Itokawa parent body >20 km in diameter as a planetesimal composed of LL chondrite material. This occurred at ~2 Myr after CAI formation (~4.565 Gys ago). (2) Thermal metamorphism with the peak temperature of ~800 °C (probably ~4 Mys later) followed by slow cooling. (3) Post-metamorphic impact heating. (4) A catastrophic impact formed Itokawa as a rubble pile asteroid although direct evidence of this has not been obtained by the sample analyses. It should be noted that neither the absolute ages of metamorphism nor the age of the catastrophic impact have been yet measured.

The Itokawa particles have been investigated in detail from various perspectives, such as the particle size distribution and the shape distribution (Tsuchiyama et al., 2011, 2014b). Submicrometer-sized impact craters were observed on the surfaces of only a limited number of Itokawa particles (Nakamura et al., 2012). They may have been created by the impact of high-speed secondary nanoparticles produced by impact into Itokawa's regolith. Tiny, flattened glass objects, which seem to be melt splashes (Nakamura et al., 2012; Matsumoto et al., 2012), also formed as a result of small-scale impacts. Two kinds of surface modifications, formation of space-weathering rims and surface abrasion, have been recognized (Noguchi et al., 2011, 2014a,b; Matsumoto et al., 2013; Keller and Berger, 2014; Thompson et al., 2014). Blisters were also recognized on the particle surfaces by FE-SEM (Matsumoto et al., 2013). Another observed surface modification is grain abrasion (Tsuchiyama et al., 2011, 2013b, 2014b): it can be regarded as a different type of space weathering with a longer timescale (called "space micro-erosion"). Solar wind implanted noble gases (He, Ne, and Ar) have been detected in Itokawa particles (Nagao et al., 2011, 2013). This clearly shows that the particles were

for some period of time located on the uppermost regolith layer. The residence time spans were estimated to be 150–550 years from the Ne concentrations.

We can construct a scenario for the Itokawa's surface as follows. (1) Formation of regolith by impacts of small objects, with selective escape of the finest-scale particles, and possibly by thermal fatigue. (2) Implantation of solar wind into the uppermost particle surfaces and formation of space-weathered rims with a timescale of $\sim 10^3$–10^4 ys. (3) Grain abrasion, probably due to seismic-induced particle motion, with time periods significantly longer than 10^4 ys. Processes (2) and (3) and impact fragmentation occurred repeatedly. (4) Final escape of some particles from the asteroid by impact(s) within the final 1 My.

6.5 Final remark

The Hayabusa mission was a huge challenge that had never been accomplished before. The Hayabusa mission for seven years was full of incidents and troubles, but it was also full of the engineers' special spirit of returning the spacecraft safely home. We have learned a lot about the technology of sample return missions and we felt that this first experience was worth the challenge. We revealed the nature of a very small asteroid for the first time, and this will lead to an improved understanding of the origin of the Solar System.

From the results of the Hayabusa mission, we can construct the following scenario. Originally a parent body of diameter about 20 km was catastrophically disrupted by a collision. Among the dispersing fragments some aggregated bodies were formed through gravitational interaction as numerically demonstrated by Michel and Richardson (2013). The rubble-piled "head" and "body" were two of these aggregates, and formed a co-rotating binary and finally came into contact by a collision at relatively low velocity, and as a result Itokawa was formed. The mutual configuration of the "head" and "body" might have changed from the initial contact of both bodies as suggested by Scheeres et al. (2007) due to various disturbances such as planetary encounters, impacts, and YORP effect. Itokawa was brought into a typical NEO orbit through $\nu 6$ secular resonance in the main belt as suggested by the numerical track-back study of the current Itokawa's orbit (Michel and Yoshikawa, 2006). Major craters had been formed before injection into the NEO orbit, and the exposure time of the surface for cratering is estimated to be at least 60–75 My (Michel et al., 2009). The duration that Itokawa spent in the NEO orbit may have been on the order of millions of years, which is equivalent to its expected lifetime against an impact with Earth (Michel and Yoshikawa, 2005).

Having such splendid results from Hayabusa, the next asteroid sample return mission Hayabusa2 was planned (Tsuda et al., 2013; Yoshikawa et al., 2014) and successfully launched on December third, 2014, arrived at its target asteroid (162173) Ryugu on June 27th, 2018, and returned to the Earth on December sixth, 2020. Hayabusa2 will bring another breakthrough in the study of asteroids and the Solar System.

Acknowledgments

Hayabusa mission was accomplished through the great effort of many people such as engineers, scientists, researchers, administrative staff, and other people who supported the Hayabusa mission so well. We are grateful to all people involved in Hayabusa mission.

References

Abe, M., Takagi, Y., Abe, S., Hiroi, T., Clark, B., Abell, P.A., Lederer, S.M., Jarvis, K.S., Nimura, T., Ueda, Y., Fujiwara, A., 2006a. Near-infrared spectral results of asteroid Itokawa from the Hayabusa spacecraft. Science 312, 1334–1338.

Abe, S., Mukai, T., Hirata, N., Barnouin-Jha, O.S., Cheng, A.F., Demura, H., Gaskell, R.W., Hashimoto, T., Hiraoka, K., Honda, T., Kubota, T., Matsuoka, M., Mizuno, T., Nakamura, R., Scheeres, D.J., Yoshikawa, M., 2006b. Mass and local topography measurements of Itokawa by Hayabusa. Science 312, 1344–1347.

Barnouin-Jha, O.S., Cheng, A.F., Mukai, T., Abe, S., Hirata, N., Nakamura, R., Gaskell, R., Saito, J., Clark, B.E., 2008. Small-scale topography of 25143 Itokawa from the Hayabusa laser altimeter. Icarus 198, 108–124.

Delbo, M.8 coauthors, 2014. Thermal fatigue as the origin of regolith on small asteroids. Nature 508, 233–236.

Demura, h, Kobayashi, S., Nemoto, E., Matsumoto, N., Furuya, M., Yukishita, A., Muranaka, N., Morita, H., Shirakawa, K., Maruya, M., Ohyama, H., Uo, M., Kubota, T., Hashimoto, T., Kawaguchi, J., Fujiwara, A., Saito, J., Sasaki, S., Miyamoto, H., Hirata, N., 2006. Pole and global shape of 25143 Itokawa. Science 312, 1347–1349.

Dombard, A.J., Barnouin, O.S., Prockter, L.M., Thomas, P.C., 2010. Boulders and ponds on the asteroid 433 Eros. Icarus 210, 713–721.

Ďurech, J., Vokrouhlichý, D., Kaasalainen, M., Weissman, P., Lowry, S.C., Beshore, E., Krugly, Y.N., Shevchenko, V.G., Gaftonyuk, N.M., Choi, Y.–J., Kowalski, R.A., Larson, S., Warner, B.D., Marshalkina, A.L., Ibrahimov, M.A., Molotov, I.E., Michłowski, T., Kitazato, K., 2008. New photometric observations of asteroids (1862) Apollo and (25143) Itokawa–an analysis of YORP effect. Astron. Astrophys. 488, 345–350.

Ebihara, M.21 coauthors, 2011. Neutron activation analysis of a particle returned from asteroid itokawa. Science 333, 1119–1121.

Ebihara, M.15 coauthors, 2015. Chemical and mineralogical compositions of two grains recovered from an asteroid Itokawa. Meteorit. Planet. Sci. 50, 243–254.

Fujiwara, A., Kadono, T., Nakamura, A., 1993. Cratering experiments into curved surfaces and their implication for craters on small satellites. Icarus, 105, 345–350.

Fujiwara, A., Kawaguchi, J., Yeomans, D.K., Abe, M., Mukai, T., Okada, T., Saito, J., Yano, H., Yoshikawa, M., Scheeres, D.J., Barnouin-Jha, O., Cheng, A.F., Demura, H., Gaskell, R.W., Hirata, N., Ikeda, H., Kominato, T., Miyamoto, H., Nakamura, A.M., Nakamura, R., Sasaki, S., Uesugi, K., 2006. The rubble-pile asteroid Itokawa as observed by Hayabusa. Science 312, 1330–1334.

Fuse, T., Yoshida, F., Tholen, D., Ishiguro, M., Saito, J., 2008. Searching satellites of asteroid Itokawa by imaging observation with Hayabusa spacecraft. Earth Planets Space 60, 33–37.

Gaskell, R., Barnouin-Jha, O.S., Scheeres, D.J., Mukai, T., Hirata, N., Abe, S., Saito, J., Ishiguro, M., Kubota, T., Hashimoto, T., Kawaguchi, J., Yoshikawa, M., Kominato, T., 2006. Landmark navigation studies and target characterization in the Hayabusa encounter with Itokawa. In: AIAA/AAS Astrodynamics Specialist Conference and Exivit. AIAA Paper, 2006–6660.

Gault, D.E., Shoemaker, E.M., Moore, H.J., 1963. Spray ejected from lunar surface by meteoroid impact. NASA TND-1767, 1–39.

Hirata, N., Ishiguro, M., 2011. Properties and possible origin of black boulders on the asteroid Itokawa. LPSC, 1821 Abstrpdf.

Hirata, N., Barnouin-Jha, O.S., Honda, C., Nakamura, R., Miyamoto, H., Sasaki, S., Demura, H., Nakamura, A.M., Michikami, T., Gaskell, R.W., Saito, J., 2009. Survey of possible impact structured on 25143 Itokawa. Icarus 200, 486–502.

Hiroi, T., Abe, M., Kitazato, K., Abe, S., Clark, B.E., Sasaki, S., Ishiguro, M., Barnouin-Jha, O.S., 2006. Developing space weathering on the asteroid 25143 Itokawa. Nature 443, 56–58.

Ishiguro, M., Hiroi, T., Tholen, D.J., Sasaki, S., Ueda, Y., Nimura, T., Abe, M., Clark, R.E., Yamamoto, A., Yoshida, F., Nakamura, R., Hirata, N., Miyamoto, H., Yokota, Y., Hashimoto, T., Kubota, T., Nakamura, A.M., Gaskell, R.W., Saito, J., 2007. Global mapping of the degree of space weathering on asteroid 25143 Itokawa by Hayabusa/AMICA observations. Meteorit. Planet. Sci. 42, 1791–1800.

Kawaguchi, J., 1986. Scientific Satellites Prospect. ISAS Report No. 43, 0285–2853 ISSN.

Kawaguchi, J., et al., 2002. launch readiness of the muses-C, a sample and returnfrom an asteroid. IAC-02-Q.5.2.04, 53rd international astronautical congress. The World Space Congress 2002, 10–19 Oct 2002/Houston, Texas.

Kawaguchi, J., 2003. muses-C launch and early operations report. AAS/AIAA astrodynamics specialists conference, AAS-03-662, big sky resort. Big Sky, Montana August 3-7, 2003.

Kawaguchi, J., 2010a. Hayabusa reentry and recovery of its capsule. COSPAR 2010, 04–10 2010, July 18-25, Bremen, Germany.

Kawaguchi, J., 2010b. Hayabusa's reentry and recovery of its capsule. International Astronautical Congress IAC-2010 IAC-10.A3.5.1, 2010 Sept.27-Oct.1, Prague, Czech.

Kawaguchi, J., Kuninaka, H., Yoshikawa, M., 2011. Return of hayabusa spacecraft and reentry of its capsule. 33rd Annual AAS Guidance and Control Conference, AAS 11-058 2011, February 5 - February 9 Breckenridge, Colorado.

Keller, L.P., Berger, E.L., 2014. A transmission electron microscope study of Itokawa regolith grains. Earth. Planets and Space 66, 71.

Kitajima, F., authors, 1.9., 2011. A micro-spectroscopic approach to the carbonaceous matter in the particles recovered by the Hayabusa mission. 42nd Lunar and Planetary Science Conference, 1855 Abstract.

Kitazato, K., Abe, M., Ishiguro, M., Ip, W.-.H., 2007. 25143 Itokawa: direct detection of the current decelerating spin state due to YORP effect. Astron. Astrophys. 472, L5–L8.

Longobardo, A., Hutzler, A., 2021. The NASA's Johnson space center astromaterials. facilities Chapter 11.

Lowry, S.C., Weissman, P.R., Duddy, S.R., Rozitis, B., Fitzsimmons, A., Green, S.F., Hicks, M.D., Snodgrass, C., Wolters, S.D., Chesley, S.R., Pittichová, J., van Oers, P., 2014. The internal structure of asteroid (25143) Itokawa as revealed by detection of YORP spin-up. Astron. Astrophys. 562, A48. doi:10.1051/0004-6361/201322602 http//dx.doi.org/.

Matsumoto, T.18 coauthors, 2012. Micro-structures of particle surfaces of Itokawa regolith and LL chondrite fragments. 43rd Lunar and Planetary Science Conference, 1969 Abstract.

Matsumoto, T.9 coauthors, 2013. Surface nano-morphologies of Itokawa regolith particles formed by space weathering processes: comparison with ion irradiation experiments. 44th Lunar and Planetary Science Conference, 1441 Abstract.

Matsumoto, T.9 coauthors, 2014. Surface micromorphologies of regolith particles from Asteroid Itokawa and its implication to space weathering. Meteoritics & Planetary Scienc 49: supplement, A266.

Michel, P., O'Brien Abe, A., Hirata, N., 2009. Itokawa's cratering record as observed by Hayabusa: implications for its age and collisional history. Icarus 200, 503–513.

Michel, P., Richardson, D.C., 2013. Collision and gravitational reaccumulation: possible formation mechanism of the asteroid Itokawa. Astron. Astrophys. 554, L1–L4.

Michel, P., Yoshikawa, M., 2005. Earth impact probability of the asteroid (25143) Itokawa to be sampled by the spacecraft Hayabusa. Icarus 179, 291–296.

Michel, P., Yoshikawa, M., 2006. Dynamical origin of Asteroid (25143) Itokawa: the target of the sample return mission Hayabusa. Astron. Astrophys. 449, 817–820.

Michikami, T., Nakamura, A.M., Hirata, N., Gaskell, R., Nakamura, R., Honda, C., Hiraoka, K., Saito, J., Demura, H., Ishiguro, M., Miyamoto, H., 2008. Size-frequency statistics of boulders on global surface on asteroid 25143 Itokawa. Earth Planets Space 60, 13–20.

Mikouchi, T.17 coauthors, 2014. Mineralogy and crystallography of some Itokawa particles returned by the Hayabusa asteroidal sample return mission. Earth, Planets and Space 66, 82.

Miyamoto, H., Yano, H., Scheeres, D., Abe, S., Barnouin-Jha, O.S., Cheng, A.F., Demura, H., Gaskell, R.W., Hirata, N., Ishiguro, M., Michikami, T., Nakamura, A.M., Nakamura, R., Saito, J., Sasaki, S., 2007. Regolith migration and sorting on asteroid Itokawa. Science 316, 1011–1014.

Mueller, T.G., Sekiguchi, T., Kaasalainen, M., Abe, M., Hasegawa, S., 2005. Thermal infrared observations of the Hayabusa spacecraft target asteroid 25143 Itokawa. Astron. Astrophys. 443, 347–355.
Mukai, T., Abe, S., Hirata, N., Nakamura, R., Barnouin-Ja, O.S., Cheng, A.F., Mizuno, T., Matsuoka, M., Scheeres, D.J., Yoshikawa, M., 2007. An overview of the LIDAR observations of asteroid 25143 Itokawa. Adv. Space Res. 40, 187–192.
Nagao, K.25 coauthors, 2011. Irradiation history of Itokawa regolith material deduced from noble gases in the Hayabusa samples. Science 333, 1128–1131.
Nagao, K., Okazaki, R., Miura, Y.N., Osawa, T., Gilmour, J., Nishimura, Y., 2013. Noble gas analysis of two Hayabusa samples as the first international A/O investigation: a progress report. 44th Lunar and Planetary Science Conference, 1976 Abstract.
Nakamura, E.17 coauthors, 2012. Space environment of an asteroid preserved on micrograins returned by the Hayabusa spacecraft. Proc. Natl Acad. Sci. 109, E624–E629.
Nakamura, T.21 authors, 2011. Itokawa dust particles: a direct link between S-type asteroids and ordinary chondrites. Science 333, 1113–1116.
Nakamura, T.22 authors, 2014. Mineral chemistry of MUSES-C Regio inferred from analysis of dust particles collected from the first- and second-touchdown sites on asteroid Itokawa. Meteorit. Planet. Sci. 49, 215–227.
Nakashima, D., Kita, N.T., Ushikubo, T., Noguchi, T., Nakamura, T., Valley, J.W., 2013. Oxygen three-isotope ratios of silicates particles returned from asteroid Itokawa by the Hayabusa spacecraft: a strong link with equilibrated LL chondrites. Earth Planet. Sci. Lett. 379, 127–136.
Naraoka, H.25 coauthors, 2012. Preliminary organic compound analysis of microparticles returned from Asteroid 25143 Itokawa by the Hayabusa mission. Geochem. J. 46, 61–72.
Noguchi, T.17 coauthors, 2011. Incipient space weathering observed on the surface of Itokawa dust particles. Science 333, 1121–1125.
Noguchi, T.23 coauthors, 2014a. Space weathered rims found on the surfaces of the Itokawa dust particles. Meteorit. Planet. Sci. 49, 188–214.
Noguchi, T.16 coauthors, 2014b. Mineralogy of four Itokawa particles collected from the first touchdown site. Earth, Planets and Space 66, 124.
Okazaki, R.9 coauthors, 2011. Noble gas recovered from the Hayabusa sample container. 42nd Lunar and Planetary Science Conference, 1653 Abstract.
Onose, N., Fujiwara, A., 2004. Mass-velocity distribution of fragments in oblique impact on gypsum. Meteorit, Planet. Sci. 39, 321–331.
Saito, J., Miyamoto, H., Nakamura, R., Ishiguro, M., Michikami, T., Nakamura, A.M., Demura, H., Sasaki, S., Hirata, N., Honda, C., Yamamoto, A., Yokota, Y., Fuse, T., Yoshida, F., Tholen, D.J., Gaskell, R.W., Hashimoto, T., Kubota, T., Higuchi, Y., Nakamura, T., Smith, P., Hiraoka, K., Honda, T., Kobayashi, S., Furuya, M., Matsumoto, N., Nemoto, E., Yukishita, A., Kitazato, K., Dermawan, B., Sogame, A., Terazono, J., Shinohara, C., Akiyama, H., 2006. Detailed images of asteroid 25143 Itokawa from Hayabusa. Science 312, 1341–1344.
Scheeres, D.J., Abe, M., Yoshikawa, M., Nakamura, R., Gaskell, R.W., Abell, P.A., 2007. The effect of YORP on Itokawa. Icarus, 188, 425–429.
Scheeres, D.J., Gaskell, R.W., 2008. Effect of density inhomogeneity on YORP: the case of Itokawa. Icarus 198, 125–129.
Sharma, I., 2010. Equilibrium shapes of rubble-pile binaries: the Darwin ellipsoids for gravitationally held granular aggregates. Icarus 205, 638–657.
Tanaka, M.12 coauthors, 2014. Crystallization temperature determination of Itokawa particles by plagioclase thermometry with X-ray diffraction data obtained by a high-resolution synchrotron Gandolfi camera. Meteorit. Planet. Sci. 49, 237–244.
Thompson, M.S., Christoffersen, R., Zega, T.Z., Keller, L.P., 2014. Microchemical and structural evidence for space weathering in soils from asteroid Itokawa. Earth, Planets and Space 66, 89.
Tsuchiyama, A.32 coauthors, 2011. Three-dimensional structure of Hayabusa samples: origin and evolution of Itokawa regolith. Science 333, 1125–1128.
Tsuchiyama, A., Matsumoto, T., Nagano, T., Matsuno, J., 2012. Microstructures of voids in Itokawa particles collected by Hayabusa. Meteorit. Planet. Sci. 47, A386.

Tsuchiyama, A.12 coauthors, 2013a. Analytical dual-energy microtomography: a new method for obtaining three-dimensional mineral phase images and its application to Hayabusa samples. Geochim. Cosmochim. Acta 116, 5–16.

Tsuchiyama, A., Matsumoto, T., Noguchi, T., 2013b. "Space erosion": a new type of space weathering process on the surface of asteroid Itokawa. 44th Lunar and Planetary Science Conference, 2169 Abstract.

Tsuchiyama, A., 2014a. Asteroid Itokawa a source of ordinary chondrites and a laboratory for surface processes. Elements 10, 45–50.

Tsuchiyama, A.16 coauthors, 2014b. Three-dimensional microstructure of samples recovered from asteroid 25143 Itokawa: comparison with LL5 and LL6 chondrite particles. Meteorit. Planet. Sci. 49, 172–187.

Tsuda, Y., Yoshikawa, M., Abe, M., Minamino, H., Nakazawa, S., 2013. System design of the Hayabusa 2 - Asteroid sample return mission to 1999 JU3. Acta Astronaut. 91, pp.356-362.

Vokrouhlický, D., Čapek, D., Kaasalainen, M., Ostro, S.J., 2004. Detectability of YORP rotational slowing of asteroid 25143 Itokawa. Astron. Astrophys. 414, L21–L24.

Wakita, S., Nakamura, T., Ikeda, T., Yurimoto, H., 2014. Thermal modeling for a parent body of Itokawa. Meteorit. Planet. Sci. 49, 228–236.

Yada, T.19 coauthors, 2014a. Hayabusa-returned sample curation in the planetary material sample. Curation Facility of JAXA. Meteoritics & Planetary Science 49, 135–153.

Yada, T.8 coauthors, 2014b. A nature of particles in the Hayabusa sample catcher and contamination controls for Hayabusa 2 sample containers. Meteorit. Planet. Sci. 49: supplement, A444.

Yano, H., Kubota, T., Miyamoto, H., Okada, T., Scheeres, D., Takagi, Y., Yoshida, K., Abe, M., Abe, S., Barnouin-Jha, O., Fujiwara, A., Hasegawa, S., Hashimoto, T., Ishiguro, M., Kato, M., Kawaguchi, J., Mukai, T., Sasaki, S., Yoshikawa, M., 2006. Touchdown of the hayabusa spacecraft at muse sea on Itokawa. Science 312, 1350–1353.

Yoshikawa, M., Watanabe, S., Tsuda, Y., Kuninaka, H., 2014. Hayabusa2 - the next asteroid sample return mission of Japan. Trans. JSASS Aerospace Tech. Japan Vol. 12 (No. ists29), 29–33.

Yoshikawa, M., Kawaguchi, J., Fujiwara, A., Tsuchiyama, A., 2015. Hayabusa Sample Return Mission Asteroids IV, 397–418.

Yurimoto, H.32 coauthors, 2011a. Oxygen isotopic compositions of asteroidal materials returned from Itokawa by the Hayabusa mission. Science 333, 1116–1119.

Yurimoto, H.32 coauthors, 2011b. Oxygen and magnesium isotopic compositions of Asteroid 25143 Itokawa returned by the Hayabusa mission. Meteorit. Planet. Sci. (46: supplement), A260.

Zolensky, M.E.23 coauthors, 2012. The shock state of Itokawa samples. 43rd Lunar and Planetary Science Conference, 1477 Abstract.

CHAPTER 7

The Hayabusa2 mission: what will we expect from samples from C-type near-Earth asteroid (162173) Ryugu?

Shogo Tachibana[a,b]
[a]UTokyo Organization for Planetary and Space Science (UTOPS), University of Tokyo, Tokyo, Japan
[b]Institute of Space and Astronautical Science, Japan Aerospace Exploration Agency (JAXA), Sagamihara, Kanagawa, Japan

Chapter Outlines

7.1 Introduction

Asteroids are the remnants of planetesimals that were the building blocks of planets in the early Solar System and record the origin and early evolution of the Solar System. The spacecraft Hayabusa (Yoshikawa et al., this book) made the first sample return from the near-Earth S-type asteroid (25143) Itokawa. Detailed mineralogical, petrological, and geochemical investigation of Itokawa particles found that Itokawa was once larger than 20 km and was heated up to ~800 °C (Nakamura et al., 2011). It was also found that active surface processes such as space-weathering, re-surfacing and particle escape occur at present even though the asteroid is thermally inactive (Tsuchiyama et al., 2011; Noguchi et al., 2011; Nagao et al., 2011). The important finding was that Itokawa

Sample Return Missions
DOI: 10.1016/C2018-0-03374-5

particles resemble equilibrated ordinary chondrites, the most common type of meteorites on the Earth, meaning that S-type asteroids are parent bodies of ordinary chondrites (Yurimoto et al., 2011; Nakamura et al., 2011; Ebihara et al., 2011).

Chondrites are undifferentiated meteorites that record processes in the early Solar System. Among chemical groups of chondrites, carbonaceous chondrites were not severely heated in their parent bodies and some carbonaceous chondrites contain hydrated silicates and organic matter. The presence of hydrated minerals and organics indicates that carbonaceous chondrites record well the origin and early evolution of the Solar System. The hydrogen isotopic compositions of carbonaceous chondrites are similar to that of the terrestrial ocean, and carbonaceous chondrites would have been a plausible deliverer of water and organic matter to the proto Earth.

C-type asteroids have been known to be spectroscopically similar to carbonaceous chondrites, but no direct linkage has been confirmed between C-type asteroids and carbonaceous chondrites. In order to find what C-type asteroids are and what they record the origin and evolution of the Solar System, the Japanese Aerospace Exploration Agency (JAXA) planned and performed the sample return mission Hayabusa2 to a near-Earth C-type asteroid. Scientific instruments on board Hayabusa2 are a laser altimeter (LIDAR) (Mizuno et al., 2017), a multi-band telescopic camera (ONC-T) (Kameda et al., 2017), wide-angle cameras (ONC-W1 and -W2), a near-infrared spectrometer (NIRS3) (Iwata et al., 2017), a thermal infrared imager (TIR) (Okada et al., 2017), a small carry-on impactor (SCI) (Saiki et al., 2017), and a sampler (SMP) for acquisition of surface materials (Tachibana et al., 2014; Sawada et al., 2017; Okazaki et al., 2017). The spacecraft brought a lander MASCOT, which was developed by DLR (Deutsches Zentrum für Luft- und Raumfahrt) and CNES (Le Centre National d'Etudes Spatiales) for in-situ surface investigation (Ho et al., 2017).

The target asteroid was (162173) 1999 JU_3, which was named as Ryugu after the launch of Hayabusa2 (Ryugu is the undersea palace in a Japanese fairy tale). The objective of sample science in the mission was summarized in Tachibana et al., 2014 before the Hayabusa2 launch. In this chapter, the objective of Hayabusa2 sample science is revisited based on Hayabusa2's findings at Ryugu.

7.2 What did Hayabusa2 find at Ryugu?

Hayabusa2 made rendezvous and proximity operation at Ryugu (Fig. 7.1) for about a year and half (June 2018–November 2019) including two landing operations for sample collection. The spacecraft first found: (1) Ryugu (mean radius of 448 ± 2 m) has a retrograde rotation with a period of 7.6326 h and an obliquity of 172 ° (Watanabe et al., 2019). (2) Ryugu has a top shape with an equatorial ridge (Watanabe et al., 2019). (3) The bulk density is 1.19 ± 0.03 g/cm^3 (Watanabe et al., 2019). (4) Many large (> 20 m) boulders are present at the surface with a number density twice as large as that of Itokawa, and there is no smooth terrain as seen in Itokawa (Sugita et al., 2019). (5) Many

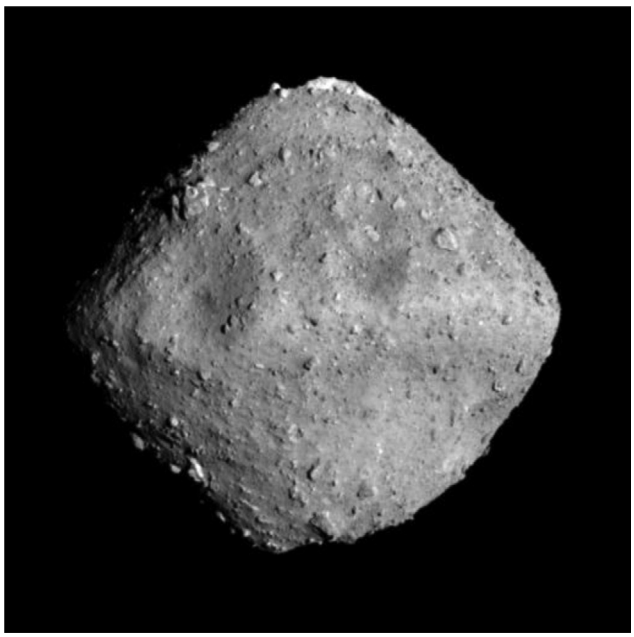

Fig. 7.1 ***C-type near-Earth asteroid (162173) Ryugu.*** Copyright: JAXA, Univ. Tokyo, Kochi Univ., Rikkyo Univ., Nagoya Univ., Chiba Inst. Tech., Meiji Univ. Univ. Aizu, AIST.

boulders are too large to be impact ejecta from craters (Sugita et al., 2019). (6) The low bulk density and the abundant large boulders suggests that Ryugu is a rubble-pile body (Watanabe et al., 2019; Sugita et al., 2019). (7) The surface has uniformity in visible spectra with very low geometric albedo (~0.043), darker than most of meteorite samples (Sugita et al., 2019). (8) A weak 2.72 μm absorption feature, observed globally, indicates the ubiquitous presence of OH-bearing hydrated minerals (Kitazato et al., 2019). The absorption is not as strong as those of typical hydrated carbonaceous chondrites and that of B-type asteroid (101955) Bennu observed by the NASAs spacecraft OSIRIS-REx (Lauretta et al., 2019, this book; Hamilton et al., 2019). The weak OH feature could be either due to partial dehydration of hydrous silicates or lack of severe aqueous alteration in the Ryugu's parent planetesimal (Sugita et al., 2019; Kitazato et al., 2019).

Further observation found that Ryugu surface shows a variety of reflectance spectra due to mixing of materials with bluish and reddish tints (Sugita et al., 2019; Morota et al., 2020). This color variation correlates with geographic features; the equatorial ridge and the polar regions are bluish, while the mid-latitude region is reddish (Sugita et al., 2019; Morota et al., 2020). The inside of relatively old craters is as reddish as the surroundings, whereas the relatively young craters have more bluish floors than the surroundings (Morota et al., 2020). These findings suggest that the reddish color results from surface alteration of bluish original materials occurring within the recent 10^6–10^7 years. Two types of bright boulders suggest the presence of ordinary chondrite-like

materials and thermally metamorphosed Ryugu materials on the surface, which could be related to the collisional evolution of the asteroid (Tatsumi et al., 2020).

The MASCOT lander on board Hayabusa2 showed that the surface is not covered with fine regolith particles (Jaumann et al., 2019) and that a ~3 cm pebble has a thermal inertia of ~280 $J\ m^{-2}\ K^{-1}\ s^{-½}$, which is much lower than chondritic meteorites (Grott et al., 2019). The low thermal inertia implies that the pebble has a porosity larger than 28 percent and that the tensile strength of the pebble is likely to be only a few hundred kPa (Grott et al., 2019). Similar low thermal inertia (~300 $J\ m^{-2}\ K^{-1}\ s^{-½}$) was also observed for many surface boulders, suggesting that Ryugu surface materials are more porous than carbonaceous chondrites (Okada et al., 2020). The artificial impact experiment with SCI produced an artificial crater with a diameter larger than 10 meter which indicates that the Ryugu surface is composed of a cohesionless material like loose sand (Arakawa et al., 2020).

7.3 Sample acquisition at Ryugu

Hayabusa2 made its first landing operation on the equatorial ridge on February 22, 2019 to collect surface samples and the second landing operation nearby the artificial SCI crater on July 11, 2019 to collect both surface samples and impact ejecta (sub-surface samples). A 5-gram tantalum projectile was shot through a 1-m long sampler horn at an impact velocity 300 ± 30 m s^{-1} at the timing of each touchdown, triggered by bending and/or shrinkage of the sampler horn (Fig. 7.2) (Sawada et al., 2017). The firing of projectiles was confirmed for two landing operations through the temperature rise near the projector due to firing. The ejecta is supposed to be put into a sample catcher through an extendable sampler horn and a conical horn under a microgravity condition (Fig. 7.2). On-ground laboratory experiments using the full-scale sampling device with 1 mm-sized glass spherules at one gravity showed that 150–250 mg of samples can be collected with a projectile shooting, which is expected to be increased under the microgravity condition because low-velocity ejecta can be effectively collected (Sawada et al., 2017).

The basic concept and design of the Hayabusa2 projectile-shooting sampling device are the same as those of the Hayabusa sampling device (Yano et al., 2006), which did not fire projectiles on Itokawa, but collected samples in alternative (unknown) ways during the mission. Two landing operations of Hayabusa2 proved for the first time that the projectile-shooting sampling device works at the asteroid surface. The firing of the projectile was supposed to be done in a closed explosive chamber of the projector to avoid contamination of explosion products (Sawada et al., 2017; Takano et al., 2020).

The sample catcher of the Hayabusa2, located at the top end of the conical horn, has three chambers to store samples, acquired at different surface locations, separately (Fig. 7.2) (Sawada et al., 2017). A rotatable inlet, connected to the conical horn, to the sample catcher was successfully rotated after the first landing operation to change the

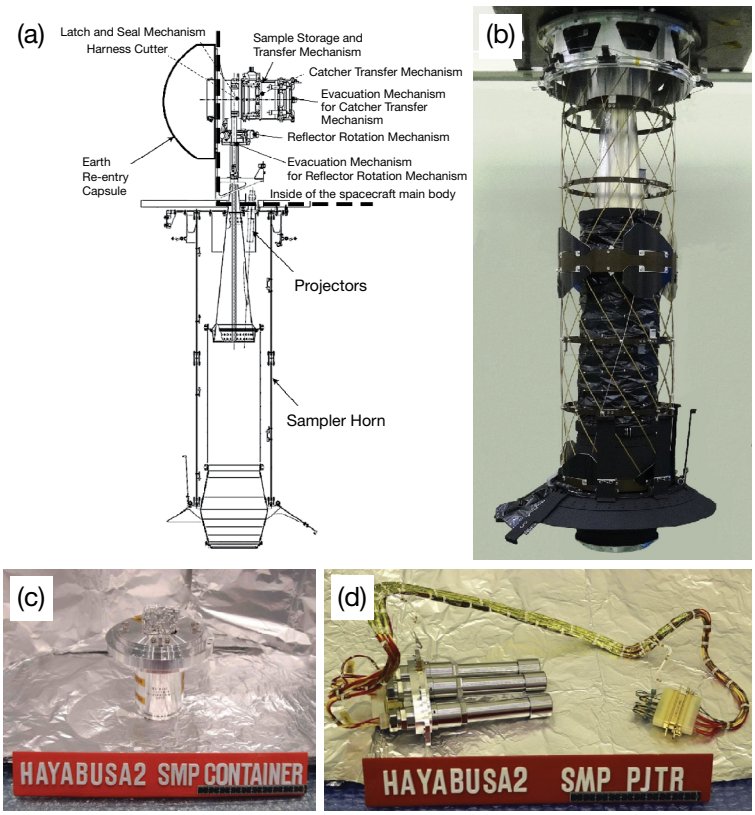

Fig. 7.2 ***Hayabusa2 Sampler (modified from Sawada et al., 2017).*** (a) Schematic illustration of the Sampler system. (b) The Sampler horn on-orbit configuration. (c) The sample container. (d) The projector system.

chamber for sample storage. The first and third chambers were used to store the samples collected during the first and second landing operations.

On August 26, 2019, the sample catcher, of which chambers were all closed, was transported into the sample container inside the Earth re-entry capsule and sealed successfully (Fig. 7.2). The container sealing method adopted for Hayabusa2 is an aluminum metal seal, where the sample catcher is sealed in the sample container by deformation of the curved surface lid with the edge of the sample container (Okazaki et al., 2017). This sealing method allows only a leak of 1 Pa air for 100 h at atmospheric pressure (Okazaki et al., 2017).

The characteristics of the Hayabusa2 sample container leads to classification of returned samples into three categories; (1) mm-sized coarse grains stored separately in three chambers, (2) <100 μm-sized fine grains that may be mixed in the sample container, and (3) volatiles components that will be released from the samples and will be extracted from the container prior to its opening.

Coarse grains should represent material properties at two sampling locations, and petrologic and mineralogical studies of them will provide important constraints on understanding the history of the asteroid and the Solar System. Fine grained samples will also provide insights into the global average surface features and surface geologic processes such as space weathering and regolith formation. Volatile components will be the first-returned extra-terrestrial volatiles and will be an important analysis target to investigate the origin and evolution of organic matter and water in the Solar System and the final evolutional state of organics in asteroids prior to the delivery to the proto Earth.

7.4 Science goals of returned sample analysis

The science goals of Ryugu sample analysis discussed in Tachibana et al., 2014 (Table 7.1) are here reviewed.

Ryugu is expected to be related to carbonaceous chondrites (Tachibana et al., 2014; Sugita et al., 2019; Kitazato et al., 2019). Carbonaceous chondrites have been investigated to study the processes occurred in the early Solar System, including the evolution of volatiles and organics. However, extraterrestrial samples recovered on the Earth are always subject to terrestrial contamination of water and organic matter. There may also

Table 7.1 Scientific objectives of Ryugu sample analysis (Modified from Tachibana et al., 2014).

Galaxy / Molecular Cloud	Protoplanetary Disk	Planetesimal	Main-Belt Asteroid	Near Earth Asteroid
Presolar Grains Nucleosynthesis Galactic chemical evolution **Molecular Cloud Organics** Low temperature processes Enrichment of heavy isotopes (D, ^{15}N)	**CAIs, Chondrules Metal** High temperature processes Constraint on the timing of parent body formation **Disk Organics** Evaporation/ Alteration Fischer-Tropsch type reactions	**Aqueous Alteration Thermal and Shock Metamorphism** Conditions and timing **Diversity of Organics** Mineral-Organics association L-enantiomer excess of amino acids	**Shock Metamorphism** Conditions and timing **Galactic Cosmic Ray** Exposure history **Bulk Density** Internal structure **Strength and Thermal Properties** Collisional evolution	**Space Weathering** Ages, Regolith dynamics, Space environments, SW, Surface activity, Orbital evolution **Thermal Metamorphism** Heating by sunlight
Spatial Variation/Heterogeneity of Returned Samples Planetesimal formation processes, Disk evolution Parent body size, Parent body processes				
Comparison with Meteorites, Interplanetary Dust Particles, and Bennu samples Uniqueness and commonness				

be a sampling bias for carbonaceous chondrites during the atmospheric entry because they are more fragile than ordinary chondrites (Flynn et al., 2018). Moreover, extraterrestrial materials recovered on the Earth have little information on geological processes on their parent bodies. The importance of sample return from C-type asteroids, plausible parent bodies of carbonaceous chondrites, is therefore clear.

7.4.1 Galactic chemical evolution and Sun's parent molecular cloud chemistry

Presolar grains with anomalous isotopic compositions are ancient stardust that formed in stellar envelopes of evolved stars. Their isotopic compositions have provided insights into stellar nucleosynthesis (e.g., Zinner, 2014). Moreover, circumstellar dust formation processes as well as the processes in the interstellar medium are recorded in their lattice structures and morphology (e.g., Takigawa et al., 2014, 2018). Presolar grains in Ryugu samples are an interesting science target to link the origin of the Solar System to the galactic chemical evolution. The abundances of presolar grains will also be a good indicator of thermal and/or aqueous alteration processes on Ryugu's parent body because their abundances decrease with degree of parent body processes (Floss and Haenecour, 2016). The presolar grain abundance may alternatively indicate thermal processes in the protosolar disk (Yamamoto et al., 2018, 2019).

Various microbeam analytical techniques such as isotope microscope, secondary ion mass spectroscopy (SIMS), focused ion beam (FIB) milling, and transmission electron microscopy (TEM) and their coordination are the key to investigate elemental, isotopic and mineralogical features of presolar grains (e.g., Yurimoto et al., 2003; Nagashima et al., 2004; Nguyen et al., 2010; Takigawa et al., 2018).

Organic materials enriched in heavy isotopes (D and ^{15}N) have been found in carbonaceous chondrites, micrometeorites, and interplanetary dust particles (e.g., Busemann et al., 2006). The enrichments of heavy isotopes have been attributed to chemical reactions at low temperatures (~10 K) in the Sun's parent molecular cloud.

Organic materials found in return samples from the comet Wild2 and Antarctic micrometeorites are enriched in N and O compared with insoluble organic matter in carbonaceous chondrites (Cody et al., 2008; Yabuta et al., 2017), suggesting that N- and O-rich organic materials are the most primitive organic materials in the Solar System.

The survey of such primitive organic materials in Ryugu samples and their characterization will be of significant importance. The Hayabusa2 spacecraft acquired surface samples at two locations with multi-scale geological information, and the alteration effect on the parent asteroid will be best known and both pre-accretional and post-accretional evolution of organic matter will possibly be investigated in detail. Along with microbeam analysis described above, X-ray absorption near edge structure (XANES) spectroscopy using scanning transmission X-ray microscopy (STXM) at synchrotron facilities will provide structural information of macromocular refractory organics (e.g.,

Yabuta et al., 2017). Nondestructive elemental analysis using muon beam can also be a potentially useful analytical technique to determine bulk abundances of carbon and nitrogen (Terada et al., 2014, 2017).

7.4.2 Pre-accretional chemical evolution and planetesimal formation in the protosolar disk

The chemical diversity of chondrites has been attributed to elemental and oxygen-isotopic fractionation processes in the early Solar System prior to planetesimal formation, and should have been preserved in the protosolar disk. The chemical and isotopic characteristics of Ryugu should thus be studied in detail first to compare Ryugu samples with known extraterrestrial materials. For instance, oxygen isotope microanalysis of Itokawa grains linked Itokawa to LL chondrites (Yurimoto et al., 2011). The oxygen isotope composition of Ryugu samples will be determined to find if there is any meteorite group that resembles Ryugu. It is also important to investigate the chemical diversity within Ryugu samples, which could be related to the material mixing within the protosolar disk and on a feeding zone of the asteroid. Ryugu samples may also shed light on the recent discussion on the dichotomy of early Solar System materials (Warren, 2011; Kleine et al., 2020). Bulk elemental and isotope analyses combined with in-situ microanalysis are thus a key for characterization of Ryugu samples.

Characteristic constituents within chondrites are high-temperature components formed in the protosolar disk, such as CAIs (Calcium-Aluminium-rich Inclusions) and chondrules. The abundance of CAIs and the size, chemical composition, and redox state of chondrules differs among chemical groups of chondrites, so that the properties of high-temperature components can also be used for classification of returned samples. The formation ages of high-temperature components in Ryugu samples will make contribution to pre-accretional material evolution in the protosolar disk and will constrain the formation age of Ryugu's parent planetesimal as well. A coordinated mineralogical, petrological, and geochemical analysis using a variety of microbeam analysis techniques will be important to explore pre-accretional processes recorded in Ryugu samples (e.g., (Kita et al., 2010); (Ushikubo et al., 2012); (Kawasaki et al., 2018).

7.4.3 Planetesimal processes: properties of the planetesimal and final evolutional stage of volatiles prior to delivery to planets

The presence of hydrated silicates on a ~1-km-sized asteroid Ryugu suggests that aqueous alteration should have occurred inside the Ryugu's parent planetesimal, which may have been larger than the present size of the asteroid. Combination of analyses of returned samples from two different surface locations and multi-scale remote-sensing observations is expected to provide us the first opportunity to study aqueous alteration processes in an asteroidal scale. If carbonates are found in the samples, they may record the timing of aqueous alteration (Fujiya et al., 2012; Doyle et al., 2015) and would be a target for ^{53}Mn-^{53}Cr

dating. A systematic study of the degree and variety of aqueous alteration and its age will invoke discussion on the timing of planetesimal formation and the size and structure of the planetesimal. The degree of thermal metamorphism, recorded in mineralogy and petrology of returned samples, should also put constraints on the heat source, the maximum temperature, and the duration. Synchrotron X-ray diffraction and X-ray computed tomography (CT) will provide mineralogical and petrological information nondestructively as in the case of Itokawa particles (e.g., Nakamura et al., 2011; Tsuchiyama et al., 2011). A coordinated microanalysis with field-emission scanning electron microscope (FE-SEM), field emission electron microprobe (FE-EPMA), FIB, TEM, and SIMS will be useful to investigate the planetesimal processes and their chronology.

Diversification of organic matter is one of the most important scientific themes of returned sample analyses. Molecular diversity should represent the processes that organic matter experienced (Naraoka et al., 2017; Orthous-Daunay et al., 2019). It has been known that the relative abundance of amino acid (isovaline) is correlated with the abundance of phyllosilicates, products of asteroidal aqueous alteration (Pizzarello et al., 2003). Experimental work has shown that various organic molecules including amino acids can form by hydrothermal reactions from simple molecules (e.g., Kebukawa et al., 2017; Isono et al., 2019). Moreover, excess of L-enantiomer of isovaline in carbonaceous chondrites has been known to positively correlate with the degree of aqueous alteration (Glavin and Dworkin, 2009). A systematic study of variations in the mineralogy, petrology, and soluble and insoluble organic matter in Ryugu samples should be systematically studied to understand the final evolutional stage of organic matter prior to the delivery to larger bodies. Liquid chromatography-Orbitrap mass spectrometry (Orbitrap LC-MS) will be a useful tool to explore the molecular diversity (e.g., Schmitt-Kopplin et al., 2010; Naraoka et al., 2017; Orthous-Daunay et al., 2019). This technique has been recently applied by Naraoka and Hashiguchi (2019) to in-situ analysis of organic molecules in carbonaceous chondrites.

7.4.4 Geological evolution of the parent asteroid in the solar system

Because Ryugu is a C-type aqueously-altered asteroid (Kitazato et al., 2019), it would have been once a larger body in which fluids circulated, and would have been destructed and re-accumulated as a rubble-pile body (Watanabe et al., 2019; Sugita et al., 2019). The timing of impact events could be determined by Ar-Ar dating of samples and/or Pb-Pb dating of phosphates as in the case of Itokawa particles (Park et al., 2015; Jourdan et al., 2017; Terada et al., 2018) although the shock ages may not correspond exactly to the timing of formation of the present Ryugu.

The bulk density of returned samples should be measured to determine the micro-porosity of Ryugu. The strength of returned samples will also be an important parameter to understand the internal structure of the asteroid and its evolution. Volume measurements of Ryugu grains with synchrotron X-ray CT will be useful to determine the grain density.

7.4.5 Surface geological processes of near-Earth asteroid

Ryugu is a near-Earth asteroid, of which surface has been heated by sunlight and has been space-weathered by solar winds more than at its original orbit in the asteroid belt. Itokawa particles well preserve space-weathering processes on their surfaces (e.g., Noguchi et al., 2011, 2014; Nagao et al., 2011). The space weathering rim, surface structure and noble gas compositions of Ryugu particles will be carefully investigated using FIB-TEM, FE-SEM, and noble gas mass spectroscopy to understand space-weathering on the surface of C-type asteroids for the first time. Particle morphology, which will be determined by synchrotron X-CT, could be related to surface geological processes as discussed for Itokawa particles (Tsuchiyama et al., 2011), and could give insight into particle movement on Ryugu (Sugita et al., 2019; Morota et al., 2019). The thermal metamorphism at the surface of near-Earth asteroid will also be studied, which could put a constraint on the orbital evolution of Ryugu (e.g., the maximum temperature and duration). Comparison between surface samples and sub-surface SCI ejecta samples, which could be distinguished by galactic cosmic-ray produced cosmogenic nuclides, will be important for this purpose.

7.4.6 Integration of multiscale data from atomic-scale to asteroidal scale, and comparison with meteorites, interplanetary dust particles, and future return samples

Detailed micro-scale information obtained from Ryugu samples should be tightly combined with on-site remote sensing data obtained at asteroidal- to regional-scale. Integrated data set from atomistic to asteroidal scale will be a key to constructing the entire history of Ryugu.

It is also particularly important to compare Ryugu samples with meteorites, interplanetary dust particles, and future return samples in order to expand the knowledge obtained in the mission to all aspects of cosmochemistry. The comparison with samples from the B-type near-Earth asteroid Bennu, which is supposed to be back to the Earth in September 2023 (Lauretta et al., 2019; Lauretta et al., this book), is crucial for better understanding of the commonness and uniqueness of Ryugu.

7.4.7 Expected sample science from Ryugu based on Hayabusa2 findings

The expected science from Ryugu samples based on the results obtained by detailed observation of Ryugu by Hayabusa2 is summarized in Table 7.1.

The remote sensing observation by scientific instruments on board the spacecraft and in-situ surface observation by the MASCOT lander found that samples from C-type asteroid Ryugu would be 'atypical' compared to typical hydrated carbonaceous chondrites in the terrestrial collection.

The low albedo and the weak 2.72 μm absorption feature of Ryugu could be attributed to thermal and/or shock-induced dehydration of hydrated carbonaceous chondrite-like materials on the asteroid because mildly dehydrated carbonaceous chondrites have an albedo as low as Ryugu (Sugita et al., 2019). If Ryugu samples are dehydrated

carbonaceous chondrites, the sample analysis will reveal alteration and metamorphic processes on the Ryugu's parent planetesimal or on the current Ryugu. If sub-surface materials are identified from the samples collected nearby the artificial crater by sample analysis (e.g., analysis of galactic cosmic ray-produced nuclides), the petrology, mineralogy, and volatile chemistry of sub-surface samples would put constraints on the surface dehydration process that would be induced by solar heating.

Even if the Ryugu samples experienced dehydration, they are expected to contain hydrated minerals that cause the 2.72 μm absorption feature, suggesting that the samples were not heated like Itokawa samples. The Ryugu samples should thus provide us with the information of material evolution prior to planetesimal accretion in the Sun's protoplanetary disk as well.

The MASCOT observation implies that the surface pebble is more fragile than typical carbonaceous chondrites and would be too fragile to survive when it enters into the Earth's atmosphere as a meteor (Grott et al., 2019). The Ryugu sample may thus represent pristine Solar-System materials that experienced only weak aqueous alteration on the Ryugu's parent body like weakly altered Antarctic micrometeorites (Noguchi et al., 2017; Yabuta et al., 2017).

If this is the case, the Ryugu samples could contain abundant pristine components that formed in the Sun's protoplanetary disk, in the Sun's parent molecular cloud, and even in outflows from evolved stars prior to the Solar System formation. The samples may contain abundant amorphous silicates, which are commonly found in the matrix of least altered carbonaceous chondrites (e.g., Davidson et al., 2019). Amorphous silicate can be used a thermometer of parent body processes because it crystallizes through annealing (e.g., Yamamoto and Tachibana, 2018).

The low albedo of Ryugu could be due to the presence of abundant macromolecular organic components that may have formed through low temperature photochemical processes in the Sun's parent molecular cloud (e.g., Piani et al., 2017; Tachibana et al., 2017). Pristine volatile materials such as H_2O, CO_2, CH_4, NH_3 and organic molecules could also be released from the fragile samples that might be broken inside the sample catcher. Extracted gases, which would be the first volatile component returned from space, and their isotopic compositions would be an important analysis target to understand the evolution of volatiles in the early Solar System and the delivery of volatiles to the inner Solar System.

At present it is not clear whether Ryugu with the weak -OH vibration feature is dehydrated or weakly altered, detailed analysis of Ryugu samples will reveal the history of Ryugu and the Solar System from the beginning to the present.

7.5 Summary

Hayabusa2, an asteroid exploration mission to return surface samples of a near-Earth C-type asteroid Ryugu, found that Ryugu (mean radius of 448 ± 2 m) has a top shape with an equatorial ridge and has a retrograde rotation with a period of 7.6326 h and an

obliquity of 172 ° Its bulk density (1.19 ± 0.03 g cm^{-3}) suggests that Ryugu is a rubble-pile body with a large macro-porosity of ~50–60 percent considering a typical density of carbonaceous chondrites. The surface has a very low geometric albedo, darker than most of meteorite samples in the terrestrial collection, and shows a weak but ubiquitous 2.72 μm absorption feature of OH vibration in hydrous minerals. The absorption feature at 2.72 μm is weaker than those of hydrated carbonaceous chondrites and that of B-type asteroid Bennu. The surface boulders have lower thermal inertia than chondrites. The spacecraft succeeded two landing operations for sample collection and just recently delivered the re-entry capsule to the Earth (December, 2020).

The returned Ryugu samples will be investigated non-destructively without exposure to air at the JAXA Planetary Material Sample Curation Facility, described in detail by Abe (this book). Ten percent of the sample mass will be delivered to the NASA Johnson Space Center one year later from the Earth re-entry capsule recovery (Longobardo and Hutzler, this book). The returned samples will be investigated by the Hayabusa2 project for one year after the six-month investigation at the JAXA Planetary Material Sample Curation Facility. State-of-the-art analytical techniques, described above, will be used for sample analysis to understand the long history of the Solar System, especially focusing on (1) galactic chemical evolution and Sun's parent molecular cloud chemistry, (2) pre-accretional chemical evolution and planetesimal formation in the protosolar disk, (3) planetesimal processes: the final evolutional stage of volatiles prior to the delivery to planets, (4) geological evolution of asteroid in the solar system, and (5) orbital evolution and surface geological processes of near-Earth asteroid. It is not clear at present whether Ryugu is composed of thermally altered carbonaceous chondrite-like materials or weakly aqueously altered pristine samples, but the samples will tell us what C-type asteroids are and stimulate discussion on the early evolution of the Solar System and small bodies.

Avcknowledgement

I am grateful to members of the Hayabusa2 Sampler team, especially H. Sawada, R. Okazaki, Y. Takano, Y. N. Miura, K. Sakamoto, C. Okamoto, and H. Yano, for the development and operation of the Hayabusa2 sampler system. I also thank the Hayabusa2 Project team for the wonderful and successful exploration.

References

Abe, M., The JAXA Planetary Material Sample Curation Facility, this book, Chapter 12.

Arakawa, M., et al., 2020. An artificial impact on the asteroid 162173 Ryugu formed a crater in the gravity-dominated regime. Science. doi:10.1126/science.aaz1701.

Busemann, H., et al., 2006. Interstellar chemistry recorded in organic matter from primitive mete- orites. Science 312, 727–730.

Cody, G.D., et al., 2008. Quantitative organic and light-element analysis of comet 81P/wild 2 particles using C-, N-, and O-μ-XANES. Meteorit. Planet. Sci. 43, 353–365.

Davidson, J., et al., 2019. Mineralogy and petrology of dominion range 08006: a very primitive CO3 carbonaceous chondrite. Geochim. Cosmochim. Acta 265, 259–278.
Doyle, P.M., et al., 2015. Early aqueous activity on the ordinary and carbonaceous chondrite parent bodies recorded by fayalite. Nat. Commun. 6, 7444. doi:10.1038/ncomms8444.
Ebihara, M., et al., 2011. Neutron activation analysis of a particle returned from asteroid Itokawa. Science 333, 1119–1121.
Floss, C., Haenecour, P., 2016. Presolar silicate grains: abundances, isotopic and elemental compositions, and the effects of secondary processing. Geochem. J. 50, 3–25.
Fujiya, W., et al., 2012. Evidence for the late formation of hydrous asteroids from young meteoritic carbonates. Nat. Commun. 3, 627. doi:10.1038/ncomms1635.
Flynn, G.J., et al., 2018. Physical properties of the stone meteorites: implications for the properties of their parent bodies. Geochemistry 78, 269–298.
Glavin, D.P., Dworkin, J.P., 2009. Enrichment of the amino acid L-isovaline by aqueous alteration on CI and CM meteorite parent bodies. Proc. Natl. Acad. Sci. USA 106, 5487–5492.
Grott, M., et al., 2019. Low thermal conductivity boulder with high porosity identified on C-type asteroid (162173) Ryugu. Nature Astronomy 3, 971–976.
Hamilton, V.E., et al., 2019. Evidence for widespread hydrated minerals on asteroid (101955) Bennu. Nature Astronomy 3, 332–340.
Ho, T.-.M., et al., 2017. MASCOT—the mobile asteroid surface scout onboard the hayabusa2 mission. Space Sci. Rev. 208, 339–374.
Isono, Y., et al., 2019. Bulk chemical characteristics of soluble polar organic molecules formed through condensation of formaldehyde: comparison with soluble organic molecules in Murchison meteorite. Geochem. J. 53, 41–51.
Iwata, T., 2017. NIRS3: the near infrared spectrometer on hayabusa2. Space Sci. Rev. 208, 317–337.
Jaumann, R., et al., 2019. Images from the surface of asteroid Ryugu show rocks similar to carbonaceous chondrite meteorites. Science 365, 817–820.
Jourdan, F., et al., 2017. Collisional history of asteroid Itokawa. Geology 45, 819–822.
Kameda, S., et al., 2017. Preflight calibration test results for optical navigation camera telescope (ONC-T) onboard the hayabusa2 spacecraft. Space Sci. Rev. 208, 17–31.
Kawasaki, N., et al., 2018. Crystal growth and disequilibrium distribution of oxygen isotopes in an igneous Ca-Al-rich inclusion from the Allende carbonaceous chondrite. Geochim. Cosmochim. Acta 221, 318–341.
Kebukawa, Y., et al., 2017. One-pot synthesis of amino acid precursors with insoluble organic matter in planetesimals with aqueous activity. Sci Adv 3, e1602093.
Kita, N.T., et al., 2010. High precision SIMS oxygen three isotope study of chondrules in LL3 chondrites: Role of ambient gas during chondrule formation. Geochim. Cosmochim. Acta 74, 6610–6635.
Kitazato, K., et al., 2019. Surface composition of asteroid 162173 Ryugu as observed by the hayabusa2 NIRS3 instrument. Science 364, 272–275.
Kleine, T., et al., 2020. The non-carbonaceous–carbonaceous meteorite dichotomy. Space Sci. Rev. 216, 55.
Lauretta, D.S., et al., 2019. The unexpected surface of asteroid (101955) Bennu. Nature 568, 55–60.
Lauretta D.S. et al., OSIRIS-REx at Bennu: Overcoming Challenges to Collect a Sample of the Early Solar System, Chapter 8, this book.
Longobardo A. and Hutzler A., The NASA's Johnson Space Center Astromaterials Facilities, Chapter 11, this book.
Mizuno, T., et al., 2017. Development of the laser altimeter (LIDAR) for hayabusa2. Space Sci. Rev 208, 33–47.
Morota, T., et al., 2020. Sample collection from asteroid (162173) ryugu by hayabusa2: implications for surface evolution. Science 368, 654–659.
Nagashima, K., et al., 2004. Stardust silicates from primitive meteorites. Nature 428, 921–924.
Nakamura, T., 2011. Itokawa dust particles: a direct link between S-type asteroids and ordinary chondrites. Science 333, 1113–1116.
Nagao, K., et al., 2011. Irradiation history of Itokawa regolith material deduced from noble gases in the hayabusa samples. Science 333, 1128–1131.
Naraoka, H., et al., 2017. Molecular evolution of N-containing cyclic compounds in the parent body of the murchison meteorite. ACS Earth and Space Chemistry 1, 540–550.

Naraoka, H., Hashiguchi, M., 2019. Distinct distribution of soluble N-heterocyclic compounds between CM and CR chondrites. Geochem. J. 53, 33–40.
Nguyen, A., et al., 2010. Coordinated analyses of presolar grains in the allan hills 77307 and queen elizabeth range 99177 meteorites. Astrophys. J. 719, 166–189.
Noguchi, T., et al., 2011. Incipient space weathering observed on the surface of Itokawa dust particles. Science 333, 1121–1125.
Noguchi, T., et al., 2014. Space weathered rims found on the surfaces of the Itokawa dust particles. Meteorit. Planet. Sci. 49, 188–214.
Noguchi, T., et al., 2017. Variation of mineralogy and organic material during the early stages of aqueous activity recorded in Antarctic micrometeorites. Geochim. Cosmochim. Acta 208, 119–144.
Okada, T., et al., 2017. Thermal infrared imaging experiments of C-type asteroid 162173 ryugu on hayabusa2. Space Sci. Rev. 208, 125–142.
Okada, T., et al., 2020. Highly porous nature of a primitive asteroid revealed by thermal imaging. Nature 579, 518–525.
Okazaki, R., et al., 2017. Hayabusa2 sample catcher and container: metal-seal system for vacuum encapsulation of returned samples with volatiles and organic compounds recovered from C-type asteroid Ryugu. Space Sci. Rev. 208, 107–124.
Orthous-Daunay, F.-.R., et al., 2019. Ultraviolet-photon fingerprints on chondritic large organic molecules. Geochem. J. 53, 21–32.
Park, J., et al., 2015. $^{40}Ar/^{39}Ar$ age of material returned from asteroid 25143 itokawa. Meteor. Planet. Sci. 50, 2087–2098.
Piani, L., et al., 2017. Evolution of morphological and physical properties of laboratory interstellar organic residues with ultraviolet irradiation. Astrophys. J. 837. doi:10.3847/1538-4357/aa5ca6.
Pizzarello, S., et al., 2003. Nonracemic isovaline in the Murchison meteorite: chiral distribution and mineral association. Geochim. Cosmochim. Acta 67, 1589–1595.
Saiki, T., et al., 2017. The small carry-on impactor (SCI) and the Hayabusa2 impact experiment. Space Sci. Rev. 208, 165–186.
Sawada, H., et al., 2017. Hayabusa2 sampler: collection of asteroidal surface material. Space Sci. Rev 208, 81–106.
Schmitt-Kopplin, P., et al., 2010. High molecular diversity of extraterrestrial organic matter in murchison meteorite revealed 40 years after its fall. Proc. Natl. Acad. Sci. USA 107, 2763–2768.
Sugita, S., et al., 2019. The geomorphology, color, and thermal properties of Ryugu: implications for parent-body processes. Science 364, 1–11 eaaw0422.
Tachibana, S., et al., 2014. Hayabusa2: scientific importance of samples returned from C-type near-earth asteroid (162173) 1999 JU_3. Geochem. J. 48, 571–587.
Tachibana, S., et al., 2017. Liquid-like behavior of UV-irradiated interstellar ice analog at low temperatures. Sci. Adv. 3, eaao2538.
Takano, Y., et al., 2020. Chemical assessment of the explosive chamber in the projector system of Hayabusa2 for asteroid sampling. Earth Planet. Space 72, 97.
Takigawa, A., et al., 2014. Morphology and crystal structures of solar and presolar Al_2O_3 in unequilibrated ordinary chondrites. Geochim. Cosmochim. Acta 124, 309–327.
Takigawa, A., et al., 2018. High-temperature dust condensation around an AGB star: evidence from a highly pristine presolar corundum. Astrophys. J. Lett. 862, L13.
Tatsumi, E., et al., 2020. Collisional history of Ryugu's parent body from bright surface boulders. Nature Astronomy. doi:10.1038/s41550-020-1179-z doi.org/.
Terada, K., et al., 2014. A new X-ray fluorescence spectroscopy for extraterrestrial materials using a muon beam. Sci. Rep. 4, 5072.
Terada, K., et al., 2017. Non-destructive elemental analysis of a carbonaceous chondrite with direct current Muon beam at MuSIC. Sci. Rep. 7, 15478.
Terada, K., et al., 2018. Thermal and impact histories of 25143 Itokawa recorded in Hayabusa particles. Sci. Rep. 8, 11806.
Tsuchiyama, A., et al., 2011. Three-dimensional structure of Hayabusa samples: origin and evolution of Itokawa regolith. Science 333, 1125–1128.
Ushikubo, T., et al., 2012. Primordial oxygen isotope reservoirs of the solar nebula recorded in chondrules in Acfer 094 carbonaceous chondrite. Geochim. Cosmochim. Acta 90, 242–264.

Warren, P.H., 2011. Stable-isotopic anomalies and the accretionary assemblage of the Earth and Mars: a subordinate role for carbonaceous chondrites. Earth Planet. Sci. Lett. 311, 93–100.
Watanabe, S., et al., 2019. Hayabusa2 arrives at the carbonaceous asteroid 162173 Ryugu——A spinning top-shaped rubble pile. Science 364, 268–272.
Yabuta, H., et al., 2017. Formation of an ultracarbonaceous Antarctic micrometeorite through minimal aqueous alteration in a small porous icy body. Geochim. Cosmochim. Acta 214, 172–190.
Yamamoto, D., Tachibana, S., 2018. Water vapor pressure dependence of crystallization kinetics of amorphous forsterite. ACS Earth Space Chem. 2, 778–786.
Yamamoto, D., et al., 2018. Oxygen isotopic exchange between amorphous silicate and water vapor and its implications to oxygen isotopic evolution in the early Solar System. Astrophys. J. 865, 98.
Yamamoto, D., et al., 2019. Survivability of presolar oxygen isotopic signature of amorphous silicate dust in the protosolar disk. Meteorit. Planet. Sci. 55, 1281–1292.
Yano, H., et al., 2006. Touchdown of the hayabusa spacecraft at the muses sea on itokawa. Science 312, 1350–1353.
Yoshikawa M. et al., The Hayabusa mission, Chapter 6, this book.
Yurimoto, H., et al., 2011. Oxygen isotopic compositions of asteroidal materials returned from Itokawa by the Hayabusa mission. Science 333, 1116–1119.
Yurimoto, H., 2003. T. High precision isotope micro-imaging of materials. Appl. Surf. Sci. 203-204, 793–797.
Zinner, E., 2014. Presolar grains. meteorites and cosmochemical processes. In: Davis, A.M. (Ed.), Treatise on Geochemistry 12nd edition. Elsevier, pp. 181–213.

CHAPTER 8

OSIRIS-REx at Bennu: Overcoming challenges to collect a sample of the early Solar System

Dante S. Lauretta, Heather L. Enos, Anjani T. Polit, Heather L. Roper, Catherine W.V. Wolner
Lunar and Planetary Laboratory, University of Arizona, Tucson, AZ, USA

Chapter Outline

8.1 Introduction

Primitive asteroids are planetesimal remnants of the early Solar System that have avoided melting and differentiation. Their exploration casts light on Solar System evolution and interrogates the origin of our own habitable planet. They may carry organic compounds necessary for the beginnings of life, as well as water and other volatiles that could serve as resources for future space missions. Some are potentially hazardous, with small but non-negligible chances of colliding with Earth.

The Origins, Spectral Interpretation, Resource Identification, and Security–Regolith Explorer (OSIRIS-REx) mission contends with all of these aspects in its target, primitive near-Earth asteroid (101955) Bennu. The OSIRIS-REx spacecraft

Sample Return Missions
DOI: 10.1016/C2018-0-03374-5

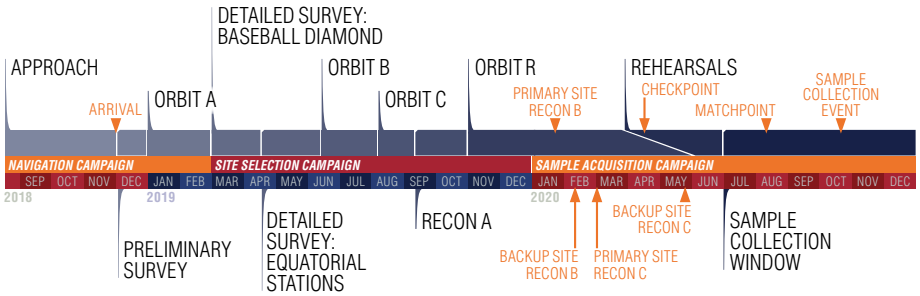

Fig. 8.1 ***Timeline of OSIRIS-REx proximity operations at asteroid Bennu, spanning August 2018 to December 2020.*** Mission phases (indicated with dark blue tick marks) and significant events (indicated with orange arrows and arrowheads) are described in the sections that follow. *(Credit: University of Arizona)*

launched in September 2016, rendezvoused with Bennu in December 2018 (Fig. 8.1), and will return a sample of Bennu's regolith to Earth in September 2023. Although Bennu was carefully characterized by telescopes before the spacecraft's arrival, OSIRIS-REx operations in proximity to the asteroid illuminated a very different surface than expected, posing challenges for the multifaceted mission.

8.1.1 Mission objectives

The prime objective of the OSIRIS-REx mission is to return a sample of more than 60 g of regolith from Bennu (Lauretta et al., 2015). Bennu is a dark asteroid spectrally classified as a B-type. It was selected as a mission target on the basis of a spectral linkage inferred from ground-based telescopic data to primitive, organic-rich, hydrated carbonaceous chondrite meteorites (Clark et al., 2011), a link that was later confirmed by spacecraft observations (Hamilton et al., 2019). The aim is to return a pristine sample of Bennu, i.e., not contaminated by the processes that compromise meteorites when they fall on Earth (Lauretta and DellaGiustina et al., 2019). The sample will be analyzed to understand the role that primitive Solar System objects like Bennu may have played in delivering life-enabling organic molecules and volatiles to Earth.

One of the great values of sample return lies in the knowledge of sample context. To achieve this, the mission has two related science objectives: (i) to develop a series of global maps of Bennu's surface and (ii) to perform detailed, local-scale characterization of specific sites. Analyses at both of these scales were used extensively in the mission's sample-site selection process and have enabled testable predictions about the nature of the returned sample. They have also significantly advanced the understanding of small Solar System bodies (e.g., Lauretta and DellaGiustina et al., 2019; Barnouin et al., 2019; Daly et al., 2020; DellaGiustina and Emery et al., 2019; DellaGiustina et al., 2020; Rozitis et al., 2020; Hamilton et al., 2019; Simon et al., 2020; Kaplan et al. 2020; Scheeres et al., 2019, 2020; Walsh et al., 2019).

Another mission objective is to constrain the probability of a potential collision between Bennu and Earth, which was known pre-encounter to be nonzero (Chesley et al., 2014). This objective requires an understanding of the interaction between the asteroid's thermal properties and its orbital dynamics, a phenomenon known as the Yarkovsky effect.

Lastly, the mission has the objective of improving asteroid astronomy. The many telescopic studies of Bennu that took place before the spacecraft encounter make it the best astronomically characterized asteroid in the Solar System (Lauretta et al., 2015). Thus, interpretations of astronomical data from other objects can be informed by evaluating the pre-encounter knowledge of Bennu against the data returned by the spacecraft (Lauretta and DellaGiustina et al., 2019; Hergenrother et al., 2019) and, ultimately, the returned sample.

8.1.2 Payload overview

The scientific instruments onboard the OSIRIS-REx spacecraft include the OCAMS imaging camera suite (Rizk et al., 2018), the OVIRS visible and near-infrared spectrometer (Reuter et al., 2018), the OTES thermal emission spectrometer (Christensen et al., 2018a), the OLA scanning laser altimeter (Daly et al., 2017), and the student-built REXIS X-ray-emission spectrometer (Masterson et al., 2018). The TAGCAMS camera suite (Bos et al., 2018), designed for navigation and sample stow operations, has also been used in practice to collect scientific data.

The TAGSAM sample acquisition mechanism (Bierhaus et al., 2018) can ingest particles 2 cm and smaller. "TAG" stands for Touch and Go, describing the concept of operations for sample collection. TAGSAM was designed to make contact with Bennu's surface for 6 to 16 s, during which time it injects high-purity nitrogen gas to fluidize the regolith and carry it into the collection chamber within the sampler head. In addition, 24 contact pads with diameters of 1.75 cm on the baseplate of the TAGSAM head can acquire fine-particulate material from the asteroid surface. Upon successful collection, the TAGSAM arm places the head in the Sample Return Capsule (SRC) for return to Earth.

8.1.3 Planning tools

One of the key challenges of the OSIRIS-REx mission is precision navigation in the microgravity environment around Bennu (Williams et al., 2018). This challenge required the development of mission-specific planning tools to achieve the spacecraft targeting for data collection. J-Asteroid is the primary planning tool of the OSIRIS-REx mission. It is an extension of the JMARS (Java Mission-planning and Analysis for Remote Sensing) geospatial information system (GIS) developed by Arizona State University's Mars Space Flight Facility (Christensen et al., 2018b). J-Asteroid was developed for scientific 3D data visualization of a small, irregularly shaped target (Bennu) and for planning scientific observations. It allowed the team to design the spacecraft pointing

and attitude profile, integrate detailed instrument commands for the science payload, and model the instrument systems to ensure correct command timing. A suite of pre-programmed observation types is tailored to the needs of each mission phase (Fig. 8.1) and supported by a library of instrument command blocks (repeatable functions). With each mission phase being unique in its observation strategy, development of J-Asteroid continued post-launch in a stepwise fashion, phase by phase, once the strategy for each phase became well-defined.

J-Asteroid computes image or spot geospatial data to ensure that observations comply with science, spacecraft, and instrument requirements. This built-in compliance-checking provides early warning of necessary design changes and decreases the risk of last-minute changes or delays to observation execution. Navigation uncertainties are rotated into the observer frame, allowing scan regions to be sized for spacecraft location errors, and plans can be inspected with updated spacecraft trajectories to assess the impact to spacecraft safety and observing conditions. J-Asteroid produces target and instrument sequences that the science operations team delivers to the spacecraft control center for integration into uplink products.

8.1.4 Adapting to the as-built Bennu

Before the OSIRIS-REx spacecraft's arrival at its target, the team developed a detailed set of assumptions about Bennu that were used to inform mission design (Lauretta et al., 2015, 2017). These assumptions were based on the asteroid's orbit, shape, mass, rotation state, radar response, and photometric, spectroscopic, and thermal properties, as observed telescopically. OSIRIS-REx data have shown that many of Bennu's global properties closely match those determined pre-encounter, e.g., shape, size, rotation state, mass (Lauretta and DellaGiustina et al., 2019). However, there were some surprises that had a substantial impact on mission operations (Fig. 8.2). These included higher-than-expected albedo variation, surface roughness, and boulder coverage (see Section 8.2), which made characterizing and sampling the surface more complicated than anticipated.

8.2 Mission operations

8.2.1 Outbound cruise

8.2.1.1 Trojan asteroid survey

The spacecraft launched on September 8, 2016, on an Atlas V rocket in the 411 configuration (Leonard et al., 2017). For the first year, the spacecraft was on a 0.78 au × 1.23 au × 1.6° orbit (Wibben et al., 2017). The spacecraft approached within

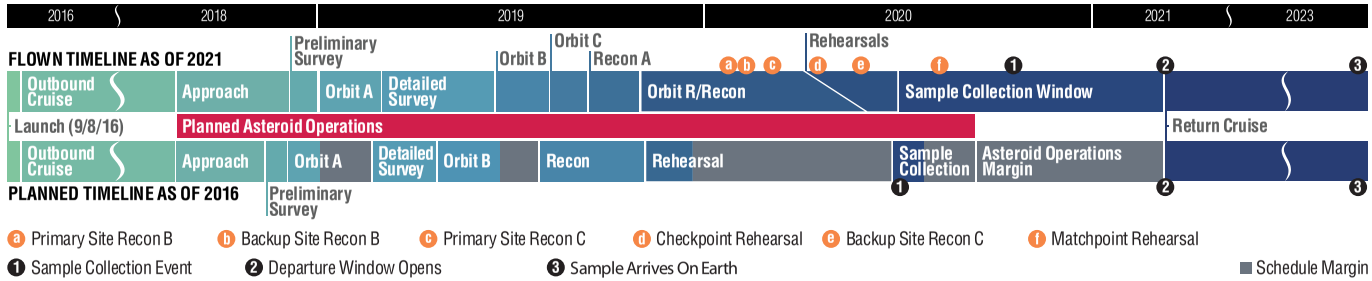

Fig. 8.2 Comparison of the as-flown (top row) and planned (bottom row) mission timelines, beginning with launch in September 2016 and extending to sample return in September 2023. *(Credit: University of Arizona)*

0.17 au of the Sun-Earth L4 Lagrange point on February 16, 2017. It has been proposed that the combined gravitational influences of the Sun and Earth could trap so-called "Trojan asteroids" around Earth-Sun Lagrange points for billions of years. To test this idea, on 10 dates between February 9 and 20, 2017, the MapCam imager (part of the OCAMS suite) surveyed the sky for Earth Trojan asteroids near opposition relative to the spacecraft. Although no such asteroids were discovered, the survey yielded many main-belt asteroid detections, demonstrating MapCam's sensitivity down to magnitude 13.8. More importantly, the survey provided a real-time operational test of the mission's science observation planning system.

The search for Earth Trojan asteroids proved to be an essential operational readiness test that revealed deficiencies in the planning and implementation process. For example, during development, it was thought that there was no need for sophisticated resource-tracking tools because the spacecraft had plenty of margin on key resources such as power and data volume. However, the challenge of the Earth Trojan asteroid survey showed that the mission needed these tools to strategically release margin, optimize science return, and reduce risks. To capture and build on the lessons learned from this activity, the team documented a concept of operations and refined the tools necessary for the OSIRIS-REx tactical planning and implementation process (Fig. 8.3).

In addition, the Earth Trojan asteroid survey highlighted the need for a kernel management plan. Kernels are files that describe the state of the spacecraft, instruments, asteroid, and other key elements throughout the mission timeline. They are critical for planning observations and generating data products. On this mission, kernels were produced by four proximate sources: the NASA Navigation and Ancillary Information Facility (NAIF) and the mission's navigation, operations, and science teams. Several direct interdependencies between the kernels from these four sources became evident, with consequences for the fidelity of observation plans, spacecraft command sequences, and data products. A comprehensive kernel management process was created with stringent configuration control.

8.2.1.2 Spacecraft debris

Although no Trojan asteroids were discovered, the MapCam imager recorded high-angular-rate streaks, indicative of small, fast-moving particles (Rizk et al., 2019), and Doppler tracking of the spacecraft revealed a small but measurable acceleration when the SRC was first placed in sunlight (Sandford et al., 2019). The streaks were determined to be water-ice particles translating across the imager's field of view, originating from the spacecraft itself. The accelerations were attributed to water outgassing from the SRC. These phenomena demonstrated that the OSIRIS-REx spacecraft has micro-climatic zones including hot regions and cold traps that pass volatiles back and forth. This outgassing had the potential to impact spacecraft navigation performance around Bennu and contaminate the collected samples. The team implemented a series of bake-out maneuvers to deliberately expose the cold traps to sunlight and drive off

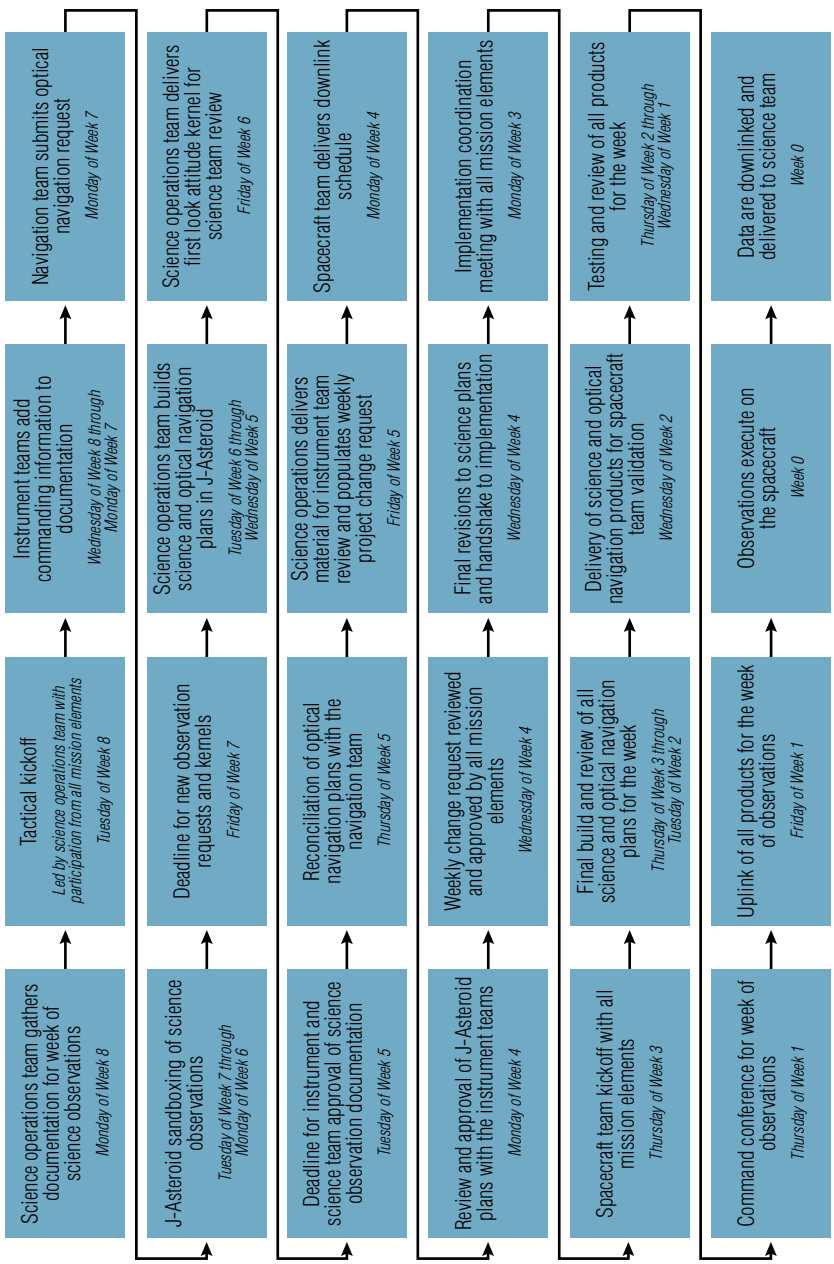

Fig. 8.3 Flow diagram of the OSIRIS-REx science planning and implementation process, illustrating the eight-week timeline and the interaction between multiple mission elements. *(Credit: University of Arizona)*

the condensed volatiles before arrival at Bennu, mitigating the risks to operations and the collected sample.

8.2.1.3 Earth gravity assist

The mission design incorporated a gravitational assist at Earth about a year after launch to match Bennu's orbital inclination of ~6°. The closest approach to Earth occurred on September 22, 2017, at a range of 17,237 km over the southern Pacific Ocean (latitude, 74.73°S; longitude, 271.94°E), with OSIRIS-REx approaching Earth from its night side. This flyby permitted observations of Earth and the Moon. Data were acquired after the gravitational assist as part of an extended instrument checkout campaign from September 22 through October 2, 2017. Within hours of the flyby, the first images received on the ground showed that they were precisely on target. The observations allowed the team to calibrate and characterize OCAMS, OTES, OVIRS, and TAGCAMS and provided an opportunity to determine alignment of instruments (Simon et al., 2018, 2019; Golish et al., 2020a; Doelling et al., 2019).

The Earth gravity assist was also vital for continuing the development of processes and tools for proximity operations. It was the first opportunity to apply the end-to-end planning and implementation process that had coalesced since the Earth Trojan asteroid survey (Fig. 8.3). The team developed in greater detail the observation change request and approval process and the chain of communication for planning the collection of optical navigation (OpNav) images (Jackman et al., 2017). The team also identified the need to integrate the instrument teams early in the observation planning process.

8.2.1.4 Ephemeris late updates

Owing to the challenges of spacecraft navigation and precision observation targeting in a microgravity environment, most science observations during proximity operations would turn out to require a "late update" to compensate for navigation uncertainties. A late update involves a complex handoff between the navigation team, the science operations team, and the spacecraft control center in the 24 hours leading up to execution to retarget the science observations. Detailed planning of asteroid proximity operations began during the outbound cruise phase. It became clear in the early stages of this planning that more asteroid observations would require late updates than originally thought. This increase in targeting complexity led the team to proceed with nadir and time-relative targeting instead of the original baseline of absolute targeting. This change facilitated the repointing of observations by simply uploading a new ephemeris as opposed to generating a new observation targeting file.

8.2.2 Approach: Welcome to the rubble

The scientific characterization of Bennu began with the Approach phase in late August through early December 2018 (Fig. 8.4) (Drozd et al., 2019). During this phase, the team used OCAMS to image the asteroid surface (Lauretta and DellaGiustina et al.,

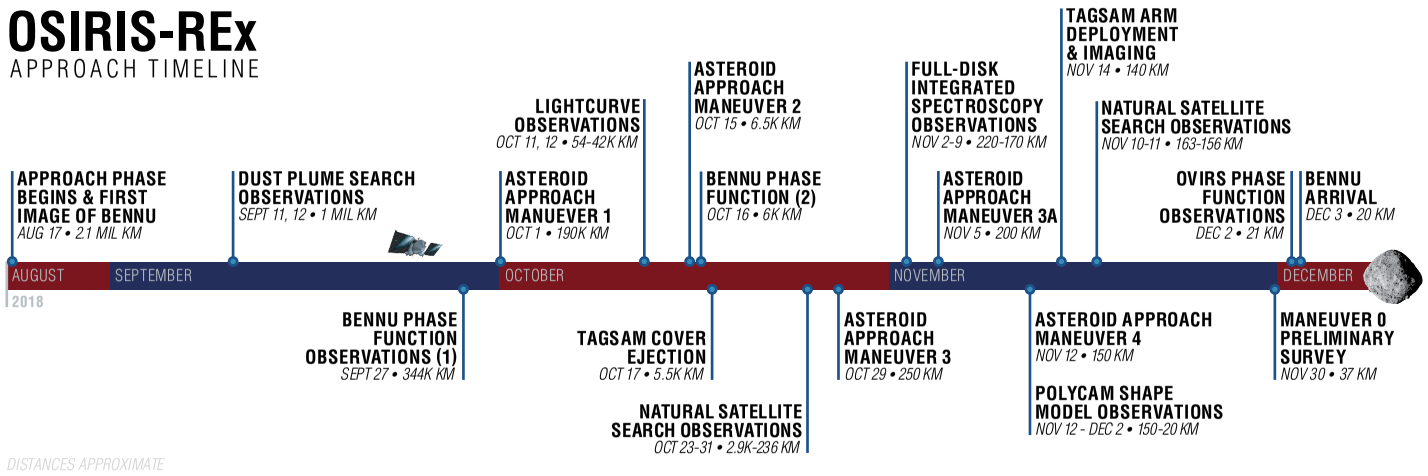

Fig. 8.4 Detailed timeline of the OSIRIS-REx spacecraft's approach to Bennu, including science observations and spacecraft maneuvers. *(Credit: University of Arizona)*

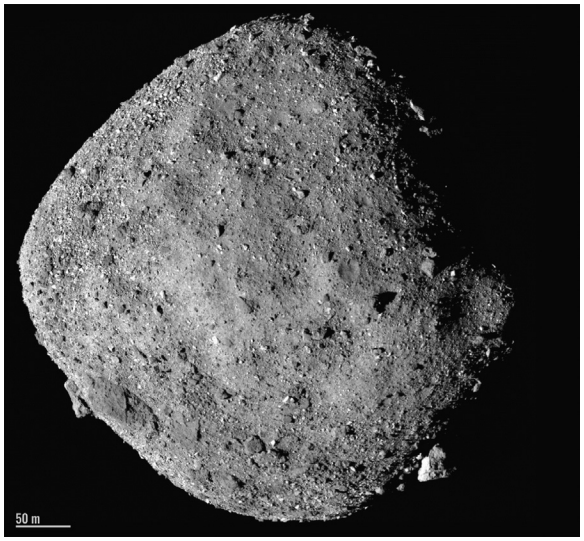

Fig. 8.5 ***A full-disk mosaic of Bennu composed of 12 images acquired by PolyCam on December 2, 2018.*** The phase angle is about 50°. *(Credit: NASA/Goddard/University of Arizona)*

2019; DellaGiustina and Emery et al., 2019), acquire data for a stereophotoclinometric shape model (Barnouin et al., 2019), and search the operational environment for hazards such as natural satellites and dust plumes, which were not detected (Hergenrother et al., 2019). OVIRS and OTES collected data to characterize the asteroid's global spectral properties (Hamilton et al., 2019).

Early in the Approach phase, Bennu appeared as a point source in images acquired by the OCAMS PolyCam instrument. The OCAMS detectors do not have 100 percent fill factor on their pixels owing to electronic structures on and below the surface of the silicon (Golish et al., 2020a). Thus, Approach-phase point-source data of Bennu must be treated carefully when determining precision radiometry.

Bennu's rotation state, size, and shape had been determined pre-encounter from lightcurve observations (Hergenrother et al., 2013) and radar images (Nolan et al., 2013). The inference of a spheroidal asteroid undergoing retrograde rotation was confirmed during early Approach. Bennu has a "spinning top" shape with a bulge at the equator and a mean diameter of 490.06 ± 0.16 m (Lauretta and DellaGiustina et al., 2019) (Fig. 8.5), consistent with expectations. However, the pre-encounter inference of a smooth asteroid surface turned out to be incorrect.

Before the OSIRIS-REx spacecraft launch, thermal infrared spectroscopy (Emery et al., 2014) and radar polarization ratio measurements (Nolan et al., 2013) were analyzed to constrain the particle size on the asteroid surface (Lauretta et al., 2015). From the thermal data, a thermal inertia of 310 ± 70 $J\ m^{-2}\ K^{-1}\ s^{-½}$ was derived (Emery et al., 2014), lower than that assumed on the basis of other planetary materials (>2000 $J\ m^{-2}\ K^{-1}\ s^{-½}$). This implied the presence of centimeter-scale particles. This inference

was consistent with radar polarization ratios. Bennu's shape and geomorphology were interpreted as additional evidence of the presence of loose particulate regolith: a subdued slope distribution was inferred at the spatial resolution of the radar shape model (7.5 m per pixel), with the average slope estimated to be 15 to 24°, depending on the bulk density of the asteroid (Scheeres et al., 2016). Together, these results led the team to conclude that Bennu's surface was largely composed of loose centimeter-scale material that was concentrated in the geopotential low region at the equator.

The original sampling strategy therefore was designed to target patches of loose regolith 50 m in diameter with particles smaller than 2 cm (Lauretta et al., 2017; Bierhaus et al. 2018). Upon arrival, however, it became clear that Bennu in fact has a rough, rugged, boulder-rich surface (Lauretta and DellaGiustina et al., 2019; DellaGiustina and Emery et al., 2019; Walsh et al., 2019) with only a small number of hazard-free regions, on the order of 5 to 20 m across. Even within these regions, initial topographic data indicated that local tilts exceeded 14°, the mission safety requirement over small areas. Such a rough surface, combined with abundant large boulders, presents tip-over and back-away hazards for the spacecraft during sampling. The team thus was faced with the challenges of improving the guidance accuracy of the spacecraft and identifying additional capability to maintain spacecraft safety during contact with the surface, at the same time as tactically planning and executing the subsequent mission phases.

8.2.3 Preliminary Survey: The triple bypass solution

The goal of the Preliminary Survey, which began on December 3, 2018, was to execute several flybys (Fig. 8.6) to determine Bennu's mass, refine the spin state model, and collect sufficient data to generate a global shape model with a resolution of 75 cm. This phase was extremely operationally challenging owing to the high cadence of observations and maneuvers. During trajectory design, it was discovered that the uncertainties on spacecraft position were too large to facilitate the necessary science imaging. The navigation team determined that the insertion of two additional north-pole flyovers would significantly reduce the positional errors, setting up a well-constrained third north-pole flyover and subsequent equatorial and south-pole flyovers for science observations. This "triple bypass" redesign resulted in a four-day extension of the Preliminary Survey phase.

The mass of Bennu measured during Preliminary Survey ($7.329 \pm 0.009 \times 10^{10}$ kg; Scheeres et al., 2019) and the 75-cm shape model (Barnouin et al., 2019), combined with the rotation state, yielded information about the geopotential of the asteroid surface, with implications for surface processes and internal structure. A transition occurs in Bennu's surface slopes within its rotational Roche lobe, a low-latitude band where material is energetically trapped to the surface. This finding implies that material should be migrating from higher latitudes and accumulating in

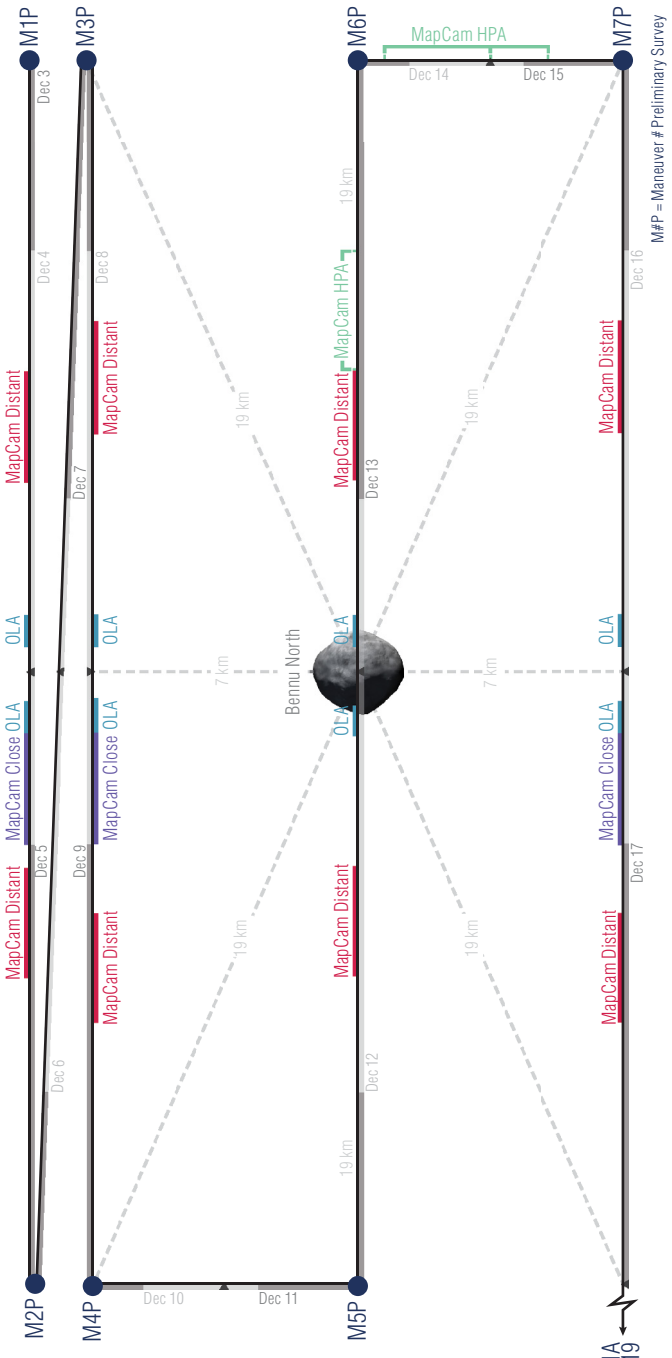

Fig. 8.6 Diagram of the Preliminary Survey flybys, highlighting the primary observations by MapCam and OLA (HPA, high phase angle). *(Credit: University of Arizona)*

the equatorial region, which has been supported by geomorphological assessments (Walsh et al., 2019; Barnouin et al., 2019; Jawin et al., 2020). The mass and density (1,190 ± 13 kg m^{-3}) of Bennu indicate that its interior is a mixture of voids and boulders, validating the hypothesis that this asteroid is a rubble pile (Scheeres et al., 2019; Barnouin et al., 2019; Walsh, 2018).

On December 27, 2018, as the team was preparing for the mission's first orbital insertion, the internet provider for the spacecraft control center experienced a nationwide outage, which prohibited normal ground activities including uplink, downlink, and moving data between elements. However, a team member was able to use the ground equipment at the Jet Propulsion Laboratory to connect to the Deep Space Network for uplink. The team was able to build products, process time-critical OpNav data, and uplink all the necessary files to the spacecraft just in time for orbit insertion.

8.2.4 Orbit A: Bennu strikes back

On New Year's Eve 2018, the spacecraft carried out a single 8 second burn of its thrusters and entered into orbit around Bennu, setting a record for the smallest object ever orbited by a spacecraft and a then-record for the closest orbit achieved (broken by subsequent OSIRIS-REx mission phases) (Fig. 8.7). This first orbital phase, Orbit A, was intended as time for the navigation team to probe the operational environment around Bennu and optimize the proximity operations plans based on those data.

Six days after orbital insertion, TAGCAMS OpNav images captured evidence of rock particles being ejected from Bennu's surface, demonstrating that Bennu is an active asteroid (Lauretta and Hergenrother et al., 2019; Hergenrother et al., 2020). Although it had been suspected pre-encounter that Bennu might be active given its spectral similarity to other asteroids in this category (Lauretta et al., 2015), the serendipitous discovery of particle ejection in navigation images came as a surprise, particularly after the null results of the Approach-phase searches for dust plumes and satellites (Hergenrother et al., 2019).

In response, the team scrambled to assess the safety of the spacecraft and add observations to characterize the activity, and ultimately determined that the ejected particles did not represent hazards to the vehicle. From this point forward, TAGCAMS particle monitoring observations were added to mission phases to acquire the largest and longest possible dataset.

From Orbit A observations of three large ejection events, the particles were determined to range from millimeters up to about 10 cm in diameter, ejecting at speeds up to a few meters per second, from various latitudes but usually in the late afternoon or early evening local solar time (Lauretta and Hergenrother et al., 2019). A persistent background of particles in the Bennu environment was also identified. More detailed characterization using data collected through Orbit C (Fig. 8.7), capturing Bennu's full

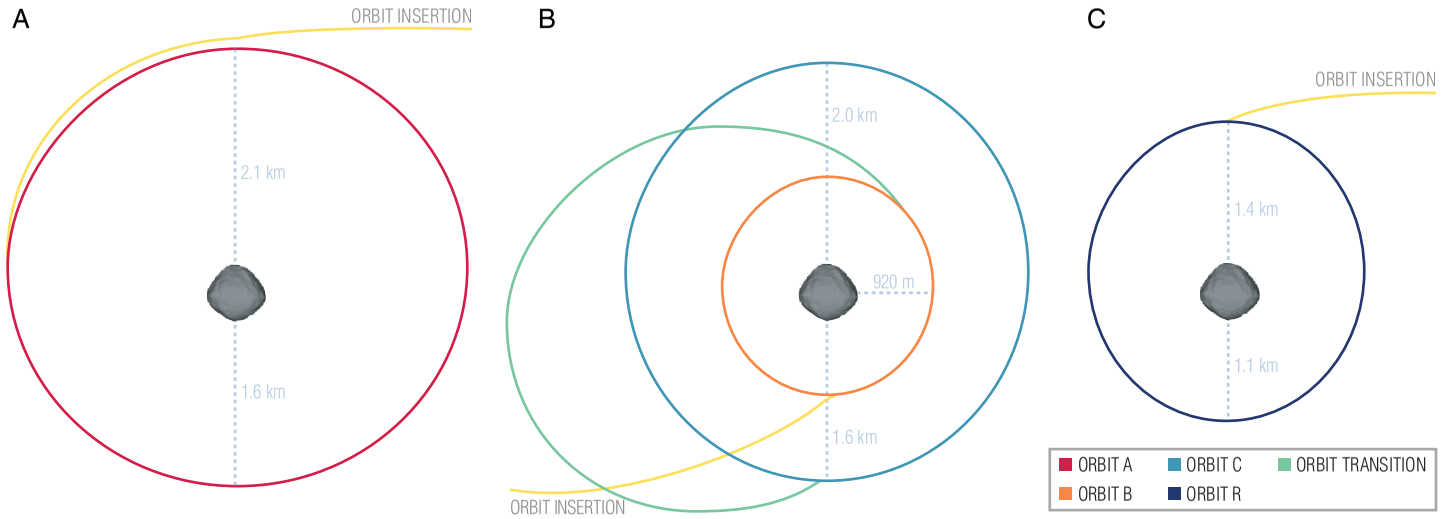

Fig. 8.7 ***Diagrams of the orbital phases of the mission*** — (A) Orbit A, (B) Orbit B, and (C) Orbit C — and (D) the safe-home orbit during the Reconnaissance phase, Orbit R. *(Credit: University of Arizona)*

range of heliocentric distance, was broadly consistent with these initial findings but offered a nuanced view of the particle dynamics, shapes, and ejection timing and origin (Hergenrother et al., 2020, and references therein). The team evaluated several hypotheses for the mechanism of particle ejection and found meteoroid impacts, thermal stress fracturing, phyllosilicate dehydration, and (for the smallest events) ricochet to be the most plausible (Lauretta and Hergenrother et al., 2019; Hergenrother et al., 2020).

One of the highest-value results from this unexpected science campaign came from the tracking of long-lived particle trajectories, which served as natural probes of Bennu's gravity field (Chesley et al., 2020; Scheeres et al., 2020). This outcome was fortuitous as the team was struggling with how to meet the primary mission requirement to measure the gravity field to degree and order 4 (McMahon et al., 2018), which was rendered difficult by the small mass of Bennu. The proposed modifications to the gravity field observation plan initially involved a lower orbit, but concerns about spacecraft safety outweighed the benefits. Instead, the team applied a novel approach: tracking and modeling of particles ejected from Bennu's surface into sustained orbits (Chesley et al., 2020). This particle-based gravity field, which used data collected from Preliminary Survey through Orbit C, is statistically significant up to degree and order 9, exceeding the mission requirement (Scheeres et al., 2020).

8.2.5 Detailed Survey–Baseball Diamond: A new ball game

The Detailed Survey phase, beginning in late February 2019 and divided into the Baseball Diamond and Equatorial Stations subphases, was designed as the primary science phase for global mapping of Bennu using OCAMS, OVIRS, and OTES. During verification and validation of the science requirements, the team found that the original observation plan (Lauretta et al., 2017) was not sufficient to generate a higher-fidelity stereophotoclinometric shape model (35 cm resolution, required for navigation; Jackman et al., 2017), and the imaging plan to create a global mosaic did not include sufficiently varied geometries. Baseball Diamond was thus completely redesigned and evolved away from the flight-path shape that had given it its name (Fig. 8.8). The science, operations, and navigation elements of the mission worked together to define a series of seven hyperbolic flybys that would meet the necessary geometric constraints, combining similar viewing geometries whenever possible.

These seven flybys constituted a significant increase from the two in the initial design, and the team was able to produce a global mosaic at ~ 5 cm per pixel (Bennett et al., 2020), the highest resolution at which a planetary body has been globally mapped to date (Fig. 8.9).

In addition to expected updates such as new kernels, observation planning for this subphase required the incorporation of new knowledge of spacecraft performance (e.g.,

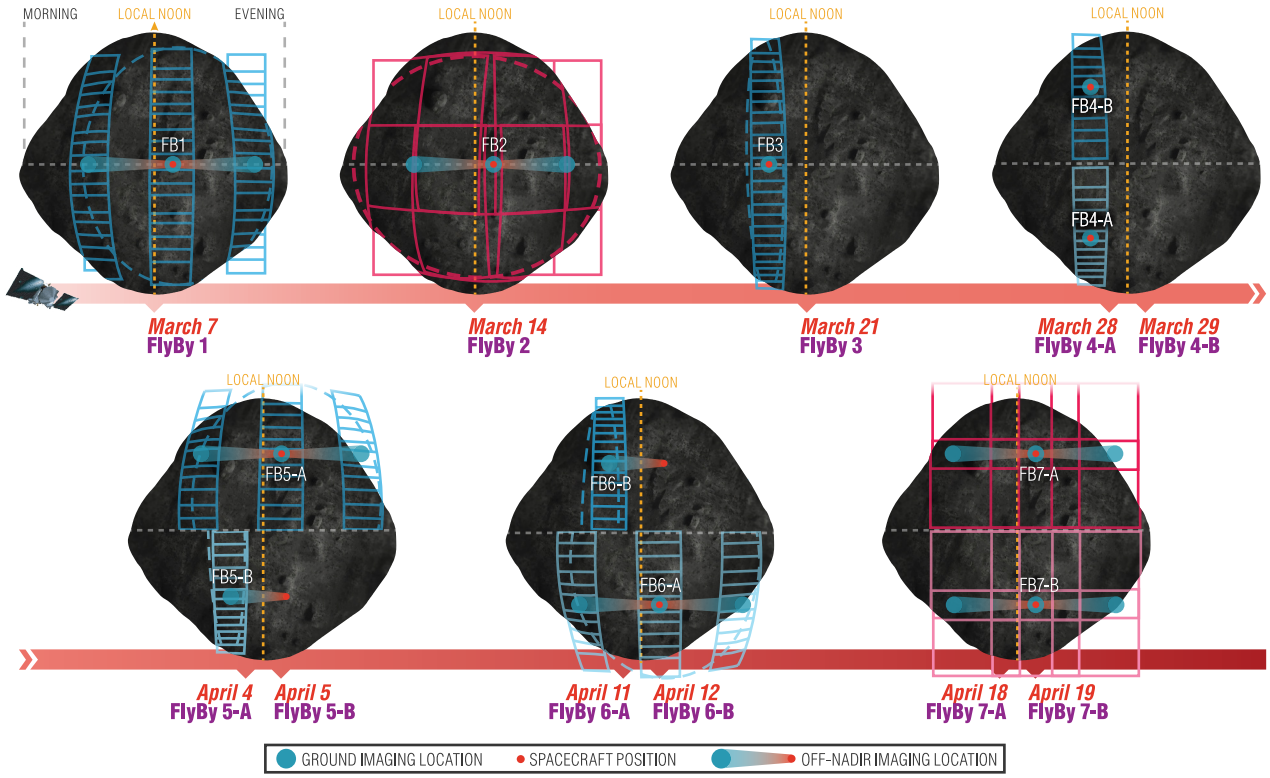

Fig. 8.8 Diagram of the Baseball Diamond flybys (FB), in chronological order from left to right and top to bottom. *(Credit: University of Arizona)*

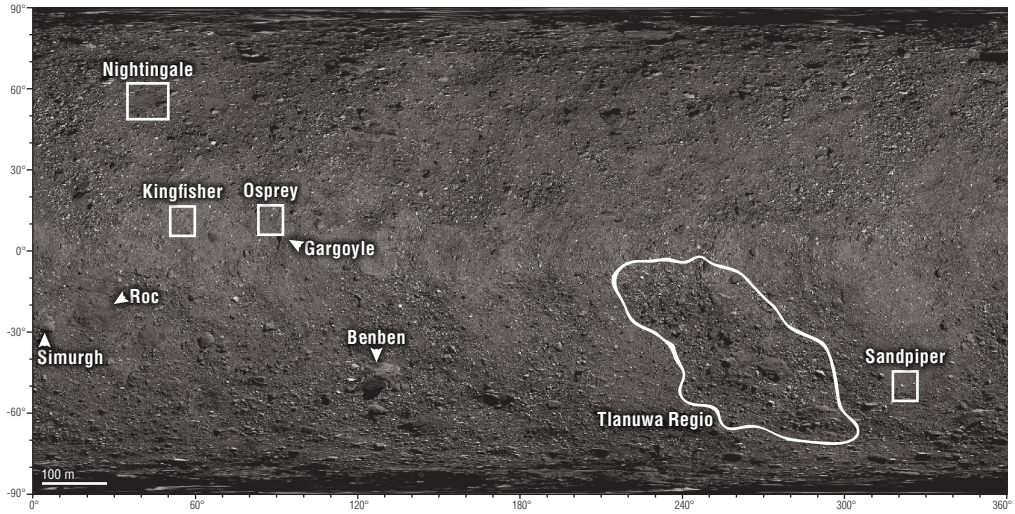

Fig. 8.9 ***Global mosaic of Bennu produced from PolyCam images collected during Baseball Diamond flybys (Bennett et al., 2020).*** White arrows and the curved white outline respectively indicate the examples shown in Fig. 8.11 of large boulders and a boulder-covered region. The white rectangles correspond to the images of the final four candidate sites for sample collection shown in Fig. 8.13. *(Credit: NASA/Goddard/University of Arizona)*

navigational uncertainties) and of Bennu itself. For instance, the albedo variation of Bennu's surface is greater than expected (Lauretta and DellaGiustina et al., 2019), which necessitated OCAMS imaging at different exposure times.

During the execution of Baseball Diamond Flyby 2 (Fig. 8.8), a bomb cyclone hit Denver, CO, where the spacecraft control center is based. The spacecraft team was unable to process the late update, re-anchor the observation to the desired latitude and time, and uplink the ephemeris to the spacecraft. Unfortunately, this missed update resulted in targeting that focused on the southern hemisphere instead of being centered at the equator, significantly limiting the MapCam color coverage and the off-nadir looks for shape model generation. Other data were found to be able to compensate for the shape model requirements; however, re-flying Flyby 2 between Orbit C and Recon A was necessary to recover color data in the northern hemisphere. The re-fly proved worth the added effort: the resultant global map revealed unexpected diversity in color among and even within Bennu's boulders and craters (DellaGiustina et al., 2020). This diversity is thought to originate from differences in both primordial composition and exposure to the space environment.

8.2.6 Detailed Survey–Equatorial Stations: Mission pay dirt

The mission transitioned to the Equatorial Stations subphase in late April 2019. Each week, the spacecraft observed Bennu from a different local solar time station (Fig. 8.10). During planning, the station sequence was reordered to prioritize the observations needed to inform sample-site selection. For each station, the observation window was centered on the equator at a distance of 5 km and lasted for one full Bennu rotation (4.3 h). These observations contributed to OVIRS and OCAMS photometric models (Golish et al., 2020b; Zou et al., 2021); global spectral (Simon et al., 2020), temperature, and thermal inertia maps (Rozitis et al., 2020); and the global 35-cm shape model required for optical navigation. At Stations 2 and 6, Bennu was backlit by the Sun. These images provided the opportunity to search again for dust plumes; none were found.

Early spectral data from the Approach phase had revealed evidence for abundant hydrated minerals on the surface of Bennu, in the form of a near-infrared absorption near 2.7 μm, and thermal infrared spectral features that are most similar to those of aqueously altered CM-type carbonaceous chondrites (Hamilton et al., 2019). With the Equatorial Stations data, the team was able to map these spectral features across the surface of Bennu. The Equatorial Stations data also revealed a 3.4-μm absorption attributable to organics and carbonates (Simon et al., 2020), validating the choice of Bennu as the mission target to achieve the goal of returning carbonaceous material to Earth. The 3.4-μm absorption varies over the surface of Bennu but does not appear to correlate with the hydration feature or other surface properties such as brightness (Simon et al., 2020).

8.2.7 Orbit B: Laser sharp

The mission's Orbit B phase began in early June 2019 with orbit insertion at ~ 680 m above Bennu's surface (Fig. 8.7), setting another record for closest orbit. The first two weeks of Orbit B focused on investigating the causes of Bennu's particle ejection events by taking frequent images of the asteroid's horizon, and the remaining five focused on observing the asteroid from a close range with OLA, OCAMS, REXIS, and OTES.

The original mission plans called for complex operations during Orbit B with numerous observations of candidate sample sites to inform the site selection process (Lauretta et al., 2017). However, later analysis showed that the imaging quality from the terminator orbit would not be suitable for this purpose. The team therefore decided to proceed with a simplified global mapping strategy for this phase. Nevertheless, the requirement for OLA that the spacecraft maintain a constant distance from the surface and precision nadir pointing resulted in a period of intense operations.

OLA measured the entire asteroid in a series of overlapping scans at a variety of incidence angles. This dataset contains almost 3 billion individual measurements, resulting in a laser altimetry–based global shape model with 20-cm facets (Daly et al., 2020).

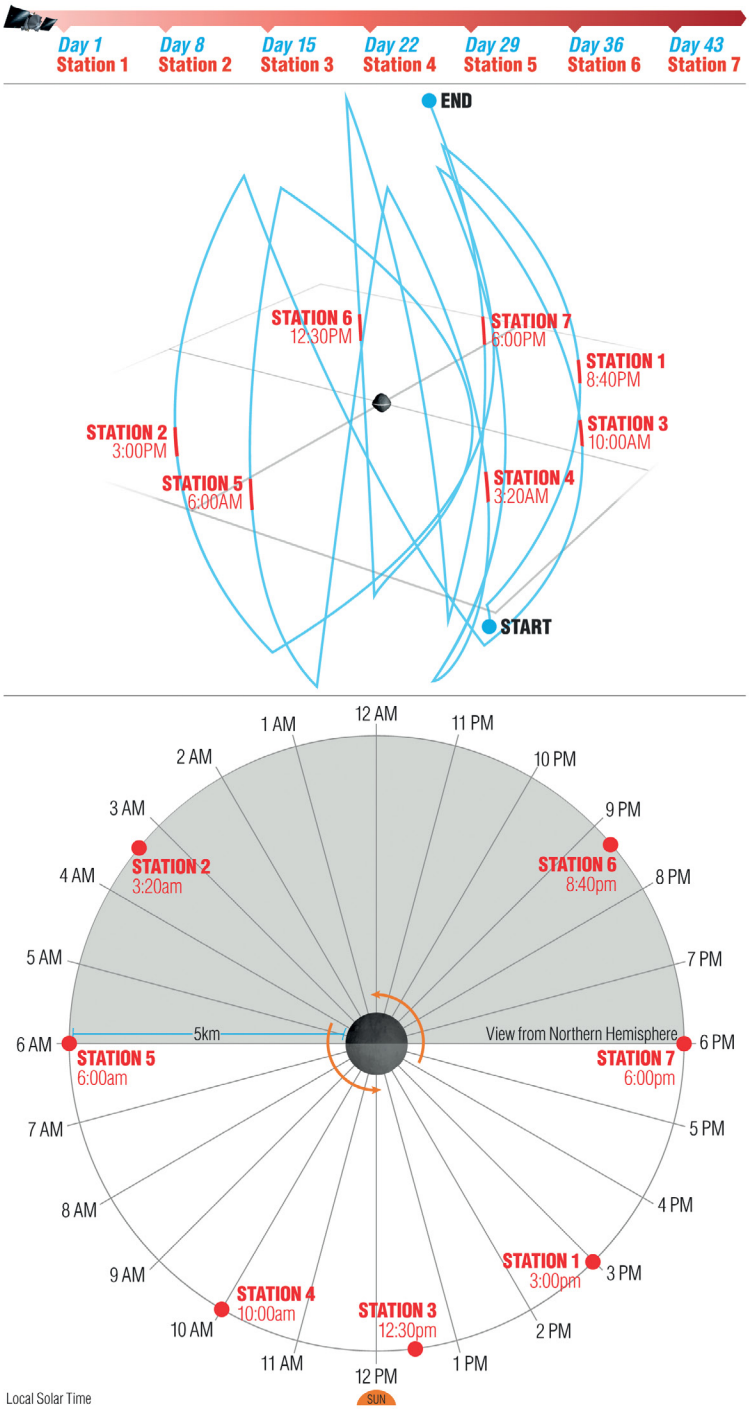

Fig. 8.10 ***Diagrams of the Equatorial Stations.*** Each station occurred at a different local time of day. Top, timeline, where Day 1 is the first Equatorial Station. Middle, spacecraft trajectories over the course of these observations. Bottom, view of the observing stations from the north pole. *(Credit: University of Arizona)*

PolyCam returned images of Bennu's surface at spatial scales down to ~ 1 cm per pixel. This campaign obtained at least one image per 10 × 10° bin on the surface to ensure wide sampling of surface geologies at a higher resolution than obtained in Detailed Survey. These images resolved circular cavities on boulders, which the team determined to be small impact craters and measured in detail using OLA data. From these measurements, the impact strength of meter-sized boulders on Bennu was estimated to be 0.44 to 1.7 MPa (Ballouz et al., 2020) — weak compared to solid terrestrial materials. This finding is consistent with global thermophysical evidence indicating that Bennu's boulders are more porous and weaker than expected (Rozitis et al., 2020).

Orbit B was also intended as the prime science collection phase for REXIS. Unfortunately, the REXIS data have not shown a definitive detection of any element X-ray fluorescence lines from the surface. Data collected later in the mission revealed that this lack of X-ray detections was not due to the instrument performance, but rather to Bennu's X-ray flux being much lower than predicted. On November 11, 2019, a bright uncatalogued soft X-ray transient source was serendipitously detected by REXIS (Allen et al., 2020). The data suggest that the source is a black hole or neutron star binary.

8.2.8 Orbit C: A welcome rest

In early August 2019, a series of maneuvers placed the spacecraft into Orbit C, a frozen orbit with a semi-major axis of 1.8 km (Fig. 8.7). This orbit, which was not part of the original mission plan, required a much less intense cadence of operations than Detailed Survey and Orbit B; the only science activity was TAGCAMS monitoring of the near-Bennu environment for particles ejected from the surface.

8.2.9 Sample-site selection: Target Nightingale

8.2.9.1 An arduous search

With the global data collection campaign completed, the team turned to the task of selecting a sample site. Global observations were integrated into thematic maps of four decision-informing properties: safety, deliverability, sampleability, and science value. The team began with assessments of the first two.

The safety map algorithm took as input digital terrain models (DTMs) with 15 cm resolution derived from OLA data, which were analyzed for regions with surface tilts < 14°, relative to the spacecraft approach vector, over a radius of 25 m. No site on Bennu met this criterion. Instead, regions of interest had safety radii of only 3 to 8 m.

The deliverability map strategy was initially based on the spacecraft design requirement of delivery to within 25 m of a selected point on the surface with greater than 98 percent probability (Williams et al., 2018). To meet this requirement, the spacecraft is equipped with two independent autonomous guidance systems for the final closure with the asteroid surface (Lauretta et al., 2017): LIDAR and Natural Feature Tracking

(NFT). The LIDAR guidance system is the less complex of the two, with little onboard processing of data. The NFT solution has better guidance accuracy but requires intense computational resources. With the smaller-than-expected radii of safety, it became clear that NFT would be needed to ensure the accuracy required for sample collection (Berry et al., 2020).

NFT uses a catalog of known features built from an asteroid shape model produced during flight (Olds et al., 2015; Mario and Debrunner, 2016). During sample collection, the features are rendered using a predicted camera pointing and Sun position and correlated against real-time images of the asteroid surface. This process results in a state update of the spacecraft's position and velocity relative to the asteroid surface, which is then used to autonomously calculate the required corrections to the sampling propulsive maneuvers. The change from LIDAR to NFT as the primary mode of guidance for sample collection required reprioritization in the imaging campaign to ensure that a natural feature catalogue could be built and tested in advance. The team found that guidance accuracies of 5 to 8 m could be achieved with NFT, depending on the chosen site. Even with this improved capability, Bennu still presented challenges.

Bennu's boulder-covered surface is far more hazardous than expected (Fig. 8.11). This drove the development of a flight software upgrade to the NFT system, called the hazard map, that makes it possible to perform autonomous hazard detection. During the final descent to the surface, the spacecraft uses the trajectory solution provided by NFT to predict the contact point. If the probability of encountering a hazard is too high, the spacecraft backs away from the surface to maintain safety and allow for another attempt.

However, obstacles remained for the site selection process. The uncertainties in the DTMs did not meet the safety map precision requirements. In addition, the back-away corridors needed to be evaluated for possible spacecraft escape trajectories vs. large obstacles to ensure that the spacecraft would not collide with a boulder on its way out. Image co-registration was therefore prioritized.

The key lesson from this process was that the project schedule had not budgeted sufficient time for data analysis and assessment. To address this problem, the Reconnaissance (Recon) phase for final site selection was redesigned (Fig. 8.12) and split into three parts (A, B, and C), the first of which involved observations that had not previously been envisioned.

After months grappling with the rugged reality of asteroid Bennu's surface, the team selected four potential sample sites, based on safety, sampleability, and deliverability criteria, to investigate further during Recon A in October 2019 (Fig. 8.13). These final four sites, named for birds, are diverse in geographic location. Nightingale is the northernmost site, situated at 56°N in a crater 20 m in diameter. Kingfisher is located in a small crater 8 m in diameter near Bennu's equator at 11°N. Osprey is also set in a small crater, 20 m in diameter, at 11°N. Sandpiper is located in a relatively flat area on the wall of a large crater 63 m in diameter at 47°S.

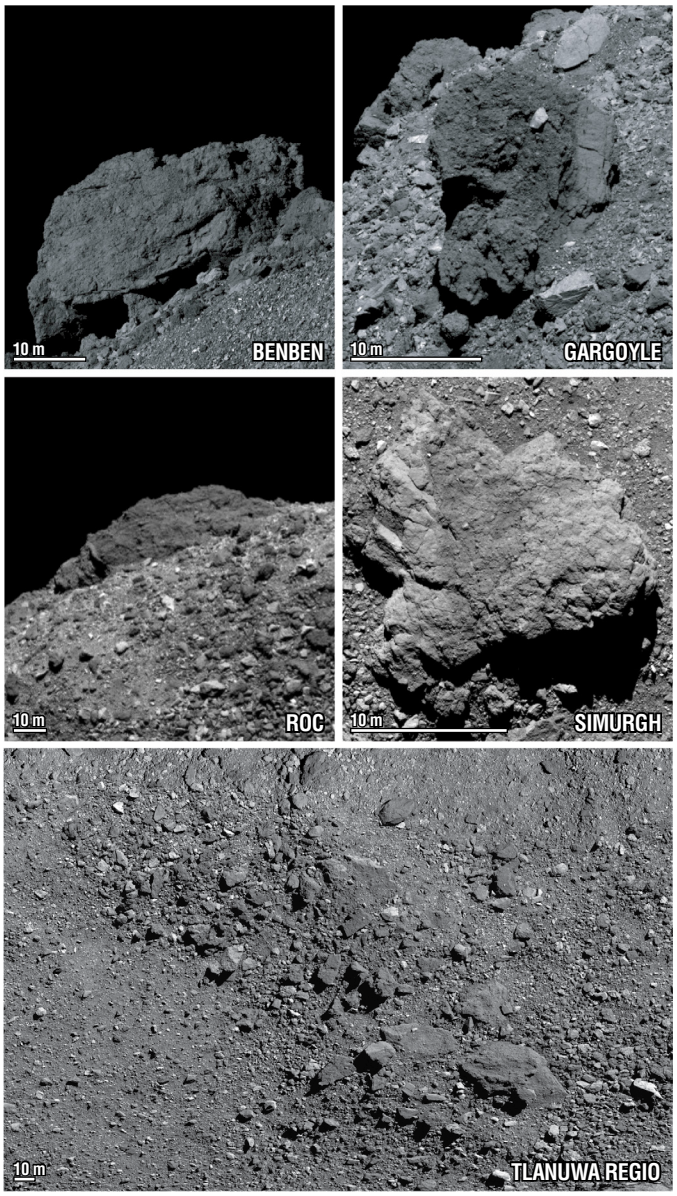

Fig. 8.11 The top four panels show examples of large boulders on Bennu's surface, and the bottom panel shows an example of a boulder-dense region (see Fig. 8.9 for locations). *(Credit: NASA/Goddard/University of Arizona)*

8.2.9.2 Recon A

Recon A comprised four hyperbolic flybys ranging in altitude from 1000 to 1250 m, one for each of the final four candidate sample sites. The primary goal of these new flybys was to observe an area with appropriate viewing geometry such that NFT features could be

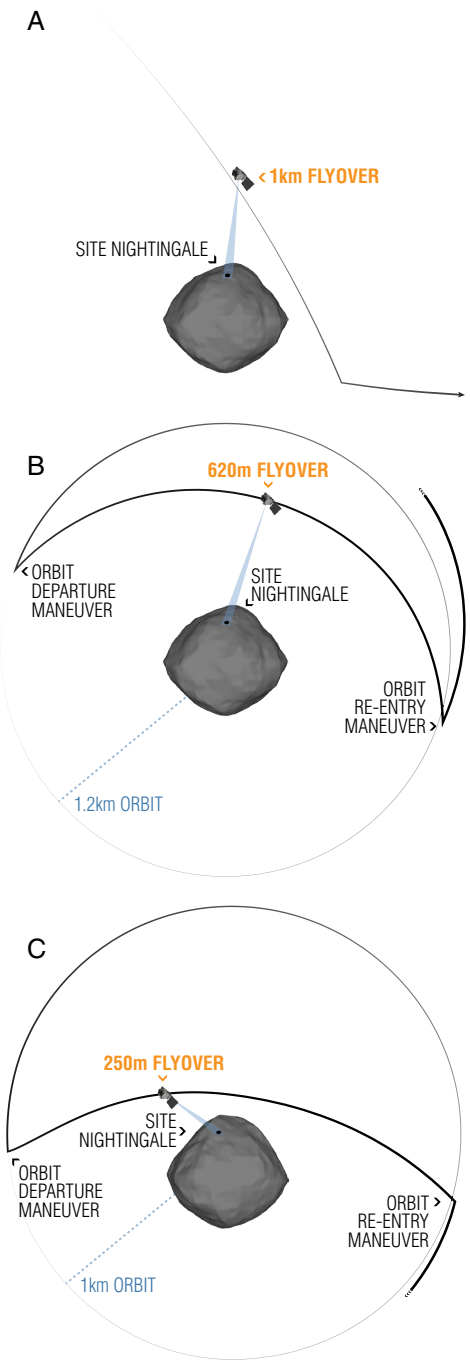

Fig. 8.12 Diagrams of the Recon flyovers of candidate sample site Nightingale: (A) Recon A, (B) Recon B, and (C) Recon C. The flyovers were performed at progressively lower altitudes. *(Credit: University of Arizona)*

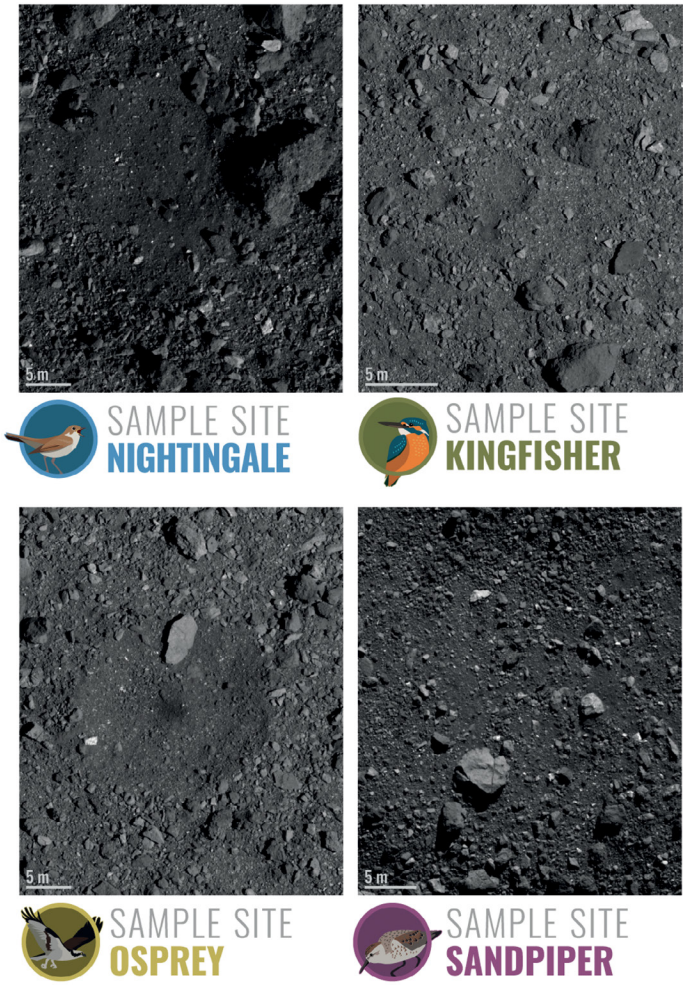

Fig. 8.13 ***The final four candidate sites for sample collection.*** These sites were selected from Detailed Survey and Orbit B data to be further investigated during Recon A. Their locations are shown in Fig. 8.9. *(Credit: NASA/Goddard/University of Arizona)*

built for spacecraft guidance. Two of the observations were optimized for topography and one for albedo; the other two viewing geometries needed for NFT were scheduled for Recon B. Imaging data to assess the sampleability of the candidate sites were also acquired. MapCam, OTES, and OVIRS observations of the sites were fit in on a best-effort basis.

This campaign was the first of the mission to focus on specific sites on the surface. While the general observation strategy was site-agnostic, the final trajectory and observation designs depended on the exact locations targeted.

On October 11, 2019, the Madrid Deep Space Network (DSN) complex went offline. As a result, OSIRIS-REx missed its high-gain DSN pass and did not downlink

OpNav images. This particular OpNav set was critical to perform a 24-hour late update of the spacecraft trajectory for the next day's Recon A flyby of the Osprey site. Without the late update, the spacecraft would instead observe an unknown spot on the asteroid surface.

The team attempted a "super late update" that entailed performing what had been treated thus far as a 24-hour activity within a single 4-hour DSN pass and pulled together seamlessly to execute this very-low-margin activity and salvage the Recon A observations of Osprey.

In addition to providing data for NFT and sampleability assessments, Recon A observations also yielded scientific results, such as the identification of carbonates and bright, meter-long veins in boulders (Kaplan et al., 2020). The dimensions of the veins indicate that hydrothermal deposition and crystallization on Bennu's parent body occurred at a near-global scale in a chemically open system (Kaplan et al., 2020).

8.2.9.3 Downselection

A site selection board comprising representatives from the operations, science, and leadership elements of the team used the Recon A data products to rank the final four candidate sites (Fig. 8.14). They chose Nightingale as the primary sample site. Nightingale offered the highest probability of collecting sufficient sampleable material, thanks to relatively unobstructed regolith at small enough particle sizes to be ingested by TAGSAM, and had the highest science value owing to a greater presence of organics. Given the site's northern location (56°N), temperatures are lower than elsewhere on the asteroid, so the regolith has been exposed to less thermal processing. The crater in which Nightingale is situated is thought to be relatively young, that is, the regolith is freshly exposed. These characteristics increased the likelihood of collecting a pristine sample.

Although Nightingale was the best sampling location on Bennu, the site still posed challenges for sample collection. The safe area for the spacecraft to touch was only about 16 m in diameter, much smaller than the 50 m diameter originally envisioned. There is also a building-size boulder situated on the crater's eastern rim, which posed a hazard to the spacecraft while backing away after contacting the site.

The spacecraft has the capability to perform multiple sampling attempts. However, any significant disturbance to Nightingale's surface would modify both the NFT features and the hazard map, making it difficult to collect a sample from that area on a later attempt. Thus, a backup site was necessary. The selection board chose Osprey for this purpose. Osprey is a lower-latitude (higher-temperature) site than Nightingale and exhibits less sampleable material; however, it may be more accessible due to fewer hazards.

8.2.9.4 Recon B and C

The next step was to further characterize the primary and backup sites for NFT catalog development and the final sampleability assessments via sortie-style flyovers in

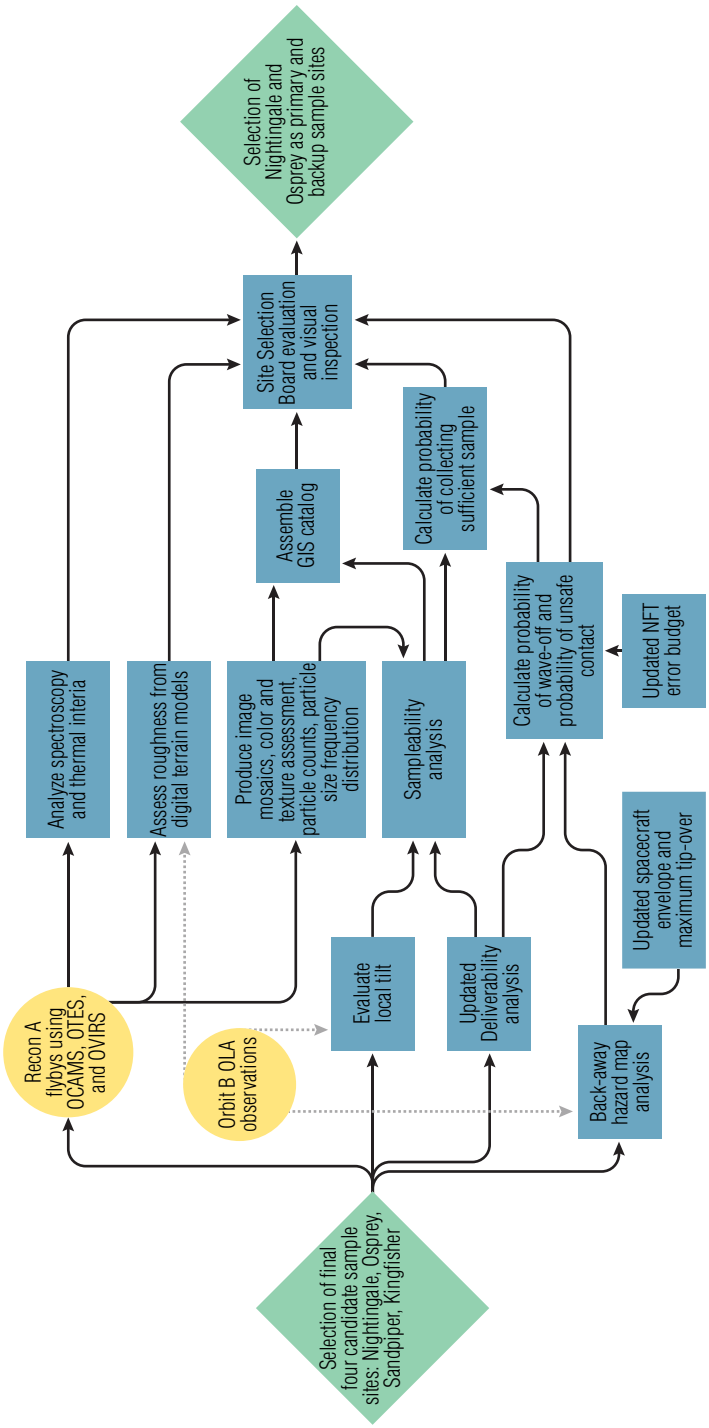

Fig. 8.14 Flow chart of the process of downselecting from four candidate sample sites to two: a primary and a backup. *(Credit: University of Arizona)*

Recon B and C (Fig. 8.12). During a sortie, the spacecraft departs orbit to fly over a specific site and inserts back into orbit at the conclusion of the observation. The original intent of these observations was to acquire color and spectral data of the primary and backup sites. With the necessity of transitioning from LIDAR- to NFT-guided sample collection, the sorties were redesigned to satisfy the NFT viewing geometries, providing the last two topography looks required to generate features for navigation to the surface.

The Recon B sorties took place at a "medium" altitude of about 620 m, whereas Recon C sorties were flown at a "low" altitude of about 250 m. The medium sortie to Nightingale executed nominally, but for the Osprey medium sortie, the sudden unexpected failure of the Low-Energy Laser Transmitter of the OLA instrument, whose ranging data were used to focus PolyCam, compromised the resolution and thus the utility of the images acquired. Fortunately, the High-Energy Laser Transmitter could be used to focus PolyCam for the remaining observations. The team considered replacing the Osprey low sortie scheduled for Recon C with a re-fly of the medium sortie, but, to avoid losing the extremely high-resolution low-sortie data, a modified plan was developed for the Osprey low sortie that would meet NFT requirements.

Another critical goal of these observations was to characterize in detail the sampleability of the sites on the basis of rock counts. Rock counts were performed initially at the comparatively coarse resolution of 5 cm in Recon A; sampleable material (2 cm or smaller in diameter) was inferred from the presence of areas with no resolvable rocks to count. By Recon C, sampleable objects down to less than a centimeter (pixel scale of 0.38 cm) were identifiable.

With the highest-resolution data from Recon C — including imaging, rock counts, and maps of sampleable material and hazards (Fig. 8.15) — the mission was as prepared as possible to attempt sample collection.

8.3 Sample acquisition and a look forward to Earth return

On April 14, 2020, the mission executed a checkpoint rehearsal – a trial run of the initial steps of the sample collection sequence (Fig. 8.16). The spacecraft departed its 1-km safe-home orbit, performed the checkpoint maneuver to reach an altitude above Bennu of 65 m, and executed the back-away burn as expected. This was the first time that the spacecraft used its onboard NFT system to autonomously correct its course. The next trial run, matchpoint rehearsal (August 11, 2020), brought the spacecraft even closer to the surface (~40 m) before backing away. The matchpoint rehearsal was a real-time test of the hazard map software designed to keep the spacecraft from contacting an unsafe area of the surface.

The sample collection event took place on October 20, 2020. NFT safely navigated the spacecraft such that TAGSAM contacted a sampleable point within 1 meter of the center of site Nightingale. The TAGSAM nitrogen gas bottle fired after 1 second of

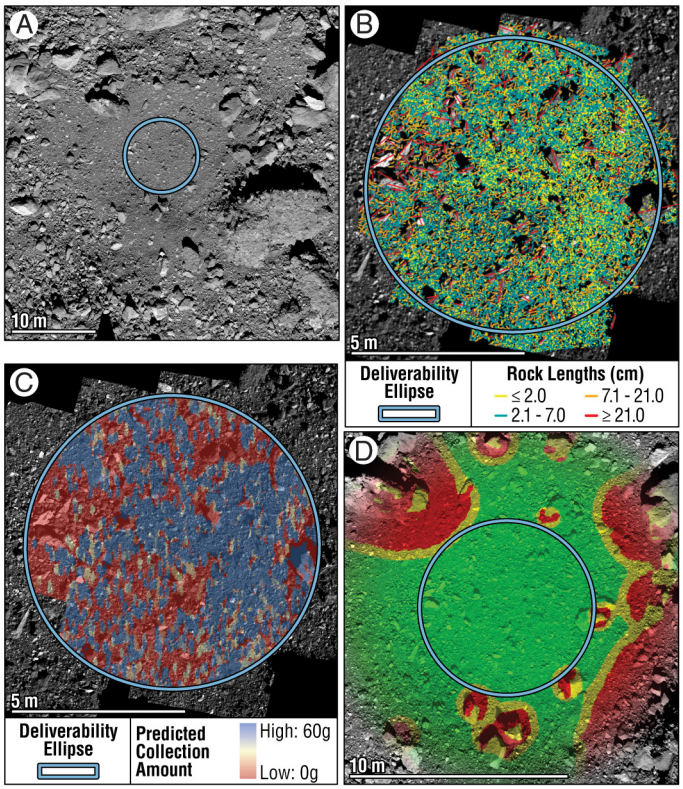

Fig. 8.15 ***The Nightingale sample site with rock count, sampleability, and hazard map data from Recon C.*** The blue ellipse indicates the target area with an 80 percent chance of spacecraft delivery. (A) Mosaic of Nightingale from PolyCam images. (B) Rock counts color-coded by the length of the long axis of each particle. (C) The sampleability map incorporating the rock counts from (B) along with an efficiency score based on surface tilt and converted to predicted collection amount. (D) Hazard map, where green indicates a safe location for the spacecraft to touch, red indicates a hazard that could potentially damage the spacecraft, and yellow is margin added to hazards to accommodate uncertainties in the NFT calculations. *(Credit: NASA/Goddard/University of Arizona)*.

contact, and the back-away burn initiated 5 seconds later. An extensive imaging campaign with multiple cameras made it possible to characterize the event and its aftermath. The surface of Bennu responded to contact in a manner consistent with weak, essentially cohesion-less material: even before the nitrogen gas bottle fired, the head descended several centimeters into the surface, filling with regolith. Material was lofted and excavated during the event and as the spacecraft backed away, degrading the signal of some instruments due to dust accumulation on the optics.

Post-sampling imaging of the TAGSAM head showed visual evidence of a large mass of sample collected, as well as particles clinging to the contact pads. In another challenge for the team, several particles ~1 to 3 cm in long dimension were wedged in the

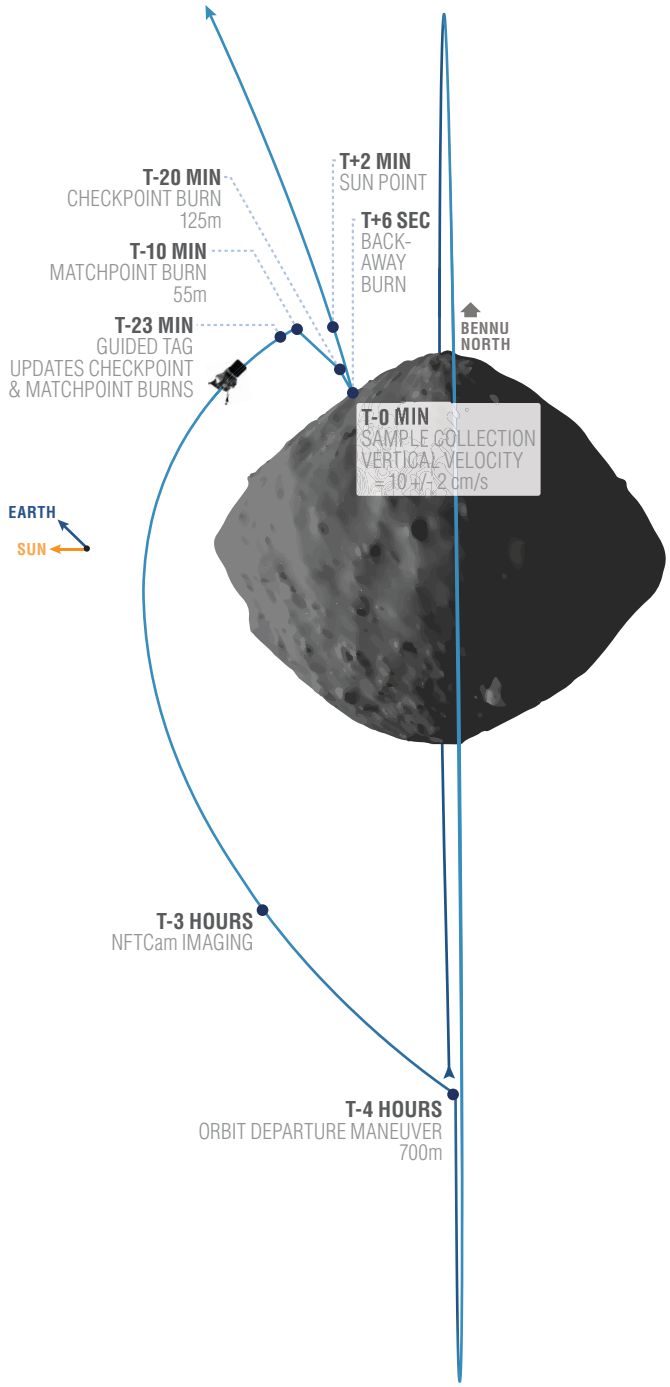

Fig. 8.16 Diagram of the spacecraft's descent trajectory to Bennu for sample collection. *(Credit: University of Arizona)*.

mylar flap that was intended to seal off the head after sampling. As a result, small flaky particles leaked from the head whenever TAGSAM moved. Mission leadership decided to accelerate the process of stowing the TAGSAM head in the SRC and thereby minimize any loss of scientific return. The spacecraft team worked around the clock to meet this challenge, and the sample was safely stowed by October 28 (if needed, additional sampling attempts could have been performed in late 2020 and early 2021 using two back-up nitrogen gas bottes).

The spacecraft's departure from Bennu is planned for May 2021. The SRC will land at the Utah Test and Training Range (UTTR) west of Salt Lake City on September 24, 2023. After field recovery, it will be airlifted to a temporary clean room at UTTR. From there it will be flown to Ellington Field, Texas, then transported by truck to the NASA Johnson Space Center. Construction of the curation facility is ongoing and will be ready at least one year in advance of sample return.

Planning is already underway for analysis of the returned sample. The plan lays out a framework for a coordinated system of analyses, defines equipment and techniques to be applied, sets baseline protocols for a co-registration and coordinated analysis of the sample data, establishes a data archiving system, provides guidance for the transfer of sample from curation facilities to analysts, and outlines the resource profile. Further, the SRC itself will be analyzed to provide context for the returned sample and to assess its performance during long-term space exposure and re-entry and descent through Earth's atmosphere.

8.4 Summary: To Bennu and back

The OSIRIS-REx spacecraft rendezvoused with asteroid Bennu in December 2018. Over the course of 2019, the mission team was presented with substantial obstacles to globally characterizing the asteroid's surface and finding a suitable site for sample collection. The rugged nature of Bennu defied expectations and exceeded the design specifications of the spacecraft. Through diligence, close coordination between different mission elements, and strategic allocation of technical and schedule margin, the team overcame these challenges and collected a substantial sample from site Nightingale. Data collected in proximity to the asteroid indicate a high likelihood that the collected sample contains water in the form of hydrated minerals, as well as carbon in the form of organic compounds and carbonate minerals. Successful return of this material promises exciting new insights into the role of carbonaceous asteroids in creating the habitable world known as Earth.

References

Allen, B., et al., 2020. Detection of MAXI J0637-430 by the regolith X-ray imaging spectrometer (REXIS) onboard OSIRIS-REx. The Astronomer's Telegram, 13594 ATel #.

Ballouz, R.-.L., et al., 2020. Asteroid Bennu's boulders record near-earth history of impacts by millimeter- to centimeter-scale objects. Nature. doi:10.1038/s41586-020-2846-z.

Barnouin, O.S., et al., 2019. Shape of (101955) Bennu indicative of a rubble pile with internal stiffness. Nat. Geosci. 12, 247–252.

Bennett, C.A., et al., 2020. A high-resolution global basemap of (101955) Bennu. Icarus, 113690.

Berry, K., et al., 2020. Revisiting OSIRIS-REx touch-and-Go (TAG) performance given the realities of asteroid Bennu. 43rd Annual AAS Guidance, Navigation and Control Conference, January 30 – February 5, 2020. Breckenridge, CO, AAS 20-088.

Bierhaus, E.B., et al., 2018. The OSIRIS-REx spacecraft and the touch-and-go sample acquisition mechanism (TAGSAM). Space Sci. Rev. 214, 107.

Bos, B.J., et al., 2018. Touch and go camera system (TAGCAMS) for the OSIRIS-REx asteroid sample return mission. Space Sci. Rev. 214, 37.

Chesley, S.R., et al., 2014. Orbit and bulk density of the OSIRIS-REx target asteroid (101955) Bennu. Icarus 235, 5–22.

Chesley, S.R., et al., 2020. Trajectory estimation for particles observed in the vicinity of (101955) Bennu. J. Geophys. Res. Planets 125, e2019JE006363.

Christensen, P.R., et al., 2018a. The OSIRIS-REx thermal emission spectrometer (OTES) instrument. Space Sci. Rev 214, 87.

Christensen, P.R., et al., 2018. J-asteroid: JMARS for asteroids and other small bodies. 49th Lunar and Planetary Science Conference. LPI Contrib 2083.

Clark, B.E., et al., 2011. Asteroid (101955) 1999 RQ36: spectroscopy from 0.4 to 2.4 μm and meteorite analogs. Icarus 216, 462–475.

Daly, M.G., et al., 2017. The OSIRIS-REx laser altimeter (OLA) investigation and instrument. Space Sci. Rev. 212, 899–924.

Daly, M.G., et al., 2020. Hemispherical differences in the shape and topography of asteroid (101955) Bennu. Sci. Adv. 6, eabd3649.

DellaGiustina, D.N., Emery, J.P., et al., 2019. Properties of rubble-pile asteroid (101955) Bennu from OSIRIS-REx imaging and thermal analysis. Nat. Astron. 3, 341–351.

DellaGiustina, D.N., et al., 2020. Variations in color and reflectance on the surface of asteroid (101955) Bennu. Science 370, eabc3660.

Doelling, D., et al., 2019. Inter-calibration of the OSIRIS-REx NavCams with earth-viewing imagers. Remote Sens 11, 2717.

Drozd, K., et al., 2019. Modeling imaging uncertainty for OSIRIS-REx's asteroid approach observations. In: Topputo, F. et al (Ed.), Advances in the Astronautical Sciences. Spaceflight Mechanics 2019. Univelt, AAS 19-509 vol. 168.

Emery, J.P., et al., 2014. Thermal infrared observations and thermophysical characterization of OSIRIS-REx target asteroid (101955) Bennu. Icarus 234, 17–35.

Golish, D.R., et al., 2020a. Ground and in-flight calibration of the OSIRIS-REx camera suite. Space Sci. Rev. 216, 12.

Golish, D.R., et al., 2020b. Disk-resolved photometric modeling and properties of asteroid (101955) Bennu. Icarus. doi:10.1016/j.icarus.2020.113724.

Hamilton, V.E., et al., 2019. Evidence for widespread hydrated minerals on asteroid (101955) Bennu. Nat. Astron. 3, 332–340.

Hergenrother, C.W., et al., 2013. Lightcurve, color and phase function photometry of the ORIRIS-REx target asteroid (101955) Bennu. Icarus 226, 663–670.

Hergenrother, C.W., et al., 2019. The operational environment and rotational acceleration of asteroid (101955) Bennu from OSIRIS-REx observations. Nat. Commun. 10, 1291.

Hergenrother, C.W., et al., 2020. Introduction to the special issue: exploration of the activity of asteroid (101955) Bennu. J. Geophys. Res. Planets 125, e2020JE006549.

Jackman, C.D., et al., 2017. Optical navigation concept of operations for the OSIRIS-REx mission Advances in the Astronautical Sciences. Spaceflight Mechanics 2017. Univelt, AAS 17-489 vol. 160.

Jawin, E.R., et al., 2020. Global patterns of recent mass movement on asteroid (101955) Bennu. J. Geophys. Res. Planets 125, e2020JE006475.
Kaplan, H.H., et al., 2020. Bright carbonate veins on asteroid (101955) Bennu: implications for aqueous alteration history. Science 370, eabc3557.
Lauretta, D.S., et al., 2015. The OSIRIS-REx target asteroid (101955) Bennu: constraints on its physical, geological, and dynamical nature from astronomical observations. Meteorit. Planet. Sci. 50, 834–849.
Lauretta, D.S., et al., 2017. OSIRIS-REx: sample return from asteroid (101955) Bennu. Space Sci. Rev. 212, 925–984.
Lauretta, D.S., DellaGiustina, D.N., et al., 2019. The unexpected surface of asteroid (101955) Bennu. Nature 568, 55–60.
Lauretta, D.S., Hergenrother, C.W., et al., 2019. Episodes of particle ejection from the active asteroid (101955) Bennu. Science 366, eaay3544.
Leonard, J.M., et al., 2017. OSIRIS-REx launch orbit determination analysis and TCM-1 reconstruction. In: Rohrschneider, R.R. (Ed.), Advances in the Astronautical Sciences, vol. 159, Guidance, Navigation, and Control 2017. Univelt, AAS 17-061.
Mario, C., Debrunner, C., 2016. Robustness and performance impacts of optical-based feature tracking to OSIRIS-REx asteroid sample collection missionBull Trimest Plan FamAdvances in the Astronautical Sciences. Guidance, Navigation, and Control 2016. Univelt, AAS, pp. 16–087 vol. 157.
Masterson, R.A., et al., 2018. Regolith X-Ray imaging spectrometer (REXIS) aboard the OSIRIS-REx asteroid sample return mission. Space Sci. Rev. 214, 48.
McMahon, J.W., et al., 2018. The OSIRIS-REx radio science experiment at Bennu. Space Sci. Rev. 214, 43.
Nolan, M.C., et al., 2013. Shape model and surface properties of the OSIRIS-REx target asteroid (101955) Bennu from radar and lightcurve observations. Icarus 226, 629–640.
Olds, R., et al., 2015. The application of optical based feature tracking to OSIRIS-REx asteroid sample collectionAdvances in the Astronautical Sciences. Guidance, Navigation, and Control 2015. Univelt, AAS 15-114 vol. 154.
Reuter, D.C., et al., 2018. The OSIRIS-REx visible and infrared spectrometer (OVIRS): spectral maps of the asteroid Bennu. Space Sci. Rev. 214, 54.
Rizk, B., et al., 2018. OCAMS: the OSIRIS-REx camera suite. Space Sci. Rev. 214, 26.
Rizk, B., et al., 2019. OSIRIS-REx low-velocity particles during outbound cruise. Adv. Space Res 63, 672–691.
Rozitis, B., et al., 2020. Asteroid (101955) Bennu's weak boulders and thermally anomalous equator. Sci. Adv. 6, eabc3699.
Sandford, S.A., et al., 2019. Outgassing from the OSIRIS-REx sample return capsule: characterization and mitigation. Acta Astronaut. 166, 391–399.
Scheeres, D.J., et al., 2016. The geophysical environment of Bennu. Icarus 276, 116–140.
Scheeres, D.J., et al., 2019. The dynamic geophysical environment of (101955) Bennu based on OSIRIS-REx measurements. Nat. Astron. 3, 352–361.
Scheeres, D.J., et al., 2020. Heterogenous mass distribution of the rubble-pile asteroid (101955) Bennu. Sci. Adv. 6, eabc3350.
Simon, A.A., et al., 2018. In-flight calibration and performance of the OSIRIS-REx visible and IR spectrometer (OVIRS). Remote Sens 10, 1486.
Simon, A.A., et al., 2019. OSIRIS-REx visible and near-infrared observations of the moon. Geophys. Res. Lett. 46, 6322–6326.
Simon, A.A., et al., 2020. Widespread carbon-bearing materials on near-earth asteroid (101955) Bennu. Science 370, eabc3522.
Walsh, K.J., 2018. Rubble pile asteroids. Ann. Rev. Astron. Astrophys 56, 593–624.
Walsh, K.J., et al., 2019. Craters, boulders and regolith of (101955) Bennu indicative of an old and dynamic surface. Nat. Geosci. 12, 242–246.
Wibben, D.R., et al., 2017. Early operational maneuvers for OSIRIS-REx: design and early performance assessment. In: Rohrschneider, R.R. (Ed.), Advances in the Astronautical Sciences. Guidance, Navigation, and Control 2017. Univelt, AAS 17-062 vol. 159.
Williams, B., et al., 2018. OSIRIS-REx flight dynamics and navigation design. Space Sci. Rev. 214, 69.
Zou, X.D., et al., 2021. Photometry of asteroid (101955) Bennu with OVIRS on OSIRIS-REx. Icarus 358, 114183.

CHAPTER 9

The Chang'e-5 mission

Long Xiao[a], Yuqi Qian[a], Qian Wang[b], Qiong Wang[b]
[a]Planetary Science Institute, School of Earth Sciences, China University of Geosciences, Wuhan, China
[b]Lunar Exploration and Space Engineering Center, China National Space Administration, Beijing, China

Chapter Outlines

9.1 Mission overview

The Chang'e-5 mission (CE-5) is the last step of the three-step Chinese Lunar Exploration Program (CLEP), designed to orbit, land, and return samples from the Moon (Zheng et al., 2008). The Chang'e-1 and Chang'e-2 missions successfully launched and orbited the Moon in October 2007 and October 2010, respectively, beginning China's lunar and space explorations and achieving the goal for Step 1. Chang'e-3 and Chang'e-4 missions achieved the goal for Step 2, by accomplishing successful soft landing and robotic rover explorations. Chang'e-3 landed in Mare Imbrium (northern hemisphere) in December 2013, and placed the Yutu rover on the Moon 37 years after the last robotic visit (Luna 24). In January 2019, Chang'e-4 landed on the farside of the Moon in Von Kármán Crater within the South Pole-Aitken Basin. At the time of writing (January 2021), Chang'e-4 and its rover Yutu-2 are still carrying on scientific observations and have just passed its 600-m milestone. The Chang'e-5 and Chang'e-6 missions, belonging to Step 3, aim at collecting lunar samples and bringing them back to the Earth >40 years after the Apollo and Luna missions. Since 2017, the launch date of the Chang'e-5 mission was postponed two times due to launch vehicle issues, and it finally launched in November 2020.

The China National Space Administration (CNSA) has set several ambitious engineering and scientific goals for the Chang'e-5 mission (Pei et al., 2015).

The main engineering objectives of the Chang'e-5 mission are: (1) to improve China's space capabilities by developing key technologies such as narrow window

Sample Return Missions
DOI: 10.1016/C2018-0-03374-5

multi-orbit binding launch, automatic lunar sampling and packaging, lunar sample storage, lunar surface takeoff, lunar orbit rendezvous and docking, Moon-Earth transfer, high-speed re-entry into the Earth's atmosphere, and multi-target high-precision measurement and control; (2) to realize China's first automatic sample return from an extraterrestrial body; (3) to optimize China's lunar exploration engineering system, form a high-level talent team of scientists and engineers and construct solid technology foundations for future crewed lunar missions and deep space explorations.

The main scientific objectives of the Chang'e-5 missions are: (1) to characterize the geological backgrounds of the landing site, (2) to study lunar samples *in-situ*, and connect *in-situ* data with laboratory analyses of the returned samples; and (3) to deepen the understanding of the formation and evolutionary history of the Moon by comprehensive studies of the returned samples, including geophysical and geochemical characterizations.

The Chang'e-5 spacecraft is composed of an orbiter, a lander, an ascender, and a returning capsule. It launched on November 24, 2020 from the Wenchang Satellite Launch Center, Hainan Island, and landed on the Moon on December 1, 2020 at 43.1°N, 51.8°W in Northern Oceanus Procellarum. Chang'e-5 has collected 1731 g of lunar samples, including ~1 m of drilling core, and returned to the Earth on December 17, 2020. The Chang'e-5 landing site is ~170 km ENE of Mons Rümker, and is characterized by some of the youngest mare basalts on the Moon (Qian et al., 2021a, 2021b). The scientific package of Chang'e-5 includes a Landing Camera, a Panoramic Camera, a Lunar Mineralogical Spectrometer and a Lunar Regolith Penetrating Radar in order to assist sampling operations and landing site investigations (Pei et al., 2015).

The mission profile of the Chang'e-5 mission, from launch to orbit transfer, lunar surface sampling, lunar surface takeoff, and back to the Earth, is shown in Fig. 9.1.

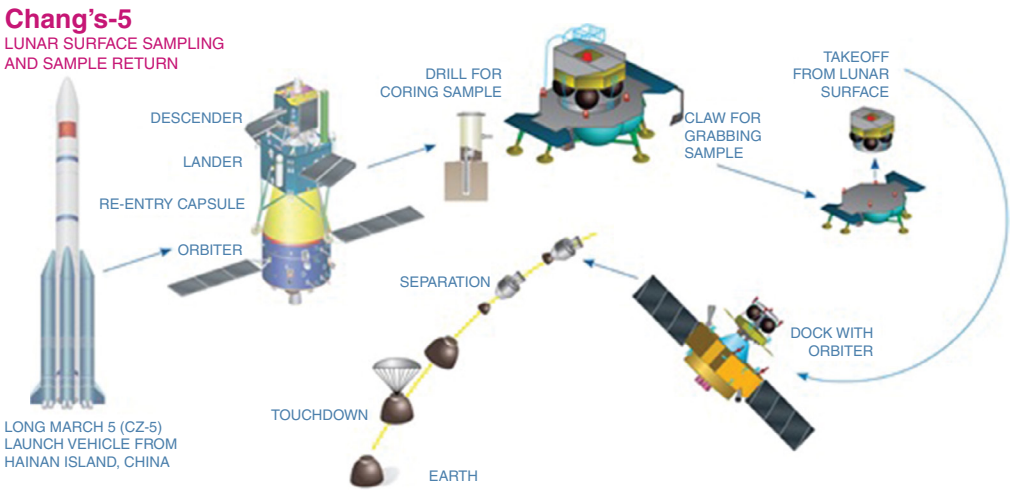

Fig. 9.1 An overview of the Chang'e-5 mission *(Xiao, 2018)*.

9.2 Sampling and science operations

9.2.1 Landing site

The pre-selected CE-5 landing region (41°–45°N, 49°–69°W) is located in Northern Oceanus Procellarum, in the northwest nearside of the Moon (Fig. 9.2). Northern Oceanus Procellarum is within the Procellarum KREEP Terrain (PKT; Jolliff et al., 2000), westward of Mare Imbrium, characterized by elevated heat-producing elements (Prettyman et al., 2006), extended volcanism (Hiesinger et al., 2011), and thin crust (Wieczorek et al., 2013). This region was selected as it has some of the youngest lunar mare basalts (Hiesinger et al., 2003, 2011; Liu et al., 2021; Qian et al., 2018, 2021a). Sampling these young mare basalts could profoundly improve our knowledge of lunar impact history and late thermal history (Qian et al., 2018, 2021a), and may solve some of the fundamental scientific questions raised recently (National Research Council, 2007).

Chang'e-5 landed within the Rümker region. It has an area of ~53,000 km^2 and is named after Mons Rümker, the most prominent feature in this area. It is a generally smooth mare plain (Fig. 9.2), covered by widespread mare basalts (Fig. 9.2 & Fig. 9.3). The mean slope of the mare surface is 1.1° with a baseline length of 354 m; only 10% of the surface, corresponding to impact features, has a slope larger than 2°. The mean elevation of the region is ~2145 m and wrinkle ridges could raise the mare surface about 100–200 m locally. The western part of the CE-5 landing region is ~200–300 m higher than the eastern part.

The landing site region includes a large number of volcanic features, such as a volcanic complex (Mons Rümker), a silicious dome (NW Mairan Dome), and a sinuous rille (Rima Sharp). Mons Rümker is one of the three largest volcanic complexes on

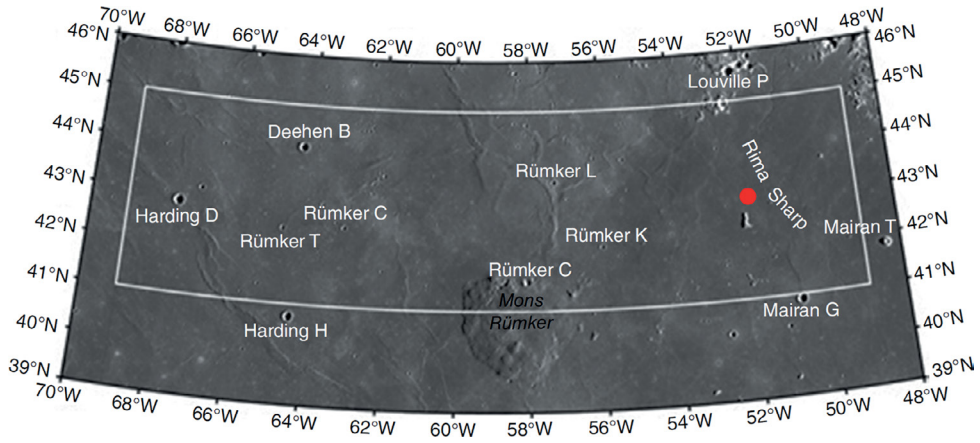

Fig. 9.2 ***Chang'e-5 landing region (white box) in Northern Oceanus Procellarum.*** The red point represents the CE-5 landing site.

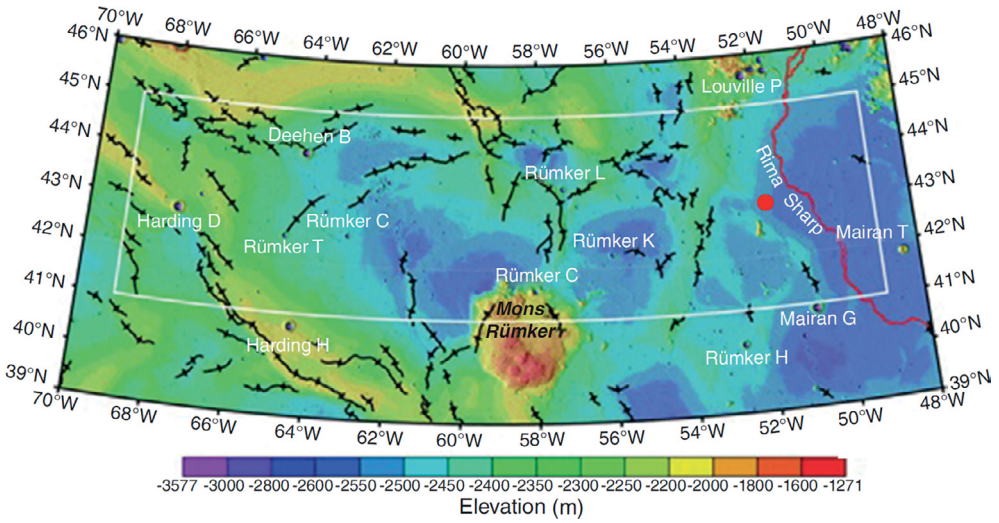

Fig. 9.3 ***Topography map of the Chang'e-5 landing region (white box).*** Black lines denote wrinkle ridges. Red lines denote Rima Sharp. The red point represents the CE-5 landing site.

the Moon (Fig. 9.2) (Head and Gifford, 1980). It is an almost circular feature, with a diameter of ~70 km and the highest point is ~1300 m above the mare surface. Because Mons Rümker formed before the surrounding mare basalts, its original size maybe even larger. Zhao et al. (2017) studied the geology and evolution history of Mons Rümker in detail. They identified 22 independent domes on the Rümker plateau and classified them into shallow domes (**ld**, Fig. 9.4) and steep-sided domes (**sd**, Fig. 9.4), representing different eruption stages. In addition, Zhao et al. (2017) divided the Rümker plateau

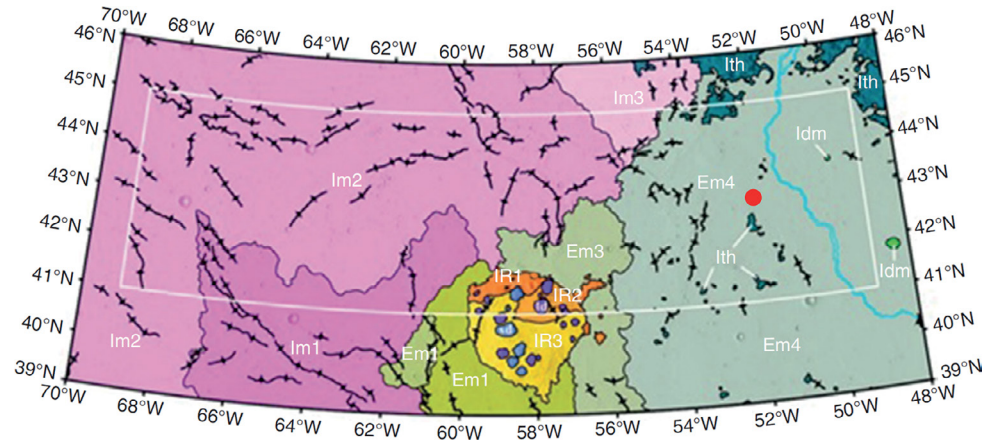

Fig. 9.4 ***Geological map of Chang'e-5 landing region (white box).*** Blue lines indicate the Rima Sharp. Ith indicates highland materials. Idm indicates silica-rich Mairan domes. IR1, IR2, and IR3 indicate Rümker plateau units. Im1, Im2, Im3, Em1, Em2, Em3, and Em4 are Imbrian-aged and Eratosthenian-aged basaltic mare units, respectively. The red point represents the CE-5 landing site.

into three units, i.e., **IR1**, **IR2**, **IR3** (Fig. 9.4). Their ages are estimated by crater size-frequency distribution to be 3.71 Ga, 3.58 Ga, and 3.51 Ga, respectively.

Rima Sharp (red line in Fig. 9.3, blue line in Fig. 9.4) is located in the east of the CE-5 landing region. It was described as the longest lunar sinuous rille (Hurwitz et al., 2013). It has a length of ~566 km, an average width of ~840 m, an average depth of ~76 m, and a regional slope of –0.008°. Because lunar sinuous rilles are formed by thermal and mechanical erosion of lava flows (Head and Wilson, 2017; Williams et al., 2000), some of the lavas that carved the rille channel may have been emplaced and distributed in the area nearby the rille and have been sampled by CE-5 (Qian et al., 2021a).

Highland material remnants (**Ith**, Fig. 9.4) are scattered in the eastern part of the landing region. They have a hilly to hummocky appearance with various shapes, and are up to 500 m higher than the mare surface. Some of them are thought to be possible ring materials of the Imbrium Basin embayed by mare lavas (Wilhelms and McCauley, 1971).

Mare basalts are the dominant materials in the CE-5 landing region. Wrinkle ridges (black lines, Fig. 9.4) develop on the mare surface across the entire area. They have three preferred orientations, i.e., NW, NNW, NE. In the western part of the landing region, wrinkle ridges range up to 6 km in width and 110 km in length and are 200 m higher than the surrounding mare. The eastern part wrinkle ridges are much smaller.

The mare basalts and the scientific significance of the younger ones have been studied in detail by Qian et al. (2018, 2021a). They found that the CE-5 landing region has two types of mare basalts, distributed in the western and eastern part of the landing region, respectively (and thus named western maria and eastern maria). The western maria have a very-low-Ti to low-Ti composition (TiO_2 content lower than 5 wt%) and low FeO content (15.8 wt% on average); the eastern maria have higher TiO_2 contents (4.7 wt% on average) and FeO content (6.7 wt %, mean content) than the western maria, excluding areas contaminated by low-Ti crater ejecta materials (Qian et al., 2021b). Both western maria and eastern maria spectra are characterized by high-Ca pyroxenes, with absorption features at <1000 nm and >2000 nm (Qian et al., 2020). However, the eastern maria pyroxenes are probably richer in iron or calcium, because of the shorter absorption Band II center (2200 nm against 2300 nm). By combining elemental composition, mineralogy, and geomorphology, Qian et al. (2018) divided the mare basalts in the region into six units. Their geologic ages are estimated by crater size-frequency distribution measurements, which are 3.42 Ga, 3.39 Ga, 3.16 Ga, 2.30 Ga, 1.51 Ga, 1.21 Ga and then labeled as **Im1**, **Im2**, **Im3**, **Em1**, **Em2**, **Em3**, **Em4** (Fig. 9.4) respectively, according to their formation sequence. Therefore, it is clear that the differences in the western maria and eastern maria are caused by two stages of volcanic activities, each with different compositions, occurred in the Imbrian Period (older than 3 Ga) and in the Eratosthenian Period (younger than 3 Ga), respectively.

The Eratosthenian-aged mare basalts are among the youngest mare basalts on the Moon. These young basalts have never been sampled by Apollo or Luna sample return missions, and thus the returned Chang'e-5 samples will provide enormous potentials for solving some basic lunar scientific questions. Qian et al. (2021a) has summarized the 27 fundamental questions that may be answered by the returned CE-5 samples, including

questions about chronology, petrogenesis, regional setting, geodynamic & thermal evolution, and regolith formation (Tab. 1 in Qian et al. 2021a), especially calibrating the lunar chronology function, constraining the lunar dynamo status, unraveling the deep mantle properties and assessing the Procellarum KREEP Terrain structures and significance.

In summary, the CE-5 landing region experienced the following geological events, from older to younger:

1. The Imbrium impact occurred at ~3.92 Ga ago (Snape et al., 2016) and generated a complex multiring system, forming the Ith unit in the area.
2. Basaltic activities were active from 3.71 to 3.51 Ga on the Rümker plateau and formed plateau basaltic units IR1 (3.71 Ga), IR2 (3.58 Ga), and IR3 (3.51 Ga).
3. The most extensive phase of basaltic volcanism occurred in the Late Imbrian Period, forming very low-Ti to low-Ti mare basalts (Im1, 3.42 Ga; Im2, 3.39 Ga; Im3, 3.16 Ga) in the western maria.
4. The extended phase of mare volcanism started at ~2.30 Ga and ceased at ~1.21 Ga, and formed four mare units (Em1, 2.30 Ga; Em2, 2.13 Ga; Em3, 1.51 Ga; Em4, 1.21 Ga). The youngest mare eruption formed the Em4 mare basalts, with higher Ti contents.

9.2.2 Sampling technologies

Chang'e-5 has collected lunar samples by using two methods, i.e., collecting subsurface samples using a drill, and collecting surface samples using a scooping device.

The drill is developed by Beijing Spacecrafts (Pang et al., 2012). It is composed of a drilling mechanism, a loading device, and a coring system. The drill stem has an internal and an external drilling pipe. During drilling operations, the external pipe rotates, while the internal drilling pipe is static to the lunar regolith. The internal drilling pipe is designed as a thin-walled hollow pipe to better preserve the original stratigraphic layers of the lunar regolith. The external pipe is a hollow pipe with helical blades to discharge drilling chips and dissipate heat. The coring mechanism uses a soft sampling bag technique to take and store samples. First, the soft sampling tube bag is installed on the inner wall of the internal pipe. The sampling bag then surrounds lunar regolith when it enters the hollow pipe. Then, the sampling bag is extracted and convolved into the primarily package device for drilling samples, and finally transfered to the sealing capsule on the top of the ascender. The goal is to penetrate and recover ~2 m of lunar regolith in the nominal sequence and Chang'e-5 has collected a ~1 m core by drilling finally.

The scooping device (Surface Sampling System) is developed by Hong Kong Polytechnic University. It consists of four joints, two samplers, and a close-range camera. Following landing and prior to sampling operations, camera images from the Sampling Monitoring Cameras, Panoramic Cameras, Far-range Camera, and Close-range Camera have been used to establish a sampling plan. Then, the robotic arm has scooped the surface regolith and rock fragments using two samplers with the help of camera images. Collected samples have then been placed into the primary package device for surface samples on the top of the lander. The scooping device has conducted 12 times of samplings, and ~1.5 kg samples have been gathered around the lander. Then, the primary

package device closed and the samples have been transported to the sealing capsule on the top of the ascender.

In summary, CE-5 conducted the following sampling workflow during the mission operations Fig. 9.5:

1. Unlock the drilling system and scooping system after landing.
2. The drilling system conducted drilling and coring. Samples were then separated and transferred to the primary package device for drilling samples. Finally, the samples were transported to the sealing capsule.
3. The robotic sampling arm conducted surface sampling. Samples were then transferred to the primary package device for surface samples on top of the lander, where it underwent primary packaging. Finally, the robotic sampling arm transported the primary package device to the sealing capsule on the top of the ascender.
4. The sealing capsule was then sealed. The package consisted of both of the drilling samples and the surface samples, which remained separately.

9.2.3 *In-situ* exploration

The Chang'e-5 mission has two key scientific payloads onboard its lander, i.e., the Lunar Mineralogical Spectrometer (LMS) and the Lunar Regolith Penetrating Radar (LRPR).

The Lunar Mineralogical Spectrometer was designed to obtain in-situ visible and ultra-violet spectra of the lunar surface both before and after sampling operations. The acquired spectra would be helpful to understand the mineralogical composition of the CE-5 landing site, especially hydrated minerals, providing information on water-rock interaction and lunar volatiles.

LMS employs acousto-optic tunable filters (AOTFs). An aluminum plate and an Infragold plate are used for calibrating the VIS/NIR and IR spectra, respectively. The visible spectrometer can acquire images of the drilling and sampling sites. The measuring capabilities of LMS are listed below (Li et al., 2015; Cai et al., 2019).

1. Spectral range: 480 ~3200 nm, covered by a VIS/NIR and an IR module. The VIS/NIR module is composed of visible (480 ~950 nm) and near-infrared (900 ~1450 nm) spectrometers, and the IR module is composed of short-infrared (1400 ~2450 nm) and middle-infrared (2400 ~3200 nm) spectrometers.

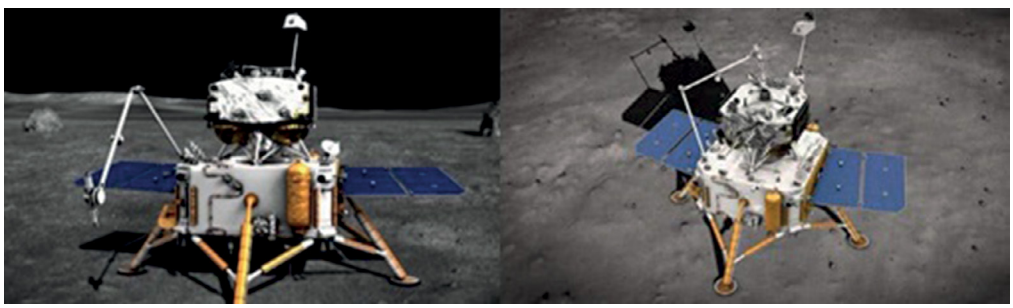

Fig. 9.5 Chang'e-5 samples the lunar surface with a robotic arm (artistic impression).

2. Spectral resolution: 3 ~25 nm
3. Detection range: 2 ~5 m
4. Field of view (FOV): 4.24°×4.24°

The Lunar Regolith Penetrating Radar was used to detect and analyze lunar regolith structure and thickness at the landing site, supporting drilling and sampling operations, and further stratigraphic analysis (Qian et al., 2021b).

LRPR is an ultra-wideband array-based ground penetrating radar (Feng et al., 2019; Y. Li et al., 2019; Xiao et al., 2019). It is composed of a high-frequency antenna array, cables, and an electronics box. The antenna array consists of 12 bow-tie antennas with a working frequency range of 1 ~3 GHz; these are asymmetrically mounted around the drill (90 cm above the ground). The LRPR works in the time domain and transmits carrier-free pulses with a Full Width at Half Maximum of 200 ps. During its operation, one of the antennas sends a pulse signal into the lunar subsurface and the other antennas receive the echo signals. The 12 antennas work taking turns, providing 132 traces of data recorded in an operation period. Each trace has a time window of 55 ns, with a temporal sampling interval of 18.3 ps. The measuring capabilities of LRPR are listed below:

1. Detection depth: ≥2 m
2. Vertical spatial resolution: ≤5 cm
3. Detection area: sampling site
4. Frequency range: 1~3 GHz

9.3 Landing, recovery and transport procedures

The sample return capsule landed in the desert area of Inner Mongolia, North China, on December 17, 2020, a traditional landing field for China's crewed and robotic space exploration missions. The recovered sample capsule was then packaged and sealed in a transfer box (filled and protected by nitrogen) and transferred to the Lunar Sample Laboratory at Ground Research Application System (GRAS), Beijing, the primary sample storage and curation center.

9.4 Sample storage and analysis

9.4.1 Sample storage and curation

The returned samples are managed by the Lunar Exploration and Space Engineering Center (LESEC), CNSA (China National Space Administration, 2020). LESEC has been entrusted to carry out the management of lunar samples, with main responsibilities including: 1) reviewing standards and operating procedures formulated by the curatorial agencies; 2) establishing an expert committee on lunar samples; 3) reviewing applications for requesting lunar samples; 4) supervising and coordinating the process of unsealing, classification, preparation, documentation, storage, application, distribution, transportation, use, return, dispositioning, management of information, and documentation of results.; 5) publishing dynamic information on lunar samples on a regular basis through data

information platform; and 6) implementing the monitoring of science returns and its applications, and preparing and publishing a list of publications and achievements.

Sample prelimary analysis and curation. The primary storage center (GRAS) is responsible for sample classification and cataloging. The general procedure is as follows (Zhang et al., 2020): 1) GRAS would receive the sealed package from the spacecraft system; 2) sample bags would be unsealed. Both scooped and drilled samples would be taken out and cataloged separatly in two unsealed containers inside the unsealed package; 3) drilled samples soft bag would be cut into several sections of 15 cm each, while scooped samples would be put into a squared container and classified into different types; and 4) after classification, the permanent storage samples will be transferred to the permanent storage glove box in the long-term storage room, and the research and backup permanent samples will be transferred to the temporary glove box waiting for further utilization.

Preliminary analysis includes physical properties, mass, grain size of the samples, and etc. GRAS is equipped with balances, microscopes, glove boxes, cryogenic freezer, etc. All the tools that will contact with lunar samples are made of stainless steel, teflon, quartz glass or materials of known composition that do not contaminate the samples and therefore do not affect subsequent scientific analysis. The pure nitrogen pressure in the glove box will be strictly monitored to prevent the lunar samples contamination from the Earth contaminations (Zhang et al., 2020).

Sample storage. Returned samples will be stored in CNSA-designated storage facilities (GRAS). Two storage types are planned: primary storage and remote disaster-tolerant backup storage. The primary storage institution has the responsibilities of (China National Space Administration, 2020): 1) formulating standards and operating procedures related to lunar samples; 2) implementing the unsealing, classification, preparation, documentation, and storage of lunar samples; 3) Implementing the distribution, return and dispositioning of lunar samples in accordance with the procedures; 4) Building and maintaining the lunar sample storage facilities, to make sure that these facilities have the capability to carry out the necessary work; and 5) Establishing a lunar sample curation catalog, thus to secure the information safety of the lunar samples.

The remote backup storage institution has the responsibilities of (China National Space Administration, 2020): 1) participating in the formulation of the standards and operating procedures related to lunar samples; 2) building and maintaining storage facilities; and 3) establishing a lunar sample information catalog to guarantee the security of lunar samples stored.

Allocation of samples for research purposes. Several specific procedures will be applied for allocation of samples for study and analysis (China National Space Administration, 2020). The institution of the applicant is the legal entity responsible for the agreement for sample allocation. At the same time, the legal entity should have safe storage conditions and research capabilities. LESEC shall accept applications all year round and shall conduct evaluations on the applications once every three months. The approved applicant shall sign the "Lunar Sample Loan Agreement" with the LESEC, and the primary

curation center shall issue the allocated samples in accordance with the procedures. The sample preparation and distribution shall be completed within 30 working days, and the relevant information shall be returned to LESEC in a timely manner. For the purpose of research, the sample allocation period will not be generally longer than 1 year. If the sample allocation apply for an extension, an agreement will need to be renewed, the renewal period will be no longer than 6 months, and the application for renewal shall be submitted to the engineering center at least 30 days in advance. Due to the preciousness and uniqueness of the samples, the allocated research samples shall be used sparingly. For destructive experiments, it will be necessary to carefully design a plan to reduce the consumption of samples and document a detailed demonstration and explanation in the sample allocation research plan. For public outreach or education purposes, the sample allocation period will be generally no longer than 2 months. If the sample agreement shall be renewed, the renewal will be no longer than 1 month, and the application for renewal shall be submitted to the LESEC at least 15 days in advance.

The person requesting allocation of a sample (the borrower) will have to maintain a record of the entire process on the samples, and video recording will be requested to ensure the traceability of the use of destructive and consumable samples. The borrowing institution shall accept inspection of facilities by the LESEC and shall not provide the samples to a third party for use. If the borrower violate the provisions of the allocation agreement, the LESEC may terminate the loan and require the immediate return of the sample. When the period of normal use expires, the records and remaining samples of the user shall be returned to the primary curation center. If there are no remaining samples, a complete video record of sample usage shall be provided.

9.4.2 International collaboration

The management and utilization of lunar samples will comply with relevant international conventions. CNSA supports joint science-based research work and promotes the international sharing of scientific results. CNSA is responsible for signing the relevant international cooperation agreements.

The LESEC undertakes and organizes the joint research, exchange, display and allocation of lunar samples, and encourages foreign research institutions and domestic research institutions and universities to set up research teams for joint researches.

9.5 Conclusions

The Chang'e-5 mission is the China's first attempt to collect samples from an extraterrestrial body, as well as the first attempt to collect lunar samples since Luna 24 in 1976, after nearly a half century. Chang'e-5 has landed in Northern Oceanus Procellarum on December 1, 2020, far from previous landing sites and having distinct geological backgrounds and especially young mare basalts. The returned samples could be used to

calibrate lunar chronology function by dating the young basalts, trace the lunar magmatic history and disclose the potential genetic link between young volcanism and the PKT terrains, using state-of-art technologies (Qian et al., 2021a). At the same time, China welcomes science teams from all around the world to jointly work to study the new returned samples with Chinese scientists and to promote lunar science toward a big step after Apollo and Luna era.

References

China National Space Administration, 2020. Lunar Sample Management Regulation. Procedures for Requesting Lunar Samples. http://www.cnsa.gov.cn/english/n6465645/n6465648/c6811126/content.html.

Cai, T., Li, C., He, Z., Ren, X., Liu, B., Xu, R., 2019. Experimental ground validation of spectral quality of the chang'E-5 lunar mineralogical spectrometer (in Chinese). Spectroscopy and Spectral Analysis, *039* (*001*), 257–262.

Feng, J., Su, Y., Li, C., Dai, S., Xing, S., Xiao, Y., 2019. An imaging method for Chang'e−5 lunar regolith penetrating radar. Planetary and Space Science, 167, 9–16.

Head, J.W., Gifford, A., 1980. Lunar mare domes: classification and modes of origin. The moon and the planets *22* (2), 235–258.

Head, J.W., Wilson, L., 2017. Generation, ascent and eruption of magma on the Moon: New insights into source depths, magma supply, intrusions and effusive/explosive eruptions (Part 2: Predicted emplacement processes and observations). Icarus 176–223.

Hiesinger, H., Head III, J.W., Wolf, U., Jaumann, R., Neukum, G., 2011. Ages and stratigraphy of lunar mare basalts: a synthesis. In: Ambrose, W.A., Williams, D.A. (Eds.), Recent Advances and Current Research Issues in Lunar Stratigraphy. Geological Society of America Vol. 477, p. 0.

Hurwitz, D.M., Head, J.W., Hiesinger, H., 2013. Lunar sinuous rilles: distribution, characteristics, and implications for their origin. Planet. Space Sci. *79-80*, 1–38.

Jolliff, B.L., Gillis, J.J., Haskin, L.A., Korotev, R.L., Wieczorek, M.A., 2000. Major lunar crustal terranes: surface expressions and crust-mantle origins. Journal of Geophysical Research: Planets *105* (*E2*), 4197–4216.

Li, H., Liu, B., Ren, X., Liu, J., Li, C., Xu, X., Xu, R., Tian, M., 2015. Ground Verification Test of Lunar Mineralogical Spectrometer on the Chang'e 5 Lunar Sample Return Lander. Paper presented at the 2015 AGU Fall Meeting, San Francisco, California.

Li, Y., Lu, W., Fang, G., Zhou, B., Shen, S., 2019. Performance verification of lunar regolith penetrating array radar of chang'E-5 mission. Adv. Space Res. *63* (7), 2267–2278.

Liu, J., Zeng, X., Li, C., Ren, X., Yan, W., Tan, X., Zhang, X., et al., 2021 Landing Site Selection and Overview of China's Lunar Landing Missions. Space Science Reviews. *217* (6).

National Research Council (2007). *The Scientific Context for Exploration of the Moon*.

Pang, Y., Liu, Z., Li, X., 2012. Design and analysis of automatic drilling sampling mechanism for lunar exploration (in Chinese). Chinese Space Science and Technology 32 (6), 16–22.

Pei, Z., Wang, Q., Tian, Y., 2015. Technology roadmap for Chang'E program (In Chinese). Journal of Deep Space Exploration *2* (2), 99–110.

Prettyman, T.H., Hagerty, J.J., Elphic, R.C., Feldman, W.C., Lawrence, D.J., McKinney, G.W., Vaniman, D.T., 2006. Elemental composition of the lunar surface: analysis of gamma ray spectroscopy data from Lunar Prospector. Journal of Geophysical Research: Planets *111*, E12.

Qian, Y., Xiao, L., Zhao, S., Zhao, J., Huang, J., Flahaut, J., Wang, G., 2018. Geology and scientific significance of the rümker region in northern oceanus procellarum: china's Chang'E-5 landing region. Journal of Geophysical Research: Planets *123* (6), 1407–1430.

Qian, Y., Xiao, L., Head, J.W., van der Bogert, C.H., Hiesinger, H., Wilson, L., 2021a. Young lunar mare basalts in the Chang'e-5 sample return region, northern Oceanus Procellarum. Earth and Planetary Science Letters *555*, 116702.

Qian, Y., Xiao, L., Wang, Q., Head, J.W., Yang, R., Kang, Y., et al.,2021b. China's Chang'e-5 Landing Site: Geology, Stratigraphy, and Provenance of Materials. Earth and Planetary Science Letters, In Press.

Qian, Y., Xiao, L., Yin, S., Zhang, M., Zhao, S., Pang, Y., et al., 2020. The regolith properties of the Chang'e-5 landing region and the ground drilling experiments using lunar regolith simulants. Icarus, 337, 113508.

Snape, J.F., Nemchin, A.A., Bellucci, J.J., Whitehouse, M.J., Tartèse, R., Barnes, J.J., Joy, K.H., 2016. Lunar basalt chronology, mantle differentiation and implications for determining the age of the Moon. Earth Planet. Sci. Lett. *451*, 149–158.

Wieczorek, M.A., Neumann, G.A., Nimmo, F., Kiefer, W.S., Taylor, G.J., Melosh, H.J., Zuber, M.T., 2013. The crust of the moon as seen by GRAIL. Science *339* (6120), 671.

Wilhelms, D.E., McCauley, J.F., 1971. Geologic Map of the Near Side of the Moon.

Williams, D.A., Fagents, S.A., Greeley, R., 2000. A reassessment of the emplacement and erosional potential of turbulent, low-viscosity lavas on the Moon. Journal of Geophysical Research: Planets *105* (E8), 20189–20205.

Xiao, L., 2018. Farside landing and nearside sample return: china's new lunar missions are on the way. The Planetary Report, September Equinox 2018, 13–17.

Xiao, Y., Su, Y., Dai, S., Feng, J., Xing, S., Ding, C., Li, C., 2019. Ground experiments of Chang'e-5 lunar regolith penetrating radar. Adv. Space Res. *63* (10), 3404–3419.

Zhao, J., Xiao, L., Qiao, L., Glotch Timothy, D., Huang, Q., 2017. The mons rümker volcanic complex of the Moon: a candidate landing site for the Chang'E-5 mission. Journal of Geophysical Research: Planets *122* (7), 1419–1442.

Zhang, G., Li, C., Liu, D., Liu, B., Zhou, Q., Gao, F., Zhang, H., Kong, D., Ren, X, 2020. Storage, processing and preparation methods for China's returned lunar samples, Paper presented at the 51st Lunar and Planetary Science Conference. The Woodlands, Houston.

Zheng, Y., Ouyang, Z., Li, C., Liu, J., Zou, Y., 2008. China's Lunar Exploration Program: Present and future. Planetary and Space Science, *56*, 881–886.

CHAPTER 10

Future missions

Elizabeth J. Tasker[a], **Jonathan I. Lunine**[b]
[a]Institute of Space and Astronautical Science, Japan Aerospace Exploration Agency
[b]Department of Astronomy, Cornell University

Chapter Outlines

10.1 The JAXA Martian Moons eXploration mission

The "Martian Moons eXploration Mission" (MMX) will be the third Japan-led sample return mission, following the asteroid explorers Hayabusa and Hayabusa2. MMX is a five-year round-trip mission to the Martian system (Fig. 10.1) to establish the origin of the Martian moons, and gain new insight into the circumplanetary environment and surface evolution of the planet. The mission will return a sample to Earth from the innermost moon, Phobos.

Sample return missions have to carefully consider contamination issues, both to the sample whose scientific value would be undermined by terrestrial contamination, and also the potential risk that the returned samples present to Earth. While the Phobos sample may contain volatile-baring phases and organics, simulation work showed a minimal chance of Mars extant micro-organisms being brought to Earth by MMX (Fujita, et al., 2019; Kurosawa, et al., 2019). This resulted in the Committee on Space Research (COSPAR) classifying MMX as an unrestricted Earth-return mission, the same as all the sample return missions performed so far.

Mission launch is planned for 2024 JFY (Japan Financial Year: April 2024 – March 2025). While led by the Japan Aerospace Exploration Agency (JAXA), the mission includes multiple contributions from international partners.

The science objectives of the MMX mission are focused on understanding volatile delivery to the terrestrial planets. Planet formation theories suggest that the rocky

DOI: 10.1016/C2018-0-03374-5

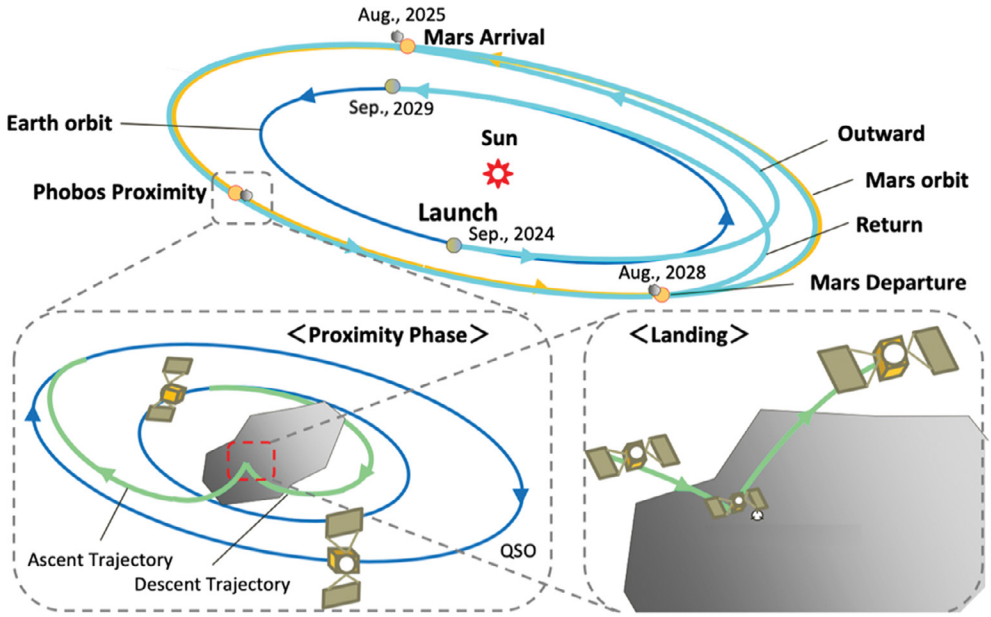

Fig. 10.1 ***MMX mission overview.*** The dates listed are approximate subject to change as the mission develops. *(Credit: JAXA).*

planets should have formed dry, as the inner Solar System was likely too warm for solid ice to be present in planetary building material. Water was then delivered via impacts from asteroids and/or comets that formed beyond the snowline (where water freezes into ice), and were scattered inwards during gravitational interactions with the giant planets.

Records of this time are preserved in the small bodies of the Solar System. While the planets have undergone substantial evolution since formation, asteroids, comets and small moons have experienced significantly less change. Their bulk composition reflect how and where they were formed, while surface conditions provide insight into changes within their surrounding environment.

The moons of Mars are of particular importance as they are situated at the gateway between the inner and outer Solar System. These two small bodies are capsules from the epoch of volatile movement in the Solar System, and could give information for the transition of Mars from a possibly habitable world into a barren landscape.

The two main mission goals for MMX are therefore:

1. Reveal the origin of the Martian moons and increase understanding of planetary system formation and the primordial transport of material between the inner and outer Solar System.
2. To understand conditions in the circum-Martian environment and the evolution of the surface of both Mars and its moons.

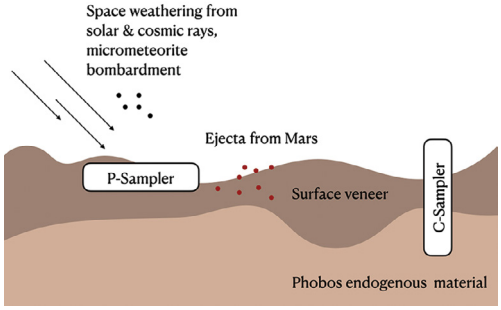

Fig. 10.2 The MMX spacecraft is equipped with two sampling mechanisms: the P-Sampler that will gather material from the top veneer of Phobos and the C-Sampler that will collect material down to a depth of at least 2cm.

These two goals tie directly into the mission plans for sampling Phobos. The spacecraft is equipped with two sampling mechanisms: the C- (coring) Sampler and the P- (pneumatic) Sampler. The two samplers will collect material from different depths from the moon's surface, which is expected to probe different aspects of the Martian system evolution (Fig. 10.2).

10.1.1 The C-Sampler and related scientific goals

The C-Sampler is designed by JAXA and aims at collecting subsurface material down to a depth of at least 2 cm. The sampler consists of a robotic arm and cylindrical corer that can drive through the surface regolith on Phobos and return a core soil tube containing more than 10 g of material.

The ability to gather from the subsurface will allow the C-Sampler to collect material from the endogenous Phobos that has been unaffected by space weathering or contamination. This sample is therefore directly linked to the origin of the moons.

Exactly how Phobos and Deimos formed is actively debated. The two main proposed mechanisms are that the moons are captured asteroids or that they formed during a giant impact with Mars (e.g. Higuchi and Ida, 2017; Hyodo, et al., 2017, Craddock, 2011).

The two satellites resemble asteroids, both in their non-spherical shape and in their reflectance spectrum that is similar to the D-type asteroids which populate the outer part of the asteroid belt (Murchie, et al., 1991). If the captured scenario is true, the moons would be examples of the small bodies that were scattered inwards to deliver volatiles to the inner Solar System.

The composition of captured asteroids would be distinct from Mars, and depend on where the moons originally formed. The heliocentric gradients for element isotopes and volatile abundances (e.g. CO_2/H_2O, D/H, $^{15}N/^{14}N$, O, Cr and Ti) provides a mechanism for linking the composition of the sample to the moon's formation location (Fig. 10.3) (Warren, 2011). If the moons were formed beyond the snowline where

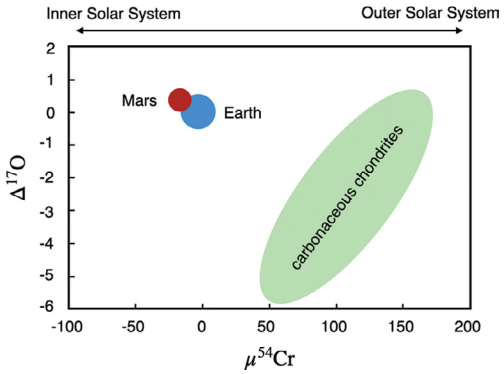

Fig. 10.3 Isotopic abundances of O and CR can clearly differentiate between reservoirs present either side of Jupiter's orbit. *(Credit: Data collected from Usui, et al., 2020).*

ice can exist, then they may also contain organic material and evidence of water-rock reactions that may have taken place on a larger parent asteroid that later fragmented to form Phobos (Alexander, et al., 2012).

Alternatively, if the moons formed during a giant impact, their composition should reflect both Mars and the (unknown) impactor. Evidence for this formation scheme is the orbit of the two moons, which both circle Mars in the planet's equatorial plane on near-circular paths. This would be achieved if the pair coalesced from debris ejected during a major collision (Craddock, 2011).

Simulations of the impact suggest that this process results in between 35 percent - 65 percent of the material forming the moons originating from the crust and mantle of Mars (Hyodo, et al., 2017). Compared to carbonaceous chondritic abundances that may be similar to those found in the captured asteroid scenario, bulk silicates on Mars are strongly depleted of volatile elements such as potassium, but slightly enriched compared to the Earth. Siderphiles in Martian silicate such as iron are also higher for Mars than any of the other terrestrial planets (Taylor, 2013; Usui, et al., 2020).

The high temperatures (around 2000K) experienced during the impact would likely destroy any organic material originally in either source of rock and instead result in shocked or recrystallized phases (Hyodo, et al., 2017).

Material returned by the C-sampler will contain both surface and subsurface material from Phobos. To separate out the surface regolith from endogenous moon material, a comparative sample will be used, that will be gathered by the P-Sampler.

10.1.2 The P-Sampler and related scientific goals

The P-Sampler is being designed by NASA and will gather material using a pneumatic system that applies pressurized gas to push the soil into the sample container. Unlike the C-Sampler which will gather from a range of depths, P-Sampler material will consist of regolith from the top layers of the moon.

The pneumatic system will work effectively in all conceivable surface conditions. In a possible case where use of the C-Sampler is disrupted by the presence of a hard bedrock layer beneath the regolith, the P-Sampler could still successfully return material.

Comparison between material collected between the P-Sampler and C-Sampler will allow subsurface endogenous Phobos material gather by the C-Sampler to be separated from grains that may have undergone alteration or have a different origin. The veneer of Phobos is expected to include both material altered from external effects such as space weathering and also that ejected from the Martian surface.

Simulations of material ejected from the Martian surface suggest impacts from meteorites over the last 500 million years should have resulted in a minimum of 1×10^9 kg of material from Mars being deposited on Phobos. This quantity could triple if Mars experienced a particularly large impact capable of forming a crater of order 260 km across during that time. Since the MMX spacecraft plans to gather more than 10 g of material from Phobos, there should be an estimated 110 grains from Mars in that sample (Hyodo, et al., 2019).

The Martian grains found on Phobos would have arrived over the course of millions of years of evolution on Mars from locations distributed globally over the planet. Radioactive isotopes in the grains can provide a timeline of Martian history. This would make the sample unique compared to in-situ studies by rovers, which are limited to a single spatial location and epoch.

Phobos's proximity to Mars is also expected to result in a wider variety of materials deposited on the moon surface, compared to that found in Martian meteorites. Interplanetary distances and atmospheric entry mean that Martian meteorites consist of hard igneous rock that has experienced pressures between 5–50 GPa (Hyodo, et al., 2019).

However, more fragile material cannot survive the journey to Earth, but could reach the Martian moons. This may include sedimentary rock that includes materials such as clays that form through contact with water. A recent discovery of organics in one of the two known meteorites from the Noachian period on Mars also suggests that organic material may be present on the surface of Phobos. Material from the P-Sampler will therefore probe the transformation of Mars's terrain, mapping any development and loss of habitability (Koike, et al., 2020).

10.1.3 Remote observations and landing

The MMX spacecraft will use a Quasi-Satellite Orbit (QSO) to study Phobos remotely. If observed from Mars, the spacecraft will appear to follow Phobos with Mars at the center of the orbit. From the perspective of Phobos, the orbit will move around the moon to allow study of the satellite's surface from the onboard remote sensing suite.

The scientific instruments onboard the MMX spacecraft will provide essential geologic context for the sample gathered from Phobos. Instruments developed at

JAXA consist of the narrow-angle camera TENGOO (TElescopic Nadir imager for GeOmOrphology), for capturing high-resolution images of the moon surface, the wide-angle multi-spectral camera, OROCHI (Observation of surface Reflectance by Optical CHromatic Imager) for identifying hydrated minerals and organic matter, the LIDAR laser altimeter for topology, the Circum-Martian Dust Monitor (CMDM), the Mass Spectrum Analyzer (MSA) to detect charged ions around the moons, the radiation environment monitor, IREM and a high resolution camera.

Instruments developed by partner agencies are also onboard. The near-infrared spectrometer, MIRS (MMX InfraRed Spectrometer), is being designed by CNES for identifying mineral compositions. NASA is contributing the gamma-ray and neutron spectrometer, MEGANE (Mars-moon Exploration with GAmma rays and Neutrons) that will also provide information about the elemental abundances in subsurface material (Lawrence, et al., 2019). A rover is also planned to explore the surface of Phobos, that is being developed in a joint project between CNES and DLR.

In addition to the global perspective, these instruments will also be used to select the landing site. At least two samplings will be considered for sample collection, with material collected each sampler stored separately for return to Earth.

The spectral slope is one of the considerations for the landing site selection. This parameter is similar to D-type asteroids for the two moons. Neverthess, Phobos contains regions that show a shallower slope, which may indicate the presence of different minerals, or exposure of subsurface material (Ballouz, et al., 2019). This was one of the reasons that Phobos was chosen for sample collection, despite being more challenging to reach than the uniform Deimos.

10.2 JAXA/OKEANOS

Beyond the MMX mission, JAXA is considering a solar power sail mission to the Jupiter Trojan asteroids. The "Oversize Kite-craft for Exploration and AstroNautics in the Outer Solar System" (OKEANOS) will rendezvous with the Trojan asteroids and deploy a lander for in-situ analysis (Okada, et al., 2018; Mori, et al., 2019). The mission is currently under study and different scenarios are being discussed, in which the most extended plan involves returning a sample from one of the Trojans to Earth.

The Jupiter Trojan asteroids are in long-term stable orbits situated at the Sun-Jupiter Lagrange points (L4 and L5). The Nice Model and other formation theories support an origin as Kuiper Belt objects intruding into these regions during the migration of the giant planets (Levison, et al., 1997, 2008; Jewitt, et al., 2004). Their location beyond the present snowline in the Solar System suggests they are volatile rich and therefore of key interest in understanding the passage of water and organics between the outer and inner Solar System (Morbidelli, et al., 2005). The OKEANOS mission therefore extends JAXA's goal to explore habitability through mapping the movement of small bodies.

The solar power sail generates electrical power using a large number of thin-film solar cells attached to a membrane with a large surface area (> 1000 m^2). The generated electric power can then be used to propel the spacecraft, for example through the operation of electric propulsion, in order to rendezvous with the Trojans asteroids even at a solar distance of 5.2 AU. The solar power sail is distinct from a solar sail, where the thrust comes entirely from the momentum transfer from solar photons, as it can take advantage of both solar photon acceleration while near the Sun, and electric propulsion operation when at larger distances.

Solar sail technology was first demonstrated for interplanetary cruise by the JAXA/IKAROS (Interplanetary Kite-craft Accelerated by Radiation of the Sun) mission, launched in 2010 (Mori, et al., 2010). The IKAROS sail was a square membrane with an approximate surface area of 200 m^2. The sail was deployed by spinning the main body of the spacecraft so that the centrifugal forces expanded the sail. Post deployment, the spacecraft continued to spin at a lower rate to maintain tension in the sail. This mechanism avoided the need for rigid structural support for the sail and allowed the use of a lighter and therefore larger membrane.

To generate sufficient power for electric propulsion in the outer Solar System, the OKEANOS sail requires a sail size ten times larger than that of IKAROS. The sail would power high specific impulse ion engines to rendezvous with the Jupiter Trojan system, where chemical thrusters will be used for position control in the proximity of the asteroids. The use of a solar power sail would allow electrical power-demanding exploration of the outer Solar System without the need to use a radioisotope thermoelectric generator (RTG).

As a large rotating sail would make landing highly risky for the spacecraft, a separate battery-powered daughter lander would be deployed and perform the landing, sampling and in-situ analysis on the asteroid, before returning part of the collected samples to the mother spacecraft for return to Earth.

The lander would employ two complementary sampling system to acquire both surface and sub-surface samples. For the surface sampling, a projectile-impact sampling mechanism that was used by Hayabusa and Hayabusa2 is being considered, with a sampler horn to gather material from the surface (Sawada, et al., 2017; Yano, et al., 2006, 2002). For the sub-surface sampling, a pneumatic drill mechanism that employs high pressure gas would mobilize the sub-surface regolith layer as deep as 1 m, in order to collect possible volatile and organic-rich samples. In-situ analysis performed by the lander would vaporize part of the collected samples for examination with a high-resolution mass spectrometer, which could measure isotopic ratios of D/H and other light elements of interest such as C, H, O and N as well as organic molecules (Toyoda, et al., 2003). If the sample return option will be taken, the remaining samples would be then transferred to a vacuum container and returned to the mother spacecraft.

Detailed research of a Trojan asteroid by global remote sensing and lander investigation including surface and sub-surface sample analyses by OKEANOS would complement NASA's Lucy mission which is planned for launch in 2021 under the agency's Discovery Program in 2017 to make multiple, fast flybys of the L4 and L5 Jupiter trojan asteroids.

As opposed to a heavy spacecraft propelled by chemical propulsion and heavy lifter rocket, a spacecraft with low thrust continuous propulsion like OKEANOS would take ~13 years for outbound trip to the Jupiter Trojans and almost 30 years for a round trip back to Earth. However, during the interplanetary cruise phase, OKEANOS would provide a platform for multiple science experiments, including continuous measurements of the interplanetary magnetic field and dust environment from 1 AU to 5.2 AU, allowing the spacecraft to start producing scientific results soon after its launch. Astronomy applications are also planned, with deep sky surveys in the infrared to take advantage of the low infrared foreground due to zodiacal dust scattering beyond the main asteroid belt. as well as gamma ray interferometry with ground stations on Earth to create a very long baseline.

10.3 The NASA Comet Astrobiology Exploration Sample Return

10.3.1 Scientific rationale

Comets are thought to be among the most primitive samples of planetary building blocks still existing in the Solar System today. A significant challenge in returning cometary samples is that much of the unique value of this material lies in its most volatile content—water ice and species with higher vapor pressure than water. These species provide the only practically accessible record of the material that supplied the giant planets with their enrichment of elements heavier than helium, as well as the ices present in the moons of the giant planets and Kuiper Belt objects like Pluto. Because giant planet growth beyond the snowline may have been dramatically affected by the size distribution of planetesimals (Bitsch et al. 2018), and ices may have contained very different amounts of volatiles as a function of time and radial position in the disk (Mousis et al., 2019), the cometary chemical and isotopic record is of unique value. Comets are unparalleled in the range of volatility of materials in a sample, from high temperature silicate condensates to noble gases, and the isotopic record can be used to trace the points of origin of the various components (Lauretta et al., 2018). Comet 67P is a member of the Jupiter family of comets, which are thought to have their origin in the Kuiper Belt beyond the orbit of Neptune (Lowry et al., 2008). Despite their current aphelion is comparable to the Jupiter heliocentric distances, their origin occurred at a distance ten times farther from the Sun than asteroids accounts for the high scientific value of such objects. Such bodies therefore are highly relevant to the question of giant planet formation and, hence, that of the terrestrial planets whose growth and inventory of water were profoundly affected by the giant planets (Morbidelli et al., 2012 and ref. therein).

10.3.2 Precursor I: Rosetta

The Rosetta investigation of comet 67P/Churyumov-Gerasimenko (hereafter, 67P) represented a watershed in the study of comets. Designed, built and operated by the European Space Agency (ESA), Rosetta is one of the most capable planetary robotic missions ever conducted. Rosetta rendezvoused with 67P on August 6, 2014, and remained with it for the next two years, terminating its mission with a landing on the nucleus of the comet on September 30, 2016. The main spacecraft deployed a small lander, Philae, which despite technical issues returned data of key importance to the rationale for and planning of comet sample return missions (Boenhardt et al., 2017). While Rosetta itself contained a sophisticated mass spectrometer that returned a wealth of compositional data (Altwegg et al., 2019), it could only sample gases already released from the nucleus, and therefore spatially and temporally averaged. To inform sample collection missions it is necessary to establish that volatile material is present in a specific type of terrain suitable for sample collection. This is precisely what Philae was able to do.

In particular, as Philae bounced on its first touchdown in a so-called smooth terrain (Fig. 10.4), loosely consolidated material was pushed up into the exhaust pipes of the COSAC (Cometary Sampling and Composition) mass spectrometer. Some of this material evidently then evaporated or sublimated into the instrument, which produced mass spectra that included a range of species more volatile than water ice, including methane, carbon monoxide, hydrogen cyanide, and other organic compounds containing varying amount of nitrogen and oxygen (Goesmann et al., 2015). These volatile materials suggest formation temperatures below 50 K (Mousis et al., 2016), and provide

Fig. 10.4 The highest resolution Philae image of smooth terrain at Agilkia on Comet 67P Scale across image is 9.7 m. *(Credit: Copyright: ESA/Rosetta/Philae/ROLIS/DLR).*

compelling evidence that on at least one comet, terrain benign enough for a landing contains material more volatile than water ice.

10.3.3 Precursor II: Stardust

The Stardust spacecraft, a NASA Discovery program mission returned the first samples from a comet, Wild 2, in January 2006 (Sandford et al., this book). This was a high speed flythrough in which coma material was captured and slowed in low density aerogel. The high speed (6 km/s) meant that only refractory solids were collected, with little or no organic and volatile material, though trapped gases were present. The grains showed a mineralogy distinct from IDPs, calling into question the long-held assumption that these derived from comets (Brownlee 2014). The high concentration of noble gases, presence of high temperature minerals and preponderance of crystalline material in the grains all suggested that inner Solar System material was mixed outward to the Kuiper Belt beyond the giant planets.

The value of the volatile-limited sample from Stardust combined with the compelling evidence for volatile-rich material in accessible sites on 67P from Rosetta and Philae made the case for a sample return mission to extract material directly from the nucleus of a comet. The investigations by Rosetta of the coma composition revealed variations in abundances of key species, including noble gases, and D/H ratios, that underscore the need for an independent measurement of ice from the nucleus itself. Comparison of refractory grain composition and isotopic data from 67P with other comets, IDPs, meteorite components, OSIRIS-REx samples, Hayabusa2 samples, and Genesis solar wind material provides a comprehensive look at the various solids present during the formation of the Solar System (Lauretta et al., 2018). First order observations will reveal if 67P is a primordial fossil from the early Solar System or a fragment from a disrupted KBO. Detailed investigation will elucidate the distinct history of the solid materials.

10.3.4 Overview of the CAESAR mission

Three comet nucleus sample return missions were proposed to NASA for the New Frontiers 4 ("NF4") opportunity which opened in January 2017. Of these, one - the Comet Astrobiology Exploration Sample Return (CAESAR) mission - was selected in 2017 for a Phase A study conducted in 2018–19. It was not selected for flight, but may be re-proposed for a later flight opportunity. It was proposed by Prof. Steve Squyres, then at Cornell University, with Goddard Spaceflight Center providing project management, Northrup Grumman the spacecraft bus, and JAXA the Sample Return Capsule. A sample acquisition system, described below, was developed by Honeybee Robotics. Other major contractors included Malin Space Science Systems for the cameras, NASA Johnson Space Center for sample recovery and curation, Kinetx Aerospace for Navigation and flight dynamics, and Motiv Space Systems for the robotic arm.

CAESAR was designed to return a sample from a comet, volatiles included. However, because of the cost cap under which New Frontiers missions are proposed (roughly, 800 million US dollars up through launch), development of a cryogenic return capsule was infeasible. Instead the approach taken was to allow the water and more volatile sample fraction to be captured into a separate gas reservoir (Squyres et al., 2018). Another cost-effective feature of the mission is that it is designed specifically to land on and sample 67P, which Rosetta and Philae have thoroughly characterized. By selecting this target, the mission's sample acquisition system was designed for the specific surface properties of the smooth terrain on 67P, candidate landing sites were already selected and validated, and the considerable risks associated with going to a poorly known or unknown comet eliminated. The experience of OSIRIS-REx at the near-Earth asteroid Bennu, where unexpectedly hazardous surface properties have delayed sample collection, illustrates how important a consideration this is for small bodies.

Another advantage of 67P is its dynamical history. In 1959 the comet encountered Jupiter which lowered the former's perihelion from 2.74 to 1.28 AU. Dynamical simulations indicate that perihelion values for the 10,000 years before were 2–5 AU (Maquet 2015). Sublimation-driven processes in the inner Solar System may be much less important for 67P than many JFCs, making it a particularly well-suited comet for sampling processes in the protoplanetary disk.

10.3.5 Sample goals and collection

CAESAR would acquire and return to Earth for laboratory analysis a minimum of 80 g of surface material from the nucleus of comet 67P The mission would characterize the surface region sampled, preserve the collected sample in a pristine state, and return evolved volatiles by capturing them in a separate gas reservoir. The sample return would allow laboratory analyses on Earth to determine the nature and abundances of dust particles and gases that may have had their origin in the interstellar medium and molecular clouds. It would trace the origin and ages of rocky condensates from the solar nebula, as well as the history of volatile reservoirs. This would allow quantification of the chemical pathways that transformed simple chemical building blocks into complex and prebiotic molecules. The samples would constrain the evolution of the comet as a geologic body in the Solar System, evaluating the potential role of comets in delivering water and organics to the early Earth. CAESAR would achieve these goals by bringing back a sample that, subjected to analysis with the most sensitive analytic laboratory devices on Earth, would link the large scale properties of the comet with the mineralogy, chemistry, and isotopic studies of volatiles and solids on a particle and grain scale.

Sample collection begins with a camera suite, providing images to allow the final sample site selection, permitting optical navigation, and documenting the site geologic context and the sample at all stages of the collection process. The sample

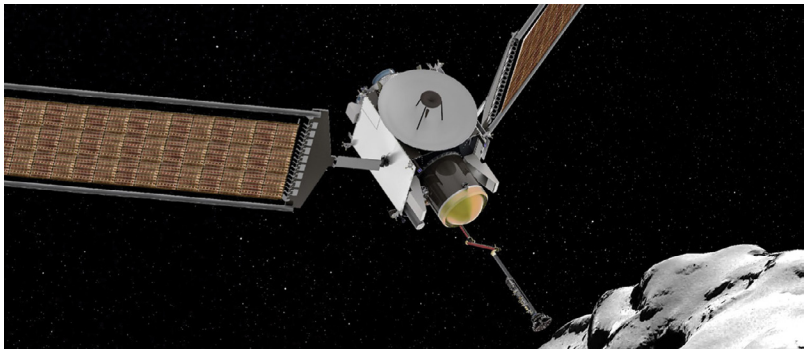

Fig. 10.5 ***CAESAR obtaining a sample***. The TAG arm has extended and the sample acquisition system can be seen at its end, just at the bottom of the frame. *(Credit: https://www.nasa.gov/sites/default/files/thumbnails/image/caesar-concept.png)*.

is collected by the "Sample Acquisition System" (SAS), which was designed for the properties of the smooth terrain on comet 67P as determined by the Rosetta/Philae mission. The SAS contacts the comet surface at the end of a Touch-and-Go (TAG) arm as the spacecraft drifts down to proximity with the nucleus (Fig. 10.5). During the at least 5 s of surface contact, pneumatic jets direct the nucleus sample into a sample container (Squyres et al., 2018). The sample is collected away from comet perihelion.

The system verifies that at least 80 g of sample has been collected. While the sample is still cold, the TAG arm puts the sample container into a containment system (Fig. 10.6) which is located in the capsule that performs the entry, descent and

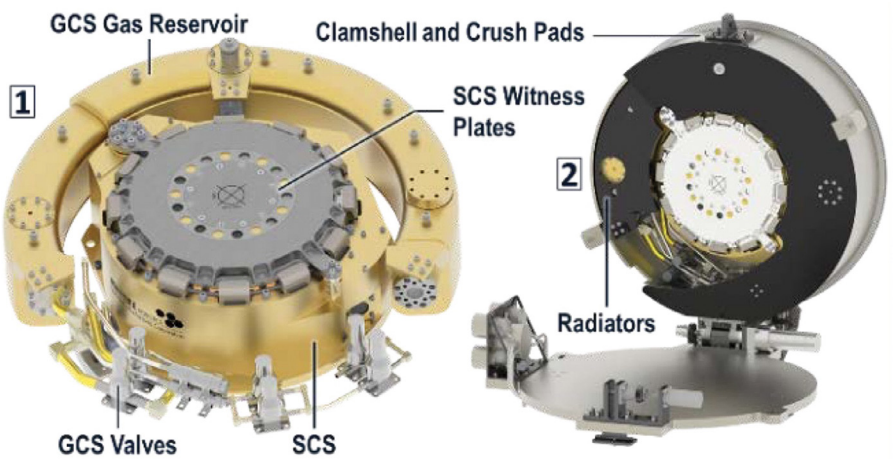

Fig. 10.6 ***Panel 1 shows the sample containment system and gas containment system***. Panel 2 shows them mounted in a clamshell mechanism. *(Credit: Glavin, D. et al., 2018. The CAESAR New Frontiers mission:. 4. Sample acquisition and preservation. 49th Lunar and Planetary Science Conference, abstr. 1337).*

landing on Earth. The sample containment system is designed to immediately seal the sample, preventing more volatile components from escaping into space (Glavin et al., 2018). The requirement to store the sample under conditions that prevent alteration, yet still achieves the science associated with comet volatiles, leads to the need for the gas containment system. The solids in the sample must be kept dry and hence below the melting point of water to avoid reactions between gases and solids, and between liquid water and solids. One of the science goals of the mission is to determine if aqueous alteration has occurred on the comet, and this requires no exposure to liquid water. Furthermore, organic reactions or isotopic reequilibration could occur if liquid water were present.

To avoid these possibilities without the expense and complexity of a cryogenic sample container, the water and more volatile species are separated from the refractory sample by sublimation into a separate reservoir (Glavin et al., 2018). After sealing the sample container, the sample is warmed to temperatures approximating those at 67Ps perihelion, allowing volatiles, including water, to sublimate. The sublimated volatiles are then passively cryopumped into a separate compartment called the gas containment system. Once the outgassing tails off, valves seal the gas containment system. That system is maintained at well below the freezing point of water and key organics, while the highly volatile species such as methane and molecular oxygen remain in the gas phase in the gas containment system. Careful work has been done to determine the optimal temperature for gas transfer that allows for a sufficiently rapid rate while avoiding melting.

The spacecraft systems are designed to maintain the solid and volatile samples well below the water freezing point throughout entry, descent, landing and recovery under the worst case conditions for environment and recovery at the planned Utah Test and Training Range (UTTR), so as to preserve the returned comet solids and volatiles to the mission requirements dictated by the science (Squyres et al., 2018). At Earth approach, the main spacecraft releases the sample return capsule using a spin-separation mechanism. After a 4-hr free coast, the capsule enters the Earth's atmosphere. A two-stage subsonic parachute system keeps shocks due to deployment low, to preserve the integrity of the sample. The heat shield jettison and parachute deployment sequence are designed to ensure that the sample inside remains well below the freezing point of water. Landing speed is 7.5 m/second (Squyres et al. 2018). The capsule is retrieved and put in cold storage; phase change material mounted in the housings allow for recovery delays of hours in case of an off-nominal descent (Fig. 10.7).

The pristine nature of the sample is preserved using stringent cleanliness and documentation protocols from fabrication through all mission phases, and careful mission design during spacecraft operations. Ground and flight witness materials thoroughly document any contamination.

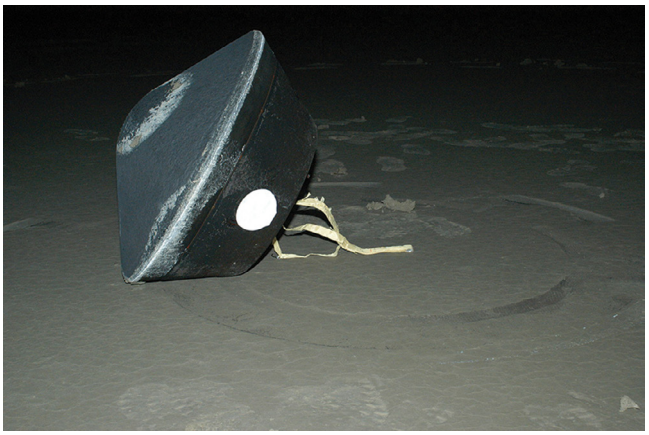

Fig. 10.7 ***The Stardust capsule, found by helicopter search some 45 min after it landed in the UTTR in January 2006.*** Strong winds had blown the parachute several miles downrange. *(Credit: NASA).*

A dedicated CAESAR sample curation facility would be built at NASA Johnson Space Center (JSC), factoring in decades of experience from Apollo and other sample return missions as well as curation by the University of Alberta of Tagish Lake meteorite samples which are kept cold (Nakamura-Messenger et al., 2018). The entire payload is delivered without onsite processing to the JSC curation facility, eliminating possible landing site contamination. Decades of sample analysis of this most pristine sample of the comet nucleus by investigators from around the world would then begin, with over 75 percent of the volatile and non-volatile components reserved for scientists worldwide beyond the CAESAR team.

References

Alexander, C.M.O., et al., 2012. The provenances of asteroids, and their contributions to the volatile inventories of the terrestrial planets. Science 337, 721.

Altwegg, K., Balsiger, H., Fuselier, S., 2019. Cometary chemistry and the origin of icy solar system bodies: the view after Rosetta. Annu. Rev. Astron. Astrophys. 57, 113.

Ballouz, R.L., et al., 2019. Surface refreshing of Martian moon Phobos by orbital eccentricity-driven grain motion. Nat. Geosci. Volume 12, 229.

Bitsch, B., Morbidelli, A., Johansen, A., Lega, E., Lambrechts, M., Crida, A., 2018. Pebble-isolation mass: scaling law and implications for the formation of super-Earths and gas giants. Astron. Astrophys. Volume 612, A30.

Boehnhardt, H., et al., 2017. The Philae lander mission and science overview. Phil. Trans. R. Soc. A 375, 20160248.

Brownlee, D., 2014. The stardust mission: analyzing samples from the edge of the solar system. Ann. Rev. Earth and Planetary Sci. 42, 179.

Craddock, R.A., 2011. Are Phobos and Deimos the result of a giant impact?. Icarus 211, 1150.

Fujita, K., et al., 2019. Assessment of the probability of microbial contamination for sample return from Martian moons I: departure of microbes from Martian surface. Life Sci. Space Res. 23, 73.

Glavin, D.P., et al., 2018. The CAESAR new frontiers mission: 4. Sample acquisition and preservation. Lunar Planet. Sci. Conf. 49, 1337 abstr.

Goesmann, F., et al., 2015. Organic compounds on comet 67P/Churyumov-Gerasimenko revealed by COSAC mass spectrometry. Science 349, 3 aab0689.
Higuchi, A., Ida, S., 2017. Temporary capture of asteroids by an eccentric planet. Astron. J. (N.Y.) 153, 155.
Hyodo, R., Genda, H., Charnoz, S., Rosenblatt, P., 2017. On the impact origin of phobos and deimos. I. Thermodynamic and physical aspects. Astrophys. J. 845 (2), 125.
Hyodo, R., et al., 2019. Transport of impact ejecta from Mars to its moons as a means to reveal Martian history. Sci. Rep. 9, 19833.
Jewitt, D.C., Sheppard, S., Porco, C., 2004. Jupiter's outer satellites and Trojans. In: Bagenal, F., Dowling, T.E., McKinnon, W.B. (Eds.), Jupiter. The Planet, Satellites and Magnetosphere. s1: University Press, Cambridge, pp. 263–280.
Koike, M., et al., 2020. In-situ preservation of nitrogen-bearing organics in Noachian Martian carbonates. Nat. Commun. 11 (1).
Kurosawa, K., et al., 2019. Assessment of the probability of microbial contamination for sample return from Martian moons II: the fate of microbes on Martian moons. Life Sci. Space Res. 23, 85.
Lauretta, D., et al., 2018. The CAESAR new frontiers mission: 2. Sample science. Lunar Planet. Sci. Conf. 49, 1334 abstr.
Lawrence, D.J., et al., 2019. Measuring the elemental composition of phobos: the mars-moon exploration with GAmma rays and NEutrons (MEGANE) investigation for the martian moons eXploration (MMX) mission. Earth and Space Science 6, 2605.
Levison, H.F., et al., 2008. Origin of the structure of the Kuiper belt during a dynamical instability in the orbits of Uranus and Neptune. Icaros 196 (1), 258–273.
Levison, H.F., Shoemaker, E.M., Shoemaker, C.S., 1997. Dynamical evolution of Jupiter's Trojan asteroids. Nature 385, 42–44.
Lowry, S., et al., 2008. Kuiper Belt objects in the planetary region: the Jupiter-family comets. In: Barucci, M.A. (Ed.), The Solar System beyond Neptune. University of Arizona Press, Tucson, pp. 397–409.
Maquet, L., 2015. The recent dynamical history of comet 67P/Churyumov-Gerasimenko. Astron. Astrophys. 579 (A78), 5pp.
Morbidelli, A., Levison, H.F., Tsiganis, K., Gomes, R., 2005. Chaotic capture of Jupiter's Trojan asteroids in the early Solar System. Nature 435, 462.
Morbidelli, A., Lunine, J.I., O'Brien, D.P., Raymond, S.N., &Walsh, K.J., 2012. Building terrestrial planets. Annual Review of Earth and Planetary Science 40, 251.
Mori, O., et al., 2019. Solar power sail mission of OKEANOS. Astrodynamics, 1–16.
Mori, O., et al., 2010. First solar power sail demonstration by IKAROS. Transactions of the Japan Society for Aeronautical and Space Sciences, Aerospace Technology Japan 8.
Mousis, O., et al., 2016. A protosolar nebula origin for the ices agglomerated by comet 67P/Churyumov–Gerasimenko. Astrophys. J. Letters 819 (L33), 5pp.
Mousis, O., Ronnet, T., Lunine, J.I., 2019. Jupiter's formation in the vicinity of the amorphous ice snowline. Astrophys, J 875 (9), 6pp.
Murchie, S.L., et al., 1991. Color heterogeneity of the surface of Phobos: relationships to geologic features and comparison to meteorite analogs. J. Geophys. Res. 96, 5925.
Nakamura-Messenger, K., et al., 2018. The CAESAR New Frontiers Mission: 5. Contamination, recovery, and curation. Lunar Planet. Sci. Conf. 49, 1339 abstr.
Okada, T., et al., 2018. Science exploration and instrumentation of the OKEANOS mission to a Jupiter Trojan asteroid using the solar power sail. Planet. Space Sci. 161, 99.
Sandford, S.E. et al., this book. The Stardust Sample Return mission, Chapter 4.
Sawada, H., et al., 2017. Hayabusa2 sampler: collection of asteroidal surface material. Space Sci. Rev. 208 (1–4), 81–106.
Squyres, S., et al., 2018. The CAESAR new frontiers mission: 1. Overview. Lunar Planet. Sci. Conf. 49, 1332 abstr.
Taylor, G.J., 2013. The bulk composition of Mars. Chemie der Erde / Geochemistry 73, 401.
Toyoda, M., Okumura, D., Ishihara, M., Katakuse, I., 2003. Multi-turn time-of-flight mass spectrometers with electrostatic sectors. J. Mass Spectrom. 38 (11), 1125–1142.
Usui, T., et al., 2020. The Importance of phobos sample return for understanding the mars-moon system. Space Sci. Rev. 216, 49.

Warren, P.H., 2011. Stable-isotopic anomalies and the accretionary assemblage of the Earth and Mars: a subordinate role for carbonaceous chondrites. Earth Planet. Sci. Lett. 311, 93.
Yano, H., Hasegawa, S., Abe, M., Fujiwara, A., 2002. Asteroidal surface sampling by the MUSES-C spacecraft. In: B. Warmbein, ed. Asteroids, Comets, and Meteors (s.l.), 103–106 ESA SP-500.
Yano, H., et al., 2006. Touchdown of the hayabusa spacecraft at the muses sea on itokawa. Science 312 (5778), 1350–1353.

PART II

Facilities

CHAPTER 11

The NASA's Johnson Space Center Astromaterials facilities

Andrea Longobardo[a], **Aurore Hutzler**[b,c]
[a]INAF-IAPS, Rome, Italy
[b]Lunar and Planetary Institute, USRA, Houston, TX, USA
[c]Astromaterials Research and Exploration Sciences, NASA JSC, Houston, TX, USA

Chapter Outlines

11.1 Introduction

In 1961 the US plan to start a human space flight program led to the creation of a NASA center which would have guided it: the NASA's Manned Spaceflight Center, in 1973 renamed the Lyndon B. Johnson Space Center (JSC), was founded in Houston, Texas. The center was the main lead for the Apollo Program (1961–1972), with astronaut training and flight capabilities, as well as the famous Mission Control Center (commonly still referred to as "Houston"). The JSC was also tasked with curating and analyzing the samples returned from the Moon by the Apollo astronauts. Building on this expertise, the Johnson Space Center stores all of the NASA-held astromaterials collections.

At the time of writing (May 2020), NASA has seven extraterrestrial sample collections, cared for by the Astromaterials Acquisition and Curation Office, part of the JSCs Astromaterials Research and Exploration Science Division (ARES). These collections include: the Apollo Lunar collection, the Antarctic Meteorite collection, the Cosmic

Sample Return Missions
DOI: 10.1016/C2018-0-03374-5

Dust collection, the Microparticle Impact collection, the Genesis collection, the Stardust collection and a subset of the JAXAs Hayabusa collection. Four of these are directly returned from space: Apollo samples from the Moon, Genesis solar wind atoms, Stardust particles from the coma of the Wild-2 comet, and Hayabusa samples from the Itokawa asteroid. Antarctic Meteorites are extraterrestrial objects collected on Earth. The Cosmic Dust collection consists of particles collected in the stratosphere, and the Microparticle Impact collection is a repository for spacecraft components that have been impacted by micro-particles in space. In addition, the Acquisition and Curation Office is curating contamination knowledge samples for the upcoming Mars 2020 mission.

Two emerging astromaterials collections are going to be added to that list in the next few years: Hayabusa2 (led by JAXA) in 2020 and OSIRIS-REx in 2023.

In this chapter, we describe curation at the Johnson Space Center (Section 2), the current (Section 3) and emerging (Section 4) extraterrestrial collections returned directly from space and their corresponding facilities. Finally, we explore how the Astromaterials Acquisition and Curation Office is getting ready for future curation needs (Section 5).

11.2 Principles of astromaterials curation

The primary goal of curation is to protect and preserve the samples while maximizing the science return. To achieve that goal, curation encompasses activities from the inception of the sample return mission, to the landing of the sample return capsule, to long-term storage and sample allocation.

Overall principles of curation of returned samples are given in other chapters of the book (e.g., Brunetto et al. and Meneghin et al., this book). In this section, we describe how astromaterials are curated at the NASA's JSC followed by specifications for each collection in Section 3. For further details, we refer the reader to McCubbin et al. (2019).

Curation infrastructure. Laboratory environmental parameters (differential pressure, airflow, temperature and relative humidity) are monitored to ensure they stay within defined ranges (McCubbin et al., 2019).

In order to minimize contamination, all laboratories are kept at a slightly higher pressure than the outside to prevent the entrance of external air and particles. Differential pressure should be maintained between 5 Pa (between two cleanrooms) and 20 Pa (between a cleanroom and an unclassified room) (Sakraida, 2008; Whyte, 2001). If differential pressure drops below 5 Pa, external air might enter the cleanroom. If differential pressure exceeds 20 Pa, it could produce a turbulent airflow when doors or airlocks open, potentially compromising laboratory cleanliness.

All input air goes through HEPA filters to ensure particulate cleanliness. Following ISO standard 14,644–1, curation laboratories at JSC ranges from ISO Class 4 (the cleanest)

to ISO Class 7. The airborne particle abundance for particles ranging from 0.3 to 10 μm is monitored weekly using handheld particle counters.

Temperature stays between 15 °C and 24 °C, relative humidity between 35 percent and 65 percent.

Laboratories and equipment are built from a known set of low-shedding and easily cleanable materials from which contamination can easily be traced.

Gowning protocols are in place to limit human contamination and range from smocks and overshoes to full body gowning for ISO Class 4–5 cleanrooms. Cleanroom floors and surfaces are cleaned daily with isopropyl alcohol (IPA) or other accepted cleaning agents, depending on the laboratory.

More in-depth contamination monitoring analyses of the cleanrooms are conducted periodically: molecular organic and inorganic contamination on witness plates and air samples (Hutzler et al., 2019) and biological loads on surfaces and in the air (Regberg, 2019). These studies assess the impact of specific materials or activities on the cleanrooms and are being developed to answer the upcoming challenges of organic-rich collections.

Curation protocols. To limit terrestrial contamination, pristine samples are stored and handled in cabinets or gloveboxes made from a limited set of materials (stainless steel, aluminium, glass) and under constant flow of a high-purity inert gas (nitrogen, or more rarely argon or helium). The high-purity gaseous nitrogen (GN2) comes from a high-purity liquid nitrogen (LN2) tank and is filtered for particulates before reaching the laboratories. It is monitored continuously for oxygen and moisture and measured periodically for particles and organic molecules.

In order to avoid cross-contamination, each collection has its own tools and containers that are cleaned in the Pre-Clean and Final Clean laboratories during separate cleaning sessions, except for Genesis which has a dedicated precision cleaning laboratory. If needed, a first cleaning procedure is performed.

For small, everyday tools, the cleaning protocol uses successive baths with detergent and surfactant followed by ultra-pure water (UPW). The cleanliness is checked to certify the part for use before the final rinse with UPW, drying under GN2 and triple-bagging (in nylon or Teflon bags depending on the collection). NASA uses the IEST-STD-CC1246E (NASA, 2013) standard for particles and non-volatile residue. Ultra-pure water is monitored continuously to ensure a resistivity of 18.18 MΩ−cm and total organic carbon under 3 ppb. Once a year, a full analysis of inorganic elements and bacterial load is conducted (McCubbin et al., 2019).

For large pieces of equipment that are cleaned less often, equipment is disassembled and cleaned with a larger variety of degreasing agents adapted to the material. The required cleanliness level depends on the collection. For example, Genesis protocols require Level 25 cleanliness, meaning no particles > 50 μm/0.1 m^2. Laboratories hosting organic and organic-rich samples for emerging and future collections (e.g., OSIRIS-REx

and Hayabusa2 collections) may require a more stringent, organic cleaning level. Techniques that could be used to accomplish this are UV-ozone, plasma, supercritical fluid and CO_2 snow cleaning (McCubbin et al., 2019 and references therein).

Basic and preliminary examination of samples. After recovery of the samples, and all through during the collection lifetime, the curation team catalogues the samples to allow scientists to request a relevant part of the collection. Basic and preliminary examination is done using mostly non-destructive techniques (photography, optical and electron microscopes, FTIR). Recently, an X-ray Computed Tomography (XCT) Laboratory has been acquired, allowing for 3D X-ray visualization and characterization on select Apollo samples (Eckely et al., 2020).

Handling and analysis of samples smaller than 100 μm. The Acquisition and Curation Office is actively using and developing small particle handling techniques. This allows the curation team to make the most out of a collection (e.g. the Apollo lunar regolith) or to work with collections exclusively composed of small particles (e.g. Hayabusa). The handling of small particles is different from macro samples due to the influence of electrostatic and intermolecular forces. Mitigating mechanisms, both environmental and through protocols, are needed to minimize the loss of particles, which could occur during transfer due to electrostatic binding to tools. Stainless steel tweezers and glass/quartz needles are commonly used, often in combination with remote or motorized manipulators. Stereo microscopes with 500x magnification and microscope stages allowing three-directional movement are used to image samples. However, optical imaging usually does not provide sufficient characterization for subsequent science. Imaging techniques involving scanning electron microscopy (SEM) are then needed, but these pose a challenge as they can lead to loss of particle due to electrostatic charging from electron beam bombardment.

Allocation. Collections are available to scientists worldwide through a proposal-based allocation process. The Curation and Analysis Planning Team for Extraterrestrial Materials (CAPTEM), an independent scientific committee, assesses each research project and issues recommendations to NASA. For approved proposals, the requested samples are then processed, packaged, and shipped. Material remains property of NASA and must be returned to JSC unless destroyed in the analytical process.

Remote access. In order to minimize movement of samples and scientists, a procedure for remote processing of returned samples was developed in 2006 for the Preliminary Examination of Stardust and in 2014 for an Apollo 16 glovebox (Calaway, 2015). In the case of Apollo 16 samples, a camera is mounted on the outside of the glovebox hosting the samples, allowing the researcher to follow the work of a processor.

Remote storage. To avoid a total loss due to natural or other disasters, a portion of each collection is kept in a secure location at NASA's White Sands Test Facility in New Mexico. Samples are stored under dry nitrogen in stainless steel cabinets and are not processed or studied.

11.3 Current astromaterials collections and laboratories

11.3.1 Lunar Curatorial Facility

Apollo (1961–1972) was the first program to return extraterrestrial materials from space. Between 1969 and 1972, six Apollo missions successfully completed a human landing on the Moon and brought back to the Earth 382 kg of lunar materials in 2200 specimens and 110 thousands samples, forming the widest collection of returned samples. An overview on the Apollo Program and the results from analysis of lunar samples in given in the Apollo chapter (Jerde et al., this book).

At the time, it was believed there could be life on the Moon and that it could be a potential hazard to terrestrial organisms. For that reason, a designated facility, the Lunar Receiving Laboratory (LRL, Building 37) was built in 1967 at the Manned Spaceflight Center. The goal of the facility was to quarantine the astronauts and the samples, while studying them. The LRL initially had a network of connected vacuum chambers held at a pressure of 10^{-4} Pa (Calaway et al., 2014) to store and analyze the samples. The curation environment had been chosen to be close to the lunar environment and vacuum was a good way to keep potential biohazards under containment. However, working under vacuum was challenging and frequent leaks lead to sample contamination.

The theory of lunar organisms was abandoned after Apollo 14 (the third Apollo mission to return samples in 1971) and quarantine deemed unnecessary. Following this, and due to the large volume of expected samples, the vacuum chambers were replaced by a series of positive pressure nitrogen gloveboxes (e.g., Simoneit et al., 1993). The collection was then moved to a retrofitted cleanroom in Building 31 between 1973 and 1979, to finally be placed in the dedicated, designed to withstand a Category 4 hurricane, high-security Lunar Curatorial Facility in Building 31-N (Fig. 11.1). The Lunar Curatorial Facility is currently the largest suite of curation cleanrooms and laboratories at JSC, including 30 nitrogen cabinets (10 for processing and 20 for storage).

Fig. 11.1 Building 31 picture. *(Credits: A. Hutzler).*

Contamination was a concern of the curatorial and scientific team early on. Materials that would be in contact with the Moon rocks were carefully selected and cleaning protocols were developed to minimize organic and inorganic contamination. All materials in the LRL and Lunar Curatorial Facility (including walls, floors, paints, etc.) were selected to minimize contamination levels, favoring low outgassing materials such as stainless steel and Teflon. Contamination monitored through the use of witness plates and analogue samples provided information about the parts of the samples that may have been contaminated. The most recent estimate concerning the levels of contamination is on the order of μg/g (McCubbin et al., 2019 and references therein). The major sources of organic contamination identified in Apollo samples include the box and hand tools used on the Moon surface, exhaust products, and, after the return to Earth, exposure to vacuum or nitrogen chambers and sample processing tools (Simoneit et al., 1993). Some materials initially used in curation, like Xylan (Wright, 1992), were later found out to be a source of contamination and subsequently eliminated.

The Lunar Curatorial Facility's design has been optimized for staff and sample workflows and for cleanrooms operations, with increased cleanliness in each subsequent room. The Apollo storage and processing facilities are split into two sections, a pristine section (ISO Class 6) and a returned section (ISO Class 7). The sections correspond to two categories of samples: the pristine section includes samples that have never been exposed to the terrestrial atmosphere and the returned section contains samples that were allocated to other laboratories around the world then sent back to JSC.

When entering the facility, staff and visitors must remove any jewelry and unnecessary items. Items that can be kept (like cameras, cellphones and working tools) must be wiped down to reduce particulate contamination and left in a pass-through in the Observation Room. The Observation Room has windows overlooking the Pristine Sample Laboratory and Change Rooms and is used to review documentation and to monitor oxygen and water content inside the laboratory/vault cabinets and rooms.

Staff and visitors must go through the two Change Rooms. In these rooms, smocks, hats and two pairs of overshoes must be worn. Gowning protocols are more stringent, including a special nylon cleanroom suit, if going to the pristine part of the facility.

A laminar airflow air shower is then used to access the pristine part of the facility. This part is composed of the Sample Laboratory for sample handling, the Sample Vault for sample storage and a corridor allowing samples to be transferred between vault and laboratory.

The Pristine Sample Laboratory is an ISO Class 6, 100 m^2 room where samples are processed and prepared for allocation in stainless steel gloveboxes (Fig. 11.2). Each glovebox stores lunar samples from a specific Apollo mission to avoid cross-contamination. The only exception is the display cabinet that contains two Apollo 15 samples (a breccia and a basalt), two Apollo 16 samples (from lunar highlands) and one Apollo 17 sample (a basalt): this cabinet can be viewed from the Lunar Viewing Area, an area

Fig. 11.2 ***Apollo samples are handled in gloveboxes under high-purity gaseous nitrogen in the Pristine Sample Laboratory.*** Each stainless steel glovebox is dedicated to a specific Apollo mission to avoid cross-contamination. *(Credits: A. Hutzler).*

external to the facility facing the laboratory and thought for visitors. Each cabinet has its own tools and containers with which to work on the samples. Instruments, like scales, that are physically inside of the glovebox have been retrofitted to remove all unacceptable materials, such as copper. Lighting, binocular microscopes and some cameras are placed outside the gloveboxes to observe samples through a window. Three layers of gloves are required to handle the samples: two Neoprene layers and a Teflon layer that is in contact with the samples.

Soil cores are contained in tubes and include material sampled on the Moon surface down to a depth of 3 m. Fifty-four cores, taken from 24 locations on the moon, are stored in the Pristine Sample Vault, four of which have still to be opened. The standard procedure for analyzing these soil cores is the following: X-ray imaging for porosity and clast distribution, transfer to a receptacle where samples are imaged and separated in slices, and storage of dissected samples in separate containers. The entire process lasts 4–6 months. A small part of the samples is distributed for analysis, while residual material in the core is embedded in epoxy and stored.

For samples that cannot be divided within a glovebox, they are taken to the saw room attached to the Sample Laboratory. This is a fundamental operation to study radiation effects at different depths or to analyze heterogeneous rocks such as breccias. Rocks are clamped and cut by a stainless steel bandsaw equipped with diamonds on the cutting edge. The operation is performed slowly and under dry GN2, in order to prevent overheating and moisture contamination. After the sawing procedure, all generated dust and fragments are collected and, as with all sample processing, the total mass of the sample

must remain unchanged. Materials that have been in contact with the Apollo samples are discarded in a specific bin that is subsequently inspected carefully for lunar particles.

All the operations in the Pristine Sample Laboratory must be recorded and documented (e.g., with photographs).

The Pristine Sample Vault is an ISO Class 6, 110 m^2 room where the samples are stored in GN2 cabinets (specific to each Apollo mission), packages in stainless steel containers or in Teflon bags. Samples are contained in sealed stainless steel trays. In addition to the building being hurricane-proof, the vault is equipped with a waterproof door that can be bolted to the entrance door.

There is a strict protocol for transporting a sample from the Vault, through the pristine corridor, to the Sample Laboratory. Each glovebox in the Sample Laboratory has a pass-through chamber with two interlocked doors, one facing the corridor (outer door) and one the cabinet (inner door). The procedure to put samples inside the cabinet is the following: open the outer door, remove the sample container's outermost bag, place the still-wrapped samples in the airlock (in this operation, double gloves must be worn), seal the outer door, purge for five minutes with dry nitrogen, open the inner door, and transfer the sample. This is usually done by two processors, one in the corridor and the other one in the sample laboratory. To bring a sample back to the vault, the process is reversed. The same protocol is used for tools and instruments needed inside of a glovebox.

The second half of the facility is dedicated to returned samples. One goes through the change room to access the Experiment Laboratory and then the Return Sample Vault.

The Experiment Laboratory is dedicated to tests and measurements from visiting scientists, including microscopy, spectroscopy, and heat conduction across unopened cores. Among the available instruments are an emission spectrograph, a gas mass spectrometer, an optical microscope and a radiation counting bunker.

The Return Sample Vault (75 m^2) is where the samples are stored in stainless steel cabinets under terrestrial atmosphere. The samples are accompanied by the list of analyses performed on them and packaged in a two-layer container. The Return Sample Vault's cabinets are composed of two stacks of drawers, in turn including plastic boxes containing the samples. Returned samples are not required to be protected from terrestrial atmosphere, because they have been already exposed to terrestrial environment during their permanence out of JSC. Currently, 48 000 samples are stored in the Return Sample Vault. The Vault is also used as a safe storage location for the other astromaterials collections in case a hurricane threatens the center.

The JSC lunar sample catalogue, together with related documentation, is available at https://curator.jsc.nasa.gov/lunar/index.cfm. All samples have been catalogued using the criteria described in Section 7 of the Apollo chapter (Jerde et al., this book). More recently, the Acquisition and Curation Office collaborated with an artist on a project to showcase Apollo samples in 3D utilizing high-resolution precision photography, micro

computed X-ray tomography and structure-from-motion photogrammetry (SFM) (https://ares.jsc.nasa.gov/projects/astromaterials-3d/). Some lunar samples are on loan, or have been donated as diplomatic samples, and are stored and displayed in museums and institutions all over the world, i.e., Europe (Austria, Denmark, France, Germany, Netherlands, Switzerland and United Kingdom), Asia (Japan and Philippines), America (U.S.A. and Mexico). For details, see Jerde et al. (this book) and https://curator.jsc.nasa.gov/lunar/displays/lunarsampledisplays.pdf.

11.3.2 Genesis Curation Laboratory

NASA's Genesis mission (2001–2004) studied solar chemistry by collecting more than ten thousands Solar Wind (SW) fragments from the Earth-Sun L1 Lagrangian point and returning them to Earth. The Genesis spacecraft was equipped with four collectors, able to collect three types of sample: low-speed or interstream wind, high-speed or coronal-hole wind, and coronal mass ejections (Neugebauer, 1991). Some of these samples were contaminated due to the crash landing of the return capsule at Utah Test and Training Range (UTTR) (Wiens et al., this book).

The Genesis Curation Laboratory was built in 1999 by retrofitting part of the Lunar Laboratory in order to assemble the Genesis container in a clean environment before the launch. To date, it consists of two adjacent ISO Class 4 clean rooms, both characterized by a perforated nickel-coated floor which guarantees a laminar flow from ceiling to floor. In both environments cleanroom suits (including hat, overshoes and gloves) are mandatory, jewellery is prohibited and a strict hygiene protocol must be followed before entering the laboratory.

The first clean room is dedicated to the cleaning of equipment and samples, such as the removal of surface particles from SW samples. To accomplish this, a megasonic bath of UPW is generated at 30 liters per minute and its temperature is controlled to avoid material corrosion.

The second clean room is used for experiments and samples' storage. The available instrumentation includes a FTIR spectrometer, a stereo microscope, an automated microscope (capable of resolving particles down to 300 nm) and a spectrometric ellipsometer (to evaluate contamination). Several reference materials are used to evaluate contamination of Genesis samples: flight-like collector substances (5000 pieces available), 200 science canister duplicate components, 100 assembly room material coupons, 8 UTTR soil samples from 5 sites, return capsule components (included sample canister), and tools and containers used for recovery.

SW samples are stored inside stainless steel cabinets filled with pure nitrogen. The JSC catalogue of the Genesis samples, with related information (e.g., size and SW regime), is available on https://curator.jsc.nasa.gov/gencatalog/index.cfm.

The Genesis Curation Laboratory is completed by a corridor (ISO Class 6) to transfer the samples and a change room (ISO Class 7). The corridor includes a cabinet

on wheel to remove the samples in case of an emergency and an emergency door facing the environment where HEPA filters are activated in case of transfer. Emergency procedure rehearsals occur once a year (Hutzler et al., 2016).

11.3.3 Stardust Laboratory

NASA's Stardust mission (1999–2006) collected and returned dust particles from the comet 81P/Wild2 as well as from the interstellar/interplanetary medium (Sandford et al., this book, and references therein). Thousands of cometary particles (hundreds of μm in size) and about 100 interstellar/interplanetary micron-sized particles were returned, for a total mass of about 1 mg. Most of the particles were collected by trapping them into an aerogel substance (Tsou et al., 2003), consisting of microporous silicon material cells embedded in trays: 126 aerogel tiles (4 × 2 × 3 cm) are included in the Stardust collection. Cometary and interstellar/interplanetary dust particles are also embedded in 120 aluminium foils (1.7 × 35 and 1.7 ×15 mm), as well as in surfaces of sample trays and sample return capsule components exposed to the outer space (Allen, 2006).

After landing at UTTR in 2006, the samples were immediately transferred to the JSC Stardust Laboratory. The Stardust Laboratory is a 65 m^2 area retrofitted in Building 31 and composed of an anteroom with a window observing the curation room, a changing room, and an ISO Class 5 curation and storage room.

Preliminary operations (return capsule opening, extraction of sample canister and aerogel tiles, initial inspection and sample processing) were performed in the curation room, with witness plates for contamination monitoring (Fig. 11.3).

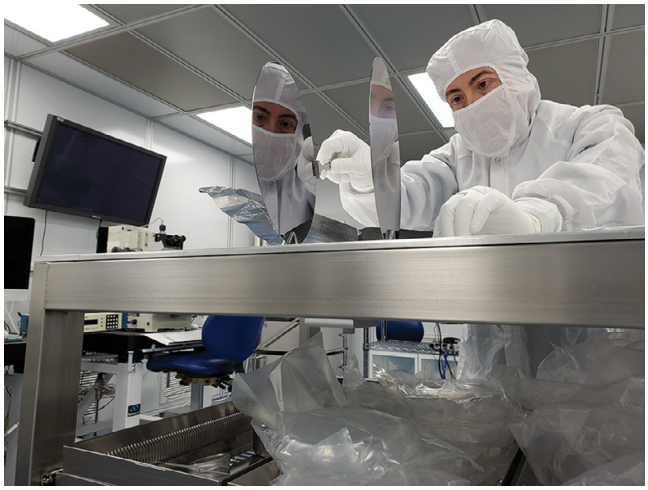

Fig. 11.3 ***Silicon wafers for airborne organic contamination are being exposed by Dr Hutzler in the Stardust curation laboratory.*** The operator is wearing a full cleanroom gown as well as double nitrile gloves and using baked-out tools to limit contamination on the wafers. *(Credits: J.A. Lewis).*

Particle extraction and photography are the only processes performed in the Stardust Laboratory. Several techniques are used for aerogel and samples extraction, such as needle, microtoming and focused ion beam etching.

Four levels of photographic documentation exist, on the basis of resolution and purpose (Nakamura-Messenger et al., 2007): Level 1 is a low-resolution record of aerogel cells in pristine conditions as obtained by means of a camera; Level 2 consists of high-resolution mosaics of areogel cells and aluminium foils obtained by a Primary Scanning System; Level 3 is the 3D high-resolution photodocumentation of cells after extraction from the trays; Level 4 documents the individual tracks extracted from hosting cells and gives the highest details of collected particles.

Samples and aerogel collectors are stored in stainless steel GN2 cabinets. The Stardust catalog is available on http://curator.jsc.nasa.gov/stardust/.

The Stardust collection includes also reference materials for contamination: spacecraft control materials (sapphire disk, aluminium disk, aerogel block), aerogel witness coupons (i.e., aerogel exposed to space but not to comet coma), and unflown aerogel tiles (Allen, 2006). The capsule components exposed to space contamination and micro-impacts are studies and stored in ISO Class 5 facilities different than the Stardust Laboratory, i.e., the Space-Exposed Hardware Laboratory and the Microparticle Impact Curation (MIC) Laboratory.

The analyses of Stardust samples, contamination reference materials and witness plates (both those located inside the sample return capsule and those used for monitoring preliminary operations in the Stardust Laboratory) allowed the identification of the main contamination sources of samples, i.e., materials in the silica aerogel, spacecraft outgassing and return capsule recovery procedure.

The identification of organic material in aerogel different than the organics of cometary origin was of crucial importance, because it avoided misinterpretation of scientific results (e.g., Sandford et al., 2010). While the organic molecules preexisting in the aerogel before the mission launch did not produce tracks and hence are easily recognizable (McCubbin et al., 2019), other terrestrial organic (and inorganic) materials, e.g., propellents, materials outgassed from spacecraft components, and secondary materials from impacts on spacecraft components, impacted aerogel tiles. These contaminants were recognized by X-ray absorption near-edge spectra (XANES) analysis and by track orientations: cometary dust particles impacted perpendicuarly to forward direction, while oblique tracks can be due to interplanetary dust particles or to secondary impacts (Westphal et al., 2008).

Concerning post-flight contamination, landing site soil samples revealed that landing was not a critical contamination issue, whereas the polypropylene bag used to package the return capsule became a source of contamination (e.g., Dirri et al., this book, and references therein).

11.3.4 NASA Hayabusa Laboratory

The JAXA/Hayabusa mission (2003–2010) sampled the S-type Itokawa asteroid in 2005, returning to Earth 1500 micron-sized (up to 100 μm) samples, for a total mass of almost 1 mg. Particles were removed from the collector by swapping with a Teflon spatula or by tapping the collector.

10 percent of the Hayabusa collection has been delivered to NASA JSC and includes both entire particles and slices, Sample containers used for the sample transfer from JAXA to NASA have an external layer consisting of stainless steel vacuum flanges and an internal case made of synthetic quartz glass plates.

The NASA's Hayabusa samples are currently stored under dry nitrogen in a stainless steel and glass cabinet in the NASA Hayabusa Cleanroom (ISO Class 5, 12 m^2). The Hayabusa curation room, derived from an existing laboratory and finished in 2011 (De Gregorio et al., 2012), is accessed through an anteroom and a changing room.

The list of Hayabusa samples available at JSC is published on https://curator.jsc.nasa.gov/hayabusa/available.cfm.

11.3.5 Other curation laboratories

In addition to samples returned from space missions, meteorites and cosmic dust are collected and studied.

The collection of Antarctic meteorites is among the largest in the world. Each year, an expedition returns hundreds of specimens from Antarctica. Meteorites are brought back frozen to JSC to the Meteorite Processing Lab, a suite of ISO Class 6 to ISO Class 7 cleanrooms. They are then thawed in a controlled, dry GN2 environment. Rare types of meteorites (typically martian and lunar) are characterized, processed and stored in dedicated GN2 cabinet and wrapped in Teflon bags. More common meteorites are initially processed on a flowbench followed by basic characterization. Depending on the size and hardness of the sample, the meteorite is chipped or cut to produce a polished section for classification.

Cosmic dust is collected in the stratosphere using high altitude airplanes. Collection campaigns typically last one month and could be performed during meteor showers in order to collect cometary particles. For example, the Perseid and Draconid meteoric showers are likely made of dust released from the Swift-Tuttle and Giacobini-Zinner comets, respectively. However, terrestrial dust has been also collected during volcanic eruptions (Rietmeijer, 1997).

Cosmic dust is processed and stored in a 7 × 4 m ISO Class 5 cleanroom. Silicone oil is generally used to coat dust (due to its chemical inertia) and to transfer particles during laboratory processes. Epoxy resins could be used to bond particles to containers.

11.4 Emerging collections

In the next few years, the Acquisition and Curation Office is going to receive organic-rich samples from the asteroids Ryugu (Hayabusa2 mission) and Bennu (OSIRIS-REx mission), prompting the need for different protocols and new facilities. Plastic and outgassing materials should be strictly limited, Teflon is used less, whereas glass and metals (stainless steel and aluminium) are preferred. Protocols for reducing organics on surface and in the air are being developed, from precision cleaning protocols to baking-out tools and containers at 500 °C (e.g., Grosjean and Logan, 2007; Sherman et al., 2007).

The curation facilities for these two collections are being built in Building 31 at the time of writing (Hutzler et al., 2019). Construction should be completed in September 2020.

11.4.1 OSIRIS-REx collection

NASA's OSIRIS-REx mission was launched in 2016 to flyby and sample the Bennu near-Earth asteroid. About sixty grams of samples are expected to be returned in 2023. The landing will occurr at UTTR, where preliminary operations, including assessment of spacecraft's contamination level, will take place in a temporary clean room. The samples will be then transported to JSC, which will conduct initial characterization and cataloguing of the samples.

The curation laboratory is under construction and will be ready before the OSIRIS-REx return.

A comprehensive contamination control plan, including studies of materials, hydrazine and witness plates, has been already performed (McCubbin et al., 2019), taking into account the NASA requirements (non-volatile residues < 500 ng/cm^2, amino acids < 180 ng/cm^2 for materials in contact with the samples [Dworkin et al., 2018], Total Mass Loss <1 percent, Collected Volatile Condesned Materials < 0.1 percent). The contamination studies performed at JSC resulted in:

- widening of the list of prohibited materials (for both spacecraft components and laboratories) and the identification of appropriate substitutes;
- an estimation of the hydrazine deposition on collectors and samples;
- the archiving of possible contaminating materials used for spacecraft/instruments assembling and for packaging, as well as of witness plates used for monitoring cleanrooms and flight components. UTTR soil samples will be added to this archive.

11.4.2 Hayabusa2 collection

JAXA'a Hayabusa2 mission was launched in 2014 to rendezvous and sample the C-type Ryugu near-Earth asteroid. JAXA will deliver 10 percent of the total sample mass to JSC within one year. A new cleanroom is under construction for receiving these

samples. The cleanroom is being constructed with the same criteria applied to the cleanroom that will host OSIRIS-REx samples.

11.5 Conclusions and future perspectives

The JSCs Astromaterials Acquisition and Curation Office has overseen the curation of NASA-held samples since 1969. Its expertise in handling, processing and storing a variety of extraterrestrial samples has grown over the years while refining existing protocols and innovating for future challenges.

New cleanrooms to develop advanced curation and advanced cleaning protocols are being built in Building 31 and facilities and cleanrooms are being designed and planned for the MMX (Martian Moons eXploration) mission (led by JAXA) and cold (−20 °C) or cryogenic (−150 °C) samples returned from the Moon (Artemis program) or from comets. The difficulty for humans to work in contact of cold, cryogenic or biohazardous is prompting the development of remote manipulation techniques. A Mars Sample Return campaign, in collaboration with ESA, is more advanced than ever and will need to keep the samples pristine but also contained in case of biohazards.

Acknowledgements

Jonathan A. Lewis (NASA Johnson Space Center) is thanked for manuscript revision and proofreading.

References

Allen, C., 2006. Stardust sample: investigator's guidebook Technical Report, NASA/STI Accession Number: 20060049068.

Brunetto, R. et al., this book. Techniques and instruments to analyze, characterize and study returned samples, Chapter 16.

Calaway, M.J., 2015. Lunar processing cabinet 2.0: retrofitting gloveboxes into the 21st century. 46th LPSC, 1492.

Calaway, M.J. et al., 2014. Organic Contamination Baseline Study in NASA Johnson Space Center Astromaterials Curation Laboratories, NASA TP-2014-217393, Lyndon B. Johnson Space Center, Houston (2014), p. 108.

De Gregorio, B.T., et al., 2012. Developing the new hayabusa curation facility at johnson space center. 43rd LPSC, 2020.

Dirri, F.et al., this book. Recovery and transport of samples, Chapter 15.

Dworkin, J.P., et al., 2018. OSIRIS-REx contamination control strategy and implementation. Space Sci. Rev. 214, 53.

Eckley, S.A., et al., 2020. Applicability and utility of the astromaterials X-Ray computed tomography laboratory at johnson space center. 51th LPSC, 2182.

Grosjean, E., Logan, G.A., 2007. Incorporation of organic contaminants into geochemical samples and an assessment of potential sources: examples from Geoscience Australia marine survey S282. Org. Geochem. 38, 853–869.

Hutzler, A., et al., 2016. Preliminary conceptual design. Deliverable 3.1 of the Horizon2020 EURO-CARES Project.

Hutzler, A., et al., 2019. Contamination control and knowledge during construction of new curation facilities at NASA Johnson Space Center. 50th LPSC, 2900.
Jerde, E.A., this book. The Apollo Program, Chapter 2.
McCubbin, F.M., et al., 2019. Advanced curation of astromaterials for planetary science. Space Sci. Rev. 215, 48.
Meneghin, A. et al., this book. Preservation of samples, Chapter 17.
NASA, 2013. IEST-STD-CC1246E: product cleanliness levels – applications, requiremenrs and determination.
Nakamura-Messenger, K., et al., 2007. Stardust curation at Johnson space center: photo documentation and sample processing at submicron dust samples from comet wild2 for meteoritics science community. 38th LPSC, 2191.
Regberg, A.B., et al., 2019. Microbial monitoring of astromaterials curation labs reveals inter-lab diversity. Conference Paper, AbSciCon, 2019.
Sakraida, V.E., 2008. Cleanroom Design in 10 Easy Steps. Engineered Systems Magazine, Troy, MI.
Sandford, S.A., et al., 2010. Assessment and control of organic and other contaminants associated with the Stardust sample return from comet 81P/Wild 2. Meteoritics & Planetary Sciences 45, 406–433.
Sandford, S.A. et al., this book. The Stardust Sample Return Mission, Chapter 4.
Sherman, L.S., et al., 2007. Improved methods for isolating and validating indigenous biomarkers in Precambrian rocks. Org. Geochem. 38, 1987–2000.
Simoneit, D.A., et al., 1993. Organic contamination monitoring and control in the lunar receiving laboratory, analytical methods developed for application to lunar samples analyses, american society for testing and materials. ASTM STP 539, 16–34.
Tsou, P., et al., 2003. Wild 2 and interstellar sample collection and Earth return. J. Geophysical Research: Planets 108, 21.
Westphal, A.J., et al., 2008. Discovery of non-random spatial distribution of impacts in the Stardust cometary collector. Meteoritics & Planetary Sci. 43, 415–429.
Whyte, W., 2001. Cleanroom design, 2nd Edition. Wiley, New York.
Wiens, R.C., this book. The Genesis Solar-Wind mission: first deep-space robotic mission to return to Earth, Chapter 5.
Wright, I.P., 1992. Xylan: a potential contaminant for lunar samples and antarctic meteorites, Proceedings of Lunar and Planetary Science, 22, 449–458.

CHAPTER 12

The JAXA Planetary Material Sample Curation Facility

Masanao Abe
Japan Aerospace Exploration Agency, Institute of Space and Astronautical Science, Astromaterials Science Research Group

Chapter Outlines

12.1 Introduction

JAXA conducted and is conducting sample return missions, such as Hayabusa and Hayabusa2, to bring back samples of extraterrestrial materials from asteroids (Itokawa and Ryugu, respectively). In addition, Japanese scientists will also receive part of the samples returned by the NASAs OSIRIS-REx missions from the Bennu asteroid. The returned materials are scientific valuable samples that can provide scientific knowledge about the origin and evolution of the Solar System (Tachibana et al., 2014).

Prior to sample return, meteorites were the only extraterrestrial material samples considered by planetary scientists to unravel the history of the Solar System. However, meteorites are affected by heating when they cross the Earth's atmosphere, and, after dropped on the ground, they are contaminated by terrestrial atmosphere, water and materials, changing their properties. On the other hand, sample return missions allow to store the sample in a sealed container and protect them from terrestrial contamination and from heat and shock during re-entry to the Earth.

Returned samples are very valuable scientifically, and it is extremely important to handle them without compromising their scientific characteristics.

Sample Return Missions
DOI: 10.1016/C2018-0-03374-5

12.2 Scientific requirements of the JAXA's Curation Center

Due to the sample return high scientific value, the curation center that accepts the returned samples has the following scientific requirements: 1) Do not expose the sample to the Earth's atmosphere; 2) Do not lose the sample; 3) Do not destroy the sample.

The first one is a requirement that the sample does not react with the Earth's material to be altered. If the terrestrial compounds are mixed into the sample, the reliability of the sample's analysis results is not ensured.

If returned samples are lost (second requirement), it is impossible to go back to the explored target body and bring back the samples again.

The third requirement is not strict but refers only to preliminary analyses on returned samples. The curation team performs the preliminary sample characterization at the JAXA curation center and provides it to the project team that carries out the sample return mission. The destructive analysis of the sample should not be performed in this stage because morphological observation is needed first.

12.3 Role of the Curation Center

The curation center is responsible for the initial acceptance and preliminary analysis (hereafter "initial description") of returned samples while satisfying the above requirements. Examples of the initial description mainly include description of size and shape by optical observation, measurement of sample mass by weighing, retrieval of chemical composition (mineral composition) by spectroscopic observations.

In the case of Hayabusa, the total amount of sample brought back was small (i.e., about 1 mg) and spectroscopic observation was difficult. To compare with the data of the X-ray fluorescence spectrometer installed on the Hayabusa spacecraft (Yoshikawa et al., this book), chemical composition analysis was also carried out by SEM/EDS during the initial description stage (Yada et al., 2014).

All these preliminary analyses have the important role to provide a scientific link between the sample brought back and its parent body.

Normally, the returned samples are stored in a special storage container, and it is necessary to take out the sample from the container by a special procedure (see Section 12.6).

Except a part of the sample stored separately for future use, around half of samples is distributed for detailed analysis, for example the initial analysis and the international AO (Announcement of Opportunity) research. The sample distribution also requires curational work, such as taking out samples and storing them in a distribution/transport container.

12.4 Curation Center facility design

In consideration of the above roles, JAXA designed clean rooms and clean chamber for each sample return mission (Fig. 12.1, Fig. 12.2). This to avoid mixing of samples

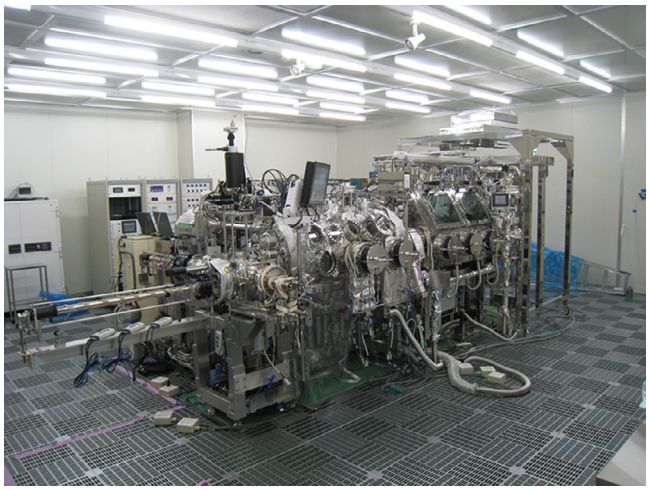

Fig. 12.1 Clean chamber for Hayabusa returned sample. *(Credit: JAXA).*

from different targets but it is also because the method of taking out the samples from the container and the contents of the initial description are different for the two missions.

Facility design for the curation center started about 5 years before the sample returned to Earth. This is because it took one year for designing, two years for manufacturing, one year for confirming functions after manufacturing, and one year for rehearsal of the operation for receiving the returned sample.

At the design stage, the specification study team formed by the JAXA curation members, the design team of the spacecraft sampler and the researchers of sample analysis played a central role in establishing the required specifications. After that, the

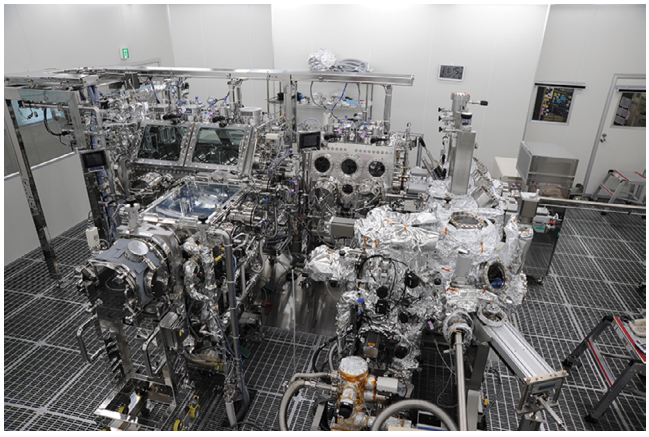

Fig. 12.2 Clean chamber for Hayabusa2 returned sample. *(Credit: JAXA).*

manufacturer was decided by bidding after receiving the specification approval from the curation steering committee and the sample return mission project team.

12.5 Clean room specifications

The specifications of the clean room at the JAXA Curation Center are almost the same for Hayabusa and Hayabusa2. The cleanliness of the clean room where the clean chamber is installed is Class 1000 (US federal standard), equivalent to Class 6 in ISO 14,644–1 standard. The floor has a grating structure, and the return airflow travels from the bottom of the grating through the back of the wall to the ceiling and circulates from the ceiling using a ULPA filter to remove dust in the air. The clean room is maintained at a pressure larger than the outside to prevent contamination from external environment. Positive pressure control is performed with the adjacent downstream room, and the shortage is taken in from the outside air through a filter by approximately 10 percent of the circulating air volume.

Temperature and humidity are controlled and maintained at 24 ± 2 °C and at 50 ± 10 percent RH, respectively. The reason why the humidity is particularly high is also to suppress the generation of static electricity.

A clean chamber is installed in the clean room. The supply pipes for exhaust gas, purified gas, cooling water, compressed air, etc. are connected to the clean chamber through a grating floor. Equipment that degrades the environments (for example, rough grinding pump) are installed in isolated areas outside of the clean room.

12.6 Clean chamber specifications

The clean chamber of the JAXA curation center is designed to perform all the operations on samples in an atmosphere-free environment, i.e., extraction from sample storage container, initial description and analysis, distribution and storage. In particular, since the structure of the sample storage container of Hayabusa and Hayabusa2 is complicated (Della Corte and Rotundi, this book; Yoshikawa et al., this book), the clean chamber is required the interface with sample container opening mechanism.

The inner surface of the chamber is based on complex electrolytic polishing for quick cleaning recovery and to avoid contamination of the sample in the chamber as much as possible.

Several types of clean chambers are prepared for the purpose of work after opening the sample storage container, and they are connected to each other through a gate valve.

In principle, the sample container opening work is performed in a vacuum environment, but the sample removal, initial description, and distribution work can be performed through a glove in a high-purity nitrogen environment.

Viton gloves were initially used based on the advice of organic matter analysis researchers, but due to the difficulty in obtaining them due to the discontinuation of production, nowadays mainly Viton coated butyl gloves are used.

Regarding the materials used for the jigs used in the clean chamber and the materials of chamber itself, in order to control the samples contamination, it was decided to avoid materials other than those used in the sampling device of the spacecraft as much as possible. In particular, the sample container is basically made of synthetic quartz glass, and it is partially permitted to use stainless steel, aluminum, or Teflon. The use of copper- or gold- plated sample holders for certain analyses such as SEM/EDS is also allowed.

12.7 Operations at Curation Center

The curation center is operated by the Astromaterials Science Research Group (ASRG) of ISAS, which is responsible for curational work (receipt, description, utilization, storage) on extraterrastrial returned samples and for facility maintenance.

ASRG was established in 2015, and, until then, it was operated by a team of technical staff and Solar System science researchers.

At the beginning of the investigation of Hayabusa's clean room and clean chamber specifications, the curation team consisted of one dedicated technical staff and two concurrent teaching staff. Currently, there are a total of 10 or more staff in the curation facility,

The tasks handled by the group are: (1) Distribution for International AO research for Hayabusa samples. (2) Research and development on acceptance of Hayabusa2 samples, (3) Research and development on OSIRIS-REx sample acceptance, for the US Asteroid Exploration Program (Lauretta et al., this book). (4) Research and development of Mars satellite sample return mission (MMX) promoted by JAXA (Tasker and Lunine, this book). (5) Contribution to research and development for future sample return mission, human resource development, and contribution for astromaterials science research community.

12.7.1 Facility maintenance

Maintenance of curation facility is an important work. In particular, the clean chamber, which stores valuable return samples, is required to operate stably 24 h a day, so that if a problem occurs in the equipment, the staff can immediately rush to it. In addition, the environment of the clean chamber where the sample is stored can be monitored remotely.

It is also important to control the cleanliness of clean rooms and clean chambers, in order to maintain a high-purity nitrogen environment in the clean chamber. Multiple nitrogen purifiers are available, regeneration is regularly performed and large-scale maintenance work was executed once a year

Maintenance and inspection of air conditioning utilities and scheduled power outages on campus are also conducted once a year.

12.7.2 Equipment cleaning and environmental assessment

The greatest care is taken in the design and operation of clean rooms and clean chambers in order to avoid contamination of the scientifically valuable return samples with terrestrial materials. ASRG pays the utmost attention to cleaning the sample handling device and to the environmental assessment.

As mentioned above, there are restrictions on the materials of the sample handling devices in the clean chamber. In this facility, as a part of the cleanliness control, the sample handling devices are basically cleaned by the staff. Specifically, ultrasonic cleaning is performed using an organic solvent and ultrapure water to remove fine particles and organic substances attached to the device. Ultrasonic cleaning uses multiple frequency bands to remove fine particles in a wide size range.

Furthermore, in addition to ultrasonic cleaning, containers and plates made of synthetic quartz glass used to store samples are also cleaned by boiling with acid and alkali solutions. If necessary, baking in a high-temperature heating furnace, plasma cleaning, ozone cleaning, may be combined.

Cleaning methods are evaluated by measuring the remaining amount of organic and inorganic substances. In addition, the environment cleanliness of the clean room and of the desiccator that stores the sample handling devices is regularly assessed and monitored to ensure the cleanliness management of the returned samples.

12.8 Current status of Hayabusa samples

Hayabusa returned samples from the asteroid Itokawa. So far, we have succeeded in extracting more than 1000 particles from the sample container.

The information of initial description on Itokawa particles is published as a sample catalog all over the world on the Internet and at the same time as a publication once a year (Yada et al., 2020).

Proposals for analytical research using Hayabusa return samples are accepted at any time as international announcement of opportunity (AO). If the research proposal is approved by the examination, ASRG will distribute and ship the samples at any time.

The results of the research adopted by the International AO will be reported by the researchers as a status report. The results will also be announced at regular symposiums (Symposium of Solar System Materials: Hayabusa symposium) sponsored by JAXA. Every year, more than 100 researchers participate in this symposium.

12.9 New challenges and preparation for Hayabusa2

The return of Hayabusa 2 samples occurred in December 2020.

At the Curation Center, the clean room and clean chamber for the Hayabusa2 return sample acceptance have been completed, and the rehearsal for sample acceptance and curation work were carried out using JAXA's new curation facility.

Rehearsals were repeated until around October, and finally the clean chamber used in the rehearsal was rehabilitated and cleaned, before the return sample arrival.

Whereas in the Hayabusa sample curation work, after opening the sample storage container in a vacuum environment, the chamber is kept in a nitrogen environment, and the curation work is performed by using gloves, the Hayabusa2 science team requires extraction and storage of some samples in a vacuum environment, to ensure that the sample will be stored for future analytical studies without ever being exposed to nitrogen gas (that could affect, e.g., N isotope analysis). Therefore, at the JAXA Curation Center, the clean chamber of Hayabusa2 has the new function of observing the inside of the sample storage container and taking out a part of the sample in a vacuum environment.

Future analyses on Ryugu samples returned by Hayabusa2 will provide new insights into the origin and evolution of the Solar System.

12.10 Conclusion

JAXA currently owns a return sample receiving facility for Hayabusa and Hayabusa2. After that, it is planned to accept returned samples by OSIRIS-REx and MMX, and the facility will play a central role as a place for accepting returned samples and performing initial description in Japan for a long time to come. ASRG members would like to continue to accumulate curation work technology and contribute deeply to the research communication of extraterrestrial materials.

References

Yada, T., Kumagai, K., Tachibana, S., Abe, M., Okada, T., Nishimura, M., Yogata, K., Yoshitake, M., Sakamoto, K., Nakato, A., Furuya, S., Miyazaki, A., Yamamoto, D., Hayashi, T., Iwamae, A., Yurimoto, H., 2020. Hayabusa Asteroid Sample Catalog 2019. JAXA Special Publication JAXA-SP-19-005E (2020), pp. 1–1209.

Della Corte, V. and, Rotundi, A., Sample Collection, Chapter 14, this book.

Lauretta, D., Enos, H.L., Polit, A.T., Roper, H.L., Wolner, C.W.V., OSIRIS-REx at Bennu: Overcoming Challenges to Collect a Sample of the Early Solar System, Chapter 8, this book.

Tachibana, S., Abe, M., Arakawa, M., Fujimoto, M., Iijima, Y., Ishiguro, M., Kitazato, K., Kobayashi, N., Namiki, N., Okada, T., Okazaki, R., Sawada, H., Sugita, S., Takano, Y., Tanaka, S., Watanabe, S., Yoshikawa, M., Kuninaka, H., 2014. Hayabusa2 project team, hayabusa2: scientific importance of samples returned from near-earth C-type asteroid 1999 JU3. Geochem. J. 48, 571–587.

Tasker, E., Lunine, J., Future missions, Chapter 10, this book.

Yada, T., Fujimura, A., Abe, M., Nakamura, T., T.Noguchi, R.O., Nagao, K., Ishibashi, Y., Shirai, K., Zolensky, M.E., Sandford, S., Okada, T., Uesugi, M., Karouji, Y., Ogawa, M., Yakame, S., Ueno, M., Mukai, T., Yoshikawa, M., Kawaguchi, J., 2014. Hayabusa-returned sample curation in the planetary material sample curation facility of JAXA. Meteorit. Planet. Sci. 49, 135–153.

Yada, T., Kumagai, K., Tachibana, S., Abe, M., Okada, T., Nishimura, M., Yogata, K., Yoshitake, M., Sakamoto, K., Nakato, A., Furuya, S., Miyazaki, A., Yamamoto, D., Hayashi, T., Iwamae, A., Yurimoto, H., Hayabusa Asteroid Sample Catalog 2019. JAXA Special Publication JAXA-SP-19-005E (2020), pp. 1–1209. doi:10.20637/JAXA-SP-19-005E/0001.

Yoshikawa, M., Kawaguchi, J., Fujiwara, A., Tsuchiyama, A., The Hayabusa Mission, Chapter 6, this book.

CHAPTER 13

A roadmap for a European extraterrestrial sample curation facility – the EURO—CARES project

Caroline L. Smith[a,b], Sara S. Russell[a], Aurore Hutzler[c,d], Andrea Meneghin[e], John Robert Brucato[e], Petra Rettberg[f], Stefano Leuko[f], Andrea Longobardo[g], Fabrizio Dirri[g], Ernesto Palomba[g], Alessandra Rotundi[h], Ludovic Ferrière[i], Allan Bennett[j], Thomas Pottage[j], Luigi Folco[k,l], Vinciane Debaille[m], Jérôme Aléon[n], Matthieu Gounelle[n], Yves Marrocchi[o], Ian A. Franchi[p], Frances Westall[q], Jutta Zipfel[r], Frédéric Foucher[q], Lucy Berthoud[s,t], John Vrublevskis[t], John C. Bridges[u], John Holt[u], Monica M. Grady[p]

[a]Department of Earth Sciences, The Natural History Museum, London, UK
[b]School of Geographical and Earth Sciences, University of Glasgow, Glasgow, UK
[c]Lunar and Planetary Institute, USRA, Houston, TX, USA
[d]Astromaterials Research and Exploration Sciences, NASA JSC, Houston, TX, USA
[e]Istituto Nazionale di Astrofisica - Osservatorio Astrofisico di Arcetri (INAF-OAA), L.go E. Fermi, Firenze, Italy
[f]German Aerospace Centre, Institute of Aerospace Medicine, Radiation Biology, Köln, Germany
[g]INAF-IAPS, Rome, Italy
[h]Università degli studi di Napoli Parthenope, Napoli, Italy
[i]Naturhistorisches Museum Wien, Vienna, Austria
[j]Public Health England, Porton Down, Wiltshire, UK
[k]Dipartimento di Scienze della Terra, Università di Pisa, Pisa, Italy
[l]CISUP, Centro per l'Integrazione della Strumentazione dell'Università di Pisa, Pisa, Italy
[m]Laboratoire G-Time, Université Libre de Bruxelles (ULB), Département Géosciences, Environnement et Société, Bruxelles, Belgium
[n]Institut de Minéralogie, de Physique des Matériaux et de Cosmochimie, Sorbonne Université, Museum National d'Histoire Naturelle, CNRS, Université Pierre et Marie Curie, Institut de Recherche pour le Développement, Paris
[o]CRPG, CNRS, Université de Lorraine, Vandoeuvre-lès-Nancy, France
[p]PSSRI, The Open University, Milton Keynes, UK
[q]CNRS, Centre de Biophysique Moélculaire, CNRS, Centre de Biophysique Moléculaire, Orléans, France
[r]Senckenberg Gesellschaft für Naturforschung, Frankfurt am Main, Germany
[s]University of Bristol, Queen's Building, University Walk, Clifton, UK
[t]Thales Alenia Space UK Limited, Bristol
[u]Space Research Centre, Michael Atiyah Building, University of Leicester, Leicester, UK

Chapter Outlines

Sample Return Missions
DOI: 10.1016/C2018-0-03374-5

13.1 Requirements for a European facility

EURO—CARES (European Curation of Astromaterials Returned from the Exploration of Space) was a European Commission funded project under the Horizon 2020 Research and Innovation program and ran between January 2015 and December 2017. The core project team was made up of academic and industry experts from 14 different organisations from the United Kingdom, France, Italy, Germany, Austria and Belgium, in addition to European and international collaborating partner organisations.

To date, EURO—CARES has been the unique European attempt to create a roadmap for the implementation of a European Extra-terrestrial Sample Curation Facility (ESCF), with the aim of improving European competitiveness in this field by identifying the required steps and highlighting areas requiring new research and innovation. This work took into account the specificities of receiving potential lunar, martian and asteroidal samples in order to adequately serve future sample return missions that are planned, or are likely to take place with European involvement e.g. Hayabusa 2 (Watanabe et al., 2017) and Mars Sample Return (Beaty et al., 2019).

Previous studies on the development and/or proposed designs for European curation facilities have been carried out, but were country-specific (e.g., Counil et al., 2002) or mission/target specific, e.g. for Marco Polo-R (Michel et al., 2014) and for Mars Sample Return (Beaty et al., 2009). Thus, the needs for curating both 'unrestricted' (i.e. lunar and asteroidal samples) and 'restricted' samples (e.g., those from Mars) (Kminek et al., 2017) together rather than in isolation. The EUROCARES project was therefore designed to build on these specific studies but to focus more on the challenges and opportunities for creating a holistic European facility that would be suitable for the curation of samples from *all* possible return missions likely over the next few decades.

In a decadal timeframe, there are clear opportunities to collaborate with other countries and also for European-led own sample return missions (Table 13.1). Future missions in which European participants can be involved (and potentially receive samples from) include Phobos sample return (JAXAs MMX mission (Kuramoto et al., 2018)), Lunar sample return from the Oceanus Procellarum and South Pole Aitken Basin regions (Chinese National Space Administration Chang'e 5 and 6 missions (Williams, 2018; Xu, Zou and Wu, 2018)) and the NASA-ESA Mars sample return campaign to Mars' Jezero Crater (ESA, 2020b; Farley, 2020). In order to achieve this, it is essential that the sample receiving and curation facility(ies) are considered as a critical element of the mission architecture and that planning and design requirements are fully incorporated during the

Table 13.1 Past, operational (current) and potential future sample return missions.
Note that the Mars 2020 mission is the first step in a planned Mars Sample Return 'campaign' and the amount and types of materials that will be collected and subsequently returned is not yet decided. The MMX and Heracles mission concepts are currently under study and so launch dates and amounts of material returned are indicative.

Mission	Year of Earth Return or launch	Target Body	Return Material	Lead Country or Agency
Apollo	1969-1972	Moon	382 kg of rocks, regolith and cores	USA
Luna	1970-1976	Moon	326 g of regolith	Russia
Genesis	2004	Sun	Implanted Solar wind particles	USA
Stardust	2006	Comet (Wild 2)	~1 mg of cometary and interstellar particles	USA
Hayabusa	2010	Asteroid (25143 Itokawa)	~1000s particles of surface regolith	Japan
Operational missions				
Hayabusa 2	Returned 2020	Asteroid (162173 Ryugu)	>0.1 g (possibly up to 10 g) of surface and near sub-surface regolith	Japan
Chang'e 5	Returned 2020	Moon	>2 kg of regolith	China
OSIRIS-REx	2023	Asteroid (101955 Bennu)	60-2000 g of regolith	USA
Future missions				
Mars 2020	Launch July 2020, Earth return ~2032	Mars	~500 g of rock cores and regolith	USA and European Space Agency (ESA)
Change'e 6	Launch 2023 or 2024	Moon	>2 kg of surface and sub-surface core	China
MMX	Launch 2024-2025	Phobos	>10 g regolith	Japan
Heracles	Launch late 2020s	Moon	≤15 kg	ESA, Japan, Canada

earliest phases of planning for each sample return mission. For example, previous studies have indicated that from site selection to full readiness for receiving Mars samples would take 8–11 years (Beaty et al., 2008, 2009; Space Studies Board, 2009; Haltigin et al., 2018).

Europe has 250 years of experience of curating meteorites that we now know to have originated on asteroids, the Moon and Mars, and much information about the best curatorial practice for these precious samples is already well understood. Internationally, humans have more than 50 years of experience in curating material brought back from space missions (e.g., Allen et al., 2011; McCubbin et al., 2019) and some aspects of the work are at a mature stage. However, other aspects of the curatorial work necessary for sample return missions in the 21st century will require innovation and significant advances from our current curatorial practice. These include (but are not limited to):

13.1.1 Planetary Protection considerations

There have been no sample return missions to Mars and so this area poses particular challenges given the stringent planetary protection requirements for Mars returned samples. Although lunar/asteroidal meteorites and returned samples, and Martian meteorites exhibit no evidence of containing life, this might not necessarily be the case for returned Martian samples. It will be necessary to address the risks involved in storing and handling possibly biogenic material and to examine how we can mitigate this. Mars Sample Return mission planning, including sample receiving and curation, requires a high level of planetary protection, to break the chain of contact between Mars and the terrestrial biosphere. For instance, new technologies such as portable receiving technologies (from the landing site on Earth to a Sample Receiving/Curation Facility) are required.

A strategic document published by the European Science Foundation (Ammann et al., 2012) has developed a risk assessment framework that can be utilized for the design of a curation facility to handle these samples. They state that any sample returned to Earth should be handled as being equivalent to a Biosafety level 4 agent, the most hazardous microbial pathogen, in addition to the requirement that the probability of an unintended release of a Martian particle into the Earth's biosphere is less than 10^{-6} (Ammann et al., 2012). This means that any facility built to house Mars returned samples will need to be built to the highest standard of containment laboratory with new and challenging requirements, whilst also protecting against terrestrial contamination of the sample (Bridges and Guest, 2011; Meyer et al., 2019). This unique combined requirement needs input from specialists in curation, high-containment microbiology, and clean room sectors. This requires a Facility to assess the potential threat to the terrestrial biosphere prior to releasing from containment samples for investigation by the wider scientific community.

13.1.2 Small sample handling

While the Apollo missions brought back hundreds of kilograms of rocks, this scale of sample collection will be prohibitively expensive and technically extremely challenging for future robotic sample return missions. However, with modern analytical techniques, tiny grains as small as a few micrometres in size can be analyzed on scales down to atomic levels, and therefore a substantial sample collection is not essential to answer the many outstanding scientific questions.

Most future missions will aim to typically bring back a few tens of grams of samples (Table 13.1), although contingencies will have to be made in case the amount of successfully returned material turns out to be lower than this (e.g., the Hayabusa mission returned less material than originally envisaged and modeled, Yano et al., 2006), or potentially larger amount (e.g., the OSIRIS-REx mission is expected to return between 60 g and ~2000 g of regolith, Bierhaus et al., 2018). The Stardust mission returned thousands of cometary particles, embedded in low density aerogel, and enabled the first analyses of *bona fide* cometary material, but the particles were of the order of micrometres in size, creating considerable technical challenges for sample han-

dling and analysis (Brownlee et al., 2006; Zolensky et al., 2008), a situation that is likely to be repeated with future sample return missions. The Mars 2020 rover 'Perseverance' sampling system contains 42 sample tubes, of which 37 are allocated for collection of rock core and regolith samples from the Martian surface (Beaty et al., 2019). Pre-flight tests indicate the tubes can contain ~16.5 g of material, meaning that ~610 g of material could potentially be sampled and collected. The remaining 5 sample tubes are witness samples, that will be flown pre-sealed with a number of different witness materials to assist in assessing and characterizing round trip contamination (Beaty et al., 2019).

However, the curatorial techniques used for Apollo samples and meteorites are not always appropriate. In particular, we need innovative solutions to ensure that micron-sized samples can be handled, characterized, and catalogued appropriately; assessing the risks and opportunities provided by robotic and/or human manipulation techniques is thus important to consider. An excellent example of innovation in curatorial facilities and protocols, which can be used as an exemplar for the curation of small samples in very clean conditions is the Extraterrestrial Sample Curation Centre (ESCuC) at JAXAs Sagamihara Campus, which was purpose-built to curate the Hayabusa mission samples (Yada et al., 2014). In the case of Mars samples, atmospheric gases are also planned to be collected, either as head-gases within the sample tubes that also contain rock fragments and regolith, or possibly as a separate dedicated sample(s) (Beaty et al., 2019), so it will also be imperative that the necessary hardware and protocols are designed to successfully extract and sample these gases without any detrimental effects e.g. isotopic fractionation or terrestrial contamination (e.g. Vacher et al., 2020).

13.1.3 Analogue samples

It is essential to understand the diversity of the physical and chemical properties of any expected returned sample in the context of its extra-terrestrial parent body. These properties will differ vastly between geologically distinct sites on the same body and between the different targets.

Ensuring that the ESCF incorporates the most appropriate handling and analytical capabilities requires the development of a coherent set of functional sample analogues, that appropriately recreate the expected sample properties, to establish and verify the technical and operational constraints on the sample curatorial facility. Furthermore, these tests and analyses are important to serve as means for assessing the best way to provide for handling/manipulation, analytical, biohazard and sterilization testing. The overall properties of the returned samples will strongly govern the requirements necessary for adequate sample handling, storage, and analyses. Meteorites, terrestrial rocks and synthetic materials can serve as sample analogues of solid rocks, loose materials (i.e. regolith), icy, dry and hydrated materials, and material formed by impact such as melted clasts – all types of materials expected to be found at the surfaces or near-sub-surfaces of the different Solar System target bodies of interest.

Design of future sample return missions would benefit from having access to a collection of well-characterized analogue samples representing a variety of different

Solar System bodies and different regions of a single body. With appropriate analogues, 'end to end' testing protocols can be developed, whereby instruments designed for sample collection (e.g., drills) can be tested as well as ground-based handling and analytical methods, within the curatorial facility or individual laboratories.

13.1.4 Analytical instrumentation

Our understanding of extra-terrestrial materials that could be returned to Earth has been greatly increased by the results obtained from in-situ missions (e.g., NASA Mars Science Laboratory, ESA-NASA Cassini-Huygens, ESA Rosetta cometary orbiter, ESA Mars Express, NASA Mars Reconnaissance Orbiter). However, there is a wealth of information that cannot be obtained from remote sensing instrumentation or payload on planetary landers, and so we also require sample return missions in parallel with these. Despite the great advances in robotic instrumentation, there are still many analytical techniques that cannot be utilized in situ by planetary landers or orbiters. For instance, electron microscopy techniques, which are routinely used to study in detail the mineralogy and chemistry of geological materials, are not possible. Similarly, high-precision radioisotope analyses for geochronology (age-dating) and stable isotope investigation are also impossible. Sample return missions afford the possibility to use the most innovative and technically advanced analytical techniques available in laboratories around the world to fully characterize the physical, chemical, and isotopic characteristics of different Solar System materials.

A key question in the design considerations for an ESCF is the types of instrumentation that would be required to enable the curatorial and sample management tasks and activities to be carried out. Instruments required for contamination knowledge of the sample are also essential.

13.1.5 Sample recovery and transport to and on Earth

Much work is required in the field of sample transport. Once the Earth Return Capsule lands on Earth, it is imperative that it is recovered, handled and transported in a way that the scientific integrity of the pristine samples within is maintained. In the case of returned material from Mars, the need for biocontainment will make these steps even more challenging. This key part of the samples' journey must be well understood and documented in case of potential problems, such as unplanned hard-landing of the Genesis return capsule (Stansbery, 2005). It should be noted that for Mars Sample Return, to satisfy the Planetary Protection requirements, the Earth Return Capsule is engineered to hard-land (Beaty et al., 2019).

13.1.6 Public perception and engagement

A significant risk to the development of an ESCF is the public perception of extra-terrestrial materials, potentially containing biological entities, being deliberately returned to Earth without going through the "sterilizing" process of long-term exposure to cosmic

rays and atmospheric entry. This could be of great concern to many people and could lead to major delays in the establishment of the ESCF. By demonstrating the ability to correctly handle and prepare extra-terrestrial samples, such that the integrity of the samples is maintained and that there is no danger to either the researchers or the general public, it should be possible to allay potential public anxiety about the existence of such materials on Earth. It is therefore crucial that at all stages in the development plans for the ESCF and during ongoing operation of the Facility, there is a transparent and honest outreach program that can explain the strategies for safeguarding the terrestrial ecosystem from potential exogenous pathogens and highlighting the benefits of being able to conduct research on the precious materials returned from mission to asteroids, the Moon and Mars.

13.2 The EURO-CARES project

Considering the above key areas where knowledge gaps exist and where there is great opportunity for innovation, the EUROCARES project developed seven key activities or 'work packages' (WP) to enable the development of a robust roadmap for the design of the ESCF. Six of the seven work packages (WP2 to WP6) were technical activities, which involved experts from academia and industry, working together to share knowledge, best practice and provide scenarios and potential solutions for the roadmap. There was also a cross-cutting work package (WP8) dedicated to outreach and dissemination of project information for a wide variety of stakeholders, including educational resources for school and college/university students and for policy makers and agency representatives.

All WPs were connected each other and results and information gathered during the different WP tasks were shared. This section provides a summary of the key activities and recommendations from each technical work package. For further information, the reader is referred to the EUROCARES project website (http://www.euro-cares.eu/reports).

13.2.1 Work Package 2 – Planetary Protection

Stringent requirements regarding planetary protection (PP) and *in-situ* biological and organic molecule contamination control are now recognized as a major factor in samples returned from space, both in respect of spacecraft hardware design and also in the design of sample curation facilities. In addition to fulfilling all the forward contamination (i.e., terrestrial contamination of extra-terrestrial samples) control requirements for the mission, there will be a variety of measures aimed at avoiding back contamination of Earth. Thus, facilities require design input from specialists in high containment microbiology and the pharmaceutical/clean room sector as well others involved in, e.g., robotic handling of hazardous materials and the sterilization/cleaning of sensitive materials. The requirements for a combination high containment and ultraclean facility will naturally lead to the development of a highly specialized facility requiring the use of novel scientific and engineering methods and processes.

The Planetary Protection WP included several activities that were required to provide key input for the roadmap and for input into other work packages.

Whilst the most stringent PP requirements are for Mars Sample Return and are concerned with the critical aspects of being able to detect any putative Martian life and/or biohazards in the returned samples, many complementary aspects of PP activity are also relevant to other sample return missions. These include cleaning and sterilization of spacecraft components and good contamination control and knowledge (e.g. Dworkin et al., 2018). The same approach applies for the curation facility and its design and operation, to prevent the inadvertent contamination of the samples during the curation process.

Major activities covered during WP2 were Life Detection and Biohazard Detection, Biohazard Security, Sterilization Techniques, Sample Transfer, and Facility Requirements. Key recommendations and areas for further investigation/technology development included:

- The development and application of a correlative approach to assess data and relationships for Life Detection and Biohazard Detection, including the different types of instrumentation and methods required (Brucato et al., 2018) (Fig. 13.1).
- The recommendation that a minimal amount of 1.5 g of a given sample is required to fulfil the needs for the Life and Biohazard Detection testing as identified through the correlative approach *and* ideally the amount of material should not exceed 10 percent of the mass of any given sample.
- Biohazard requirements and considerations must ensure the facility design includes both primary and secondary containment functions, but also critical is the impor-

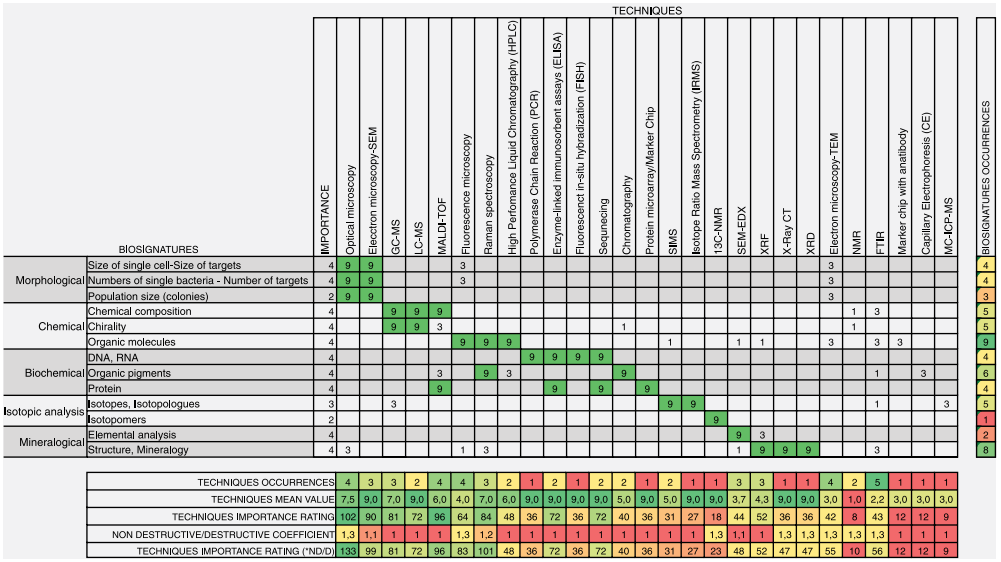

Fig. 13.1 ***Correlation matrix approach as applied to the different types of scientific investigations and techniques relevant to biohazard testing as part of planetary protection protocols.*** The higher the number indicates the higher the correlation (or applicability) of a technique for a specific investigation.

tance of 'people factors' such as high-levels of staff training and the physical and mental effects of working under challenging conditions.
- Special attention should be given to the validation of the facility and processes carried out to ensure they are functioning as required – this is a critical step that must be carried out prior to any sample return samples entering the facility.
- The evaluation of different decontamination/sterilization techniques and trade-off and how these would be applied during different operations of the facility, e.g., for cleaning sample storage environments between different samples.
- The evaluation of different materials and possible designs for use in sample holders for transfer between different areas of the facility (e.g., between different instruments/laboratories) and for transfer of samples outside the facility.

13.2.2 Work Package 3 – Facilities and Infrastructure

The main objective of this WP was to define the state-of-the-art for facilities required to receive, contain, and curate extra-terrestrial samples whilst guaranteeing planetary protection. All the aspects of building design, ranging from sample reception to sample storage and curation were covered by this WP. As a guiding principle the curation facility should enable long-term, high quality research, either by providing pristine samples to the science community, or by planning fully functional laboratories within the facility.

The main activities identified that would be conducted within the ESCF are: 1) to receive the return capsule, 2) to extract the sealed sample container(s) from the spacecraft, 3) to open and to recover the sample(s) from the sample container(s), 4) to store the sample(s), 5) to curate and characterize the sample(s), as to allow further science activities, 5) for restricted samples, to conduct life detection/biohazard tests, 6) to allocate samples for research, after appropriate biohazard assessment and sterilization (if required).

Major activities covered during WP3 were evaluation of different design and operational requirements for existing high-containment facilities, preliminary design concepts including a 'Design Studio' with architectural students from the Institute of Architecture and Design at the Vienna University of Technology, advanced and final design concepts developed using key inputs from the other technical work packages (Hutzler et al., 2017). Key recommendations and areas for further investigation/technology development included:
- Evaluation and identification of different design and operational requirements for high-containment facilities and comparison of these against the types of operations required for both restricted and unrestricted samples.
- The concept of identifying the key operational activities and workflows carried out in the building and assigning them to different 'Functional Units' (Fig. 13.2), hence using the activities to inform the design scenarios and concepts rather than a design-led solution.
- The recognition that in defining a given Functional Unit a major consideration is the number of staff and the skills sets required to carry out the given operation(s) safely and successfully. This applies for both restricted and unrestricted samples.

PRF Unrestricted	PRF Restricted	Assessing, cleaning and packaging the spacecraft on the landing site. Delivery of the spacecraft to SRF.
SRF Unrestricted	SRF Restricted	Receiving, the sample container, cleaning and opening of the outer layers and delivery of the unopened sample canisters to the curation facility. Clean environment. For restricted samples, containment environment required.
SCF Unrestricted	SCF Restricted	Receiving of the sample canister, accessing the samples Preliminary Examination (sample and hardware) and Sample Early Characterisation Curation and Dissemination. For restricted sample, Life Detection and Biohazard Assessment Protocol. Ultra-clean environment. For restricted samples, high containment environment required.
Work Space		Support space for workers (offices, meeting rooms, social rooms, restaurant, etc.).
Public Outreach		Space accessible to the public (different categories of public, TBD) to promote the activities of the ESCF.
AMUF		Personnel training, instruments and protocols testing on analogue samples. Meterial testing for cleanliness and containment suitability.
Remote Storage Unrestricted	Remote Storage Restricted	Storage under dead-mode of a TBD part of the samples. Clean environment. For restricted samples, contained environment.

Fig. 13.2 ***Different Functional Units as identified for the ESCF.*** Red indicates Functional Units carrying out scientific operations on restricted samples and blue for unrestricted samples. Yellow is used for the Analogue Mockup Facility, which will host only terrestrial samples. Functional Units colored green are those identified that do not carry out scientific operations but are critical for the running of the facility.

- Phasing of the design and delivery of the ESCF into main steps with inbuilt adaptability to 'future-proof' the facility and to allow for testing and verification of different operations in each Functional Unit. The inclusion of a Functional Unit dedicated to testing different operations on a dedicated set of analogues is a key feature of this concept.
- The ESCF should be a new facility and therefore there would be no constraints by repurposing an existing building, which would ensure the building concept is driven by operational requirements for each Functional Unit, however, it could be co-located with (an) existing facility(ies) on an existing site.

13.2.3 Work Package 4 - Instruments and Methods

The objective of this WP was to understand the most appropriate analyses and corresponding types of instrumentation to be performed within the ESCF whilst ensuring minimal contamination/minimal damage to the sample and rapid distribution of

samples to the scientific community as appropriate. Specific topics addressed included: determining the types of analyses necessary for preliminary examination and curation functions in the facility, the types of analyses that may be carried out on 'pristine' samples within sample containers and those that would require samples to be removed from their containers, evaluation of whether destructive analyses are required and to assess the risks and opportunities of carrying out of such analyses within the facility. Owing to the different biohazard constraints between restricted and unrestricted samples, the instrumentation required for both types of samples was evaluated. Key recommendations and areas for further investigation/technology development included:

- Identifying and defining the differences between 'Sample Early Characterization' and 'Preliminary Examination'. Sample Early Characterization (SEC) corresponds to the minimal characterization and is performed within the ESCF upon opening of the sample return capsule, by the facility staff. Preliminary Examination (PE) corresponds to the first scientific investigations aiming at reaching the missions' scientific goals. This could be done by science teams selected prior to the sample arrival on Earth, for example by including scientists based on analytical or scientific experience that would be required during the PE phase. After these two phases it can be anticipated that the samples would be available for the wider scientific community upon calls for proposals to answer different or unanticipated questions or to perform newly developed specific analyses. Experience gained from previous missions, notably the Stardust mission, shows that the scientific output is maximal if the analyses in the ESCF are minimal and as rapid as possible (Burnett, 2006; Space Studies Board, 2019).
- The analytical infrastructure required for investigation of unrestricted samples and restricted samples should be kept separated in the ESCF, in order (1) to avoid biohazard cross-contamination issues, (2) to ease as far as possible the maintenance of instruments for the unrestricted samples. Keeping the two separated, eventually with duplication of similar instruments, allows continued working on unrestricted samples, even if quarantine is required for different restricted samples. In the framework of the infrastructures evaluated by WP3, this corresponds to separated facilities, even though they can be located at the same place to optimize, e.g., staff expertise and associated infrastructure.
- Identification of different instruments and methods to be employed during the 'Sample Early Characterization' (SEC) phase carried out in the ESCF Fig. 13.3, their conditions of operations, staffing levels required to operate and maintain those instruments.

13.2.4 Work Package 5 - Analogue Samples

The overall objective of WP5 was to create a list of different types of analogue samples that would be required for the curation facility for the testing and verification of various operations and processes in the different Functional Units, and to create a preliminary

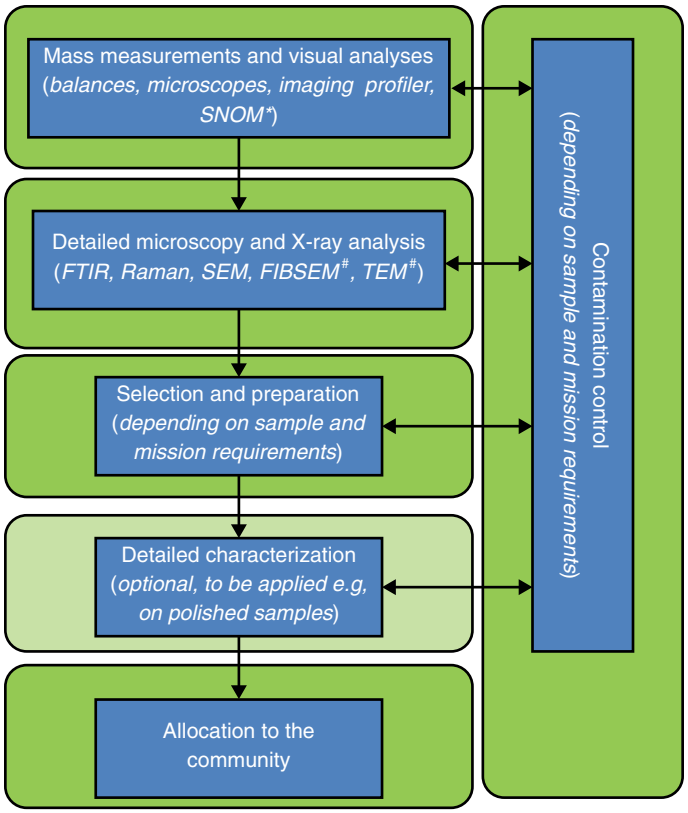

Fig. 13.3 ***Summary overview of sample processing and instrumentation required for each for each step.*** Contamination knowledge is generally not associated with direct measurement of samples but runs parallel to all aspects of sample processing. Techniques marked with an asterisk are particularly suited to small sample analyses and can perform sub-micrometer scale resolution, however all involve sample preparation to be carried out before analyses.

list of analogue materials already available (Fig. 13.4). These lists, including recommendations for the creation of new artificial analogues, were completed over the course of the EUROCARES project in response to the requirements established by the other work packages. Specific topics investigated during WP5 included the evaluation of specific storage conditions and handling procedures during curation and analysis of extraterrestrial materials, the identification of analogue samples crucial for evaluating and defining the protocols necessary to accomplish safe and sustainable handling of extraterrestrial materials, the understanding the different types of analogue samples required for the different operations in the sample curation facility (e.g. analogues, standards, witness plates), and the evaluation of analogue materials and types already available and in use. Key recommendations and areas for further investigation/technology development included:

Fig. 13.4 Example from the EURO—CARES Analogue Database (Euro-Cares Consortium - WP5, 2017).

- The early creation of a robust set of analogues is a critical part of the planning and development of the ESCF. It is imperative that the analogue collection (including appropriate witness plates) is ready early enough for protocol testing and ideally during the preparatory phase of a mission and/or the building phase of the curation facility.
- Curation should accompany mission planning and development from the start with the science team making recommendations regarding suitable standards and functional analogue materials to be used in the curation facility at the start of the mission.
- Analogues used for testing and validation of operations in the ESCF could also be used for space mission instrument validation and for testing ground-based instruments to aid in interpretation of data from mission payload instruments.
- The analogues need to cover a wide range of physical and chemical properties and will include simple to complex materials to demonstrate that the end-to-end workflow is flawless. However, specific analogues will be needed for specific processes, therefore, it will not be necessary or appropriate that one analogue serves the whole end-to-end flow.

13.2.5 Work Package 6 – Sample Transport Receiving Technologies

The objective of this WP was to propose methods for the recovery and transport of Mars or lunar and asteroid samples from the landing site to the Facility. The Earth re-entry capsule from any given sample return mission would be targeted at a specific landing ellipse on the Earth, possibly at a considerable distance from the Facility. Before the capsule arrives, considerable preparations for the recovery need to be made and many different scenarios rehearsed. Once the capsule has landed, an assessment of the state of the spacecraft would lead to an appropriate recovery procedure. A temporary receiving facility near to the landing site may be used as a safe location to inspect, document and package the sample capsule/container. The samples would then be transported to a permanent facility using a safe and secure method. The entire process is summarized in Fig. 13.5.

Specific topics that were investigated during WP6 included: identification of possible worldwide landing sites for both restricted and unrestricted sample return and how this classification may inform an ideal site, identification of the risks and quantifying the impact of a compromised sample at landing, determining the necessary procedures to prepare for sample recovery, assessment of the tasks and facilities necessary for recovery and initial inspection of the sample(s) and how procedures for recovery would differ between unrestricted and restricted mission samples.

Key recommendations and areas for further investigation/technology development included:

- Determining the general requirements and a basic design of a transportation box, which could be used to transport samples from the landing site to the ESCF. Most of the concepts are at a low readiness level in Europe, but they are not substantial technical challenges. Some concepts have already been demonstrated by other agencies.
- Identification of the sequence of actions for different Earth Return Capsule landing scenarios, ranging from nominal unrestricted missions through to non-nominal restricted missions. The identification and understanding of the different scenarios allow for the training of staff in the different recovery processes envisaged. This will then help to ensure any deviance from the mission plan has been catered for and there is a process to deal with it safely and efficiently.
- Identification and evaluation of different potential landing sites worldwide, including a possible European site: the Esrange Space Centre in Sweden
- The importance of identifying "non-technical" readiness: the entirely novel nature of the ESCF and recognizing that the capability it delivers is not solely due to equipment and physical infrastructure alone. Important issues of non-technical readiness include, for example, staff recruitment and training, which must also be addressed since lack of preparedness in this area would have just as much impact as lack of technology readiness.

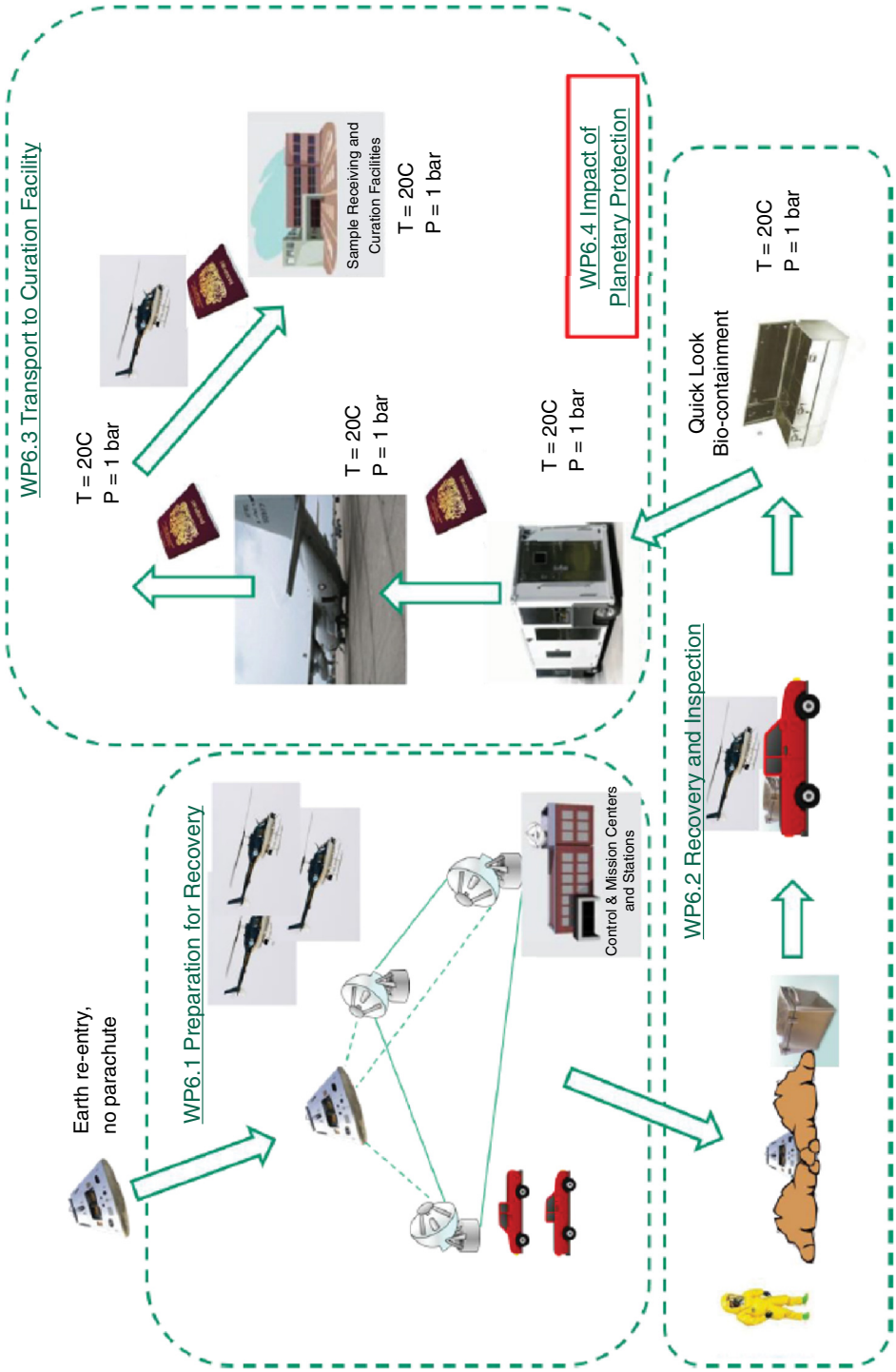

Fig. 13.5 Summary of the initial concept of operations during the recovery procedure for a sample return mission.

13.3 Summary and key recommendations

The EUROCARES project resulted in the following major recommendations and suggestions for the next stage of work to be carried out in order to develop a fully functional facility (Fig. 13.6):

- There is an **urgent need to update the Planetary Protection Protocols**. The most recent published protocol for assessing Mars samples for potential hazards was issued in 2002 (Rummel et al., 2002; Rummel and Kminek, 2018), although other teams have considered some of the relevant issues (e.g., Beaty et al., 2008; Space Studies Board, 2009; Haltigin et al., 2018; Meyer et al., 2019). Whilst the philosophical approach and many of the broad concepts are still valid, our scientific knowledge and analytical capabilities have changed significantly in the last decade (Kminek et al., 2014; Space Studies Board, 2018, 2019, 2020). **We strongly recommend a cross-European effort with significant, wider international participation** to update the Planetary Protection protocols, utilizing the significant expertise in the life and Earth sciences as well as analytical instrumentation innovation that exists within Europe.
- **Funding for a European Sample Curation Facility must be budgeted.** Estimated that the required time to build an ESCF is a minimum of 7 years, and perhaps longer in view of the administrative barriers that must be overcome, it is essential that a funding line for an ESFC is identified as soon as possible. **We strongly recommend that a European Sample Curation Facility becomes part of the ESFRI** (European Strategy Forum on Research Infrastructures) **roadmap**. This then provides a route for funding.
- **Appropriate training of staff working in the facility is critical.** The amount of time required should not be underestimated and is a major part of the 7-year (minimum) facility development time. We also have a need to promote links between European researchers and combine efforts around Europe to take advantage of complementary skill sets and expertise and to avoid duplication of work or knowledge gaps. **We strongly recommend that a training programme for curators is established**. This could be achieved through the ECs Marie Skłodowska-Curie or International Training Network actions program, although it would be advantageous to widen the focus beyond Europe, to draw on international expertise.
- **We recommend that a well-defined and fully characterized suite of analogue materials is assembled for the ESCF before the arrival of material returned from space.** There are several complementary activities involving terrestrial analogues in Europe that have a direct link to curation facility development, funded by ESA, CNES and European Union, respectively (Smith et al., 2018; Martin and Duvet, 2019; ESA, 2020a; Bost et al., 2013; Veneranda et al., 2019).
- As the major European space agency, **ESA should be a leading stakeholder in the curation effort**, enabling technological development and scientific studies to

oversee work undertaken and to develop products that match their future space mission requirements. Individual national space agencies also have their own priorities and bilateral agreements with other space-faring nations.

- **We recommend that the building that houses the ESCF is built as a series of modules, to maximize flexibility.** We considered various building designs in terms of separate functional units, each one with its own purpose, such as curatorial space, communications, analogue samples etc. This maximizes flexibility and allows for growth of the facility as more missions are returned to Earth.
- **We recommend that a more detailed evaluation of the Esrange Space Center's feasibility as a landing site is undertaken**. Six potential landing sites across the world, and the strengths and weaknesses of each in terms of weather/climate, accessibility and population were considered. The best site for landing a European sample return mission appears to be the Esrange Space Center, Sweden. However, specific considerations for each individual mission may favor another site.
- Early characterization of the samples returned must be undertaken in the ESCF as part of curatorial best practice, and in view of the requirements for handling restricted samples. However, owing to potential planetary protection constraints, **we recommend that detailed examination of returned samples is undertaken by specialists outside the ESFC.** This enables the broader science community to engage in the missions and is more cost effective, as it negates the need for multiple large laboratories (see also recommendations in Space Studies Board, 2019).
- **Engagement with the public and with decision makers is essential for the ongoing support of the facility.** Methods for outreach, education and communication with the public should be at the heart of the ESCF.
- We have **identified a series of technological innovations that are required,** including:
  - Robotics. New generation curation facilities would be greatly aided by robotics. Robotic instrumentation can perform tasks such as sample movement and manipulation to great accuracy, and can work in a variety of conditions, including, e.g., very cold environments. **We recommend the development of sample manipulation robotics, using robots already available in industry as a starting point**. However, issues such as potential contamination by moving parts and lubricants need to be addressed.
  - **Detailed design of the transport container for restricted mission samples**. One of the biggest challenges of working with restricted samples is to break the chain of contact between Earth and Mars. A requirement for restricted samples is that the probability of contamination to Earth by a particle ≥ 0.1 μm in size shall be less or equal to 1×10^{-6} (Ammann et al., 2012). To meet this requirement, we have considered suitable designs for containers and these now need to be further developed.

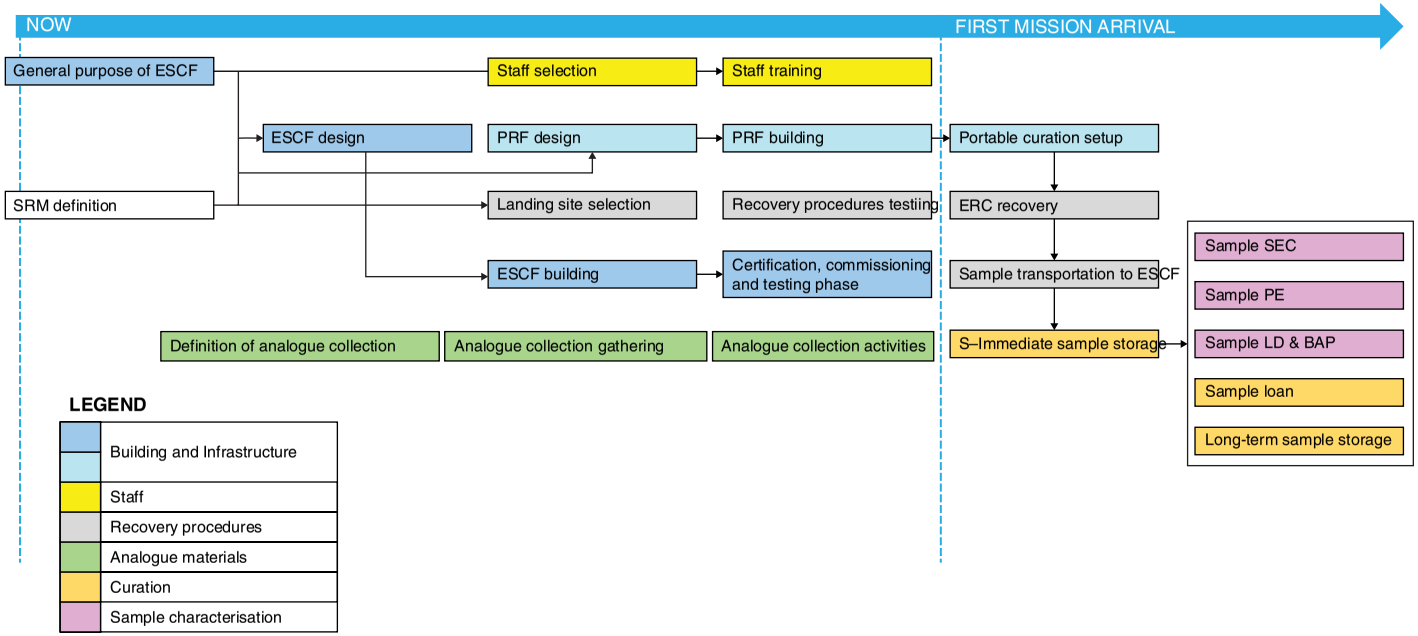

Fig. 13.6 Overview of timeline of key activities and timeline as identified in the EURO—CARES project for the development and implementation of a fully functional and operational ESCF.

Acknowledgements

This project was funded through the European Union's Horizon 2020 Research and Innovation programme under grant agreement No 640,190. We would like to thank the many European and international colleagues who attended the different EUROCARES workshops, hosted visits to existing facilities and organisations, listened to our presentations at international conferences and provided very helpful feedback and insights, which significantly assisted in our work. We would also like to thank the EUROCARES reviewer, Ian Lyon (University of Manchester, UK) for his detailed work and very constructive comments and our EU Desk Officer, Sally Taylor.

References

Allen, C, et al., 2011. Curating NASA's extraterrestrial samples—past, present, and future. Chem. Erde 71 (1), 1–20. doi:10.1016/j.chemer.2010.12.003.

Ammann, W. et al. (2012) *Mars Sample Return backward contamination – Strategic advice and requirements*. Available at: https://www.essc.esf.org/fileadmin/user_upload/essc/MarsSampleReturn_2012.pdf.

Beaty, D.W, et al., 2008. Preliminary planning for an international mars sample return mission report of the international mars architecture for the return of samples (iMARS). Working Group. Available at https://mepag.jpl.nasa.gov/reports/iMARS_FinalReport.pdf.

Beaty, D.W, et al., 2009. Planning considerations for a mars sample receiving facility: summary and interpretation of three design studies. Astrobiology 9 (8), 745–758. doi:10.1089/ast.2009.0339.

Beaty, D.W, et al., 2019. The potential science and engineering value of samples delivered to earth by mars sample return: international MSR objectives and samples team (iMOST). Meteoritics and Planetary Science 54 (S1), S3–S152. doi:10.1111/maps.13242.

Bierhaus, E.B, et al., 2018. The OSIRIS-REx spacecraft and the touch-and-go sample acquisition mechanism (TAGSAM). Space Sci. Rev. 214 (7). doi:10.1007/s11214-018-0521-6. The Author(s).

Bost, N, et al., 2013. Missions to mars: characterisation of mars analogue rocks for the international space analogue rockstore (ISAR)Planetary and Space Science82–83. Elsevier, pp. 113–127. doi:10.1016/j.pss.2013.04.006.

Bridges, J.C., Guest, M., 2011. Planetary protection and mars sample return. Proc. Inst. Mech. Eng. Part G J. Aerosp. Eng. 225 (2), 239–246. doi:10.1177/09544100JAERO900.

Brownlee, D, et al., 2006. Comet 81P/wild 2 under a microscope. Science 314 (5806), 1711–1716. doi:10.1126/science.1135840.

Brucato, J, et al., 2018. Use of the correlation matrix approach to define the life detection techniques in a sample curation facility. European Planetary Science Congress 12, p. Abstract #690.

Burnett, D.S., 2006. NASA returns rocks from a comet. Science 314 (5806), 1709–1710. doi:10.1126/science.1137084.

Counil, J., Bonneville, R., Rocard, F., 2002. The french involvement in mars sample return program. in 34th COSPAR Scientific Assembly, 3166.

Dworkin, J.P, et al., 2018. OSIRIS-REx contamination control strategy and implementation. Space Sci. Rev. 214 (1), 19. doi:10.1007/s11214-017-0439-4.

ESA, 2020. ESA's Sample Analogue Curation Facility. Available at https://sacf.esa.int/.

ESA, 2020. Mars Sample Return. Available at https://www.esa.int/Science_Exploration/Human_and_Robotic_Exploration/Exploration/ESA_and_NASA_to_investigate_bringing_martian_soil_to_Earth.

Farley, K.A., 2020. MARS 2020 MISSION: Science Rover. Available at https://mars.nasa.gov/mars2020/.

Haltigin, T., et al., 2018. iMARS phase 2Astrobiology18. Mary Ann Liebert, Inc., publishers, pp. S-1-S-131. doi:10.1089/ast.2018.29027.mars.

Hutzler, A, et al., 2017. EURO-CARES extraterrestrial sample curation facility : architecture as an enabler of science. 47th International Conference on Environmental Systems.

Kminek, G, et al., 2014. Report of the workshop for life detection in samples from Mars Life Sciences in Space Research2. Elsevier Ltd, pp. 1–5. doi:10.1016/j.lssr.2014.05.001.
Kminek, G, et al., 2017. COSPAR's planetary protection policy. Space Res. Today 200, 12–25. doi:10.1016/j.srt.2017.11.010.
Kuramoto, K., Kawakatsu, Y., Fujimoto, M., 2018. Martian Moons eXploration (MMX) : an overview of its science. European Planetary Science Congress 12, 1036. EPSC2018-Available at https://meetingorganizer.copernicus.org/EPSC2018/EPSC2018-1036.pdf.
Martin, D., Duvet, L. (2019) 'ESA's sample analogue curation facility (SACF), and expanding ESA'S exploration sample analogue collection (ESA2C).', in 50th Lunar and Planetary Science Conference *(LPI Contrib. No. 2132)*, p. 2663.
McCubbin, F.M, et al., 2019. Advanced curation of astromaterials for planetary science. Space Sci. Rev. 215 (8). doi:10.1007/s11214-019-0615-9 The Author(s).
Meyer, M.A, et al., 2019. MSR science planning group (MSPG) workshop #1 report: the relationship of MSR science and containment, Ninth International Conference on Mars 2019, *No. 2089. LPI Contrib*, pp. 6385.
Michel, P, et al., 2014. MarcoPolo-R: near-earth asteroid sample return mission selected for the assessment study phase of the ESA program cosmic vision. Acta Astronaut. 93, 530–538. doi:10.1016/j.actaastro.2012.05.030.
Rummel, J.D, et al., 2002. A draft test protocol for detecting possible biohazards in martian samples returned to earth. NASA/CP *20020211842*, 127.
Rummel, J.D., Kminek, G., 2018. It's time to develop a new "draft test protocol" for a mars sample return mission (or Two…). Astrobiology 18 (4), 377–380. doi:10.1089/ast.2018.1823.
Smith, C.L, et al., 2018. The european space agency exploration sample analogue collection (ESA2C) and curation facility-present and future, 49th Lunar and Planetary Science Conference, *No. 2083. LPI Contrib*, pp. 1623.
Space Studies Board, 2009. Assessment of planetary protection requirements for Mars sample return missions. National Academies Press. doi:10.17226/12576.
Space Studies Board, 2018. Review and Assessment of Planetary Protection Policy Development Processes. National Academies Press. doi:10.17226/25172.
Space Studies Board, 2019. Strategic Investments in Instrumentation and Facilities for Extraterrestrial Sample Curation and Analysis. National Academies Press. doi:10.17226/25312.
Space Studies Board, 2020. Assessment of the Report of NASA's Planetary Protection Independent Review Board. National Academies Press. doi:10.17226/25773.
Stansbery, E.K., 2005. Genesis recovery processing, Lunar and Planetary Science Conference, XXXVI, 2179.
Vacher, L.G, et al., 2020. Hydrogen in chondrites: influence of parent body alteration and atmospheric contamination on primordial components. Geochim. Cosmochim. Acta 281, 53–66. doi:10.1016/j.gca.2020.05.007.
Veneranda, M, et al., 2019. Planetary terrestrial analogues library (PTAL) project: raman data overview. J. Raman Spectrosc., 5652. doi:10.1002/jrs.5652 jrs.
Watanabe, S, et al., 2017. Hayabusa2 mission overviewSpace Science Reviews208. Springer Science+Business Media, Dordrecht, pp. 3–16. doi:10.1007/s11214-017-0377-1.
Williams, D., 2018. Future Chinese Lunar Missions. Nasa. Available at nssdc.gsfc.nasa.gov/planetary/lunar/cnsa_moon_future.html.
Xu, L., Zou, Y., Wu, J., 2018. Preliminary imagines for the planning and its scientific objectives of china's lunar research station, 49th Lunar and Planetary Science Conference, 1856.
Yada, T, et al., 2014. Hayabusa-returned sample curation in the planetary material sample curation facility of JAXA. Meteoritics and Planetary Science 49 (2), 135–153. doi:10.1111/maps.12027.
Yano, H, et al., 2006. Touchdown of the Hayabusa spacecraft at the muses sea on Itokawa. Science 312 (5778), 1350–1353. doi:10.1126/science.1126164.
Zolensky, M, et al., 2008. Curation, spacecraft recovery, and preliminary examination for the Stardust mission: a perspective from the curatorial facility. Meteoritics and Planetary Science 43 (1–2), 5–21. doi:10.1111/j.1945-5100.2008.tb00607.x.

PART III

Techniques and technologies

CHAPTER 14

Collection of samples

Vincenzo Della Corte[a], **Alessandra Rotundi**[b]
[a]INAF-IAPS, Rome, Italy
[b]Università degli studi di Napoli Parthenope, Napoli, Italy

Chapter Outlines

14.1 Introduction

Sample return provides fundamental chronological and geochemical ground truth that enhances the value of both orbital and surface observations well beyond their stand-alone importance. It provides a unique perspective not offered by in situ space missions, as the variety of the state-of-the-art analytical techniques for the returned sample analyses (Westphal et al. 2017) are not limited by the constraints – e.g., power, mass, duration, accuracy - imposed by in-situ analyses. In particular, sample return missions allow analyses at small spatial scale (down to angstroms), sample manipulation and the possibility to modify analytical experiments with evolving technology. Returned samples will be available for a long time after the end of the spacecraft mission and their analyses will be revisited as both our scientific understanding and analytical techniques will improve (Sandford, 2011). Sample return is also essential for the human exploration program to identify resources as well as human health and safety issues.

Example of sample return mission profiles and related operations are given in Table 14.1 and Table 14.2. They represent the closest approximation to human flight in overall goals, as a sample return shall complete a series of complex and linked tasks: each step of the mission must be completed successfully and connected to subsequent stages.

Sample Return Missions
DOI: 10.1016/C2018-0-03374-5

Table 14.1 Examples of Flyby, Touch-and-Go, and Surface Collections Missions.

Type	Planetary Body or Process	Sample type
Flyby		
	Mars, Venus	Atmospheric sample (dust, gas)
	Impact or volcanic plumes	Plume (dust, gas)
	Comet	Cometary dust
	Planetary Rings	Dust
	Solar Wind	High-energy particles
Touch-and-go		
	Moons	Regolith
	Asteroids	Regolith, organics
	Comets	Regolith, ices, organics
Surface Sampling		
	Comets	Regolith, ices, organics
	Asteroids	Regolith, rocks
	Moon/Mercury	Regolith, rocks, ices
	Mars, Phobos, Deimos	Regolith, rocks, ices, organics
	Venus	Regolith, rocks, atmosphere
	Moons of the outer planets	Regolith, rocks, atmosphere, organics

A scheme of the required operations and their interconnections is illustrated in the flow diagram in Fig. 14.1. The diagram highlights the similarities among all sample return missions, the differences due to mission configuration and to sample types, as well as the connections among technologies. The used technologies can have different complexity (Table 14.3), cost and risk.

The main issue associated with sample return missions is the high cost and risk, that require to be minimized, especially in view of conduction of sample return from a wide range of planetary bodies (asteroids, comets, small moons, Moon, Mars, Venus) on a regular basis. A cost and risk mitigation strategy consists in developing technologies, with different complexity, that could be appropriate for different mission profiles and targets (Table 14.4): this will increase the rate of success of sample return missions and will lower the overall cost. There are several types of technology/capability linkages that either are appropriate for several missions with minor modifications or feed forward to more complex missions: 1) linkages among different mission configurations (flyby, touch-and-go, surface landing) such as hard-landing on Earth and preserving environmentally sensitive samples; 2) linkages between a certain mission configuration

Table 14.2 Operations in different sample return mission types.

Mission Stage		Mission Type			
		Flyby	**Touch & go**	**Surface (static)**	**Surface (mobile)**
Pre-Lunch:					
	Sterilization protocols & verification procedures	x	X	x	x
Sampling:					
	Autonomous Positioning/Hazard Avoidance	/	X	x	x
	Pi-Poin Landing Capability	/	x	x	x
	Multiple Sampling Acquisition	/	x	x	x
	Multiple sites sampled	/	x	x	x
	Sample Acquisition & transfer mechanism	/	x	x	x
	Sample acquisition verification procedures	x	x	x	x
	Environ. Control on sample storage	(x)	(x)	(x)	(x)
(x) =related to the samples					

to a variety of planetary bodies, e.g. sample collection, manipulation, and storage on a planetary surface, or sample collection and verification of success during a touch-and-go mission, or inert collection material on a flyby mission.

The Moon, a close planetary body, should be a training field to test such technologies (except for gathering an atmospheric or volcanic plume sample during a flyby). In addition, it is a target of high scientific value for testing sample return.

14.2 Asteroid sampling systems

14.2.1 Sampling technologies for asteroids soil: state of art

Concerning the sample return missions from asteroids, a range of sampling methods have been investigated for the different kinds of mission listed in Table 14.3. The amount

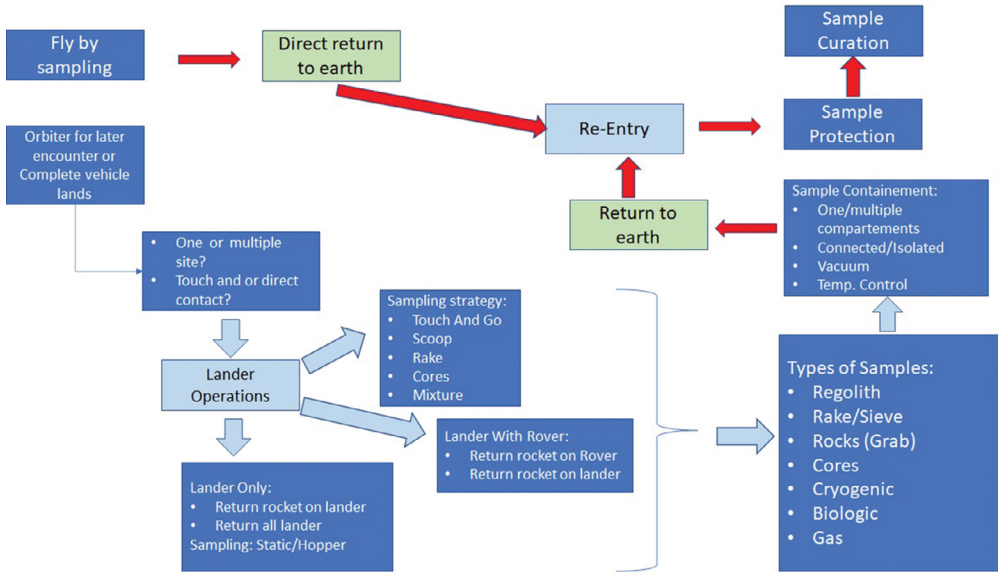

Fig. 14.1 Flow diagram schematizing the operations required for a sample return and their interconnections.

of sample material in the fly-by mission configuration is limited from the unique sampling site allowed, because of the high relative spacecraft speed with respect to the small body. On the other side, surface landing may be possible only as large missions (high cost cap) due to the difficulty of landing and performing mechanical operations in a low gravity environment. However, missions to asteroid surfaces are much simpler than those to comet nuclei (Section 3) due to the hazardous conditions presented by material ejection in cometary environments.

Asteroid sample return missions include a return capsule and a separation system, in addition to imaging, compositional analysis and physical properties testers payload and a sample handling system. The sampled material comes from the shallow surface to variable depths: millimeters to centimeters or decimeters, depending on the surface properties of the specific planetary body. Milligrams to grams of regolith and icy fines or plugs are collected. To allow the spacecraft to stay at a safe distance from the planetary body, proposed samplers can use either tethers, booms, or a release & recapture method.

Bartlett et al. (2007) proposed a classification of the sampling systems based on the interaction duration. The non-landed samplers, grouped as "*Sub-Second Interaction*" samplers, which engage and disengage from the surface almost instantaneously, have the lowest complexity and operational risk. This group of samplers include:

- *Impactors & collectors,* the simplest and coarsest method for surface sampling, using a mean to disturb the asteroid surface to observe the effects. Missions are proposed to send an impactor and a second spacecraft that collects and analyzes the ejected material.

Table 14.3 Simple, Intermediate, and Complex Sample Return Mission Concepts.

	Simple	Intermediate	Complex
Flyby sampling			
Spacecraft	Orbiter	Orbiter	Orbiter
Sample Type	Dust	Dust	Atmospheric/volcanic gases and dust
Mode	Fly through plume produced by projectile fired from spacecraft	Fly through plume/ atmosphere	Fly through volcanic plume
Sampling Mechanism	Aerogel (or Aerogel equivalent capture)	Aerogel (or Aerogel equivalent capture)	Canister+aerogel (or Aerogel equivalent capture
Touch-and-go sampling			
Spacecraft	Orbiter	Orbiter	Orbiter
Sample Type	Regolith	Regolith	Regolith+Rock. Ice
Mode	1 descent & grab	>1 descent & grab	>1 descent & grab at different sites
Sampling Mechanism	Tether & Scoop	Tether & Scoop	Tether, scoop, mechanical "hand"
Landed sampling			
Spacecraft	Lander (no rovers)	Fetch Rover	Sampling rover or hopper
Sample Type	Regolith	Regolith + rocks	Regolith, rocks, ices, gases
Mode	Sampling from lander on site	Sampling from lander multiple sites	Sampling from lander multiple sites
Sampling Mechanism	Scoop/Rake/Sieve	Sampling Cache	Scoop. "mechanical hand" corer, rake, or sieve.

- *Tethered harpoon,* offering high reliability even in cryogenic ices and on tilted surfaces. A tethered harpoon is fired to the surface, where it enables exchangeable robust tips to collect samples: this operation is feasible not only on loose granular material but also on consolidated ices, icy soils and brecciated soils. The material is then ejected into a sample handling device for analyses.
- *Adhesives*, feasible only for very brief encounter, using sticky substances to collect loose fines and small rocks on the surface of the planetary body.

Other samplers are used for the "Multiple Second Interaction", i.e. when acquisition of multiple samples and/or materials of higher strength, e.g. rock, is necessary, thus the sampler must be designed for a longer duration interaction. This scenario is satisfied by the:

- *Touch & Go Surface Sampler*, which includes high speed counter-rotating cutters to break into material and draw it into a sample cavity. A similar design has been

Table 14.4 Enabling Technologies for Sample Return.

1. Technologies that impact all sample acquisition types and all sample return mission scenarios:	
Pre-Launch	Sterilization protocols and verification procedures.
Sampling	Autonomous Positioning/Hazard Avoidance; Multiple sample acquisition; Sample acquisition and transfer mechanisms; Sample acquisition verification procedures. Sample Container Separation/isolation of separate samples to prevent cross contamination; Unreactive, strong sample containers; Sealing/resealing mechanisms for sample container; Sealing verification procedures.
Sample Return	Low mass lander/ascent vehicle infrastructure.
2. Technologies that impact most of sample types and of mission scenarios:	
Sampling	Pin-point landing capability.
Sample Container	Environmental monitoring (and control if appropriate) during time on the surface and during return; Abrasion between samples and the container needs to be minimized; Gas containment at different pressures to 1 bar;
Sample Return	Low mass lander/ascent vehicle infrastructure. Curation Development of cold/cryogenic curation and storage protocols; Development of gas curation and storage protocols.
3. Technologies required for specialized sampling/sample targets.	
Sampling	Ability to sample multiple sites.
Sample Container	Encapsulation: regular cores vs. irregular rocks vs. loose regolith samples vs. ice samples vs. astrobio samples vs. gas/atmospheric samples; Development of non-silicate aerogel for dust sampling.
Sample Return	Autonomous vertical alignment of ascent vehicle return.

developed for sample return cometary mission at JPL (see Section 3). Another sampler, adopting a brush-wheel sampler concept, was developed for the study of the Gulliver sample return mission to Deimos (Britt 2003). Both designs require booms to reach the mission target surface and to draw the sample to be returned back to the spacecraft.

14.2.2 Sampling systems used in past and present asteroid sample return mission

The JAXA/Hayabusa mission sampled the near-Earth asteroid Itokawa in 2005. The Hayabusa probe adopted the "touch and go" sampling scheme and used the combination of a shooting projectile and a fragment catcher to retrieve fragments from the surface ejected by the projectile shot.

The Hayabusa rendezvous spacecraft carried a horn that was designed to be brought up to the surface of Itokawa during the closest asteroid approaches. During each of these touch-and-go "landings", a 5 gram projectile was fired onto the surface at a velocity of a 300 m per second in order to blast a small quantity of material from the surface (2-A). The explosive-type system consists of three projectors, each of which had a stainless steel (SUS304) barrel with a diameter of 17 mm, a 4.85 g tantalum projectile with an aluminum alloy (A1070) sabot, and an explosion room. The projectile with the sabot was accelerated by explosion up to 300 ± 30 m/s inside the barrel. When the projectile hit a stopper, the sabot was halted at the end of the barrel and the projectile was separated from the sabot and shot to the asteroid surface. The surface dust and fragments from the impact were then captured by the horn (Fig. 14.2B) and funneled into a sample container (Fig. 14.2C) (Kubota et al. 2008). During the sampling, the catcher inlet surface covered the shot area, that was concealed from the main body of the spacecraft, in order to avoid fragments and dust hits on the spacecraft.

Fig. 14.3 shows a close-up of the sample transfer mechanics and the tube connecting with the sampler horn. Fragments ejected from the surface reached the sample catcher inside the spacecraft through the sample collection device, which was an extendible funnel-like cylinder mounted at the bottom of the spacecraft.

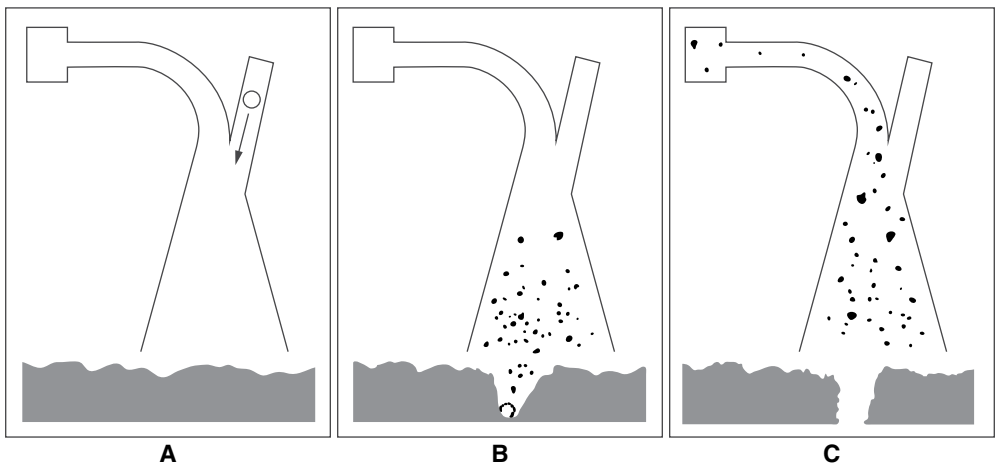

Fig. 14.2 ***Diagram showing the Hayabusa sample collection process.*** A projectile is fired at the asteroid and the fragments are then collected by the sampling system.

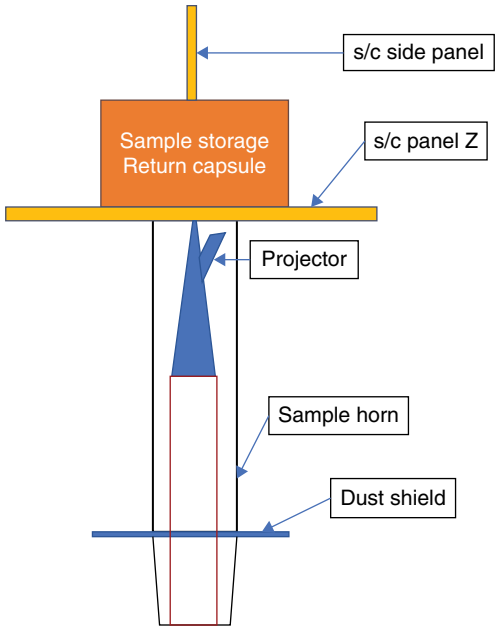

Fig. 14.3 Scheme of the sample recovery mechanics and the tube connecting with the sampler horn.

The JAXA/Hayabusa2 mission reached the asteroid Ryugu on 27 June 2018, and mapped the asteroid till 21 September 2018, when the spacecraft ejected the first two rovers, Rover-1A and Rover-1B, from about a 55 m altitude. The rovers worked nominally and transmitted data until 26 October Rover 1A and 24 September Rover 1B On 3 October 2018 the MASCOT (Mobile Asteroid Surface SCOuT) rover was deployed successfully and operated for about 16 h, as planned. The first surface sample retrieval took place on 21 February 2019. On 5 April 2019, Hayabusa2 released an impactor on the asteroid surface creating an artificial crater and exposing the sub-surface that was sampled on 11 July 2019.

The sampler system mounted on Hayabusa2 is based on a very simple but effective and reliable concept. It is composed of three main parts: 1) a sample storage and transfer mechanism; 2) a sampler horn, protruding from the bottom face of the spacecraft; 3) a projector.

The sampling operation foresaw the following phases: 1) a 5 g tantalum projectile was shot from the projector at a speed of 300 m/s inside the sampler horn as soon as sampler horn tip touched the asteroid surface; 2) the ejected material rose up through the sampler horn to a sample catcher; 3) closing of the sample catcher; 4) the reflector rotation mechanism was evacuated to allow the sample catcher to be transferred into a sample container enclosed in the Earth re-entry capsule.

The sampler system concept will allow an easy extraction after its return to the Earth. In addition to the soil sampler, a gas sampling interface is attached to the bottom

face of the sample container, which, when on Earth, can be attached to a vacuum line to extract volatile components by piercing the thinned part with a tungsten carbide needle (Okazaki et al., 2017).

The horn of the sampler is a cylinder 1007 mm long and a base of diameter of 140 mm, which is the area touching the asteroid surface during collection. When the sampler horn tip touched the surface, millimeter-sized pebbles were picked up by the scoop-up part, regardless of whether a projectile is fired or not. Even in case of positively charged surface pebbles (up to ~5 V; Colwell et al., 2005), particles larger than 100 micrometers could have been detached and collected in the sample catcher during the spacecraft deceleration operation.

The sample catcher is a cylindrical container divided in three chambers that store samples collected in different locations. With respect to Hayabusa, an extra chamber was added without changing the total volume, as the sample catcher size is constrained by the volume allocation in the re-entry capsule. The total volume of the three chambers is 48 cm^3: the catcher can thus store about 10 g of material, assuming a bulk density of 2 g/cm^3 and a yield coefficient of 10 percent. Each chamber is closed by the rotatable reflector itself after every sampling operation. As the same sampler horn is used for three touchdown operations, due to existent gaps between the rotatable inlet and the chamber walls, particles could have been mixed during successive samplings, especially those smaller than 100 μm, which are thus considered a global feature of the asteroidal surface (e.g., due to space weathering effect) (Tachibana et al. 2014).

In order to avoid contamination from the explosive system and projector itself, a sabot method was used for projectile shooting. Shapes and way to shooting the projectile have been investigated by Yano et al. (2009), but the final configuration selected use the same projectile-shooting sampling system used for Hayabusa.

Another present sample return mission from an asteroid is the NASA/OSIRIS-REx (Origins, Spectral Interpretation, Resource Identification, and Security–Regolith Explorer), whose target is the near-Earth asteroid Bennu. The spacecraft incorporates a Camera Suite (Rizk et al., 2018), a Visible and near- IR Spectrometer (Reuter et al., 2018), a Thermal Emission Spectrometer (Christensen et al., 2018), a Laser Altimeter (Daly et al. 2017), a student experiment and measurements of the asteroid gravity derived from the spacecraft communications system. In addition, a Touch-and-Go Sample-Acquisition Mechanism (TAGSAM) is mounted on the spacecraft to collect asteroid sample. TAGSAM is the product of Lockeed Martin internal research and development activities that explored a wide variety of techniques to sample the surfaces of small bodies. Following cleanliness protocols, the bulk of TAGSAM is made of aluminum alloy and includes stainless-steel parts and Mylar flap. The Touch-and-Go architecture was designed to: 1) minimize the contact time; 2) reduce sample handling complexity in the proximity of the surface; 3) reduce the variability of thermal states when in contact with the object; and 4) avoid the need to ensure long-term communications

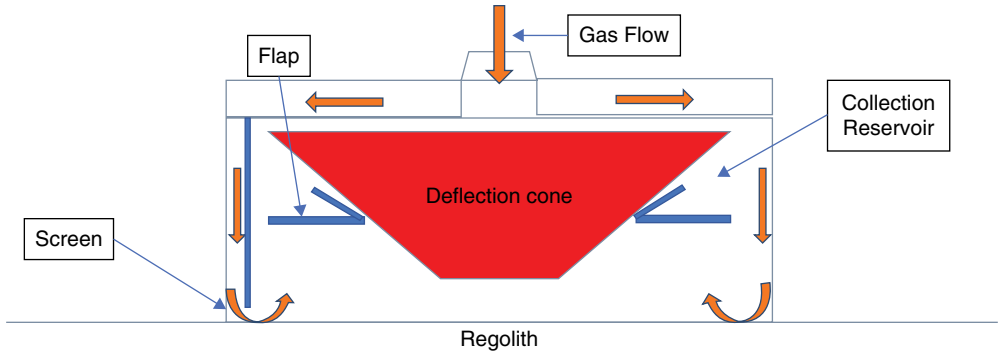

Fig. 14.4 TAGSAM scheme with labels identifying the components.

to Earth while on the surface. On-ground tests were performed to evaluate collection performance as a function of material type and grain sizes. They demonstrated a significant collection capability in a wide variety of materials and gravities, from 1-g and near zero-g (experienced during the parabolic airplane flights).

TAGSAM, shown in Fig. 14.4, consists of: 1) an arm with telescoping spring; 2) three pressurized bottles containing curation-grade nitrogen gas, with a small amount of helium (to check leaks prior to launch); 3) the sample collection "head"; 4) a u-joint between the arm and the head, optimizing the contact between the head and the local surface; 5) a container housing the head to maintain cleanliness during final ground processing, launch, and initial spacecraft outgassing.

The TAGSAM working principle is based on high-pressure gas flows through a feedline to the head into the regolith via an annular aperture. This process mobilizes the asteroidal material underneath the head as the gas expands into the regolith and support the sample collection.

A sample collection event starts with the arm positioning the collection head along the spacecraft center of mass, ~3 m far from the science deck plane. When the spacecraft touches the asteroid, the spring mounted in the arm mitigates the contact dynamics between the spacecraft and the surface and the control system starts the gas release (lasting 5 s), beginning the collection phase. On-ground tests demonstrated that TAGSAM requires a collection time <1 s (Bierhaus et al., 2018).

14.3 Cometary material sampling systems

14.3.1 Sampling technologies for cometary nuclei: state of art

The NASA Decadal Survey identified a Comet Surface Sample Return concept as a high priority mission for the next decade. This selection led to the study, development and tests of several mechanism and sampling tools to be used in future Touch-and-Go sample return mission. Starting from a comet surface strength within the range

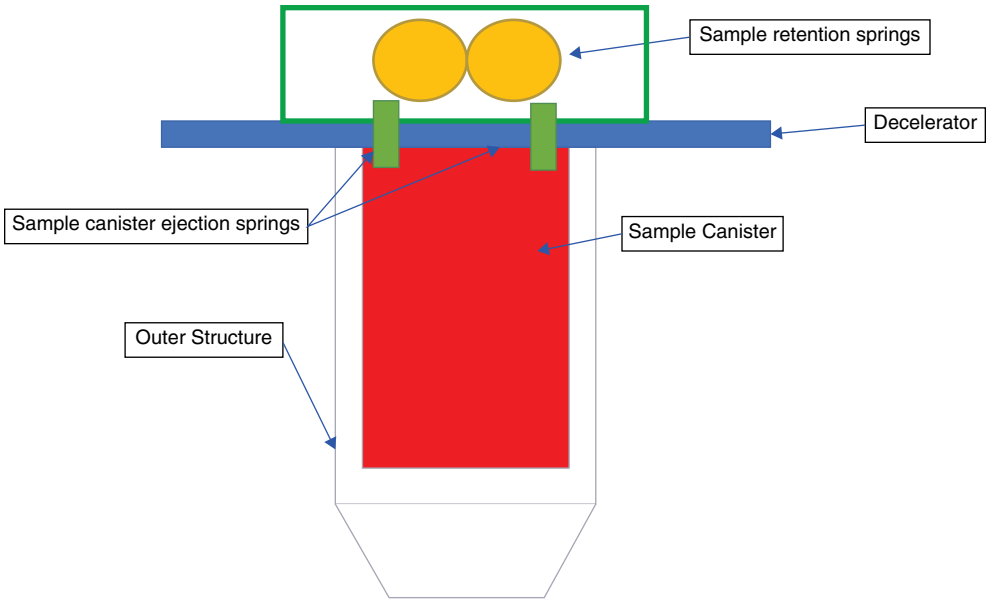

Fig. 14.5 Reactionless Drive Tube sampler design.

of 1 – 100 kPa, the requirements associated with sampling are to: 1) return a single ≥500 cm^3 sample from the surface of any comet nucleus; 2) preserve the sample complex organics (using a "soft" technique); 3) prevent sample aqueous alteration (maintaining the sample at ≤−10 °C). Additional requirements could be to capture evolved gases from the sample and to return material from depth >10 cm, maintaining sample stratigraphy.

Several technical solutions have been studied and tested for the Touch-And-Go configuration.

The Brush-Wheel-Sampler (BWS), developed at Jet Propulsion Laboratory, has two or three counter-rotating brushes capturing the surface material and drive it up and into a sample canister. The robotic arm deploys the BWS to the surface and, after collection, transfers the sample canister to a chamber mounted in the Sample Return Capsule. The BWS has the benefit of quickly capturing a large volume of sample (Bonitz et al. 2012).

The Reactionless Drive Tube (RDT) was developed to sample down to 10 cm depth maintaining the stratigraphy of the soil, but also minimizing reacted force to the spacecraft. The concept is to eject a sacrificial mass providing the reacted force for an impulsive sampling event. The RDT sampler (Fig. 14.5) consists of an outer shell structure, an inner sample canister, a decelerator, a sample retention mechanisms, and a sample canister ejection mechanisms (Zacny et al. 2015).

The Clamshell Sampler system (Fig. 14.6) is designed to acquire a cometary surface sample by driving two quarter-sphere buckets. A linear piston drives a linkage that

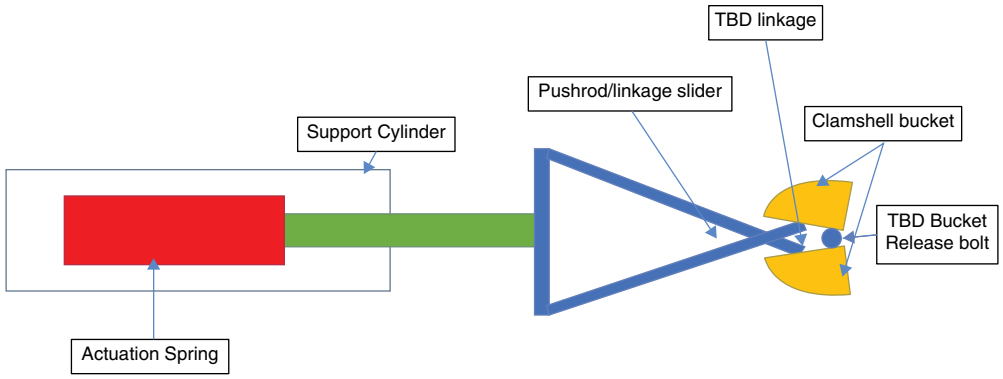

Fig. 14.6 Clamshell Sampler mechanism.

causes the two buckets to rotate around a common axis to close the buckets into each other. This mechanism allows to acquire and retain the sample in a single action. The thin walls of the sampler buckets guarantee a minimum sampling energy due to the very low volume displacement during the sampling event. Since the sampling action retains samples, there is no need for additional retention mechanisms within the sampler walls as would be required from drive tube sampling tools (Backes et al., 2014).

The BiBlade sampler (Fig. 14.7), supposed to be mounted at the end of a robotic arm, uses two blades controlled by sprigs to be driven into the cometary surface. The arm connection to the spacecraft is studied to let the forces react through the spacecraft center of mass, in order to safely push the spacecraft away from the comet during samples collection. The blades, once closed, encapsulate the sample before measurements and final deposition in the sample chamber. The sampling time is about 0.1 s, allowing the spacecraft to thrust away from the comet as soon as the sampling operation start (Backes et al., 2017).

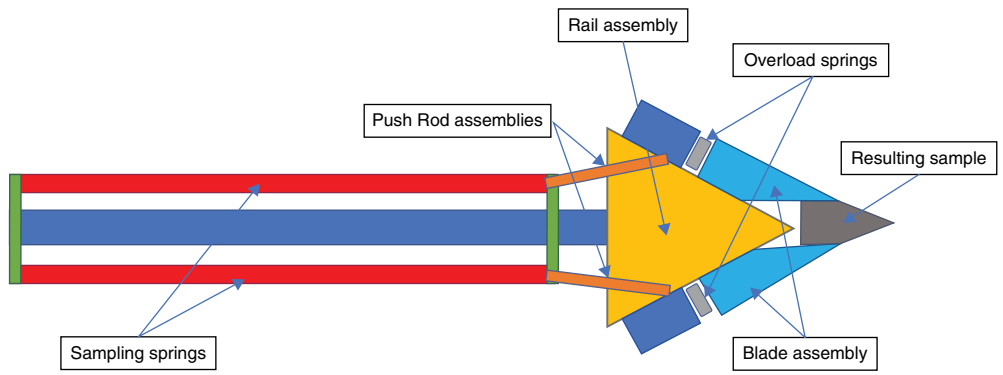

Fig. 14.7 BiBlade sampling system scheme.

14.3.2 Sampling technologies for cometary comae: state of art

Extensive laboratory experimentation and space flight testing demonstrated the feasibility to sample hypervelocity particles, i.e. >7 km/s: while hypervelocity particles impacting on metallic collector are mostly atomized, retaining only the original elemental compositions, Tsou (1990) spotted that they can survive in a low-density capture medium. Their experiment showed that the shock pressure of an aluminum particle impacting at 6 km/s a 16 mg/ml styrofoam is about 0.8 GPa, i.e., two orders of magnitude below the pressure inducing aluminum melting.

Polymer foams and fairly high-density aerogel (Tsou et al., 1990) were tested and proved to be successful capturing media for hypervelocity projectiles. However, foams were not compatible with space environment, but low density aerogels was successfully applied in Stardust space mission (see next subsection) and the returned dust particles were extracted and extensively analyzed (e.g. Brownlee et al., 2006; Sandford et al., 2006; Rotundi et al., 2008; 2014). The aerogel density threshold to prevent samples damage was determined to be about 50 mg/ml at impact speeds of around 6 km/s (Tsou, 1995).

14.3.3 Past comet sample return missions and recent mission studies

In 2006 the NASA/Stardust mission returned to Earth dust samples collected in the coma of the comet Wild 2 (Brownlee et al., 2006). Its sampling system (Fig. 14.8) contained three sets of flight components: the Sample Return Capsule (SRC), the Sample Canister (SC), and the Sample Tray Assembly (STA).

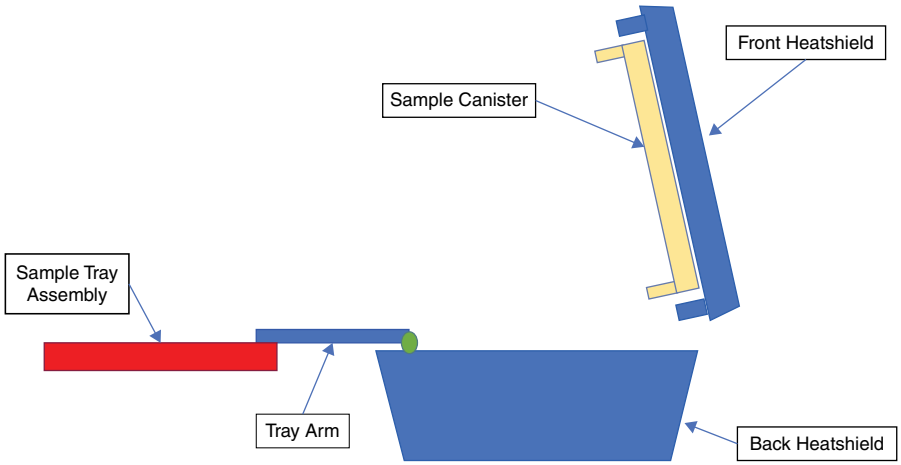

Fig. 14.8 ***NASA/Stardust's Sample Return Capsule scheme shown in the fully deployed position.*** The Sample Tray Assembly, consisting in two trays mounted back-to-back, for cometary dust and for interstellar dust collection, respectively, are made of an aluminium structure holding 130 aerogel blocks.

The SRC, about 80 cm in diameter and 50 cm in height, included a mechanism consisting of: 1) two clamshell latches; 2) one clamshell hinge; 3) two wrist motors to deploy the STA and associated gears.

The Sample Canister (SC) consisted of an aluminum honeycomb plate with aluminum face sheets, with a base 2.5 cm thick and about 60 cm wide, which served as an anchor surface for the STA and SRCs related mechanisms. The inner canister face sheet was 0.08 cm thick and made of bare aluminum. The SC aluminum cover, 50.3 cm in diameter and 10.2 cm in height, was sealed around the edges to prevent STA contamination.

The STA, mounted at the end of a tabular aluminum arm, 2.5 cm wide and 45.5 cm long, consists two different trays, made of non-anodized aluminum, mounted back-to-back for cometary and interstellar dust collection. Each tray holds 130 rectangular (4 × 2 cm) and two trapezoidal aerogel (microporous silicon material) capture cells, the most critical components. The cell thickness is the only difference between the two trays, being 3 cm for the cometary tray and 1 cm for the interstellar one. The cell rectangular shape, with four 0.635 cm rounded corners, was selected because it guaranteed: 1) a good mechanical strength; 2) a short optical path across one dimension, simplifying post-flight particle detection, analyses and removal; 3) low damage risk during installation (Tsou et al., 2003).

Other three missions proposed to the NASAs New Frontiers Program planned a cometary sample return.

The Comet Astrobiology Exploration Sample Return (CAESAR) mission was proposed to collect and return to Earth at least 80 g from a smooth terrain of the 67P/Churyumov-Gerasimenko comet nucleus (Lauretta et al., 2018). The sampling system was conceived to protect the volatile and the non-volatile component from contamination or alteration. The Sample Acquisition and Sample Containment Systems (SAS/SCS) mounting on a two degree-of-freedom compliant end joint would allow sampling surface sloped up to ± 15° A set of spring loaded would be included in the SAS/SCS to break up particles held together by cohesion. A pneumatic system, mounted on a robotic arm, would provide high purity nitrogen gas that would reach the surface by passing the sampling cone through pneumatic nozzles, and would funnel cometary particles into a centralized sample container: this operation would be performed by shaking nucleus surface particles by means of gas nozzles mounted near the sampling chambers outer perimeter, and then by directing them towards the inner gold-plated sample container. Then, another nozzle, closer to the funnel throat, would open a flexible Kapton flap, allowing the sample to flow into the sample container. Once stopped the gas flow, the flap would be closed, entrapping particles within the sample container (Lauretta et al. 2018).

The Comet Rendezvous, Sample Acquisition, Investigation, and Return (CORSAIR) mission was proposed to return a sample from a comet using a tethered

ballista or "harpoon" approach (Sandford et al., 2017). The ballista would be attached to the spacecraft by means of a spooled boom, which would provide bending stiffness to prevent the harpoon impact on the spacecraft. This sampling system would offer the following advantages: 1) absence of direct interaction with the comet surface; 2) ability to sample hard surfaces; 3) considerable depth of penetration, allowing the access to more pristine material with respect to the surface. The sampling operation would foresee: 1) a slow spacecraft descent toward the pre-selected sampling site down to a sampling altitude as detected by a laser altimeter; 2) firing the ballista into the cometary nucleus to encapsulate the sample; 3) retracting the harpoon while the spacecraft thrusts away from the comet (Sandford et al. 2017).

The COmet Nucleus Dust and Organics Return (CONDOR) mission was proposed to collect $a \geq 50$ g sample from the surface of comet 67P/Churyumov-Gerasimenko and bring it back to the Earth within 12.4 years and curated at ≤ −80 °C. In addition, it would foresee an onboard payload, i.e., a narrow angle camera and a mm-wave radiometer, to check for possible 67P changes with respect to the ESA/Rosetta mission (ended in 2016) observations of the same comet, to select a sampling site and to perform gravity science investigations. The sampling system (described in sub-Section 2.1), a BiBlade tool studied by JPL and constructed by Honeybee Robotics, is designed to acquire up to 590 cm^3 of comet material down to a 15 cm depth in a Touch-and-Go mission configuration. The sample would be stored inside the blades at temperature lower than −80 °C, within the CONDOR Sample Return Capsule (SRC), which would contain two sample vaults (each storing a 67P sample). Molecular sieves are integrated in the sample vault lids to capture volatiles potentially released by the samples (Choukroun et al. 2017).

14.4 Sampling dust in space and in the upper Earth stratosphere

The presence of interstellar dust dynamically coupled to the interstellar gas stream in the inner heliosphere has been confirmed by several spacecraft missions, such as NASA/Ulysses, NASA/Galileo (Gruen et al., 1993) and NASA-ESA/Cassini (Altobelli et al. 2016). This dust comes into the heliosphere from an ecliptic longitude of about 252. and an ecliptic latitude of about 2.5. with a 26 km/s velocity.

The Stardust probe collected and returned to Earth some interstellar particles (Westphal et al. 2014). Sampling occurred in the spacecraft orbit arc characterized by the lowest relative velocity between interstellar dust and spacecraft, minimizing the capture speed and therefore maximizing the probability to maintain sample particles intact. The collection of individual interstellar particles is affected by forces acting on them (solar gravity acceleration, solar radiation pressure and other forces playing a minor role, e.g., Lorentz forces) and by dust properties (i.e., charge, initial speed, size, density and sublimation rates). To simplify the instrument design, the sampling was focused

on those particles upon which acted a solar pressure equal to the solar gravity, i.e., the ratio between the two forces, b, was 1. Basing on calibration activities at the Max Plank Institute which demonstrated the submicron carbony iron sphere capture in aerogel at speeds higher than 10 km/s, it was concluded that the interstellar particles could have been collected by Stardust at encounter speeds below 15 km/s. Therefore, the Stardust orbit offered the opportunity to sample interstellar particles with $b = 1$, size between 0.1 and 0.9 mm, and encounter speeds between 7 and 15 km/s, during the infall arcs of three orbits (Tsou et al., 2003). Due to the larger speed of interstellar particles with respect to cometary dust particles, a lower aerogel density was considered, i.e. 20 mg/ml.

Interplanetary dust particles (IDPs) are usually collected in the terrestrial stratosphere. Solid and condensed nano- and micrometric particles in the stratosphere originate from both terrestrial and extra-terrestrial sources, but it is generally thought that upper stratosphere is dominated by extraterrestrial particles, such as samples of comets and asteroids, and lower stratosphere by terrestrial debris, mostly volcanic ash ejecta. Condensed particles can also be the result of meteor ablation. Meteoric dust in bolides is occasionally deposited into the lower stratosphere around 20 km altitude (Jenniskens, 2006).

IDPs collected in the stratosphere are distinct from meteorites and micrometeorites collected on the Earth's surface (Brownlee 1985; Sandford 1987). These differences can be attributed to a combination of selection effects, in particular the lower deceleration from cosmic velocities at high altitudes (~100 km), where the ram pressure is low (Whipple 1951). In fact, only a fraction of incoming extra-terrestrial mass is recovered at the Earth's surface because meteoroids decelerating in the atmosphere will typically loose about 85 percent of their mass but they are not completely vaporized ('shooting stars') (Rietmeijer, 2000; Rietmeijer et al. 2016). Consequently, fragile materials may survive atmospheric entry as small particles (<50 μm) but do not reach the ground. Stratospherically collected IDPs are therefore a unique and important class of extraterrestrial materials, also due to their chemical and mineralogical characteristics.

The stratospheric collection of IDPs followed decades of unsuccessful ground-level, sounding rocket, balloon, and aircraft collection efforts that were overwhelmed by terrestrial contaminants (Brownlee, 1978). In fact, the low accretion rate of cosmic dust particles (~1 m^{-2} day^{-1}) coupled with pervasive and abundant terrestrial dust necessitates sampling high volumes of very clean air to collect IDPs with a manageably low background (Brownlee 1985). This was first achieved by high altitude (~35km) balloon flights that pumped and filtered massive amounts of air (the so-called "Vacuum Monster" collector), followed by high altitude (~20 km) U2 aircraft flights (Brownlee et al., 1973; 1976).

IDPs are currently collected by NASA high-altitude WB-57 aircraft using essentially the same techniques established over 40 years ago (Warren and Zolensky, 1994), i.e.,

inertial impact onto flat-plate collectors. The collectors consist of flat Lexan™ surfaces coated with highly viscous (500,000 centistokes) silicone oil that prevents particles from bouncing off during impact (Brownlee et al., 1976). Silicone oil is applied in a dilute mixture with Freon in several stages, ultimately leaving a uniform ~10 μm-thick coating on the collector surface after Freon evaporation. Impacting particles are effectively trapped and localized in the silicone oil, even if they can be broken during collection. However, concerns have been raised about influence of silicone oil on compositional measurements of GEMS (Glass with Embedded Metal and Sulphides) (Keller et al. 2011) grains in IDPs (Bradley et al., 2011). Silicone oil could have been deleterious especially for IDP organics analyses, because it exhibits infrared C-O and C-H spectral bands that overlap the IDP organic phases bands, including the important aliphatic C-H stretching band at 3.4 μm. p polyurethane foam substrate for the first oil-free stratospheric collection of IDPs.

Polyurethane foam substrate is a recent alternative to silicone oil (Kavouras and Koutrakis, 2001). Collected particles adhere to the polyurethane foam substrate by van der Waals and electrostatic forces and no other surface treatments are used to enhance particle collection or retention: this process, referred to as "dry collection", does not require to clean the collected particles with solvents prior to analysis. In a detailed set of laboratory analog impact experiments, Kavouras and Koutrakis (2001) showed that open pore polyurethane foam substrates systematically outperformed oil-coated metal in collection efficiency (>97 percent versus 92 percent) of small particles and collected smaller particles (1.1 versus 2.5 μm) for impact velocities of ~20 m/s (Messenger et al. 2015).

Extraterrestrial dust particles can be collected in the Earth upper stratosphere also by balloon-borne instruments (Testa et al., 1990, Della Corte et al., 2012). The DUSTER (Dust from the Upper Stratosphere Tracking Experiment and Retrieval) instrument (Fig. 14.9) was designed to collect nanometer to micrometer scale solid aerosol particles in the upper stratosphere (between 30 and 40 km) on board balloons (Della Corte et al., 2012). It performed six successful flights (2008–2019), collecting dust particles, whose laboratory study confirmed their extraterrestrial origin.

The use of balloons as a mean to reach the upper stratosphere requires active systems for stratospheric aerosol sampling and decoupling from the air stream. The inertial separation is a well-established technique to this aim: a particle moving in a gas stream can be separated from the flow and deposited on a target in its path. As the gas stream deflects around the obstacle, the particle continues toward the target stitching on the collecting surface.

The DUSTER design aimed at overcoming the limitations identified in the previous collections such as contamination control and the use of sticking material to entrap

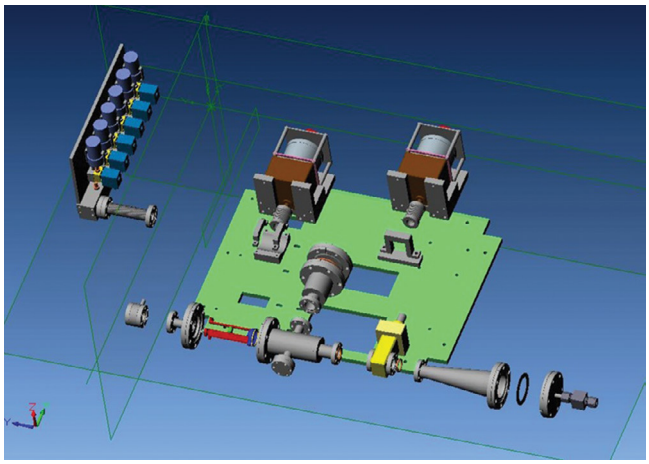

Fig. 14.9 DUSTER sampling system design.

particles. Prior the DUSTER experiment, the major contamination sources of dust collected by means of balloons were exhaust from pumping systems and dust deposited on the balloon and equipment during launch and ascent. Additional contamination would be possible at the landing site. Addressing these problems, DUSTER included a collection chamber that could be sealed by Ultra-High Vacuum (UHV) valves when in non-sampling mode and a one shot mechanism that sealed the inlet pipe prior to reaching 20 km of altitude (Della Corte et al., 2012; 2014).

14.5 The future: planetary sampling systems

14.5.1 Technologies for soil sampling in future Mars & Moon space mission

The Mars Sample Return Campaign is an effort to return samples of Martian rocks and soil to be investigated in unprecedented detail, using the state-of-the-art analytical laboratory techniques. It is part of the NASAs Mars Exploration Program, a long-term plan of Mars robotic exploration. NASA is collaborating with the European Space Agency (ESA) to develop the advanced technologies and hardware needed for the campaign.

The main scientific objectives achievable by the Mars Sampling return campaign have been identified in interpretation of geologic processes and their relation to volatiles, assessment of biological history, determination of evolutionary timeline, preparation for future human exploration by identifying environmental hazards and in-situ resources (Beaty et al. 2019).

The NASA/Mars2020, to be launched at time of writing, is preparatory to future sample return from Mars. It plans to acquire approximately 20–40 cores, each with a

mass of approximately 10 gs, and place them in a cache for future return (Backes et al., 2011). When an average rock density of 2.5 g/cm^3 will be considered, the resulting required rock volume will be 4 cm^3, that would imply core dimensions of 1 cm in diameter and 5 cm long. The most important payload is the Sample Acquisition and Cache system, formed by a drill, a robotic arm to deploy the drill, and a Sample Handling and Caching system. The nominal operational sequence is: i) acquisition of a rock core or regolith sample, ii) depositing the sample inside the Sampling handling and caching system, and iii) picking up a new bit (if necessary) for the next sampling sequence.

To help in-situ investigations, rocky samples could be brushed and abraded whereas small cores acquired from a rock could be inspected along its length via non-contact instruments. The sample selection tasks for the Mars 2020 mission may be identified as reported in Table 14.5.

The Sample Acquisition and Cache system is equipped with four different bits, that will allow the operation listed above and are described in detail below. All four types of bits can be deployed using the same drill.

Brushing and Abrading Tool (BAT), Bit #1 and #2: this bit is a combination of two bits into one system. Inherited from the Mars Exploration Rovers Rock Abrasion Tool concept (Gorevan et al. 2003), this system is driven by a rotary actuator, consisting of a gearbox containing a number of nested gears and high velocity rotating brushing and abrading bits revolving at the same time. BAT has two operational modes: 1) abrading the rock and brushing it continually to clear the powder off the rock; 2) purely brushing the rock surface, with the grinding bit rotating above the surface.

Core Pre-ViewBit (CPVB), Bit #3: this bit is designed to acquire short cores for in-situ analysis and to cache samples of great scientific value (Pratt et al., 2010). The CPVB has side slots in the break-off tube, which is rotated during the drilling process to open each side slot. During the break-off stage, the inner tube is rotated again to close the side slot and contemporarily to shear and captures the core avoiding its fall out. To dispense the core onto a tray, the breakoff tube is rotated 180° upside down.

Table 14.5 Scenario for the Mars 2020 mission.

Task #	Description
1	Brushing rocks for in situ analysis (as done by the Rock Abrasion Tool on MER and will be done by the Dust Removal Tool on the Mars Science Laboratory (MSL) rover)
2	Abrading rocks for in situ analysis (as done by the Rock Abrasion Tool on MER)
3	Acquiring rock powder and regolith for in situ analysis and/or sample return (as will be done on the MSL)
4	Acquiring a 1 cm diameter by 2 cm long preview core for in situ analysis and/or sample return
5	Acquiring a 1 cm diameter by 5 cm long core for return back to earth

Powder and Regolith Acquisition Bit (PRAB), Bit #4: As for the Mars Science Laboratory rover drill (Okon, 2010), the PRAB can be used to acquire regolith and rock cuttings during the drilling process. The acquired sample can be either dispensed into an instrument inlet port to be analyzed in situ or cached for sample return.

Caching Bit (SLOT), Bit #5: The SLOT acquires cores that will be returned to Earth. It is a fourth generation of rotary percussive core bits, based on Honeybee Robotics most recent core bit designs (Zacny et al., 2014). In the framework of the Mars Sample Return, it should collect at least 10 gs: this means that, considering an average rock density of 2.5 g/cm^3, the required core volume is approximately 4 cm^3, i.e. a cylindrical core with 1 cm of diameter and 5 cm of length. However, the development of the tool results in a smaller diameter and longer core (Zacny et al., 2012), e.g., 0.8 cm of diameter and 7.8 cm of length.

SLOT, once closed along length of the coring bit, allows simple visual inspection of entire core sample before caching, enabling in-situ analysis critical to determine the core volume before its caching.

The detachable scoop for planetary surfaces, currently designed for Mars, is an alternative solution for planetary surface sampling systems. In its current design, it should be mounted and operate on board a rover platform. It consists of a detachable titanium scoop, a motorized scoop clamping mechanism, to attach and detach scoops, and a cache container. The detachable titanium scoops, cut from a single titanium block, allows sampling up to 68 cm^3 of material. The scoop clamping mechanism, positioned on top of the scoops, allows to grip onto sample scoops, to hold them during scooping operations, and to release them for sample caching (Younse et al., 2009).

Another example of planetary surface sampling system is the device designed for Chinese Lunar exploration (Lin et al. 2018). This exploration program is operating in three stages: 1) orbiting; 2) landing; 3) sample return. In stage 1, the satellite orbited and probed the Moon along a 200 km orbit. In stage 2, a lander and a rover were deployed on the lunar surface for in-situ exploration. The next step is the stage 3 (the CNSA/Chang'e 5 mission was launched in November 2020, see Xiao et al., this book) which used a Surface Sample Acquisition and Caching Device (SSACD) (Fig. 14.10), consisting of:

1. Scoop & Funnel, i.e., the sampling mechanism and the pipe used to transfer the sample from the scoop to the container, respectively.
2. Shell & Linker, i.e., the external shield preventing contamination of the actuation system.
3. Actuation System, to vibrate the scoop and to detach the sample container from the sample acquisition device.
4. Sample Container, to cache the collected sample.
5. Locking System, i.e., a triggered passive mechanism to seal the Sample Container during return.

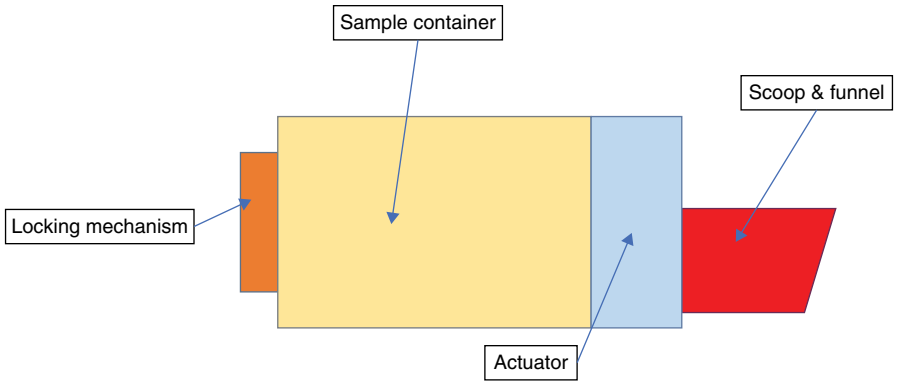

Fig. 14.10 Scheme of the Surface Sample Acquisition and Caching Device that will be used for CNSA/Chang'e5 mission.

The scoop design is compliant with the stringent requirements on mass, on power compatibly with low digging resistance and on high collection efficiency. A bionic design might improve the digging efficiency up to 30 percent (Zhang et al. 2013): three typical shapes of animals' claw (pangolin, field mouse and mole) have been simulated to check for the best scoop performances. The field mouse claw shape was selected as the one having the lowest digging resistance.

The sample container design, consisting of an upper lid, a container body, and a lower lid, allows an easy manufacture and assembling (Li et al. 2013).

Sample collection devices can also use pressurized gas to collect sample from a planetary surface, as in the case of PlanetVac (Fig. 14.11). The instrument can be separated into two distinct parts: the sampler cone and the sample container. The sampler cone is where the sampling process induced by nuzzles occurs. In particular, pneumatic nozzles push high pressure gas into the surface in order to stir the regolith up and move the sample towards the sample container. A flap nozzle, pointed towards the sample container, enhances the sample collection into the container. The successive gas evacuation from the sample container is allowed through a dedicated filter. These nozzles are designed to maximize the sample movement towards the container but preventing the "blow out" around the edge in contact with the planetary surface, which would reduce the collection efficiency.

Depending on the regolith characteristics, the sample motion to the sample container follows two different transport methods: rules of particle transport in fluid for sub-cm particles and motion dominated by the momentum imparted by the gas for particles larger than 1 cm. The dominant transport method is a strong driving factor in the sampling system design, thus the PlanetVac needs to be customized for the planetary body, target of the mission (Spring et al., 2019).

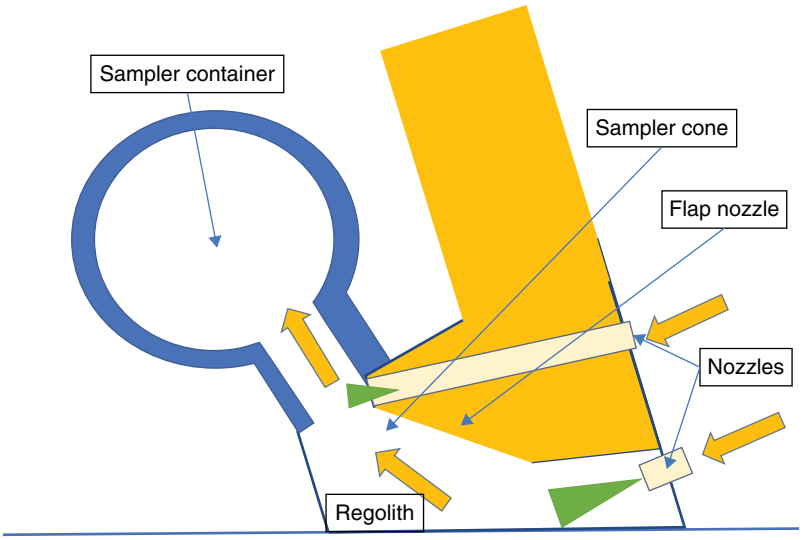

Fig. 14.11 Left panel: PlanetVac Xodiac sampler structure. Right panel: visualization of the collection process scheme.

14.5.2 Technologies for atmosphere sampling in future Mars space missions

Sampling Mars atmosphere would be critical to understand Mars origin and its ability to support life. However, it is a very complex task with several requirements. The Mars Exploration Program Analysis Group (Beaty et al., 2019) recommends a minimum amount of 1.9×10^{-5} Mole of atmosphere, which corresponds to a volume of 50 m^3, following the ideal gas law at Mars ambient temperature and pressure. In addition, a second sampling at a different pressure would be desired. MEPAG fixed the minimum size of the sampler, by considering the capabilities of mass spectrometers available and taking into account that 50 percent of the sample should be available for future science. Starting from the dimensions of the existing Mars Sample Return design lid, a preliminary sample canister was designed. The sample is supposed to be collected in two steps: 1) the atmospheric sample is collected by releasing the first valve allowing air to flow into the chamber; 2) after the valve is closed the sample is drawn into the canister via holes in the valve mounting surfaces.

14.6 Conclusions

Sample return missions have proven their value allowing scientific advances not reachable by in-situ space missions. These results represent the driving force to endure the challenge and provide incentives for the development of new sampling systems optimized for specific sample return mission profiles. This optimization will lead to

increasingly important discoveries that will allow us to continue the path towards understanding the two fundamental questions of Solar System formation and life birth on the Earth.

References

Altobelli, N., Postberg, F., Fiege, K., Trieloff, M., Kimura, H., Sterken, V.J., Hsu, H.W., Hillier, J., Khawaja, N., Moragas-Klostermeyer, G., Blum, J., Burton, M., Srama, R., Kempf, S., Gruen, E., 2016. Flux and composition of interstellar dust at Saturn from Cassini's cosmic dust analyzer. Science 352 (Issue 6283), 312–318. doi:10.1126/science.aac6397 15 Apr.

Backes, P., 2011. Experimental results of rover-based coring and caching, Aerospace Conference, 2011. Big Sky, MT, pp. 1–14. doi:10.1109/AERO.2011.5747263.

Backes, P., 2017. BiBlade sampling tool validation for comet surface environments, IEEE Aerospace Conference, 2017. Big Sky, MT, pp. 1–20.

Backes, P., et al., 2014. Sampling system concepts for a touch-and-go architecture comet surface sample return mission, AIAA SPACE 2014 Conference and Exposition.

Bartlett, P.W., et al., 2007. Asteroid & comet surface sampling methods from non-landed spacecraft. Workshop on Spacecraft Reconnaissance of Asteroid and Comet Interiors(LPI Contribution No. 1325). 1325.

Beaty, D.W., et al., 2019. The potential science and engineering value of samples delivered to earth by mars sample return: international MSR objectives and samples team (iMOST). Meteorit. Planet. Sci. 54, S3–S152.

Bierhaus, E.B., et al., 2018. The OSIRIS-REx spacecraft and the touch-and-go sample acquisition mechanism (TAGSAM). Space Sci. Rev. 214 (7), 107.

Bin, Z., Min, Y., Huayong, Y, 2013. A review of encapsulation techniques for planetary samples [J]. Spacecraft Environment Engineering, 1.

Bonitz, R., 2012. The brush wheel sampler — a sampling device for small-body touch-and-go missions, IEEE Aerospace Conference, 2012. Big Sky, MT, pp. 1–6.

Bradley, J.P., Wozniakiewicz, P.J., Ishii, H.A, 2011. Constraints on the cosmochemical significance of element/si ratios and oxygen isotopic compositions of GEMS from IDPs collected in silicone oil. Lunar and Planetary Science Conference 42.

Britt, D.T., 2003. The gulliver mission: sample return from the martian moon deimos. Lunar and Planetary Science Conference. 34.

Brownlee, D.E., 1978. Microparticle studies by sampling techniques. Cosmic dust, 295–336.

Brownlee, D.E., et al., 1973. Some physical parameters of micrometeoroids, Lunar and Planetary Science Conference Proceedings, 4.

Brownlee, D.E., Ferry, G.V., Tomandl, D, 1976. Stratospheric aluminum oxide. Science 191 (4233), 1270–1271.

Brownlee, D.E., 1985. Cosmic dust: collection and research. Annu. Rev. Earth Planet. Sci. 13 (1), 147–173.

Brownlee, D., et al., 2006. Comet 81P/wild 2 under a microscope. Science 314 (5806), 1711–1716.

Choukroun, M., Raymond, C., Wadhwa, M., 2017. for the CONDOR science team EPSC, COmet nucleus dust and organics return (CONDOR): a new frontiers 4 mission proposal abstracts vol. 11, EPSC2017-413. European Planetary Science Congress, 2017.

Christensen, P.R., et al., 2018. The OSIRIS-REx thermal emission spectrometer (OTES) instrument. Space Sci. Rev. 214 (5), 87.

Colwell, J.E., et al., 2005. Dust transport in photoelectron layers and the formation of dust ponds on Eros. Icarus 175 (1), 159–169.

Daly, M.G., et al., 2017. The OSIRIS-REx laser altimeter (OLA) investigation and instrument. Space Sci. Rev. 212 (1–2), 899–924.

Della Corte, V., Rietmeijer, F.J.M., Rotundi, A., Ferrari, M., 2014. Introducing a new stratospheric dust-collecting system with potential use for upper atmospheric microbiology investigations. Astrobiology 14 (Number 8). doi:10.1089/ast.2014.1167 Mary Ann Liebert, Inc.

Della Corte, V., Palumbo, P., Rotundi, A., et al., 2012. In situ collection of refractory dust in the upper stratosphere: the DUSTER facility. Space Sci. Rev. doi:10.1007/s11214-012-9918-9.

Gorevan, S.P., et al., 2003. Rock abrasion tool: mars exploration rover mission. Journal of Geophysical Research: Planets 108 (E12).
Grün, E., et al., 1993. Discovery of Jovian dust streams and interstellar grains by the Ulysses spacecraft. Nature 362 (6419), 428–430.
Jenniskens, P.Petrus Matheus Marie Jenniskens, 2006. Meteor showers and their parent comets. Cambridge University Press.
Li, C., Xie, Z., Liu, H., 2013. Surface Sample Acquisition and Caching Device for Chinese lunar sample return plan, IEEE International Conference on Robotics and Biomimetics (ROBIO), 2013. Shenzhen, pp. 2599–2604.
Kavouras, I.G., Koutrakis, P, 2001. Use of polyurethane foam as the impaction substrate/collection medium in conventional inertial impactors. Aerosol Science & Technology 34 (1), 46–56.
Keller, L.P.Scott Messenger, 2011. On the origins of GEMS grains. Geochim. Cosmochim. Acta 75 (18), 5336–5365.
Lauretta, D.S., et al. "The CAESAR new Frontiers Mission: 2". Sample Science. (2018).
Lin, X.U., Yongliao, Z.O.U., Yingzhuo, J.I.A, 2018. China's planning for deep space exploration and lunar exploration before 2030. 空间科学学报 38 (5), 591–592.
Messenger, S., Nakamura-messenger, K., Keller, L.P., and Clemett S.J., Pristine stratospheric collection of interplanetary dust on an oil-free polyurethanefoam substrate, meteoritics & planetary science 50, Nr 8, 1468–1485 (2015) doi:10.1111/maps.12473.
Okazaki, R., et al., 2017. Hayabusa2 sample catcher and container: metal-seal system for vacuum encapsulation of returned samples with volatiles and organic compounds recovered from C-type asteroid Ryugu. Space Sci. Rev. 208 (1–4), 107–124.
Okon, A.B. "Mars Science Laboratory Drill." (2010).
Pratt, L.M., et al., 2010. The mars astrobiology eXplorer-Cacher (MAX-C): a potential rover mission for 2018. Astrobiology.
Reuter, D.C., et al., 2018. The OSIRIS-REx visible and infrared spectrometer (OVIRS): spectral maps of the asteroid Bennu. Space Sci. Rev. 214 (2), 54.
Rietmeijer, F.J.M., 2000. Interrelationships among meteoric metals, meteors, interplanetary dust, micrometeorites, and meteorites. Meteorit. Planet. Sci. 35 (5), 1025–1041.
Rietmeijer, F.J.M., et al., 2016. Laboratory analyses of meteoric debris in the upper stratosphere from settling bolide dust clouds. Icarus 266, 217–234.
Rizk, B., et al., 2018. OCAMS: the OSIRIS-REx camera suite. Space Sci. Rev. 214 (1), 26.
Rotundi, A., et al., 2008. Combined micro-Raman, micro-infrared, and field emission scanning electron microscope analyses of comet 81P/wild 2 particles collected by Stardust. Meteorit. Planet. Sci. 43 (1208), 367–397 2.
Rotundi, A., et al., 2014. Two refractory Wild 2 terminal particles from a carrot-shaped track characterized combining MIR/FIR/Raman microspectroscopy and FE-SEM/EDS analyses. Meteorit. Planet. Sci. 49 (4), 550–575.
Sandford, S.A., Chabot, N.L., Dello Russo, N., Leary, J.C., Reynolds, E.L., Weaver, H.A., Wooden, D.H.The CORSAIR Team, 2017. CORSAIR (COmet Rendezvous, Sample Acquisition, Investigation, and Return): a New Frontiers Mission Concept to Collect Samples from a Comet and Return them to Earth for Study, 80th Annual Meeting of the Meteoritical Society. LPI Contrib. No. 1987.
Sandford, S.A. "The collection and analysis of extraterrestrial dust particles." (1987).
Sandford, S.A., et al., 2006. Organics captured from comet 81P/wild 2 by the stardust spacecraft. Science 314 (5806), 1720–1724.
Sandford, S.A., 2011. The Power of Sample Return Missions - Stardust and Hayabusa, The Molecular Universe, Proceedings of the International Astronomical Union, Volume 280. IAU Symposium, pp. 275–287. doi:10.1017/S174392131102504X.
Spring, J., et al., 2019. Planetvac xodiac: lander foot pad integrated planetary sampling system, IEEE Aerospace Conference, 2019. Big Sky, MT, USA, pp. 1–9.
Tachibana, S., et al., 2014. Hayabusa2: scientific importance of samples returned from C-type near-earth asteroid (162173) 1999 JU3. Geochem. J. 48 (6), 571–587.
Kubota, T., Otsuki, M., Hashimoto, T., 2008. Touchdown dynamics for sample collection in hayabusa mission, IEEE International Conference on Robotics and Automation, 2008. Pasadena, CA, pp. 158–163. doi:10.1109/ROBOT.2008.4543202.

Testa, John P., Jr., Stephens, John R., Berg, Walter, Cahill, Thomas A., et al., 1990. Collection of microparticles at high balloon altitudes in the stratosphere. Earth and Planetary Science Letters. 98 (3–9), 287–302. doi:10.1016/0012-821X(90)90031-R.

Tsou, P, 1990. Intact capture of hypervelocity projectiles. Int. J. Impact Eng. 10 (1–4), 615–627.

Tsou, P, 1995. Silica aerogel captures cosmic dust intact. J. Non Cryst. Solids 186, 415–427.

Tsou, P., Brownlee, D.E., Sandford, S.A., Ho¨rz, F., Zolensky, M.E., 2003. Wild 2 and interstellar sample collection and earth return. J. Geophys. Res. 108 (NO. E10, 8113). doi:10.1029/2003JE002109.

Warren, J.L., Zolensky, M.E, 1994. Collection and curation of interplanetary dust particles recovered from the stratosphere by NASA, *AIP Conference Proceedings*. Vol. 310. American Institute of Physics No. 1.

Westphal, J., Bridges, J.C., Brownlee, D.E., Butterworth, A.L., Gregorio, B.TD.E., Dominguez, G., Flynn, G.J., Gainsforth, Z., Ishii, H.A., Joswiak, D., Nittler, L.R., Ogliore, R.C., Palma, R., Pepin, R.O., Stephan, T., Zolensky, M.E., 2017. The future of stardust science. Meteorit. Planet. Sci. 52 (Nr 9), 1859–1898. doi:10.1111/maps.12893.

Westphal, A.J., et al., 2014. Evidence for interstellar origin of seven dust particles collected by the stardust spacecraft. Science 345 (6198), 786–791.

Whipple, F.L., 1951. The theory of micro-meteorites: part II. In heterothermal atmospheres. Proc. Natl. Acad. Sci. U.S.A. 37 (1), 19.

Xiao, L. et al., this book. The Chang'e 5 mission, Chapter 9.

Yano, H., et al., 2009. Development of sampling systems for small solar system bodies onboard the hayabusa follow-on missions, Proceedings of the 27th International Symposium on Space Technology and Science.

Younse, P., et al., 2009. Sample acquisition and caching using detachable scoops for mars sample return, IEEE Aerospace conference, 2009. Big Sky, MT, pp. 1–12.

Zacny, K., Avanesyan, A., Paulsen, G., Craft, J., Chu, P., Szwarc, T., 2012. Mars drill for the mars sample return mission with a brushing and abrading bit, regolith and powder bit, core preview bit and a coring bit, IEEE Aerospace Conference, 2012. Big Sky, MT, pp. 1–8.

Zacny, K., Chu, P., Davis, K., Paulsen, G., Craft, J., 2014. Mars2020 sample acquisition and caching technologies and architectures, IEEE Aerospace Conference, 2014. Big Sky, MT, pp. 1–12.

Zacny, K., et al., 2015. Pyramid comet sampler (PyCoS). AIAA SPACE 2015 Conference and Exposition.

CHAPTER 15

Recovery and transport of samples

Fabrizio Dirri[a], Andrea Longobardo[a], Ernesto Palomba[a], Lucy Berthoud[b,f], Aurore Hutzler[c,d], Caroline L. Smith[e,g], Sara S. Russell[e]

[a]INAF-IAPS, Rome, Italy
[b]Thales Alenia Space UK Limited, Bristol
[c]Lunar and Planetary Institute, USRA, Houston, TX, USA
[d]Astromaterials Research and Exploration Sciences, NASA JSC, Houston, TX, USA
[e]Department of Earth Sciences, The Natural History Museum, London, UK
[f]University of Bristol, Queen's Building, University Walk, Clifton, UK
[g]School of Geographical and Earth Sciences, University of Glasgow, Glasgow, UK

Chapter Outlines

15.1 Introduction

Sample Return Missions (SRMs) allow for the availability to the scientific community of samples coming directly from a planetary body or interplanetary medium. To ensure the best possible science outcome, the samples must be kept pristine, without any

Sample Return Missions
DOI: 10.1016/C2018-0-03374-5

interference from the terrestrial environment (as occurs, for example, in meteorites). This means that Earth Return Capsule (ERC) recovery and transport of samples, both from landing site to curation facility and subsequently among laboratories, must have as their primary duty to preserve the samples from terrestrial contamination (forward contamination).

In the case of restricted samples, i.e., returned from bodies with an astrobiological potential as defined by COSPAR (Kimnek et al. 2017) (such as Mars, Europa or Enceladus), these operations must take into account the backward contamination, which is the interaction between non-terrestrial and terrestrial organisms. With at least one Mars sample return mission being moved forward with the upcoming launch of NASAs Mars 2020, and others in the making (e.g. CNSA missions), the scientific community is getting ready for this challenge and, in particular, how the recovery and transport samples should take place. These procedures must take into account the Planetary Protection requirements specific for each body and, in specific cases, the indications given by the World Health Organization (WHO).

The present chapter describes how previous and upcoming SRMs (e.g. Osiris-REx) recovered the ERC, and lists lessons learned from the missions. It also describes techniques and technologies first for transporting ERCs and samples.

Section 2 introduces the landing sites considered for previous and upcoming SRMs and how their environmental conditions have influenced the transportation box design and recovery and transport operations. Section 3 describes the landing site operations, the transportation methods and the lessons learned from the various SRMs performed so far. Section 4 is devoted to requirements for restricted samples and to regulatory issues concerning packaging and transport of potentially hazardous samples.

15.2 Landing sites

The landing sites of SRMs have stringent rules in terms of climate, presence of population and buildings, and military restrictions. The best candidate of an SRM landing site should be isolated and a remote area sparsely populated, like military areas, desert and steppe regions. Military areas, e.g. Utah Test and Training Range in the US, would give more advantages in terms of signal and visual control of re-entry capsule (by using military facilities), but it is not always accessible.

This section describes the following landing sites (Fig. 15.1), either selected in the past or candidate for future SRMs, and their influence on re-entry capsule recovery, based on their environmental conditions: Kazakh steppe (KZ), Siberia area (RUS); UTTR (Utah Test and Training range, USA), WAS (White Sand Area, USA), WFF (Wallops Flight Facility, USA), WPA (Woomera Prohibited Area, AUS), VTR (Vidsel Test Range, SWE), MNG (Siziwang Banner Area, CHN).

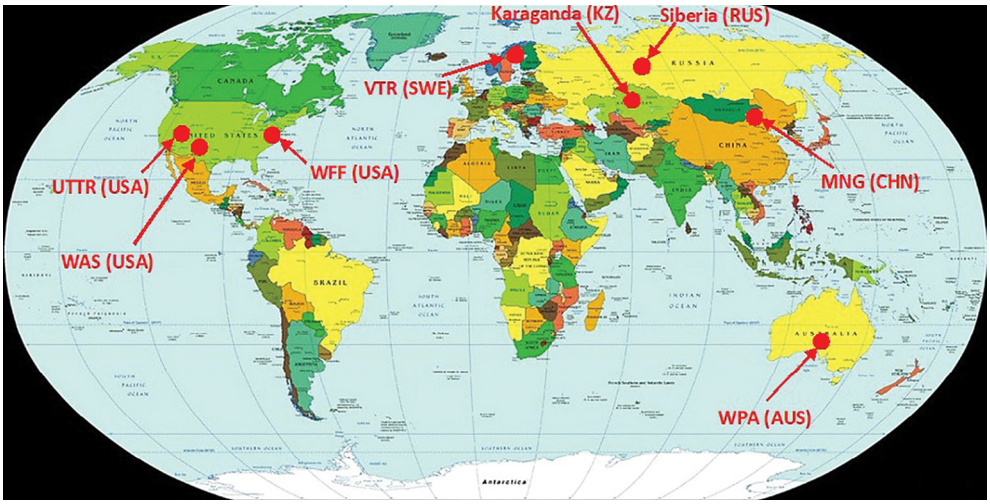

Fig. 15.1 Landing sites described in this chapter.

15.2.1 Karaganda Area (KZ)

Karaganda Area is a flat steppe located in Kazakhstan, central Asia, used for example for International Space Station (ISS) crew members return. This area has a humid continental climate with warm summer and very cold winters. The average temperature goes from −18 to + 26 °C with lowest and highest records of −43 °C and + 40 °C (2019 data, http://www.pogodaiklimat.ru/climate/35394.htm). The semiarid region, the climate and flat terrains would be useful for the recovery and transportation phase at landing site. Nevertheless, the low temperature might be critical for samples transport in winter season, while a possible contamination from dust, also moved by very high wind, could be an issue during recovery operations. Finally, travel time to reach a selected area inside Karaganda could last hours.

15.2.2 Siberia Area (RUS)

Siberia Area is an extensive geographical region in North Asia extending from Ural Mountains to Pacific Ocean. It was used during the Soviet Space Program for capsule re-entry of Luna SRMs. For instance, on the 22nd of August 1976, Luna 24 landed at about 200 km southeast the Surgut city in western Siberia (Wesley and Mikhail, 2011). Siberia Area has a low population density (mainly living in the South of Siberia) and is characterized by a variable climate. The abundance of soil variety (steppe, taiga, permafrost) and the mild temperatures (in the summer season) make it suitable as landing site.

Specifically, the Eastern Siberia has been excluded so far as a landing site due to low temperatures (−70 °C) and because of peat and marshy surfaces caused by suppression of microflora. North and South Siberia are tundra and sod soils, respectively. Western Siberia cover an

area from the Ural mountain in the west to the Yenisei River in the east and is outside the normal agricultural and developed strip of Russia so that it is sparsely populated area, e.g. the city of Surgut is the largest one in the interior and it has three hundred thousand inhabitants.

15.2.3 Utah Test and Training Range (USA)

Utah Test and Training Range (UTTR) is a vast and unoccupied salt flat controlled by US Army and Air Force located in Utah's West Desert. This area has been used as landing site for Genesis and Stardust mission and will be the landing site of the OSIRIS-REx mission (Lauretta et al. 2014). The site was chosen because its wide area could compensate the aerodynamic uncertainties on the capsule direction due to winds (https://www.nasa.gov/mission_pages/genesis/spacecraft/faq-2.html). In addition, UTTR gives the advantage to easily localize the landing site of the ERC, thanks to the semiarid terrain and the already available facilities, including buildings for temporary clean room or vehicles (helicopter and ground vehicles). Precipitation is usually low (150 mm/year). Temperatures spans from −3 °C (winter) up to +26 °C (summer) with an average relative humidity of 35 percent in the summer and 65 percent in the winter. The UTTR area should not affect the conditions of returned samples due to the stable temperature during the day.

The UTTR disadvantages are instead local mud and water depressions, including some contaminated areas by biological and chemical compounds and high temperature excursion, as well as military restrictions.

15.2.4 White Sands Area (USA)

White Sands Area (WSA) is a 710 km^2 region located on the west slope of the San Andres mountains between Las Cruces, New Mexico and the White Sands Missile Range, a component of the NASA Johnson Space Center (JSC) in Houston, Texas (https://www.nasa.gov/Directorates/heo/rpt/white-sands-test-facility.html). This region is a US government rocket test facility for space flight materials and rocket propulsion system and comprises sand dunes of gypsum crystals, a relatively rare dune-forming mineral. The WSA shows groundwater contamination, e.g. N-nistrosodimethylamina (NDMA), N-nitrodimethylamine (DMN) and other volatile compounds (Strepo et al. 2001), due to historical operations using propellants and industrial solvents. WSA is subjected also to strong winds which can move the dust particles from the valley floor to more than 1200 m over the mountains. Moderate Resolution Imaging Spectroradiometer (MODIS) on NASAs Aqua satellite also captured wider, regional view of the plumes (https://earthobservatory.nasa.gov/images/77775/white-sands-dust-storm).

15.2.5 Wallops Flight Facility (USA)

Wallops Flight Facility (WFF) is located in the Eastern Shore of Virginia (USA) and is the NASAs principal facility for suborbital and small orbital research missions. This area is provided for rocket launch site to support science and exploration missions for NASA

and it is equipped with fixed location instrumentation assets with radar, telemetry receivers and command transmitters (NASA Report by URS Group Inc., 2010 (Wallops Flight Facility Shoreline Restoration and Infrastructure Protection program 2010)).

The Aircraft Office at Wallops provides for the operation, maintenance, airworthiness, and mission support of assigned NASA aircraft as well as the planning and conducting of Airborne Science missions. (https://www.nasa.gov/centers/wallops/missions/index.html).

The climate exhibits a substantial annual variation but a fairly uniform precipitation rate (distributed around 1100 mm per year). The temperature spans from 4 °C in January to 32 °C in summer while the wind speed is comprised between 4 to 6 m/s.

15.2.6 The Woomera Prohibited Area (AUS)

The Australia's Woomera Prohibited Area (WPA) is regulated by the Defense Act 1903, Defense Force Regulations 1952 and the WPA Rule 2014 (http://www.defence.gov.au/woomera/about.htm). It is a globally unique military testing range, the largest in the world declared prohibited on 1947. As a declared prohibited area, the access to WPA for non-defence use requires Commonwealth approval, provided that the Defence activities will be not unduly compromised (https://www.defence.gov.au/woomera/about.htm).

It was the landing site for JAXAs Hayabusa mission and JAXAs Hayabusa2 mission.

WPA is a desert isolated area with sparsely population with high summer and cool winter temperatures. Rainfall is rare while the climate is generally warm and dry. The area's stable climatic conditions virtually ensure the ability to conduct ground and recovery operations (Strom, 2005). WPA offers some advantages for the recovery phase regarding SRM, e.g., stable weather conditions, low population density and strict security system. The disadvantages would be dust contamination, temperature and humidity variations, unexploded ordinance (UXO) due to military activity, and the strong winds (critical for re-entry phase).

15.2.7 Vidsel Test Range (SWE)

Vidsel Test Range (VTR) is a Swedish strategic national test Area managed by the Swedish Defence Material Administration (FMV) and situated about 900 km north of Stockholm. It is located in the north of Sweden, in a region with extremely low population and little air-traffic and with a restricted airspace (7.200 km^2 in size). The installation includes a military base and is used as a Swedish and European missile test site (UXO can be present).

The climate is generally cold: the average temperature is below 0 °C in January and snowfalls are common. The air is generally dry (with a visibility up to 100 km), while the terrains are varying, including forest, hills, lakes, marshland and rivers (http://www.vidseltestrange.com/europe%E2%80%99s-largest).

The SRM recovery procedure should be followed by military team with a few restrictions from air or ground activities while the facilities are well suited for testing the re-entry capsule. Snowfalls and low temperatures could make the recovery difficult.

15.2.8 Siziwang Banner (CHN)

Siziwang Banner is in the Ulanqab region of the China's Inner Mongolia Autonomous Region, bordering the Republic of Mongolia to the Northwest. It is located about 80 km north of the capital of Inner Mongolia and is the primary landing site adopted in the Chinese Space Program for manned Shenzhou spacecrafts.

Siziwang Banner area is a semi-arid desert steppe with an average elevation of 1400 m. The climate is windy in spring, with low precipitation in summer, and dry and cold throughout winter (Nadin et al., 2013). The annual average temperature, precipitation and evaporation are 4.1 C, 305 mm and 2213 mm, respectively (Li et al., 2002). The population of the county seat, i.e. Wulanhua town is about two hundred thousand people.

For Chinese space program, a special road has been constructed from Wulanhua to Honggor to support the recovery of the Shenzhou spacecraft at pasture land called Amugulang. This allows the Chinese recovery team to track the progress of re-entry near the landing site and to quickly reach the site (about 40 min from facility base).

15.3 Transport of samples in previous missions

To keep the samples as pristine as possible, it is fundamental to minimize contamination. At the moment, robotic SRMs have all been unrestricted, and did not have to deal with Planetary Protection. In order to characterize the contamination environment and to preserve rock/dust samples, the contaminants (specially organics) should be recognized when possible and their amount should be characterized and minimized.

To this end, containers and transportation boxes of various size and shape were considered from Apollo missions up to Hayabusa mission. In the following, a description of each SRM is given, based on landing site and related contamination due to ground impact or to environment, transportation method used to move the sample from landing site to temporary facility, e.g. Temporary Clean Room (TCR), and transportation box used.

15.3.1 Apollo Program (NASA, 1961–1975)

The NASA Apollo Program was the first to achieve a large collection of extra-terrestrial materials returned to Earth (up to 382 kg of lunar rocks and soil), as well as to land humans on the Moon and return them safely to Earth. The first missions were considered restricted, as the scientific community was considering the possibility the

Fig. 15.2 Apollo 16 LSRC upon opening in the Lunar Receiving Laboratory with a large rock inside *(Credits: NASA, 372–36,984 photo)*.

Moon was life-bearing. This requirement was dropped after the Apollo 14 (McCubbin et al., 2019).

The main difficulties of samples containment were to avoid contamination and to respect the NASA stringent scientific requirements. The ALSRC (Apollo Lunar Sample Return Container) was used to store the returned materials (Fig. 15.2): it consisted of an aluminium box with a triple seal to preserve the lunar like-vacuum around samples and to protect them from shock environment of the Earth return flight. The aluminium mesh helped to absorb the shock impact while the box was closed under vacuum in order to not contain pressure higher than the lunar ambient pressure. The outer envelope of an ALSRC was 48 × 30 × 20 cm, hinges and latches included. The exterior box dimensions were 48 × 27 × 20 cm, with wall thickness of about 2 mm and capacity of about 16,000 cm^3.

The ALSRC came from a single block of 7075 AA aluminium alloy. The soft metal sealing surface was an alloy of 90 percent indium and 10 percent silver. The two sealing O-rings were made of L608-6 fluorosilicone. The indium seal protector lid spacer, used prior to final sealing on the moon, were made of Teflon. Two ALSRCs were used on each Apollo mission and were produced by Union Carbide, Nuclear Division, Oak Ridge (TN) (Allton, 1989).

The ALSRC shown in Fig. 15.2 was used on Apollo 12. It contained two Teflon bags with the planned "selected sample" of 20 rocks and fine grained material (https://airandspace.si.edu/collection-objects/alsrc-apollo-lunar-sample-return-container-apollo-12/nasm_A19772507000).

The Apollo samples are curated at the NASA JSC in ISO Class 6 cleanrooms. Starting in 2019, under the ANGSA program, unopened pristine samples in their original containers will be open and processed. Of the 382 kg returned samples by Apollo program, 52 kg are stored at the NASA White Sands Test Facility site in New Mexico.

15.3.2 Luna Program (USSR, 1959–1976)

Luna 16, Luna 20 and Luna 24 (1970, 1972, 1976) were three successful soviet SRMs flown as a part of Luna program as a competitor of Apollo Missions. Luna 16 was the first robotic probe to sample the Moon as well as the third SRM (after Apollo 11 and 12). It came back with 101 gs of collected material of lunar soil.

Each spacecraft was equipped with an extendable arm with a drilling rig for the collection of a lunar soil sample. The samples were placed in a hermetically sealed soil sample container inside a re-entry capsule.

The Luna 16 re-entry capsule landed on approximately 80 km SE of the city of Dzhezkazgan in Kazakhstan at 03:26 UT

Luna 20 was launched on the 14th of February 1972, carried back about 55 gs of collected lunar samples from lunar highlands and landed in the Soviet Union on the 25th of February 1972 (Wesley and Mikhail, 2011). In particular, the Earth-return vehicle landed in Kazakhstan and was recovered from the mission team about 24 h later. The delay was due to ice, wind and snow which raised severe difficulties for the recovery phase. When opened, the return capsule proved to contain only 55 gs of lunar soil (Wesley and Mikhail, 2011). Sampled material was anorthosite from ancient lunar highlands rather than basalt returned from Luna 16 (Slyuta et al., 2020).

Luna 24 was launched more than 4 years after Luna 20 on the 14th of August 1976. The probe sampled Mare Crisum and on the 22nd of August 1976 returned with 170.1 gs of lunar soil. It landed on Soviet Union (Badescu, 2012). A small portion of returned samples was shared with NASA in December 1976 (Slyuta et al., 2020).

Information about the transportation boxes used, the vehicles and methods used to transfer the samples are not represented in the literature.

15.3.3 Genesis mission (NASA, 2001–2004)

NASA/Genesis was the fifth Discovery-class spacecraft, aimed at collecting and returning to Earth solar wind samples (Lo et al. 2012). The collection device, fixed inside the sample return capsule, was made of a stack of four circular metallic trays, one continuously exposed and the other three deployed depending on particular solar wind characteristics. A suite of fifteen types of ultra-pure materials was distributed among several locations, in turn mounted on deployable panels ('collector arrays') (Jurewicz A.J.G. et al. 2003).

The capsule unfortunately suffered a hard landing at the Dugway Proving in UTTR on the eighth of September 2004. A following investigation proved that the accident was due to design defects that allowed an incorrect orientation during assembly of the gravity switch (Genesis Mishap Investigation Board Report, 2006). The science canister was breached, and the collectors were broken into thousands of shards.

The initial recovery plan involved two helicopters that were waiting to transfer the Genesis capsule from landing site to TCR close to the landing site. If the landing had been nominal, the capsule would have been caught by its parachute on the end of a five

meters' hook and then would have been soft landed close to TCR. The damage due to the high velocity impact was less severe than expected probably because of fall into fairly soft muddy ground. Fortunately for the mission, alternative recovery plans had been planned for and rehearsed by the curation team. The returned capsule was taken to a TCR for inspection where the ground team rolled the cradle hold up by metal support and covered by several aluminium foil and collected fragments and samples of local desert soil to serve as a reference to identify possible contaminants in the future. Four weeks was needed by Genesis Team for inspecting, cataloguing and packaging processes. The shattered sample canister was taken to a clean room and carefully disassembled during the subsequent month. Teams eventually tagged 15,000 fragments of the return capsule. Because NASA categorized Genesis samples as "unrestricted" from the Planetary Protection point of view, a specific biosafety transportation box was not used (https://solarsystem.nasa.gov/missions/genesis/in-depth/).

Thanks to the contamination knowledge and curation protocols, all primary science goals were achieved. Scientists obtained a significant amount of data from recovered debris which allowed the identification of argon and neon isotopes in samples of three types of solar wind captured by the spacecraft (Wiens et al., 2020). The Genesis solar wind samples are stored at NASA Johnson Space Center in an ISO Class 4 cleanroom and available to the worldwide scientific community.

15.3.4 Stardust mission (NASA, 1999–2011)

Stardust was the fourth low-cost exploration mission of the NASAs Discovery Program, the first to sample a comet (81P/Wild2) and the second robotic mission after Genesis. The mission was launched on the seventh of February 1999. The primary goal of the mission was to fly by 81P/Wild 2 at a distance of 150 km from the nucleus and to collect coma dust and interstellar particles (Brownlee et al. 2003; Brownlee et al. 1997).

The samples were collected by using aerogel, a low density microporous silica-based substance, to "soft-catch" and preserve the cometary materials. The Stardust Sample Return Capsule (SRC) was released from the mother spacecraft and successfully landed at 10:10 UT of 15 January 2006 within a 30 × 84 km landing zone in UTTR. Due to high winds, the capsule drifted north of the ground track, but fortunately, a locator beacon allowed recovery teams to find the capsule 44 min after landing. Then, the SRC temperature was measured with an IR gun (60 °C). First efforts of the recovery team were aimed at minimizing all the possible exposures to contaminants by using double plastic bags for the SRC transportation, a specific cradle as support and a positive pressure N_2 purge on the sample canister once it was returned on TCR (Sandford et al., 2006). A SO_2 gas detector was placed with the capsule between the two bags in order to confirm the SRC transponder battery had not shorted out and it came into no further contact with local soil (Sandford, 2011). The plastic bags themselves have successively revealed to be a source of organic contaminations.

Fig. 15.3 Left: container used for Sample Return Canister arriving at Ellington Field (JSC2006-E-00,880, 17 January 2006, image credit: NASA). Right: Donald Bronwlee, the Stardust principal investigator with the University of Washington; JSCs Mike Zolensky, curator and co-investigator for the project; Friedrich Horz, JSC, and Peter Tsou while are studying the returned Stardust material after its canister is opened in la laboratory at Johnson Space Center *(Jet Propulsion Laboratory, credits: NASA)*.

In order to ensure the contaminants identification, soil samples in the vicinity and under the Sample Return Capsule (SRC), water and vegetation samples were collected. Soils samples were initially stored in polyethylene bags and later transferred to cleaned glass tubes and dried (Sandford, 2011).

The SRC was moved to an ISO class 7 modular cleanroom located in a facility close to landing site where the pyros, electronics and Sample Canister (SC) were removed and placed into an especially clean designed container (Fig. 15.3). The SC was placed under ultra-pure nitrogen atmosphere by using a dedicated container with purge system, temperature monitored environment and then flown to the Stardust Laboratory at the NASA (JSC) for preliminary examination of returned samples (Barrow et al., 2007). A police escort followed the samples from Houston's Ellington Airport to JSC curation facility (Zolensky et al., 2008). The aerogel cells were examined at NASA/JSC in an ISO Class 5 cleanroom (Zolensky et al. 2008), showing that the capsule had returned more than 10,000 particles larger than 1 μm with the presence of a wide range of organic compounds. In August 2014, NASA announced that seven rare, microscopic interstellar dust particles dating from the very origins of the Solar System were among the samples collected by Stardust (https://solarsystem.nasa.gov/missions/stardust/in-depth/).

15.3.5 Hayabusa Program (JAXA, 2003–2010)

The JAXAs Hayabusa mission was the first to successfully land and take off from the surface of an asteroid.

It was launched on the ninth of May 2003 at 04:29:25 UT on an M-5 solid fuel booster from the Kagoshima launch center. The primary scientific objective was to collect a surface sample from asteroid 25,143 Itokawa (1998 SF36) and return the sample

Fig. 15.4 Transportation boxes used for the Hayabusa mission (left) and their transport at the landing site (right) *(Credits: Australian Science Media Centre)*.

to Earth for analysis after a touchdown. The re-entry capsule was detached from the main spacecraft at 300–400 thousand km from Earth and re-entering in the Earth's atmosphere on 13th June 2010 via parachute in Woomera area (WPA), Australia.

The SRC was found in the planned landing site, thanks to the weak winds (Kawaguchi et al., 2010). The team on board the helicopter located the capsule and recorded its position with GPS. At the landing site, photography documentations and collection of soil samples were performed in order to identify possible contaminants. Then, the re-entry capsule was placed into a temporary plastic bag, in turn placed in a specially designed transportation box (Fig. 15.4) to Woomera Headquarters building (within a TCR facility), where explosive devices, batteries and contaminants adhering to the capsule were removed.

The transportation box had a purge function of pure nitrogen gas and a temperature logger attached externally in order to monitor the thermal condition of the re-entry capsule (Yada et al., 2014). On the 17th of June, the capsule was flown from Woomera's airfield in Australia to Haneda airport in Japan through a direct flight (Abe et al., 2011).

Successively, in the JAXA Planetary Sample Curation Facility in Sagamihara, de-integration of re-entry capsule from transportation box (Fujimura et al., 2013), sample extraction and preliminary examination were performed. Due to the failure of sampling system, only 1500 asteroid particles were collected (up to 100 gs were planned).

The landing procedure and Return Capsule of Hayabusa 2 was similar to Hayabusa, including the transportation box design. The mission returned the Sample Container with three filled sample catchers to Earth at Woomera Test Range in Australia. About 5.4 grams of dark material have been found in the first sample chamber that exceeds the mission goal of 0.1 mg (the amount required for the initial scientific analysis).

15.3.6 OSIRIS-REx mission (NASA, 2016–2023)

OSIRIS-REx (Origins, Spectral Interpretation, Resource Identification, Security-Regolith Explorer) is the third major planetary science mission for NASA's New Frontiers Program, launched on September 2016 on an Atlas V411 from Cape

Canaveral Air Station. The main aim of this mission is to collect a sample of about 60 gs from the Near Earth Asteroid 101,955 Bennu and to bring it to Earth (Lauretta et al. 2017). After collection of high-resolution imagery to allow the mission team the selection of the sampling site, the spacecraft approached Bennu and the robotic arms, i.e., the TAGSAM instrument (Touch-And-Go Sample Acquisition Mechanism) collected regolith samples by releasing a burst of nitrogen to kick up the regolith particles from the surface and collecting these particles with the sampler head (Bierhaus et al., 2018; Lauretta et al., this book). Then, the TAGSAM sampler has been stowed in the sample return capsule.

The approach to Earth and the release of the capsule containing the asteroid sample by means of a parachute landing is planned on 24th September 2023 (Beshore et al., 2015). The capsule will enter in the Earth's atmosphere at more than 12 km/s, will deploy its parachute at an altitude of 3 km for a soft landing at UTTR about 130 km West of Salt Lake City, Utah.

The capsule will be tracked with UTTR radar system and then recovered and transported to a staging area at UTTR to prepare the transport to JSC (Ajluni et al. 2015). Air samples would be collected at both landing site and staging area to test for SRC outgassing. Soil samples would be collected from landing site, too, because they could have a contact with the re-entry capsule. The recovery team will have a portable clean enclosure (ISO Class 7,) and initiate a purge on the sample canister before transport to JSC (Righter et al., 2013). The capsule will be sent to JSC in Houston, Texas, where the canister will be opened in a dedicated facility. There, the scientists at the Astromaterials Acquisition and Curation Office will catalogue the sample and set aside some portions for partners in the Japanese and Canadian space agencies. After about six months, NASA will distribute parts of the sample to research groups around the world. A portion of the sample will also be stored remotely at the NASA White Sands Test Facility site in New Mexico to avoid complete loss of the collection (https://solarsystem.nasa.gov/missions/osiris-rex/in-depth/).

15.3.7 Chang'e 5-T1 and Chang'e 5 missions (CNSA, 2014–2020)

Chang'e 5-T1 Test Vehicle was designed as a test of the strategy planned for the CNSA/Chang'e 5 lunar SRM. The mission goal was a flight test to validate the atmospheric re-entry design of a sample return capsule, crucial to China's plans of launching a complex lunar sample return mission (Chang'e-5). After leaving on the 24th October 2014, the Chang'E-5-T1 spacecraft travelled around the Moon and then, at 5000 km from Earth, released a capsule which returned to Earth on the 31st of October, landing in China's Inner Mongolia Autonomous Region site. The returned capsule at landing site is a scaled-down type design of Shenzhou capsule used in China's manned space

program. A heat shield is on the capsule bottom, while at the top there is an access hatch and sample transfer mechanism that can be moved robotically to enable the transfer of sample material. The Return Vehicle includes batteries, a guidance system, attitude control thrusters, communication systems including GPS and parachutes. From the images released, the capsule is on the order of 1.5 m tall.

The capsule landed at Siziwang Banner Landing Site in Inner Mongolia and was recovered in a few minutes by the recovery team which performed the photography documentation and packaging into a special cradle. The transfer of the capsule was performed by helicopter and then with aero-cargo to Beijing for study. This test validated the heat shield technology, trajectory design and recovery procedures for Chinese SRM

The next CNSA SRM, i.e. Chang'e 5, launched in November 2020, landed in the Mons Rumker Region of Oceanus Procellarum and returned up to 2 kg of lunar regolith. It is in progress at time of writing.

15.4 Guidelines and regulatory issues for restricted samples packaging

All the SRMs performed so far returned/are returning unrestricted samples, but we cannot rule out that return of restricted samples will take place in the next future.

Past and upcoming SRMs have sampled unrestricted bodies only. However, restricted SRMs should be happening in the next decade or so. In this section, we give guidelines for restricted samples packaging during transport from landing site to curation facility and then between laboratories. These guidelines are based on the World Health Organization (WHO) directives of transport of hazardous/infectious substances (WHO, 2012).

According to the WHO, substances can be classified as:

Category A: *An infectious substance which is transported in a form that, when exposure to it occurs, is capable of causing permanent disability, life-threatening or fatal disease in otherwise healthy humans or animals.*

Category B: *An infectious substance which does not meet the criteria for inclusion in Category A*, i.e. is capable to cause "minor" disease.

Moreover, as stated by WHO standard "*if there are doubt as to whether or not a substance meets the criteria it shall be included in Category A"*. Thus, according to WHO definitions, restricted samples should be treated as "Category A" samples, because it cannot be excluded the presence of simple forms of life causing disease to humans. On the other hand, unrestricted samples (e.g., sterilized Mars and Europa samples, asteroid and lunar samples) should be treated as "not hazardous" and are not included in the WHO classification (Longobardo et al. 2016).

15.4.1 Transport from landing site to curation facility

According to WHO guidelines, the system of packaging of Category A samples must be based on a three layers packaging.

1. The first one is the inner layer, i.e. a *primary receptacle* that must be watertight and leak-proof and contain the samples (it could coincide with ERC).
2. The second one, i.e. a *secondary package* must be durable, leak-proof and watertight too. This packaging can also contain more than one primary receptacle: in the case this occurs, more absorbent material is needed to absorb the fluid (if present) in case of leakage and/or breakage. Both primary and secondary packages have to survive to a differential pressure of 95 kPa and to the temperature range from −55 °C to 40 °C.
3. The third packaging layer, i.e. the *outer package*, needs to be rigid and sufficiently cushioned to avoid outside influence (e.g., physical damage).

If real-time samples monitoring is required, an outer package can be enclosed in an ISO container, that can include additional instrumentation for contamination and environmental control, e.g. accelerometers, temperature sensors, microbalance sensors for organics contaminants (Dirri et al. 2016).

15.4.2 Transport between laboratories

A vital role of curation is to allow the scientific community to access the samples, through allocation. A part of the sample is transferred from the curation facility to the laboratory that requested it. If the science done on the sample doesn't consume it entirely, the sample is then shipped back to the curation facility, where is it is stored again. For the current astromaterial collections, the only requirement for transport was to keep a level of cleanliness consistent with the collection requirements, and with the science to be done on the sample. For restricted collections, samples will need to be kept under containment at all times to avoid backward contamination, on top of the cleanliness requirements described above.

It is also advisable that the samples be kept at the same storage conditions (temperature, pressure, cleanliness, humidity) during transport.

In particular, the restricted samples should be included in a complex, three-layered package, according to WHO guidelines:

1. The sample container would be the most internal layer and should be surrounded by an absorbent material in the case of fluid leakage (e.g. phase transition in Martian samples).
2. A layer consisting of a non-outgassing plastic material bag would be the second layer. This is needed to prevent backward contamination, whereas in the case of unrestricted samples a double packaging (sample containers + metallic box) would be sufficient to prevent contamination.

3. Rigid and cushioned box would be the most external layer. Low temperature inside the box, if needed, would be guaranteed by a cooling system, involving liquid nitrogen or a refrigeration plant. The box pressure should be monitored during the transport due to the possibly pressure change caused by box leakage or forward contamination.

15.5 Conclusions and future perspectives

The past SRMs returned to the Earth range from thousands of particles (Stardust mission) up to hundreds of kilograms (Apollo Program) of extra-terrestrial materials. We provided a description of past, current and planned SRMs recovery and transport procedures. Each recovery procedure is related to a scenario involving landing site characteristics (i.e., environmental conditions and military restrictions) and returned samples.

As an ideal landing site, the desert and steppe regions would be the best candidates for SRM due to stable climate and weather conditions. Otherwise, the landing sites subjected to dust storm and strong wind should be avoided in order to make the recovery procedure easier. Military areas, for example UTTR, would give more advantages in terms in real time controlling of the re-entry capsule.

The extra-terrestrial returned samples are stored at JAXA's Extraterrestrial Sample Curation Center (ESCuC) and NASA's Astromaterials Research and Exploration Science Directorate (ARES) (Allen et al. 2011; Abe et al. 2014). The Luna Soviet Mission samples are stored at the Vernadsky Institute of Geochemistry and Analytical Chemistry at the Russian Academy of Science (Slyuta et al., 2020).

Possible returned restricted samples, e.g., from Mars, Europa, Enceladus, must be curated and studied under strict requirements of cleanliness and containment. The current agreement within the community is that the containment level must be at least similar to a Biosafety Level 4 (BSL-4) facility. Transport of these samples will require a triple packaging, according to WHO guidelines.

The scientific community has been periodically studying best practice for curation facilities both for restricted and unrestricted SRMs, e.g., H2020 EC EUROCARES Project (Hutzler et al. 2017) and NASA Mars Sample Return Receiving Facility (Harrington et al. 2019; Atlas 2008; National Research Council 1997).

Acknowledgements

Part of this research was done during the EUROCARES Project, which has received funding from the European Union's Horizon 2020 research and innovation programme under grant agreement No 640,190.

References

Abe, M., et al., 2011. Recovery, transportation and acceptance of the curation facility of the hayabusa *re*-entry capsule. 42nd LPSC, LPI Contribution (No. 1608), 1638.

Abe, M., Yada, T., Uesugi, M., et al., 2014. Current status of JAXA's extraterrestrial sample curation center. 46th LPSC Abstract, 1245 pdf.

Ajluni, T., Everett, D., Linn, T., Mink, R., Willcockson, W., Wood, j, 2015. OSIRIS-REx, returning the asteroid sample, Aerospace Conference. IEEE, pp. 13.

Allen, C., Allton, J., Lofgren, G., et al., 2011. Curating NASA's extraterrestrial samples—past, present, and future. Chem. Erde 71 (Issue 1), 1–20. doi:10.1016/j.chemer.2010.12.003.

Allton, J.H., 1989, Catalog of APOLLO Lunar surface geological sampling tools and containers, prepared for NASA/JSC Solar System Exploration Division Contract NAS 9-17900, Job Order J2-J60.

Atlas, R., 2008. "Mars Sample Return Receiving Facility"; NASA.

Barrow, K., et al., 2007. sample return primer and handbook, D-37294 report, pasadena, jet propulsion laboratory. National Aeronautics and Space Administration.

Beshore, E., et al., 2015. The OSIRIS-REx Asteroid Sample Return Mission. IEEE 978-1-4799-5380-6/15.

Bierhaus, E.B., Clark, B.C., Harris, J.W, et al., 2018. The OSIRIS-REx spacecraft and the touch-and-go sample acquisition mechanism (TAGSAM). Space Sci. Rev. 214, 107. doi:10.1007/s11214-018-0521-6.

Brownlee, D.E., et al., 1997. The stardust mission: returning comet samples to earth. Met. And Plan. Science 32, A22.

Brownlee, D.E., et al., 2003. Stardust: comet and interstellar dust sample return mission. J. Geophys. Res. 108 (E10), 8111. doi:10.1029/2003JE002087 2003.

Badescu, V., 2012. Polytechnic university of bucharest, moon: prospective energy and material resources. Springer Science & Business Media, 749 March 2012.

Dirri, F., et al., 2016. Piezoelectric crystal microbalances measurements of enthalpy of sublimation of C2-c9 dicarboxylic acids. Atmos. Meas. Tech. 8, 7127–7160.

Fujimura, A., et al., 2013. Hayabusa-returned sample curation in the Planetary Material Sample Curation Facility of JAXA. JAXA Special Publication JAXA-SP-12-012E.

Genesis Mishap Investigation Board Report, 2006. https://ntrs.nasa.gov/search.jsp?R=20060008607.

Harrington, A., et al., 2019. The Acquisition, Containment, and Curation of Mars Samples on Earth21st EGU General Assembly, EGU2019 Proceedings. Vienna, Austria, pp. 19086 id.

Hutzler, A., Kilic, E., Bennett, A., et al., 2017. Extraterrestrial Sample Curation Facility: architecture as an enabler of science, EUROCARES project, 47th International Conference on Environmental Systems, 16–20 July 2017. Document ICES, Charleston, South Carolina, pp. 2017–2323.

Kawaguchi, et al., 2010. Hayabusa re-entry and recovery of its capsule - quick report. Abstract for 38th COSPAR Scientific Assembly.

Kimnek, g, et al., 2017. COSPAR planetary protection policy. Space Res. Today 200, 14–15.

Lauretta, D.S., Bartels, A.E., Barucci, M.A., et al., 2014. The orisis-rex target asteroid 101955 bennu: constraints on its physical, geological and dymanical nature from astronautical observations. M&P Science 50 (issue 4), 834–849. doi:10.1111/maps.12353.

Lauretta, D.S., Balram-Knutson, S.S., Beshore, E, et al., 2017. OSIRIS-REx: sample return from asteroid (101955) bennu. Space Sci. Rev. 212, 925–984. doi:10.1007/s11214-017-0405-1.

Lauretta, D. et al., this book. OSIRIS-REx at Bennu: Overcoming challenges to collect a sample of the early Solar System, Chapter 8, this book.

Li, Z., et al., 2002. Identifying management strategies to improve sustainability and household income for herders on the desert steppe in inner mongolia, china, jan 2014Agricultural Systems NASA Technical Standards, Standard for Lifting Devices and Equipment. NASA-STD, pp. 9.

Lo, M., Williams, B., Bollman, W., et al., 2012. Genesis mission design. AIAA/AAS. doi:10.2514/6.1998-4468.

Longobardo, A. et al. (2016), Transport to curation facility, Deliverable to European Community released under the Horizon2020 EURO-CARES project.

Jurewicz, A.J.G., et al., 2003. The Genesis Solar-Wind Collector Materials. The Genesis Mission. Springer, Dordrecht. doi:10.1007/978-94-010-0241-7_2 In: Russell C.T. (eds).

McCubbin, et al., 2019. Advanced Curation of Astromaterials for Planetary Science. Space Science Review 215, 48. doi:10.1007/s11214-019-0615-9.
Nadin, R., et al., 2013. Climate risk and resilience in China, 14 ottobre 2015. RoutledgeProc Natl AcadSci U S A 110 (21), 8369–8374. doi:10.1073/pnas.1208063110 2013 May 21PMCID: PMC3666733.
National Research Council, 1997. Mars Sample Return: Issues and Recommendations. The National Academies Press, Washington, DC. doi:10.17226/5563.
Righter, K., et al., 2013. Curation of OSIRIS-REx asteroid samples. 76th Annual Meteoritical Society Meeting.
Sandford, S.A., 2011. The Power of Sample Return Missions - Stardust and Hayabusa. The Molecular Universe Proceedings IAU Symposium (No. 280).
Sandford, S.A., et al., 2006. The recovery of the Stardust sample return capsule. Lunar and Planetary Science, 1123 XXXVII.
Slyuta, E. et al., 2020. The Luna Program, this book.
Strepo, M.W., Giles, G.C., Pierson, J.W., 2001. Contaminated groundwater interception and remediation within the mid-plume constriction areaNASA White Sands Test Facility. Proc. Containment and Remediation Technologies, Florida, USA.
Strom, S.R., 2005. International site launch guideThe Aerospace Corporation with the American. Institute of Aeronautics and Astronautics, El Segundo, California and Reston, Virginia.
Wesley, T.H., Mikhail, Y.M., 2011. Soviet Robots in the Solar System: Mission Technologies and Discoveries. Springer Science & Business Media, pp. 453.
Yada, T., et al., 2014. Hayabusa-returned sample curation in the Planetary Material Sample Curation Facility of JAXA. Meteoritics& Planetary Science 49 (Nr 2), 135–153. doi:10.1111/maps.12027.
WHO, 2012. Guidance on Regulations for the Transport of Infectious Substances. WHO/HSE/GCR/, pp. 2 2012.
Wallops Flight Facility Shoreline Restoration and Infrastructure Protection program, 2010, vol.2, Report prepared for NASA by URS Group Inc.
Wiens, R.C. et al., 2020, The Genesis Solar-Wind Mission: First Deep-Space Robotic Mission to Return to Earth, this book, Chapter 5.
Zolensky, M., et al., 2008. Curation, spacecraft recovery and preliminary examination for the stardust mission: a perspective from the sample return facility. MAPS 43 (1–2), 5–21.

CHAPTER 16

Techniques and instruments to analyze, characterize and study returned samples

Rosario Brunetto[a], Jérôme Aléon[b], Alice Aléon-Toppani[a], Janet Borg[a], Zahia Djouadi[a]

[a]Université Paris-Saclay, CNRS, Institut d'Astrophysique Spatiale, Orsay, France
[b]Institut de Minéralogie, de Physique des Matériaux et de Cosmochimie, Sorbonne Université, Museum National d'Histoire Naturelle, CNRS, Université Pierre et Marie Curie, Institut de Recherche pour le Développement, Paris

Chapter Outlines

16.1 Introduction: historical background

Since the beginning of the study of meteorites, progress in the understanding of extra-terrestrial (E.T.) materials has been linked to progress in the development of analytical techniques. Further developments of analytical techniques enabled sample analyses, while further requirements for sample analysis drove the development of new analytical techniques.

The first E.T. samples analyzed in dedicated laboratories were the various "stones fallen from the sky" identified across the world. These analyses began at the end of the 18th century when reliable scientific instruments started to be available. In 1794, a German chemist, Ernst Chladni published a booklet claiming that the "iron and stone falls" did come from space. Chladni also advanced the hypothesis that such stones

Sample Return Missions
DOI: 10.1016/C2018-0-03374-5

originated either from a planet that did not form or from the destruction of a planet. In 1803, thousands of stones fell on the little town of L'Aigle in Normandy (France). The chemist Jean-Baptiste Biot confirmed the E.T. origin of the analyzed stones and a new discipline was born: cosmochemistry. Collections of E.T. samples began to be maintained and studied in Natural History Museums all around the world.

The analysis of meteorites marked the beginning of the analysis of returned E.T. samples. In the 19th century, scientists could only observe cm-sized samples of polished sections of meteorites through optical microscopes (using either ordinary or polarized light), study their reactions to various chemical reagents, or characterize some physical properties (density, magnetism, color and interaction with light). Today, scientists can study down to nm-sized samples extracted from meteorites, from individual dust particles collected in space (interplanetary dust particles, IDPs) or on Earth (micrometeorites), and from grains collected by sample return missions. Modern imaging techniques cover now a large range of sizes, from the bulk specimen to the μm-sized sections of individual grains. The remarkable progress of the analytical techniques over the last century marked a transition from the limited information obtained on big samples to the detailed information extracted from sub-micron entities.

In the 20th century, two techniques were invented, that can be considered the precursors of many of the instruments installed today in the laboratories working on the characterization of returned samples. (i) Transmission electron microscopes using electron-beams instead of photon-beams were first designed in 1931, and scanning electron microscopes followed shortly afterwards. (ii) The first mass spectrometers were designed in the 1910s and many technical improvements followed, like in 1948 the development of the time of flight mass spectrometer. Elemental and isotopic mapping of smaller and smaller samples became possible.

All along the 20th and 21st centuries, spectacular improvements of the analytical techniques were achieved, thanks to technical and scientific innovations. At the same time, more and more samples were collected on Earth (micrometeorites) and from the stratosphere (cosmic dust), and from the Moon and some small bodies (sample return missions). The first samples of cosmic dust collected were the small metallic spherules captured in the deep sea by the HMS Challenger oceanic mission in 1872 – 1876. The samples were identified as cosmic dust and analyzed only in the 1970s (Ganapathy et al., 1978), at the time when knowledge of our Solar System started to expand. The collection of cosmic dust ignited progress in the transportation, curation and handling of the samples. Clean rooms were built, handling tools were developed, sample preparation methods became more and more sophisticated.

A big step in sampling and analyzing E.T. materials took place when it became possible to fetch samples at the surface (Moon and asteroid regolith) or in the vicinity (cometary dust) of the sample's parent body. The exploration of the Solar System started in the 1960s, with the space race between the USA and the former USSR to be the first in space, around the Earth, around and on the Moon. New space agencies were

born to drive space exploration and study planetary bodies. Planetary science developed, thanks to remote sensing observations, spacecrafts to celestial bodies, and in some cases dedicated sample return programs.

Numerous analytical developments were linked to the expansion of space exploration. A good example is the development of secondary ion mass spectrometry (SIMS or ion probe), tightly linked to the *Apollo* lunar missions. At that time, SIMS was a newborn technique developed as an extension of electron probe microanalysis to perform ion microscopy (Liebl and Herzog, 1963; Slodzian, 1964). The urge to prepare for the upcoming lunar samples quickly led NASA to fund the development of a prototype instrument specifically dedicated to the analysis of lunar samples. This first generation of SIMS allowed for instance spatially resolved analysis of uranium, thorium and rare earth elements (REE) in Moon rocks (Andersen and Hinthorne, 1973) and served as basis for the development of commercial instruments in the 1970's.

Extraterrestrial samples analysis has made tremendous progress since then. The laboratory analyses of samples retrieved from comet Wild2 by the *Stardust* (NASA) mission and from asteroid Itokawa by the *Hayabusa* (JAXA) mission largely benefited from the emergence of the third generation of synchrotron light sources all around the globe and the *Hayabusa2* (JAXA) and *OSIRIS-REx* (NASA) missions will benefit from new and improved analytical methods, of which a non-exhaustive list is presented here.

16.2 General presentation of the analytical techniques

The analytical techniques applied to E.T. matter are used to characterize the structure and morphology, and/or to detect the presence of a given species or chemical compound in a sample, and possibly to estimate its relative and/or absolute abundance. Two main categories of analyses can be defined: bulk methods measuring the sample general properties and in-situ methods targeting localized and small-scale properties. Bulk methods have made tremendous progress and now allow high precision analysis of subtle properties in increasingly smaller samples. For instance, the isotopic composition of many elements present in the sub-percent range can now be measured with ppm precision in sub-mg samples. The ever-increasing quality of analytical blanks also allows measurement of noble gas isotopes with ‰ precision in mg to sub-mg samples (Bekaert et al., 2020). Noteworthy applications have been reported in the analysis of Stardust samples (Palma et al., 2019). In the last ten years, such mass spectrometric progresses revolutionized the classification of E.T. material (Kruijer et al., 2020). However, many bulk methods are destructive, which implies a limited use in the analysis of rare and small samples. In this chapter, we decided to focus on in-situ methods. These are less destructive than bulk methods and allow 2D and 3D characterizations, which make them particularly useful for the analysis of rare samples.

In order to summarize the main characteristics of modern in-situ analysis techniques, we will consider them as a function of the incident beam necessary to extract

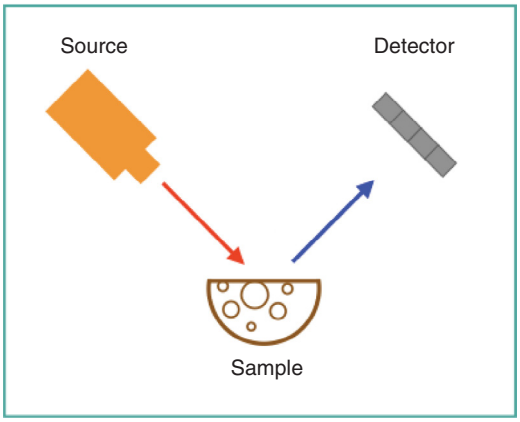

Fig. 16.1 The general idea behind most of the analytical techniques relies in combining the appropriate source and detector to investigate the composition of a given sample.

information on the properties of the sample or its sub-units. The sample is generally exposed to a primary flux (of particles or light) and the interaction between the flux and the sample produces a secondary flux that is revealed by a detector. The detection of this secondary flux provides information on the sample composition and / or structure, thanks to the calibration of the technique often through standard samples of known composition. Each technique requires a specific sample preparation, which has to be performed with great care as the amount of available material is usually limited. The sample preparation plays a very important role in the triangle "source - sample - detector", in which the sample composition is determined by using a particular combination of source and detector (Fig. 16.1).

This general idea seems obvious nowadays, but it was not so in the 19th century when the principles of spectroscopy were established and the quantitative measurement of light was standardized. The process was generalized at the end of the 19th century / beginning of the 20th century, when first, individual ions, and then sub-atomic particles were discovered and isolated, and it was established that they could be used as source beams for investigating the composition of a sample. Today, most analytical techniques used for the analysis of small E.T. samples determine the sample composition by using this method, and the combination of source and detector is chosen to address a specific scientific question.

In many cases, modern analytical techniques used to study E.T. matter are based on techniques that were developed by other communities for investigations in various fields (physics, chemistry, geology, biology, etc.), and that were adapted to the peculiar characteristics of E.T. samples. One of the specificities of these analyses is usually the low amount of available E.T. materials, requiring constant improvement to push the chosen techniques to their limits, which also benefits the analysis of terrestrial samples. For example, micro-imaging has been subject of important improvements, because it

plays a key-role in all modern techniques applied to primitive E.T. materials, like some grains from asteroids and comets, that are very heterogeneous and complex.

In the following (Sections 3–6), we provide a non-exhaustive review of significant in-situ analytical techniques that have been successfully applied to E.T. materials collected by sample return missions. We present and group the techniques based on the choice of the analytical source (photon-based, electron-based, ion-based, others). Each technique has advantages and disadvantages, which are a direct consequence of the chosen physico-chemical process used by that specific analysis. Section 7 is devoted to the possibility of combining some of these techniques in a multi-analytical sequence, to deepen the characterization of the samples.

16.3 Photon-based analytical techniques

16.3.1 Visible and infrared light

When speaking of photon-based methods, one immediately thinks of optical microscopy and spectroscopy, either using visible (~0.4–0.7 μm) or infrared (IR) light (~0.7–100 μm) as source of excitation for the sample. The use of optical images is in most cases the first technique of observation of the samples, and an optical microscope is essential for a first characterization. Spectroscopic analyses in these spectral ranges are typically performed using light either reflected from or transmitted through the sample. Quantitative analyses are easier in transmittance than in reflectance. While transmittance measurements require some extent of sample preparation (e.g., sectioning, crushing, welding, etc.), reflectance and Raman measurements can be performed on almost any kind of surface.

Fourier Transform Infrared spectroscopy (FTIR) has long been used to study collected E.T. materials (e.g., in the case of *Stardust* samples, (Keller et al., 2006), and references therein). It is a nondestructive analytical tool, as it is totally non-invasive (it does not modify the intrinsic characteristics and composition of the analyzed samples). This technique allows to detect and study the molecular vibrations associated to specific chemical bonds between the elements present in the samples. Thus, FTIR can also infer the chemical elements present in the samples. For instance, in the mid-IR range (~2.5 – 15 μm) it is relatively easy to identify the silicate features (~10 μm) and those associated to the aliphatic organics (~3.4 μm). FTIR also allows direct comparison with astronomical data, obtained when telescopes are equipped with IR spectrometers. The majority of space missions studying asteroids and comets are equipped with IR spectrometers or microscopes (e.g., the VIRTIS instrument onboard the ESA *Rosetta* mission, (Capaccioni et al., 2015)). The resolutions of the laboratory instruments are usually higher than those of the on-board spectrometers, both spectrally (typically 5–10 times better) and spatially (up to several orders of magnitude).

Analyses using IR light can be extended down to the visible spectral range, in order to perform micro-spectral analysis in a range that is the most common in

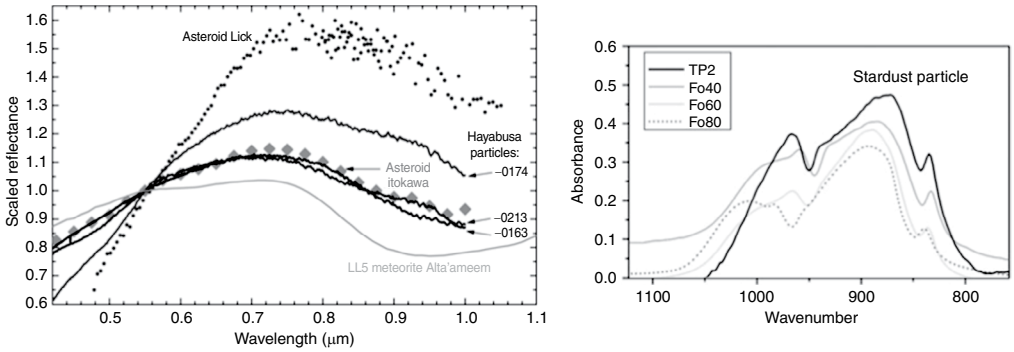

Fig. 16.2 Left: the scaled micro-reflectance spectra of three *Hayabusa* particles compared with the ground-based observation of asteroid Itokawa and asteroid Lick, and with the laboratory spectrum of an LL5 ordinary chondrite meteorite. From Bonal et al. (2015), reprinted with permission of Wiley. Right: the micro-IR absorbance spectra of a small (11 μm) *Stardust* terminal particle (TP2) measured at the SMIS beam-line of synchrotron SOLEIL (France), compared with laboratory olivine standards of different Mg/Fe content (Fo number). Adapted from Rotundi et al. (2014), *(reprinted with permission of Wiley)*.

planetary remote sensing. If the measurements are performed in reflectance, the laboratory data can be compared with the observational data. An example is provided by Bonal et al. (2015), who analyzed three *Hayabusa* particles, studied their mineralogy, and compared the laboratory data with the remote sensing spectral measurements of their Itokawa parent body, to investigate the weathering suffered in space (see Fig. 16.2, left panel).

Since the establishment of IR beam-lines in synchrotron, it has been possible to replace the internal source of the spectrometers by synchrotron light to excite the sample. The high coherence and brilliance of the synchrotron radiation allow to probe weak absorption features at μm-sized analytical spots down to the diffraction limit, as shown in Fig. 16.2 (right panel) in the case of a *Stardust* particle (Rotundi et al., 2014). Thanks to modern Focal Plane Array detectors, it is also possible to perform 3D spectral imaging of the chemical bonds distribution in the volume of the samples and their co-localization, with a spatial resolution defined by the diffraction limit. We then speak of 3D FTIR micro-tomography (or **IR-CT** for infrared computed tomography), a technique initially developed to analyze biological samples (Martin et al., 2013), and successfully used to analyze grains of CM carbonaceous meteorites and of asteroid Itokawa (Dionnet et al., 2018, 2020; Yesiltas et al., 2017). IR-CT has the advantage of providing a totally non-destructive characterization of the molecular composition of an isolated grain. The drawbacks include the diffraction-limited spatial resolution, the fact that the sample has to be smaller than 50 μm to avoid saturation and needs to be mounted on a needle.

More recent advances include the coupling of FTIR with an Atomic Force Microscope (AFM), giving birth to the **NanoFTIR** (FTIR at nanometer scale). This

scanning probe technique is based on the use of an AFM tip to back-scatter the light coming from a FTIR spectrometer. Hyper-spectral imaging can be performed by scanning the tip on a flat surface of the sample. NanoFTIR pushes the spatial resolution below 100 nm, beating the diffraction limit of the IR light. Dominguez et al. (2014) analyzed primitive meteorites and *Stardust* samples using NanoFTIR, and started a new era of IR nano-spectroscopy applied to small E.T. samples.

A spectroscopy technique complementary to IR spectroscopy is **Raman spectroscopy**. It is a non-destructive method of observation and characterization of the molecular vibrations (lattice vibrations in a crystal) of the samples. In a typical Raman spectrometer, a monochromatic visible light is sent to the sample, the inelastic diffused light is collected and then sent to a grating and analyzed by a CCD detector. UV, visible or near-IR lasers can be used as source of sample excitation. To preserve the samples from heating and avoid modifications, it is necessary to apply low laser powers (typically less than 2 mW). Raman spectrometers can be easily coupled to visible microscopes, in order to perform Raman micro-spectral imaging analyses with spatial resolution of the order of the laser wavelength (typically less than 1 μm).

Selection rules are different for IR and Raman spectroscopies, so the two techniques are very complementary. Thanks to a resonant interaction with poly-aromatic molecular units, Raman spectroscopy is a technique very sensitive to the presence of aromatic-rich carbonaceous materials in the samples. Raman micro-spectroscopy has the advantage of a better spatial resolution than IR micro-spectroscopy. The combination of Raman and IR micro-spectroscopies was successfully applied to the investigation of the *Stardust* samples (Rotundi et al., 2008; Sandford et al., 2006). Recent advances allow mapping the Raman bands in samples at different depths (Merouane et al., 2018) and thus studying the distribution of the components in 3D.

Overall, the main advantage of IR and Raman micro-spectroscopic techniques is their ability to provide molecular information of E.T. materials with limited sample preparation in a totally non-destructive way. They are valuable tools for a first characterization of returned samples and for the comparison with planetary observations. The derivation of the molecular abundances from the measured spectra is however not straightforward as it requires first a general understanding of the global spectrum, which is influenced by the scattering properties of granular materials related to the sample roughness, porosity and structure. Some phases have little or no active modes in the IR and Raman spectra (e.g., metals), but they can affect the spectral continuum, which in turn affects the determination of the other components. The result is that, in general, it is hard to quantify the abundances of active functional groups below a few percent. Another intrinsic disadvantage is the limited spatial resolution in imaging mode, which can however be bypassed by coupling spectroscopy to AFM or by the use of lasers.

16.3.2 X-ray light

X-rays consist in photon radiation with energies from hundreds of eV to a few MeV (0.01–10 Å). X-ray-based analyses are diverse and very versatile, including scattering, absorption and fluorescence. Here we focus on a few examples of successful application to the analysis of E.T. materials, in particular thanks to the synchrotron light sources which produce intense and highly coherent X-ray beams (either monochromatic or in a given spectral range) at the μm to mm scale. Synchrotron-based X-ray techniques tend to be well adapted to the analysis of E.T. samples in the 1–100 μm size range, depending of course on the photon wavelength and on the studied process. This is why they have been successfully applied both to *Stardust* and *Hayabusa* samples. Depending on the technique, the sample preparation can be as simple as the deposition of individual grains on a substrate (e.g., for micro-tomography) or more invasive as the production of thin sections by ultramicrotomy or by focused ion beam (FIB) microscopes (e.g., for scanning transmission microscopy).

X-ray Computed Tomography (X-CT) is a 3D imaging technique based on the use of an X-ray beam source (either monochromatic or polychromatic) and of a 2D matrix-detector. The sample is mounted on a rotating stage, in order to acquire 2D projections of the X-ray linear attenuation coefficient (LAC), which are reconstructed in a 3D volume distribution. X-CT provides quantitative information about density and internal structure of the sample, but also qualitative about compositional heterogeneity. X-CT is the best technique for the non-invasive study of a sample in 3D without destroying its structure. X-CT is generally considered non-destructive, although the X-ray interacting with the sample may induce damage (Sears et al., 2016). It is particularly efficient when combined with other microanalytical techniques.

Since X-CT can achieve μm- or sub-μm sized spatial resolution, it is sometimes referred to as Computed Microtomography (CMT), X-ray microtomography (XMT), or synchrotron computed microtomography (SCMT) when using a synchrotron source. Thanks to its capability of combining relatively large fields of view with relatively high spatial resolution, X-CT has been successfully used to analyze various E.T. materials from individual grains to large macroscopic fragments. A recent and exhaustive review of principles and applications of X-CT to planetary materials is provided by Hanna and Ketcham (2017).

The fall of CV meteorite Allende in 1969 triggered an ensemble of dedicated studies, especially thanks to its CAIs (Arnold et al., 1983). Since then, X-CT has routinely been applied to the study of meteorites (Ebel and Rivers, 2007). The establishment of dedicated X-CT beam-lines in third generation-synchrotrons (Uesugi et al., 2006, 1999) opened the way to the analysis of μm-sized E.T. dust (Tsuchiyama et al., 2004) and returned samples. The beam-lines at synchrotron SPring-8 (Japan, see Fig. 16.3 top panel) played a major role in the X-CT analysis of *Stardust* samples (Nakamura et al., 2008b; Rietmeijer et al., 2008; Tsuchiyama et al., 2009) and later of *Hayabusa* samples

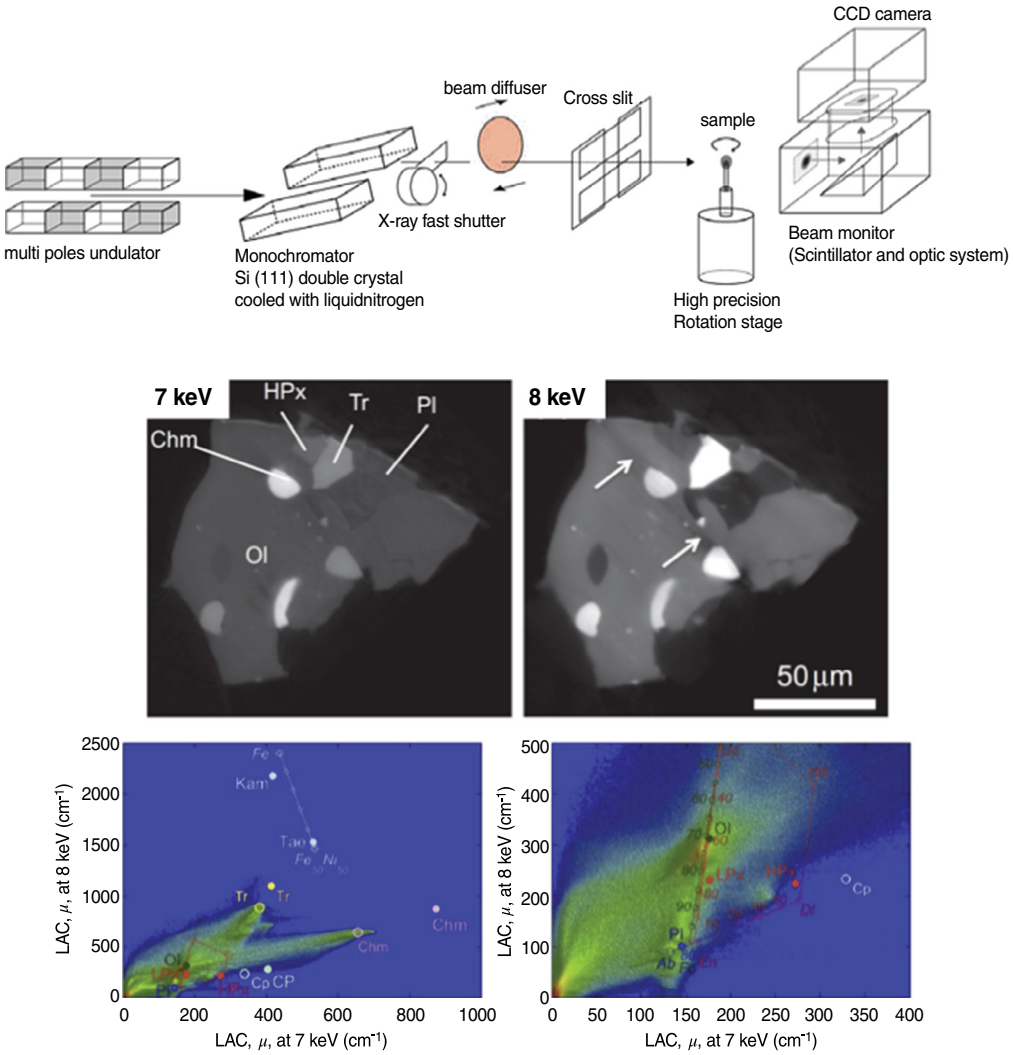

Fig. 16.3 Top: illustration of parallel beam XMT at the beam-lines BL20XU and BL47XU of the synchrotron SPring-8 (Japan). From Uesugi et al., 2009, reprinted with permission of IOP Publishing. Center: MCT slice images of one Itokawa particle measured at SPring-8, with a gray scale showing the LAC at 7 keV (left) and 8 keV (right). Bottom: a plot of the LAC at 8 and 7 keV for the same Itokawa particle, allows the identification of different mineral phases (olivine, plagioclase, troilite, etc.). Adapted from Tsuchiyama et al. (2013), *(reprinted with permission of Elsevier)*.

(Tsuchiyama et al., 2014, 2011). The Itokawa samples showed how X-CT can be used not only to study the internal structure and inclusions of a sample, but also interesting surface structures that are formed on Solar System surfaces by space weathering processes (Matsumoto et al., 2016). In terms of analytical developments, it is worth mentioning the establishment of dual-energy XMT as a new method for obtaining 3D

mineral phase images (see Fig. 16.3 center and bottom panels), which was successfully applied to Itokawa grains (Tsuchiyama et al., 2013).

X-ray Diffraction (XRD) is a noteworthy example of X-ray scattering techniques. The incident beam is elastically scattered by the electrons of the target atoms into many specific directions which are characteristic of the atomic and molecular structure of the crystals, thus allowing a direct and quantitative access to the crystallography of the sample. In some beam-lines, the X-ray spot on the sample can be as small as a few microns, allowing the analysis of very small particles. Fruitful applications have been reported on *Stardust* (Hicks et al., 2017) and on *Hayabusa* (Tanaka et al., 2014) samples. In particular, the use of high resolution Gandolfi camera at the Japanese synchrotron SPring-8 allowed to obtain pseudopowder diffraction patterns from single crystals or an agglomerate of single crystals in Itokawa particles. Some beam-lines have arranged experimental stations allowing to measure XRD and X-CT on the same sample, as both techniques can be applied to isolated grains mounted on needles.

X-ray Absorption Near Edge Structure (XANES) is an analytical technique based on the use of synchrotron X rays as an excitation beam that allows to investigate the absorption of a material in the neighborhood (typically ~100 eV on each side, with a spectral resolution that can be as low as 0.1 eV) of its absorption front. XANES provides information on the local order of the compounds, differently from classical methods of X-ray diffraction that give information on the crystalline structure of a material. From XANES spectra it is possible to obtain relative elemental and molecular abundances (for instance normalized to the total carbon content in the case of organic functional groups), in some sense complementary to IR or Raman spectroscopy.

Thanks to XANES measurements, the oxidation state of a given element is identified and it is used to investigate the environmental conditions during formation and history of E.T. material. This method has been successfully used to analyze *Stardust* samples, to study the unexpected presence of crystalline silicates in the coma of the comet Wild2 (Westphal et al., 2009) and to compare the Fe valence state of different grains extracted from a bulbous track in the aerogel (Stodolna et al., 2013). Using XANES, Cody et al. (2008) compared the organics found in organic rich particles of Wild2 with the insoluble organic matter found in chondrites, revealing considerable diversity and chemical complexity in the Wild2 organics, and a wide range in heteroatom content such as O and N. In the case of *Hayabusa* particles, Fe K-edge XANES measurements have been reported (combined to other analytical techniques) by Noguchi et al. (2014a) to determine the mineralogy of asteroid Itokawa, and by Mikouchi et al. (2014) who showed that the plagioclase found in the particles has been formed in a relatively oxidizing environment based on their relatively high abundance of Fe^{3+}.

Scanning Transmission X-ray Microscopy (STXM) is an imaging technique based on the interaction between a monochromatic X-ray beam produced by synchrotron radiation with a thin specimen, generating both microscopic observations (e.g.,

contrast images) and spectroscopic measurements (e.g., XANES) with a 15–20 nm spatial resolution. It is now routinely used for the study of organic matter in extraterrestrial matter (Chan et al., 2018; Le Guillou et al., 2013; Nittler et al., 2019).

Finally, **X-ray Fluorescence (XRF)** is based on the emission of X-rays from a material that is excited with high-energy X-rays or gamma rays. This phenomenon is particularly useful in the identification of the main and trace elements in the analyzed material. Similarly to X-CT, XRF micro- and nano-tomography can also be performed, in order to determine the fully 3D distribution of the elements at sub-μm spatial resolutions. Silversmit et al. (2009) have demonstrated the possibility to perform XRF tomography at the nm-scale on a *Stardust* cometary particle. They obtained the 3D distribution of the elements from calcium to selenium with a spatial resolution of 200 nm within a unique ~2 μm terminal particle in a track of aerogel (the collector of the *Stardust* mission). Thanks to the use of reference materials, XRF can provide quantitative measurements with detection limits for the abundance ranging from few to hundreds of ppm, depending on the element. Recent improvements include the possibility of performing fast 2D/3D imaging and spectroscopy (absorption, differential phase contrast, dark field and fluorescence) on the same beam-line (Medjoubi et al., 2018), a highly promising option for the next generation sample return.

In summary, synchrotron based X-ray techniques are currently an essential part of the in-situ analysis of returned samples. They provide a very rich scope of quantitative information about the elemental composition, oxidation state, structure, morphology, and mineralogy of E.T. materials. Disadvantages include potential modifications of the molecular composition by the X-ray photons, and in some cases, an invasive sample preparation.

16.4 Electron-based analytical techniques

Electron microscopes have been developed to achieve a much higher spatial resolution than optical microscopes that are diffraction-limited at the wavelength of the visible light. Two main types of electron microscopes are used to observe E.T. materials, with different energy of the incident beam: from 1 to 30 keV for a Scanning Electron Microscope (SEM) with a spatial resolution down to a few nm, and from 120 to 300/1000 keV for a Transmission Electron Microscope (TEM) with an atomic spatial resolution.

Electron based analysis relies on electron-matter interactions which produce different secondary emissions, used to analyze properties of the sample: secondary, back scattered, Auger, diffracted and transmitted electrons and X-ray photons, whose energy depends on the nature of the excited elements. Sources of incident electrons have improved in the last 20 years and field-emission guns are now routinely used, allowing better signal/noise ratio and higher spatial resolution.

16.4.1 Scanning electron microscopy

After optical microscopy, **Scanning Electron Microscopy (SEM)** is one of the first steps in the observation of the sample, allowing imaging and chemical characterization. This is why SEM observations are routinely performed on returned samples, also as a context for subsequent analytical techniques. Image of the sample's topography can be obtained using secondary electrons while Z-contrast (atomic number) images can be obtained using back-scattered electrons. **Energy Dispersive X-ray Spectroscopy (EDS)** uses the primary electron beam of a SEM to study the secondary X-rays emitted from the sample and to perform μm-sized chemical analysis (with an interaction volume that goes from one to several microns, depending on the elements) or chemical mapping. Chemical elements can be detected down to 0.1 percent but EDS-analysis remains semi-quantitative. Modern EDS detectors provide a better spectral resolution, which allows to work at lower electron energy and thus obtain also a better spatial resolution.

SEM microscopes and electron microprobes usually require a flat polished conductive sample. However, small micron-sized particles can just be deposited on a conductive sample holder. As meteorites are not conductive, gold or carbon coatings are usually required, except in low-vacuum environmental SEMs, albeit with limited spatial resolution. SEM observations can even be performed on isolated grains mounted on conductive needles (see the example of a *Hayabusa* particle shown in

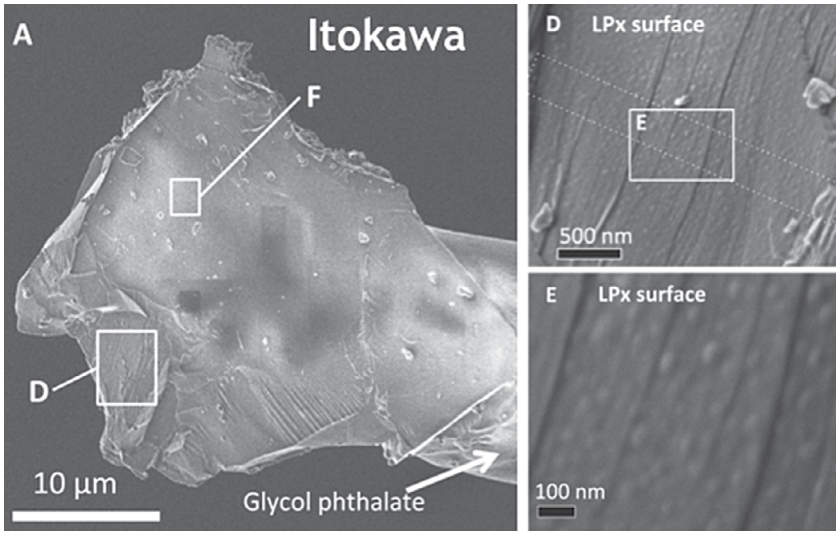

Fig. 16.4 (A) Secondary electron field-emission SEM image of an Itokawa particle (RB-QD04-0043) mounted on a carbon fiber with glycol phthalate. (D) Image of low-Ca pyroxene surface indicated by the square in (A). The dots indicate an area sectioned later. (E) Close-up image of an area rich in spotted structures probably due to space weathering. Adapted from Matsumoto et al. (2015), *(reprinted with permission of Elsevier)*.

Fig. 16.4, Matsumoto et al., 2015), a useful sample preparation that is compatible with other techniques (e.g., IR-CT, X-CT, XRD, see above).

The de-excitation of the atoms of the surface, excited by a primary electron beam can result in the emission of very low energy "Auger electrons" which are characteristic of the excited atoms. It is therefore possible to obtain information on the composition of the sample (**Auger spectrometry**). Auger electron detectors are now routinely used in the analysis of circumstellar grains trapped in meteorites during solar system formation (presolar grains, Floss 2018).

Another possibility in the use of SEM is to have 5–25 keV electrons (with penetration depth of 1–3 μm) impact on a luminescent material like phosphorus, causing the emission of a photon (**Cathodoluminescence, CL**) in UV, visible or IR ranges. This analytical method is particularly useful to investigate shocked minerals. Cathodoluminescent detectors are newly used in the study of chondrules to provide information on the trace elements present or on the growth history of the crystals in the young Solar System (Libourel and Portail, 2018). It has also been used to obtain information about weathering processes on asteroid Itokawa (Gucsik et al., 2017).

Electron Back Scattered Diffraction (EBSD) can be performed with a SEM equipped with an EBSD detector. This technique provides crystallographic information down to 30 nm spatial resolution on samples prepared with a high quality polishing (Bland et al., 2011; Watt et al., 2006).

In **Electron Microprobe Analysis (EMA)**, 2 to 5 **Wavelength Detector Spectroscopy (WDS)** detectors collect photons of given wavelengths corresponding to different elements. Such selected collection allows a better sensitivity down to ~100 ppm in specific analytical conditions, and μm-scale spatial resolution. Thanks to the use of standards, the obtained chemical analyses are quantitative.

16.4.2 Transmission electron microscopy

In a **Transmission Electron Microscope (TEM)**, direct images are obtained using transmitted electrons through the sample. With a 200–300 keV TEM, high resolution imaging can be performed. For TEM, thin samples around 50 to 120 nm thickness have to be prepared using ultramicrotomy of epoxy or sulfur embedded sample (see the example of *Stardust* samples shown in Fig. 16.5), ion milling or more recently, FIB in a SEM. Focused ion-beams of Gallium are used to extract thin samples from a selected site (Giannuzzi and Stevie, 1999; Heaney et al., 2001). A new generation of FIB using more energetic Xe ions is now beginning to be used to cut larger samples (Delobbe et al., 2014). Such TEM sample preparations are difficult and can damage the sample (irradiation effects, loss of structure).

Similarly to SEM, different methods of analysis of the transmitted beam can be performed.

Electrons diffracted by the crystallographic network provide information such as crystal structure parameters or crystal defects. X-photons emitted during electronic

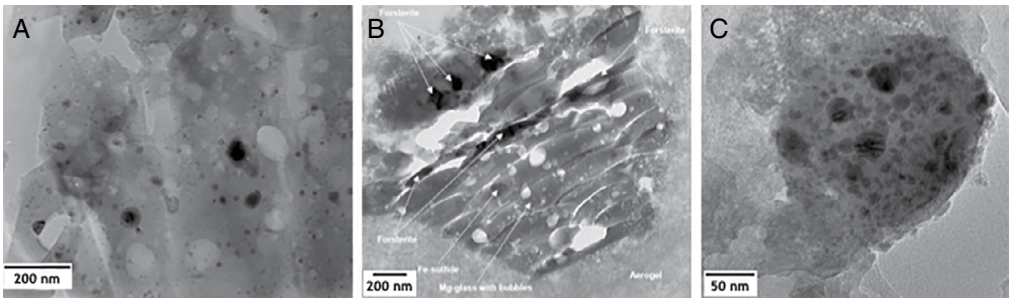

Fig. 16.5 ***Bright-field TEM images of Wild 2 grains.*** (A) Compressed and vesicular melted aerogel surrounding grains. Dark gray and black objects are admixed silicates, Fe-Ni metal, and Fe-Ni sulfides. (B) Captured Wild2 grain composed predominantly of forsterite and Fe-sulfides, mantled by compressed aerogel. (C) Glassy body from a *Stardust* track, resembling similar structures commonly found in IDPs; rounded dark inclusions are predominantly Fe-Ni metal, Fe-Ni sulfides, and ferromagnesian silicates. The cometary samples were embedded in high-purity S and sliced into 50–70 nm-thick sections with an ultramicrotome equipped with a diamond knife. Adapted from Zolensky et al. (2006), original data were kindly provided by M. Zolensky.

inelastic interactions can be detected by EDS detectors and give chemical information about the sample. **Scanning transmission electron microscopy (STEM)** using a focused beam combined with EDS provides Z-contrast images and chemical mapping.

Electron energy loss spectroscopy (EELS) provides information about chemical bonding or valence state for low-atomic elements. Recent improvements in optics and in the reduction of the energy dispersion of the electron beam allows a better energy resolution in EELS down to 0.03 eV, allowing detection of isotopes, of oxygen (Bradley et al., 2014), and of trace elements (Bernatowicz and Gibbons, 1990; Stroud et al., 2011).

TEM-EELS can be considered complementary to STXM-XANES (Section 3.2). Both techniques provide chemical, speciation or bonding information. STXM observes at nanometer scales whereas TEM gives chemical and structural information at an atomic-scale resolution. Radiation damages are less important with STXM (Rightor et al., 1997), and, compared to TEM, the spectral resolution is better (~0.1 eV using soft X-rays compared to ~1 eV with TEM-based EELS).

To summarize, electron beam techniques, both by reflection at the surface of the sample and by transmission through the sample, are powerful techniques although several disadvantages can be cited: material loss and damages associated with sample preparation, irradiation damage, volatiles loss and even isotopic fractionation during analysis. SEM and/or TEM are instruments commonly used to observe E.T. samples and study their composition and structure. They contributed enormously in maximizing the scientific outcome of the *Stardust* (Leroux et al., 2008; Westphal et al., 2014; Zolensky et al., 2006) and *Hayabusa* (Nakamura et al., 2011; Noguchi et al., 2014b, 2011) missions, and will certainly play a major role in the next sample returns analyses.

16.5 Ion-based analytical techniques

Analytical methods using ion bombardment are all surface methods. They can use either high or low energy incident ions.

16.5.1 High energy methods: nuclear microprobe

Proton or nuclear microprobe analyses use primary protons or helium nuclei accelerated to energies in the few MeV range. The nuclei hit a sample prepared as a conductive polished section with low to grazing angle incidence. These techniques include **Proton (or Particle) Induced X-ray Emission (PIXE)**, **Rutherford Backscattering (RBS)** and **Elastic Recoil Detection Analysis (ERDA)**.

In PIXE analysis, interactions between the incident ions and the target atoms induce excitation of electrons in the target, which emit X-ray photons upon returning to the ground state. As in electron microprobe techniques, these X-ray photons have energies depending on the nature of the excited elements. Quantitative EDS or WDS detection of these X-rays allows a complete analysis of the sample chemistry. PIXE can be performed in imaging mode using a pixel size of 10–20 μm (micro-PIXE, e.g., Noun et al., 2019). Typical detection limits vary between few ppm to tens of ppm, depending on the element. In RBS analysis, the energy loss of incident protons backscattered during interactions with the target depends on the chemistry of the target and is used to determine the elemental composition. ERDA is an extension of these methods aiming at measuring the hydrogen content of a sample. The H content is deduced from the number of H atoms ejected from the sample by elastic collisions with incident ions. ERDA can detect H present in abundances as low as a few ppm (Bureau et al., 2009).

These techniques allow measurements of elemental abundances down to the ppm level with a lateral resolution ranging from a few μm to a few 100 μm. The sample depth affected by the bombardment is ~ 1–10 μm. Nuclear microprobes are considered relatively non-destructive because the erosion of target atoms is extremely low, although some damage can be produced especially at the end of the ion tracks. The analyses last from a few minutes for major elements to a few hours for H in trace amounts.

Compared to other methods used for measuring elemental composition, nuclear microprobe methods tend to have lower spatial resolution but higher sensitivity. While PIXE and RBS are limited to the measurement of elements heavier than Na and B, respectively, light elements can be measured by the direct observation of particles emitted during nuclear reactions with the incident particles. ERDA is especially powerful for the determination of H abundances, as it does not require the use of standards compared to SIMS and FTIR (Withers et al., 2012). These methods have not previously been used for the analysis of returned samples but yielded volatile element abundances in glass inclusions from chondritic olivine (Varela et al., 2003) and ERDA is used to measure H standards for the SIMS analysis of E.T. material (e.g., Lévy et al., 2019).

16.5.2 Low energy methods: SIMS and SNMS/RIMS

Secondary Ions Mass Spectrometry (SIMS) is a mass spectrometric method whereby an ion beam (primary ions) accelerated to ~10 keV is used to sputter a small area in a solid sample prepared as a conductive polished section. Ionized atoms extracted from the very first atomic layers of the sample (secondary ions) are accelerated to comparable energies and sent to the mass spectrometer. With the exception of noble gases, all elements from the periodic tables can be detected depending on their electron affinity and their ionization potential.

Two SIMS modes are recognized: static SIMS whereby the incident ion flux is low enough to consider that the system returns to ground state between two collisions. This mode is often associated to time-of-flight mass spectrometry (Stephan, 2001) and ion imaging allowing molecular mass spectrometry up to several 1000 atomic mass units, e.g. for analysis of organic material, and simultaneous detection of a large number of elements. TOF-SIMS analysis of sub μm cometary *Stardust* samples indicated a nearly chondritic chemical composition for most major elements and revealed indigenous polycyclic aromatic hydrocarbons (Stephan et al., 2008). By contrast, dynamic SIMS uses a much higher primary ion flux, with the advantage of a much higher sensitivity allowing isotopic analysis. Three types of dynamic SIMS instruments have been used for the analysis of E.T. materials.

(1) "Conventional" SIMS instruments mostly use large radius magnetic sectors nowadays. They have a lateral resolution of a few μm and can detect simultaneously up to five isotopes in a small mass range. They are usually used for high precision spot analyses of isotopes with a precision reaching 0.1‰.

(2) NanoSIMS instruments have a specific optical design allowing very efficient collection of secondary ions and enhanced lateral resolution down to 50 nm. The geometry of the magnet allows simultaneous detection of 5 to 7 masses along a large mass range. NanoSIMS analyses are highly sensitive to the properties of the sample surface and have a reproducibility at most in the ‰ range.

(3) The UCLA MegaSIMS is an exotic instrument specifically designed for the analysis of O isotopes in the solar wind samples returned by the NASA *Genesis* mission (McKeegan et al., 2011). It is based on a conventional SIMS coupled with a Tandem accelerator along the secondary ion optics to separate ^{17}O from the ^{16}OH interference, followed by a custom multicollector to detect simultaneously high energy O isotopes.

As for most mass spectrometric methods, chemical and isotopic fractionations of instrumental origin are calibrated with reference materials of known composition and structure (standards). SIMS can be used for isotopic analysis at high mass resolution and imaging in both scanning or microscope modes. SIMS is a destructive method, it also allows depth profiling with time since collisions with primary ions affect only a layer <10 nm, whereas the typical thickness of ablated samples range from 100 nm to several μm. Depending on the ion yields of the various elements, the detection limit can be as low as a few ppb. Major drawbacks in SIMS analysis are instrumental effects

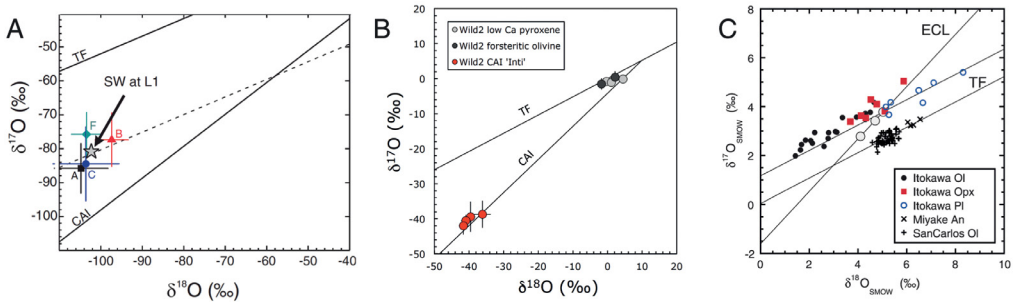

Fig. 16.6 ***Example of SIMS analysis of returned samples, focused on the oxygen isotopes.*** Left: solar wind isotopic composition measured in *Genesis* samples (McKeegan et al., 2011)), reprinted with permission of The American Association for the Advancement of Science. Center: grains of comet Wild2 collected by *Stardust* (adapted from (McKeegan et al., 2006). Right: Itokawa particles collected by *Hayabusa* (Yurimoto et al., 2011), reprinted with permission of The American Association for the Advancement of Science.

known as matrix effects between samples of different chemistry/mineralogy and interferences requiring a high mass resolving power. Most of these interferences can be resolved (hydrides, oxides) but not strict isobars. Although it is a surface analysis, it is usually considered destructive at the μm scale. In spite of these limitations, the strength of SIMS is the in-situ isotopic analysis at the μm to sub-μm scale. It is notably the only method that allows in-situ isotopic analysis of light atmophile elements (H, C, N, O) often of major importance in cosmochemistry.

As a result SIMS is widely used for the analysis of returned samples (Fig. 16.6). The O and N isotopic compositions of the solar wind were notably determined from the *Genesis* samples by SIMS (Marty et al., 2011; McKeegan et al., 2011) bringing insights on the composition of the initial solar nebula. O isotopes measured by SIMS also established the link between *Stardust* cometary samples and inner Solar System materials (McKeegan et al., 2006; Nakamura et al., 2008a) and the link between *Hayabusa* samples from S-type asteroid Itokawa and ordinary chondrites (Yurimoto et al., 2011).

Sputtered Neutral Mass Spectrometry (SNMS) and Resonant Ionization Mass Spectrometry (RIMS) use in-situ sputtering by an ion beam, thus sharing many similarities with SIMS. During sputtering, only a small fraction of the sample atoms are efficiently ionized, typically a few percent. Most sputtered materials are ejected as neutral atoms and cannot be accelerated to the mass spectrometer. In order to gain sensitivity and achieve high precision isotopic analysis of trace elements, SNMS and RIMS use additional lasers to ionize these neutral atoms above the sample surface. Depending on laser energy and wavelength, secondary ions can be produced by resonant ionization (RIMS) or tunneling ionization. While RIMS is element selective and allows complete separation of isobaric interferences, tunneling ionization allows ionization of noble gases. Two notable instruments have been developed for the study of E.T. materials: CHILI is a very large RIMS instrument developed at the University of

Chicago, USA, for the isotopic analysis of trace metals in presolar grains (Stephan et al., 2016) and LIMAS is a tunneling ionization instrument at the University of Hokkaido, Japan, developed specifically for the in-situ analysis of noble gases (Ebata et al., 2012) allowing measurement of implanted solar wind in the *Genesis* returned samples (Bajo et al., 2015). Both instruments have μm to sub-μm spatial resolution and can analyze isotopes of elements present at the several ppm level.

16.6 Others

Several other methods of E.T. matter in-situ analysis exist. Here we cite two examples based on mass spectrometry.

The most commonly used is probably **Laser-Ablation Inductively-Coupled-Plasma Mass Spectrometry (LA-ICP-MS)**. This method combines a laser-ablation chamber, where the samples are ablated using pulsed lasers, with an ICP mass spectrometer. Most of the laser-ablated material consists of neutral species aerosols that are sent to the mass spectrometer by flowing a carrier gas (He or Ar). The most frequently used lasers are Nd:YAG lasers with a 1064 nm wavelength, which can be multiplied to reach 266, 213 and 193 nm wavelengths (UV lasers). Their pulses are typically ~3–5 ns. Femtosecond lasers producing ultrashort pulses are now used to reduce sample heating. LA-ICP-MS is increasingly used for imaging by scanning the laser beam on the sample surface. The spatial resolution is given by the laser beam diameter, typically between 10 and 250 μm, although resolutions down to 2 μm are possible (Zitek et al., 2014). Depth profiling can also be combined with imaging to provide 3D information in a similar way to SIMS. The depth resolution is typically of a few μm or more. LA-ICP-MS is probably the most destructive in-situ technique with ablated volumes up to a few tens of μm^3 and does not allow measurements of atmophile elements because of the use of carrier gases. However, because of these large ablated volumes, its sensitivity is excellent and allows measurements of elements in sub-ppm abundances. Although standards are required, LA-ICP-MS is usually less sensitive to matrix effects than SIMS. It is commonly used to measure trace element (e.g. REE) abundances in meteoritic components (e.g., Ingrao et al., 2019; Tissot et al., 2016) and would become a method of choice for such analyses on returned samples provided there are sufficient amounts of material.

Owing to developments in **tomographic atom probes (TAP)** in the 2000s, all atoms within a small volume (100 nm) can now be detected and counted as a function of their 3D distribution. The sample is prepared, usually by FIB, as a 50 nm radius tip. TAP is a mass spectrometric method based on evaporation of a sample submitted to an electric field which triggers the extraction and ionization of sample atoms that are sent to a 2D detector via a TOF-mass spectrometer. On this detector the position of the ions depends directly on their initial position at the surface of the sample. It is thus possible to make a 2D chemical map of the sample surface, the time of flight giving the mass

of the ions. The 3D distribution is obtained with time as the tip evaporates. A specificity of TAP is the lack of instrumental fractionation because all atoms are detected. The measurement precision and the detection limit depend on the amount of atoms in the sample, they are limited by the small volume analyzed. With an atomic spatial resolution, this technique is especially useful for the 3D characterization of nm-sized inclusions in minerals and materials. Initially developed for metallurgy and nano-electronics, it was recently used to study the effects of impacts in lunar samples (Gopon et al., 2017) and martian meteorites (Moser et al., 2019).

16.7 Complementary techniques in a multi-analytical sequence

We discuss here how to combine different techniques for the analysis of the same sample.

Each of the different analytical techniques described above requires a specific sample preparation. The dimensions of the chosen specimen and its surface conditions are important parameters of the sample preparation, as well as the interface to a sample holder. The loss of E.T. samples during preparation may in some cases be significant. Some analytical techniques may themselves be invasive or destructive to some extent, and this may seriously affect the possibility of analyzing the same sample later with other techniques.

Potential terrestrial contamination is also a limiting factor, which often implies specific preparation protocols depending on the specific techniques to be used. Terrestrial contamination may be present in collection, transportation, curation, manipulation, and analysis steps, and can also be a function of the sample size. Different techniques are sensitive to different kinds and amounts of contaminants, and each technique has its own methods of addressing or removing the presence of contaminants.

All these considerations apply to individual techniques and imply that a specific analysis needs a dedicated strategy of sample preparation, handling and examination, with the general goal to maximize the scientific output of the chosen technique and to minimize the loss and contamination of E.T. samples. This has been a common goal of many analytical developments in the past few decades.

Considering the limited amount of material usually retrieved by sample return missions, it becomes clear that several techniques need to be combined on the same sample in order to maximize the scientific return. The idea of a multi-analytical sequence was introduced since the very first sample returns, but it became crucial in the case of the analysis of individual grains and dust particles retrieved by *Stardust* and *Hayabusa*. To set up an efficient multi-analytical sequence one needs to consider and combine the specific sample preparation issues of the individual techniques, while minimizing sample loss and contamination at each step of the sequence. In addition, the conditions of the sample at the end of each analytical step need to remain acceptable for the subsequent technique. This is commonly achieved by ordering the techniques from less to more

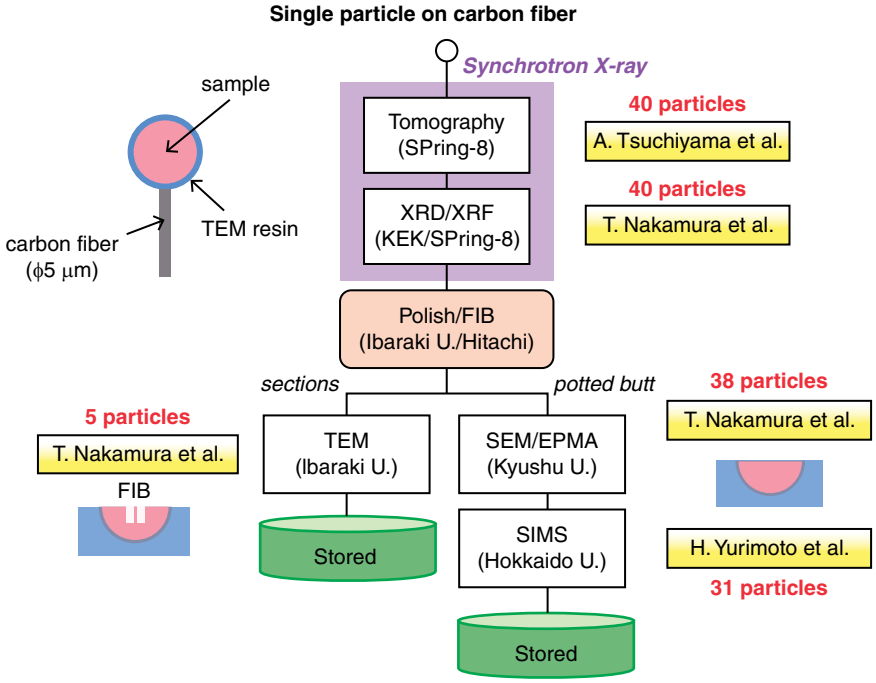

Fig. 16.7 ***Illustration of the analytical strategy developed for Itokawa samples retrieved by Hayabusa.*** The flow chart shows the synchrotron-based X-ray analyses performed as first steps, followed by electron microscopy and ion beam analyses. Each analytical step required a dedicated sample preparation. From Nakamura et al. (2011), *(reprinted with permission of The American Association for the Advancement of Science)*.

destructive, but also establishing a sequence as a function of the sample size and of the analytical spot size (from general morphological, molecular and elemental information at the large scale to specific composition at the small scale).

Fig. 16.7 shows an example of multi-analytical sequence (Nakamura et al., 2011) successfully applied to the analysis of Itokawa particles (*Hayabusa* mission). This sequence included non-destructive synchrotron X-ray analysis (tomography, diffraction and fluorescence) in the first steps, with a dedicated sample preparation of individual grains glued to carbon fibers. The subsequent steps implied additional preparations (e.g., polishing, sectioning), which allowed morphological, elemental, and isotopic analysis of portions of the same particles at a very small scale, by electron microscopy (TEM, SEM) and ion beam analysis (SIMS). The first analytical steps did not compromise the samples for subsequent analyses, and a maximum amount of scientific information was derived from the analysis of individual particles.

Similar efforts are currently being conducted in preparation of the analysis of current missions. During 2021, preliminary examinations will be conducted on samples returned from C-type asteroid Ryugu (*Hayabusa2* mission, JAXA) by international subteams organized by scientific goals and techniques (Tachibana et al., 2018). A similar

multi-analytical approach will probably be implemented for the *OSIRIS-REx* sample return mission (NASA), expected to return samples of B-type asteroid Bennu to Earth in 2023.

In the context of the multi-analytical approach described above, modern non-destructive imaging techniques are an excellent starting point, as they provide a large scale view of the sample and a structural and compositional description which acts as a support for high-resolution techniques. In the past decades, significant efforts have been conducted to upgrade the classical 2D imaging techniques to 3D volume analyses. Nowadays, most imaging techniques are available in some sort of 3D version, e.g., X-CT, IR-CT, 3D-XRF, 3D-TAP, TEM tomography. Destructive methods have also been developed for 3D volume analyses, including combination of imaging and depth profiling modes in SIMS/NanoSIMS or LA-ICP-MS and sequential FIB sectioning for electron microscopy.

In the case of the analysis of individual particles, the combination of complementary IR-CT and X-CT as a starting point in a multi-analytical sequence provides a first quick look at the composition, abundance and 3D distribution of E.T. materials at the μm-scale (Dionnet et al., 2020). Once specific regions of interest are revealed by IR and X measurements (for instance, spots with abundant organic materials or areas showing high porosity), thin sliced sections of the grains can be extracted and analyzed by more destructive techniques to retrieve the structure and the elemental and isotopic composition down to the nanometer scale. This top-down sequence puts advanced high-resolution techniques in a larger context. It is a synergic approach, which overcomes the intrinsic limitations of each technique and in some cases it allows to access scientific information that is not detectable by individual techniques. In the particular case of spectroscopy, a top-down sequence helps building a bridge between the remote sensing observations performed by telescopes and/or spacecrafts at the macroscopic scale and the chemical and physical processes operating at the nanoscale.

16.8 Perspectives

In the past 15 years, *Stardust* and *Hayabusa* have shown that high resolution synchrotron-based studies (micro-imaging, spectroscopy, fluorescence, diffraction, and micro-tomography) play an important role in maximizing the information obtained from μm- and sub-μm sized E.T. samples. This new decade witnesses the birth of the fourth generation of light sources. These new sources include different concepts for producing ultra-brilliant and highly coherent photon beams. Free-electron lasers (FEL) and diffraction-limited storage rings (DLSR) are outstanding examples (Yabashi and Tanaka, 2017). Although the DLSRs provide significant enhancement in the soft to hard X-ray range with respect to the current generation of synchrotrons, the improvement is limited in the lower energy range. In parallel, improved table-top sources and setups for "home-made" systems are being developed.

The complementary roles played by large facilities and small laboratories are particularly interesting in the case of returned sample analyses. In the case of the synchrotron analyses, for instance, the obvious fact that "the samples must go to the facility" implies a tradeoff between sample handling in non-clean room environments, and the access to a facility that allows for high resolution analyses and a rich and fertile context for the multi-analytical approach described in Section 7 (thanks to the access to several beamlines close to each other).

Differently from large-scale facilities, smaller-scale instruments can actually be moved and can "go to the sample", with the undeniable advantage of entering the curation facilities or in general the clean room environments. Analytical instruments can even be miniaturized for space studies to get even closer to the samples ("the laboratory goes to space"). Many of the instruments for in situ analysis that were used onboard the *Rosetta/Philae* (ESA) mission (Bibring et al., 2007) and onboard the *MASCOT* (DLR-CNES) lander of *Hayabusa2* (Ho et al., 2016) were miniaturized versions of larger instruments that had been successfully used for the analysis of E.T. materials in the laboratory. Every space instrument has its laboratory counterpart, connecting space exploration to analytical developments on Earth. In this regard, we expect that the return and analysis of *Hayabusa2* and *OSIRIS-REx* samples will trigger a new wave of laboratory studies, which, in turn, will inspire new developments of space instruments for future observations of Solar System bodies.

Together with the evolution of analytical instruments, we witness an evolution of communities. So far, the analysis of returned samples has essentially been conducted with tools typical of the Materials Science, Physics and (Geo)-Chemistry communities. The search for organic materials in retrieved E.T. samples has also progressed in the last decades, notably thanks to the use of sophisticated chromatography techniques which are now able to provide statistically significant detection of organics, separated from the pervasive terrestrial contaminations. A remarkable example has been provided by the detection of glycine in *Stardust* samples (Elsila et al., 2009). As our knowledge of E.T. materials deepens, and the search and analysis of organic matter in space progress, new tools typical of the (Bio)-Chemistry & Biology communities are likely to play a larger role both in the analyses in space and in the laboratory. These tools include analytical methods as well as data processing methods, such as correlative imaging techniques widely used in bio-sciences and aiming at coupling images acquired by different methods, hence carrying different and complementary informations. We anticipate that a positive feedback between complementary scientific communities and forthcoming technological developments may pave the way towards future sample return from comets, Mars and its moons.

Acknowledgements

We are grateful to M. Zolensky for providing original *Stardust* data. We thank A. Longobardo and P. Boiardi for useful comments and suggestions on the manuscript. This work has been funded by the Centre National d'Etudes Spatiales (CNES-France, *Hayabusa2* mission).

References

Andersen, C.A., Hinthorne, J.R., 1973. 207Pb/206Pb ages and REE abundances in returned lunar material by ion microprobe mass analysis. Lunar and Planetary Science.

Arnold, J.R., Testa, J.P., Friedman, P.J., Kambic, G.X., 1983. Computed tomographic analysis of meteorite inclusions. Science. doi:10.1126/science.219.4583.383.

Bajo, K.-I., Olinger, C.T., Jurewicz, A.J.G., Burnett, D.S., Sakaguchi, I., Suzuki, T., Itose, S., Ishihara, M., Uchino, K., Wieler, R., 2015. Depth profiling analysis of solar wind helium collected in diamond-like carbon film from Genesis. Geochem. J. 49, 559–566.

Bekaert, D.V., Broadley, M.W., Delarue, F., Druzhinina, Z., Paris, G., Robert, F., Sugitani, K., Marty, B., 2020. Xenon isotopes in archean and proterozoic insoluble organic matter: a robust indicator of syngenecity?. Precambrian Res. 336, 105505.

Bernatowicz, T.J., Gibbons, P.C., 1990. Electron energy loss spectrometry of interstellar diamonds. Astrophys. J 359, 246–255.

Bibring, J.-P., -P. Bibring, J., Rosenbauer, H., Boehnhardt, H., Ulamec, S., Biele, J., Espinasse, S., Feuerbacher, B., Gaudon, P., Hemmerich, P., Kletzkine, P., Moura, D., Mugnuolo, R., Nietner, G., Pätz, B., Roll, R., Scheuerle, H., Szegö, K., Wittmann, K., 2007. Philae project office and the entire philae team. The Rosetta Lander ("Philae") Investigations. Space Science Reviews. doi:10.1007/s11214-006-9138-2.

Bland, P.A., Howard, L.E., Prior, D.J., Wheeler, J., Hough, R.M., Dyl, K.A., 2011. Earliest rock fabric formed in the Solar System preserved in a chondrule rim. Nat. Geosci. 4, 244–247.

Bonal, L., Brunetto, R., Beck, P., Dartois, E., Dionnet, Z., Djouadi, Z., Duprat, J., Füri, E., Kakazu, Y., Montagnac, G., Oudayer, P., Quirico, E., Engrand, C., 2015. Visible-IR and Raman microspectroscopic investigation of three Itokawa particles collected by Hayabusa: mineralogy and degree of space weathering based on nondestructive analyses. Meteorit. Planet. Sci. doi:10.1111/maps.12496.

Bradley, J.P., Ishii, H.A., Gillis-Davis, J.J., Ciston, J., Nielsen, M.H., Bechtel, H.A., Martin, M.C., 2014. Detection of solar wind-produced water in irradiated rims on silicate minerals. Proc. Natl. Acad. Sci. U. S. A. 111, 1732–1735.

Bureau, H., Raepsaet, C., Khodja, H., Carraro, A., Aubaud, C., 2009. Determination of hydrogen content in geological samples using elastic recoil detection analysis (ERDA). Geochim. Cosmochim. Acta 73, 3311–3322.

Capaccioni, F., Coradini, A., Filacchione, G., Erard, S., Arnold, G., Drossart, P., De Sanctis, M.C., Bockelee-Morvan, D., Capria, M.T., Tosi, F., Leyrat, C., Schmitt, B., Quirico, E., Cerroni, P., Mennella, V., Raponi, A., Ciarniello, M., McCord, T., Moroz, L., Palomba, E., Ammannito, E., Barucci, M.A., Bellucci, G., Benkhoff, J., Bibring, J.P., Blanco, A., Blecka, M., Carlson, R., Carsenty, U., Colangeli, L., Combes, M., Combi, M., Crovisier, J., Encrenaz, T., Federico, C., Fink, U., Fonti, S., Ip, W.H., Irwin, P., Jaumann, R., Kuehrt, E., Langevin, Y., Magni, G., Mottola, S., Orofino, V., Palumbo, P., Piccioni, G., Schade, U., Taylor, F., Tiphene, D., Tozzi, G.P., Beck, P., Biver, N., Bonal, L., Combe, J.-P., Despan, D., Flamini, E., Fornasier, S., Frigeri, A., Grassi, D., Gudipati, M., Longobardo, A., Markus, K., Merlin, F., Orosei, R., Rinaldi, G., Stephan, K., Cartacci, M., Cicchetti, A., Giuppi, S., Hello, Y., Henry, F., Jacquinod, S., Noschese, R., Peter, G., Politi, R., Reess, J.M., Semery, A., 2015. Cometary science. The organic-rich surface of comet 67P/churyumov-gerasimenko as seen by VIRTIS/Rosetta. Science 347, aaa0628.

Chan, Q.H.S., Zolensky, M.E., Kebukawa, Y., Fries, M., Ito, M., Steele, A., Rahman, Z., Nakato, A., Kilcoyne, A.L.D., Suga, H., Takahashi, Y., Takeichi, Y., Mase, K., 2018. Organic matter in extraterrestrial water-bearing salt crystals. Sci Adv 4, eaao3521.

Cody, G.D., Ade, H., Alexander, M.O., Araki, T., Butterworth, A., Fleckenstein, H., Flynn, G., Gilles, M.K., Jacobsen, C., Kilcoyne, A.L.D., 2008. Quantitative organic and light-element analysis of comet 81P/wild 2 particles using C-, N-, and O-μ-XANES. Meteorit. Planet. Sci. 43, 353–365.

Delobbe, A., Salord, O., Hrncir, T., David, A., Sudraud, P., Lopour, F., 2014. High speed TEM sample preparation by Xe FIB. Microsc. Microanal. 20, 298–299.

Dionnet, Z., Aléon-Toppani, A., Borondics, F., Brunetto, R., Buellet, A.C., Djouadi, Z., King, A., Rubino, S., Troadec, D., 2018. FTIR Micro-tomography of five itokawa particles and one primitive carbonaceous chondrite. Microsc. Microanal. 24, 2100–2101.

Dionnet, Z., Brunetto, R., Aléon-Toppani, A., Rubino, S., Baklouti, D., Borondics, F., Buellet, A.C., Djouadi, Z., King, A., Nakamura, T., Rotundi, A., Sandt, C., Troadec, D., Tsuchiyama, A., et al., 2020. Combining IR and X-ray microtomography data sets: Application to Itokawa particles and to Paris meteorite. Meteoritics and Planetary Science 55, 1645–1664. doi:10.1111/maps.13538.

Dominguez, G., Mcleod, A.S., Gainsforth, Z., Kelly, P., Bechtel, H.A., Keilmann, F., Westphal, A., Thiemens, M., Basov, D.N., 2014. Nanoscale infrared spectroscopy as a non-destructive probe of extraterrestrial samples. Nat. Commun. 5, 5445.

Ebata, S., Ishihara, M., Uchino, K., Itose, S., Matsuya, M., Kudo, M., Bajo, K.-I., Yurimoto, H., 2012. Development of laser ionization mass nanoscope (LIMAS). Surf. Interface Anal. 44, 635–640.

Ebel, D.S., Rivers, M.L., 2007. Meteorite 3-D synchrotron microtomography: methods and applications. Meteorit. Planet. Sci. doi:10.1111/j.1945-5100.2007.tb00595.x.

Elsila, J.E., Glavin, D.P., Dworkin, J.P., 2009. Cometary glycine detected in samples returned by Stardust. Meteorit. Planet. Sci. doi:10.1111/j.1945-5100.2009.tb01224.x.

Floss, C., 2018. Auger spectroscopy in planetary science: elemental analysis of presolar silicate grains. Micros. Today 26, 12–17.

Ganapathy, R., Brownlee, D.E., Hodge, P.W., 1978. Silicate spherules from deep-sea sediments: confirmation of extraterrestrial origin. Science 201, 1119–1121.

Giannuzzi, L.A., Stevie, F.A., 1999. A review of focused ion beam milling techniques for TEM specimen preparation. Micron 30, 197–204.

Gopon, P., Spicuzza, M.J., Kelly, T.F., Reinhard, D., Prosa, T.J., Fournelle, J., 2017. Ultra-reduced phases in apollo 16 regolith: combined field emission electron probe microanalysis and atom probe tomography of submicron Fe-Si grains in apollo 16 sample 61500. Meteorit. Planet. Sci. doi:10.1111/maps.12899.

Gucsik, A., Nakamura, T., Jäger, C., Ninagawa, K., Nishido, H., Kayama, M., Tsuchiyama, A., Ott, U., Kereszturi, Á, 2017. Luminescence spectroscopical properties of plagioclase particles from the hayabusa sample return mission: an implication for study of space weathering processes in the asteroid itokawa. Microsc. Microanal. 23, 179–186.

Hanna, R.D., Ketcham, R.A., 2017. X-ray computed tomography of planetary materials: a primer and review of recent studies. Geochem. Explor. Environ. Analy. 77, 547–572.

Heaney, P.J., Vicenzi, E.P., Giannuzzi, L.A., Livi, K.J.T., 2001. Focused ion beam milling: a method of site-specific sample extraction for microanalysis of Earth and planetary materials. American Mineralogist. doi:10.2138/am-2001-8-917.

Hicks, L.J., MacArthur, J.L., Bridges, J.C., Price, M.C., Wickham-Eade, J.E., Burchell, M.J., Hansford, G.M., Butterworth, A.L., Gurman, S.J., Baker, S.H., 2017. Magnetite in Comet Wild 2: evidence for parent body aqueous alteration. Meteorit. Planet. Sci. 52, 2075–2096.

Ho, T.-.M., Baturkin, V., Grimm, C., Grundmann, J.T., Hobbie, C., Ksenik, E., Lange, C., Sasaki, K., Schlotterer, M., Talapina, M., Termtanasombat, N., Wejmo, E., Witte, L., Wrasmann, M., Wübbels, G., Rößler, J., Ziach, C., Findlay, R., Biele, J., Krause, C., Ulamec, S., Lange, M., Mierheim, O., Lichtenheldt, R., Maier, M., Reill, J., Sedlmayr, H.-J., Bousquet, P., Bellion, A., Bompis, O., Cenac-Morthe, C., Deleuze, M., Fredon, S., Jurado, E., Canalias, E., Jaumann, R., Bibring, J.-P., Glassmeier, K.H., Hercik, D., Grott, M., Celotti, L., Cordero, F., Hendrikse, J., Okada, T., 2016. MASCOT—the mobile asteroid surface scout onboard the hayabusa2 mission. Hayabusa2. doi:10.1007/978-94-024-1538-4_18.

Ingrao, N.J., Hammouda, T., Boyet, M., Gaborieau, M., Moine, B.N., Vlastelic, I., Bouhifd, M.A., Devidal, J.-L., Mathon, O., Testemale, D., Hazemann, J.-L., Proux, O., 2019. Rare earth element partitioning between sulphides and melt: evidence for Yb2+ and Sm2+ in EH chondrites. Geochim. Cosmochim. Acta 265, 182–197.

Keller, L.P., Bajt, S., Baratta, G.A., Borg, J., Bradley, J.P., Brownlee, D.E., Busemann, H., Brucato, J.R., Burchell, M., Colangeli, L., d'Hendecourt, L., Djouadi, Z., Ferrini, G., Flynn, G., Franchi, I.A., Fries, M., Grady, M.M., Graham, G.A., Grossemy, F., Kearsley, A., Matrajt, G., Nakamura-Messenger, K., Mennella, V., Nittler, L., Palumbo, M.E., Stadermann, F.J., Tsou, P., Rotundi, A., Sandford, S.A., Snead, C., Steele, A., Wooden, D., Zolensky, M., 2006. Infrared spectroscopy of comet 81P/Wild 2 samples returned by Stardust. Science 314, 1728–1731.

Kruijer, T.S., Kleine, T., Borg, L.E., 2020. The great isotopic dichotomy of the early solar system. Nature Astronomy. doi:10.1038/s41550-019-0959-9.

Le Guillou, C., Remusat, L., Bernard, S., Brearley, A.J., Leroux, H., 2013. Amorphization and D/H fractionation of kerogens during experimental electron irradiation: comparison with chondritic organic matter. Icarus 226, 101–110.

Leroux, H., Rietmeijer, F.J.M., Velbel, M.A., Brearley, A.J., Jacob, D., Langenhorst, F., Bridges, J.C., Zega, T.J., Stroud, R.M., Cordier, P., Harvey, R.P., Lee, M., Gounelle, M., Zolensky, M.E., 2008. A TEM study of

thermally modified comet 81P/wild 2 dust particles by interactions with the aerogel matrix during the Stardust capture process. Meteorit. Planet. Sci. 43, 97–120.
Lévy, D., Aléon, J., Aléon-Toppani, A., Troadec, D., Duhamel, R., Gonzalez-Cano, A., Bureau, Hélène, Khodja, H., 2019. NanoSIMS imaging of D/H ratios on FIB sections. Analytical Chemistry. doi:10.1021/acs.analchem.9b03134.
Libourel, G., Portail, M., 2018. Chondrules as direct thermochemical sensors of solar protoplanetary disk gas. Sci Adv 4, eaar3321.
Liebl, H.J., Herzog, R.F.K., 1963. Sputtering ion source for solids. J. Appl. Phys. 34, 2893–2896.
Martin, M.C., Dabat-Blondeau, C., Unger, M., Sedlmair, J., Parkinson, D.Y., Bechtel, H.A., Illman, B., Castro, J.M., Keiluweit, M., Buschke, D., Ogle, B., Nasse, M.J., Hirschmugl, C.J., 2013. 3D spectral imaging with synchrotron fourier transform infrared spectro-microtomography. Nat. Methods 10, 861–864.
Marty, B., Chaussidon, M., Wiens, R.C., Jurewicz, A.J.G., Burnett, D.S., 2011. A 15N-poor isotopic composition for the solar system as shown by genesis solar wind samples. Science 332, 1533–1536.
Matsumoto, T., Tsuchiyama, A., Miyake, A., Noguchi, T., Nakamura, M., Uesugi, K., Takeuchi, A., Suzuki, Y., Nakano, T., 2015. Surface and internal structures of a space-weathered rim of an Itokawa regolith particle. Icarus 257, 230–238.
Matsumoto, T., Tsuchiyama, A., Uesugi, K., Nakano, T., Uesugi, M., Matsuno, J., Nagano, T., Shimada, A., Takeuchi, A., Suzuki, Y., Nakamura, T., Nakamura, M., Gucsik, A., Nagaki, K., Sakaiya, T., Kondo, T., 2016. Nanomorphology of itokawa regolith particles: application to space-weathering processes affecting the itokawa asteroid. Geochimica et Cosmochimica Acta. doi:10.1016/j.gca.2016.05.011.
McKeegan, K.D., Aléon, J., Bradley, J., Brownlee, D., Busemann, H., Butterworth, A., Chaussidon, M., Fallon, S., Floss, C., Gilmour, J., Gounelle, M., Graham, G., Guan, Y., Heck, P.R., Hoppe, P., Hutcheon, I.D., Huth, J., Ishii, H., Ito, M., Jacobsen, S.B., Kearsley, A., Leshin, L.A., Liu, M.-C., Lyon, I., Marhas, K., Marty, B., Matrajt, G., Meibom, A., Messenger, S., Mostefaoui, S., Mukhopadhyay, S., Nakamura-Messenger, K., Nittler, L., Palma, R., Pepin, R.O., Papanastassiou, D.A., Robert, F., Schlutter, D., Snead, C.J., Stadermann, F.J., Stroud, R., Tsou, P., Westphal, A., Young, E.D., Ziegler, K., Zimmermann, L., Zinner, E., 2006. Isotopic compositions of cometary matter returned by Stardust. Science 314, 1724–1728.
McKeegan, K.D., Kallio, A.P.A., Heber, V.S., Jarzebinski, G., Mao, P.H., Coath, C.D., Kunihiro, T., Wiens, R.C., Nordholt, J.E., Moses Jr, R.W., Reisenfeld, D.B., Jurewicz, A.J.G., Burnett, D.S., 2011. The oxygen isotopic composition of the sun inferred from captured solar wind. Science 332, 1528–1532.
Medjoubi, K., Baranton, G., Somogyi, A., 2018. Fast full-field micro-tomography at the nanoscopium multitechnique nanoprobe beamline of synchrotron soleil. Microscopy and Microanalysis. doi:10.1017/s1431927618013612.
Merouane, S., Günther, S., Chitarra, O., Stenzel, O., Hilchenbach, M., Engrand, C., Tarcea, N., 2018. Investigation of antarctic micrometeorites and selected carbonaceous chondrites by raman sprectoscopy, electron microscopy and mass spectrometry. 81st Annual Meeting of the Meteoritical Society.
Mikouchi, T., Komatsu, M., Hagiya, K., Ohsumi, K., Zolensky, M.E., Hoffmann, V., Martinez, J., Hochleitner, R., Kaliwoda, M., Terada, Y., Yagi, N., Takata, M., Satake, W., Aoyagi, Y., Takenouchi, A., Karouji, Y., Uesugi, M., Yada, T., 2014. Mineralogy and crystallography of some Itokawa particles returned by the hayabusa asteroidal sample return mission. Earth Planets Space 66, 82.
Moser, D.E., Arcuri, G.A., Reinhard, D.A., White, L.F., Darling, J.R., Barker, I.R., Larson, D.J., Irving, A.J., McCubbin, F.M., Tait, K.T., Roszjar, J., Wittmann, A., Davis, C., 2019. Decline of giant impacts on mars by 4.48 billion years ago and an early opportunity for habitability. Nature Geoscience. doi:10.1038/s41561-019-0380-0.
Nakamura, T., Noguchi, T., Tanaka, M., Zolensky, M.E., Kimura, M., Tsuchiyama, A., Nakato, A., Ogami, T., Ishida, H., Uesugi, M., Yada, T., Shirai, K., Fujimura, A., Okazaki, R., Sandford, S.A., Ishibashi, Y., Abe, M., Okada, T., Ueno, M., Mukai, T., Yoshikawa, M., Kawaguchi, J., 2011. Itokawa dust particles: a direct link between S-type asteroids and ordinary chondrites. Science 333, 1113–1116.
Nakamura, T., Noguchi, T., Tsuchiyama, A., Ushikubo, T., Kita, N.T., Valley, J.W., Zolensky, M.E., Kakazu, Y., Sakamoto, K., Mashio, E., Uesugi, K., Nakano, T., 2008a. Chondrulelike objects in short-period comet 81P/wild 2. Science 321, 1664–1667.
Nakamura, T., Tsuchiyama, A., Akaki, T., Uesugi, K., Nakano, T., Takeuchi, A., Suzuki, Y., Noguchi, T., 2008b. Bulk mineralogy and three-dimensional structures of individual stardust particles deduced from synchrotron X-ray diffraction and microtomography analysis. Meteorit. Planet. Sci. 43, 247–259.

Nittler, L.R., Stroud, R.M., Trigo-Rodríguez, J.M., De Gregorio, B.T., Alexander, C.M.O., Davidson, J., Moyano-Cambero, C.E., Tanbakouei, S., 2019. A cometary building block in a primitive asteroidal meteorite. Nature Astronomy 3, 659–666.

Noguchi, T., Bridges, J.C., Hicks, L.J., Gurman, S.J., Kimura, M., Hashimoto, T., Konno, M., Bradley, J.P., Okazaki, R., Uesugi, M., Yada, T., Karouji, Y., Abe, M., Okada, T., Mitsunari, T., Nakamura, T., Kagi, H., 2014a. Mineralogy of four Itokawa particles collected from the first touchdown site. Earth Planets Space 66, 124.

Noguchi, T., Kimura, M., Hashimoto, T., Konno, M., Nakamura, T., Zolensky, M.E., Tanaka, M., Tsuchiyama, A., Nakato, A., Ogami, T., Ishida, H., Sagae, R., Tsujimoto, S., Matsumoto, T., Matsuno, J., Fujimura, A., Abe, M., Yada, T., Mukai, T., Ueno, M., Okada, T., Shirai, K., Ishibashi, Y., 2014b. Space weathered rims found on the surfaces of the Itokawa dust particles. Meteorit. Planet. Sci. 49, 188–214.

Noguchi, T., Nakamura, T., Kimura, M., Zolensky, M.E., Tanaka, M., Hashimoto, T., Konno, M., Nakato, A., Ogami, T., Fujimura, A., Abe, M., Yada, T., Mukai, T., Ueno, M., Okada, T., Shirai, K., Ishibashi, Y., Okazaki, R., 2011. Incipient space weathering observed on the surface of Itokawa dust particles. Science 333, 1121–1125.

Noun, M., Baklouti, D., Brunetto, R., Borondics, F., Calligaro, T., Dionnet, Z., Le Sergeant d'Hendecourt, L., Nsouli, B., Ribaud, I., Roumie, M., Della-Negra, S., 2019. A mineralogical context for the organic matter in the paris meteorite determined by a multi-technique analysis. Life 9. doi:10.3390/life9020044.

Palma, R.L., Pepin, R.O., Westphal, A.J., 2019. Helium and neon in comet 81P/Wild 2 samples from the NASA stardust mission. & planetary. Science.

Rietmeijer, F.J.M., Nakamura, T., Tsuchiyama, A., Uesugi, K., Nakano, T., Leroux, H., 2008. Origin and formation of iron silicide phases in the aerogel of the stardust mission. Meteorit. Planet. Sci. doi:10.1111/j.1945-5100.2008.tb00613.x.

Rightor, E.G., Hitchcock, A.P., Ade, H., Leapman, R.D., Urquhart, S.G., Smith, A.P., Mitchell, G., Fischer, D., Shin, H.J., Warwick, T., 1997. Spectromicroscopy of poly (ethylene terephthalate): comparison of spectra and radiation damage rates in X-ray absorption and electron energy loss. J. Phys. Chem. B 101, 1950–1960.

Rotundi, A., Baratta, G.A., Borg, J., Brucato, J.R., Busemann, H., Colangeli, L., d'Hendecourt, L., Djouadi, Z., Ferrini, G., Franchi, I.A., 2008. Combined micro-Raman, micro-infrared, and field emission scanning electron microscope analyses of comet 81P/wild 2 particles collected by stardust. Meteorit. Planet. Sci. 43, 367–397.

Rotundi, A., Rietmeijer, F.J.M., Ferrari, M., Della Corte, V., Baratta, G.A., Brunetto, R., Dartois, E., Djouadi, Z., Merouane, S., Borg, J., Brucato, J.R., Le Sergeant d'Hendecourt, L., Mennella, V., Palumbo, M.E., Palumbo, P., 2014. Two refractory wild 2 terminal particles from a carrot-shaped track characterized combining MIR/FIR/Raman microspectroscopy and FE-SEM/EDS analyses. Meteorit. Planet. Sci. 49, 550–575.

Sandford, S.A., Aléon, J., Alexander, C.M.O., Araki, T., Bajt, S., Baratta, G.A., Borg, J., Bradley, J.P., Brownlee, D.E., Brucato, J.R., Burchell, M.J., Busemann, H., Butterworth, A., Clemett, S.J., Cody, G., Colangeli, L., Cooper, G., D'Hendecourt, L., Djouadi, Z., Dworkin, J.P., Ferrini, G., Fleckenstein, H., Flynn, G.J., Franchi, I.A., Fries, M., Gilles, M.K., Glavin, D.P., Gounelle, M., Grossemy, F., Jacobsen, C., Keller, L.P., Kilcoyne, A.L.D., Leitner, J., Matrajt, G., Meibom, A., Mennella, V., Mostefaoui, S., Nittler, L.R., Palumbo, M.E., Papanastassiou, D.A., Robert, F., Rotundi, A., Snead, C.J., Spencer, M.K., Stadermann, F.J., Steele, A., Stephan, T., Tsou, P., Tyliszczak, T., Westphal, A.J., Wirick, S., Wopenka, B., Yabuta, H., Zare, R.N., Zolensky, M.E., 2006. Organics captured from comet 81P/wild 2 by the Stardust spacecraft. Science 314, 1720–1724.

Sears, D.W.G., Sears, H., Ebel, D.S., Wallace, S., Friedrich, J.M., 2016. X-ray computed tomography imaging: a not-so-nondestructive technique. Meteorit. Planet. Sci. 51, 833–838.

Silversmit, G., Vekemans, B., Brenker, F.E., Schmitz, S., Burghammer, M., Riekel, C., Vincze, L., 2009. X-ray fluorescence nanotomography on cometary matter from comet 81P/wild2 returned by stardust. Anal. Chem. 81, 6107–6112.

Slodzian, G., 1964. Étude d'une méthode d'analyse locale chimique et isotopique utilisant l'émission ionique secondaire. Ann Phys (Paris). doi:10.1051/anphys/196413090591.

Stephan, T., 2001. TOF-SIMS in cosmochemistry. Planet. Space Sci. 49, 859–906.

Stephan, T., Flynn, G.J., Sandford, S.A., Zolensky, M.E., 2008. TOF-SIMS analysis of cometary particles extracted from stardust aerogel. Meteorit. Planet. Sci. doi:10.1111/j.1945-5100.2008.tb00623.x.

Stephan, T., Trappitsch, R., Davis, A.M., Pellin, M.J., Rost, D., Savina, M.R., Yokochi, R., Liu, N., 2016. CHILI–the chicago instrument for laser ionization–a new tool for isotope measurements in cosmochemistry. Int. J. Mass Spectrom. 407, 1–15.

Stodolna, J., Gainsforth, Z., Leroux, H., Butterworth, A.L., Tyliszczak, T., Jacob, D., Westphal, A.J., 2013. Iron valence state of fine-grained material from the Jupiter family comet 81P/Wild 2 – A coordinated TEM/STEM EDS/STXM study. Geochimica et Cosmochimica Acta. doi:10.1016/j.gca.2013.08.006.

Stroud, R.M., Chisholm, M.F., Heck, P.R., O'D. Alexander, C.M., Nittler, L.R., 2011. Supernova shock-wave-induced co-formation of glassy carbon and nanodiamond. ApJL 738, L27.

Tachibana, S., Yurimoto, H., Nakamura, T., Noguchi, T., Okazaki, R., Yabuta, H., Naraoka, H., Abe, M., 2018. Initial Analysis Plan of Jaxa Hayabusa2 Returned Ryugu Regolith. University of Tokyo. doi:10.1130/abs/2018am-320240.

Tanaka, M., Nakamura, T., Noguchi, T., Nakato, A., Ishida, H., Yada, T., Shirai, K., Fujimura, A., Ishibashi, Y., Abe, M., 2014. Crystallization temperature determination of Itokawa particles by plagioclase thermometry with X-ray diffraction data obtained by a high-resolution synchrotron Gandolfi camera. Meteorit. Planet. Sci. 49, 237–244.

Tissot, F.L.H., Dauphas, N., Grossman, L., 2016. Origin of uranium isotope variations in early solar nebula condensates. Sci Adv 2, e1501400.

Tsuchiyama, A., Nakamura, T., Okazaki, T., Uesugi, K., Nakano, T., Sakamoto, K., Akaki, T., Iida, Y., Kadono, T., Jogo, K., Suzuki, Y., 2009. Three-dimensional structures and elemental distributions of Stardust impact tracks using synchrotron microtomography and X-ray fluorescence analysis. Meteorit. Planet. Sci. doi:10.1111/j.1945-5100.2009.tb01218.x.

Tsuchiyama, A., Nakano, T., Uesugi, K., Uesugi, M., Takeuchi, A., Suzuki, Y., Noguchi, R., Matsumoto, T., Matsuno, J., Nagano, T., Imai, Y., Nakamura, T., Ogami, T., Noguchi, T., Abe, M., Yada, T., Fujimura, A., 2013. Analytical dual-energy microtomography: a new method for obtaining three-dimensional mineral phase images and its application to Hayabusa samples. Geochim. Cosmochim. Acta 116, 5–16.

Tsuchiyama, A., Okazawa, T., Noguchi, T., Yano, H., Osawa, T., Nakamura, T., Nakamura, K., Nakano, T., Uesugi, K., Yasuda, H., 2004. Density and porosity measurement of Antarctic micrometeorites using microtomography. Meteorit. Planet. Sci 39.

Tsuchiyama, A., Uesugi, M., Matsushima, T., Michikami, T., Kadono, T., Nakamura, T., Uesugi, K., Nakano, T., Sandford, S.A., Noguchi, R., Matsumoto, T., Matsuno, J., Nagano, T., Imai, Y., Takeuchi, A., Suzuki, Y., Ogami, T., Katagiri, J., Ebihara, M., Ireland, T.R., Kitajima, F., Nagao, K., Naraoka, H., Noguchi, T., Okazaki, R., Yurimoto, H., Zolensky, M.E., Mukai, T., Abe, M., Yada, T., Fujimura, A., Yoshikawa, M., Kawaguchi, J., 2011. Three-dimensional structure of Hayabusa samples: origin and evolution of Itokawa regolith. Science 333, 1125–1128.

Tsuchiyama, A., Uesugi, M., Uesugi, K., Nakano, T., Noguchi, R., Matsumoto, T., Matsuno, J., Nagano, T., Imai, Y., Shimada, A., Takeuchi, A., Suzuki, Y., Nakamura, T., Noguchi, T., Abe, M., Yada, T., Fujimura, A., 2014. Three-dimensional microstructure of samples recovered from asteroid 25143 Itokawa: comparison with LL5 and LL6 chondrite particles. Meteorit. Planet. Sci. 49, 172–187.

Uesugi, K., Takeuchi, A., Suzuki, Y., 2009. High-definition high-throughput micro-tomography at SPring-8. J. Phys. Conf. Ser. doi:10.1088/1742-6596/186/1/012050.

Uesugi, K., Takeuchi, A., Suzuki, Y., 2006. Development of micro-tomography system with Fresnel zone plate optics at SPring-8, in: developments in X-Ray Tomography VPresented at the Developments in X-Ray Tomography V. International Society for Optics and Photonics, pp. 63181F.

Uesugi, K., Tsuchiyama, A., Nakano, T., Suzuki, Y., Yagi, N., Umetani, K., Kohmura, Y., 1999. Development of microtomography imaging system for rock and mineral samples, in: developments in X-Ray tomography II. Presented at the developments in X-Ray tomography II. International Society for Optics and Photonics, 214–221.

Varela, M.E., Mosbah, M.B.-., Kurat, G., Gallien, J.P., 2003. Nitrogen microanalysis of glass inclusions in chondritic olivines by nuclear reaction. Geochim. Cosmochim. Acta 67, 1255–1265.

Watt, L.E., Bland, P.A., Prior, D.J., Russell, S.S., 2006. Fabric analysis of allende matrix using EBSD. Meteorit. Planet. Sci. doi:10.1111/j.1945-5100.2006.tb00499.x.

Westphal, A.J., Fakra, S.C., Gainsforth, Z., Marcus, M.A., Ogliore, R.C., Butterworth, A.L., 2009. Mixing fraction of inner solar system material in comet 81p/wild2. Astrophys. J. 694, 18.

Westphal, A.J., Stroud, R.M., Bechtel, H.A., Brenker, F.E., Butterworth, A.L., Flynn, G.J., Frank, D.R., Gainsforth, Z., Hillier, J.K., Postberg, F., Simionovici, A.S., Sterken, V.J., Nittler, L.R., Allen, C., Anderson, D., Ansari, A., Bajt, S., Bastien, R.K., Bassim, N., Bridges, J., Brownlee, D.E., Burchell, M., Burghammer, M., Changela, H., Cloetens, P., Davis, A.M., Doll, R., Floss, C., Grün, E., Heck, P.R., Hoppe, P., Hudson, B., Huth, J., Kearsley, A., King, A.J., Lai, B., Leitner, J., Lemelle, L., Leonard, A., Leroux, H., Lettieri, R., Marchant, W., Ogliore, R., Ong, W.J., Price, M.C., Sandford, S.A., Sans Tresseras, J.-A., Schmitz, S., Schoonjans, T., Schreiber, K., Silversmit, G., Solé, V.A., Srama, R., Stadermann, F., Stephan, T., Stodolna, J., Sutton, S., Trieloff, M., Tsou, P., Tyliszczak, T., Vekemans, B., Vincze, L., Von Korff, J., Wordsworth, N., Zevin, D., Zolensky, M.E., 2014. Interstellar dust. Evidence for interstellar origin of seven dust particles collected by the Stardust spacecraft. Science 345, 786–791.

Withers, A.C., Bureau, H., Raepsaet, C., Hirschmann, M.M., 2012. Calibration of infrared spectroscopy by elastic recoil detection analysis of H in synthetic olivine. Chem. Geol. 334, 92–98.

Yabashi, M., Tanaka, H., 2017. The next ten years of X-ray science. Nature Photonics. doi:10.1038/nphoton.2016.251.

Yesiltas, M., Sedlmair, J., Peale, R.E., Hirschmugl, C.J., 2017. Synchrotron-based three-dimensional fourier-transform infrared spectro-microtomography of murchison meteorite grain. Appl. Spectrosc. 71, 1198–1208.

Yurimoto, H., Abe, K.-I., Abe, M., Ebihara, M., Fujimura, A., Hashiguchi, M., Hashizume, K., Ireland, T.R., Itoh, S., Katayama, J., Kato, C., Kawaguchi, J., Kawasaki, N., Kitajima, F., Kobayashi, S., Meike, T., Mukai, T., Nagao, K., Nakamura, T., Naraoka, H., Noguchi, T., Okazaki, R., Park, C., Sakamoto, N., Seto, Y., Takei, M., Tsuchiyama, A., Uesugi, M., Wakaki, S., Yada, T., Yamamoto, K., Yoshikawa, M., Zolensky, M.E., 2011. Oxygen isotopic compositions of asteroidal materials returned from Itokawa by the hayabusa mission. Science 333, 1116–1119.

Zitek, A., Aléon, J., Prohaska, T., 2014. Chemical imaging, in: sector field mass spectrometry for elemental and isotopic analysis. Royal Society Of Chemistry, 152–182.

Zolensky, M.E., Brownlee, D.E., Tsou, P., Hörz, F.P., Sandford, S.A., Flynn, G.J., McKeegan, K.D., Keller, L.P., 2006. Preliminary examination of the comet wild 2 samples returned by the Stardust spacecraft. Proc. Int. Astron. Union. doi:10.1017/s1743921307010873.

CHAPTER 17

Preservation of samples

Andrea Meneghin, John Robert Brucato
Istituto Nazionale di Astrofisica - Osservatorio Astrofisico di Arcetri (INAF-OAA), L.go E. Fermi, Firenze, Italy

Chapter Outlines

17.1 Planetary Protection

The definition of requirements for returned extraterrestrial samples preservation was posed by scientific community and a National Academy of Science resolution in 1958 (NAS, 1958). This was one of the reasons why in 1959 the Committee on Space Research (COSPAR) was established, with the mandate from the United Nations to maintain and promulgate internationally the Planetary Protection (PP) policies, i.e., the set of practices needed to protect bodies of the Solar System, and the Earth itself, from any possible form of cross-contamination.

According to COSPAR guidelines (COSPAR, 2002), space exploration missions are divided into five categories, in increasing order of planetary protection requirements. This classification is in agreement with article IX of 1966 Outer Space Treaty (U.S. Department of State. 2004), which in article IX states:

"States Parties to the Treaty shall pursue studies of outer space, including the Moon and other celestial bodies, and conduct exploration of them so as to avoid their harmful contamination and also adverse changes in the environment of the Earth resulting from the introduction of extraterrestrial matter and, where necessary, shall adopt appropriate measures for this purpose."

Category V concerns sample return missions and is further divided into two subcategories:

- Unrestricted Earth Return: sample return missions from bodies of the Solar System for which there is a shared scientific opinion that indigenous forms of life are not present.
- Restricted Earth Return: sample return missions from all other bodies.

Sample Return Missions
DOI: 10.1016/C2018-0-03374-5

According to the current state of knowledge, Mars, Enceladus and Europe belong to the restricted category, even if this definition can be updated on the basis of future shared scientific information.

PP has the aim to avoid two possible ways of contamination:

- Forward contamination could arise from spacecrafts launched for space exploration. Forward PP has the aim to avoid that terrestrial organisms and organic materials carried by these spacecrafts contaminate other celestial bodies in the Solar System (and consequently returned samples). This applies to both unrestricted and restricted missions.
- Backward contamination could arise from returned samples, brought back to Earth in a sample return mission. Backward PP has the aim to avoid any possible contamination of the Earth biosphere, due to extraterrestrial life or bioactive molecules. This applies to restricted missions, only.

Forward PP requires the sterilization of spacecrafts in order to reduce the possible bioburden (in particular, in landing operations) and the definition of flight plans able to avoid non-nominal impacts. Backward PP requires the definition of procedures and technologies to protect the Earth from returned extraterrestrial samples.

The set of technologies and procedures for handling returned samples must be developed within a Sample Curation Facility (SCF), i.e., a specific, isolated and protected infrastructure to recover, analyse, possibly catalogue and store the samples in a safe environment. SCF is an essential resource for the management of the samples: it must be able to operate for very long times and maximize the scientific benefits.

SCF requirements, design, building, management, procedure and containment technologies are guided from the characteristics of the samples' parent body. These characteristics are known as soon as the mission is programmed, allowing definition of the infrastructure's technological requirements in advance with respect to the sample return. In unrestricted missions the main goal is to protect the samples, while in restricted ones both samples and Earth's environment have to be protected.

In particular, for restricted missions, COSPAR states that it is necessary to conduct timely analyses in a SCF, under conditions of tight control and using the most sensitive techniques to detect any clues in support of the existence of extant or extinct forms of non-terrestrial life. As long as these analyses are not completed, the SCF must be able to hold the samples within containment that will stop any release of an unsterilized particle, that could be a source of the contamination for the terrestrial ecosystem. The PP requirements state that the probability of a single unsterilized particle of size ≥0.1 μm being released from this facility shall be $\leq 10^{-6}$ (Rummel et al., 2002a).

17.2 Sample curation facilities

Table 17.1 lists all the sample return missions performed so far. All these missions returned unrestricted samples: NASA/Apollo and USSR/Luna missions collected rocks and regolith from the Moon, NASA/Genesis returned atoms of solar wind

Table 17.1 Past sample return missions.

Mission	Returned to Earth	Target	Returned Material
Apollo 11 (USA, NASA)	1969	Moon	21.55 kg
Apollo 12 (USA, NASA)	1969	Moon	34.30 kg
Luna 16 (USSR)	1970	Moon	101 g
Apollo 14 (USA, NASA)	1971	Moon	42.80 kg
Apollo 15 (USA, NASA)	1971	Moon	76.70 kg
Luna 20 (USSR)	1972	Moon	30 g
Apollo 16 (USA, NASA)	1972	Moon	95.20 kg
Luna 24 (USSR)	1976	Moon	170 g
Apollo 17 (USA, NASA)	1972	Moon	110.40 kg
Genesis (USA, NASA)	2004	Earth-Sun Lagrange 1	> 10,000 Solar Wind fragments
Stardust (USA, NASA)	2006	Wild 2 comet	about 1 mg
Hayabusa (Japan, JAXA)	2010	25,143 Itokawa asteroid	about 1 mg

particles, NASA/Stardust cometary (81P/Wild2) and interstellar particles, and JAXA/Hayabusa Itokawa asteroid samples (see Table 17.1). Other three missions are currently in flight or just ended, i.e., NASA/OSIRIS-Rex to Bennu asteroid, JAXA/Hayabusa 2 to Ryugu asteroid and CNSA/Chang'e 5 to Moon), and also belong to the unrestricted category.

Currently, two SCFs are operating at the NASAs Johnson Space Centre (JSC) in Texas, USA (Longobardo and Hutzler, this book) and at the JAXAs Planetary Material Sample Curation Facility (PMSCF) in Japan (Abe et al., this book), respectively. While the Japanese facility only deals with the samples returned from Hayabusa mission (and Hayabusa2, that just returned its samples), JSC curates a heterogeneous collection of samples returned from NASA missions (Table 17.1). The JSC facility also curates part of the Itokawa sample collection, Antarctic meteorites (ASMET program), cosmic dust grains (collected in the stratosphere by means of aircrafts) and microparticulate matter impacted on spacecrafts.

Both the American and the Japanese facility are curating unrestricted samples. Their aim is to mitigate the sample contamination potentially arising from the Earth (particulate, organic, microbiological) by means of air control and the use of inert material for building, furniture, instruments and sample containers. Samples are manipulated and

stored inside cleanroom environments, where the air is kept at positive differential pressure (i.e., larger than the outside pressure) and filtered through high-efficiency systems. Furthermore, the curation staff wears protective clothing, worn in a changing area, and has access to the samples areas through buffer corridors (Yada et al., 2014).

To date, no restricted sample curation facilities exist. The concept of a biocontainment laboratory is well known: it requires the use of a biosafety level adequate to the managed pathogens (WHO, 2004), safe working practices and engineering controls to ensure that pathogenic organisms and agents are not released to the environment. Biocontainment is currently exploited in many microbiology laboratories, nevertheless it has not still applied to space sample curation. In this case, the challenge would be to make biocontainment and sample preservation coexist. The set of possible components of returned samples, in case of a restricted mission, could include (EURO-CARES, 2017a):

- Inorganic compounds: ferromagnesian silicates, aluminosilicates, Fe and Cr oxides, phosphates, metals, sulphides, carbides, nitrides, and hydrated silicates (e.g. clays);
- Organic compounds: soluble carbonaceous and insoluble kerogenous-like compounds, aliphatic and aromatic hydrocarbons, heterocyclic compounds, amines and amides, alcohols, carbohydrates, biomolecules and, possibly, simple life forms.

In addition, gaseous species in the headspace of the sample tubes, potentially liquids and/or ices could also be delivered within the ERC and shall be treated as subsamples.

At time of writing (April 2020), there are two proposals for the development of a restricted SCF: a European Sample Curation Facility (ESCF), proposed by Horizon 2020 EUROCARES project, devoted to generic category V samples (Meneghin et al., 2017), and a NASA Mars sample receiving facility dedicated to Martian samples.

17.3 Technologies for samples preservation in unrestricted and restricted missions

Regardless the COSPAR category of the sample return mission, the main SCF requirement is a safe sample handling and preservation of their pristine conditions. The main goal is obtained by breaking the potential contact chain between the extraterrestrial environment where the samples were taken and the Earth environment where they are brought.

This approach is applied prior the mission departure, by sterilizing spacecraft components that could be in contact and contaminate the samples, and after the Entry Return Capsule (ERC) landing, by recovering the ERC from the landing site and putting it in safe conditions before shipping to the SCF. This procedure should be done also in the event of a non-nominal landing, as happened for NASAs Genesis mission in 2004 (Wiens et al., this book).

After the samples arrival to SCF, preliminary operation and following analyses depend on the unrestricted/restricted classification of the mission and on the potential

risk associated with the management of the samples. Currently, curation experience concerns only unrestricted mission. This means that technologies and procedures used in curating unrestricted samples are robust and consolidated, while the technological constraints and the procedures to balance contamination control (CC) and PP in restricted missions have been theorised, partially implemented, but never applied. The planned NASAs Mars 2020 mission will store geological samples on Mars surface to allow a future mission to bring them to Earth, extending the current curation procedures and technologies to samples potentially able to show extinct or extant forms of life.

Currently, SCFs adopt the following unrestricted sample curation criteria, that could be extended also for restricted samples:

1. Sample preservation at landing site, to make sure the containment chain does not break.
2. Cleanrooms technologies, to isolate the working area where the samples are manipulated;
3. Appropriate tools (operated by human or robotics), to handle, transport and store the samples reducing the possibility to compromise their pristinity;
4. Contamination Control, to verify the environment cleanliness;
5. Sample degradation risk reduction, to maximize the structural integrity or even the availability of the samples;
6. Cleaning and sterilization, to keep the work environment able to preserve the samples pristinity;

The criteria 2–6 apply to SCFs, where the samples are actually handled, analyzed and stored. In accordance to these criteria, the working area must be built, equipped and served by the necessary plants in order to be physically distinct from any other area of a SCF (e.g., office, outreach, services areas), and must include specific cabinets for samples storage and handling (isolator cabinets, storage boxes etc.), where they are ideally being kept in pristine condition. The samples must be manipulated by the personnel or through robotic devices within these cabinets, by using specific tools and devices.

In the following, we give for each of the criteria identified above an overview of the current state-of-art and technology and procedure improvements that would be needed for future restricted sample return missions.

17.3.1 Sample preservation at landing sites

Preservation of samples starts at the landing site, before the sample transport to SCF. For security reasons, landing sites are usually located in remote and few-urbanized locations (Dirri et al., this book). It is necessary to keep in mind that landing is one of the most critical phases of a sample return mission, therefore the occurrence of non-nominal conditions cannot be excluded, including the ERC catastrophic damage. A non-nominal landing occurred for the Genesis mission, when the drogue parachute did not deploy over the Utah Test and Training Range (Wiens et al., this book). The Genesis

Mishap Report (NASA, 2005) identified the main failure reasons, proposed recommendations to avoid future incidents and highlighted that, during the recovery, a number of personnel were close to the return canister, being a source of potential contamination.

A portable receiving facility allows keeping the samples and their envelope in controlled conditions until their delivery to SCF (Meneghin et al., 2017). The portable receiving facility contains equipment for coarse cleaning and initial inspection of the ERC, including evaluation of possible containment chain leakage (i.e., from the sample canister to the ERC external surface). It also includes tools that are useful especially in case of non-nominal landing: specific storage and transport containers must be available to accommodate and transport any fragments of the ERC hardware, any disperse space samples, and samples representative of the landing site environment (soil, air, liquids, vegetation, etc.), necessary to carry out the necessary verification/control operations.

Some of the past recoveries involved the use of temporary cleanrooms. The Genesis ERC, after the non-nominal landing, was moved to a temporary cleanroom at Utah Test and Training Range (UTTR) to catalogue spacecraft components and collector fragments. The Stardust ERC, landed upside-down, was moved to a ISO 7 modular cleanroom at UTTR for preliminary inspection and processing (Zolenski et al., 2008). The Hayabusa ERC, after landing at Woomera Prohibited Area (Australia), was placed in a N_2 container and moved to a temporary cleanroom in South Australia.

17.3.2 Cleanroom and BSL technologies

A cleanroom is a closed space isolated from the outside, where particulate contamination is controlled to be kept under an assigned limit. Temperature, pressure and humidity are normally maintained to a constant value, according to the curation needs. Working area environmental parameters are continuously monitored and recorded to verify the maintenance of the required conditions and highlight the occurrence of non-compliances. According to International Organization for Standardization (ISO) standard (ISO 14644–4), a positive differential pressure between cleanroom and external environment is adopted to avoid samples contamination in case of sample containers leakage.

Air flow is controlled by means of High Efficiency Particulate Air (HEPA) or Ultra Low Penetration Air (ULPA) filters, capable of blocking particles down to about 0.3 μm and to about 0.1 μm, respectively. This is obtained by recirculating the cleanroom air through a number of fibrous layers. Air is usually supplied from the ceiling and collected on the floor (counter top or tables). The mechanisms blocking the particulate matter are the following:

- Impact (>10 μm): particles deviate and collide with the fibers. Efficiency increases with the air flow and with decreasing fibers distance.
- Interception (<10 μm): particles are trapped by the filter.
- Diffusion (≤0.1 μm): the smallest particles, in Brownian motion, come in contact and adhere to the fiber. Efficiency increases with decreasing flow.

Table 17.2 Conversion between ISO 14,644–1 and US FED STD 209E standards.

ISO	Maximum particles/m³						
	≥0.1 μm	≥0.2 μm	≥0.3 μm	≥0.5 μm	≥1 μm	≥5 μm	FEDSTD
ISO 1	10	2					
ISO 2	100	24	10	4			
ISO 3	1000	237	102	35	8		Class 1
ISO 4	10,000	2370	1020	352	83		Class 10
ISO 5	100,000	23,700	10,200	3520	832	29	Class 100
ISO 6	1,000,000	237,000	102,000	35,200	8320	293	Class 1,000
ISO 7				352,000	83,200	2930	Class 10,000
ISO 8				3,520,000	832,000	29,300	Class 100,000

- Air flow is controlled in order to minimize its direct interaction with the samples: there are two main flow delivery models:
- Turbulent or non-directional (flow is uncontrolled): a lower cleanliness degree is guaranteed (i.e., not better than ISO 5, see Table 17.2), being potentially dangerous for the small samples and dust, that can be lost due to the uncontrolled flow.
- Laminar (flow is unidirectional, usually at low speed): the cleanliness degree is higher (from ISO 5 to ISO 1, see Table 17.2) and environmental parameters (temperature and pressure) can be better controlled.

There are many standards to classify cleanrooms. The main ones are the ISO (ISO 14644–1) and the United States Federal Standard (FED-STD-209E 1992). The latter is still in use as classification tool, even if cancelled in 2001. The conversion between such standards is reported in Table 17.2.

The existing curation facilities at NASA JSC have the following standards: ISO 6 for lunar rocks and soil, ISO 6 for Antarctic meteorites, ISO 5 for cosmic dust from Earth's atmosphere, ISO 4 for solar wind samples, ISO 5 for cometary and interstellar particles, ISO 5 for the Itokawa asteroid subset. The curation of Itokawa asteroid samples at JAXA follows ISO 5 standard. The planned Ryugu and Bennu asteroids return mission will have ISO 5 cleanrooms.

For restricted sample return missions, cleanroom technology and biological containment approaches will have to coexist. The biosafety level is the set of technologies, equipment and practises to create a safe condition, within and outside a laboratory, when dealing with dangerous biological agents. The level can vary from BSL-1, typical of non-pathogenic agents, to BSL-4, used for very dangerous agents for humans and environment (i.e., agents for which there are no treatments or vaccines). Table 17.3 shows laboratory practises and safety equipment needed for each level.

Table 17.3 Biosafety level risk groups (WHO, 2004). BSC and GMT indicate Biological Safety Cabinet and Good Microbiological Techniques, respectively.

Level	Laboratory Type	Laboratory practises	Safety equipment
BSL-1	Basic teaching, research	GMT	None
BSL-2	Primary health services, diagnostic services, research	GMT plus protective clothing, biohazard sign	Open bench plus BSC potential aerosol
BSL-3	Special diagnostic services, research	As BSL-2 plus special clothing, controlled access, directional airflow	BSC and/or other primary devices for all activities
BSL-4	Dangerous pathogen units	As BSL-3 plus airlock entry, shower exit, special waste disposal	Class III BSC or positive pressure suits in conjunction with Class II BSCs, double ended autoclave (through the wall) filtered air

According to PP and World Health Organization (WHO) requirements, the restricted samples should be treated as dangerous for the Earth environment until it is demonstrated that they are not a risk for life on Earth or until they are properly sterilized (Rummel et al., 2002b). Beyond the debated issue about influence of early sterilization on science (i.e., possibility to discover extraterrestrial life), this requires that a restricted SCF should have a biosafety level 4 (BSL-4) (WHO, 2004).

Four planetary protection levels (PPL) were defined (Table 17.4), based on combinations of containment and cleanliness condition (Rummel et al., 2002b).

The main difficulty in the coexistence of cleanroom and BSL technologies is the pressure issue: while for a standard cleanroom a positive differential pressure is required,

Table 17.4 Proposed definition of Planetary Protection Levels (Rummel et al., 2002).

PPL	Biocontainment	Cleanliness	Environment condition	Field of use
PPL-α	Max. (BSL-4)	High	1atm, inert gas	Incoming container and materials, preliminary tests, sample bank/storage, some Life Detection analyses
PPL-β	Max. (BSL-4)	High	Earth-like	Some Life Detection, some physical/chemical analyses
PPL-γ	Max. (BSL-4)	Moderate	Earth-like	Some Biohazard Assessment Protocol testing, some physical/chemical processing and animal testing
PPL-δ	Strict BSL-3-Ag	Ambient	Earth-like	Some Biohazard Assessment Protocol; post-release tests

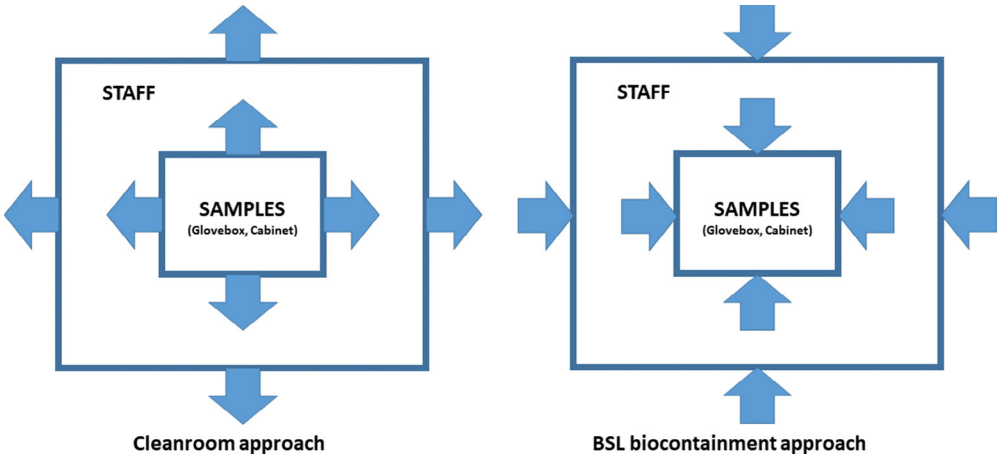

Fig. 17.1 Air flow (blue arrows) in case of leakage for a cleanroom (left) and a BSL approach (right).

in biological containment laboratories a negative pressure gradient would prevent samples from contaminating the external environment (Fig. 17.1).

A possible trade-off between the two requirements could be the double walled insulator (DWI) technique (Vrublevskis et al. 2018 and Holt et al. 2019): gloveboxes and cabinets should have an external double wall, with an interspace, filled by an inert gas (GN2, argon) kept at a pressure larger than the ones acting on both external surfaces, i.e., towards the samples and towards the staff (Fig. 17.2). This design would guarantee both biocontainment and cleanroom standard, as well as minimization of contamination

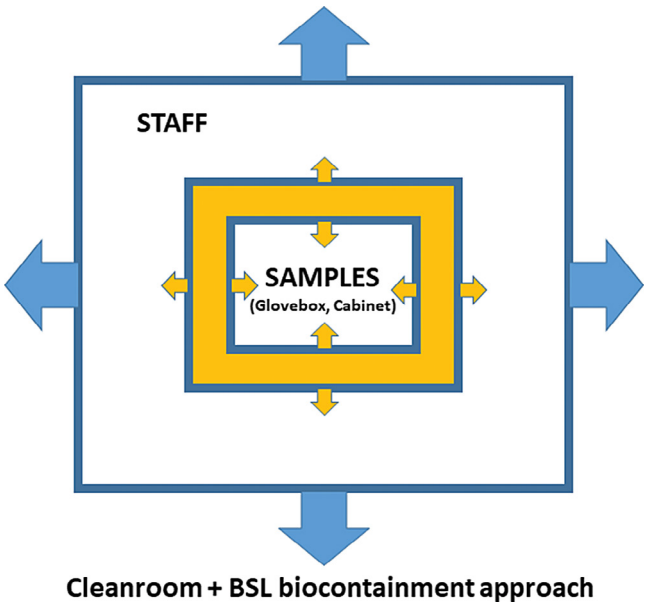

Fig. 17.2 Air flow in integrated cleanroom-BSL approach, by using the DWI design.

risk, thanks to the use of inert gases. So far, DWI prototype devices have been created. In view of future sample return missions, the next big technological challenge will be to bring this approach to maturity.

DWI would require robotics for sample manipulation because gloves could compromise sample pristinity due to material outgassing. Other techniques for handling restricted samples could be taken into account, such as cabinet lines and suited laboratories: these techniques are less efficient but commonly used in high containment biological laboratories. In the first case, the samples are confined in cabinets, having an internal air flow, whose rate and direction would prevent material leakage: however, this approach would be disadvantageous for small samples, due to their high loss risk. In the second case, the working area staff would need to wear uncomfortable positive pressure clothing and would have direct access to samples (without the interface of gloveboxes). However, both systems pose cross-contamination risks and do not guarantee the correct application of the CC plan.

17.3.3 Tools and operations

Cleanroom requirements can be applied to the only cabinets storing the samples or extended to the entire work environment. In the latter case, operators must compulsorily wear protective and sterile clothes (gloves, suits, glasses, etc.) and use changing rooms and airlocks before entering the cleanroom. The access to the cleanrooms could occur through a succession of cascade environments at increasing pressure from the outside to the inside.

Isolator cabinets contain samples, containers and generally manipulation tools and scientific instrumentation (e.g., this is the case of lunar samples stored at JSC). They allow samples isolation from the external environment and their direct manipulation by means of integrated gloves, robotics or manipulators.

When dealing with restricted samples, further considerations regarding handling procedures are necessary. Whereas in the case of unrestricted missions the approach based on the cleanroom standard allows operators to act manually on the samples, in the case of restricted missions the access to the samples should preferably carried out by using remote manipulation systems (i.e. micromanipulators, robots, cobots, automatic warehouse systems, etc.). This approach is mandatory when using a DWI cabinet. Remote operations would have the advantage of removing personnel from the direct manipulation of the samples, and hence of reducing the possible contact with any pathogens contained in the samples. The suitable technologies could be completely or partially autonomous, or completely controlled by the operators. A typical example of a fully automated system could be the transfer of sample containers to and from the storage cabinets by means of an automatic warehouse system. The use of remote-control technologies should have a positive fallout, e.g., offering a more accurate manipulation

of small samples, also on unrestricted samples, on which this approach is currently applied but with a limited extent.

Storage operations and containers depend on the sample characteristics, e.g., size (atoms, grains, regolith, rocks, etc.) and, in the case of restricted samples, phase (solid, liquid, ice, gas). A possible classification of the containers, based on their operations in a SCF, is the following:

- Sample containers, where samples are allocated for analysis out of the working area;
- Storage containers, receiving the samples for their conservation inside the storage cabinets;
- Transport containers, to transport the samples to and from external laboratories.

The containers volume and shape must comply with the samples' characteristics. Sample containers are required to keep the samples only for the time needed for preliminary and cataloguing operations and guarantee an easy access to the analysis instrumentation. Storage containers are designed for a long-term samples' sealing. Transport containers are required to prevent sample damage or loss during transfer outside SCF: in the case of restricted samples, their design must be compliant with WHO guidelines for transporting potentially hazardous samples (WHO, 2012).

17.3.4 Contamination Control

Sample contamination is the molecular, liquid and particulate material absorption, which could alter or degrade samples. Liquid contamination could originate from any compound capable of easily flowing at room temperature and pressure (water, organic, metal). Particle contamination could originate from any inorganic, organic and biological solid particle (with size ranging between 0.01 and 100 μm). Molecular contamination could originate from any gaseous chemical product, in the case contaminants do not aggregate in particles (Hutzler et al., 2019).

The main contamination sources are generated in the facility itself (infrastructure, staff, tools and materials) or in the surrounding environment, even if cleanroom is kept at a positive differential pressure (IEST Recommended Practices, 2011). A list of the main possible SCF contaminating sources, also including some biological contamination sources, is shown in Table 17.5.

Contamination control (CC) is the main guiding principle inside an unrestricted SCF. All the CC procedures aim at detecting and minimizing all the foreseen potential sources of sample contamination (Meneghin et al., 2017). A set of predefined contamination thresholds is required to avoid samples exposition to unacceptable levels of contamination and to ensure that cleaning and handling procedures meet the specification requirements.

CC is implemented through a continuous, routinely monitoring of cleanrooms and, if needed, of the surrounding environment. In-situ contamination monitoring is obtained by means of witness plates, i.e., pieces of materials left in the working area

Table 17.5 List of the main SCF contaminants.

Source	Contaminant	Type
Facility	Surface coatings: walls, floors and roofs	Particulate, liquid
	Surface desorbed water	Liquid
	Building materials	Particulate
	Air conditioning	Particulate, liquid
	Room air	Particulate, molecular
	Spills and leaks	Liquid, molecular
	Air filters	Particulate
	Packing	Particulate, liquid
	Containers	Particulate
Personnel	Skin	Biological (cells)
	Skin fat	Liquid
	Cosmetics	Molecular, particulate
	Spittle	Liquid
	Clothing fibers	Particulate
	Particles in hair or clothes	Particulate
	Hair	Biological
	Bacteria, fungi and viruses	Biological
	Water	Molecular, liquid
	Organics	Molecular
	Secondary microorganism products	Molecular (also as biofilm)
Tools	Friction and wear	Particulate
	Lubricants and emissions	Molecular, liquid
	Vibrations	Particulate
	Brooms and mops	Particulate
	Spatters	Liquid (also as solid film)
	Cleaning chemicals	Molecular, liquid
	Plasticizers	Molecular (outgases)
	Adhesive plates	Molecular
	Machine oils	Liquid
Product generated	Teflon	Particulate, molecular
	Quartz	Particulate
	Aluminium	Particulate, molecular
	Gold	Particulate, molecular
	Stainless steel	Particulate, molecular
	Coating metal	Particulate

and regularly collected to verify if biological, chemical and/or organic contamination happens. Gases, reagents, surfaces, sample handling or storage device and test samples are also monitored. Sample analogues are generally used to validate the CC plan, before beginning of returned sample curation.

17.3.5 Sample degradation risk reduction

The returned samples come from different pressure and temperature environments. The need to preserve the original conditions could induce a technological complexity not easily solved with the currently available technologies. For this reason, the axiom of keeping the samples in their original conditions is replaced by the creation of a sample manipulation environment capable of preventing the occurrence of alteration and degradation processes that may compromise the samples themselves.

Following this approach, it is possible to define risk reduction as the set of curation practises to be implemented in order to maximize the structural integrity or even the availability of the samples (e.g. micrometric-sized samples, can even get lost inside their own containers in case of a non-appropriate approach). ISO 4 Cleanrooms with a full ceiling coverage of ULPA filters, perforated floor and laminar flow maintain a low airborne particle environment and should be considered as the best practise for unrestricted samples curation, but they are not sufficient to avoid sample contamination.

The risk reduction best practises aim at creating a non-interacting layer (atmosphere and material in contact) around the samples, to prevent mechanical, chemical and biological alteration: the atmosphere inside the cleanroom/cabinets, the surfaces in direct contact and the tool used to manipulate should have a composition that do not compromise the pristine nature of samples.

Samples are normally processed in an inert atmosphere using purified gases. Inert gases do not chemically react with samples, preserving their pristinity. Gaseous nitrogen is the most commonly used inert gas for curatorial use. For example, pristine Apollo samples are stored in a dry (<5 ppm of H2O) gaseous nitrogen atmosphere. Argon and helium are also used for specific activities or experiments (Herd et al., 2016). The use of vacuum is an alternative solution, but it requires a careful evaluation. Considering the environmental outgassing and technical complexity to handle sample in vacuum (it requires constant pumping and should be disruptive for samples in case of leakage), the use of vacuum should be a working condition only for specific purposes, and not for an extended curatorial aims. Vacuum was employed for lunar samples collected during the Apollo missions and, to date, it is successfully applied only in JAXA curation of Itokawa asteroid samples (Yada et al., 2014).

To ensure the preservation of the samples it is necessary that the contact surfaces have a limited or no level of interaction with samples, so that the materials used must therefore have specific characteristics: limited outgassing, little or no thermal, magnetic and electrical conductivity, absence of permeability to gas and liquids. They must also have high mechanical resistance to impact and abrasion. Although all types of material can interact with samples to a certain extent (e.g. both the organic and inorganic portion of regolith can desorb or adsorb atoms or molecular fragments from the interface of containers), gold, Teflon, stainless steel, aluminium alloy and quartz are generally preferred as materials in contact with samples. Viscosity is another property that is taken

into account: Teflon and quartz surfaces are suitable for samples larger than 1–2 mm, while smaller, dust-like samples should be handled and stored on surfaces made with softer materials, such as gold foil. In case of manipulating systems, lubrication is not allowed. For example, pristine Apollo samples are allowed to be in contact only with 304/316 stainless steel, Teflon, 6100 aluminium alloy. All the tools, sample containers and cabinet surfaces that come into direct contact with the samples are composed only of these materials. JAXA manipulates samples at PMSCF using isolator cabinets with an integrated mechanical manipulation, using 6061 aluminium, 304/316 stainless steel, Teflon, and quartz in an ultrapure nitrogen atmosphere system (Yada et al. 2014).

Generation and accumulation of electrostatic discharge (ESD) of surfaces in direct contact with samples is another issue to face inside the SCF working area, because it can modify the sample properties or make them difficult to handle, especially when they are small. There are three categories of protective systems capable of preventing the ESD onset: antistatic, which prevents the generation of the charge, static dissipative, with a low surface electrical resistance that allows electrons to flow easily, and conductive. In a SCF, the floor should guarantee low electrical resistance, the staff should be grounded through dedicated footwear, as well as all equipment and devices should have the same electrical potential of the operators. This set of precautions allows cleanrooms, workstations and operators to reach a state of equilibrium and maximize the factors inhibiting the occurrence of ESD

17.3.6 Cleaning and sterilization

Cleaning and sterilization of isolator cabinets, manipulating tools and sample containers is one of the main drivers to reduce organic and inorganic contaminants and preserve the samples purity. There is a number of standard procedures for both cleaning (ultrapure water, isopropyl alcohol) and sterilization (dry and wet heath, hydrogen peroxide).

Cleaning should comply with the CC plan, in order to maintain a measurable level of cleanliness under the prescribed threshold. There are many international standards to verify the accuracy of cleaning activities. NASA Curation Office frequently uses the Institute of Environmental Sciences and Technology (IEST) STD-CC1246E standard (IEST, 2013), which specifies the surface cleanliness level for both particles and non-volatile residue (NVR). Particles are counted by microscopy or liquid particle counts while NVR is measured by gravity mass calculation. Particulate and NVR witness plates are commonly used to monitor the environment.

Ultrapure water (UPW) is the main cleaning agent used inside curation facilities. NASA uses the Technical Support Procedure 23 (TSP 23) standard procedure for cleaning cabinets in all curation laboratories, using UPW with resistivity larger than 18 MΩ, total organic carbon (TOC) lower than 5 ppb and heated to 70 °C, (Calaway et al., 2013 and 2014). After cleaning procedure, the particles cleanliness level should normally comply level 50 of the Military Standard (MIL-STD-1246C, 1994), as defined

Table 17.6 MIL-STD-1246C cleanliness level 50.

Level	Particle Size (μm)	Count per 0.1 m²	Count per liter
50	5	179	530
50	15	27	230
50	25	7.88	34
50	50	1.08	10

in Table 17.6. MIL-STD-1246C is the basis of STD-CC1246E standard. In some cases, the cleanliness level should be better, as for Genesis curation, where surfaces require a level 25 cleaning.

UPW cleaning was first used for curation of Apollo samples and is now a very mature approach, particularly efficient for removing inorganic compounds. The removal of organic should require additional techniques such as bake-out, UV-ozone or plasma cleaning (McCubbin F.M. et al., 2019). Megasonically energized UPW is also used for direct cleaning of samples of solar wind collected by Genesis missions and contaminated during the non-nominal landing (Calaway et al., 2009).

Sterilization is the validated process used to render product free from viable micro-organisms (ECSS-Q-ST-70-53C 2008). Both physical and chemical methods are used for sterilization. The first category includes heat and radiation, while the second one uses liquid or gaseous products. The advantage of physical methods is their ability to sterilize not only external surface layers (as chemical methods do), but also internal volumes. Chemical treatments are cheap and quick but may alter the samples, reducing their value for subsequent scientific analysis, so they are commonly used to sterilize devices and tools not in direct contact with the samples. The most used physical method is the thermostable materials heating, which can be divided into autoclave wet heat and oven dry heat. There is a number of temperature/time dependant protocols. Ionizing radiation may afford a less destructive route to sterilization, but implementation could be problematic.

In case of an unrestricted mission, sterilization processes are not required to be repeated after their implementation inside the curation working area (EURO-CARES, 2017b), differently than cleaning procedures. On the contrary, sterilization needs to be repeated when dealing with restricted samples: this would be a fundamental operation because contamination could affect life detection and biohazard analyses, leading to detection of false positives.

17.4 Conclusions

In general terms, curation of samples in a SCF requires a well-defined approach consisting of procedures and technologies, capable of preserving the sample original characteristics for long-term. To date, curation facilities are efficient in dealing with unrestricted samples:

curating approach is robust and personnel is well trained. On the other hand, future restricted missions, arising from the great challenge of seeking life outside the Earth, will need a brand new curatorial environment, that should be implemented by combining existing technologies to guarantee forward and backward planetary protection.

References

Calaway, M.J., et al., 2009. Decontaminating solar wind samples with the Genesis ultra-pure water megasonic wafer spin cleaner, 40th Lunar and Planetary Science Conference 2009. Abs, 1183.

Calaway, M.J., et al., 2013. Ultra pure water cleaning baseline study on NASA JSC astromaterial curation gloveboxes, Lunar and Planetary Sciences Institute Conference 2013.

Calaway, M.J., et al., 2014. Organic contamination baseline study in NASA Johnson space center astromaterials curation laboratories. NASA Astromaterials Acquisition and Curation Office. NASA/TP 2014, 217393.

COSPAR (2002). COSPAR Planetary Protection Policy. p 4.

Dirri, F. et al., this book. Recovery and Transport of Samples, Chapter 15.

ECSS-Q-ST-70-53C, 2008. Space product assurance - materials and hardware compatibility tests for sterilization processes. European Cooperation for Space Standardization (ECSS).

EURO-CARES - D7.1 Interim Technical Report (2017a).

EURO-CARES - D2.3 A plan for European Curation of Returned Extraterrestrial Samples (2017b).

FED-STD-209E, Federal Standard: airborne Particulate Cleanliness Classes in Cleanrooms and Clean Zones (1992).

Herd, C.D.K., et al., 2016. Cold curation of pristine astromaterials: insights from the Tagish Lake meteorite. Meteorit. Planet. Sci. 51, 499–519.

Hutzler, et al., 2019. contamination control and knowledge during construction of new curation facilities at NASA Johnson space center, 50th Lunar and Planetary Science Conference, 2019.

Holt, J.M.C., et al., 2019. Double walled isolator technology for Mars sample return facilities. Proceedings of the 50th Lunar and Planetary Science Conference 2019, 2408 #.

IEST-STD-CC1246E (2013). Product cleanliness levels - Applications, requirements, and determination.

IEST-RP-CC003.3 (2011). Garment system considerations for cleanrooms and other controlled environments (2011).

ISO 14644-1:2015 Standard, 2015. Cleanrooms and associated controlled environments - Part 1. Classification of air cleanliness by particle concentration.

ISO 14644-4:2001 Standard (2001). Cleanrooms and associated controlled environments - Part 4: design, construction and start-up.

Longobardo, A. and Hutzler, A., this book. The NASA's Johnson Space Center Astromaterials Facilities, Chapter 11.

McCubbin, F.M., et al., 2019. Advanced curation of astromaterials for planetary science. Space Sci. Rev. 215 (Issue 8), 81. doi:10.1007/s11214-019-0615-9 article id48.

Meneghin, A., et al., 2017. Euro-cares D7.2 final technical report. (Deliverable of the EURO-CARES project http://www.euro-cares.eu/reports).

MIL-STD-1246C, 1994. Military standard. Product cleanliness levels contamination control program.

NAS, 1958. Resolution adopted by the Council of the NAS, February 8, 1958. Addendum to Minutes of the Meeting of the Council of the National Academy of Sciences February 8, 1958.

NASA (2005). GENESIS Mishap Investigation Board Report. 1.

Rummel, J.D., et al., 2002a. COSPAR'S planetary protection policy: a consolidated draft. Adv. Space Res. 30 (Issue 6), 1567–1571.

Rummel, J.D., et al., 2002b. A draft test protocol for detecting possible biohazards in Martian samples returned to Earth. NASA/CP 2002, 211842.

Yada, T., et al., 2014. Hayabusa-returned sample curation in the planetary material sample curation facility of JAXA. Meteoritics and Planetary Science 49 (2), 135–153. doi:10.1111/maps.12027.

U.S. Department of State, 2004. Narrative: treaty on principles governing the activities of states in the exploration and use of outer space. Including the Moon and Other Celestial Bodies.

J. Vrublevskis, J., et al., 2018. Description of European Space Agency (ESA) double walled isolator (DWI) breadboard currently under development for demonstration of critical technology foreseen to be used in the Mars sample receiving facility (MSRF), Proceedings of the Second International Mars Sample Return Conference, 2018, 6009 #.

WHO, 2012. Guidance on regulations for the transport of infectious substances. WHO/HSE/GCR 2012, 2.

WHO (2004). Laboratory biosafety manual. 3rd ed. 186 p. ISBN: 92-4-154650-6.

Wiens, R.C., this book. The Genesis Solar-Wind mission: first deep-space robotic mission to return to Earth, Chapter 5.

Zolensky, M., et al., 2008. Curation, spacecraft recovery and preliminary examination for the stardust mission: a perspective from the curatorial facility. MAPS 43 (1–2), 5–21.

PART IV

The future

CHAPTER 18

Lessons learned and future perspectives

Andrea Longobardo
INAF-IAPS, Rome, Italy

Sample return is the last frontier of Solar System exploration: it gives not only the possibility to work on uncontaminated samples and to have them available for future analyses, but also the opportunity to investigate astrobiological issues, that is one of the main scientific goals identified by the worldwide planetary science community.

Sample collection, transport, analysis and storage techniques are quickly improving, and a further enhancement is expected in the coming years, thanks to planned missions and mission concept studies, including some very ambitious and technologically challenging.

After one human, four robotic and two ongoing missions, as well as the development of two curation facilities, we learned a lot about sample return, from mission design to sample analysis in terrestrial laboratories. The lessons learned are the starting point for the future, especially in view of missions aimed at returning samples possibly hosting life forms (hereafter restricted samples). These missions will require a particular care, because restricted samples must be considered as potentially causing fatal human disease until the reverse is demonstrated.

We give in the following a non-exhaustive list of lessons learned so far.

Mission profile. The first sample return mission was Apollo 11. Apollo missions rendezvoused the Moon, combining a lunar lander and a command/service module. This is an optimal mission configuration when landing sites is at equatorial latitudes, but not appropriate for high latitudes. Apollo missions had additional constraints, concerning human operations, such as duration and astronauts number. Luna sample return missions, that also landed at equatorial latitudes, were instead commanded from Earth.

The Genesis mission collected solar wind particles on the Earth-Sun L1 lagrangian point: its operations were affected by solar activity, with the spacecraft switching on safe mode during a solar storm. Cometary dust was instead sampled by the Stardust mission flying over the 81P/Wild comet.

Missions to small asteroids are more challenging, because of the need to work in micro-gravity environment, where the difficult touch-and-go sampling operation should take place. For instance, the OSIRIS-REx mission profile is very complex, with several stages, each with a different observation strategy: a new planning tool (JAsteroid) was developed to satisfy precision navigation, to ensure operations compliance with

Sample Return Missions
DOI: 10.1016/C2018-0-03374-5

science requirements and to decrease risks of last-minute changes. Nevertheless, a mission team must be ready to modify the mission profile during navigation, due to unforeseen incidents or in the case of target different than expected. The Hayabusa mission was disturbed by solar flares, which degraded solar cells, and emergency maneuvers were implemented to overcome incidents related to fuel, attitude and communication. During OSIRIS-REx, whose team has the possibility to implement late updates to compensate for navigation uncertainties, the mission profile was changed and the sampling plan reviewed because the target asteroid was rougher, with larger albedo variation and higher boulders coverage than expected. Another issue influencing navigation is spacecraft outgassing, therefore bake-out maneuvers have to be planned.

Landing/sampling site selection. In the crewed Apollo missions, the primary landing site requirement was the operations safety. Landing site selection was therefore based on terrains smoothness (absence of craters and boulders) and dust thickness.

Asteroid missions selected the sampling site during observations preceding the sampling. For example, OSIRIS-REx dedicated one mission stage to site selection, based on safety (inferred from the digital terrain model), deliverability (taking into account the guidance accuracy), sampleability and science value. Generally, it is very useful to plan multiple samplings, in order to overcome the failure of a touchdown operation. For example, Hayabusa2 performed two landing operations to sample the Ryugu asteroid. In particular, the second landing occurred close to an artificial crater, previously created by an impact experiment, to sample both surface and subsurface materials.

Sample collection. Whereas Apollo samples were collected in situ by astronauts using hammers, a variety of robotic sample collection techniques has been applied so far: drilling rig on Luna missions (which allowed rock density measurements), solar wind collectors (Genesis), aerogel collectors to sample cometary and interplanetary dust (Stardust), projectile shot on the surface, with fragments collected in a horn (Hayabusa and Hayabusa2), injection of high-purity nitrogen to fludize regolith and carry it into a collection chamber (OSIRIS-REx). Whatever the technique considered, all the returned missions successfully brought back samples, even if collection by means of hypervelocity impacts (Stardust) could have destroyed sample organics. Details on collection techniques, with related pros and cons, are given in Chapter 14 (Della Corte and Rotundi).

Return to Earth. The Earth landing site has stringent requirements for climate and presence of population and buildings, with additional constraints arising in the case of military areas. A detailed review of the landing sites considered so far or to be considered in the future is given in Chapter 15 (Dirri et al.).

The use of a temporary cleanroom for preliminary operations at the landing site has been demonstrated to be very useful to prevent sample contamination. This is particularly true in the case of non-nominal landing, as the occurred Genesis capsule crash: in such a scenario, capsule fragments should be packed, sent to the curation facility and archived, in order to assess the level of terrestrial contamination.

Containers and tools materials. Because materials outgassing is one of the main sample contamination sources, the low outgassing rate is a fundamental requirement of materials used for operations in vacuum (planetary and laboratory) environments. Several materials were never considered in sample return missions (lead, uranium, thorium, lithium, beryllium, boron, potassium, rubidium, strontium, noble gases, rare earths), while those used for in-flight, transport and storage containers include aluminum alloys, stainless steel, glass, fluoroplastics. Teflon is the most used plastic material. Nylon-6, used to bag Stardust samples during curation, revealed to be a source of sample contamination. Hayabusa samples also experienced contamination from terrestrial gases passed through the capsule O-ring seal.

Curation laboratories. Returned samples are accepted in curation facilities. The first operation is their removal from containers, that is performed with different methods, e.g., electrostatic needle, Teflon spatula, screwdrivers, microtomes, focused ion beams. Then the samples are handled, processed and stored.

The primary goal of curation is to protect and preserve samples from terrestrial environment (e.g., dust, atmosphere, water) while maximizing their scientific return. All the protocols and criteria adopted in the facility for samples handling, transport, analysis and storage must guarantee this principle. These include:

- Accurate selection of facility materials (including walls, floors, paints).
- Selection of tools and containers materials, such as stainless steel, teflon, quartz glass, aluminum, neoprene, Viton and other non-contaminating materials.
- Sterilization of containers, when needed.
- Samples handling and storage under vacuum, or, more frequently, in cabinets filled by high-purity nitrogen (in some cases high-purity helium), where entrance of other gases is avoided and monitored. This is guaranteed by maintaining a pressure larger than the outside (positive gradient).
- Cleanroom ISO standard between 4 and 6.
- Maintaining laboratories environmental parameters (pressure, temperature, humidity) within defined ranges.
- Contamination monitoring by witness plates and analysis of contamination reference materials (e.g., samples from the landing site, spacecraft components)
- Cleaning and gowning protocols (with ultrapure water being the most used agent for cleaning). Cleaning rooms can be separated from analysis/storage rooms, while changing room is always a distinct environment.
- Possibility of remote access to samples to minimize samples and scientists movement.

To date, curation activities identified several sources of contamination, e.g., sample collectors (Stardust), box and tools used on the Moon (Apollo), exhaust products, spacecraft-outgassed compounds, secondary materials from impacts on spacecraft components, laboratory tools. Some materials used in facilities, such as Xylan, were later found out to be a source of contamination and subsequently eliminated.

Samples from different missions are curated and stored in different laboratories to avoid their mixing. Thus a new sample return mission requires the development of a new laboratory. The development cost can be reduced by retrofitting an existing laboratory and removing all the materials not appropriate for returned samples curation. Otherwise, the development of a new curation facility could take five to seven years (see the case of the JAXA curation center).

Samples returned from the same mission may require an additional subdivision, i.e., the separation between pristine and processed samples, with the former needing a particular care. Then, samples are catalogued basing on different criteria, such as sample type (e.g., rock or fine), depth (in the case of surface drilling), grain size, composition.

Samples analysis. Returned samples are precious and their analysis must preserve their purity and minimize the risk of sample loss. Sample analysis techniques are non-destructive: photon-based (FTIR and NanoFTIR, Raman spectrocopy, emission spectrometry, and X-ray fluorescence, diffraction and tomography, scanning transmission X-ray microscopy, XANES), electron-based (SEM-EDX, i.e., scanning electron microscopy using energy-dispersive X-ray analyses, TEM, electron probe microanalysis), ion-based, both high-energy (e.g., Proton-Induced X-Ray scattering and Elastic Recoil Detection Analysis) and low-energy (SIMS is one of the most used, but other techniques are also considered). These techniques are often combined into a multi-analytical sequence. Details of these techniques, with their pros and cons, are summarized in Chapter 16 (Brunetto et al.). Destructive techniques might be applied only after a full morphological and optical characterization of the sample.

Restricted samples. Even if restricted samples have never been returned, there is some experience on their curation, because lunar samples were considered under this category until 1971: the Johnson Space Center curating the Apollo samples included vacuum systems for initial sample handling, nitrogen-purged glove boxes for additional handling and quarantine areas for astronauts and equipment.

In addition and thanks to the lessons learned, further improvements are expected in the next years. In the following, we give a non-exhaustive list of future sample return perspectives.

Ongoing missions. The samples brought back by the OSIRIS-REx and Hayabusa2 missions will give new insights into the role of carbonaceous asteroids in creating the Earth's habitability.

New laboratories are under development at the NASA's Johnson Space Center (JSC) and at the JAXA's Planetary Material Sample Curation Facility (PMSCF), that will accept and curate the samples returned from these two missions.

The JSC laboratories will adopt new protocols (Longobardo and Hutzler, Chapter 11, and references therein), limiting outgassing and plastic material (including Teflon) and preferring glass and metals (stainless steel and aluminum). As a matter of fact, contamination studies at JSC extended the list of prohibited materials and identified

appropriate substitutes. These studies also estimated the hydrazine deposit on collectors and samples. Other protocols under definition concern the reduction of organic contamination in air and on the surfaces, such as precision cleaning and baking-out of tools and containers at 500 °C.

Rehearsals for OSIRIS-Rex and Hayabusa2 samples acceptance and processing have been performed at the JAXA curation center (Abe et al., Chapter 12). The main challenge is the Hayabusa2 samples extraction and storage under vacuum (instead of in a high-purity nitrogen environment), that would protect some samples analyses (e.g., N-isotope) against the working environment.

New techniques. New tools are under study for sampling asteroids and cometary nuclei. These include tethered harpoons (appropriate even for cryogenic samples and tilted surfaces) and adhesives (applicable only for very brief encounters). Collectors based on high speed counter-rotating cutters or brush-wheels are under development to sample harder materials. Other studied and tested sample collectors are optimized for cometary nuclei, such as Reactionless Drive Tube (based on ejection of a sacrificial mass), Clamshell Sampler (based on two-quarter-sphere buckets) and BiBlade Sampler. Details of all these techniques are described in Chapter 14 (Della Corte and Rotundi).

Sample analysis techniques are improving, too, thanks to the development of a new generation of light sources, including concepts to produce ultra-brilliant and highly coherent light beams. Moreover, the possibility to miniaturize some of the currently used instruments is under study, and this could have implications for future in-situ missions on planetary bodies. Details on future perspectives of sample analysis techniques are given in Chapter 16 (Brunetto et al.).

Moon sample return. Chang'e 5 was the first sample return mission led by CNSA (China National Space Administration). It was addressed to the Moon and aimed at demonstrating the China's ability to develop key technology for sample return. At the time of writing, Chang'e 5 just returned to Earth almost 2 kg of lunar materials, sampled by means of a robotic arm and a drill from one of the youngest Moon regions. Their analysis will allow refining the lunar chronology curve. Mission details are given in Chapter 9 (Xiao et al.).

The Artemis program, led by NASA with collaboration of other space agencies (ESA, JAXA, Canadian, Italian and Australian Space Agency), plans to return samples from the Moon's South Pole: these samples could contain water ice and therefore be astrobiologically relevant. The program (under implementation while writing this book, and for this reason without a dedicated chapter) includes a series of missions preparatory to a new human landing on the Moon, specifically the first woman and the next man landing, currently scheduled in 2024. These preparatory missions will characterize the lunar South Pole's surface, with particular regard of the volatiles distribution, by means of rover and instrumentation, and will test navigation/communication techniques as well as characterize the deep space environment by means of cubesat and uncrewed/

crewed spacecrafts. The human landing is planned in the Artemis III mission, whose landing site has not been selected yet, but could be within six degrees of the South Pole. 100 kg of science tools and equipment would be carried on the Moon to collect and return 35 kg of different types of lunar samples (i.e., rock, core tubes, material inside and outside the permanently shadowed regions), whose analysis will support the comprehension of impact history, solar wind influence and volatiles role on the Moon. More details on the Artemis program plan are found in the NASAs document https://www.nasa.gov/sites/default/files/atoms/files/artemis_plan-20200921.pdf.

JSC is already planning laboratories for curation and storage of cold and cryogenic samples. It is plausible that remote manipulation techniques would be preferred, due to the difficult handling of these samples.

Whatever the target, an important asset of future sample return missions would be the adoption of a cost and risk mitigation strategy. This would imply the development of technologies appropriate for different mission configurations or for different planetary bodies. The Moon will represent the ideal target to test these technologies, mainly due to its proximity to Earth, but also given its scientific value. Moreover, multiple Moon sample return missions would allow answering unresolved issues about its evolution, such as the time elapsed from the most recent basaltic volcanism events, the compositional ranges of lunar basalts and the anorthositic crust thickness.

Mars Moon eXploration (MMX). The JAXA/MMX, to be launched in 2024, will be the first mission to sample the Martian moon Phobos and will give insights into its formation (currently still debated) and evolution. Both surface and subsurface will be sampled, by means of a pneumatic system and a driller, respectively, allowing to unveil their possible differences in origin, processing, contamination and organics' role. Both NASA/JSC and JAXA/PMSCF are planning the development of a new laboratory dedicated to MMX samples curation. Further details of the mission are given in Chapter 10 (Tasker and Lunine).

ZhengHe. ZhengHe is a CNSA mission approved while writing this book. Its launch is planned between 2024 and 2026 and its goal is the exploration of two targets, a Near-Earth asteroid (2016 HO3) and a Main Belt Comet (133P/Eelst-Pizarro).

Specifically, the mission will return a sample from the NEA and will rendezvous the Main Belt Comet. While technical details of this mission are under definition, from a scientific point of view ZhengHe will enable the understanding of issues related to formation and evolution of the Solar System, and in particular to the role of near-Earth and Main Belt objects impacts in life formation.

Mission concepts. JAXA is considering OKEANOS (Oversize Kite-craft for Exploration and AstroNautics in the Outer Solar System), a solar-power sail mission that would analyze in situ and possibly return a Trojan asteroid sample, in order to clarify the origin of these bodies. Both surface (by means of a projectile plus horn) and subsurface (pneumatic drill) would be sampled.

CAESAR (Comet Astrobiology Exploration SAmple Return) is a mission proposed to the NASA New Frontiers 4 opportunity to sample the 67P/Churyumov-Gerasimenko comet nucleus, giving the chance to determine nature and abundance of dust and gases that may have been originated in the early Solar System. Because the 67P comet has been largely observed by the ESA/Rosetta mission, the sampling site selection would be facilitated, reducing the mission costs. The sample would be collected by means of a touch-and-go maneuver, followed by a pneumatic jet. The possibility to separate volatile and refractory component of the sample through sublimation would allow the return of cometary volatile compounds without the need of developing a sample cryogenic container, further lowering mission expenses. Spacecraft systems would be a technological challenge, because they should guarantee that the sample would be maintained at temperatures below the water freezing point. In the same way, the sample return capsule should be stored at low temperatures after its recovery.

Chapter 10 (Tasker and Lunine) gives further details on these mission concepts.

Curation facility concepts. In addition to NASA's JSC and JAXA's PMSCF, the development of a European curation facility is under evaluation. The European Community funded project EUROCARES (European Curation of Astromaterials Returned from the Exploration of Space) provided requirements for a curation facility dedicated to returned samples. The project started from the state of art of curation facilities and biocontainment systems to identify the necessary steps to create a laboratories complex able to curate both unrestricted and restricted samples. The project gave key recommendations for future sample return, concerning, e.g., amount of returned samples, biohazard, facility design validation, materials, operational workflows, scientific community involvement, analogues and standards, transportation boxes. Details on the project are given in Chapter 13 (Smith et al.).

Mars Sample Return. Bringing back a sample from Mars is currently the most ambitious sample return project, as well as the main opportunity to return a restricted sample: other astrobiologically relevant planetary bodies (e.g., Europa and Enceladus) are farther and sample return missions to these bodies are less considered, even if mission concepts were proposed.

A Mars Sample Return mission would deepen our understanding of geological process and their influence on the current volatile inventory, enabling a more accurate definition of the Mars evolutionary timeline. In addition, such a mission would play an important role in view of future human exploration of Mars, because it could identify hazards and in-situ resources.

The main challenge of a Mars Sample Return mission is to keep the samples in their pristine conditions and simultaneously to contain them because of possible biohazards. According to World Health Organization (WHO) guidelines and Planetary Protection requirements, Martian samples must be considered dangerous for terrestrial environment until it is demonstrated that they are not a risk for life on Earth or until they are

properly sterilized. In other words, they require the breakage of the chain between Mars and terrestrial biosphere, by implementing both the highest planetary protection and the highest biocontainment level.

Most of the collection systems, developed and under development for sampling other planetary bodies, can be applied to Mars. Otherwise, new technologies are required for sample transport, such as portable receiving technologies. According to WHO guidelines, the transportation box to move the samples from landing site to curation facility (or between laboratories) must be based on a triple packaging system (Dirri et al., Chapter 15): the primary receptacle is the innermost layer, and could coincide with the Sample Return Capsule; the secondary package must be made of plastic material (that should be selected on the basis of outgassing rate, physical properties and compatibility with the working environment); the outer package must be rigid and must protect the inner layers from contamination and physical damage.

Curation facilities also require new technologies. For example, remote and robotic manipulation techniques should be preferred, also due to their versatility (they can be useful for unrestricted small samples, too). The main requirement of a laboratory curating restricted sample is the coexistence of contamination control and Planetary Protection approach. While a standard cleanroom requires a positive pressure gradient (that would prevent entrance of gases from outside), a biocontainment laboratory requires a negative pressure gradient (to ensure that sample do not contaminate the terrestrial environment). A possible trade-off is the Double-Walled Insulator (DWI) technique (Meneghin and Brucato, Chapter 18, and references therein), consisting in a double wall separated by an interstice filled by an inert gas. This inert gas would be maintained at a pressure larger than the pressure acting on both the external surfaces, i.e., facing toward the samples and toward the outside, respectively. The coupling of DWI and remote manipulation techniques would minimize the risk of both forward and backward contamination. New protocols for samples sterilization should be also considered, with the sterilization process performed more than once (differently than unrestricted samples).

The first step toward the Mars Sample Return is the NASA/Mars 2020 mission, launched on 30 July 2020. This mission will acquire Martian samples and will store them into a cache, that would be recovered by a following mission. The Mars 2020 Sample Acquisition and Cache System includes the following subsystems (details in Della Corte et al., Chapter 14, and references therein): Brushing and Abrading Tool (based on a rotary actuator), Core Pre-View Bit (to collect and store samples of high scientific value), Powder and Regolith Acquisition Bit (to collect samples from drilling process), Caching Bit (to store the samples). A NASA-ESA joint effort is implementing the strategy to recover the Mars 2020 samples. The current plan is the launch of two additional spacecrafts: the first would be a Mars Orbiter and the second would carry a rover and a Mars Ascent Vehicle (MAV). The samples would be retrieved by the rover, sent to the Mars Orbiter by means of the MAV and finally returned to Earth.

Planetary science community is also considering return of Martian gaseous samples. Analysis of these samples would constrain the origin of the Martian atmosphere and would clarify if it has ever been able to host life forms. The Mars Exploration Program Analysis Group (MEPAG) identified requirements to sample the Martian atmosphere and conceived a preliminary design of a sample canister. The return of Martian gases would require an update of transport, analysis and Planetary Protection protocols as well.

We conclude here the first review on the current state of sample return. Because of the several and ambitious future perspectives, as well as of our quickly improving technological and scientific knowledge, we can guess that it will be soon updated.

Index

Page numbers followed by "*f*" and "*t*" indicate, figures and tables respectively.

F

G

H

I

J

K

L

M

T

U

W

X

Z